CRANFIELD UNIVERSITY

ANA CÁTIA FERRÃO MARQUES

Investigation of the effect of structured hyaluronic acid surfaces on cell proliferation and expression of HA cellular receptors: CD44 and RHAMM

CRANFIELD HEALTH

Translational Medicine Department

PhD Thesis

CRANFIELD UNIVERSITY

CRANFIELD HEALTH

Translational Medicine Department

PhD Thesis

Academic year 2011

ANA CÁTIA FERRÃO MARQUES

Investigation of the effect of structured hyaluronic acid surfaces on cell proliferation and expression of HA cellular receptors: CD44 and RHAMM

Supervisors: Dr. Sarah L. Morgan
Professor David Cullen

March 2011

This thesis is submitted in partial fulfilment of the requirements for the degree of Doctor of Philosophy

Eles não sabem que o sonho

É uma constant da vida

Tão concreta e definida

Como outra coisa qualquer

…

Eles não sabem nem sonham

Que o sonho comanda a vida

Que sempre que um homem sonha

O mundo pula e avança

Como bola colorida

Entre as mãos de uma criança

António Gedeão

They do not know that the dream

Is constantly in life

So real defined

As anything else

…

They do not know, they not even dream

That dream commands life

Whenever a man dreams

The world jumps and progresses

As a colourful ball

At the hands of a child

António Gedeão

ABSTRACT

Hyaluronic acid (HA) is one of the major components of the extracellular matrix; and may exhibit different biological functions, dependent on polymer molecular weight (MW). The signalling events performed by HA are mediated through interactions with its main cell receptors: CD44 and RHAMM. However, the direct effect between the HA MW and the expression of CD44 and RHAMM remains unclear.

This study aimed to investigate whether different HA polymer MW alters the proliferation of tumour-derived cell lines, and whether different HA-sized has an effect on the regulation of the expression of CD44 and RHAMM.

In order to determine size-specific responses of tumour cells of defined fragment MW, this investigation was undertaken using HA-tethered culture surfaces. Four surfaces were constructed, coated with polymers of different MWs. HA (4, 234, 2590 kDa) and an oligomer mixture were tethered onto an aminosilane (AHAPTMS)-treated glass surfaces using a carbodiimide reaction. Surfaces were analysed using a toolbox of *in situ* characterisation techniques, including wettability measurements, QCM, AFM and confocal microscopy. Using the constructed surfaces was demonstrated that HA-polymer MW modulates cell proliferation of human bladder (RT112 and T24) and prostate (PC3 and PNT1A) cell lines, with low HA MW (HA_4) increasing proliferation, whereas a decrease is seen in the presence of medium (HA_{234}) and high MW fragments (HA_{2590}). The proliferation stimulus performed by HA was found to be phenotype dependent, with HA_4 surfaces stimulating an increased proliferation in those less invasive cell lines (T24 and PNT1A), while HA_{234} and HA_{2590} inducing a sharper decrease in the most malignant tumour cell lines (RT112 and PC3). It was also demonstrated that the regulation of CD44 and RHAMM transcripts expression appears to be phenotype dependent but not HA-MW dependent. HA down-regulates CD44 and RHAMM in the most malignant cell lines; with up-regulation of the expression of the cell receptors in the less invasive cell lines. In addition, the presence of exogenous HA was shown to be involved in the regulation of the expression of CD44 variants expression. The results obtained for the CD44 and RHAMM protein expression were also found to be correlated with the obtained transcripts expression. However, the significance of these findings in tumourigenesis remains unclear.

Findings from this investigation may help in the design and development of biocompatible implants with controlled surface properties to be used in cancer

therapeutics; with medium and large HA polysaccharides being potential biopolymer candidates, useful for the development of novel therapies for highly invasive cancer. In addition, implications from this work can serve as a base for future research, and can lead to ideas for drugs and methods to be used in cancer therapeutic approaches.

Key words: CD44/ extracellular matrix/ hyaluronic acid/ proliferation/ RHAMM/ surface/ tumour

ACKNOWLEDGMENTS

First of all, I would like to thank Dr. Sarah Morgan for this opportunity in working in the Translational Medicine Department. Thank you for trusted me this project, for always trying to keep me motivated, for all the critical review, advices and help during this PhD.

I would like to thank to Professor David Cullen for all the critical review and suggestions for this work.

To Dr. Steven Fowler, Dr. Iva Chianella, Joana Senra and Arnaud Lemelle for all the technical support.

To Paul Oladimeji, Dr. Wayne Mitchell, Dr. Ryan Pink, and all the people in Translational Medicine Department for all the teaching, advices and availability.

To all my friends who were always to my side, for their motivation, understanding, encouragement, and most of all for all the friendship.

Last but not the least. To my parents and my family, for their love, support, motivation and understanding. Thank you for having helped me to reach the end of this long marathon.

TABLE OF CONTENTS

LIST OF FIGURES

LIST OF TABLES

LIST OF EQUATIONS

ABBREVIATIONS

°C – Degree Celsius

aa - aminoacid

abl – Abelson murine leukemia

AFM – Atomic force microscopy

AHAPTMS – N-[6-(aminohexyl)aminopropyl]-trimethoxysilane

akt – Murine thymoma viral oncogene

APC – Adenomatous Polyposis Coli

ATM – Ataxia telangiectasia mutated

Bad – BCL2-antagonist of cell death

BAX – Bcl-2–associated X protein

bcl – B-cell CLL/lymphoma

BRAC – Breast cancer

b-raf – V-raf murine sarcoma viral oncogene homolog B1

Ca – Calcium

CAM – Cell adhesion molecule

CD – Cluster of differentiation

CD44 – Cluster of differentiation 44

Cdc37 – Cell division cycle 37 homolog

CDK – Cyclin-dependent kinases

cDNA – Complementary DNA

c-myc – Proto-oncogene myc

CSC – Cancer stem cells

Da – Dalton

DEPC H_2O – Water treated with diethyl pyrocarbonate

DMEM – Dulbeccos modified eagles medium

DNA – Desoxirribonucleic acid

dNTP – Deoxyribonucleotide

DPC4 – Deleted in pancreatic cancer, locus 4

ECM – Extracellular matrix

ECMRIII – Extracellular matrix receptor III

EDC – 1-ethyl-3-[3-dimethylaminopropyl]carbodiimide hydrochloride

EDTA – Ethylenediaminetetraacetic acid

EMD – Endoscopic mucosal dissection

EMR – Endoscopic mucosal resection

EMRSH – Endoscopic mucosal resection sodium hyaluronate

EMT – Epithelial-mesenchymal transition

erbB – v-erb-b2 erythroblastic leukemia viral oncogene

ERK – Extracellular-signal-regulated kinase

erk1 – Extracellular signal-regulated kinase 1

Fas – Fatty acid synthase

FCS – Foetal calf serum

FHIT – Fragile histidine triad gene

G1 – gap 1

G2 – gap 2

GAG – glucosaminoglycan

gip – Gastric inhibitory polypeptide

Glca – D-glucuronic acid

GlcNAc – D-N-acetylglucosamine

gp90 Hermes – Llymphocyte homing receptor

GPI – Glycosylphosphatidyl inositol

gsp – Fused glutathionylspermidine amidase/glutathionylspermidine synthetase

Gy – Gray

H_2O – Water

HA – Hyaluronic acid, hyaluronan

HAPB – HA-binding proteins

HARE – Hyaluronan receptor for endocytosis-like

HAS – Hyaluronan synthase

HBP – Heme-binding protein

HCl – Hydrochloric acid

HEPES – 4-(2-hydroxyethyl)-1-piperazineethanesulfonic acid

hox-11 – T-cell leukemia homeobox 1

hsp – Heat shock protein

HYAL – Hyaluronoglucosaminidase

IAP – Inhibitor of apoptosis

IGF – Insulin-like growth factor

IgG – Immunoglobulin G

IHABP4 – Hyaluronan binding protein 4

INK4 – Cyclin-dependent kinase inhibitor 2

IαI – Inter-α-trypsin inhibitor

kDa – Kilo Dalton

LEC – Liver-expressed chemokine

LKB1 – Serine/threonine kinase

Ly-24 – CD44 antigen

LYVE-1 – Lymphatic vessel endothelial hyaluronan receptor 1

M – mitotic

mAb – Monoclonal antibody

MAP – Mitogen activated protein

MAS – MAS1 oncogene

MEK1 – Mitogen-activated protein kinase kinase 1

MET – Mesenchymal-epithelial transition

mg – Milligram

$MgCl_2$ – Magnesium chloride

ml – Millilitre

MLH1 – mutL homolog 1, colon cancer, nonpolyposis type 2

mm – Millimetre

mM – Millimolar

mRNA – Messenger RNA

MSH – Muscle segment homeodomain protein

MTT – 3-(4,5-dimethylthiazolyl-2)-2,5-diphenyltetrazolium bromide)

MW – Molecular weight

myc – v-myc myelocytomatosis viral oncogene homolog

NaCl – Sodium chloride

NaCl – Sodium chloride

NaOH – Sodium hydroxide

NaOH – Sodium hydroxide

NF – Neurofibromin

NHS – N-hydroxysuccinimide

NKX3.1 – NK-3 transcription factor, locus 1

nm – nanometer

nm – Nanometre

Oct – Octamer-binding transcription factor

p16 – Cyclin-dependent kinase inhibitor 2A

p27 – Cyclin-dependent kinase inhibitor 1B

p53 – Tumour suppressor 53

p68 – DEAD (Asp-Glu-Ala-Asp) box polypeptide 5

pAb – polyclonal antibody

PAI-1 – plasminogen activator inhibitor-1

PARP – Poly-ADP-Ribose-Polymerase

PBS – Phosphate buffered saline

PCR – Polymerase chain reaction

PDGF – Platelet-derived growth factor beta

PDGFR – Platelet-derived growth factor receptor, alpha polypeptide

Pgp-1 – Phagocytic glycoprotein

pm – picometer

PML – Promyelocytic leukemia protein

PMS – Methionine sulfoxide reductase A

PTC – Coiled-coil domain containing 6 (CCDC6)

PTEN – Phosphatase and tensin homolog

QCM – Quartz crystal microbalance

Rac – Rat Sarcoma

Raf – v-raf murine leukemia viral oncogene homolog

RARα – Retinoic acid receptor α

ras – Rat sarcoma viral oncogene homolog

Rb – Retinoblastoma

RHAMM – Receptor for HA-mediated motility

RNA – Ribonucleic acid

RO – Reverse osmosis

RT – Reverse transcriptase

S – Synthesis

s.d. – Standard deviation

SAM – Self-assembled monolayer

SHAP – Serum-derived hyaluronan-associated protein

src – v-src sarcoma viral oncogene homolog (avian)

TBS – Tris buffered saline

TGF-α – Transforming growth factor, alpha

TLR-4 – Toll-like receptor 4

TNF – Tumour necrosis factor

TNM system – Tumour, Node, Metastases (Classification of Malignant Tumours)

TSC1 – Tuberous sclerosis 1

UICC – International Union Against Cancer

UK – United Kingdom

USA – United States of America

UV – Ultraviolet

VEGF – vascular endothelial growth factor

VHL – von Hippel-Lindau tumor suppressor

Wt1 – Wilms tumor 1 homolog

XPS – X-ray photoelectron spectroscopy

β – Beta

µl – Microlitre

µM – Micromolar

µmol – Micromoles

CHAPTER 1

“What is essential is invisible to the eye” – Antoine de Saint-Exupery

CHAPTER 1

1. INTRODUCTION

The extracellular matrix (ECM) once regarded simply as structural scaffold, is now recognised as an important modulator on cell phenotype and function, with cells requiring interactions with ECM components in order to undergo normal morphogenesis and consequently organogenesis. In certain pathological disorders such as cancer, increased synthesis of certain ECM components and/or increased breakdown with generation of ECM cleavage products can contribute to tumour progression. Hyaluronic acid (HA) is a major component of the ECM and it interacts with cells via two main receptors: CD44 and RHAMM. HA has been demonstrated to play a role in a number of processes, including embryonic development, wound healing, cell migration and proliferation and is implicated in tumour progression. The biological functions exhibited by HA are known to be dependent on the polymer molecular weight (MW), and mediated through interactions with its main cell receptors. However, the direct effect between the HA MW and the expression of CD44 and RHAMM remains unclear.

The technology platforms originally developed for tissue engineering applications, once regarded in an opposite field of cancer research, are starting to provide valuable *in vitro* and/or *in vivo* models for cancer investigation. Immobilised components on a 2D substrate may more closely stimulate cell responses within 3D scaffolds due to intimate cell contact with the substrate, rather than periodic contact with exogenous components of media supplementation. Biological surfaces have been

used in medical implants for tissue regeneration and drug delivery systems, as well as in the unleashing of the structure and function of many biological receptors. HA structured surfaces not only offer the opportunity to be used in the establishment of *in vitro* models for the investigation of factors involved in tumourigenesis, but also provide insights for potential use in cancer therapeutics applications.

1.1. THESIS STRUCTURE

This thesis is organised into six chapters of work. **Chapter 1** presents a review of the literature, aiming to provide relevant information for the understanding of this project. Therefore, this chapter gives an overview on basic cancer biology at a molecular and cellular level. It is presented hyaluronic acid and its importance in cancer biology along with the currently medical applications. The current understanding of the relation of hyaluronan with its main important cellular receptors CD44 and RHAMM is also reviewed. Finally it is given an overview of tissue engineering, and how it can meet the needs in cancer research, and as well as a summary of constructed HA biological surfaces. **Chapter 2** describes the experimental design and methodology for the construction of a variety of novel structured hyaluronic acid surfaces, used to support the adhesion and growth of cultured cell lines. This chapter also reports the characterisation of these surfaces. **Chapter 3** presents the methods used in mammalian cell culture. This chapter investigates whether HA has an effect on proliferation and apoptosis in human bladder and prostate cell lines. In **Chapter 4** whether HA has an effect on CD44 and RHAMM expression is investigated on human cell lines, at both transcriptional and translational level. **Chapter 5** presents a final discussion of the

results and **Chapter 6** gives a general conclusion of the presented investigation and the current proposed direction of future work.

1.2. INTRODUCTION TO CANCER BIOLOGY

Cancer is a major public health problem in most of developed countries, affecting people at all ages, but typically the risk increases with age. In 2007, according to the American Cancer Society, of the 10 million new cases diagnosed, 7.6 million people died from cancer in the world. This corresponds about 13% of all deaths worldwide, with one in four deaths can be attributed to cancer, being the second most common cause of death in industrialised countries after cardiovascular diseases (Van der Schueren *et al.*, 2000; WHO, 2002; Jemal *et al.*, 2007; American Cancer Society, 2008a).

1.2.1. THE MOLECULAR BASIS OF CANCER

Cancer is a group of diseases sharing common characteristics. It is considered a genetic disease, since malignant phenotype results from a genetic alteration, which is then transmitted from the mutated cell to its cellular offspring. Such alterations in the expression of genes lead to uncontrolled cell proliferation, invasion, and spread of cells from the site of origin to other sites in the body (Pecorino, 2005; Gabriel, 2007). There are a number of mechanisms by which alterations in gene expression occurs, and can occur through two routes: DNA alterations (such as mutation, translocation, amplification, deletion, loss of heterozygosity) or abnormal gene transcription or

translation. This results in an imbalance of cell replication and cell death that favours growth of a tumour cell population; whereas in normal tissues cell proliferation and death are in a state of equilibrium (Rudon, 2007). Depending on the damage abnormal cells may form either benign or malignant tumours. Benign tumours are not considered cancerous and rarely cause death, growing slowly and being limited to a specific location. Whereas, malignant tumours interfere with the normal functions of the body and being often fatal, since they can undergo metastasis, migrating through the blood or lymph vessels to distant locations throughout the body (McKee and McKee, 2008).

Cancers are classified according to the tissues affected: carcinomas, which are the vast majority of cancerous tumours, are derived from epithelial tissue cells including skin, breast, various glands and the lining of most internal organs; adenocarcinoma originates in glandular tissue; sarcomas are tumours arising from connective or supportive tissue, including bone, cartilage and muscle; leukaemias are cancers of the bone marrow, where excessive leukocytes are produced; myeloma also arises from bone marrow, being a cancer of plasma cells; in lymphomas the lymphocytes produced in the lymph nodes and spleen proliferate uncontrollably; blastoma originates from precursor cells or blasts (immature or embryonic tissue of organs), and can occur in different part of the body, including the brain, liver, kidneys, nervous system, bones and retina. (McKee and McKee, 2008).

1.2.1.a. Carcinogenesis

Carcinogenesis is the process by which cancers are generated, i.e., is the process by which normal cells are transformed into cancer cells. It is a mechanism resulting

from the accumulation of errors in vital regulatory pathways, due to dynamic changes in the genome (King, 2000; Hanahan and Weinberg, 2000). Mutations producing oncogenes with dominant gain of function and tumour suppressor genes with recessive loss of function are in the basis of genome changes (Bishop and Weinberg, 1996).

Vogelstein and Kinzler (1992), using skin painting experiments in mice have elucidated that carcinogenesis is a multistep process, constituting the first step towards neoplastic tumour development. The process by which neoplastic tumour development takes place can be split into a series of stages termed initiation, promotion and progression. Initiation is an early irreversible change produced by the single or very limited application of initiating factors (or carcinogens). Initiating agents can be chemical, physical or bacterial/viral, and generate a genetic mutation (such as transitions, transversions and deletions) within the cell. This mutation does not take effect until a secondary factor, a promoting agent, is present (King, 2000; Rudon, 2007). Cells may remain in this initiated latent stage for a number of years until acted upon by a promoter. During this time, cellular proliferation must occur, but it may originally be limited by host defences (Rudon, 2007). Promoting agents are influencing factors (not carcinogens) that enhance the effect of the damage caused during the initiation stage. These are numerous, varying from cell specific factors to hormones and normal growth factors. Promotion is a reversible stage, and commonly associated with increased mitosis, which stimulates the development of an initiated cell to a tumour (King, 2000; Rudon, 2007). Tumour development can also be promoted by chemicals that not modify DNA structure – denominated as tumour promoters, and contributing to carcinogenesis by two principal methods: by activating components of intracellular signalling pathways, in which some molecules (e.g. phorbol esters) provide the cell a growth

advantage over the neighbours; and the second method may involve transient effects such as increasing cellular Ca2+ levels or increasing synthesis of enzymes that convert procarcinogens into carcinogens. Conversely to initiating agents, the effects of tumour promoters are reversible, and only producing permanent damage only with prolonged exposure after an affected cell has undergone an initiating mutation (McKee and McKee, 2008). Once a cell begins to proliferate, it enters in the stage of progression, where tumour progression escapes from the host defence mechanisms, and vascularisation of the growing tumour ultimately occur. During this stage genetic instability occurs, leading to a number of complex genetic mutations (such as deletions, translocations and gene amplification), alteration of surrounding cells sensitivity, and loss of growth regulation. All these events lead to phenotypic instability and eventual tumour formation. The tumor progression is reversible only up to a certain point, where the accumulation of a number of genetic changes reaches a point where progression becames an irreversible stage (King, 2000; Rudon, 2007).

1.2.1.b. Cell growth and proliferation

Cellular growth and proliferation in normal tissues are events highly controlled and regulated. The cell cycle is an ordered series of events leading to cell replication, and being divided in two basic periods: mitosis and interphase (**Figure 1.1**). It is during the interphase in which cell grows; accumulating nutrients needed for mitosis and DNA replication takes place. Cell cycle events occur in an orderly manner, which is organised in four major biological and biochemical stages: G1 (gap 1), S (synthesis), G2 (gap 2) and M (mitotic) phases. G1 is the first phase within interphase, from the end of the

previous M phase until the initiation of the DNA replication. In this phase, the cell is metabolically active, producing mRNA and proteins, and continuously grows, but do not synthesise its DNA. G1 is followed by S phase, with the DNA synthesis and chromosome replication. The DNA replication is followed by G2 phase, during which cell growth continues and significant protein synthesis occurs. In G2 phase the cell checks if DNA-replication is complete and prepares for mitosis. Mitosis (M phase) consists in the nuclear division, where the separation of the daughter chromosomes takes place, and ending with cytokinesis (cell division) take place (Alberts *et al.*, 2002; Lodish *et al.*, 2004; Stein and Pardee, 2004; Cooper and Hausman, 2007).

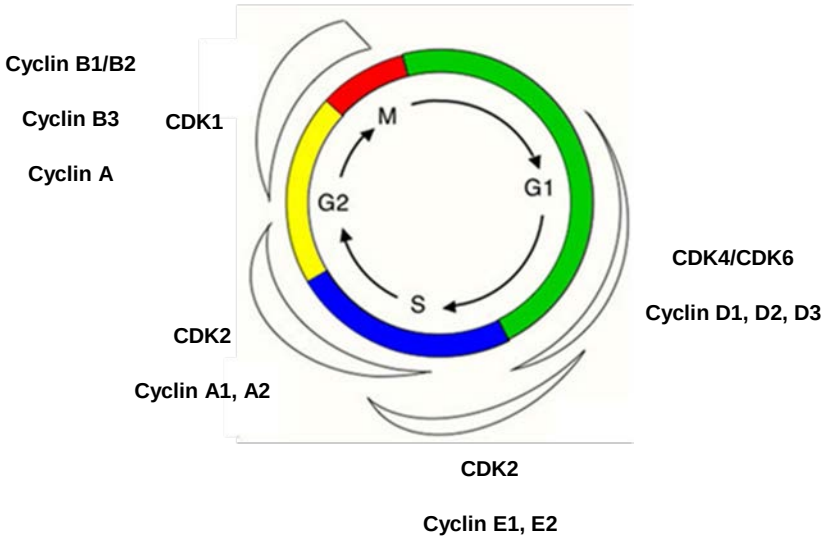

Figure 1.1 – The phases of the cell cycle. Approximate time of activity for different combinations of cyclins and CDKs. Shapes outside the cycle indicate increase and reduction of corresponding CDK/cyclin activity [Adapted from Van den Heuvel, 2005].

The typical human cell cycle takes approximately 24 hours, where the G1 phase might last about 11 hours, S phase about 8 hours, G2 phase about 4 hours and M about 1 hour. Cells in the G1 phase do not always continue through the cycle. Instead, if extracellular conditions are unfavourable, they can exit from the cell cycle and enter a

quiescent stage of the cycle (G0). The cells in G0 phase are metabolically active but no longer proliferating. They can remain in this phase for days, weeks or even years until have appropriated extracellular signals to its proliferation (Albers *et al.*, 2002; Cooper and Hausman, 2007).

The cell cycle is controlled trough the interaction of three different families of proteins: cyclins (phosphatases), cyclin-dependent kinases (CDKs) and cyclin-dependent-kinase inhibitors (INK; **Figure 1.1;** Stein and Pardee, 2004; Van den Heuvel, 2005). CDKs play key role in the phosphorylation of the proteins required for cell progression, and cyclins activate CDKs. INK bind and block activities of cyclin/CDK complexes, counterbalancing the cyclin's activation of CDKs, and in this manner affecting cycling and developing tumourigenesis (Stein and Pardee, 2004).

Uncorrected failures of DNA repair are important in the progression from normal to cancerous cells. There are some crucial steps involved in the regulation of the cell cycle: these include detection and repairing of genetic damage, and provision of various checkpoints to prevent uncontrolled cell division, delaying the entry into the next phase of the cell cycle (Albers *et al.*, 2002; Stein and Pardee, 2004; Cooper and Hausman, 2007). In the process of DNA checkpoint control a signal transduction cascade occurs (**Figure 1.2**). Therefore, if DNA replication stops for any reason and/or the DNA is damaged, a signal is detected by sensor proteins and then sent by transducer proteins to effector proteins, which block the cell cycle and elicit DNA repair (**Figure 1.2A**).

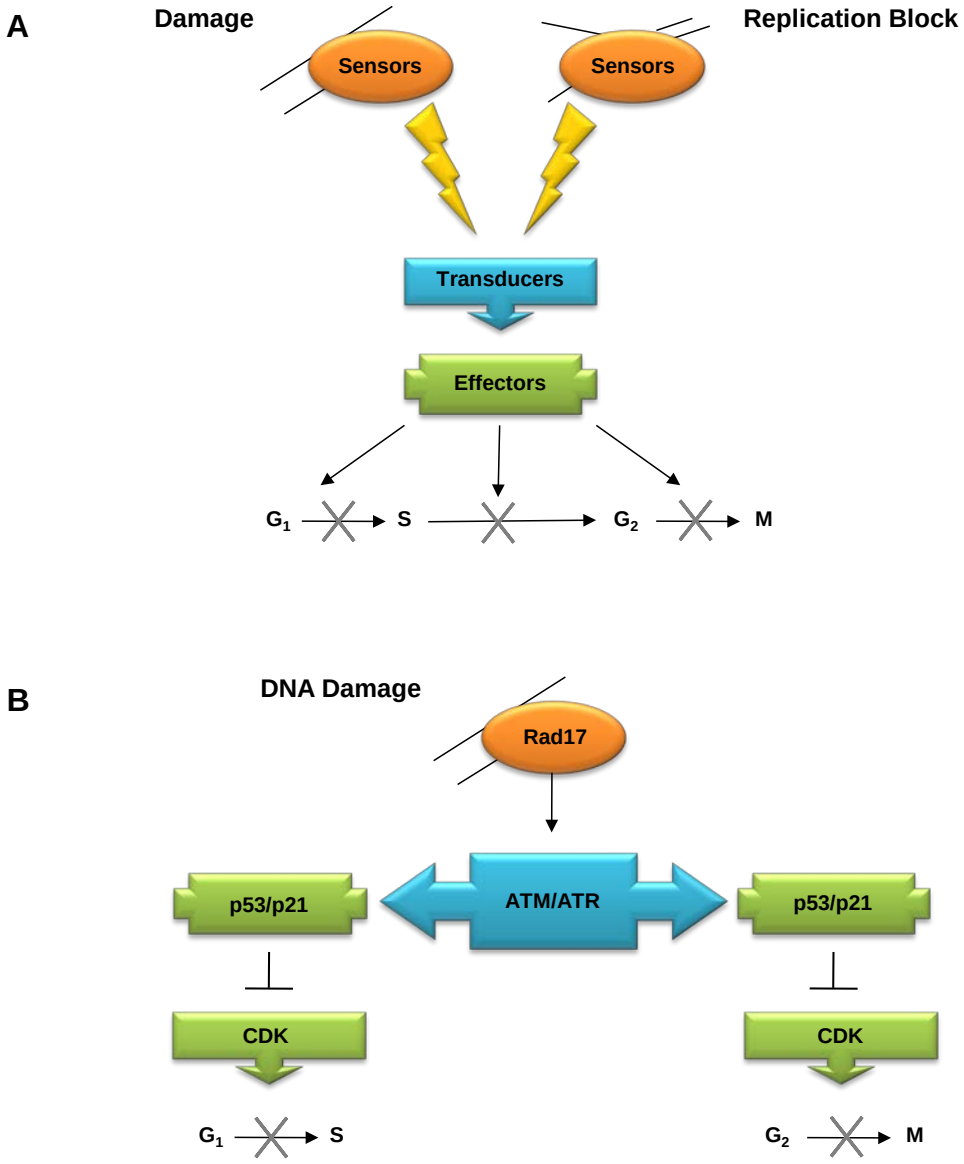

Figure 1.2 – (**A**) DNA checkpoint regulation; (**B**) DNA damage checkpoint [Adapted from Stein and Pardee, 2004].

There are three major checkpoints in this regulation control: G_1 to S transition, which prevents damaged G1 cells from beginning DNA synthesis until DNA has been repaired; S phase; and G_2/M transition. There are several molecular pathways and several proteins involved in the regulatory mechanisms of the cell cycle. One of the most important proteins implicated is p53 tumour suppressor protein (Ko and Prives,

1996), which increases its levels when DNA is damaged and acting as a transcription factor, increasing the expression of a number of important genes. As a result, p21 protein is induced (Brugarolas *et al.*, 1995; Deng *et al.*, 1995), blocking DNA synthesis by inhibiting cyclin/CDK; and this resulting in the stimulation DNA repair mechanisms. In this pathway, DNA damage signal is transduced by the ATM (ataxia telangiectasia mutated) protein (Savitsky *et al.*, 1995), which phosphorylates and increases p53, and therefore resulting in the transcription of p21. P53, known as the "guardian of the genome", stops cell cycle progression by inhibiting the CDK enzyme either at G_1/S or at G_2/M, when DNA is damaged (**Figure 1.2B**; Stein and Pardee, 2004). Rb (retinoblastoma) protein (Weinberg, 1995) is another important protein implicated in cell cycle regulation, playing key roles in the regulation of the proliferation, acting as a barrier to inappropriate cell progression. Rb is involved in G_1/S checkpoint, checking and ensuring the DNA integrity before synthesis at S phase. This process is also mediated through an interaction of p53 with Rb, and where a delay of the cell cycle progression occurs if DNA damaged is detected (Stein and Pardee, 2004). If the DNA damage is irreparable, then p53 mediates the entry of cells into apoptosis (programmed cell death; Stein and Pardee, 2004; Cooper and Hausman, 2007).

1.2.1.c. Apoptosis

In normal tissues, the number of cells is tightly regulated. This regulation occurs, not only by controlling the rate of cell division, but also by controlling the rate of cell death. Therefore, cellular proliferation occurs in balance with cell death. If cells are physiological unneeded or dangerous, they commit suicide by activating an

intracellular death program. This mechanism is denominated as programmed cell death or apoptosis, and can be divided in three phases: induction, commitment and degradation (Stein and Pardee, 1999; Vaux and Korsmeyer, 1999; Alberts *et al.*, 2002; Stein *et al.*, 2004). A cell may enter in apoptosis due a number of inducing events, such as a decrease or complete withdrawal of growth cytokines (including TGF-α, IGF, PDGF), influence of death-promoting cytokines (such as TNF), or DNA damage provoked by radiation and genotoxic agents and drugs used for chemotherapy. After induction, cells enter in an irreversible commitment phase (King, 2000). The intracellular machinery responsible for apoptosis depends on a family of proteases known as caspases (cysteine-aspartate-acid-proteases). Initially caspases are synthesized in the cell as inactive procaspases, and then are activated by other caspases proteins. Once activated, caspases alter mithocondrial function to release cytochrome C into the cytoplasm, where it activates other procaspases, and what consequently results in an amplification of proteolytic cascade (King, 2000; Alberts *et al.*, 2002). These proteins cleave other key proteins in the cell (such as endonucleases and proteases, as well as proteins involved in DNA repair, RNA splicing, signal transduction and transcription factors), leading to the degradation phase (**Figure 1.3**; King, 2000; Alberts *et al.*, 2002, Stein and Pardee, 2004). The caspase cascade is activated by either extracellular or intracellular death signals, which cause intracellular adaptor molecules to aggregate and activate procaspases (Alberts *et al.*, 2002, Stein and Pardee, 2004). The regulation of the cascade is carried out by many cellular mechanisms, including transcriptional regulation and posttranslational modification (Earnshaw *et al.*, 1999; Stein and Pardee, 2004). Bcl and IAP (inhibitor of apoptosis) protein families are involved in the regulation of caspases (Alberts *et al.*, 2002). The Bcl family consists of Bcl-2 (Cory and Adams,

2002), an anti-apoptotic protein involved in the inhibition of apoptosis; and BAX and Bad, which are pro-apoptotic, involved in the activation of apoptosis (Deveraux and Reed, 1999; Hay, 2000). The relative proportions of BAX/Bcl-2 in the cell determine the apoptosis response. Therefore, if the concentration of BAX is high enough, then the cell will enter in the degradation phase, whilst a high enough concentration of Bcl-2 will block apoptosis. On the other hand, Bad blocks Bcl-2, altering the balance in favour of BAX, and as a consequence stimulates the apoptosis (King, 2000). Cells that enter apoptosis via p53 are affected through this BAX/Bcl-2 protein balance, since p53 induces an increase of BAX (King, 2000, Stein and Pardee, 2004). IAP proteins have two mechanisms of inhibiting apoptosis: one is that they bind to some procaspases to prevent their activation, and the other is their binding to caspases inhibiting their activity (Alberts *et al.*, 2002). If a cell enters in the degradation phase, then a change in the permeability of the mitochondrial membrane results in the release of cytochrome C and calcium ions within the membrane. The release of cytochrome C results in the breakdown of membranes and cytoskeleton. The release of calcium, which is characteristic of apoptosis, leads to the degradation of DNA by calcium ion sensitive nucleases (King, 2000). Degradation is characterised by morphological changes of the cell such as shrinkage, chromatin condensation, DNA fragmentation and plasma membrane blebbing. As a result, the cell dismantles itself (apoptotic body) quickly and neatly, and it is rapidly taken up and digested by neighbouring cells (Alberts *et al.*, 2002, Stein and Pardee, 2004).

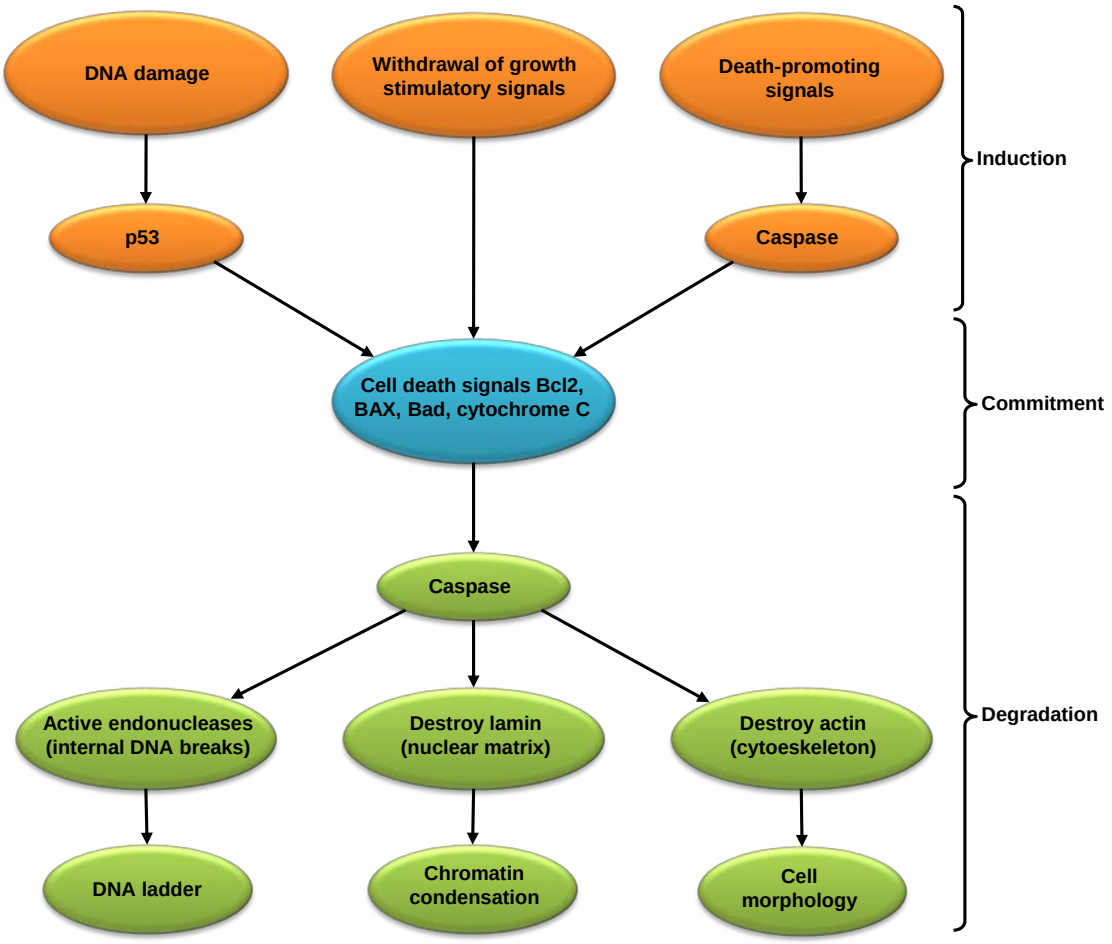

Figure 1.3 – Pathways promoting apoptosis [Adapted from King, 2000].

Defects in apoptosis process contribute to neoplastic diseases, by preventing or delaying normal cell turnover, and resulting in cell accumulation. Cell accumulation facilitates tumour progression, and as a consequence, cancer cells start becoming resistant to death mechanisms and survive beyond their normally intended lifespans. These cell alterations are due the subversion of the need for exogenous survival factors, protection from hypoxia and oxidative stress as tumour mass expands, and accumulation of genetic alterations that deregulate cell proliferation, interfering with differentiation, promoting angiogenesis, and increasing cell motility and invasiveness during tumour progression. Abnormal apoptosis also facilitates metastasis, since cells

do not attach to extracellular matrix, and promotes resistance to immune system, chemotherapy and radiation (Kufe *et al.*, 2003; Frank, 2007).

1.2.1.d. Oncogenes and tumour suppressor genes

Neoplastic transformation is dependent upon the accumulation of multiple mutations of a single cell, and where there is a loss of control favouring the increase proliferation and decrease of apoptosis (Coleman and Tsongalis, 2002). The genes involved in neoplastic transforming mutations are divided in two major classes: oncogenes and tumour-suppressor genes (Kurzrock and Talpaz, 1996; Precorino, 2005).

An oncogene is a mutated allele of normally functioning wild-type genes (proto-oncogenes). The oncogene protein product is produced in higher quantities or is an altered product that has increased activity. These quantitative and qualitative changes, or the combination of both, are due to mutations within the coding regions and/or regulatory sequences of the oncogene. According to a genetic point of view, this is referred to as a gain of function mutation, and is termed as transforming potential. Only a mutation in one allele is required for the activation of the proto-oncogene and loss of regulation of the proto-oncogene product. Thus, oncogenes act in a dominant manner (King, 2000; Coleman and Tsongalis, 2002; Precorino, 2005). Oncogenes can be referred to as either c-onc or v-onc, depending on their nature – cellular or viral, respectively (King, 2000). Oncogenes are grouped according to the function of the proto-oncogene protein product, and there are several classifications, not existing yet a widely accepted standard: growth factors (e.g. sis), receptor tyrosine kinases (e.g. PDGFR), membrane associated non-receptor tyrosine kinases (e.g. src), G-protein

coupled receptors (e.g. MAS), membrane associated G-proteins (e.g. ras), serine/threonine kinases (e.g. raf), nuclear DNA-binding/transcription factors (e.g. myc) (Kurzrock and Talpaz, 1996; Cooper and Hausmen, 2007).

Tumour-suppressor genes encode proteins that inhibit or suppress cell proliferation. Unlike oncogenes, generally tumour-suppressor genes mutations act recessively, since both alleles need to be affected. And in genetic terms, tumour-suppressor genes are referred as loss of functions mutations since they act as the cellular breaking mechanism, regulating cell proliferation in a negative manner (Coleman and Tsongalis, 2002). However, there are some exceptions for these recessive alterations in tumour-suppressor genes, such as p53 (Baker *et al.*, 1990) and p27 (Fero *et al.*, 1998). Tumour-suppressor genes encode five classes of proteins: intracellular proteins that regulate or inhibit progression through a specific stage of the cell cycle (e.g. p16 and Rb), receptors for secreted hormones that function to inhibit cell proliferation (e.g.TGF-β), checkpoint-control proteins (e.g. p53), proteins that promote apoptosis and enzymes that participate in DNA repair (Lodish *et al.*, 2004).

1.2.1.e. Cell adhesion molecules

Cells are surrounded either by other cells or by extracellular matrix (ECM), and contact tightly and interact specifically with each other. This interaction is mediated by cell adhesion molecules (CAMs), which enable cells to adhere tightly and specifically with cells of the same or similar type. CAMs are transmembrane receptor proteins that can be divided in four major families: immunoglobulin superfamily, integrins, cadherins and selectins (Lodish *et al.*, 2004; Cooper and Hausmen, 2007). Ca^{2+}, Mg^{2+} or Mn^{2+} are

required for selectins, integrins and most of the cadherins cell-mediated adhesion molecules (Cooper and Hausmen, 2007).

Integrins are involved in the attachment of the cell to the ECM, as well as in the signal transduction from the ECM to the cell (Lodish *et al.*, 2004; Cooper and Hausmen, 2007). They are chief molecules in the development of tissues during morphogenesis, maintenance of adult tissue, wound healing, and oncogenesis, as they play roles in the architecture of the cellular shape, mobility and regulation of the cell cycle (Mizejewski, 1999; Lodish *et al.*, 2004; Cooper and Hausmen, 2007). Alterations in the expression of integrins are associated with tumour growth and metastasis, and they have also been shown to mediate angiogenesis in several types of cancers (Saiki, 1997; Mizejewski, 1999).

Cadherins are key intracellular adhesion molecules in cell-cell adhesion and cell signalling, maintaining tissue architecture and playing key roles during tissue differentiation (Lodish *et al.*, 2004; Cooper and Hausmen, 2007). Cadherins are a large family of proteins, being composed for about 80 members (Cooper and Hausmen, 2007). E-cadherin is one of the most studied cadherin, being expressed in epithelial tissues, leading to selective adhesion of epithelial cells to one another; and the loss of this protein function or expression is implicated in cancer progression and metastasis (Saiki, 1997; Lodish *et al.*, 2004; Cooper and Hausmen, 2007).

Selectins are expressed on the surface of leukocytes and activated in endothelial cells. They mediate the adhesion of the leukocytes to vascular endothelial cells (Tedder *et al.*, 1995; Cooper and Hausmen, 2007). This event is followed by the formation of more stable adhesions, in which integrins on the surface of leukocytes bind to immunoglobulin superfamily molecules, and are expressed on the surface of endothelial

cells (Lodish *et al.*, 2004; Cooper and Hausmen, 2007). The immunoglobulin superfamily is composed for more than 100 proteins, which are involved in cellular processes of recognition, binding and adhesion (Cooper and Hausmen, 2007). Selectins and immunoglobulin superfamily proteins have been shown to be involved in the metastasic process, as they promote the migration of tumour cells from the site of origin (Saiki, 1997).

1.2.2. EXTRACELLULAR MATRIX AND CANCER

Unlike bacterial, fungal and plant cells, animal cells are not surrounded by a rigid cell wall. However, many animal cells in tissues are embedded in an extracellular matrix (ECM), which fills the spaces between cells and binds cells and tissues together, providing structural support to the cells. This matrix is composed of water and a variety of proteins and polysaccharides, such as collagen, fibronectin, laminin, proteoglycans and glycosaminoglycans, which are secreted locally and interact with receptors on the cell surface (**Figure 1.4**; Yang *et al.*, 1994; Alberts *et al.*, 2002; Kufe *et al.*, 2007).

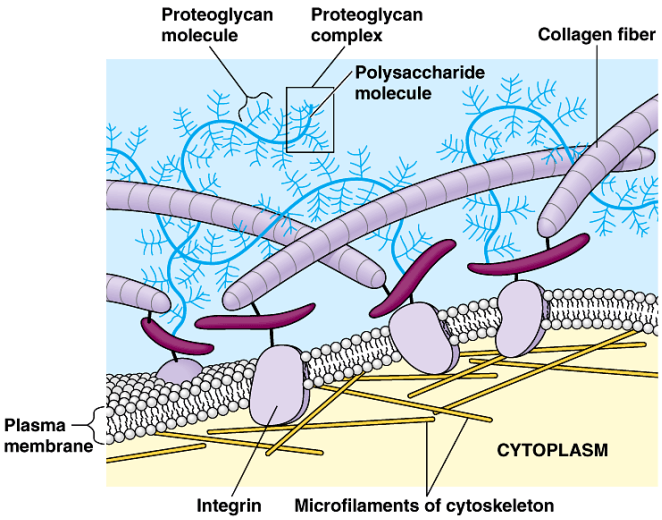

Figure 1.4 – Scheme of the extracellular matrix components (Simmons, 2007).

The composition of the extracellular matrix macromolecules and their organisation in the ECM is dependent on the type of tissue. Therefore, ECM has different forms, each adapted to functional requirements of that particular tissue (Alberts *et al.*, 2002). ECM does not only play key roles in the cell architecture control of cell behaviour, but it also have a role on the cellular survival, development, migration and proliferation (Alberts *et al.*, 2002; Kufe *et al.*, 2007). Most of normal cells are anchorage-dependent, i.e., they need to be attached to one another and to the ECM for normal growth, differentiation, and function. When normal cells are detached, they undergo apoptosis. Unlikely, cancer cells are not anchorage-dependent, being free to proliferate and having increased cell motility and potential tissues invasiveness (Kufe *et al.*, 2007).

ECM has a crucial role during the invasion of cancer cells (Herrera-Gayol and Jothy, 2002; Gosh *et al.*, 2004; Pavia *et al.*, 2005). Malignant cells produce a variety of lytic enzymes and cytokines that degrade and modify the ECM. The degradation and modification of the ECM allow the invasion of the tumour, through tissue barriers,

blood vessel and lymph channel walls, with the possible further metastatic development (Liotta and Kohn, 2001; Kufe *et al.*, 2007). Promotion of abnormal intra- and inter-cellular signalling stimulates cell migration, promotes proliferation and survival of those malignant cells (Adamia *et al.*, 2005b). On the other hand, ECM can also act as a camouflage for malignant cells, and enable them do not be recognised by the body's immune system (Pavia *et al.*, 2005).

1.3. HYALURONIC ACID

1.3.1. STRUCTURE AND FUNCTION OF HYALURONIC ACID

1.3.1.a. Physicochemical and structural properties

Hyaluronic acid (HA, also called hyaluronan or hyaluronate; Balazacs *et al.*, 1986) was first biochemically isolated and purified from bovine vitreous humour and umbilical cord tissue in the 1930s by Meyer and Palmer (Meyer and Palmer, 1934, 1936), and solved its structure in the 1950s (Weissman and Meyer, 1954).

HA is considered as a glucosaminoglycan (GAG), being the only non-sulphated member of this family (**Table 1.1**). It is a polymer composed of disaccharide units, each consisting of D-glucuronic acid (Glca) and D-N-acetylglucosamine (GlcNAc), linked together via alternating β-1,4 and β-1,3 glycosidic bonds (**Figure 1.5**; Laurent, 1970; Laurent and Fraser, 1992; Mian, N., 1986; Scott and Heatley, 2002).

Table 1.1 – Glycosaminoglycans group [Adapted from Fraser *et al.*, 1997].

Name	Constituent sugars	Sulphate	Proteoglycans
Hyaluronan	Glucoronic acid Glucosamine	-	-
Chondroitin 4-(6-) sulphates	Glucoronic acid Galactosamine	+	+
Dermatan sulphate	Iduronic acid Galactosamine	+	+
Keratan sulphate	Galactose Glucosamine	+	+
Heparan sulphate	Glucoronic and iduronic acid Glucosamine	+	+
Heparin	Glucoronic and iduronic acid Glucosamine	+	+

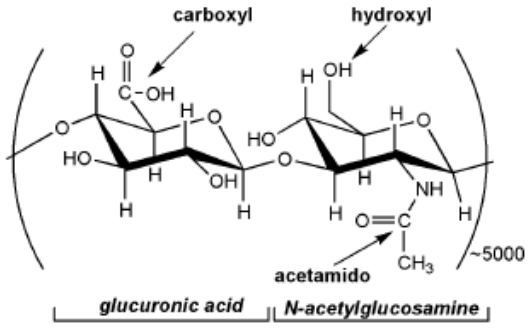

Figure 1.5 – The structure of native HA. HA is a naturally derived polymer composed of disaccharide repeats of glucoronic acid and N-acetylglucosamine. The molecular weight of native HA is typically several million. Each disaccharide contains three possible modification sites: the hydroxyl, carboxyl, and acetamido groups (Leach and Schmidt, 2004).

In the body, HA occurs in the salt form – hyaluronate, and it is found in extracellular, cell surface and intracellular environments (Leach and Schmidt, 2004; Spagnoli *et al.*; 2005). High concentrations of HA are found in several soft connective tissues, including skin, umbilical cord, synovial fluid and vitreous humour, as well as in

lung, kidney, brain and muscle tissues (**Table 1.2**; Leach and Schmidt, 2004; Sundstrom, 2006).

Table 1.2 – Concentration of hyaluronate in some tissues and body fluids [Adapted from Laurent and Fraser, 1992; Sundstrom, 2006].

Tissue / body fluid	**Concentration (mg/l)**
Human umbilical cord	4100
Normal rooster comb	7500
Human synovial fluid	1420-3600
Bovine nasal cartilage	1200
Human vitreous body	140-338
Human dermis	200
Human amniotic fluid	
at 16 weeks	20
at term	1
Human urine	0.2
Human serum (healthy young adults)	0.035
Rabbit brain	65
Rabbit muscle	27

HA is a negatively charged polysaccharide and exhibits hydrodynamic behaviour typical from a slightly stiffened random coil in dilute aqueous salt solution (Spagnoli *et al.*, 2005). Due to its highly hydrophilic properties, in the presence of water, HA molecules can expand in volume up to 1000 times to form loose hydrated matrices (Leach and Schmidt, 2004). Its viscoelasticity properties are influenced by their polymeric and polyelectrolytical characteristics. HA solutions are highly viscoelastic, providing protective functions to the synovial liquid, such as lubrication and absorption of shock (Lapick *et al.*, 1998).

HA is a megadalton molecule and its physicochemical and biological properties are dependent on its molecular weight (Laurent and Fraser, 1992; Lapick *et al.*, 1998; Lee and Spicer, 2000; Toole, 2004; Evanko *et al.*, 2007). Under normal physiological conditions it ranges in relative molecular mass from ~$2x10^5$ to ~$10x10^7$ Da (~2,000–25,000 disaccharides) with polymer lengths of 2–25 μm (Laurent and Fraser, 1992; Lee and Spicer, 2000; Toole, 2004; Evanko *et al.*, 2007). There is evidence that HA is capable of an amazing variety of conformations (Cowman *et al.*, 2005; Spagnoli *et al.*, 2005; Evanko *et al.*, 2007); for each specific biological function of HA there is a corresponding conformation and specific binding interactions (Cowman *et al.*, 2005). HA can be from extended chains, to relaxed coils, to condensed rods, and pearl necklaces of helical coils, rods, hairpins, and toroids (Spagnoli *et al.*, 2005; Evanko *et al.*, 2007). It can also self-associate to form fibers, networks, and stacks (Evanko *et al.*, 2007). The different conformations can also be affected by the local environment (e.g. ionic strength, specific ionic interactions), local dielectric constant, excluded volume effects, tethering to surfaces and fixed macromolecular assemblies, exposure to perturbing mechanical forces, and presence of interacting species (e.g. proteins and lipids; Cowman *et al.*, 2005).

Despite being classified as a glucosaminoglycan, HA differs from other GAGs regarding the molecular size; GAGs are relatively smaller in size (<50 kDa, commonly 15-20 kDa) with a short chain length comparatively to HA (Laurent and Fraser, 1992; Lee and Spicer, 2000; Toole, 2004). In addition, the cellular synthesis of HA is a unique and highly controlled process contrasting with other polymers of its family (Lee and Spicer, 2000). Most GAGs are synthesized by resident Golgi enzymes and covalently attached to core proteins, whereas HA is synthesized at the inner face of the plasma

membrane and immediately extruded out of the cell and into the ECM without any protein core (Lee and Spicer, 2000; Schumacher, 2004; Toole, 2004). HA synthesis is carried out by a group of the proteins called hyaluronan synthases (Laurent and Fraser, 1992, DeAngelis, 1999).

1.3.1.b. Synthesis

Hyaluronan is synthesized in the plasma membrane (Prem, 1984) by a class of integral membrane proteins called hyaluronan synthases (HAS, EC 2.4.1.212; Girish and Kemparaju, 2007). There are four HAS genes in most vertebrate genomes, but mammals only have three types: HAS1, HAS2, and HAS3 (**Table 1.3**).

Table 1.3 – Chromosomal location of hyaluronan synthase genes [Adapted from Girish and Kemparaju, 2007].

Family	Species	Chromosomal location	Gene	Protein
HA synthase	Human	19q13.3-13.4	HAS1	HAS1
		8q24.12	HAS2	HAS2
		16q22.1	HAS3	HAS3
	Mouse	17	Has1	Has1
		15	Has2	Has2
		8	Has3	Has3

HAS isoenzymes have unique characteristics. The HA chain synthesis is carried out on the intracellular membrane surface, in contrast with all other GAGs, which are synthesised in the rough ER attached to core proteins that together generate GAG's as end products. Also, HAS enzymes do not undergo any post-translational modifications that often take place in the Golgi, reinforcing the idea that HAS are integral membrane

proteins with an active site located in the cytoplasmic side of the plasma membrane. HAS polypeptides have both selective (β-1,4)GlcNAc and (β-1,3)GlcUA transferase activities, being thus the first identified GAGs shown to catalyse the addiction of two different monosaccharides to a polymer chain. HA polymerisation occurs by repeatedly adding GlcNAc and GlcUA to the nascent polysaccharide as it is extruded through the cell membrane into the extracellular space (Mian, N., 1986, Laurent and Fraser, 1992, DeAngelis, 1999, Lee and Spicer, 2000, Rilla *et al.*, 2005, Stern, 2005, Stern *et al.*, 2006, Girish and Kemparaju, 2007, Weigel and DeAngelis, 2007).

Mammal HAS were only identified and cloned in the 1990's (Itano and Kimata, 1996 a, b, Shyjan *et al.*, 1996, Spicer *et al.*, 1996, Watanabe and Yamaguchi, 1996, Spicer *et al.*, 1997 b, Weigel *et al.*, 1997, DeAngelis, 1999), and found to be localised in different chromosomes (**Table 1.3**; Spicer *et al.*, 1997 c; Girish and Kemparaju, 2007).

Despite HAS genes presenting a high similarity (75-87%) they have distinct expression patterns, and therefore the catalytic rate and mode of regulation for each HAS isoenzyme are different, expressing different enzymatic properties. Each mammalian HAS enzyme presents different molecular stability, kinetic characteristics and molecular sizes of HA (Spicer and McDonald, 1998, Itano *et al.*, 1999, Stern, 2005, Stern et al, 2006, Girish and Kemparaju, 2007, Weigel and DeAngelis, 2007). The different expression patterns expressed by HAS genes seem to be controlled by various growth factors and cytokines, and being tissue and cell-specific (Tzanakakis *et al.*, 1995; Tirone *et al.*, 1997; Sugiyama *et al.*, 1998, Itano and Kimata, 1996, Weigel *et al.*, 1997, Itano *et al.*, 1999, Kennedy *et al.*, 2000, Reclies *et al.*, 2001, Stern *et al.*, 2006).

HAS1 is the less active mammal enzyme, synthesizing low levels of high molecular weight HA (3.9 x 10^6 Da). HAS2 also generates high molecular weight HA,

but is more catalytically active than HAS1. HAS2 is implicated in developmental and repair processes involving tissue expansion and growth, being involved in cell proliferation and angiogenesis, as well as in the development through cell migration and invasion (Adamia *et al.*, 2005a; Stern, 2005). It is also involved in shock, septicaemia, inflammation and massive wounding. HAS3 is more active than HAS1 and HAS2, and synthesizes large amounts of shorter forms of HA molecules ($< 3 \times 10^5$ Da). These HA molecules may provide the pericellular glycocalyx, and appear to interact with cell surface receptors, triggering cascades of signal transduction events and major changes in cellular behaviour (Itano *et al.*, 1999; Stern, 2005; Girish and Kemparaju, 2007). However, the exact function of HAS isoenzymes and their role in cell signalling are assumptions and definitive functions require confirmation (Adamia *et al.*, 2005a; Stern, 2005).

Dysregulation of HAS genes appears to result in abnormal production of HA and promotion of abnormal biological process such as transformation and metastasis (Adamia *et al.*, 2005a; Girish and Kemparaju, 2007). The reason for the existence of three HAS isoforms remains unclear. However, it is believed that the existence of isoforms with different enzymatic characteristics may provide flexibility to the cells with respect to the control of HA biosynthesis and functions (Itano *et al.*, 1999).

1.3.1.c Degradation

The degradation of HA occurs in cells by a series of coordinated enzymatic reactions performed by a family of enzymes called hyaluronidases, which share a high degree of sequence homology (Meyer, 1971; Stern, 2003; Stern, 2005; Girish and

Kemparaju, 2007). According to Meyer (1971), based on biochemical analysis of their reaction products, there are three classes of hyaluronidases: 1) Endo-β-N-acetylglucosaminidases (mammalian-type hyaluronidases, e.g. testicular, lysosomal and bee venom hyaluronidase, EC 3.2.1.35) have hydrolytic and transglycosidase activities, and randomly cleave β-1-4 glycosidic linkages in HA, chondroitin and chondroitin sulfates to yield tetra- and hexasaccharides as the predominant end-products; 2) β-eliminases or lyases (include bacterial hyaluronidases, EC 4.2.2.1,) function as eliminases yielding disaccharides, and contrasting with their eukaryotic counterparts, they are specific for HA; 3) Endo-β-glucuronidases (leech hyaluronidase, EC 3.2.1.36) mainly generate tetra- and hexasaccharide end-products with glucoronic acid at the reducing end of the product (Meyer, 1971; Stern, 2004; Stern, 2005; Girish and Kemparaju, 2007; Hofinger *et al.*, 2008).

In the human genome, six hyaluronidase like gene sequences have been identified, being referred to as hyaluronoglucosaminidase (HYAL) genes. These six paralogs of HYAL genes are known to share about 40% of their identity with one another. Although, the expression of each gene has a unique tissue distribution, HYAL genes are tightly clustered at two chromosomal locations. HYAL1, HYAL2 and HYAL3 – coding for Hyal-1, Hyal-2, and Hyal-3, respectively – are located on chromosome 3p21.3; and the other set of three genes, HYAL4, PHYAL1 (a pseudogene), and sperm adhesion molecule 1 (SPAM 1) – code respectively for Hyal-4, the pseudogene transcribed but not translated in the human, and PH-20 – are clustered in a similar fashion on chromosome 7p31.3 (Stern, 2003; Stern, 2005; Girish and Kemparaju, 2007). In contrast to human genome, mouse genome has seven

hyaluronidase-like gene sequences (**Table 1.4**; Miller *et al.*, 2007; Reitinger *et al.*, 2007).

Table 1.4 – Chromosomal location of hyaluronidase genes [Adapted from Girish and Kemparaju, 2007].

Family	Species	Chromosomal location	Gene	Protein
Hyaluronidase	Human	3p21.3	HYAL1	Hyal1
			HYAL2	Hyal2
			HYAL3	Hyal3
		7p31.3	HYAL4	Hya4
			SPAM1	HPH-20
			HYALP1	-
	Mouse	9F1-F2	Hyal1	HYAL1
			Hyal2	HYAL2
			Hyal3	HYAL3
		6 A2	Hyal4	HYAL4
			Spam1	PH-20
			Hyalp1	-
			Hyal5	HYAL5

Human and mouse hyaluronidase genes are located in equivalent locations of respective chromosomes

The rapid turnover rate of HA enables its use in many physiological processes (Fraser *et al.*, 1992; Toole *et al.*, 1994). According to Stern (2003), a 70 kg individual has 15 g of HA; 5 g of which turns over daily. In the blood circulation, the $t_{1/2}$ of HA is 2-5 minutes (Fraser *et al.*, 1998), while in the skin (comprising 50% of the total HA body) it is 1-2 days, and in a inert tissue, such as cartilage, the turnover occurs in 1-2 weeks (Stern *et al.* 2003, 2004).

It is well described that the discrete sizes of HA fragments have widely different biological activities (Stern, 2003; Stern, 2005; Stern *et al.*, 2006; Girish and Kemparaju, 2007; Hofinger *et al.*, 2008), what may indicates that the HA catabolic pathway is a highly controlled process (Stern, 2003), occurring in a step-wise process generating

ever-smaller fragments (Roden *et al.*, 1989; Lepperdinger *et al.*, 2004; Stern, 2004; Stern, 2008). HA turnover in the human body occurs through three different pathways (Stern *et al.*, 2006):

1 – Cellular pathway, which includes binding by the predominant HA receptors – CD44 (Culty *et al.*, 1992; Hua *et al.*, 1993; Aguiar *et al.*, 1999; Lesley *et al.*, 2000; Ponta *et al.*, 2003) and RHAMM (Zhang *et al.*, 1998; Cheung *et al.*, 1999; Lynn *et al.*, 2001), internalisation, and degradation within cells (Stern *et al.*, 2006).

2 – Tissue pathway, where HA is released from the tissue matrices, drained into the vasculature and lymphatics, finishing its fate in liver, kidney, and possibly spleen (Stern *et al.*, 2006). This pathway, as well as the pathway described above involves HA receptors, such as HARE (Zhou *et al.*, 2000), LYVE-1 (Banerji *et al.*, 1999), and layilin (Bono *et al.*, 2005).

3 – Non-enzymatical HA degradation can occur by free radicals under oxidative conditions, yielding several intermediate end products (Myint *et al.*, 1987; Deguine *et al.*, 1998; Uchiyama *et al.*, 1990; Saari *et al.*, 1993; Noble *et al.*, 2002; Soltes *et al.*, 2005). These reactive oxygen species (ROS) includes superoxide anion radical (O_2-), hydrogen peroxide (H_2O_2) and especially by –OH radicals.

Regarding the cellular pathway, there is a putative HA metabolic scheme (**Figure 1.6**) proposed by Stern (2003, 2004), where 5 g of HA are daily degraded in the average individual, and therefore 5 g of these sugars are daily released.

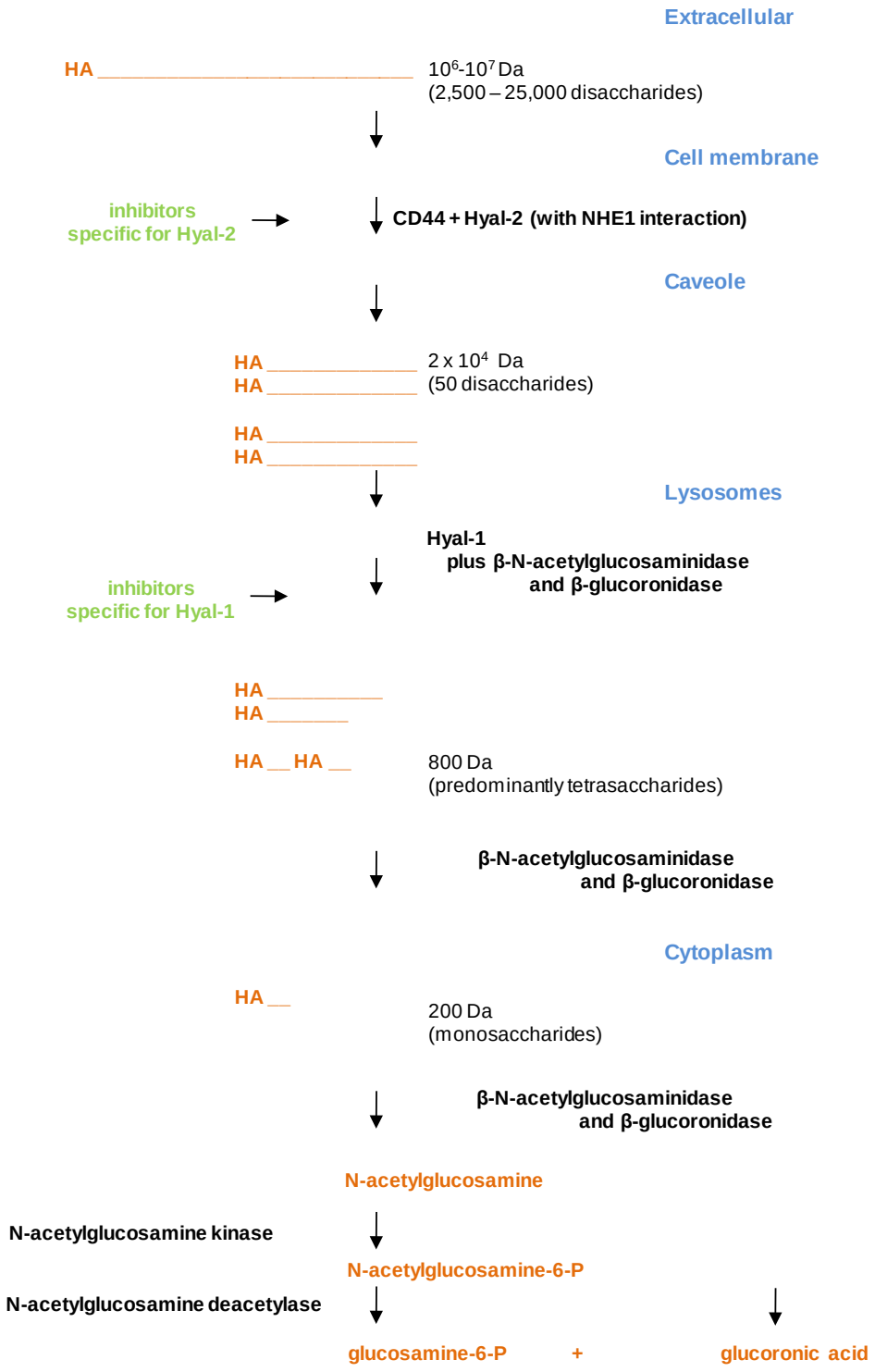

Figure 1.6 – A putative scheme for HA catabolism, beginning with a high molecular-weight extracellular polymer, and ending with single sugars that are then available for other metabolic cycles [Adapted from Stern, 2004].

In this catabolic scheme, high-molecular-weight extracellular HA is tethered to the plasma cell surface by HA receptors (CD44 and RHAMM), combined with an interaction of Hyal-2, which is the GPI-linked hyaluronidase anchored to the plasma membrane (Stern 2003, 2004). Hyal-2 cleaves HA, generating fragments of 50-100 saccharides (Stern, 2008). These fragments are internalised, delivered to endosomes, and later on to lysosomes. In the lysosomes, these HA fragments are degraded to smaller oligosaccharides, predominantly tetrasaccharides, by the action of Hyal-1 (Stern 2003, 2004, 2008). In mammals, besides hyaluronidases, two more lysosomal β-exoglycosidases, β-D-glucuronidase and β-N-acetyl-hexosaminidase, participate in this degradation (Leach and Schmidt, 2004; Stern, 2003, 2004). The single sugars that are products of HA catabolism are glucuronic acid and N-acetylglucosamine (Stern, 2004). N-acetylglucosamine is phosphorylated to N-acetylglucosamine-6-P, and glucosamine-6-P is generated (**Figure 1.6**; Stern, 2004), particularly in Kupffer and endothelial cells of the liver (Smedsrod and Pertoft, 1985; Roden *et al.* 1989).

Stern (2003, 2004) proposed that, as for glycogen metabolism there is a glycogen mini-organelle occurring in both liver and muscle (Banhegyi and Mandl, 2001), a similar mini-organelle may occur for the β-linked hyaluronan polymer – the hyaluronasome. Thus, the putative hyaluronasome may be a multi-protein membrane-associated complex, located possibly in cytoplasmic surface of plasma membranes, containing both synthetic and catabolic activities. Due to its ability to respond to extracellular and intracellular events, may contain HA receptors (such as CD44 and RHAMM), HAS and HYAL enzymes, HYAL inhibitors, β-exoglycosidases and HA-binding proteins (such as HAPB1; Stern 2003, 2004).

1.3.1.d. Biological activities of HA and HA oligomers

Although the major biological function of HA is still unsure, many roles have been correlated with this polymer. HA is predominantly present in the ECM, particularly in embryonic and malignant tissues (Stern, 2003), and performing three basic molecular functions: autocrine signalling with cell surface HA receptors on the same cell; paracrine signalling with a variety of ECM molecules on neighbouring cells, and due to its large physical structure HA can interact with more than one cell (Tammi *et al.*, 2002; Turley *et al.*, 2002; Toole, 2004; Spicer and Tien, 2004); secretion of the newly synthesized HA molecules that subsequently can interact with several cell surface receptors (such as CD44, RHAMM, LYVE-1, HARE, LEC receptor and TLR-4). This HA interaction with cell surface receptors mediates important physiological processes, including signal transduction, formation of pericellular coats and receptor-mediated internalisation (Laurent *et al.*, 1996; Vercruysse *et al.*, 1999; Toole *et al.*, 2002; Turley *et al.*, 2002; Toole, 2004; Spicer and Tien, 2004; Adamia *et al.*, 2005a; Tailor and Gallo, 2006).

HA has been shown to participate in various physiological processes, and given such complexity, distinguishing between the effects of biological activity and physicochemical properties of this polysaccharide is not straightforward. Due to its hydrophilic properties, HA plays several roles in the ECM, including space filler (probably to protect cells against lymphocytes and viruses), lubrificant and osmotic buffer. HA is implicated in pathological processes, such as immune surveillance and inflammation, since it can act as a sieve, restricting the movement of the pathogens, plasma proteins and proteases (Termeer *et al.*, 2003; George and Stern, 2004; Adamia *et*

al., 2005a; Day and de la Motte, 2005; Jiang *et al.*, 2005; Leach and Schmidt, 2005; Girish and Kemparaju, 2007). This polysaccharide also appears to be implicated in phagocytosis, increasing its concentration in monocytes and granulocytes (Shultz *et al.*, 2005; Pavia *et al.*, 2005; Girish and Kemparaju, 2007). Hyaluronan was shown to be involved in other physiological processes, including embryological development, proliferation, differentiation, migration and adhesion of cells (Manzel and Farr, 1988; Heldin, 2003; Spicer and Tien, 2004; Adamia *et al.*, 2005a; Girish and Kemparaju, 2007). During some stages of embryogenesis, the embryo is covered by a thick HA coating, which is probably important in the differentiation of the cells (Adamia *et al.*, 2005a). The production of HA is high during cell proliferation, since this polymer promotes chromatin condensation, and therefore facilitating mitosis. On the other hand, HA may help cells to detach from the matrix making it easier for them to divide. HA levels also increase during the differentiation and in the areas where cell migration begins (Adamia *et al.*, 2005a). It also plays important roles in multi-drug resistance (Toole, 2004), wound healing (Chen and Abatangelo, 1999), angiogenesis and malignant transformation (Adamia *et al.*, 2005a; Shultz *et al.*, 2005; Pavia *et al.*, 2005; Girish and Kemparaju, 2007).

It is known that the biological functions exhibited by HA depend on the chain length, molecular mass and on the conditions under which the polysaccharide is synthesized (Noble, 2002; Toole, 2004; Girish and Kemparaju, 2007). Polymers coming from the HA fragmentation in the course of the catabolic pathway occur in a variety of sizes that have a vast range of properties. High and low molecular weight HA polymers play opposite roles on cell behaviour (Girish and Kemparaju, 2007).

High-molecular-size HA polymers are space filling-molecules that are able to hydrate tissues, since they can incorporate large amounts of water into its solvent domain (Granger *et al.*, 1984), and on the other hand they are able to exclude other molecules and cells (Feinberg and Beebe, 1983; Deed *et al.*, 1997). These large molecules inhibit endothelial cell growth, and due to this physiological property they are anti-angiogenic (Chen and Abatangelo, 1999; Stern *et al.*, 2006). They also show anti-inflammatory and immunosuppresive properties (McBride and Bard, 1979; Delmage *et al.*, 1986; Day and de la Motte, 2005; Milner *et al.*, 2006). There are some evidence that high-molecular-mass HA is involved in ovulation, fertilisation, and embryogenesis processes (Stern, 2006). High concentrations of HA are present in foetal circulation (Decker *et al.*, 1989) and amniotic fluid (Dahl *et al.*, 1983), which may have some effect in the immunosuppression in the developing foetus. High levels of HA are also involved in inflammation process, being correlated with leukocyte migration and adhesion (Day and de la Motte, 2005; Milner *et al.*, 2006), and inhibition of the phagocytosis by monocytes, macrophages and peripheral polymorphonuclear neutrophils (Foster and Balazs, 1980). In addition, these large HA molecules are also involved in the promotion of cell quiescence and protection of cells against apoptosis and injury, and support of tissue integrity (Morrison *et al.*, 2001; Jiang *et al.*, 2005).

Conversly to high-molecular-size HA fragments, small polymers have angiogenic, wound healing, inflammatory and immunostimulatory properties (Noble, 2002; Termeer *et al.*, 2002; Rossler and Hinghofer-Szalkay, 2002; Stern, 2003). Several studies have shown that low-molecular-size HA fragments promote angiogenesis (West *et al.*, 1985; Kumar *et al.*, 1989; Rooney *et al.*, 1995; Horton *et al.*, 1998, 2000; Noble, 2002; Toole, 2004). These fragments stimulate endothelial cell proliferation, adhesion,

and migration by activating multiple signalling pathways, such as adhesion kinase and mitogen activated protein (MAP) kinase pathways (Rossler and Hinghofer-Szalkay, 2002; Murai *et al.*, 2004) and tyrosine kinase cascades (Lokeshwar and Selzer, 2000). Low and intermediate molecular weight (2×10^4–4.5×10^5) HA fragments activate dendritic cells (the antigen-presenting cells of the immune system), stimulating inflammatory cytokine production and adhesion molecules (Noble *et al.*, 1993; McKee *et al.*, 1996; Termeer *et al.*, 2000, 2002, 2003).

Very small HA oligosaccharides also play very important and specific roles in cell behaviour. Tetrasaccharides are anti-apoptotic, inducing expression of heat shock proteins (Xu *et al.*, 2002) and inhibiting anchorage-independent growth of several tumour cell types (Ghatk *et al.*, 2002). Whilst hexasaccharides act as antagonists to larger HA fragments, promoting, for example, differentiation of the endothelial cells induced in response to the angiogenic effect of larger HA fragments (Ohno *et al.*, 2005; Takahashi *et al.*, 2005).

Table 1.5 shows a list of HA fragments and their biological functions correlated with molecular size.

Table 1.5 – Sizes of HA with key function [Adapted from Stern *et al.*, 2006].

Size (saccharides)	Function
High-molecular-mass	Suppression of angiogenesis
HA > 1000-5000	Immune suppression
	Inhibition of phagocytosis
	Suppression of HA synthesis
HA fragments	
~1000	Induction of inflammatory chemokines Stimulation of PAI-1 Stimulation of urokinase
10-40	Induction of CD44 cleavage Promotion of tumour cell migration
8-32	Stimulation of angiogenesis Stimulation of tumour neovascularisation
~15	Suppression of smooth muscle cell proliferation
12	Endothelial cell differentiation ~Up-regulation of PTEN in tumour cells
10	Displacement of matrix HA on oocyte surface Displacement of proteoglycans from cell surface
6	Suppression of HA cable formation Induction of NO and MMPs in chondrocytes Induction of HAS2 in chondrocytes
4-6	Induction of cytokine synthesis in dendritic cells Transcription of MMPs
4	Up-regulation of Hsp 72 expression
	Suppression of apoptosis
	Induction of chemotaxis
	Up-regulation of heat shock factor-1
	Up-regulation of Fas expression
	Suppression of proteoglycan sulfation

1.3.2. HA BINDING PROTEINS AND RECEPTORS

All the previously mentioned signalling events performed by HA, such as cell migration, attachment and metastasis, are mediated through a group of HA-binding proteins denominated hyaladherins (Toole, 1990; Knudson and Knudson, 1993; Leach

and Schmidt, 2004; Girish and Kemparaju, 2007). Hyaladherins exhibit significant differences in their tissue expression, cellular localisation, specificity, affinity and regulation (Day and Prestwich, 2002). These proteins are categorised according to their molecular basis of HA recognition (sequence of HA binding site) and their location, i.e., some of them interact with HA within the ECM, whereas others interact with HA at the plasma membrane of cells, as cell-surface matrix receptors (**Table 1.6**; Knudson and Knudson, 1993; Turley and Harrison, 1999; Girish and Kemparaju, 2007).

Table 1.6– Hyaladherin family proteins [Adapted from Turley and Harrison, 1999].

Cellular		**Extracellular**	
Itinerant proteins	**Transmembrane proteins**	**ECM proteins**	**Soluble proteins**
RHAMM cdc37 p68 HBP IHABP4 TSG-6 LYVE-1 LEC	CD44 family	versican aggrecan neurocan brevican link protein fibrinogen	Inter-α-trypsin inhibitor

Most of the hyaladherins share a common structural binding domain of ~100 amino acids in length, denominated as the link module (Day and Prestwich, 2002). The link module region comprises an immunoglobulin domain, which is responsible for the link protein-proteoglycan interaction, and two contiguous link modules, which mediate binding to HA (Day and Prestwich, 2002; Spicer *et al.*, 2003). Nevertheless, there are number of hyaladherins that lack this domain and are unrelated to each other at the sequence level (**Figure 1.7**; Day and Prestwich, 2002).

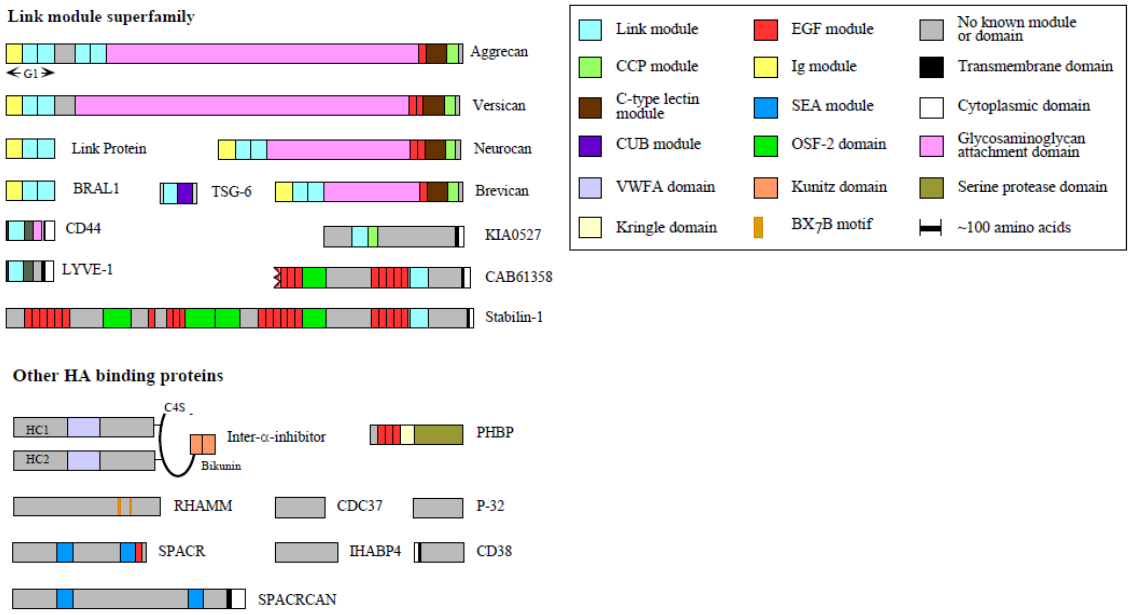

Figure 1.7 – The modular domain organization of the hyaladherins [Adapted from Day and Prestwich, 2002].

1.3.2.a. Extracellular hyaladherins

Extracellular hyaladherins include aggrecan, versican, neurocan and brevican, which constitute a gene family denominated as lectins (or hyalectins; Yamaguchi, 2000; Hartmann and Maurer, 2001; Girish and Kemparaju, 2007). These lectins are chondroitin sulphate proteins (CSPGs; Yamanda *et al.*, 1994), and they can form huge and link protein-stabilised complexes with HA (Day and Prestwich, 2002). Aggrecan is the largest proteoglycan, found predominantly in cartilage (Hardingham and Muir, 1972; Hardingham and Fosang, 1992; Knudson and Knudson, 1993), while versican is predominantly synthesised in fibroblasts and also present in another soft tissues (Knudson and Knudson, 1993; Yamanda *et al.*, 1994; Girish and Kemparaju, 2007). Neurocan and brevican are present predominantly in the central nervous system

(Yamanda *et al.*, 1994). The complexes formed between these proteoglycans and HA provide the load-bearing function in articular cartilage, give elasticity to blood vessels, while contributing to structural integrity of many tissues such as skin and brain (Watanabe *et al.*, 1997; Yamaguchi, 2000).

Link protein also has a specific and strong binding to HA, and its interaction with the polysaccharide results in the retention of aggrecan within cartilaginous tissues (Knudson and Knudson, 1993). In addition, the presence of link protein in non-cartilaginous tissues may be correlated with the stabilisation of versican and neurocan with HA (Rauch *et al.*, 1992; Knudson and Knudson, 1993).

Inter-α-trypsin inhibitor (IαI) is an atypical HA-binding protein since does not appear to use the link module as the binding domain (Huang *et al.*, 1993; Toole, 2001; Zhuo *et al.*, 2004). This protein interacts in a complex manner with HA generating the serum-derived hyaluronan-associated protein (SHAP)-HA complex (Hamerman *et al.*, 1963; Sandson *et al.*, 1965; Zhuo *et al.*, 2004). This complex is involved in the binding of HA to cell surfaces and in the assembly of pericellular matrices (Toole, 2001; Zhuo *et al.*, 2004).

1.3.2.b. Cellular hyaladherins – HA receptors

Cluster of differentiation 44 (CD44; Aruffo *et al.*, 1990; Goldstein *et al.*, 1989) and receptor for HA-mediated motility (RHAMM; Turley, 1982; Hardwick *et al.*, 1992) are the most studied hyaladherins, and are considered to be the principal HA receptors (Leach and Schmidt; 2004; Girish and Kemparaju, 2007).

CD44 is a transmembrane glycoprotein, being expressed in a number of different isoforms and on a variety of cell types including leukocytes, fibroblasts, epithelial cells, keratinocytes, and some endothelial cells (Tavernor *et al.*, 1992; Isacke and Yarwood, 2002; Sillanpää *et al.*, 2003; Leach and Schimdt, 2004; Girish and Kemparaju, 2007). It is involved in many cell-cell and cell-matrix interactions and signalling, including cell adhesion, migration, receptor-mediated internalisation/degradation of HA, and lymphocyte functions (Knudson *et al.*, 2002; Toole, 2002, 2004; Knudson, 2003; Leach and Schimdt, 2004; Spicer and Tien, 2004; Girish and Kemparaju, 2007).

RHAMM is also known as CD168 since is expressed on the cell surface. This hyaladherin is also expressed in the cytoplasm, cytoskeleton, mitochondria and nucleus (Turley *et al.*, 2002; Nedvetzki *et al.*, 2004) by several cell types, including most adult homeostatic tissues, keratinocytes, fibroblasts, smooth muscle cells, macrophages and T lymphocytes (Turley and Harrison, 1999). Similarly to CD44, RHAMM is expressed in several isoforms (Zhang *et al.*, 1998; Akyiama *et al.*, 2001; Lynn *et al.*, 2001; Turley *et al.*, 2002). The intracellular isoforms are also known as IHAPBs (intracellular HA-binding proteins; Fieber *et al.*, 1999; Lee and Spicer, 2000). Depending on which isoform present, RHAMM plays key roles in HA mediate migration and motility, cytoskeletal assembly and intracellular signal transduction (Hall *et al.*, 1996; Fieber *et al.*, 1999; Turley *et al.*, 2002; Toole, 2004; Girish and Kemparaju, 2007).

LYVE-1 (lymphatic vascular endothelial hyaluronan receptor) is a HA specific binding protein being only expressed in lymph vessel endothelium (Jackson, 2003, 2004; Girish and Kemparaju, 2007). LYVE-1 appears to play a role in HA metabolism or leukocyte trafficking within lymphatic vessels and lymph nodes (Jackson, 2004).

LYVE-1 is structurally related with CD44 presenting 43% of similarity (Banerji *et al.*, 1999; Jackson *et al.*, 2001; Jackson, 2003).

TGS-6 (tumour necrosis factor-stimulated gene-6) is a protein implicated in many physiological and pathological conditions associated with inflammation and tissue remodelling (Bayliss *et al.*, 2001; Mahoney *et al.*, 2001; Girish and Kemparaju, 2007). It plays key roles in the regulation of leukocyte migration, and its pattern of expression and ligand specificity indicate that it may be involved in extracellular matrix remodelling (Bayliss *et al.*, 2001; Day and Prestwich, 2002; Mahoney *et al.*, 2001; Girish and Kemparaju; 2007).

Table 1.7 shows the relationship of HA oligosaccharides size and hyaladherins.

Table 1.7 – Minimum size of HA oligosaccharides that bind to hyaladherins [Adapted from Stern *et al.*, 2006].

Molecular size (saccharides)	Protein
6	HAPB1
	CD44 and TGS-6 link module
	Chondrocyte CD44
	Smooth muscle cell CD44
8	IαI
	TSG-6
8-10	SHAP
10	Aggrecan
	Versican
	Link protein
50	Keratinocyte CD44 (CD44E)
	Link protein plus aggrecan

1.3.3. HA AND CANCER

It has been shown that high concentrations of HA are present in tumours, being consistent with the high levels of HA present in the serum of some cancer patients, when compared with the levels found in those normal individuals (Dahl and Laurent, 1988; Knudson *et al.*, 1989; Knudson, 1996; Auvinen *et al.*, 1997; Ropponen, 1998). HA has been implicated in migration, differentiation, progression and invasion of cancer cells leading to metastasis. Several studies have shown that HA mediates these cellular functions through interactions with specific binding proteins, previously discussed in the **subchapter 1.3.2**.

Tumour progression is accompanied by various cellular, biochemical and genetic alterations, including the interaction of tumour cells with ECM molecules, such as HA. The accumulation of HA has been found in several tumours, including bladder carcinoma (Hautman *et al.*, 2001) breast carcinoma (Auvinen *et al.*, 1997, 2000; Li *et al.*, 2007), colon carcinoma (Ropponen *et al.*, 1998; Köbel *et al.*, 2004), epithelial ovarian carcinoma (Anttila *et al.*, 2000), gliomas (Delpech *et al.*, 1993), lung carcinoma (Horai *et al.*, 1981; Pirinen *et al.*, 2001), prostate carcinoma (Lokeshwar *et al.*, 2001; Lipponen *et al.*, 2001; Aaltomaa *et al.*, 2002), thyroid carcinoma (Bohm *et al.*, 2002), and Wilm's tumours (nephroblastoma; Hopwood and Dorfman, 1978). High levels of HA are not only a characteristic seen in tumours; transformed cells, including those cells infected with oncogenic viruses, exhibit higher levels of HA production as well as abnormal acceleration of cellular growth (Hamerman *et al.*, 1965; Ishimoto *et al.*, 1966; Hopwood and Dorfman, 1977; Leonard *et al.*, 1978).

Several studies have demonstrated that the overexpression of HAS genes induces HA production and matrix formation. There is some evidence that is due the HA overproduction that cancer cells form a HA-rich matrix, providing a suitable environment for tumour growth, invasion and metastasis (Toole *et al.*, 1979; Dick *et al.*, 1983; Kimata *et al.*, 1983; Turley and Tretiak, 1985; Turley, 1992; Zhang, 1995; Knudson, 1996; Itano *et al.*, 2004). Kosaki and co-workers (1999) have demonstrated that high levels of HA induce tumour growth of fibrosarcoma cells, whereas in a study performed by Itano and co-workers (1999) the stimulation of metastatic breast cancer cells was observed. There is some evidence that HAS isoforms are involved in different stages of malignant tumourigenesis, with HAS1 overexpression correlated with poor prognosis in human colon (Yamada *et al.*, 2004) and ovarian (Yabushita *et al.*, 2004) cancers, and multiple myelomas (Adamia *et al.*, 2005b); whilst elevated expression of HAS2 and HAS3 isoforms is involved in fibrosarcomas, melanomas and mesotheliomas (Kosaki *et al.*, 1999; Liu *et al.*, 2001; Li and Heldin, 2001). Conversly, decrease of tumourigenic potential of various cell lines was seen when low levels of HA are expressed, due to suppression of HAS2 and HAS3 (Simpson *et al.*, 2002; Simpson *et al.*, 2002b; Nishida *et al.*, 2005; Udabage *et al.*, 2005). However, Ened and co-workers (2002) have shown contradictory results, demonstrating that overexpression of HAS2 inhibits tumour formation. These findings were supported by a study performed by Itano and co-workers (2004), showing suppression of the tumourigenesis, while using rat 3Y1 fibroblasts undergoing oncogenic transformation.

Degradation of HA may be involved in the control of HA accumulation, with HYALs appearing to play roles in tumourigenesis (Csoka *et al.*, 1997). However, HYALs function is not fully understood, since some results show to be ambiguous.

Hyal-1 overexpression is seen in prostate (Lokeshwar *et al.*, 2001) and bladder (Lokeshwar *et al.*, 2002) cancers; but on the other hand, low levels of Hyal-1 are shown in advanced ovarian cancer (Hiltunen, 2002).

All the findings above described suggest that HA is an effector of tumour cell behaviour, and there are a number of ways that HA can be involved in the regulation of cancer growth and spreading. Nevertheless, the relation of HA production/degradation and its functions in cancer progression remains to be elucidated.

1.3.4. MEDICAL APPLICATIONS OF HA

The clinical use of HA is rapidly increasing and estimations about its world-wide size market are around one billion dollars (Liao *et al.*, 2005; Oh *et al.*, 2010). The intrinsic physicochemical and biological properties of HA make this polymer suitable for applications in clinical therapies, diagnostics, tissue engineering, and drug delivery, for a variety of biomedical needs, including orthopedic, cardiovascular, pharmacologic and oncologic applications (Liao *et al.*, 2005). In **Table 1.8** it can be seen a list of HA products for clinical use commercially available.

Table 1.8 – Some commercial available HA products [Adapted from Liao *et al.*, 2005].

Application	Tradename	Company
Osteoarthritis	Hyalgan	Fidia
	Synvisc	Biomatrix/Genzyme
	Supartz	Seikagaku
	Hylashield	Biomatrix
	Artz	Seikagaku
	Orthovisc	Anika
Ophthalmology	Healon	Pharmacia
	Amvisc	Bausch & Lomb
	Coease, Shellgel, Staarvisc	Anika Therapeutics
	Amo Vitrax, Vitrax	Allergan/Medtronic
	Provisc, Viscoat	Alcon Laboratories
	Opegan, OpeganHi	Seikagaku
	Opelead	Shiseido
Wound healing	Bionect	Fidia
	Ialuset	IBSA
	Connettivina	Fidia
Postsurgical adhesions	Adcon	Gliatech
	Intergel	LifeCore Biomedical
	Seprafilm	Genzyme
Surgical scaffolding	Hyalomatrix	Fidia
	Hylasine	Biomatrix
Gastrourology	Deflux	Q-Med
Embryo implantation	EmbryoGlue	Vitrolife

Hyaluronan originally found in the vitreous humour of the eye, is an important agent in ophthalmic surgery, due to its viscoelasticity and hydrophilicity. It has been routinely used during cataract operations, aiming to protect the delicate corneal endothelium or to maintain the shape of the anterior eye chamber. HA has been used as well as an adjuvant to eye tissue repair and as an enhancing component of eye drops (Miller and Stegmann, 1983; Laurent *et al.*, 1995; Menzel and Farr, 1998; Lapckik *et al.*, 1998).

Due to its viscoelastic and hydrophilic properties HA has been used in orthopaedic applications, acting as a lubricant and promoting cartilage-healing in joint

diseases, such as osteoarthritis. A variety of HA materials have been developed and used in viscosupplementation treatments to treat many orthopaedic diseases, where the concentration and molecular weight of the HA naturally present in the joint decreases, contributing to stiffness and pain (Laurent and Fraser, 1992; Peyron, 1993; Pozo *et al.*, 1997).

The advent of HA derivatives and crosslinked HA has allowed the use of HA materials in drug delivery applications for drug targeting. In the administration route of HA materials are included gene delivery, and dermal, ophthalmic, nasal, pulmonary, parenteral, liposomal, and implantable drug delivery; which have a wide variety of applications ranging from wound healing and tissue regeneration, cancer, ophthalmic patologies, to diabetes (**Table 1.9**, Liao *et al.*, 2005). Hyaladherins, such as CD44 and RHAMM, are involved in the mechanisms of HA in the application of drug delivery system, not only because they are overexpressed in many diseases tissues (e.g. tumour and inflamed tissues), but because they can internalise the HA-drugs. These potential drug delivery system materials have been formulated as topical, injectable and implantable vehicles (in forms such as films, microspheres, liposomes, fibres, or hydrogels). Biocompatibility, biodegradability, stability and readily modified chemical structure are on the basis of using HA as a drug carrier. In addition, the coupling of drugs to HA provides advantages in drug solubilisation and stabilisation, allowing a controllable and localised delivery of biologically active molecules (Willoughby, 1994; Leach and Schmidt, 2004; Liao *et al.*, 2005; Yadav *et al.*, 2008). A number of studies have shown that HA has the capacity to increase the bioavailability of many drug molecules, including insulin, pilocarpine, tropicamide, timolol, gentimycin, and arecaidine propargyl ester. The bioavailability promoted by HA is the result of

bioadhesion and/or penetration enhancement, which were found to be dependent on the polysaccharide molecular-weight, with high molecular weight HA fragments (more than 300 kDa) promoting an increase in the bioavailability and low molecular weight fragments (55 kDa) having no effect (Liao *et al.*, 2005).

Table 1.9 – Summary of the drug delivery applications of HA (Liao *et al.*, 2005).

Route	Justification	Therapeutic agents
Ophtalmic	Increased ocular residence of drug that can lead to increased bioavailability	Pilocarpine, tropicamide, timolol, gentimycin, tobramycin, arecaidine polyester, (S) aceclidine
Nasal	Bioadhesion resulting in increased bioavailability	Xylometazoline, vasopressin, gentamycin
Pulmonary	Absortion enhancer and dissolution rate modification	Insulin
Parenteral	Drug carrier and facilitator of liposomal entrapment	Taxol, superoxide dismutase, human recombinant insulin-like growth factor, dexorubicin
Implant	Dissolution rate modification	Insulin
Gene	Dissolution rate modification and protection	Plasmid DNA/ monoclonal antibodies

HA has been investigated in wound healing regeneration. Despite its role in the wound healing not be fully understood, there is some evidence that HA is present in high concentrations in the skin and soft connective tissues. Furthermore, some studies have showed that exogenous HA exerts have beneficial effects on the wound healing process, accelerating skin wound healing when topically applied in hamsters and rats (Foschi *et al.*, 1990; King *et al.*, 1991; David-Raoudi *et al.*, 2008). HA forms a very readily matrix and its tissue-integrity-promoting behaviour, making this polymer an appropriate matrix to support dermal regeneration and augmentation, and also giving many possibilities in the wound repair field (Chen and Abatangelo, 1999). Several studies have shown that HA promotes cell detachment, and therefore having both

adhesive and anti-adhesive properties (Barnhart *et al.*, 1979; Abatangelo *et al.*, 1982; Koochekpour *et al.*, 1995). Crosslinked HA has been used in post-surgical applications preventing adhesions and forming barriers to cell movement (Evanko *et al.*, 2007). Injections of HA are now being used in endoscopic mucosal resection (EMR) or endoscopic mucosal dissection (EMD), instead of normal saline solution. Some studies have shown that EMRSH (endoscopic mucosal resection sodium hyaluronate) creates a more prominent and longer-lasting mucosal protrusion and complete resection can be achieved in greater numbers of cases comparatively with typical EMR. However, it is unclear if exogenous HA can increase the risk of cell growth and tumour development in case of malignant disease (Matsui *et al.*, 2004; Sohn *et al.*, 2008).

HA has been successfully used in cosmetic applications due to its ability to retain water for considerable periods, presenting properties of a moisturiser, in addition that it is highly elastic. HA gels are currently commercially available in forms of creams and injectables. These preparations have been used in soft tissue augmentation, to fill facial wrinkles and depressed scars (Duranti *et al.*, 1998; Kogan *et al.*, 2006; Stern and Maibach, 2008).

HA has been now a substitute for albumin in culture media, since sometimes albumins can be contaminated with prions and viruses (Gardner *et al.*, 1999; Simon *et al.*, 2003; Liao *et al.*, 2005). HA is a suitable component for *in vitro* fertilisation, and can act as a cryopreservative to human embryos (Gardener *et al.*, 2003).

The surface coating of medical devices is another prominent application of HA. The biopolymer coating enables devices such as catheters, guidewires and sensors, to be biocompatible and lubricated, while reducing fouling and tissue abrasion (Hoekstra, 1999).

1.4. CD44

CD44 is a family of transmembrane glycoproteins (Weber *et al.*, 1996), initially discovered on lymphocytes, and later identified on many different cell types from several mammal species (Dalchau *et al.*, 1980). It was first identified as having cell adhesion and cell homing functions, but it already has been shown to have a multiplicity of functions. CD44 is also known as Ly-24, lymphocyte homing receptor (gp90 Hermes), phagocytic glycoprotein (Pgp-1), extracellular matrix receptor III (ECMRIII), and HA receptor (H-CAM-homing cellular adhesion molecule and HUTCH-1). This variety of names is due its individual discovery by several research centres, but sequencing studies have shown that all these molecules were identical. Thus, in the Third International Workshop on Human Leukocyte Differentiation Antigens, CD44 was decided as the name of the protein (Cobbold, 1987).

1.4.1. CD44 GENE

In humans, the gene coding for CD44 is located on the short arm of chromosome 11 location p13 (Francke *et al.*, 1983; Forsberg *et al.*, 1989a, 1989b), on chromosome 2 in mice. It was first cloned in 1989 by Stamenkovic and co-workers, while using cDNA libraries prepared from hematopoietic cell lines. Screaton and co-workers (1992) have found that the gene was composed by 19 exons, 12 of which were alternatively spliced (Screaton *et al.*, 1992, 1993). However, some years later it has been shown that it is composed by at least 20 exons, spanning approximately 60 kb (Borland *et al.*, 1998; Günthert, 2001). There are two groups of 10 exons each: one group comprises exons 1-

5 and 16-20, being expressed together on all cell types and described as the standard form of the gene – CD44S; and the other group described as the variable form – CD44V – which comprises exons 6-15 that can be alternatively spliced, resulting in a large number of functionally distinct isoforms (**Figure 1.8**; Tölg *et al.*, 1993).

Among seventeen exons that code for extracellular domain, the first five exons (exon 1-5), exons 16 and 17 are present in all CD44 isoforms, whereas exons 6-15 are subjected to alternative splicing (designated as variant exons, v1-v10; van Weering *et al.*, 1993; Martin *et al.*, 2003; Thorne *et al.*, 2004; see **Figure 1.8**). The human CD44 does not contain exon v1, thus the first variant exon of human CD44 is numbered as v2 (Nedvetzki *et al.*, 2003). Exon 1 encodes the N-terminal signal sequence, exons 2 and 3 encode a link-homology hyaluronan-binding module, the membrane proximal region of the extracellular domain is encoded by exons 4, 5, 16 and 17, exon 18 encodes a short hydrophobic transmembrane domain, and the cytoplasmic domain is encoded by exons 19 and 20 (Martin *et al.*, 2003; Thorne *et al.*, 2004). It was also noticed that exons 19 and 20 can also be alternatively spliced, generating different lengths of the cytoplasmic tail of the CD44 protein. Thus, the expression of exon 19 results in a short and truncated form (additional three amino acids), while exon 20 results in a long version by the inclusion of the C-terminal exon (additional 67 amino acids). The longer form of the cytoplasmic tail is predominantly expressed, while exon 19 is normally spliced out, and therefore, the short form is only rarely expressed (Goldstein *et al.*, 1990; Screaton *et al.*, 1992; Günthert, 2001; Martin *et al.*, 2003).

The alternative splicing of CD44 can gives rise to a variety of CD44 polymorphisms (more than one thousand), but nevertheless, not all combinations of variably spliced exons are expressed (Naor et al, 1997, 2002). CD44 isoforms are

expressed in a cell-specific manner, and among these isoforms there are two occurring more frequently: haematopoietic CD44 (CD44H), which is broadly distributed in haematopoietic cells (particularly leukocytes; Stamenkovic *et al.*, 1989; Quackenbush *et al.*, 1990), and epithelial CD44 (CD44E), which appears restricted to subsets of epithelial cells (Stamenkovic *et al.*, 1991; Brown *et al.*, 1991). CD44H does not contain variably sliced exons, being encoded by constitutively expressed exons 1-5, 16-17 and 19 (Bajorath, 2000). CD44E is one of the CD44 variants, containing exons 12, 13 and 14 (Stamenkovic *et al.*, 1991).

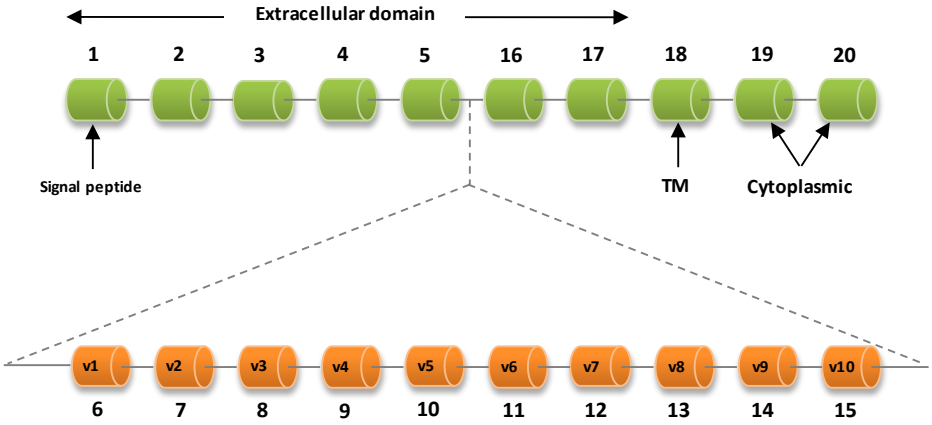

Figure 1.8 – Genomic organisation of CD44. Orange boxes represent the 10 variant exons v1–v10 which are either all spliced out to produce CD44s or inserted into the extracellular domain in multiple combinations to produce alternatively spliced CD44 isoforms (CD44v) [Adapted from Isacke and Yarwood, 2002; Martin *et al.*, 2003].

1.4.2. CD44 PROTEIN STRUCTURE

The standard isoform of human CD44 (CD44s) is a type I transmembrane molecule, i.e. the N-terminus is located outside and the C-terminus inside the cell (Bajorath, 2000). CD44s is the smallest CD44 isoform, since all variant exons are

excised. It is composed of 341 amino acids (aa) and is subdivided into three major domains: a C-terminal cytoplasmic domain (70 aa), a transmembrane domain (23 aa), and a N-terminal extracellular domain (248 aa), which can be subdivided further into two distinct regions: the N-terminal domain and the membrane proximal region of the extracellular domain (or stem region; 85 aa). The ten exons subjected to alternative splicing (v1-v10) encode up to 381 aa. They are inserted at a single site in the membrane proximal extracellular domain between exons 5 and 16 of the RNA transcript, corresponding to a position between aa 202 and 203 (**Figure 1.9**; Martin *et al.*, 2003).

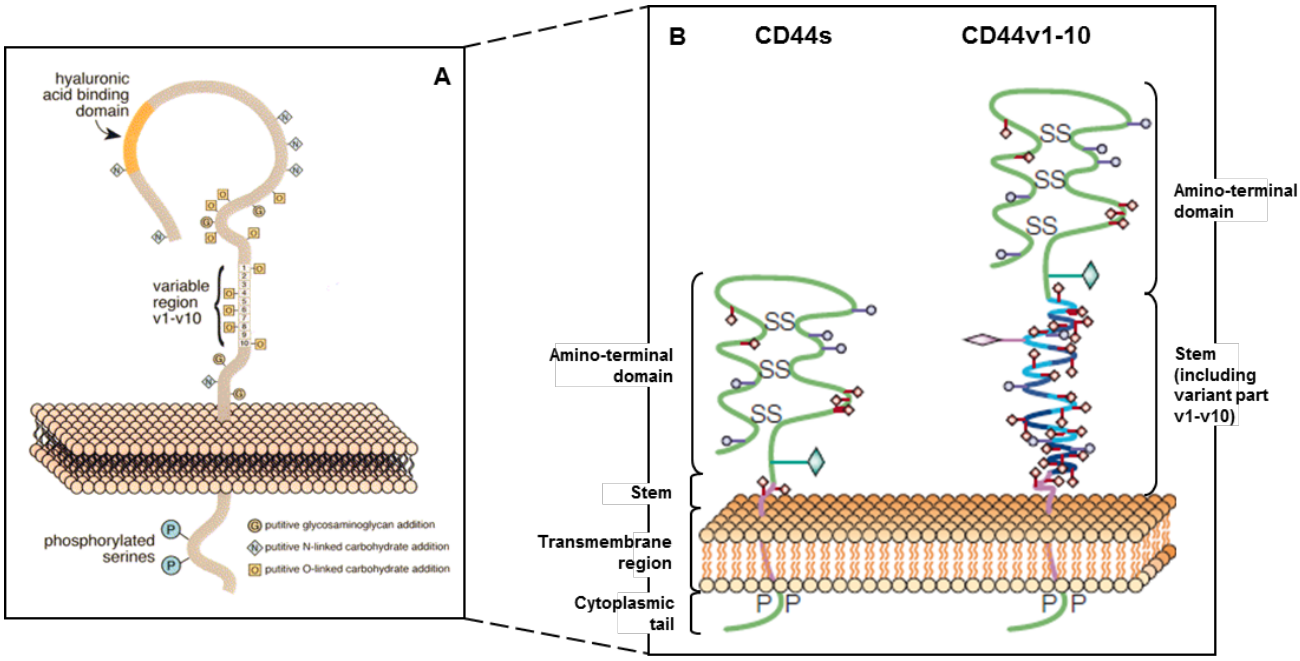

Figure 1.9 (**A**) Protein structure of CD44 [Adapted from Ponta *et al.*, 1998]. (**B**) Comparison between CD44s and the largest variant isoform CD44v1–10, which shows that the sequences encoded by the variant exons are in the stem region [Adapted from Ponta *et al.*, 2003].

The single-pass transmembrane domain encoded by exon 18 contains 23 aa. The cytoplasmic region, composed by 70 aa (residues 272-341), is encoded by exons 19 and 20, and part of exon 18 (only three aa; Martin *et al.*, 2003). CD44s is a polypeptide

synthesised as 37 kDa. However, CD44 can undergoes extensive post-translational modifications, resulting in several isoforms-specific post-translational modifications and therefore to a structural diversity. For example, the attachment of numerous carbohydrates to N- and O-linked glycosylation sites of the extracellular domain, results in a protein of 80-95 kDa, while the attachment of chondroitin sulphate results in a protein of 180-200 kDa. Glycosylation patterns of CD44 isoforms varies among different cell types and cellular context, giving rise to CD44 polypeptides ranging from 80-250 kDa (Bajorath, 2000; Martin *et al.*, 2003). Consequently, post-translational modifications modulate binding characteristics and functional properties of CD44 (Kincade *et al.*, 1997; Lesley *et al.*, 1997; Borland *et al.*, 1998).

1.4.3. CD44 LIGANDS

It is well known that HA is the principal ligand of CD44 (Lesley and Hyman, 1998). CD44 binds to HA through a link domain (previously discussed in **subchapter 1.3.2.**; Goodison *et al.*, 1999; Martin *et al.*, 2003; Banerji *et al.*, 2007). Although all CD44 isoforms contain the HA recognition site, not all cells expressing CD44 bind the HA constitutively. And in many cases CD44 only binds to its ligand when is activated by external stimuli. Cells can express CD44 in an active (can bind to HA), an inducible (which does not bind HA or binds it only weakly, but can only bind HA in presence of inducing factors), or an inactive state (unable to bind HA, even in presence of inducing factors) with respect to HA binding (Lesley *et al.*, 1993, 2000; Goodison *et al.*, 1999; Bajorath, 2000). These differences in the HA binding are cell specific and can be attributed to post-translational modification patterns. Thus, glycosylation of CD44 is

directly or indirectly required for HA binding (Goodison *et al.*, 1999; Bajorath, 2000). While reduced levels of N- and O-glycosylation enhance HA binding (Bennet *et al.*, 1995; Katoh *et al.*, 1995; Lesley *et al.*, 1995), mutation of N-linked glycosylation sites in CD44 abrogates HA binding, converting thus an inducible to an active form (Bartolazzi *et al.*, 1996). In addition, it has been shown that in certain cell types, CD44 can be induced to bind HA by specific monoclonal antibodies, cytokines growth factors or phorbol ester (Lesley *et al.*, 1993, 1995, 2000).

Due to its polymorphic nature CD44 can also bind to other ligands besides HA. These include growth factors (Yu *et al.*, 2002), matrix metalloproteinases (Yu and Stamenkovic, 1999, 2000; Mori *et al.*, 2002; Yu *et al.*, 2002), and ECM proteins, including osteopontin (Webber *et al.*, 1997), collagen (Carter and Wayner., 1988; Faassen *et al.*, 1992; Ishii *et al.*, 1993), fibronectin (Jalkanen *et al.*, 1992; Romaris *et al.*, 1995) and laminin (Ishii *et al.*, 1993). Furthermore, CD44 also interacts with a number of other non-ECM ligands, such as the major histocompatibility complex (MHC) class II (Naujocas *et al.*, 1993), addresin (Picker *et al.*, 1989) and serglycin (Toyama-Sorimachi and Miyasaka, 1994; Toyama-Sorimachi *et al.*, 1995). In addition, it was also been reported that CD44 interacts with intracellular proteins via its cytoplasmic domain; these include ankyrin (Bourguignon *et al.*, 1986; Kalomiris and Bourguignon, 1988), proteins of ERM family (such as ezrin, radixin and moesin (Sato *et al.*, 1992; Yonemura *et al.*, 1998; Legg *et al.*, 2002) and merlin, a tumour suppressor protein related to ERM proteins (Morrison *et al.*, 2001). There is some evidence that CD44 interacts with cytoskeleton through actin microfilaments binding mediated by ankyrin and ERM proteins (Tsukita *et al.*, 1994).

There is a current model for HA-dependent CD44-signalling pathways (**Figure 1.10**), in which CD44 is tightly coupled at least to two tyrosine kinases: $p185^{HER2}$ and c-src.

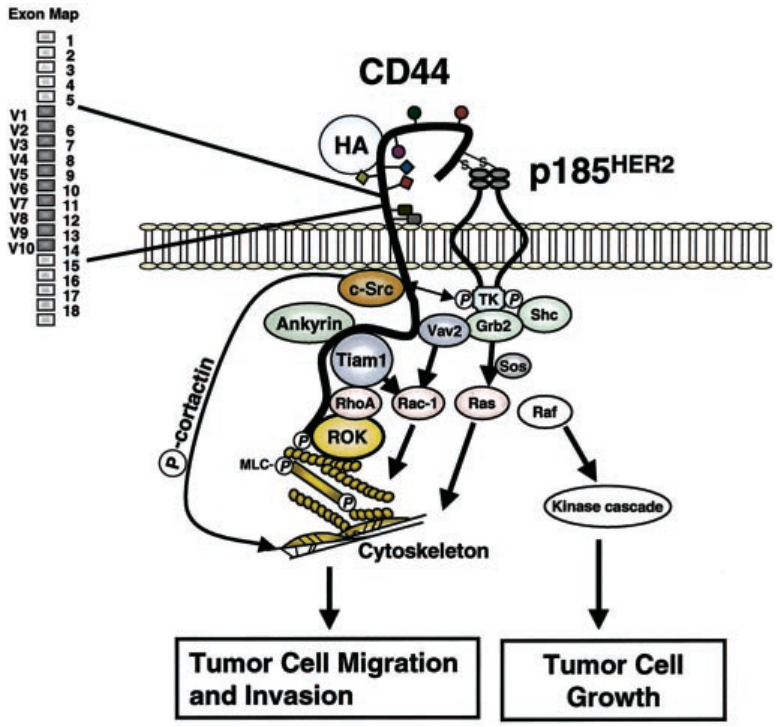

Figure 1. 10 – Current model for HA-dependent CD44-signalling pathways (Turley *et al.*, 2002).

The CD44-HA interactions can stimulate CD44-associated $p185^{HER2}$ tyrosine kinase activity, leading to an increase in the tumour growth. On the other hand, CD44-HA interactions stimulate c-src kinase activity, increasing tyrosine phosphorylation of the cytoskeletal protein (cortactin), which induces cytoskeleton-regulated tumour cell migration. CD44-HA interactions also activate Rho GTPases, such as RhoA and Rac1, which participate in the interaction between CD44 and cytoeskeletal proteins. When associated with CD44, RhoA stimulates ROK (Rho kinase) to phosphorylate several cellular proteins, promoting binding of CD44 to ankyrin. It has been proposed that CD44 and RhoA-mediated signalling is involved in membrane-cytoskeleton interactions

and tumour cell migration during cancer progression. CD44 also activates Rac1 through its binding with Tiam1 and Vav2, which are guanine nucleotide factors that catalyse GDP-GTP exchange, leading to HA-mediated tumour cell migration (**Figure 1.10**; Turley *et al.,* 2002).

Wolny and co-workers (2010) have shown that small fragments of HA (≤10 kDa) reversible bind to CD44, whereas an irreversible interaction with larger polymers is seen (Wolny *et al.,* 2010). It has also been reported that HA oligomers can stimulate different cell responses when bound to CD44, comparatively to high MW fragments, because oligomers can cause clustering of multiple CD44 receptors and thus altering the intracellular responses (Liu *et al.,* 1998). It has been suggested that the interaction of HA oligomers with CD44 promote cell proliferation, due the enhancement of vascular EC growth factor (VEGF) (Murphy *et al.,* 2005).

1.4.4. CD44 FUNCTIONS AND EXPRESSION

CD44 is a cell surface glycoprotein, playing an important role in cell-cell and cell-ECM interactions. In addition, CD44 is a cell adhesion molecule, being involved in cell motility and migration, differentiation, signal transduction, and gene transcription (Martin *et al.,* 2003). Most of the roles of CD44 are intimately associated with its capacity to promote cell attachment to HA (Naor *et al.,* 1997). CD44 is also implicated in uptake and subsequent degradation of HA (Culty *et al.,* 1992). It was also been shown that the accumulation of HA is directly correlated with the downregulation of CD44. The abnormal excess of HA is associated with lichen sclerosus at atrophicus (LSA; Kaya *et al.,* 2000), solitary cutaneous myxomas (Calikoglu *et al.,* 2002), myxoid

dermatofibroma (Calikoglu *et al.*, 2003), while high levels of HA in keratinocytes are implicated in skin and corneal lesions (Kaya *et al.*, 1997, 1999).

As previously discussed, CD44 has two important isoforms: CD44H and CD44E. The major differences presented by these isoforms are correlated with the mediation of lymphocyte homing: while CD44H can bind to HA and mediate lymphocyte homing, CD44E cannot (Berg *et al.*, 1989; Picker *et al.*, 1989; Stamenkovic *et al.*, 1991). One of the major functions of CD44 is lymph node homing (Jalkanen *et al.*, 1986, 1987; Aruffo *et al.*, 1990), playing as well key roles in lymphocyte activation and extravasation (Huet *et al.*, 1989; Shimizu *et al.*, 1989; Aruffo *et al.*, 1990). These interactions are carried out by the middle domain of CD44H in lymphocytes and a mucosal adressin. CD44E cannot perform these functions, due to an insert in the middle of domain, preventing the interaction with mucosal adressin (Underhill, 1992). Due to its involvement in homing and inflammation, CD44 has been shown to play roles in wound healing.

1.4.5. CD44 AND CANCER

The biological and physiological properties of CD44 are not only essential to the activities of normal cells, but they are also correlated with pathologic activities of cancer cells. While CD44s is ubiquitously expressed, CD44v is more restricted in normal cells, being some of the variants only expressed on malignant cells and tumour-derived cell lines (Bourguignon *et al.*, 1993, Martin *et al.*, 2003). CD44 mediates tumour-cell adhesion through its binding to several ECM components, including HA. CD44 can be correlated with the oncobiological behaviour (including tumourigenesis,

growth, metastasis and prognosis), since it is a transmembrane protein involved in the mediation of the mechanical force created by the cytoskeleton and for transmission of intracellular locomotory signals. Furthermore, high levels of CD44 are expressed in several types of tumours (Bourguignon *et al.*, 1993; Liu and Jiang, 2006).

In 1989, Stamenkovic co-workers have shown that CD44 gene was expressed in a variety of carcinoma cell lines and solid tumours. A couple of years later, Günthert and co-workers (1991), while working with a non-metastasic rat pancreatic adenocarcinoma cell line transfected with the CD44v4-7 isoform, showed that CD44 has metastatic properties, since the original tumour started to metastasing when administrated into healthy rats. These authors have shown an inhibition of metastasis upon the reaction of an antibody directly against CD44v6 (Günthert *et al.*, 1991). Furthermore, Guo and co-workers (1994) demonstrated that a mAb specific for CD44s completely inhibits the binding to hyaluronic acid of cells of a human melanoma cell line *in vitro*, inhibiting as well the metastatic capacity of the tumour cell *in vivo*. According to studies performed by Bartolazzi and co-workers (1994) there is a strong and direct relationship between HA and aggressiveness of human melanoma cell lines. This observation was achieved when working with cells transfected with CD44 mutated at arginine 41 exon s2, which is an essential site for HA recognition; resulting in the singnificantly reduction of cellular aggressiviness (Bartolazzi *et al.*, 1994). A very different behaviour of melanoma cells was observed in studies performed by Birch and co-workers (1991). These authors showed that cells exhibiting high levels of CD44 have a stronger adhesion to HA, and a more vigorous motility and homotypic aggregation, when compared to those cells expressing lower levels of CD44. In addition, cells expressing high levels of CD44 have an increased capability of colonise lungs of nude

mice, and consequently producing pulmonary nodules (Birch *et al.*, 1991). It has also been reported high levels of CD44 are correlated with the aggressiveness of lymphoid tumours (Horst *et al.*, 1990) and invasiveness of bladder carcinomas (Knudson *et al.*, 1990).

Proteolytic cleavage of the extracellular domain of CD44 is strongly related to cancer migration and signalling pathway. After the release of the extracellular domain by matrix metalloproteinases (MMPs; Nagano *et al.*, 2004) and further proteolytic cleavage by presenilin-dependent g-secretase, the intracellular domain suffers translocation to the nucleus (Okamoto *et al.*, 2001; Pelletier *et al.*, 2006). This leads to the activation of gene transcription and consequently promotion of neoplastic transformation. Despite the cleavage of the extracellular domain occurs as well in non-malignant cells; this event is clinically relevant, serving as a diagnosing parameter, since soluble CD44v can be detected in the serum of patients (Gadducci *et al.*, 1997; Goi *et al.*, 1997; Sliutz *et al.*, 1995; Saito *et al.*, 1998; Yamaguchi *et al.*, 1998; Shee-Chen *et al.*, 1999; Yamane *et al.*, 1999; Kopp *et al.*, 2001). A major problem in cancer diagnosis, using serum CD44v, is that some variant forms are also expressed in non-malignant epithelial cells, and high levels of soluble CD44v are detected in patients mainly with inflammatory diseases (Kittl *et al.*, 1997a, 1997b; Scott *et al.*, 2000).

In spite of the biological significance of CD44 in tumourigenesis starts to be elucidated, there are some aspects that need to be clarified. There are cases showing that standard CD44, rather than its variants, enhances tumour progression (Sy *et al.*, 1991; Bartolazzi *et al.*, 1994). Conversely, in prostate cancer and cervical neuroendocrine carcinoma, CD44 suppresses metastasis (Gao *et al.*, 1997; Kuo *et al.*, 2007). Furthermore, if in some cases low levels of CD44 allow the release of the tumour from

the primary site and the subsequent metastatic phase, there are studies showing that it inhibits prostate cancer progression (Desai *et al.*, 2007; Patrawala *et al.*, 2007). Therefore, the internal and external environment of the tumour appears to have an influence in the relationship of standard CD44 *vs.* CD44 variants. Consequently, this relationship must be analysed for each case and type of tumour, since heterogeneity in CD44-dependency can be detected in tumours derived from the same histological origin (Naor *et al.*, 2008).

1.5. RHAMM

RHAMM was the second characterised and cloned HA receptor. It was originally isolated in 1982 by Turley, from subconfluent fibroblasts in culture, and later cloned by Hardwick and co-workers (1992), while using mesenchymal cells. RHAMM is a unique hyaladherin, since it occurs in multiple forms, being expressed both intracellularly and at the cell surface. RHAMM is also known by different names, including hyaluronan-mediated motility receptor (HMMR), intracellular hyaluronic acid binding protein (IHABP) and CD168.

1.5.1. RHAMM GENE

RHAMM is encoded by a single gene, which in humans is located on chromosome 5 location 5q33.2 (Spicer *et al.*, 1995), and on chromosome 11 in mice. It was first cloned by Hardwick and co-workers (1992), while using a 3T3-cDNA library

from murines. The gene is composed by 18 exons, 9 of which can be alternatively spliced (Hardwick *et al.*, 1992; Entwiste *et al.*, 1995; Harrison and Turley, 1999). Thus, similarly to CD44, RHAMM can exist in multiple forms, and there are at least six described isoforms (**Figure 1.11**; Harrison and Turley, 1999).

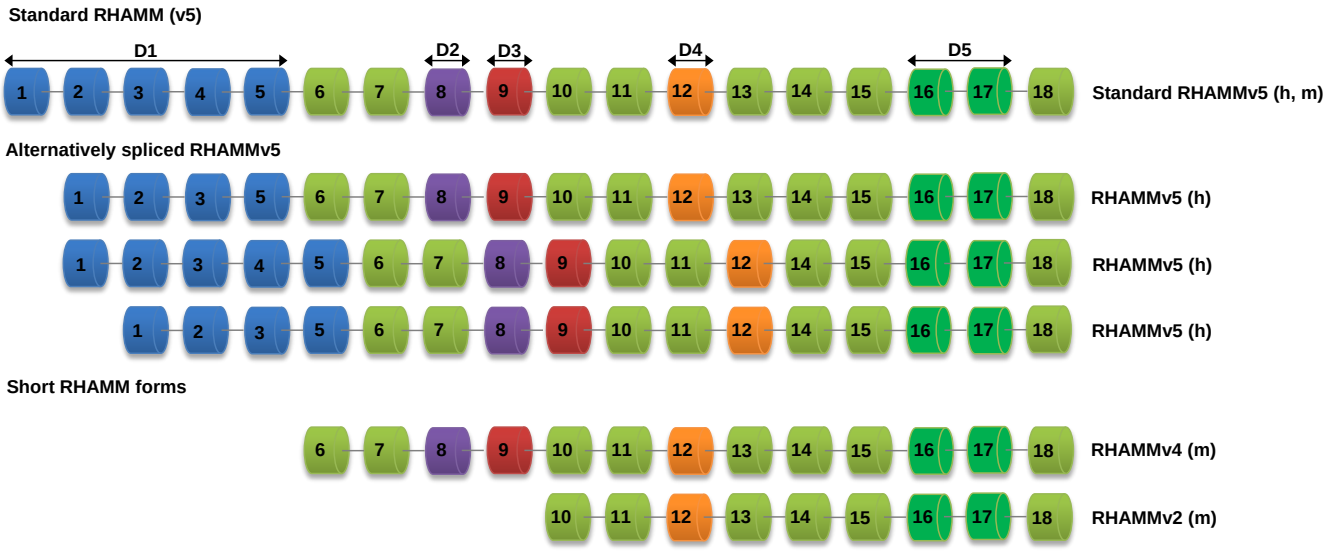

Figure 1.11 – Predicted domain structure of RHAMM in human (h) and mouse (m) [Adapted from Harrison and Turley, 1999].

Human and mouse RHAMM share 85% homology, while sharing 100% homology in HA binding domains (Pilarski *et al.*, 1999). In humans, four different transcripts were identified. These include full length RHAMM, an isoform lacking exon 4 and other lacking exon 13, and a variant reported in adherent cells lacking both exons 4 and 13 (Harrison and Turley, 1999; Assmann *et al.*, 1999). While in mice three isoforms were identified, including full length RHAMM, a variant lacking 1-5 exons and other variant lacking 1-9 exons (**Figure 1.11**; Harrison and Turley, 1999).

1.5.2. RHAMM PROTEIN STRUCTURE

RHAMM protein, originally isolated from supernatant medium of non-confluent embryonic chick heart fibroblasts (Turley *et al.*, 1992), is a unique hyaladherin occuring as multiple forms. Conversly to the others hyaladherins, RHAMM occurs intracellularly and at the cell surface. Due its lack of both signal peptide and transmembrane domain, RHAMM it is exported from the cell through putative chaperone signalling proteins involved in regulating cell cycle and motility. Associations with a GPI anchor or a linker protein allows the incorporation of RHAMM onto the cell surface (Hall *et al.*, 1995; Enwistle *et al.*, 1996; Zhang *et al.*, 1998; Crainie *et al.*, 1999).

The constitutively expressed and most common RHAMM mRNA transcript encodes the largest intracellular RHAMM protein with 85 kDa in humans and 95 kDa in murines, and which has been designated as RHAMMv5. Some isoforms are generated by alternative splicing of the longest RHAMMv5 mRNA transcript; shorter isoforms may be generated either by separate mRNA transcripts, internal start codon usage of the v5 transcript, or proteolysis of the v5 protein (**Figure 1.11**; Harrison and Turley, 1999). RHAMM protein has five functional domains **Figure 1.12**), which have been identified by structure/function analysis and are required for RHAMM-mediated cell motility and passage through the cell cycle.

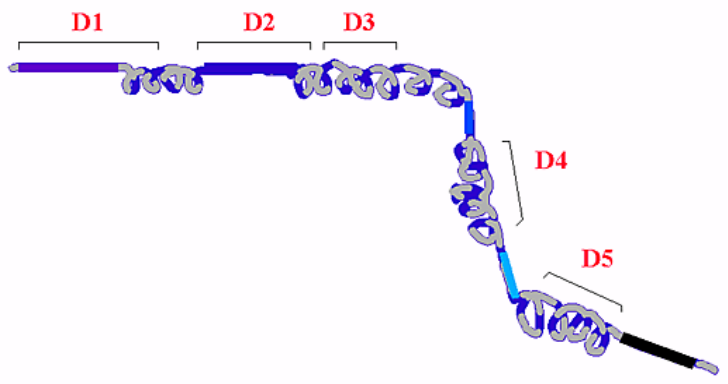

Figure 1.12 – Predicted secondary and domain structure of RHAMM (Harrison and Turley, 1999).

D1 is composed by exons 1-5, and negatively regulates the ability of RHAMM sequence to promote activation of erk1 kinase; D2 is composed by exon 8 and encodes an imperfect leucine zipper that is required for RHAMM-mediated cell motility and podosome formation; D3, which is exon 9, is involved in the interaction of intracellular RHAMM with MEK1; exon 12 gives rise to D4 which can be repeated up to 8 times in the murine protein and contributes to the binding of erk1 to intracellular RHAMM; D5, composed by exons 16 and 17, encodes hyaluronan binding motifs that are responsible for interaction of hyaluronan with cell surface RHAMM and erk1 binding to intracellular RHAMM (Harrison and Turley, 1999).

RHAMM's secondary structure analysis indicates that the sequence of this molecule, from amino acids 163 to carboxyl-terminus, is largely a coiled coil protein punctuated by small non-coiled coil stretches often preceding functional domains (**Figure 1.12**; Harrison and Turley, 1999).

RHAMM undergoes alternative splicing, containing many potential sites for post-translational modifications. These include N-glycosylation sites, myristoylation sites and notably, multiple serine-threonine phosphorylation sites. Despite being well

known that similarly to CD44, RHAMM has potential for alternative splicing and post-translational modifications, giving rise to numerous tissue- and species-specific protein isoforms, it is still unclear whether these modifications might cause effects on subcellular localisation and protein interactions (Harrison and Turley, 1999).

The classical protein export model is dependent on the secretory pathway of the Golgi/ endoplasmatic reticulum (ER), accounting for most of the constitutive export proteins. However, RHAMM is part of a heterogeneous group of cell-surface proteins that do not follow this model, since RHAMM gene does not encode a traditional leader sequence to permit it secretion via the traditional Golgi/ER export pathway (Turley *et al.*, 2002; Maxwell *et al.*, 2008). As a consequence, RHAMM lacks signal peptides and is predicted to be a cytoplasmatic protein, being exported in response to specific stimuli (e.g. non-constitutively) by unconventional mechanisms (Maxwell *et al.*, 2008).

1.5.3. RHAMM LIGANDS

HA is known to be the principal ligand for RHAMM (Leach and Schmidt, 2004; Girish and Kemparaju, 2007). Both cell surface and intracellular RHAMM forms are required for cell motility and cell cycle progression. Cell surface RHAMM acts as co-receptor that modify signalling through integral proteins (e.g. PDGF), while intracellular RHAMM forms are erk1 binding proteins (Harrison and Turley, 1999). A current proposed model for HA-dependent RHAMM mediated signalling pathways, is based on the cell surface RHAMM-HA interactions regulation signalling through src and ras (**Figure 1.13**; Harrison and Turley, 1999; Turley *et al.*, 2002). These molecules can act as oncogenes, and are involved in the regulation of cytoskeleton assembly,

proliferation and motility (Harrison and Turley, 1999). Modification of tyrosine phosphorylation of FAK and signalling of growth factors (such as PDGF) are events that result from the interaction between cell surface RHAMM with HA, and which are mediated by src and ras. As a result, these interactions alter the ability of PDGF receptor to activate erk kinase, which is a molecule involved in cell motility. Intracellular RHAMM forms are src and erk binding proteins, since they have specific recognition sites for these molecules. Cell surface RHAMM is also required for the regulation of ras, but at different points along the signalling pathway (Harrison and Turley, 1999; Turley *et al.*, 2002; Maxwell *et al.*, 2008).

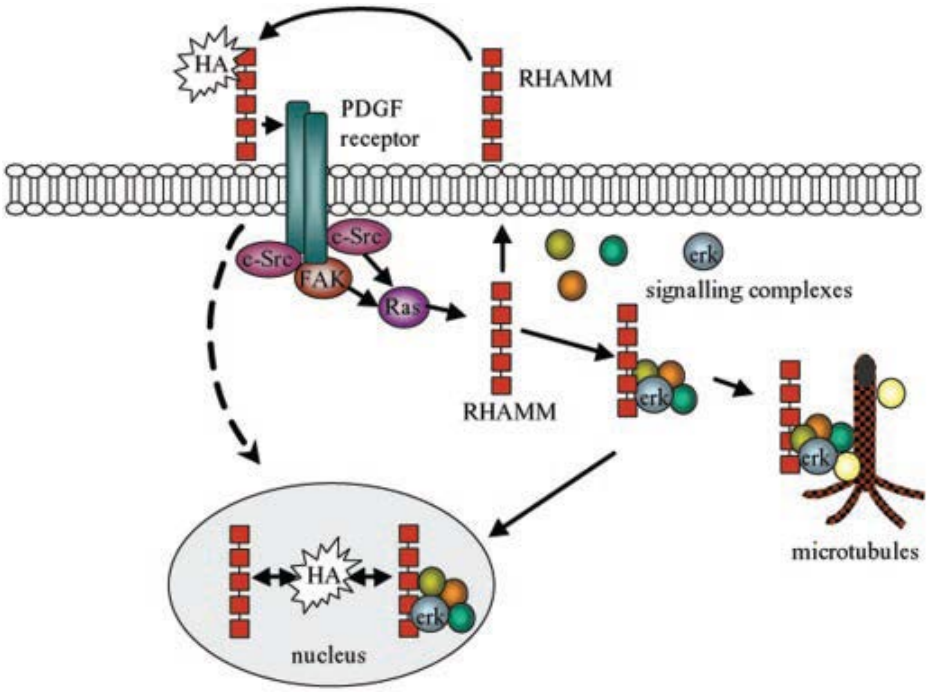

Figure 1.13 – A current model for HA-dependent RHAMM-mediated signalling pathways (Turley *et al.*, 2002).

RHAMM can bind to other ligands, including tubulin, actin, calmodulin (Assman *et al.*, 1998; 2001), heparin (Yang *et al.*, 2004), fibronectin (Yang *et al.*, 1993; Yang *et al.*, 1994a; Chang *et al.*, 1997) and laminin (Nagy *et al.*, 1995).

1.5.4. RHAMM FUNCTIONS AND EXPRESSION

RHAMM is distributed into multiple compartments, such as cell surface, cytoskeleton, mitochondria, and cell nucleus, depending on alternative splicing of the transcript (Turley *et al.*, 2002). This molecule is expressed in several cells and tissues, including fibroblasts, smooth muscle cells, endothelial cells, macrophages, immature thymocytes, B cell lineages, bone marrow stromal cells, keratinocytes, sperm, astrocytes, astrocytomas, central nerve cells, microglial cells, sprouting olfactory nerve cells. Moreover, it is also observed in some malignant tumours (Harrison and Turley, 1999).

RHAMM has two major isoforms: cell surface and intracellular (usually referred to as intracellular HA binding protein [IHAPB]) variants. Cell surface RHAMM is implicated in promotion of the cellular motility and invasion. While IHAPB, localised in the centrosome, it is involved in the cell cycle control and mitotic spindle formation. IHAPB is also associated with actin and microtubule cytoskeletal elements (Turley *et al.*, 2002; Girish and Kemparaju, 2007).

As previously described, RHAMM is part of an unconventionally exported protein, performing unexpected extracellular functions that are not defined by protein-structure rules. This protein is exported in response to specific stimuli, and stimulating on the other hand, cell adhesion and/or motility upon export (Maxwell *et al.*, 2008). The

RHAMM's promotion of the cellular motility and invasion is signalled via an association with HA-CD44 complexes, promoting the activation of signalling cascades. In the presence of HA, RHAMM partners with CD44, activating erk1/2 and resulting in the expression of genes, which are required for cell motility and invasion (**Figure 1.14**; Turley *et al.*, 2002; Toole *et al.*, 2004; Maxwell *et al.*, 2008).

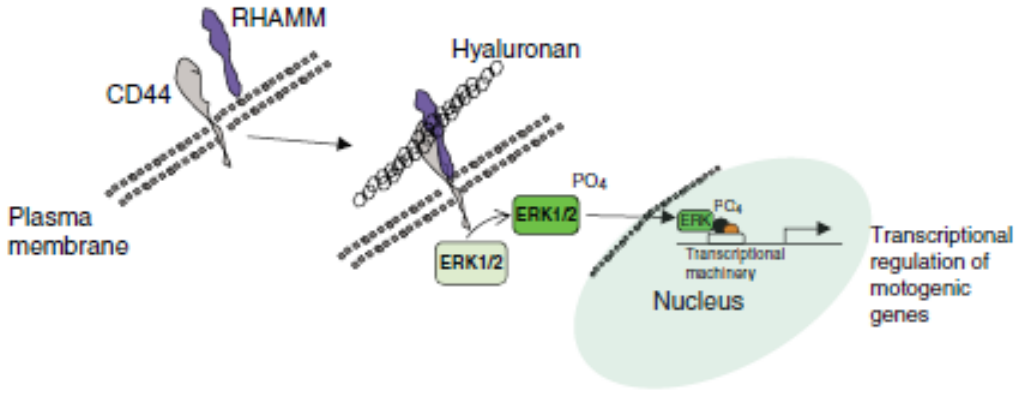

Figure 1.14 – Extracellular functions of RHAMM. erk1/2 is indicated as phosphorylated (PO_4) ERK1,2, (Maxwell *et al.*, 2008).

Physiologically, RHAMM plays key roles in the processes of development (Boudreau *et al.*, 1991) and wound repair (Savani *et al.*, 1995); while pathologically, is involved in restenosis (Savani and Turley, 1995) and tumour progression (Hall and Turley, 1995; Masellis-Smith *et al.*, 1996). In most of normal tissues RHAMM mRNA and protein expressions are low or undetectable. However, an upregulated expression of RHAMM is seen following both wounding *in vivo* and in fibroblasts and smooth muscle cells *in vitro*, in response to hypoxia and fibrogenic factors, such as TGFβ1(Savani *et al.*, 1995; Mohapara *et al.*, 1996; Tolg *et al.*, 2003; Maxwell *et al.*,

2008). In contrast, a genetic delection of RHAMM results in a slow healing of skin wounds (Tolg *et al.*, 2006).

High levels of RHAMM are also seen in culture at low confluence *in vitro* in the presence of growth factors or upon neoplastic transformation both *in vitro* and *in vivo* (Tolg *et al.*, 2003). Furthermore, RHAMM it is also involved on the progression of diseases such as arthritis (Maxwell *et al.*, 2008).

1.5.5. RHAMM AND CANCER

High levels of RHAMM are seen in tumour cells, and they are also correlated with the neoplastic progression of a variety of tumours (Maxwell *et al.*, 2008). In some tumours a high expression of RHAMM can be a prognostic of a poor outcome; whereas many aggressive human neoplasms are characterised by having high levels of RHAMM, including aggressive human fibromatoses (desmoid) tumours, terminally differentiated multiple myelomas, breast carcinoma cells, blood tumours, adenocarcinomas, small lung carcinoma cells, squamous cell carcinomas, and late stage astrocytoma (Turley *et al.*, 1993; Teder *et al.*, 1995; Mohapara *et al.*, 1996; Assman *et al.*, 1998; Greiner *et al.*, 2002; Tolg *et al.*, 2003).

IHAPB plays key roles in the mitotic-spindle stability, which is important for the regulation of the mitosis (Adamia *et al.*, 2005a; Maxwell *et al.*, 2008). It has been suggested that RHAMM-centrosome-mitotic-spindle associations promotes gene instability, having implications on cell transformation and tumour progression (Maxwell *et al.*, 2008).

There is some evidence of RHAMM and CD44 interplaying, with cell surface RHAMM having a role in the activation of CD44-dependent signalling. It has been suggested that this partnership can confer malignant potential in breast cancer, by activating the extracellular HA binding (Maxwell *et al.,* 2008). Moreover, this partnership was also seen in invasive breast cancer cell lines, where extracellular RHAMM-CD44 complexes coordinate HA-dependent erk1/2-mediated cell transformation (Hamilton *et al.,* 2007). In advanced prostate cancer RHAMM seems to compensate the loss of CD44. Thus, partnering with other integral HA receptors, RHAMM can maintain the activation of HA-signalling pathways (Maxwell *et al.*, 2008).

Some studies have shown that suppression of normal HA-RHAMM interactions and genetic delection of RHAMM inhibit the cell locomotion and proliferation, leading to an inhibition and decrease of tumour growth (Hall *et al.*, 1995; Mohapara *et al.*, 1996; Tolg *et al.,* 2003). Moreover, mutations of key basic residues in the C-terminus of RHAMM, lead to a disruption in HA binding, which in turn inhibits the transforming capacity of RHAMM and ras transformation (Maxwell *et al.,* 2008). Conversly, RHAMM-transfected cells are able to metastasize (Hall *et al.*, 1995).

RHAMM appears to be a promising target for immunotherapeutic approaches and have shown some potentialities in clinical use. Currently, a vaccine for acute myeloid leukaemia and multiple myeloma using RHAMM is being carried out in phase I of clinical trials (Schmitt *et al.*, 2007).

1.6. EXPLOITATION OF HA AT THE BIO-INTERFACE

Surfaces play a key role in biology and medicine, with most biological reactions occurring at surfaces and interfaces. Interfaces of biological importance include cell surface/biomaterial, ECM/biomolecule and ECM/cell (Castner and Ratner, 2002). Therefore, the development of biomaterials for tissue engineering applications has been focused on the design of biomimetic materials, which are an attempt to make the materials able to interact with surrounding tissues by biomolecular recognition, eliciting specific cell responses (Shin *et al.*, 2003). The introduction of surface methods of biological interest has had a considerable impact on molecular and cellular biology and medicine (Castner and Ratner, 2002). Surfaces have been used in medical implants for tissue regeneration and drug delivery systems. Furthermore, the structure and function of many biological receptors have been determined along with their mechanism of cell binding activation (Castner and Ratner, 2002; Shin *et al.*, 2003). In the last years, the investigation of the processes relating biointerfaces and cancer biology has been increasing (Peramo *et al.*, 2008).

Body tissue is composed of cells and the surrounding environment, which includes the extracellular matrix (ECM) and biosignalling molecules. However, sometimes tissue repairing cannot be achieved only by the single or combinatory effect of the use of ECM components and biosignalling molecules in an appropriate way. Therefore, it is necessary to biomedically contrive the way to combine, what can be achieved by biomaterial technology (Tabata, 2009). Biomaterial technology plays an important role in the tissue engineering therapeutics strategy, providing cells with a local environment that regulates cellular proliferation, differentiation, angiogenesis and

apoptosis (Tabata, 2009; Tilkorn *et al.*, 2010). Biomolecular recognition of materials by cells has been achieved by surface with bioactive molecules, including ECM components that can incur specific interactions with cell receptors (Shin *et al.*, 2003). Tethering biomolecules onto solid substrates can provide the construction of interesting models that can be used in biological applications, including controlled cellular adhesion and growth, biosensors and immunoassays (Peramo *et al.*, 2008).

Tissue engineering is a multidisciplinary field and applies knowledge of clinical and life sciences with engineering. This field has been attracting many scientists and clinicians with a hope to treat patients in a minimal invasive and less painful way. It offers unique opportunities to investigate aspects of the structure-function relationship and to predict the clinical outcome of the specific medical treatment. This can be achieved by the use of biomimetic materials, which are designed for eliciting specific cellular responses and biomolecular recognition (Shin *et al.*, 2003).

1.6.1. TISSUE ENGINEERING IN CANCER RESEARCH

Tissue engineering and cancer research once regarded as in opposite fields concerning their proclaimed goals, start now suggesting that the cross-disciplinary research will benefit both fields (Tilkorn *et al.*, 2010). Technology platforms originally developed for tissue engineering applications produce valuable *in vitro* and/or *in vivo* models for cancer research (**Figure 1.15**). These models mimic tissue organisation and function allowing the understanding of cell/tissue function under normal and pathological situations, and unleashing the mechanisms of morphogenesis, differentiation and cancer. In addition, these models have started now to be used in the

investigation of angiogenesis, apoptosis and factors in tumourigenesis, in order to establish ways of targeting angiogenesis and inducing apoptosis in tumours (Hutmacher *et al.*, 2010). These models have been established by the use of well-defined synthetic hydrogels or scaffold-based tissue engineered constructs that generate tightly controlled microenvironments typical from *in vivo* environment (Hutmacher *et al.*, 2010). Naturally-derived matrices used in cancer research include collagen and laminin-rich gels (Kleinman *et al.*, 1986; Benton *et al.*, 2009; Kleimen and Martin, 2005). Kleiman and co-workers (1986) firstly demonstrated the great value of reconstituted basement membrane as a culture substract (Kleinman *et al.*, 1986). This basement membrane was mainly constituted by type IV collagen, laminin and heparan sulphate proteoglycan, and allowed the development of new products, including Matrigel™ (which consists of mainly type IV collagen and laminin). Later on, alternative systems, such as type I collagen gels, have also been used in cancer models (Jedeszco *et al.*, 2008; Moss *et al.*, 2009; Sabeh *et al.*, 2009; Wozniak *et al.*, 2010). Although these gels can be easily produced, their structure can be affected by minor changes in several factors, including their source, crosslinking chemistry, temperature, pH, ionic strength and ion stoichiometry, and monomer concentration, what can lead to alterations in the properties of the resultant matrices and variations of results obtained from different work groups (Sabeh *et al.*, 2009).

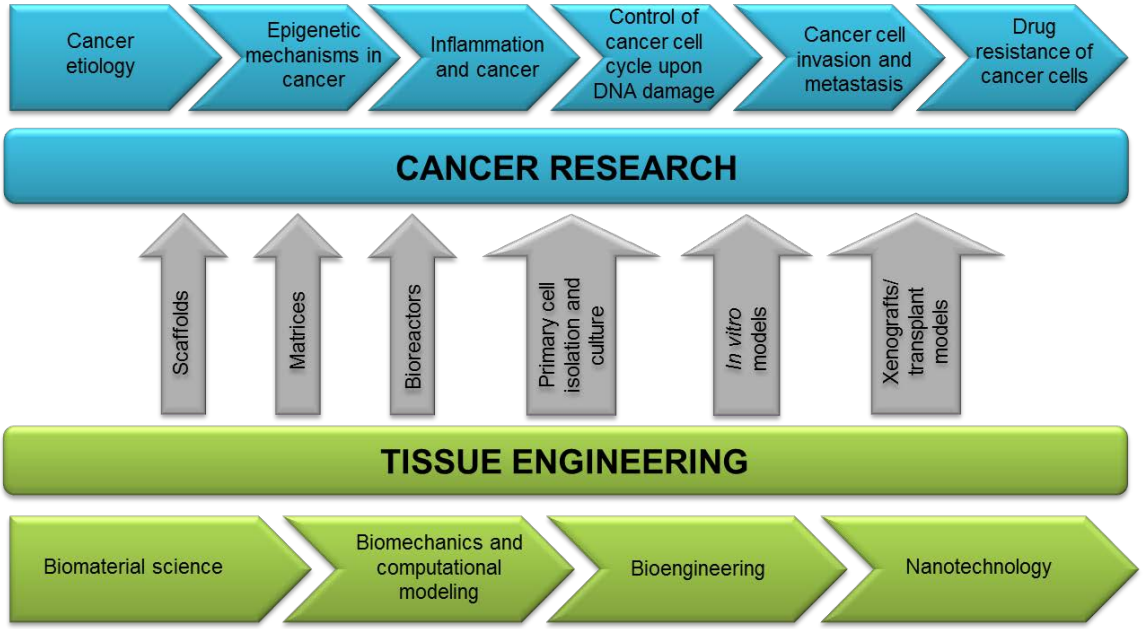

Figure 1.15 – Schematic illustration of how technology platforms originally developed for tissue engineering applications produce valuable models that mimic tissue organisation and function by replicating physiological and pathological conditions of cancer as close as possible [Adapted from Hutmacher *et al.*, 2010].

In the last years, tissue engineering has been focusing in the development of alternatives to naturally derived matrices, and therefore trying to overcome their limitations. As a result, synthetic hydrogel-like materials and scaffolds that biomimetic ECM have been developed. These synthetic materials provide the possibility of controlling characteristics, including as matrix morphology and porosity, gel formation and cross-linking dynamics, degradation rates and mechanical properties (Hutmacher *et al.*, 2010). Currently, there are several alternative gel systems, including those based in polyethylene glycol (PEG; Schneider *et al.*, 2006), RGD-peptides coupled to alginate (Fischbach *et al.*, 2009), poly(lactide-co-gylcolide acid) (PLGA; Fischbach *et al.*, 2007), and HA (Liu *et al.*, 2007; David et al., 2008; Choi *et al.*, 2010).

1.6.2. HYALURONIC ACID STRUCTURED SURFACES

Hyaluronic acid is of great biological interest, and due to its physiochemical characteristics it is an advantageous polysaccharide for biomaterial fabrication and applications. It is naturally derived, enzymatically degradable and non-immunogenic, and in addition can be easily and controllably produced in large quantities through microbial fermentation, enabling the scale-up of HA-derived products and avoiding the risk of animal-derived pathogens (Leach and Schimidt, 2004). Therefore, HA appears to be a good candidate for incorporation in biological surfaces aimed to favour cell adhesion, tissue repair, or drug delivery (Picart *et al.*, 2001).

Several approaches have been taken aiming to construct HA-coated surfaces. Most of them rely on the self-assembled methodology, while using crosslinked HA. Picart and co-workers (2001) fabricated films based on poly(L-lysine) and HA (PLL/HA), aiming to investigate the interaction of the surfaces with chondrocytes and study the interaction of HA with CD44. PLL/HA films were also investigated in other works aiming to study the interaction of the surfaces with chondrosomas (Richert *et al.*, 2004a), hepatocytes (Khademhosseini *et al.*, 2004), fibroblasts (Khademhosseini *et al.*, 2004, Schneider *et al.*, 2007a), smooth muscle cells (Richert *et al.*, 2004c) and myoblasts (Ken *et al.*, 2008; Váskez *et al.*, 2009). Surfaces based on the alternate deposition of chitosan (CHI) and HA were also investigated, since the low cost of CHI when compared to PLL makes it a better candidate for industrial applications (Richert *et al.*, 2004b). Scheneider and co-workers (2007) also investigated CHI/HA films for drug diffusion (Schneider *et al.*, 2007b). Porous collagen-HA matrix was produced by Park and co-workers (2003) to be used as a scaffold for dermal tissue regeneration (Park et

al., 2003). An investigation of the size-specific effects of HA on aortic endothelial cells was carried out using surfaces coated with a wide range of HA fragment sizes (Ibrahim *et al.*, 2007). David and co-workers (2008) produced an HA hydrogel used for the evaluation of anticancer drug sensitivity, while using lung cancer cell lines. These authors showed that the crosslinked HA matrix was a good model for the evaluation of the efficiency of cytotoxic drugs on the growth and invasion of tumour cells (David *et al.*, 2008).

1.7. AIMS AND OBJECTIVES

The biological functions exhibited by HA are known to be dependent on the polymer molecular weight (MW), and mediated through interactions with its main cell receptors: CD44 and RHAMM. However, the direct effect between the HA molecular weight and the expression of CD44 and RHAMM remains unclear. The overall aim of this project is to investigate whether different HA polymer MW alters the proliferation of tumour-derived cell lines, and whether different sizes of HA have an effect on the expression of CD44 and RHAMM, and on the alternative splicing patterns commonly seen for these cell receptors. In order to perform this investigation, this project also aims to immobilise HA polymer to glass coverslips, designed to support cell adhesion and therefore allowing the permanent contact of the cells with the substrate, rather than periodic contact with exogenous HA of media supplementation.

The initial objective of this work is the development of a protocol to construct a variety of novel HA structured surfaces to support adhesion of tumour-derived cell lines. In order to determine size-specific responses of tumour cells of defined fragment

MW, surfaces coated with a range of polymers of different MWs will be constructed and analysed using a toolbox of *in situ* characterisation techniques. After the establishment of well-defined *in vitro* model systems, the effect that HA has on cell proliferation and apoptosis will be evaluated. Once cell biology studies have been assessed, the study will move to the last objective of the project, the investigation of the interaction of HA with CD44 and RHAMM cell receptors. This investigation will be carried out at both transcriptional and translational levels. Transcription studies include the quantification of the CD44 and RHAMM transcript levels, and to look at the alternative splicing patterns commonly seen for these cell receptors. Transcriptional studies will be carried out in order to investigate the immunolocalisation of CD44 and RHAMM proteins. These objectives will each be achieved through a defined chapter of work previously described in **section 1.1**.

CHAPTER 2

“Impossible is just a big word thrown around by small men who find it easier to live the world they've been given than to explore the power they have to change it. Impossible is not a fact. It's an opinion. Impossible is not a declaration. It's a dare. Impossible is potential. Impossible is temporary. Impossible is nothing.” – Muhammed Al

CHAPTER 2

2. CONSTRUCTION OF A VARIETY OF NOVEL STRUCTURED HYALURONIC ACID SURFACES

2.1. INTRODUCTION

The present work deals with the construction of hyaluronic acid (HA)-coated surfaces designed to support cell adhesion. Immobilised components on a 2D substrat may more closely stimulate cell responses within controlled surfaces, due to intimate cell contact with the substract-bound HA, rather than periodic contact with exogenous HA of media supplementation (Ibrahim *et al.*, 2007). Due to its physiochemical characteristics, HA is an advantageous polysaccharide for biomaterial fabrication and applications. It is naturally derived, enzymatically degradable and non-immunogenic, and in addition can be easily and controllably produced in large quantities through microbial fermentation, enabling the scale-up of HA-derived products and avoiding the risk of animal-derived pathogens (Leach and Schimidt, 2004).

Soluble HA has been used in several clinical applications, such as ophthalmology (Miller and Stegmann, 1983; Laurent *et al.*, 1995; Menzel and Farr, 1998; Lapckik *et al.*, 1998), cartilage and wound repair (Chen and Abatengelo, 1999), wound regenerative healing (Foshi *et al.*, 1990; King *et al.*, 1991; David-Raoudi *et al.*, 2008), viscosupplementation for osteoarthritis (Laurent and Fraser, 1992; Peyron, 1993; Pozo *et al.*, 1997), anti-adhesion applications (Barnhart *et al.*, 1979; Abatangelo *et al.*,

1982; Koochekpour *et al.*, 1995; Evanko *et al.*, 2005), drug delivery systems (Liao *et al.*, 2005), and binding onto tumour cells and metastases (Toole and Hascall, 2002). However, uncrosslinked soluble HA presents some characteristics that limit its use in many biomedical applications. HA can be chemically modified or crosslinked in order to improve its poor mechanical properties and rapid degradation in an aqueous environment (Segura *et al.*, 2005; Collins and Birkinshaw, 2007). Crosslinking is the most common modification of HA to form a hydrogel, while attempting to maintain its biocompatibility and biological activity (Leach and Schimidt, 2004; Collins and Birkinshaw, 2008). The functional groups which are mainly responsible for the crosslinking of HA molecules are hydroxyl and carboxyl groups, with hydroxyl groups crosslinked via an ether linkage and carboxyl groups via an ester linkage. If desired, HA may be chemically modified prior to crosslinking to form other chemically reactive groups. The structural integrity of HA hydrogels is determined by the chemical bonds and by physical interactions formed during crosslinking, and such gels are processed easily, are generally biodegradable and can be delivered in a minimally invasive manner (Collins and Birkinshaw, 2008).

Many strategies exist for crosslinking HA (**Figure 2.1**; Leach and Schmidt, 2004; Collins and Birkinshaw, 2008), of which carbodiimide-mediated crosslinking was chosen for the present investigation, for its simplicity to induce intermolecular crosslinks on HA, and in contrast with conventional crosslinking agents does not chemically bind to HA polysaccharide molecules (Tomihata and Ikada, 1997; Wrobel *et al.*, 2002). EDC modifies the side groups of polysaccharides to make them reactive with other side groups, including ester linkages between the carboxyl groups of HA and the hydroxyl groups of HA (Richert *et al.*, 2004). The carbodiimide-mediated crosslinking

is also often used for immobilisation of different biological molecules on solid supports, where the reaction of activated carboxylic sites with primary amino groups in the presence of water soluble carbodiimide (EDC) and of N-hydroxysuccinimide takes place (NHS; Schneider *et al.*, 2007). EDC catalyses the formation of amide bonds between carboxylic acids and amines. Briefly, EDC reacts first with a carboxyl group, forming an amine-reactive *O*-acylisourea intermediate that quickly reacts with an amino group to form an amide bond and releasing an isourea by-product in the process (Staros *et al.*, 1986; Schneider *et al.*, 2007; NHS instructions). The intermediate is unstable in aqueous solutions. Thus, the carboxyl groups of the component HA disaccharide monomers are activated with EDC into the chemically reactive and unstable *O*-acylisourea. This complex can either react with a primary amine to form stable amide bonds or undergo hydrolysis in the presence of water to reform the carboxyl (**Figure 2.1;** Schneider *et al.*, 2007; NHS instructions).

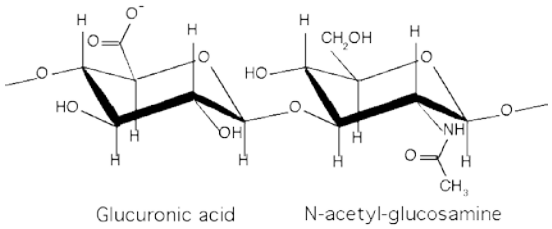

Figure 2.1 – The repeating disaccharide unit of hyaluronic acid.

To prevent the hydrolysis of *O*-acylisourea, NHS is added to the solution. NHS combined with *O*-acylisourea produces a more stable amine reactive NHS-ester intermediate, increasing the efficiency of EDC-mediated coupling reactions, which

consequently gives a greater reaction yield (**Figure 2.2**; Staros *et al.*, 1986; Schneider *et al.*, 2007; NHS instructions).

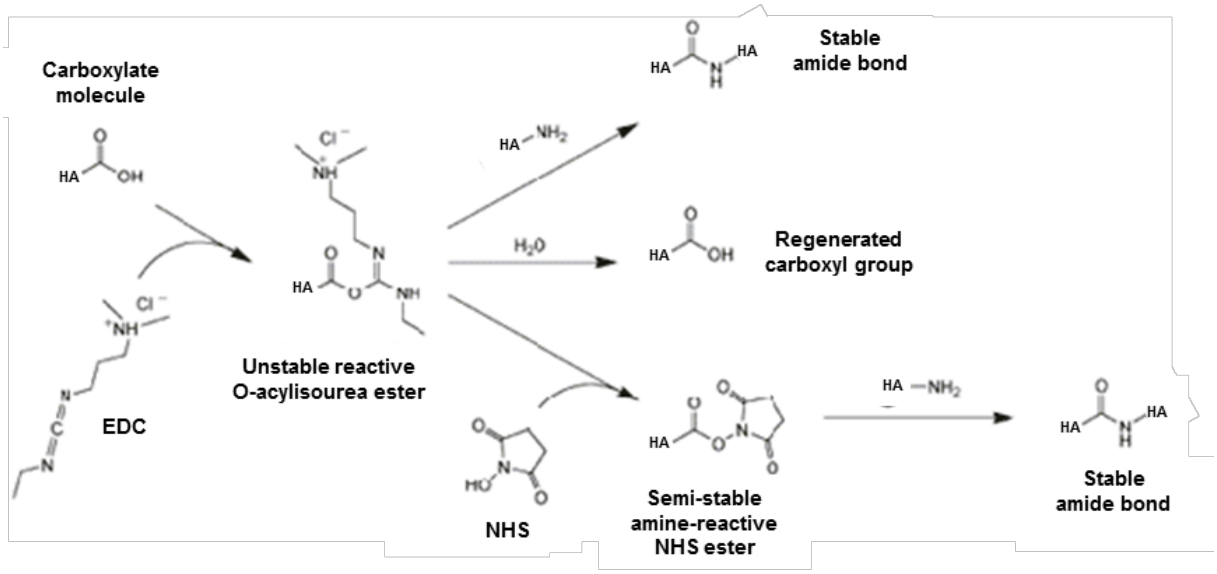

Figure 2.2 – HA crosslinking reaction by carbodiimide-mediated crosslinking using EDC as crosslinker. EDC reacts with a carboxylic group (**1**). The activated complex is conversed into an active ester with NHS (**2**). The activated ester reacts with a primary amine to form an amide bound (**3**). The unreacted sites are hydrolysed giving a regeneration of the carboxyls (**4**) [Adapted from Richert *et al.*, 2004].

The optimisation of the construction process for HA-coated surfaces represents another important stage in their design. It is an overall complex experimental approach, dependent upon multiple parameters. In the field of biomaterials, controlling the surface properties of the material is of crucial importance, as these properties can influence cell behavior, including recolonisation, adhesion, migration, and differentiation. Cell/material interactions are influenced by a large number of parameters, which include surface chemistry and topography, and mechanics of the substrate (Wong *et al.*, 2004; Ren *et al.*, 2008). Matrix stiffness was found to have an effect on cell morphology, adhesion, proliferation, and migration; and several studies have demonstrated the influence of the substrate rigidity on the cell adhesion and movement (Ren *et al.*, 2008).

It was also found that cells show different morphologies and motility rates when cultured on substrates of identical chemical properties but different rigidities (Pelham and Wang, 1997).

This chapter describes the protocol development and optimisation of the construction of 2D structured hyaluronic acid surfaces designed to support cell adhesion. These are well defined HA surfaces, coated with a range of different sized-polymers. In addition, in order to investigate the influence of crosslinker on the concentration of the surfaces, HA films of different polymer chain lengths were crosslinked to various degrees.

The work presented in this chapter can be divided into three main parts:

- Experimental design and optimisation of the construction of HA-coated surfaces;
- Characterisation of the surfaces;
- Choice of the surfaces to support cell adhesion.

In **Figure 2.3** is summarised the steps involved in the construction and characterisation of HA-coated surfaces.

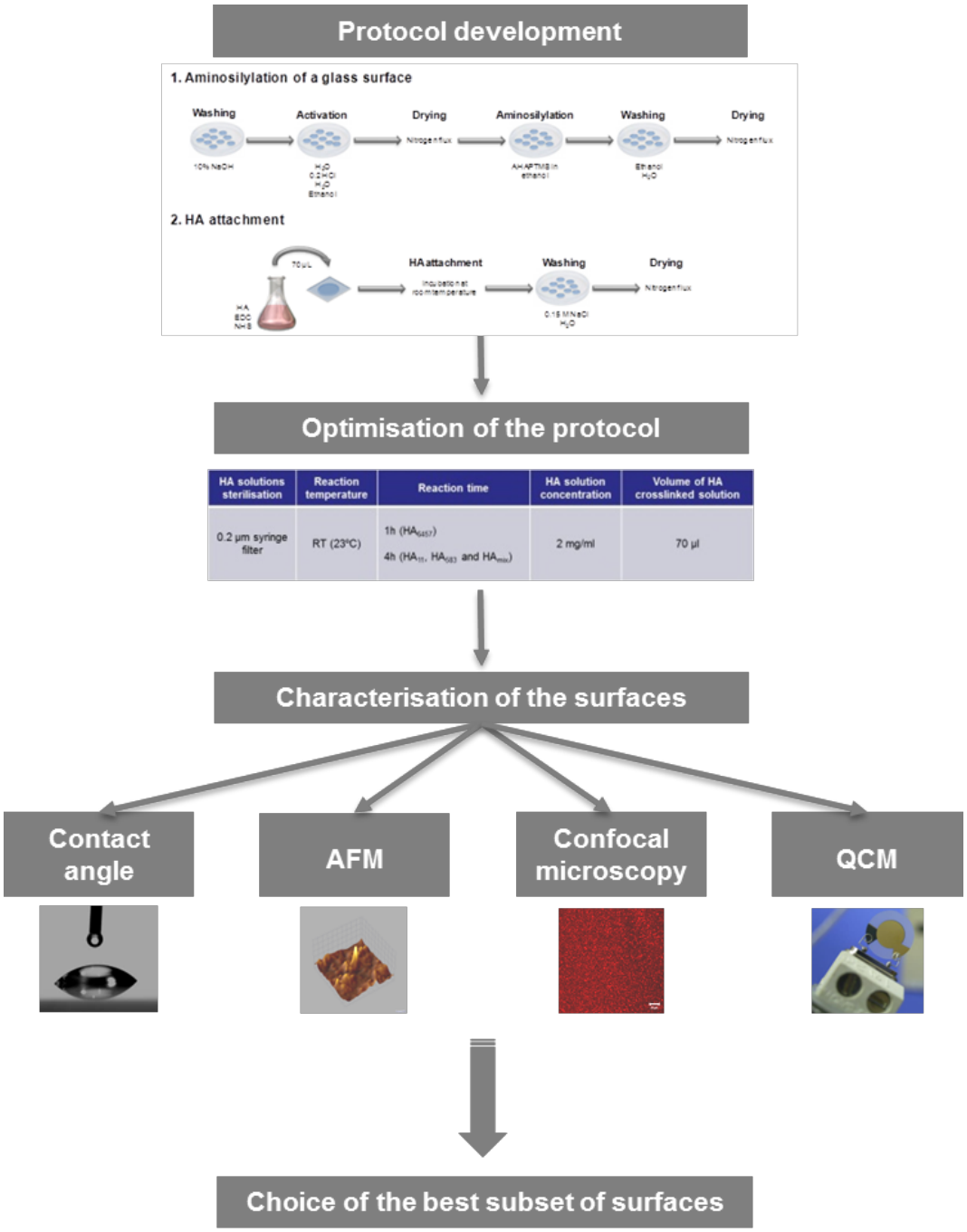

Figure 2.3 – Summary of the steps involved in the construction and characterisation of HA structured surfaces.

2.2. MATERIAL AND METHODS

2.2.1. PREPARATION OF HA FILMS ON GLASS COVERSLIPS

In the present work hyaluronan sodium salt from microbial (*Streptococcus pyogenes*) fermentation process (Lifecore, USA) was used. Hyaluronan (HA) was anchored on glass coverslips (19 mm diameter – nº0 thickness, Raimond A Lamb Limited, UK) through aminosilane monolayers. Glass coverslips were first immersed in 10% NaOH overnight. The cleaning procedure was then followed by four washing steps of 5 minutes each to hydrate the surfaces: first with RO water, followed by 0.2 M HCl, RO water, and the last step performed in absolute ethanol. The coverslips were dried under nitrogen flux and then immersed in an absolute ethanol solution containing 1 µl/ml AHAPTMS (N-(6-aminohexyl)-aminopropyltrimethoxysilane) 95% (Fluorochem Ltd, UK) overnight. This was followed by two washing steps with absolute ethanol and RO water as previously described, and drying with a nitrogen flux. The dried coverslips were stored for later use at room temperature.

Four different HA-films were prepared: low-molecular-size – HA_4 (4.3 kDa), medium-molecular-size – HA_{234} (234 kDa), high-molecular-size – HA_{2590} (2590 kDa), and a mix of all -polymers in an equal ratio – HA_{mix} (**Appendix XIX**). Each HA solution was prepared at 2 mg/ml in 10 mM HEPES buffer (pH 7.0; Fisher) and gently stirred overnight. All HA solutions were sterilised with a syringe filter (0.2 µm, Nalgene, Thermo Fisher Scientific Inc.). EDC (1-ethyl-3-[3-dimethylaminopropyl]carbodiimide hydrochloride; Thermo scientific) and NHS (N-

hydroxysuccinimide; Pierce) were added to the HA solution previously described and reacted for 5 minutes at room temperature (23ºC). Three different crosslinker concentrations were tested (**Table 2.1**).

Table 2.1 – EDC and NHS concentrations used for crosslinking reaction.

	EDC	NHS
C1	0.2 M	0.05 M
C2	0.4 M	0.10 M
C3	0.6 M	0.15 M

To create a thin and flat film, 70 µl of the gelation solution were dropped onto a square glass slide (22 x 22 mm, Thermo Scientific) previously subjected to UV radiation for sterilisation and covered with an aminosilanised glass coverslip. The HA attachment was carried out at room temperature for 1 hour in case of HA_{2590} surfaces and for 4 hours for the rest of the surfaces. Then the entire coverslip assembly was placed in 0.15 M NaCl solution pH 6.0, and they were carefully separated in parallel directions. The HA coated-coverslips were first washed with 0.15 M NaCl solution pH 6.0 for 30 minutes, followed by a RO water washing step for 10 minutes. Coverslips were dried under nitrogen flux and stored at 4ºC until use.

Figure 2.4 shows a schematic representation of HA-coating protocol.

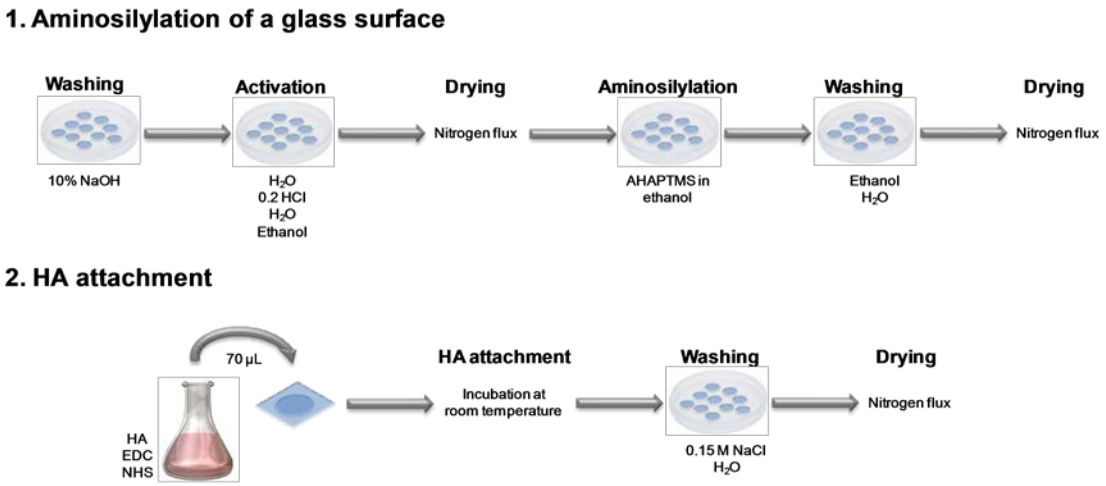

Figure 2.4 – Scheme summarising the steps involved in the protocol for coating HA to glass coverslips.

2.2.1.a. Optimisation of the construction of HA structured surfaces

For the optimisation of the construction of HA-coated surfaces, preliminary experiments were carried out, in order to facilitate an appropriate selection of the experimental ranges of investigation:

- Sterilisation of HA solutions
- Reaction temperature
- Reaction time
- Volume of HA solution drop in each coverslip

In order to reach different matrix stiffness, different crosslinker concentrations were tested. The chosen crosslinker concentrations were based on a study performed by Ladam and co-workers (2003), and according to EDC solubility in water (> 200 g/l).

2.2.2. CONTACT ANGLE

To estimate the quality of stable monolayers and multilayer films, wetting measurements can be used. One of the most commonly used techniques is contact angle, which is a quantitative technique that measures the wetting of solid surfaces by a liquid. It can be used to gauge the surface tension between a liquid and a surface, thus shedding light on a surface's hydrophobicity. To verify the modification of the surface, static contact angle measurements were performed using a KSV cam 100 (KSV Instruments Ltd) with RO water.

2.2.3. ATOMIC FORCE MICROSCOPY*

Atomic force microscopy (AFM) is a scanned probe technique, which reveals the surface topography on a very fine scale. In the present work AFM was performed in glass, aminosilane and HA-tethered coverslips in order to determine the roughness and gauge the uniformity of the coatings. A PicoScan SPM (Molecular Imaging, USA) was used, and samples were imaged under non-contact mode, and analysed with Gwyddion and ImageJ software. Three samples were analysed for each HA-coated surface and one sample for glass and aminosilane surfaces. Five points per sample were analysed for the calculation of the roughness.

*Atomic force microscopy image capture was undertaken by Dr. Steven A. Fowler, with data analysis and interpretation carried out by the author of the present thesis.

2.2.4. CONFOCAL MICROSCOPY

The detection of surface bound-HA fragments was carried out by immunofluorescence. Briefly, dried coverslips were immersed into PBS for 5 minutes. This was followed by incubation with primary antibody solution reacting with HA-tethered surfaces for 1 hour at room temperature. The primary antibody was HABP polyclonal sheep IgG (AbD Serotec, UK) diluted 1:100 in 1% goat serum in PBS, and the excess was removed by rising the coverslips with PBS. Then coverslips were immersed in a secondary antibody solution and incubated for 30 minutes at room temperature. Secondary antibody was donkey anti-sheep IgG-biotin conjugate (Sigma, UK) diluted 1:200 in 1% goat serum in PBS, and the excess was removed by rising the coverslips with PBS. Coverslips were then immersed in strepavidin-alexa fluor 555 conjugate diluted to 1 μg/ml in PBS, and incubated at room temperature in the dark for 20 minutes, followed by a rinse step in PBS. Coverslips were mounted in a slide using glycerol fixer (glycergel, DAKO, UK). For the control, the same protocol was followed except the incubation with the primary antibody. Slides were imaged using an Axioskop2plus LSM 510 confocal scanning fluorescence microscope (Zeiss, Germany).

2.2.5. QUARTZ CRYSTAL MICROBALANCE

Quartz crystal microbalance (QCM) is a technique for the assessment of a mass per unit area, by the measuring the change in frequency of a quartz crystal resonator, and thus giving the rate of deposition in thin film deposition. QCM experiments were carried out

using 10 MHz AT-cut quartz crystals (16 mm diameter, International Crystals Manufacturing co, Inc, USA) with gold electrodes (6 mm diameter) on both sides. Prior to the experiments the electrode surfaces were cleaned for 5 minutes using oxygen plasma at 40 W in a plasma chamber (Emitech, UK) and rinsed in absolute ethanol for 5 minutes. The electrodes were dried with nitrogen flux and immersed in a 5 mM 2-mercapto-ethylamine (Sigma, UK) solution in absolute ethanol overnight. This was followed by two washing steps with absolute ethanol and RO water for 5 minutes, and drying with nitrogen flux. HA attachment was performed as previously described for the preparation of HA films on glass coverslips. The frequency variations of the quartz crystals were monitored using a Techno Biochip frequency counter model Libra V3.0.

Theoretical backgrounds for using quartzes as mass sensors take origin in Sauerbrey equation (**Equation 2.1**), which takes into account the frequency shift due to mass deposition on quartz surfaces:

$$\Delta f = -2n{f_0}^2 \frac{\Delta m}{A\sqrt{\rho_q \mu_q}} \qquad \textbf{(Equation 2.1)}$$

Where Δf corresponds to the frequency shift, n is the overtone number, f_0 is the unloaded quartz frequency, A is the piezoelectric active area and Δm is the mass deposited/adsorpted. ρ_q and μ_q are respectively the density (2.648 g/cm^3) and shear modulus (2.947 10^{11} g/cm s^2) the density and and shear modulus of the quartz.

According to Sauerbrey equation, for a 10 MHz crystal, a Δf of 1 Hz corresponds to a Δm/A of 4.41ng/cm^2 (**Appendix XX**).

2.2.6. STATISTICAL ANALYSIS

Analysis of variance (ANOVA) was performed using Tukeys' multiple comparison test. A probability value of < 0.05 was considered statistically significant. Data are reported as mean ± 1 standard deviation (s.d.) of the mean.

2.3. RESULTS

2.3.1. CONSTRUCTION OF HA-COATED SURFACES

This section of work had deal with the establishment of a protocol to construct 2D HA-coated surfaces to support cell adhesion. For this purpose, an investigation of immobilising HA on glass surfaces was carried out.

The protocol for coating surfaces with HA can be divided into two parts: firstly, the aminosilylation of a glass coverslip and secondly, the covalent immobilisation of hyaluronic acid. The aminosilylation of a glass coverslip aims to attach a silane coupling agent to the glass, which in turn will allow the attachment of HA to the surface. The aminosilane used in this investigation was AHAPTMS (N-(6-aminohexyl)-aminopropyltrimethoxysilane). The formation of monolayers via the self assembly of silane compounds to activated surfaces is well known (Matinlinna *et al.*, 2004). For AHAPTMS ($C_{12}H_{30}N_2O_3Si$), this self-assembly occurs by a condensation reaction between the hydrolysed methoxylsilane and the activated surface's hydroxyl groups

(**Figure 2.5**). This resulting in AHAPTMS's terminal amino group being exposed at the surface and changing the surface functionality (Fowler, 2009).

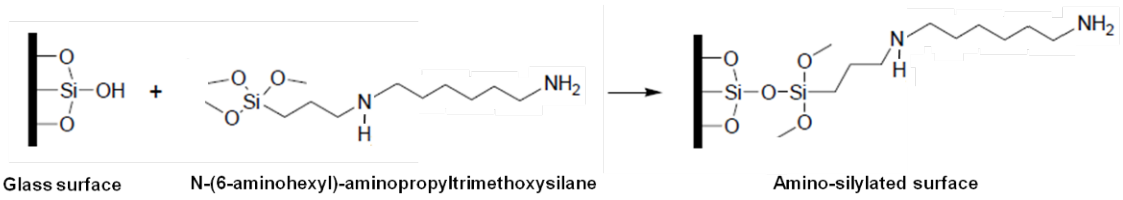

Figure 2.5 – Reaction of AHAPTMS with glass surface [Adapted from Thermo Fisher Scientific].

The amino functionality provided by the AHAPTMS monolayer allows the covalent binding of HA via an amino-carboxyl coupling (Matinlinna *et al.*, 2004; Fowler, 2009). Briefly, the conjugation of HA with AHAPTMS involves the formation of an amidic bond between the carboxylate groups of the polysaccharide and the primary amino of the silane (**Figure 2.6**; Pasqui *et al.*, 2007).

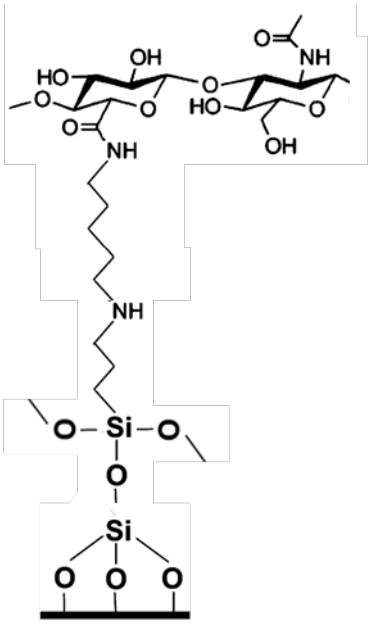

Figure 2.6 – Final product between the reaction of AHAPTMS with hyaluronic acid [Adapted from Pasqui *et al.*, 2007].

In this work carbodiimide-mediated crosslinking was the method of choice for crosslinking hyaluronic acid (**Figure 2.3**). Carbodiimide-mediated crosslinking is commonly used for reactions between carboxylic acids and amines. EDC is used as carbodiimide agent and the addition of NHS increases the efficiency of EDC-mediated coupling reactions and thus promoting a greater desired yield (Staros *et al.*, 1986; Schneider *et al.*, 2007; NHS instructions).

For the optimisation of this protocol, preliminary experiments were carried out. Regarding the sterilisation of the HA solutions, autoclaving and the use of a 0.2 µm filter syringe were compared. It was observed upon autoclaving that HA solutions lost their viscosity properties. Therefore, the sterilisation method relied on filtration. The incubation time, at which the hyaluronic acid reacts with the aminosilane surface, is dependent on the temperature at which this occurs. Several preliminary experiments were carried out in order optimise the tethering of HA molecules to aminosilane surfaces. Incubation was first carried out at 4ºC for 48h, then at room temperature (23ºC) for 12h, and later still reacting at room temperature but decreasing the time for 4h in case of HA_4, HA_{234} and HA_{mix} surfaces and 1h for HA_{2590} surfaces. This choice was based on the crosslinking properties of hyaluronic acid. It was observed that for HA_{2590}, and depending on the crosslinker concentration, this polymer starts to be crosslinked in less than 1h, quickly becoming gelatinous. The rest of polymers required longer incubation periods to get crosslinked. Preliminary experiments were also carried out in the presence and absence of crosslinker. From this results, it was observed that gelatinisation of HA was due the crosslinking, as in the absence of crosslinker gelatinisation did not occur.

Table 2.2 summarises the parameters optimised for the construction of HA-coated surfaces.

Table 2.2– Factors involved on the construction and optimisation of HA-coated surfaces.

HA solutions sterilisation	Reaction temperature	Reaction time	HA solution concentration	Crosslinker concentration		Volume of HA crosslinked solution
				EDC	NHS	
0.2 µm syringe filter	RT (23ºC)	1h (HA_{2590})	2 mg/ml	0.2 M	0.05 M	70 µl
		4h (HA_4, HA_{234} and HA_{mix})		0.4 M	0.10 M	
				0.6 M	0.15 M	

2.3.2. SURFACE CHARACTERISATION

2.3.2.a. Surface wettability

Changes in the surface wettability were assessed using static contact angle measurements at each stage of the HA immobilisation: from glass, through activated glass, aminosilane, and HA-coated coverslips. To verify the modification of the surface, three samples were used for each step, and contact angle was performed at several points on each surface (**Figure 2.7**; **Appendix II**). The contact angle measurement was taken by placing a drop of pure water onto each surface. The contact angle can be defined as the angle formed between the solid/liquid interface and the tangent at the liquid/vapour interface where the three phase boundaries intersect. This angle provides information about the relationship between the cohesive forces of the liquid and the adhesive forces

between the surface and the liquid. Therefore, a relationship can be directly related to the hydrophobicity of solid surface: when the angle tends towards 0º (the adhesive forces are greater than the cohesive forces) then the surface is hydrophilic and if the angle is greater than 90º the surface is hydrophobic.

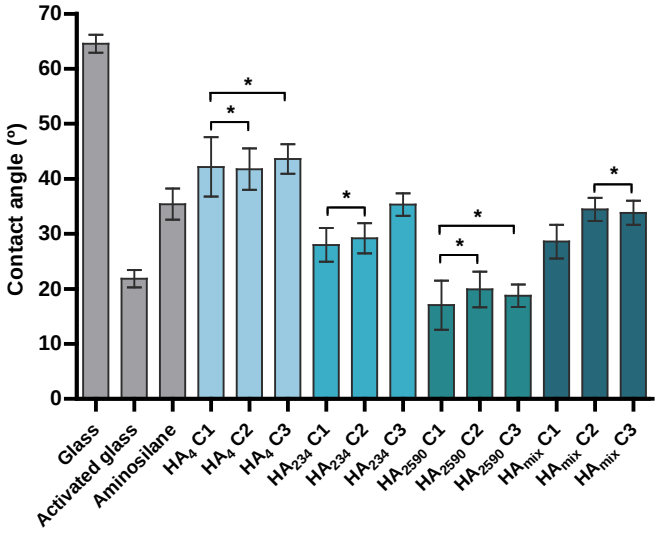

Figure 2.7 – Surfaces wettability measurements assessed by contact angle. Data are reported as means ± 1 s.d. Statistical comparisons were based on ANOVA analysis and Tukey's test for pairwise comparisons ($p<0.05$ was considered significant; n=3). The conditions linked by (*) are statistically similar.

The surface wettability of the glass coverslips was 64.78º, whereas the contact angle formed on the activated coverslips was 22.16º. The activated glass coverslips were treated with AHAPTMS, and the contact angle of the surface increased from 21.86º to 35.41º after silination (**Appendix II**). This means that the surface became less hydrophilic. The immobilisation of HA increased the hydrophilicity of the surfaces, except for the HA_4, which an increase of the wettability can be seen. HA_4-coated coverslips appeared to be the less hydrophilic comparatively to the rest of HA-coated surfaces. From HA_4 surfaces it can be seen that only C2 formed a contact angle significantly different from C3, the other surfaces being similar; with C2 being the most

hydrophilic surface of the HA_4 subset. The contact angle values for HA_{234} C1 and C2 were found to be significantly similar, with C3 being the less hydrophilic surface of this subset. HA_{2590}-coated coverslips were found to be the most hydrophilic subset of surfaces, with only C2 and C3 not having contact angle values significantly similar. The contact angle formed on HA_{mix} C2 and C3-coated coverslips was also found to be significantly similar. HA_{234} and HA_{mix}-coated surfaces were found to have similar contact angle values.

2.3.2.b. Surface topography

Surface topography was assessed by AFM demonstrating the presence of tethered aminosilane and HA molecules (**Figure 2.8**). The increase in roughness (Ra) of aminosilane-tethered surface (236.0 ± 32.86 pm) in comparison to untreated glass (56.0 ± 5.48 pm) confirmed the successful immobilisation of the aminosilane. There is a direct relationship between film stiffness and film roughness: as the crosslinker concentration increases, so does the film roughness. The roughness of the HA-coated surfaces showed an inverse correlation to molecular weight of HA fragments. In accordance, HA_{2590} appears smoother than HA_4 and HA_{234}. HA_{mix} presents the smoother surface overall (**Figure 2.8**).

From the comparison of each HA molecular weight subset it was found that C3-coated surfaces were significantly rougher than the correspondent C1 surface, with no topographical significant difference seen between C1 and C2, and C2 and C3 surfaces. The only exception was observed for HA_{mix} surfaces, were C3 was also found to be significantly rougher than C2 surface. Therefore, a greater increase in crosslinker

concentration can lead to significant difference in roughness, and hence topography changes. The MW was also found to significantly change the topography of the surfaces. Regarding C1 subset, was observed that HA_4 presents a significant increased roughness than HA_{2590} and HA_{mix}; with HA_{234} also presenting a rougher surface comparatively to HA_{mix}. The same results found for C1 were also observed for C2 surfaces subset. Regarding C3 surface subset, only HA_{2590}-coated surface was found to present a significantly different topography comparatively to the rest of the surfaces, presenting the smoothest surface (**Figure 2.8**, **Appendix XVIII**).

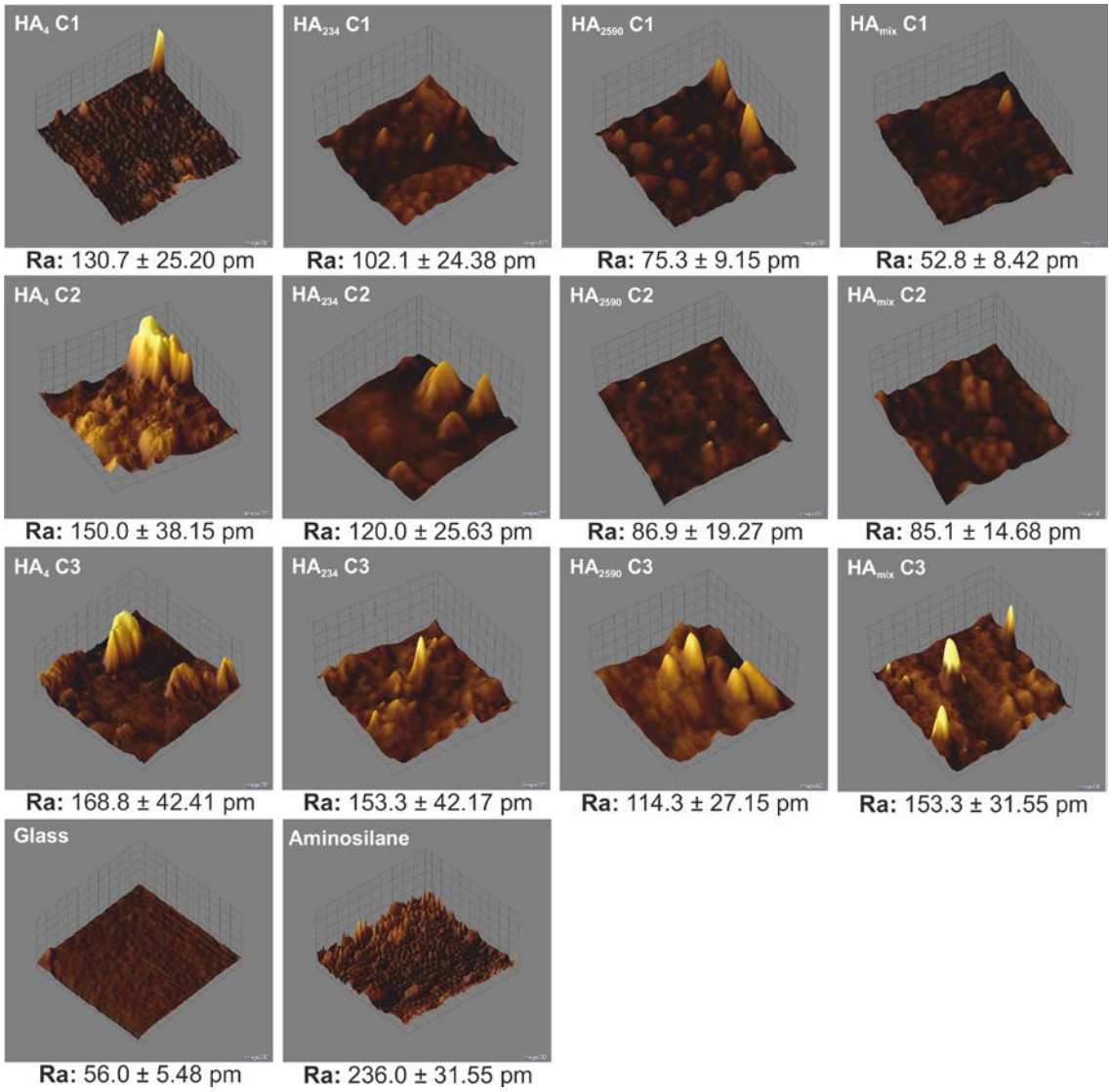

Figure 2.8 – AFM topographies of glass, aminosilane and HA-coated surfaces. Image range 1µm x 1µm x 15nm. Ra refers to roughness of the surface, representing the arithmetic average of the absolut values.

2.3.3.c. Surface homogeneity

The presence of HA tethered to amine-modified surfaces was confirmed by immunofluorescent using an anti-HA antibody and detected by fluorescence labelling with strepavidin-Alexa Fluor 555 bioconjugated. HA_4 C3 surface not treated with anti-

HA antibody was used as negative control, and did not exhibit non-specific binding (**Figure 2.9**).

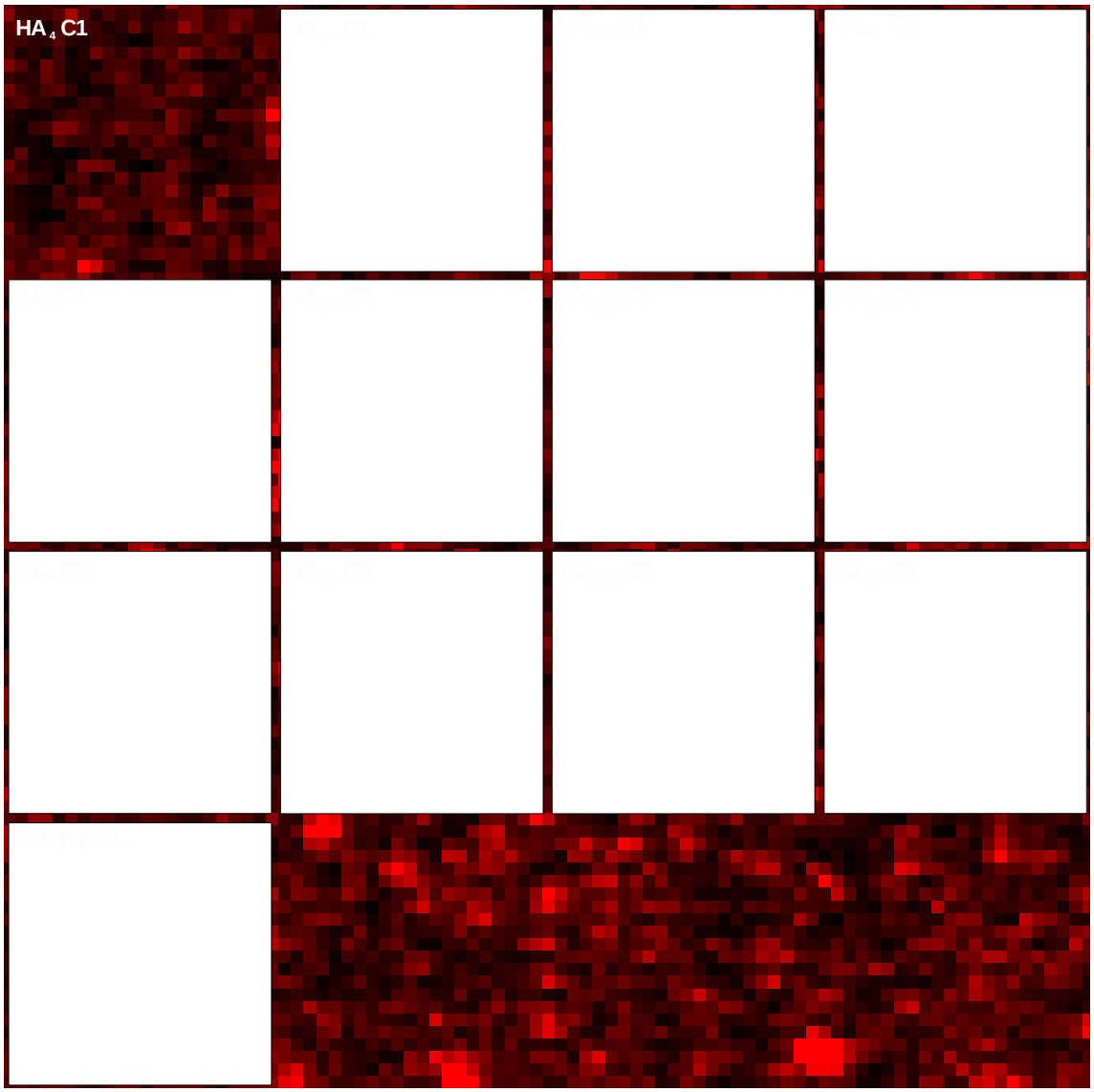

Figure 2.9 – Immunofluorescence (IF) detection of surface-immobilised HA, using anti-HA antibody, and confirmed by fluorescence labelling with strepavidin-Alexa Fluor 555 bioconjugated. For the control a HA_4 C3 surface was not treated with anti-HA antibody, and not exhibiting non-specific binding. Scale bar refers to 20 μm.

From the figure above it can be seen that there appears to be a direct relationship between the homogeneity of the surfaces and film stiffness. Surfaces coated with highly

crosslinked films (C3) appear to be the most homogeneous, showing fewer gaps between the polymer fragments. HA_{2590} and HA_{mix} surfaces appeared somewhat less homogeneous with some gaps between areas of intense fluorescence, while HA_4 and HA_{234} surfaces fluoresced more uniformly (**Figure 2.9**).

2.3.3.d. HA density

Figure 2.10 shows the frequency shift values for each HA-coated surface obtained from QCM measurements. These values were used to calculate the respective densities of HA and the total amount of HA in each surface (**Table 2.3**). QCM was not a valid method to estimate the densities of HA of C1 and C2-coated surfaces, as it was not possible to obtain the respective frequency shifts.

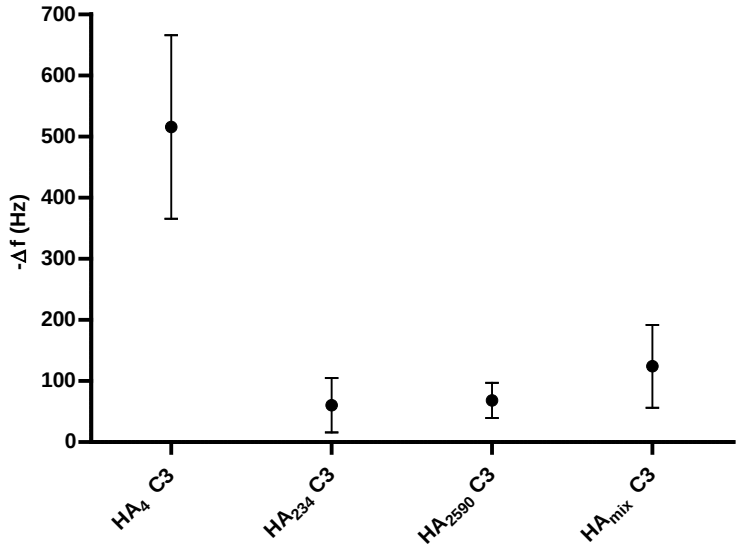

Figure 2.10 – QCM frequency shift vs HA-coated surface. Data are reported as means ± 1 s.d (n=3).

QCM showed that HA_4 C3 surface presents a considerably higher polymer density than the rest of the surfaces. HA_{234} C3 and HA_{2590} C3 present similar densities,

with a small amount of HA being tethered onto these surfaces. HA_{mix} C3 surface presents a relatively small increase of tethered polymer in comparison to HA_{234} and HA_{2590} surfaces (**Table 2.3**).

Table 2.3– HA densities and total amount of HA per surface.

Surface	Density of HA (μg/cm^2)	Total amount of HA per surface (μg)
HA_4 C3	2.27	6.45
HA_{234} C3	0.27	0.75
HA_{2590} C3	0.30	0.85
HA_{mix} C3	0.55	1.55

2.4. DISCUSSION

The main goal of this chapter was the construction of 2D hyaluronic acid structured surfaces designed to support cell adhesion. Therefore, in the present chapter it is presented the experimental design and optimisation of a protocol to construct HA-coated surfaces. Four surfaces were constructed, coated with different sized-polymers and over a range of different crosslinker concentrations. After the characterisation of the surfaces, the best subset was chosen in order to support cell adhesion and to be used in *in vitro* studies.

2.4.1. CONSTRUCTION OF HA-COATED SURFACES

The development of self-assembled monolayers (SAMs) methods presents a major advance in materials fabrication technology. SAMs provide well defined structures and chemistries, being used to immobilise biomolecules to the surfaces required for well-defined biological experiments (Castner and Ratner, 2002).

Here it was presented a simple method to create HA films that are well-defined in their molecular attachment to the substrate (glass coverslip). The confinement to a solid support made these coats accessible to characterisation with a range of techniques that are not easily applicable to living cells. Therefore, the first decision to be made was the choice of a surface that could be both coated with hyaluronic acid, and easily adapted for cell culture vessels, making it suitable for analysis. A number of different materials, including glass, quartz, metal oxide and polymers have been modified with biomolecules and characterised for cellular interaction with their surfaces (Shin *et al.*, 2003). The choice of round glass coverslips was made on the basis of their ability to be placed on cell growth plates and removed from plates for analysis, in addition to their low cost when compared to other materials. A suitable protocol for the hyaluronic acid tethering to glass coverslips was the second decision to be made. The protocol for coating surfaces with HA can be divided in two parts: firstly, the aminosilylation of a glass surface, and secondly the covalent immobilisation of hyaluronic acid. The aminosilylation of a glass surface aims to attach a silane coupling agent to the glass, which in turn will allow the attachment of HA to the surface. As mentioned previously, the formation of monolayers via the self assembly of silane compounds to activated

surfaces has already been well established (Matinlinna *et al.*, 2004). Silane coupling agents are often used as they can provide organic functionality to inorganic compounds (Matinlinna *et al.*, 2004). The aminosilane used in the present investigation was AHAPTMS (N-(6-aminohexyl)-aminopropyltrimethoxysilane). This choice was based on work performed by Ladam and co-workers (2003) and due the hydrolytic stability of AHAPTMS shown elsewhere (Ladam *et al.*, 2003; Matinlinna *et al.*, 2004).

Soluble HA has some characteristics that limit its use in many biomedical applications; these include poor mechanical properties and rapid degradation in an aqueous environment. These limiting characteristics can be overcome by crosslinking HA (Segura *et al.*, 2005; Collins and Birkinshaw, 2007). Crosslinking individual HA polymer chains together decreases their degradation rates (Leach and Schimidt, 2004). Crosslinking is the most common modification of HA to form a hydrogel (Leach and Schimidt, 2004; Collins and Birkinshaw, 2008). There are many strategies employed to crosslink HA, a process where the chemical modification of one or more of HA's available reactive groups (hydroxyl, carboxyl, and acetamido) is performed while attempting to maintain biocompatibility and biological activity: diepoxy crosslinking, carbodiimide-mediated crosslinking, aldehyde crosslinking, divinyl sulfone crosslinking, photocrosslinking (Leach and Schimidt, 2004). However, carbodiimide-mediated crosslinking was the method of choice. This choice relied on the literature, where carbodiimide-mediated crosslinking is often utilised in reactions between carboxylic acids and amines. In addition, since EDC is a zero length crosslinker, it does not introduce additional molecules that may be toxic in *in vitro* and *in vivo* applications (Richert *et al.*, 2004).

The optimisation of the second part of this protocol (the covalent immobilisation of hyaluronic acid to aminosilane coverslips) was not straightforward. Several issues had to be dealt with. First was the sterilisation of HA solutions, concerning the necessity of producing pathogen-free surfaces. The easiest way would be the exposition of the HA-coated coverslips to UV irradiation. However, large HA fragments are broken into smaller fragments when exposed to UV radiation (Trommer *et al.*, 2003). Consequently, an investigation of the use of filtration and autoclaving methods was carried out. As the HA molecular-weight increases, so does the polymer viscosity. In a work performed by Ito and co-workers (2004), HA solutions have been autoclaved at 128ºC for 20 minutes; however, in this study loss of viscoelastic properties was observed when autoclaving HA solutions at 121ºC for 20 minutes (Ito *et al.*, 2004). Therefore, filtered HA solutions using a 0.2 μm syringe filter as described by others (Baier, 2003) was the method of choice.

Since it has been described that HA concentrations can influence cell behaviour (Liu *et al.*, 2004), the choice of the HA solution concentration was another important factor to consider. Depending on the application, different concentrations have been used, ranging 1–4 mg/ml. The choice of 2 mg/ml was made on the basis of the expensive price of HA polymer. One mg/ml was not the chosen concentration, since this concentration is typically used in applications where multilayered films are constructed (Picart *et al.*, 2001; Etienne *et al.*, 2004; Richert *et al.*, 2004; Schneider *et al.*, 2006).

The incubation conditions for the immobilisation of HA with the aminosilane surfaces were crucial in the optimisation of this protocol, especially regarding time and temperature. In different studies, different conditions have been used. Incubations are reported to be performed either at 25ºC, room temperature or 4ºC; for 2h, 4h, 16h, 12h

or 120h, under normal atmosphere, vacuum, or humid conditions (Picart *et al.*, 2001; Etienne *et al.*, 2004; Richert *et al.*, 2003; Schneider *et al.*, 2006; Landam *et al.*, 2003; Collins and Birkinshaw, 2006; Morra *et al.*, 2006 Ibrahim *et al.*, 2007). In the present study, pre-experiments have been carried out in order to optimise the reaction time and temperature. Incubation was first carried out at 4ºC for 48h, then at room temperature (23ºC) for 12h, and later still at room temperature; but decreasing the time to 4h in case of HA_4, HA_{234} and HA_{mix} surfaces, and 1h for HA_{2590} surfaces. These different times relied on the differences on crosslinking times, since for HA_{2590} it was observed that this polymer becomes crosslinked more rapidly than the rest. Thus, in the present work it was deduced that there was no need to incubate for as a long period as in other studies.

Other considered factors were the volume drop in each aminosilane-tethered surface and how to make a homogenised HA film. First 200 µl of each HA solution was drop on each coverslip, and later on this volume was reduced to 120 µl. Nevertheless, the problem of achieving a homogenised HA still persisted. Therefore, to create a thin and flat film, a square glass coverslip was used to make an assembly of coverslips, allowing for the construction of a much more homogenised surface and requiring the use of less HA solution. Seventy µl of solution was fixed as final volume.

2.4.2. CROSSLINKING AND HA-POLYMER MOLECULAR WEIGHT INFLUENCE THE CONSTRUCTION OF THE SURFACES

Changes in surface wettability were assessed using static contact angle measurements at each stage of the HA immobilisation: from glass, through activated

glass, aminosilane, and HA-coated coverslips. The increase in the wettability seen from glass to activated glass coverslips can be attributed to the hydration of the surfaces. An increase in the contact angle was observed after the treatment of activated glass coverslips with AHAPTMS, meaning that the surface becomes less hydrophilic. The immobilisation of HA was found to increase the hydrophilicity of the surface, except for HA_4. This increase is probably due to the hydrophilic nature of hyaluronic acid. The decrease in wettability of HA_4 surfaces may be related with the size of HA, as smaller fragments can lead to a more closely-packed structure, and consequently reducing water-surface interactions and the exposure of hydrophilic groups at the interface (Pasqui *et al.*, 2007). The great wettability seen for HA_{2590} surfaces might be related to the highly hydrophilic properties presented by HA. In the presence of water, HA molecules can expand in volume up to 1000 times to form hydrated matrices (Leach and Schmidt, 2004). Thus, as larger fragments can absorb more water, the presence of HA_{2590} molecules presented a more hydrophilic surface. Interestingly, HA_{234} and HA_{mix}-coated surfaces were found to have similar contact angle values. Therefore, the contact angle value obtained for surfaces coated with different MW polymers in an equal ratio (HA_{mix}), were found to be intermediate between HA_4 and HA_{2590} films.

There is some evidence that the surface hydrophilicity/hydrophobicity can be important for cell adhesion and growth. Depending on the cell line, cellular growth can be improved by increasing the hydrophilicity of the surfaces, whereas the optimal rates were obtained using an intermediate degree of hydrophilicity. Nevertheless, cell growth on highly hydrophobic surfaces has also been stated (Larsson and Ocklind, 2000). Since it is still unclear how the chemistry of material surfaces affects cell adhesion, spreading and growth, conclusions cannot be made regarding the relationship between the

obtained contact angle measurements and the adhesion and proliferation of the cell lines used in the present work (see **Chapter 3**). The use of wettability measurements relied on the simplicity and fast method to estimate the quality of monolayers. In addition, contact angle is an inexpensively technique. The use of contact angle gave information regarding the modifications occurred on the coverslips along the protocol.

Analysis of the HA surfaces by AFM and confocal microscopy indicate that film stiffness modulates the topography and construction of the surfaces. Highly crosslinked films present the most homogenous and rough surfaces. Ren and co-workers (2007) also observed these findings, showing that film roughness increases as a function of film stiffness (Ren *et al.*, 2007). In addition, the construction of the surfaces is also influenced by the HA polymer-size. The roughness of the HA-coated surfaces showed an inverse correlation to molecular weight of HA fragments, which was also observed by Ibrahim and co-workers (2007). All of these AFM observations were supported by confocal microscopy analysis. It was found that there is a direct relationship between the homogeneity of the surfaces and film stiffness. Surfaces coated with highly crosslinked films (C3) appeared to be the most homogeneous, showing fewer gaps between the polymer molecules. Also, homogeneity was found to be related with polymer size. HA_{2590} and HA_{mix} surfaces appeared somewhat less homogeneous with some gaps between areas of intense fluorescence, while HA_4 and HA_{253} surfaces fluoresced more uniformly. A possible explanation lies in the fact that the strands of larger HA fragments cause substantial strand entanglement producing a compact zone of HA close to the aminated surface, and creating sporadic gaps devoid of HA. On the other hand, this can also be related with the fact that the strands of larger HA fragments might prevent other strands from binding to aminosilane molecules in the local vicinity

by directly binding to them or sterically inhibiting their interaction with other strands, therefore this resulting in a less efficient binding of HA to aminosilane-tethered surface (Ibrahim *et al.*, 2007). Ibrahim and co-workers (2007), while performing a study where a range of different HA fragments (1000, 200, 20 kDa and 4 HA oligomers) was immobilised onto aminosilane-coated surfaces using carbodiimide reaction, also observed that HA_{1000} and HA_{200} surfaces appeared less homogeneous and formed greater gaps between HA coatings (Ibrahim *et al.*, 2007).

QCM showed that HA_4 C3 surface presents a higher polymer density than the rest of the surfaces. HA_{253} and HA_{2590} present similar densities, where a small amount of HA is tethered onto these surfaces. HA_{mix} presents a few increase of polymer amount, comparatively to HA_{253} and HA_{2590} surfaces. Similar findings were found by by Richter and co-workers (2007), reporting that HA-film density increases strongly as molecular weight decreases (Richter *et al.*, 2007). However, QCM was not a valid and sensitive method for estimating the density of HA on C1 and C2-coated surfaces. This might be related with the small amount of HA present in the quartz. In addition, it can also be related with the viscosity and flexibility of the films, and being not stiff enough to vibrate along with the quartz, and therefore not possible to be analysed by QCM (Chianella, 2010).

2.5. CONCLUSIONS

This chapter describes the attempts made in order to immobilise hyaluronic acid on 2D glass surfaces, in a wide range of HA fragment sizes and crosslinker

concentrations. A protocol to construct homogeneous HA-coated surfaces was successfully developed. In this protocol HA is tethered onto aminosilane (AHAPTMS)-treated glass surfaces using a carbodiimide reaction (EDC and NHS). Four surfaces were constructed, coated with polymers of different molecular weights (HA_4, HA_{253}, HA_{2590} and HA_{mix}). In addition, three different crosslinker concentrations were investigated. After a characterisation of these surfaces using contact angle, AFM and confocal microscopy it was concluded that the most homogeneous surfaces were those coated with films of higher stiffness (C3 crosslinker concentration). Therefore, C3 surfaces were chosen to be used in *in vitro* experiments. The construction and characterisation of these surfaces represented a crucial step in the overall project. These surfaces were used as cell growth support, and were used in the evaluation of the effect that exogenous HA has on cell proliferation (**Chapter 3**).

To the present knowledge, this represents the first study where surfaces coated with HA polymers of varying molecular weights have been constructed over a range of film stiffness.

CHAPTER 3

“Essentially, all models are wrong, but some are useful.” – George E. P. Box

CHAPTER 3

3. STUDY OF THE GROWTH AND PROLIFERATION OF TUMOUR-DERIVED CELL LINES ON A RANGE OF HA STRUCTURED SURFACES

3.1. INTRODUCTION

The extracellular matrix (ECM), although once regarded simply as structural scaffold, is now recognised as an important modulator of cell phenotype and function, and the glycosaminoglycan hyaluronic acid (HA) one of the chief components. Although the major biological function of HA remains unclear, many roles have been attributed to this polymer. HA is present predominantly in the ECM, particularly in embryonic and malignant tissues (Stern, 2003). It has been shown to be involved in various physiological processes, including embryological development, proliferation, differentiation, migration and adhesion of cells (Manzel and Farr, 1988; Heldin, 2003; Spicer and Tien, 2004; Adamia et al., 2005a; Girish and Kemparaju, 2007). It has been reported that the production of HA is high during cell proliferation, since this polymer is involved in the promotion of chromatin condensation, and therefore facilitating mitosis. On the other hand, HA may help cells to detach from the matrix making it easier for them to divide. HA levels also increase during the differentiation and in the areas where cell migration begins (Adamia *et al.*, 2005a). It also plays important roles in multi-drug resistance (Toole, 2004), wound healing (Chen and Abatangelo, 1999), angiogenesis

and malignant transformation (Adamia *et al.*, 2005a; Shultz *et al.*, 2005; Pavia *et al.*, 2005; Girish and Kemparaju, 2007).

It is well reported that the biological functions exhibited by HA depend on the chain length, molecular mass and on the conditions under which the polysaccharide is synthesized (Noble, 2002; Toole, 2004; Girish and Kemparaju, 2007). Polymers coming from the HA fragmentation in the course of the catabolic pathway occur in a variety of sizes that have a vast range of properties; with high and low molecular weight HA polymers playing opposite roles on cell behaviour (Girish and Kemparaju, 2007). High-molecular-size HA polymers are reported to inhibit endothelial cell growth and being anti-angiogenic (Chen and Abatangelo, 1999; Stern *et al.*, 2006); showing anti-inflammatory and immunosuppressive properties (McBride and Bard, 1979; Delmage *et al.*, 1986; Day and de la Motte, 2005; Milner *et al.*, 2006). In addition, these large fragments are also involved in the promotion of cell quiescence and protection of cells against apoptosis and injury, and support of tissue integrity (Morrison *et al.*, 2001; Jiang *et al.*, 2005). Conversely to high-molecular-size HA molecules, small polymers have angiogenic, wound healing, inflammatory and immunostimulatory properties (Noble, 2002; Termeer *et al.*, 2002; Rossler and Hinghofer-Szalkay, 2002; Stern, 2003).

The main goal of this chapter was to investigate whether surfaces constructed with HA polymers of different molecular weight can influence the growth and proliferation of tumour-derived cell lines. The development and maintenance of multicellular biological systems depends on a sophisticated interplay between cell proliferation and physiological cell death, in order to maintain homeostasis in terms of constant cell numbers (Gewies, 2003). Therefore, this chapter of work also aimed to investigate whether HA has as effect on apoptosis of tumour-derived cell lines.

Quantitation in cell culture is required for the characterisation of the growth properties of different cell lines for experimental analyses (Freshney, 2005). Knowledge of the growth state of a culture and its kinetic parameters is critical in the design of cell culture experiments, with measurements of kinetic parameters often used to determine the response of cells to a particular stimulus or toxin. This work is focused upon human bladder and prostate cell lines, using two cell lines of each tissue type. The use of two cell lines of each tissue type may provide insights into the variability of expression within tumours of differing stage and grade. The first part of this chapter presents cell proliferation assays using cells growing under normal conditions (i.e., cells growing on uncoated wells) in order to compare cell lines and establish the optimal conditions to be used in tissue culture. The comparison of cells growing under normal conditions with cells growing in the presence of HA made possible the assessment of the effect that HA has on cell proliferation and apoptosis. Therefore, this chapter can be divided in three different parts: firstly the establishment of the optimal conditions to be used in the culture of the cell lines, secondly the assessment of the effect that HA has on cellular proliferation, and in the last part the assessment of the effect that HA has on apoptosis. The work presented in this chapter can be illustrated by **Figure 3.1**, summarising all the stages involved in this investigation.

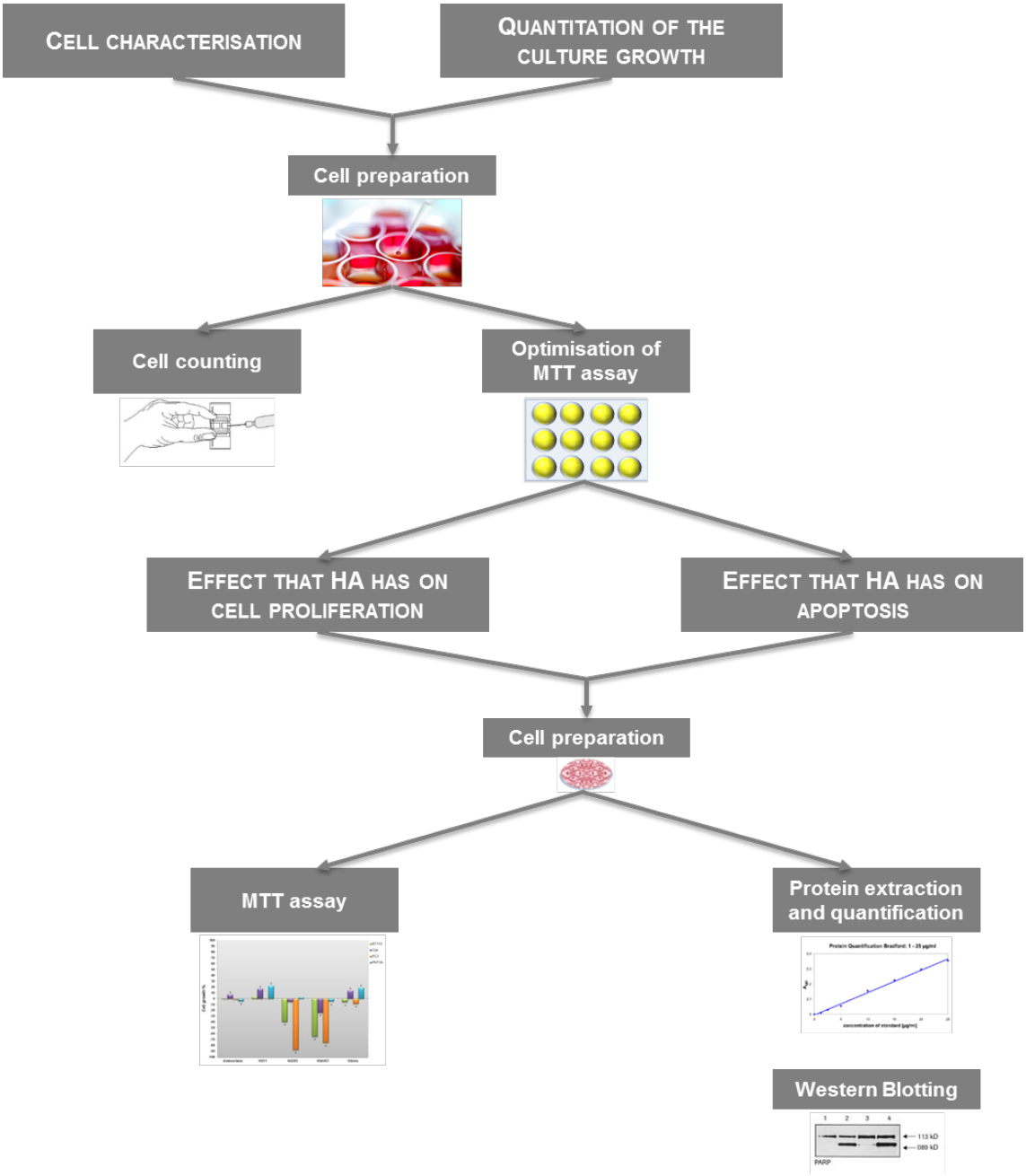

Figure 3.1 – Summary of all the stages of work involved in Chapter 3.

3.2. MATERIAL AND METHODS

3.2.1. CELL CULTURE

3.2.1.a. Cell lines and cell culture

Four cell lines were used as model systems for CD44 and RHAMM expression, all human in origin. The bladder cell lines were RT112/84 (derived from a human bladder carcinoma with epithelial morphology – ECACC: 85061106) and T24/83 (derived from a human bladder carcinoma with epithelial morphology from an 81 year old Caucasian female – ECACC: 85061107, also known by the names EJ138 and MGH-U1). The prostate cell lines were PC3 (derived from a human prostate adenocarcinoma grade IV from a 62 years old Caucasian male – ECACC: 90112714) and PNT1A (derived from a human post pubertal prostate normal, from a 35 years old male at post mortem, immortalised with SV40 – ECACC: 95012614).

All cells were grown from seed culture stored under liquid nitrogen and cultured in Dulbeccos modified eagles medium (DMEM) containing HAM's F12 (1:1) 1x nutrient mix plus 15 mM HEPES & L-glutamine medium (GIBCO, Invitrogen, UK). The media was supplemented with 10% heat inactivated foetal calf serum (FCS; GIBCO, Invitrogen, UK), 200 mM L-glutamine (Invitrogen, UK), 1000 units of penicillin and 1 mg streptomycin (GIBCO, Invitrogen, UK) per bottle. Cultures were grown at 37ºC in a 5% CO_2 atmosphere and were maintained by passage when they had grown to 80-90%.

3.2.1.b. Cell passage and maintenance

Once all four lines were adhered, passaging required the use of trypsin/EDTA to detach the cells from the surface of the culture flasks. Cultures were first washed in 10 ml of sterile PBS followed by the addition of 5 ml of 1x 0.5% trypsin/EDTA solution (GIBCO, Invitrogen, UK) to each flask. This was incubated at 37ºC for approximately one minute, or until detachment could be detected, upon which the cells were removed from the flask and placed into a centrifuge tube containing 5 ml of media to inactivate the trypsin. This was then centrifuged at 1,300 g at 4ºC for 5 minutes. The supernatant was discarded and the cells resuspended in DMEM and subcultured into each fresh flask.

3.2.1.c. Cell Storage

Cell lines were frozen for long term storage. When cell monolayers reached approximately 90% confluence, cells were detached as described in section 2.2.1.c. The trypsin/EDTA solution was neutralised in full media and the suspension was then centrifuged at 1,300 g for 5 minutes at 4ºC. The supernatant was removed and the cell pellet was resuspended in freezing medium (10% DMSO in FCS). DMSO prevents the formation of intracellular ice crystals during the freezing process and consequently aids in maintaining cellular integrity. The cell and freezing medium suspension was aliquoted into 1.5ml cryovials (Greiner Bio-one, Frickenhausen, Germany). The cryovials were placed in a cryofreeze container (Nalgene, Milton Keynes, UK)

containing propan-2-ol and then stored at -80°C. After at least 24 hours at -80°C, the cryovials were transferred to liquid nitrogen dewars, at -196°C, for long term storage.

3.2.1.d. Cell Thawing

To revive cells after storage in liquid nitrogen, it is essential to thaw the cells rapidly. The cryovial was warmed to 37°C and the cell suspension was resuspended in 10 ml warmed culture media. The suspension was centrifuged at 1,300 g for 5 minutes at 4ºC and the supernatant containing the DMSO was removed. The pellet was resuspended in full culture media and transferred to a culture flask, which was then placed in the incubator so the cells could adhere.

3.2.2. CELL PROLIFERATION ASSAYS

To seed the wells with a required number of cells, a T75 flask was treated as if for passage. Cells were centrifuged at 307 g at 4ºC for 5 minutes. The supernatant was discarded and the cell pellet resuspended in 1 ml of media before the cells were counted using a haemocytometer (Neubauer Assistant, Germany). The number of cells in the 1 ml suspension was then calculated before being diluted to a desired concentration and seeded into 12-well plates to give a final volume of 2 ml/well. The 12-well plates were incubated at 37ºC with 5% CO_2.

3.2.2.a. Cell counting

Permeability assays involve staining damaged cells with a dye and counting viable cells that exclude the dye. Counts can be performed manually using a haemocytometer, and this method is normally used to determine the cell density (cell number/ml) in batch cell cultures.

For each cell line, eight 12-well polystyrene plates were prepared, and cells were seeded with a final concentration of 5 x 10^4 cells/ml. This assay was performed over eight days, and every 24 hours cell counting was performed as described: media was removed from wells, followed by washing with 1 ml PBS. Then 500 µl of 1x 0.5% trypsin/EDTA solution was added and the cells were incubated for 1-2 minutes. Cells were detached from the bottom of the well using a cell scraper, and the cell solution was placed into a microcentrifuge tube and centrifuged at 1,300 g at 4ºC for 5 minutes. The supernatant was discarded and the cells resuspended in 1 ml of PBS. 50 µl of the cell suspension was mixed with 50 µl of trypan blue (Sigma-Aldrich, UK). Cell counting was assessed using 20 µl of the cells/PBS/trypan blue placed onto a haemocytometer. The number of cells was then counted using an x10 objective lens (Nikon microscope). The average number of cells from three replicates was calculated and plotted against the number of days the cells had been allowed to grow, for the construction of a growth curve.

3.2.2.b. MTT assay

Metabolic assays measure the mitochondrial activity, relying on the basis that cellular damage will inevitably result in loss of the ability of the cell to maintain and provide energy for metabolic cell function and growth. MTT cell proliferation assay is one of these metabolic assays. It is a quantitative colourimetric assay, which has been used to study the mammalian cell survival and proliferation. On the basis of MTT assay there is the assessment of mitochondrial activity through the measure of succinate dehydrogenase enzymatic activity of metabolically active cells. These enzymes reduce the yellow tetrazolium MTT salt (3-(4,5-dimethylthiazolyl-2)-2,5-diphenyltetrazolium bromide) to a purple formazan product. This resulting intracellular insoluble formazan product is then dissolved and the colour produced quantified spectrophotometrically. MTT assay detects living, but not dead cells and the signal generated is dependent on the degree of activation of the cells (Mosmann, 1983; Davey and Lord, 2002).

For each cell line, eight 12-well polystyrene plates were prepared. Four different cell densities were used: $5x10^4$, $2.5x10^4$, $1.25x10^4$ and $6.25x10^3$ cells/well. Three replicates were used for each cell density. Plates were incubated at 37ºC with 5% CO_2. One thousand and five hundred ml of the supernatant from each well were removed and 650 µl of MTT solution pipetted into each well. MTT solution was prepared as described: 1mg MTT powder (Sigma-Aldrich, UK) was dissolved in 1ml of PBS, and filtered with a 0.45 µm syringe filter (NALGENE Labware, Thermo Fisher Scientific, UK). The plate was incubated at room temperature for three hours in the dark and 1340 µl of acidified isopropanol (100 µl concentrated HCl in 100 ml isopropanol) were added to each well and vigorously mixed to solubilise the formazan salts. This procedure was

performed over eight days, and the absorbance of each well was then read in a plate reader (Varioskan Flash, Thermo Fisher Scientific) at $\lambda = 570$ nm each 24 hours.

3.2.2.c. Assessment of the effect that HA has on cell proliferation

In order to assess the effect that HA has on cellular proliferation, MTT assay was performed on cells cultured on HA and aminosilane-coated surfaces. Briefly, cells were trypsinized, pelleted by centrifugation at 4ºC (1,300 g, 5 minutes) and resuspended in DMEM. Two ml of cell suspension were cultured on surfaces previously placed onto 12-well plates. Cultures were grown at 37ºC in a 5% CO_2 atmosphere over 8 days. MTT assay was performed in three wells per film condition, and cells growing on tissue culture polystyrene wells were used as control.

3.2.3. CALCULATION OF KINETIC GROWTH PARAMETERS

The understanding of the growth state of a culture and its kinetic parameters are critical factors in the design of cell culture experiments. Thus, using the data collected from the curve fitting, kinetic parameters were calculated.

The log phase is a period of exponential increasing in cell number, which can be represented by **Equation 3.1**:

$$N = N_0 \times 2^X \quad \textbf{(Equation 3.1)}$$

where N_0 = initial cell concentration of the log phase; N = final cell concentration of the log phase; X = number of generations of cell growth. The generation time (X) refers to the average time it takes between two cell divisions.

The population doubling time (D) during cell growth, which is the time taken for the culture to increase two-fold in the middle of the exponential phase, can be calculated using **Equation 3.2**:

$$D = \frac{T}{X} \quad \textbf{(Equation 3.2)}$$

where T = total elapsed time of the log phase.

The specific growth rate (μ), which is the measure of the rate of increase of cell number at certain cell concentration, can be calculated from **Equation 3.3**:

$$\mu = \frac{logN - logN_0}{T_1 - t_1} \quad \textbf{(Equation 3.3)}$$

Where t_1 = initial time of the log phase and T_1 = final time of the log phase.

The growing percentage can be achieved by **Equation 3.4**:

$$Growing\ \% = \frac{Final\ nº\ of\ cells}{Nº\ of\ seeded\ cells} \times 100 \quad \textbf{(Equation 3.4)}$$

3.2.4. APOPTOSIS ASSAY

Apoptosis was assessed by Poly-ADP-Ribose-Polymerase (PARP) cleavage. Detection of the 89 kD PARP fragment with anti-PARP serves as an early marker of apoptosis. Western blotting was carried out in order to detect cleaved PARP. β-actin antibody was used as positive control, to ensure integrity of protein. Protein extract from OE21 (Caucasian oesophageal squamous cell carcinoma) cells 10 Gy irradiated (kind gift from Joana Senra, Manchester University) was also used as positive control.

3.2.4.a. Protein extraction and quantification

Two ml of cell suspension were cultured onto surfaces previously placed on 12-well plates and seeded to the same concentrations as optimised for MTT assay (section **3.2.2**). Protein extraction was performed after 8 days of cell growth, into 12 wells per film condition, and cells growing on tissue culture polystyrene wells were used as control. Culture media was removed and cells were washed in PBS. This was followed by the addition of protease inhibitor cocktail produced (MP Biomedicals, UK; **Appendix I**) and scraping of cells off the surface of wells. Once all cells were removed from 12 wells, the solution was transferred into a 15 ml centrifuge tube and cells pelleted by centrifugation at 554 g for 10 minutes at room temperature. The supernatant was discarded and the pellet resuspended in 1.5 ml of protease inhibitor cocktail. Cell suspension was transferred to an Eppendorf tube and centrifuged at 12073 g for 15 minutes at room temperature. The supernatant was discarded and the pellet resuspended in 1.5 ml of CHAPS lysis buffer (**Appendix I**) and snap frozen. This was then thawed

and incubated on ice for 1 hour and centrifuged at 12,073 g for 30 minutes. The resulting supernatant is the cellular protein extract and after quantification was stored at -80ºC.

Protein quantification was carried out in a 96-well plate using the Micro-BCA protein assay (Pierce, Thermo Scientific, UK) according to manufacturer's guidelines. One hundred and fifty µl of Micro BCA Working Reagent were added to 150 µl of each sample and the plate thoroughly mixed on a plate shaker for 30 seconds. This was incubated at 37ºC for 2 hours and the absorbance of each sample was read in a plate reader (Varioskan Flash, Thermo Fisher Scientific) at λ = 562 nm. For the protein quantification, a standard curve was constructed using a BSA protein standard (100 µg/ml; Pierce, Thermo Scientific, UK; **Appendix XVII**).

3.2.4.b. Western Blotting

Preparation of Samples for Electrophoresis

After protein concentrations were determined, the volume of sample needed to give the 10 µg of protein was calculated and transferred to an Eppendorf tube. An equal volume of 2x sample buffer was added and the samples were then boiled at 100°C for 5 minutes to ensure denaturation of the proteins. Samples were briefly centrifuged then kept on ice to prevent protein clumping.

SDS-PAGE (Poly-Acrylamide Gel Electrophoresis)

Denatured protein samples were separated on discontinuous polyacrylamide gels on the basis of size. 10% resolving gels, determined by the concentration of acrylamide (BioRad, UK), were used to separate and isolate the proteins in question. A Mini-Protean II Cell (BioRad, UK) gel electrophoresis equipment was assembled according to manufacturer's instructions. The resolving gel was loaded between the glass plates and distilled water was immediately loaded afterwards to prevent oxidation at the gel surface, as well as to aid in reducing bubble formation and to ensure an even surface while solidifying. Excess water was blotted away using filter paper once the gel had set and the stacking gel was then poured. Well-forming combs were quickly yet carefully inserted between the glass plates to form loading wells in the stacking gel.

When solidified, the gels were fitted onto the tank equipment to form the central chamber and 1x running buffer was poured into the tank to completely immerse the gels. The well-forming combs were removed and the wells were washed by pipetting running buffer into them. A molecular weight protein marker (BioRad Kaleidoscope Pre-stained Standards Cat. No. 161-0324 range 6-197 kDa) was loaded in the gel as well. The anode and cathode of the Mini-Protean II Cell were connected to a power supply and set at 150 volts. The electrophoresis was carried out at 150 V for approximately 10 minutes until the samples had stacked and passed through to the resolving gel. At this time the voltage was reduced to 100 V for approximately 1 hour.

Immunoblotting Procedure

To transfer the separated proteins to polyvinylidene fluoride (PVDF) membrane (Millipore, Hertfordshire, UK) for antibody detection, a wet protein transfer method was employed. The PVDF membrane was cut to the appropriate size, the top left hand corner was cut off and the membrane was activated in 100% methanol for 1 minute until it became translucent and ready to accept proteins. Cold 1x transfer buffer was used to wet sponge pads, 3mm filter paper (Whatman Plc, Brentford, UK) and the activated membrane. The electrophoresis equipment was dismantled and the gel was removed. The stacking gel was cut away and the top left hand corner of the gel was cut off to align with the membrane and aid in orientation.

The cassette containing the sandwich of sponge pads, filter paper, gel and membrane was placed into the transfer tank containing 1x transfer buffer. An ice block was also inserted and the tank was then placed on ice. This was to ensure a cool environment lasted for the entire transfer process to prevent protein denaturation from electrical heat generated. Electrode connections were attached to the power supply and the proteins transferred overnight at 30 volts.

Probing the Membrane

To ensure successful transfer of the proteins, once the membrane was removed from the transfer cassette it was washed in Ponceau S solution. Ponceau S reversibly binds to proteins present on the membrane and allows quick visualisation of any protein bands present. The membrane was washed in PBS supplemented with 0.1% (v/v)

Tween-20 (PBST), on a rotating gyrorocker mixer (Stuart Scientific, Staffordshire, UK), to remove the Ponceau S solution. It was then blocked for 1 hour in 5% (w/v) non-fat dried milk (NFDM, Marvel) solubilised in 0.1% (v/v) PBST to mask non-specific binding sites. Primary antibodies were prepared in 5% (w/v) NFDM at the dilutions specified in **Table 3.1**. Membranes were incubated in cleave PARP antibody solution at overnight at 4ºC on a roller mixer (Stuart Scientific, UK). After antibody incubation, the membrane was washed with 0.1% (v/v) PBST three times for 15 minutes to ensure complete removal of the primary antibody. Secondary antibody was incubated with the membranes for 1 hour at room temperature on the roller mix. The membrane was then washed again with 0.1% (v/v) PBST three times for 15 minutes to ensure complete removal of the secondary antibody. β-actin was used as a loading control for every membrane. Membranes were incubated in β-actin antibody solution 1 hour at room temperature, followed by the same as for cleaved PARP antibody.

Table 3.1– Primary and secondary antibodies used in western blotting.

Primary Antibody	**Dilution**	**Secondary antibody (HRP-conjugated)**	**Dilution**
Cleaved PARP (New England Biolabs, UK)	1:1,000	anti-mouse (New England Biolabs, UK)	1:10,000
β-actin (Sigma Aldrich, UK)	1:40,000	anti-rabbit (New England Biolabs, UK)	

Antibodies were diluted in 5% (w/v) NFDM

Chemiluminescent Detection

To detect and visualise the proteins, the Enhanced Chemiluminescence (ECL) kit (GE Healthcare, Buckinghamshire, UK) was used according to manufacturer's guidelines. The membrane was immersed in activated ECL solution for 1 minute and

then blotted and transferred to an autoradiography hypercassette (Kodak, UK). HRP-conjugates present on the membrane react with the luminol in the ECL solution and emit blue light at 480nm, which is detected by blue-light-sensitive film. The membrane and cassette were transferred to the dark room where a piece of hyperfilm (Fuji Medical X-ray film; Fuji, UK) was removed from the packaging, in the red light environment, and placed over the membrane. The cassette was sealed and the film was exposed to the membrane for the required amount of time. The film was then developed using the automated developer (Xograph Imaging Systems, UK). On removal from the developer, the film was placed back in the cassette to identify the protein bands based on the pre-stained marker standards.

3.2.5. STATISTICAL ANALYSES

Data were analysed using GraphPad Prism 5.0 software with significance at $p < 0.05$. Statistical comparisons between treatment and control were performed using a paired Student's T-Test. Data are reported as mean ± 1 standard deviation (s.d.) of the mean. Curve fitting was performed for best-fit data using SigmaPlot 10.0 software, using Piecewise nonlinear regression to test the fit of the regression line.

3.3. RESULTS

Biologists often utilise growth experiments to analyse basic properties of a given organism or cellular model. To investigate the specific effect of a given experimental set

up or condition (e.g., a compound or substrate), characteristic parameters of the growth curves are derived. Curve fitting is finding a curve that matches the best fit to a series of data points, possibly subjected to constraints. It is often used in science to visualise and plot the curve that best describes the shape and behaviour of the interested data. The data collected for the construction of cell growth curves are usually at regular intervals, with mammalian cell growth curve being represented by different phases: lag phase, exponential (log) phase and stationary phase. In this context, application of one linear model for the whole data is not justified. Frequently biologists use exponential linear regression in order to fit cell growth curves. However, the growth of mammalian cells is characterised by different phases, and the exponential model does not take into account the different phases. It is therefore necessary to exploit the possibility of using a model to suit the available data. The model representing the growth curve in piecewise model can then be split into linear pieces that can represent the different phases of a mammalian cell growth curve. The use of piecewise nonlinear regression allows multi-line fit equations to be defined over different independent variable (x) intervals. This data measures the number of viable cells as function of time, with the shape of a cell growth curve consisting of three segments (see **Figures 3.2B** and **C**, **3.3B** and **2C**).

$$f = \begin{cases} \dfrac{x_1\,(T_1 - t) + x_2\,(t - t_1)}{T_1 - t_1}, & t_1 \le t \le T_1 \quad \rightarrow \textbf{region 1} \\ \dfrac{x_2\,(T_2 - t) + x_3\,(t - T_1)}{T_2 - T_1}, & T_1 \le t \le T_2 \quad \rightarrow \textbf{region 2} \\ \dfrac{x_3\,(T_3 - t) + x_4\,(t - T_2)}{T_3 - T_2}, & T_2 \le t \le t_3 \quad \rightarrow \textbf{region 3} \end{cases}$$

The three *x* intervals can be defined by the time points t1 < T1 < T2 < T3. The "region" equations are defined so that the end points of each segment meet.

3.3.1. CELL LINES COMPARISON

Cell counting, performed over eight days, allowed the construction of growth curves for each cell line (see **Appendices IV** and **V**). The mean values of the replicates were plotted and a nonlinear regression was performed for best-fit data. This procedure was carried out using piecewise nonlinear regression using three linear segments and kinetic parameters were calculated (Chandrasekaran *et al.*, 2005; **Appendix VI**).

3.3.1.a. RT112 and T24 cell lines

In **Figure 3.2A** is shown the comparison of cell growth curves for RT112 and T24. **Figures 3.2B and C** show the curve fitting for both cell lines, with the respective kinetic parameters calculated in **Table 3.2**.

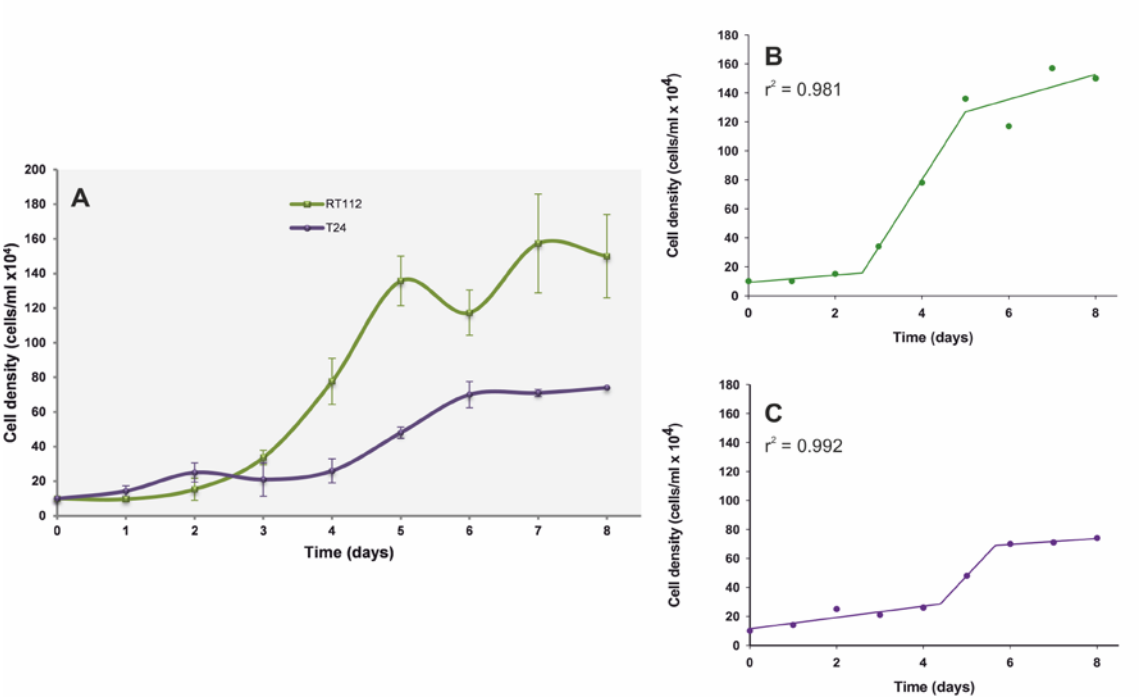

Figure 3.2– Comparison of the cell growth curves for RT112 and T24 cell lines, using viable cell counting method (**A**). Graphs of nonlinear regression, using piecewise with 3 linear segments, of RT112 (**B**) and T24 (**C**) cell lines.

Table 3.2 – Kinetic growth parameters calculated for RT112 and T24 cell lines.

Parameter	RT112	T24
N_0 (cells/ml x 10^4)	15.74	28.52
N (cells/ml x 10^4)	126.88	68.98
t_1 (days)	2.62	4.39
T_1 (days)	5.00	5.66
X (generations/day)	3.01	1.27
D (hour)	18.94	23.88
μ (hour^{-1})	0.016	0.013
Growing %	1500.00%	740.00%

Where N_0 = initial cell concentration of the log phase; N = final cell concentration of the log phase; t_1 = initial time of the log phase; T_1 = final time of the log phase; X = number of generations of cell growth; D = doubling time; μ = specific growth rate.

It can be seen from **Figure 3.2** that RT112 has a higher cell growth rate than T24. Using values obtained by the nonlinear regression (**Appendix VI**) it can be observed that RT112 has a lag phase of about two and a half days, from which cells enter into exponential phase until day 5. While T24 has a lag phase of approximately four and half days, and having the exponential phase until almost the day 6, followed by a plateau. The comparison of cell growth curves between RT112 and T24 has shown that a higher cell growth rate is seen in RT112. RT112 had an increase of 1500% in the cell growth, while in T24 was observed an increase of 740%. The calculated kinetic parameters (**Table 3.2**) also show that the number of generations per day (X) and the specific growth rate (μ) are higher for RT112. Furthermore, the doubling time (D) for RT112 is lower than for T24.

3.3.1.b. PC3 and PNT1A cell lines

Figure 3.3A shows a comparison between cell growth curves for PC3 and PNT1A, and **Figures 3.2B** and **C** the respective fitting curves. In **Table 3.3** is shown the respective kinetic parameters.

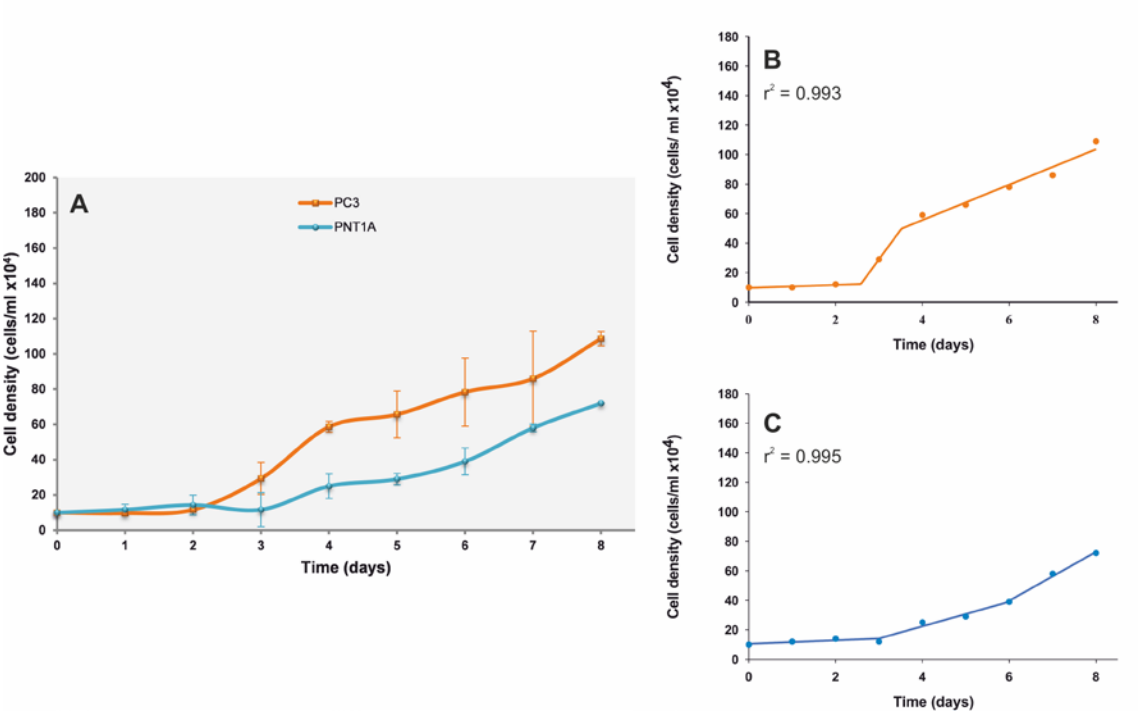

Figure 3.3 – Comparison of the cell growth curves for PC3 and PNT1A cell lines, using viable cell counting method (**A**). Graphs of nonlinear regression, using piecewise with 3 linear segments, of PC3 (**B**) and PNT1A (**C**) cell lines.

Table 3.3 – Kinetic growth parameters calculated for PC3 and PNT1A cell lines.

Parameter	PC3	PNT1A
N_0 (cells/ml x 10^4)	12.25	14.11
N (cells/ml x 10^4)	49.84	38.32
t_1 (days)	2.58	3.00
T_1 (days)	3.52	5.92
X (generations/day)	2.02	1.44
D (hour)	11.12	48.54
μ (hour^{-1})	0.027	0.0062
Growing %	1086.67%	720.00%

In **Figure 3.3** is shown that PC3 has a higher cell growth rate than PNT1A. According to piecewise regression (**Figure 3.3, Appendix VI**) PC3 has a lag phase of about two and half days, followed by a growth phase of one day. PNT1A has an

exponential phase starting on day 3 and followed by three more days. From **Table 3.3** can be observed that all the calculated kinetic parameters, X and μ, are higher for PC3 than PNT1A, being observed a much lower D value for PC3. A higher growing efficiency was also achieved in PC3, being respectively 1090%, while a growth of 720% was observed for PNT1A cell line.

3.3.2. OPTIMISATION OF MTT ASSAY

MTT assay was another approach to assess cell proliferation. In order to optimise MTT for each cell line, this assay was carried out over eight days, and four different cell dilutions were used for each cell line. Different cell concentrations were used not only aiming for the optimisation of MTT assay for each cell line, but also allowed the observation of the cell growth behaviour under different seeding concentrations (see **Appendices VII** and **VIII**). Conversely, for viable cell counting assay, cell growth percentage was not calculated, since OD values were not obtained for day 0.

3.3.2.a. RT112 cell line

Figure 3.4 shows the growth curves for RT112, where the mean of OD values of the replicates were plotted against day. **Table 3.4** shows the respective kinetic growth parameters calculated for each initial cell concentration (see **Appendix IX**).

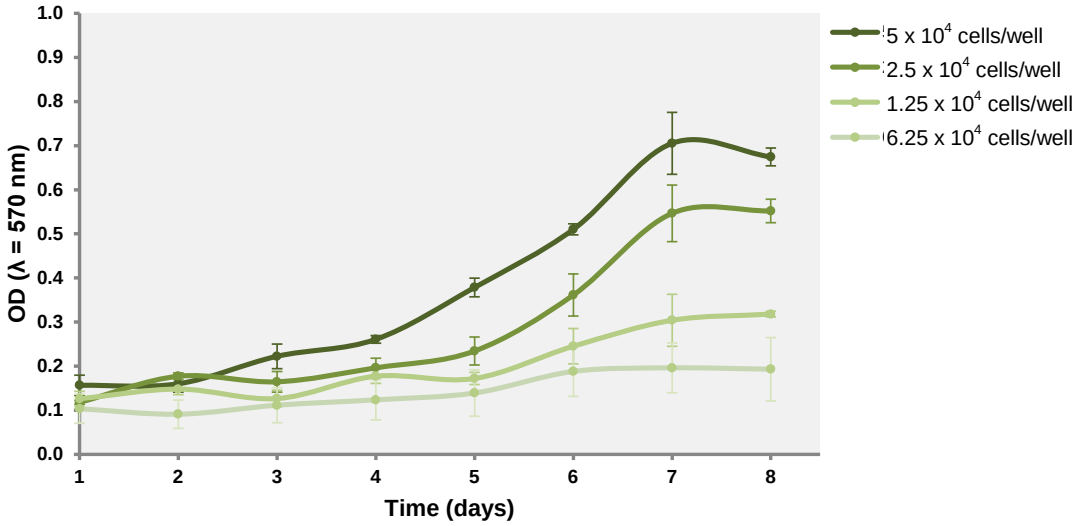

Figure 3.4 – Cell growth curves of RT112 cell line under normal conditions measured by MTT optical density readings at λ = 570 nm.

Table 3.4 – Kinetic growth parameters calculated for RT112 cell line, according to the different seeded cell concentrations.

Parameter	$5x10^4$ cells/well	$2.5x10^4$ cells/well	$1.25x10^4$ cells/well	$6.25x10^3$ cells/well
N_0 (OD)	0.27	0.24	0.19	0.13
N (OD)	0.78	0.57	0.32	0.20
t_1 (days)	4.41	5.35	5.01	4.72
T_1 (days)	7.52	7.13	7.22	6.22
X (generations/day)	1.52	1.25	0.76	0.66
D (hour)	49.05	34.30	69.56	54.13
μ ($hour^{-1}$)	0.0061	0.0088	0.0043	0.0056

From the data analysis it can be observed that the best initial concentration for the MTT assay is $2.5x10^4$ cells/well. This conclusion was based on the population doubling time (D) and on the specific growth rate (μ). Regarding the population doubling time, this initial concentration has the lower value – approximately 34 hours. Whereas, for the specific growth rate is seen the higher value. This means that with this

concentration is reached the higher rate of increase of cell number. The exponential phase was achieved in approximately two days, being observed between days 5 and 7.

3.3.2.b. T24 cell line

In **Figure 3.5** it can be seen the growth curves for T24 and in **Table 3.5** the respective kinetic growth parameters calculated for each initial cell concentration (see **Appendix IX**).

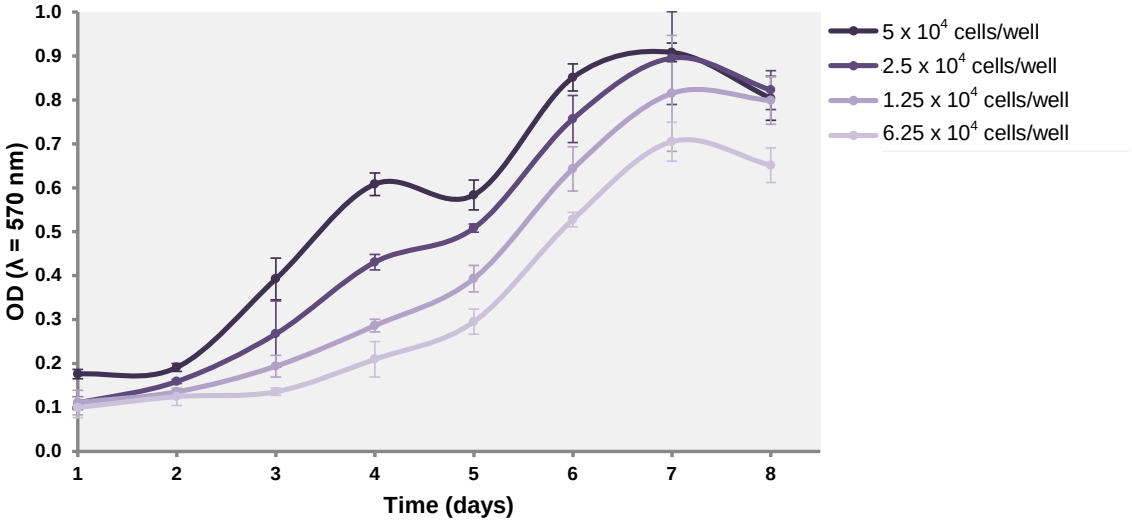

Figure 3.5 – Cell growth curves of T24 cell line under normal conditions, measured by MTT optical density readings at $\lambda = 570$ nm.

Table 3.5 – Kinetic growth parameters calculated for T24 cell line, according to the different seeded cell concentrations.

Parameter	$5x10^4$ cells/well	$2.5x10^4$ cells/well	$1.25x10^4$ cells/well	$6.25x10^3$ cells/well
N_0 (OD)	0.19	0.51	0.31	0.22
N (OD)	0.94	0.92	0.82	0.72
t_1 (days)	1.76	5.00	4.66	4.66
T_1 (days)	6.73	6.66	6.71	6.81
X (generations/day)	2.32	0.85	1.41	1.73
D (hour)	51.27	46.48	34.78	29.83
μ ($hour^{-1}$)	0.0059	0.0065	0.0087	0.010

From the data analysis it can be observed that the best initial concentration for for T24 cell line is $6.25x10^3$ cells/well. This concentration shows a better specific growth rate and a lower population doubling time. The log phase for this concentration has approximately two days, being seen between days 4.7 and 6.8.

3.3.2.c. PC3 cell line

Figure 3.6 shows the cell growth curves for PC3 cell line and **Table 3.6** the respective kinetic growth parameters calculated for each initial seeded cell concentration (see **Appendix IX**).

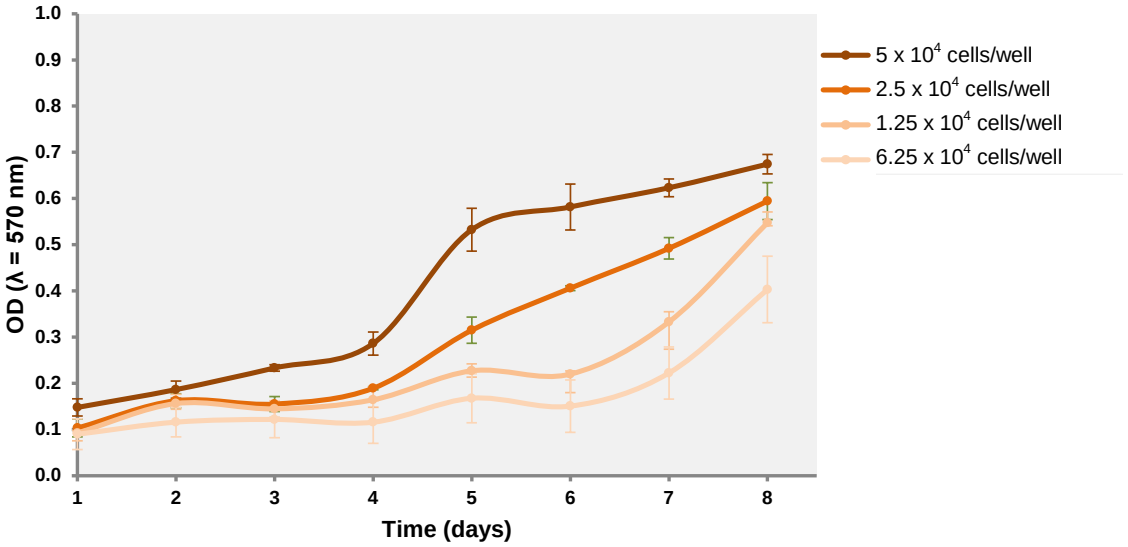

Figure 3.6 – Cell growth curves for PC3 cell line under normal conditions, measured by MTT optical density readings at λ = 570 nm.

Table 3.6 – Kinetic growth parameters calculated for PC3 cell line, according to the different seeded cell concentrations.

Parameter	$5x10^4$ cells/well	$2.5x10^4$ cells/well	$1.25x10^4$ cells/well	$6.25x10^3$ cells/well
N_0 (OD)	0.27	0.19	0.13	0.11
N (OD)	0.53	0.27	0.24	0.17
t_1 (days)	3.94	3.98	1.61	1.49
T_1 (days)	5.01	4.55	6.55	6.68
X (generations/day)	0.97	0.54	0.83	0.65
D (hour)	26.24	25.17	142.06	192.13
μ ($hour^{-1}$)	0.012	0.012	0.0021	0.0016

From the data analysis, $5x10^4$ cells/well was the chosen concentration to be used in further MTT assays. This choice was based on the specific growth rate and in the number of generations per day. Despite being seen a slightly lower doubling time for the concentration of $2.5x10^4$ cells/well, a lower X is also observed. Since the difference of D between the concentrations of $5x10^4$ and $2.5x10^4$ cells/well it is only one hour, the

highest concentration was the selected one for the MTT assay. Thus, for $5x10^4$ cells/well a log phase of approximately one day is seen between days 4 and 5.

3.3.2.d. PNT1A cell line

In **Figure 3.7** is shown the cell growth curves for PNT1A cell line and in **Table 3.7** the respective kinetic growth parameters calculated for each initial cell concentration (see **Appendix IX**).

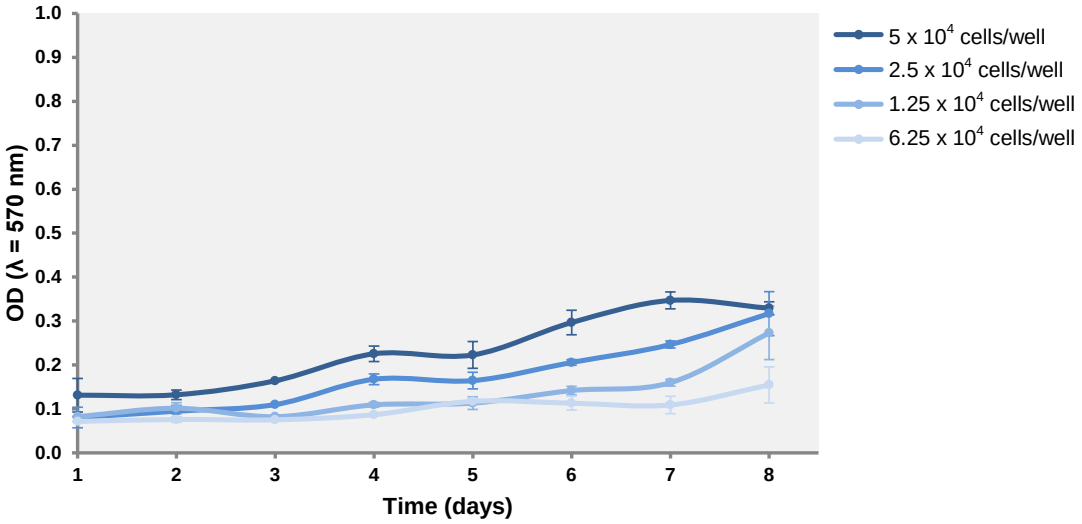

Figure 3.7 – Cell growth curves for PNT1A cell line under normal conditions, measured by MTT optical density readings at $\lambda = 570$ nm.

Table 3.7 – Kinetic growth parameters calculated for PNT1A cell line, according to the different seeded cell concentrations.

Parameter	$5x10^4$ cells/well	$2.5x10^4$ cells/well	$1.25x10^4$ cells/well	$6.25x10^3$ cells/well
N_0 (OD)	0.27	0.11	0.09	0.08
N (OD)	0.78	0.22	0.16	0.13
t_1 (days)	4.41	2.60	3.00	3.00
T_1 (days)	7.52	6.68	7.25	7.65
X (generations/day)	1.52	1.06	0.91	0.71
D (hour)	49.05	92.70	112.51	158.17
μ ($hour^{-1}$)	0.0061	0.0032	0.0027	0.0019

From the data analysis it can be seen that the best initial concentration for PNT1A cell line is $5x10^4$ cells/well. This concentration shows a better specific growth rate and a lower population doubling time. The exponential phase for this concentration is at approximately three days – between days 4.4 and 7.5.

3.3.3. EVALUATION OF THE EFFECT THAT HA HAS ON CELL GROWTH AND PROLIFERATION OF TUMOUR-DERIVED CELL LINES

To investigate whether HA polymer MW has an effect on proliferation of tumour-derived cell lines, cells were seeded and cultured on HA-coated surfaces. All four cell lines used in this project were found to adhere and growth onto the different structured surfaces, although different growth patterns were observed. All cell lines growing on HA_4 can spread along the surface, appearing to show similar cell morphology to the controls; whereas cells growing on HA_{234} and HA_{2590} surfaces showed a markedly increased capacity for self-aggregation, leading to enhanced cell

clumping. Cells growing on HA_{mix} presented a mix of morphologies but mainly forming cell aggregates (**Figure 3.8**). However, when removed and placed on tissue culture polystyrene, these cellular clumps started to spread along the surface and presented similar cell morphology as the controls (data not shown).

MTT assay was performed in order to assess the effect that HA polymer molecular weight has on proliferation of tumour-derived cell lines. Using tissue culture polystyrene as control, the proliferation of RT112, T24, PC3 and PNT1A on the coated surfaces was evaluated. The cells were seeded and cultured *in vitro* over eight days, and cell viability was determined (see **Appendix X**). Using the obtained OD values, for each cell line cell proliferation percentages (**Figure 3.9**) and kinetic parameters were calculated (**Tables 3.8** to **3.11**; **Appendix XII**).

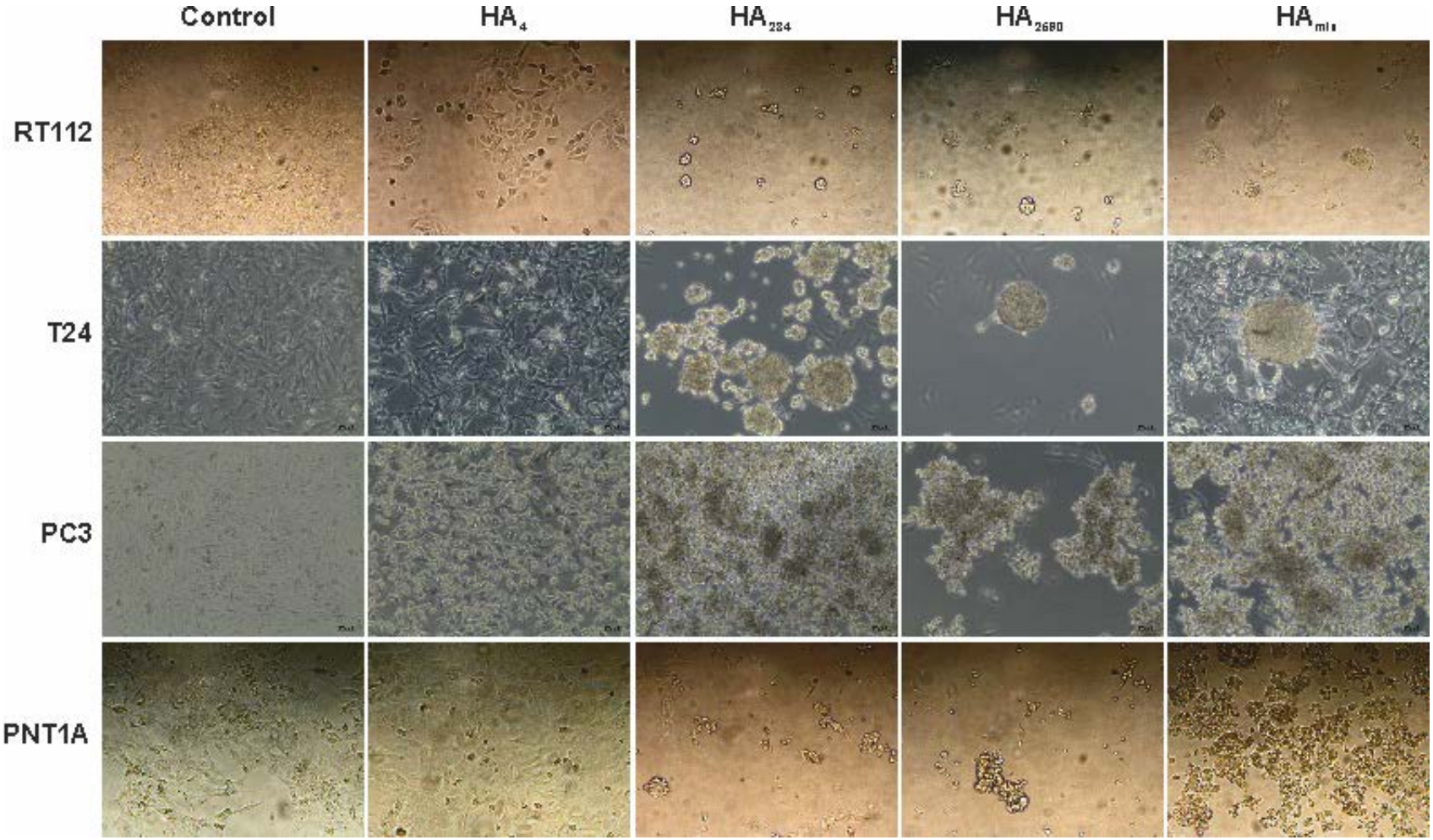

Figure 3.8 – Effect of HA on cell growth of RT112, T24, PC3 and PNT1A cell lines after 5 incubation days in growth medium.

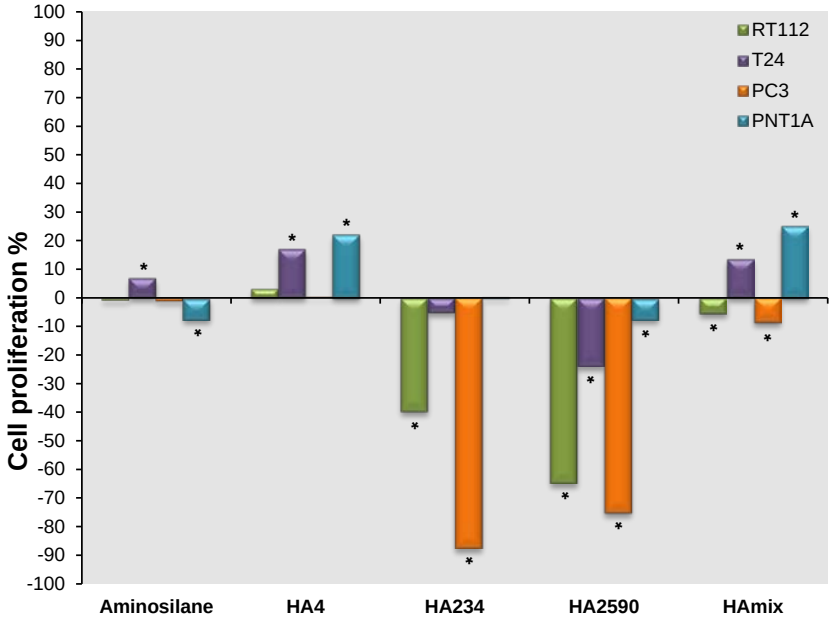

Figure 3.9 – Effect of HA on cell proliferation of tumour-derived cell lines. Cell proliferation percentages when compared to the respective control (cells growing on tissue culture polystyrene) after 8 incubation days in growth medium. Measurements were performed by MTT optical density reading at $\lambda = 570$ nm. Statistical comparisons were based on t student test for two-tailed P value ($p < 0.05$ was considered significant; n=3). The conditions linked by (*) are statistically different to the control, the other one being similar.

In **Figure 3.9** is shown the cell proliferation percentages obtained for all four cell lines when compared to the respective controls after 8 days of cell growth. Cell proliferation percentage values were calculated using data obtained from the OD measurements. HA-tethered surfaces induced significant proliferation of tumour-derived cell lines over 8 days of culture, although different growth patterns were observed depending on the molecular weight of HA chain (**Figure 3.9**; **Appendix XI**). For all cell lines, an increase in the proliferation was seen for cells growing on HA_4 surfaces, whilst a decrease was observed in those cells growing on HA_{234} and HA_{2590} surfaces. This cell proliferation decrease was very sharp for RT112 and PC3 cells. For RT112 cells growing on HA_{234}, a decrease of 40% can be seen, whereas a decrease of 65% is

observed for those cells growing on HA_{2590}. Regarding PC3 cell line, a decrease of 88% can be observed when cells grow on HA_{234}, while a decrease of 75% is seen on those cells growing on HA_{2590}. For T24 cells, it can be seen that HA_4 and HA_{mix} stimulated a proliferation of 17% and 14%, respectively, when compared to control, whereas a decrease was observed for those cells growing on HA_{2590} (24%) and HA_{234} (5%). For PNT1A cells growing on HA_4 and HA_{mix}, the highest proliferation increase when compared to the rest of cell lines is seen; 22% and 19% respectively. Conversely to the other cell lines, HA_{234} did not induce significant changes in the proliferation of PNT1A cells. In addition, for PNT1A cells growing on HA_{2590}, the smallest decrease in proliferation (4%) when compared to the other cell lines is seen. Aminosilane surfaces were used as a control to show that the differences seen in cell proliferation were not due to the construction of HA-coated surfaces, but due to the properties of HA.

Quantitation in cell culture is required for the characterisation of the growth properties of different cell lines for experimental analyses (Freshney, 2005). Knowledge of the growth state of a culture and its kinetic parameters is critical in the design of cell culture experiments. Measurements of kinetic parameters are often used to determine the response of cells to a particular stimulus or toxin. The calculated kinetic parameters were found to be related to the cell proliferation percentages obtained (**Figure 3.8**). For RT112 cells growing on HA_4 surfaces, it can be seen that the doubling time value (D) is lower and the specific growth rate (μ) and number of generations/day (X) values are higher than for the control. Whilst for cells growing on the other surfaces, higher D values, and lower X and μ values are observed when compared to the control (**Table 3.8**). Regarding T24, PC3 and PNT1A cell lines this correlation between cell growth

and kinetic parameters is also observed (**Tables 3.8 to 3.11**). The only exceptions are seen for PC3 cells growing on HA_4, and PNT1A growing on HA_{mix}.

Table 3.8 – Kinetic growth parameters calculated for RT112 cell line. Cells were seeded at a concentration of 2.5 $x10^4$ cells/well.

Parameter	Control	Aminosilane	HA_4	HA_{234}	HA_{2590}	HA_{mix}
N_0 (OD)	0.23	0.63	0.40	0.44	0.30	0.34
N (OD)	0.79	1.11	0.89	0.67	0.65	0.64
t_1 (days)	1.91	4.22	4.40	4.19	1.96	2.71
T_1 (days)	4.79	5.83	5.61	5.63	6.00	4.51
X (generations/day)	1.77	0.81	1.15	0.61	1.13	0.90
D (hour)	38.90	47.34	25.43	56.71	85.84	48.05
μ ($hour^{-1}$)	0.008	0.0064	0.012	0.0053	0.004	0.0063

Table 3.9 – Kinetic growth parameters calculated for T24 cell line. Cells were seeded at a concentration of 6.25$x10^3$ cells/well.

Parameter	Control	Aminosilane	HA_4	HA_{234}	HA_{2590}	HA_{mix}
N_0 (OD)	0.37	0.28	0.34	0.26	0.25	0.37
N (OD)	0.91	0.93	0.81	0.37	0.38	0.96
t_1 (days)	4.68	4.47	4.79	3.00	3.00	5.46
T_1 (days)	7.04	7.03	6.37	5.05	5.54	6.90
X (generations/day)	1.31	1.74	1.27	0.53	0.58	1.36
D (hour)	43.30	35.35	29.79	92.11	104.57	25.35
μ ($hour^{-1}$)	0.0070	0.0085	0.0101	0.0033	0.0029	0.0119

Table 3.10 – Kinetic growth parameters calculated for PC3 cell line. Cells were seeded at a concentration of $5x10^4$ cells/well.

Parameter	Control	Aminosilane	HA_4	HA_{234}	HA_{2590}	HA_{mix}
N_0 (OD)	0.73	0.76	0.62	0.39	0.52	0.58
N (OD)	1.10	0.98	1.01	0.77	0.83	1.05
t_1 (days)	5.20	5.21	5.06	4.47	4.72	5.47
T_1 (days)	5.84	5.75	5.94	6.32	6.00	6.82
X (generations/day)	0.59	0.36	0.70	0.99	0.68	0.85
D (hour)	25.59	36.74	30.47	44.85	45.17	37.91
μ ($hour^{-1}$)	0.0118	0.0082	0.0099	0.0067	0.0067	0.0079

Table 3.11 – Kinetic growth parameters calculated for PNT1A cell line. Cells were seeded at a concentration of $5x10^4$ cells/well.

Parameter	Control	Aminosilane	HA_4	HA_{234}	HA_{2590}	HA_{mix}
N_0 (OD)	0.51	0.51	0.46	0.37	0.35	0.32
N (OD)	0.80	0.85	0.67	0.67	0.56	0.63
t_1 (days)	4.98	5.19	5.90	5.38	5.69	4.33
T_1 (days)	5.74	6.18	6.23	6.50	6.63	7.03
X (generations/day)	0.63	0.74	0.55	0.87	0.67	0.97
D (hour)	29.03	31.73	14.43	30.68	33.39	67.03
μ ($hour^{-1}$)	0.010	0.0095	0.021	0.0098	0.009	0.0045

3.3.4. EVALUATION OF THE EFFECT THAT HA HAS ON APOPTOSIS OF TUMOUR-DERIVED CELL LINES

To investigate whether HA polymer MW induce apoptosis, cells were immunoblotted for the 89 kDa, carboxy-terminal catalytic domain fragment of cleaved PARP. Using tissue culture polystyrene as control, the apoptosis of RT112, T24, PC3 and PNT1A cells growing on the coated surfaces was evaluated. The cells were seeded and cultured *in vitro* over eight days, and apoptosis was determined by western blotting. The amount of cleaved PARP produced following treatment can indicate the extent to which the cells have undergone apoptosis. β-actin antibody was used as positive control, to ensure integrity of protein. Protein extract from OE21 cells 10 Gy irradiated was also used as positive control.

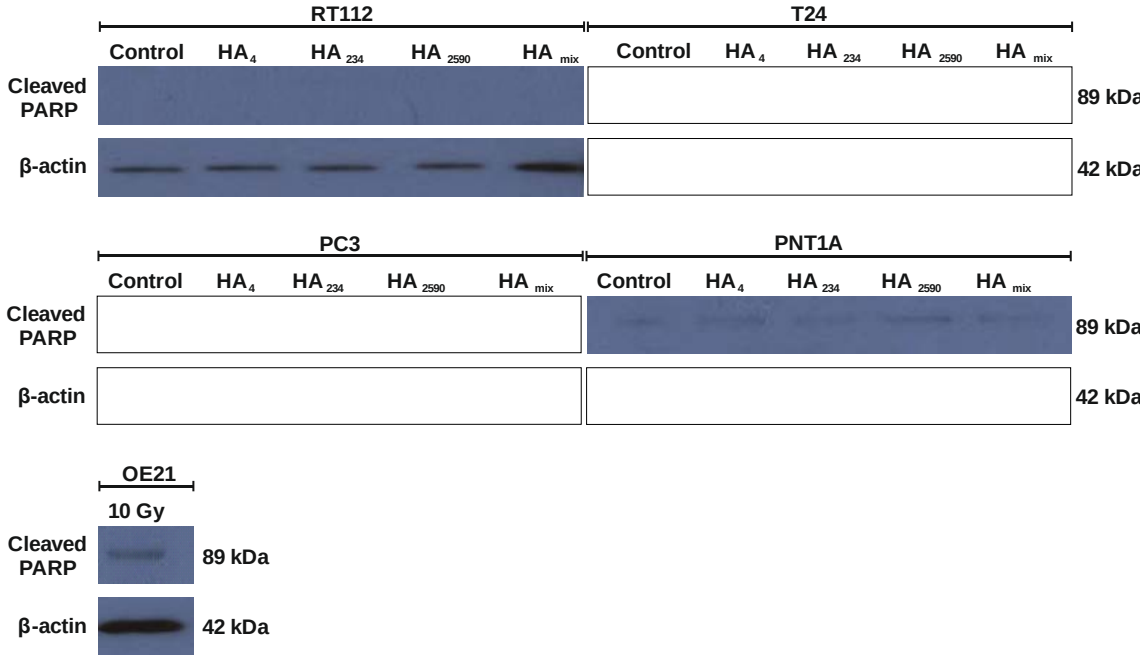

Figure 3.10 – Effect of HA on the expression of apoptotic marker protein. Lysates from RT112, T24, PC3 and PNT1A cells growing on HA-coated surfaces were immunoblotted, probing for cleaved PARP.

β-actin was used as a loading control. Lysate from OE21 10 Gy irradiated cells was used as positive control for apoptosis.

The data shown in **Figure 3.10** indicate that HA did not induce apoptosis. Cleaved PARP was not detected on cell lines growing on HA-coated surfaces. The only exception is seen on PNT1A cells, where samples have undergone apoptosis. Since similar expression of cleaved PARP was also found in control cells, it can therefore be assumed that HA did not have an effect on apoptosis.

3.4. DISCUSSION

The data shown in **Figure 3.10** indicate that HA did not induce apoptosis. Cleaved PARP was not detected on cell lines growing on HA-coated surfaces. The only exception is seen on PNT1A cells, where samples have undergone apoptosis. Since similar expression of cleaved PARP was also found in control cells, it can therefore be assumed that HA did not have an effect on apoptosis.

3.4.1. QUANTITATION OF THE CULTURE GROWTH

One of the goals of this project was to assess whether different HA molecular weight has on proliferation of tumour-derived cell lines. For this purpose, the studies firstly carried out in this chapter aimed to construct cell growth curves viewing a better knowledge of the cell lines characteristics, and to establish reproducible conditions for the experiments and maintenance of the cultures. The construction of growth curves from cell counts provides information about a number of parameters that should be

characteristic of the cell line under a given set of culture conditions, including cell growth vessel area, cell concentration, and media. Quantitation of the culture growth is not only an important factor in routine maintenance, but also a crucial element for monitoring the consistency of the culture and knowing the most appropriate time to subculture. It is very important to observe when it is the exponential phase of a cell culture, since it is in this stage that the cell growth is high (usually 90-100%) and the culture is in its most reproducible form. Consequently, this is the optimal time for sampling, as the population is at its most uniform and the viability is high (Freshney, 2005).

A variety of assays are currently available providing information on the proliferation and capability of cell populations: cell counting, measurement of metabolic activity, measurement of DNA synthesis, measurement of cell cycle regulatory molecules (Rode *et al.*, 2006). Of these available methods, two different assays were chosen, focusing on a direct and an indirect technique. Viable cell count is a direct measure of proliferation, while MTT assay is an indirect method based on the measurement of the cell metabolic activity. The direct cell counting in a haemocytometer is the most straightforward method for quantifying the number of viable cells in a culture. The cell viability is measured by the ability of viable cells exclude a dye such as trypan blue, while cells with compromised membrane integrity are stained. This is an inexpensive technique and requires only a small fraction of total cells from a cell population (Rode *et al.*, 2006). However, it is a laborious and time consuming procedure (Lin *et al.*, 1999). MTT assay is a colourimetric method, being less laborious than cell counting and widely used in evaluation of viable cell numbers *in vitro* experiments (Lin *et al.*, 1999). In MTT assay, the use of a tetrazolium dye as the

end point relies on the ability of cells to reduce the dye in a quantitative manner, and thus estimate of surviving cell numbers (Plumb *et al.*, 1989). Whereas MTT is an assay where the metabolic activity measures the cell health, cell viable counting gives an absolute measure of cell proliferation. In addition, MTT assay is a widely used method, being inexpensive and supported by an extensive literature base. Thus, combining these assays, a more detailed view of the cell activity can be reached (Genetic Engineering & Biotechnology News, 2006).

This work focused upon human bladder and prostate cell lines, using two cell lines of each tissue type. The use of two cell lines of each tissue type may provide insights into the variability of expression within tumours of differing stage and grade. Regarding the comparison of cell growth curves between RT112 and T24 (bladder) cell lines , it was observed that RT112 presents a higher cell growth rate. This is likely to be related to with the more invasive phenotype presented by RT112 cells; and therefore being observed a higher cell proliferation rate than T24 cells (Nixdorf *et al.*, 2004). From the comparison between PC3 and PNT1A (prostate) cell lines, it was shown that PC3 presents a higher cell growth rate. These data might be correlated with the malignant phenotype presented by PC3 cells; the PNT1A cell line is derived from normal prostate cells immortalised with SV40 viral genome, hence their non-malignant phenotype (Cussenot *et al.*, 1991; Scaltriti1 *et al.*, 2004).

Findings from this work suggest that piecewise nonlinear regression with three linear segments can represent the different growth phases of a mammalian cell culture. Piecewise nonlinear regression has been used for the analysis of trends in cancer rate incidence (Kim *et al.*, 2000; Tiwari *et al.*, 2005), to estimate size- and age-related mortality rates of fish (Maceina, 2007), and to fit stock-recruitment and individual

growth curves for fish (Borrowman and Myers, 2000). In this chapter of work is proposed the use of piecewise nonlinear regression with three linear segments as a good tool for the calculation of growth kinetic parameters of mammalian cell lines (Chandrasekaran *et al.*, 2005).

3.4.2. HA-POLYMER MOLECULAR WEIGHT MODULATES GROWTH AND PROLIFERATION OF TUMOUR-DERIVED CELL LINES

Tumour progression is accompanied by various cellular, biochemical and genetic alterations, including the interaction of tumour cells with ECM molecules, including HA (Laurent and Fraser, 1992). The effects of HA on cell adhesion are controversial and dependent on cell type. It has been reported promotion or inhibition of cell adhesion in inflammatory cells, hepatic cells, myoblast cells or stabilised cell lines (Cho *et al.*, 2004; Ken *et al.*, 2008). The differential effects of HA on tumour cells attachment, proliferation and migration have not been completely studied. In particular, the effects of different HA polymer molecular weight (MW) have not been explored. To the present knowledge, this represents the first study were HA polymer MW has been suggested to modulate cell adhesion and differentiation of tumour-derived cell lines. Here it was reported that the MW of the polysaccharide plays a pivotal role in adherence and morphology of tumour-derived cell lines. It was observed that HA with medium and large molecular weights prevent tumour cells from attaching to the matrix, and consequently cells do not acquire their normal morphology. Hence, these findings may suggest that cell behaviour of tumour cells is HA MW-dependent.

The next stage of work was the evaluation of the effect that HA has on cell proliferation. Cells were seeded and cultured *in vitro* over 8 days, and cell viability was determined by MTT assay. HA-tethered surfaces induced proliferation of tumour-derived cell lines over eight days of culture, although different growth patterns were seen. It was observed that cells respond to HA low MW fragments more exuberantly than to high MW fragments. Small HA fragments (HA_4) increase proliferation, whereas a decrease is seen in the presence of medium (HA_{234}) and large fragments (HA_{2590}). Interestingly, HA_4 stimulated an increased proliferation in those less invasive cell lines (T24 and PNT1A), while HA_{234} and HA_{2590} induced a sharper decrease in the most malignant tumour cell lines (RT112 and PC3). An increase in cell proliferation was observed for T24 and PNT1A cells growing on HA_{mix} surfaces, whereas a small decrease was observed for RT112 and T24 cell lines. These observations might be related with the antagonist effect that small HA polymers have in the presence of larger fragments (Ohno *et al.*, 2005; Takahashi *et al.*, 2005). The cell growth results are comparable to the kinetic values obtained. These observations were also found in a work performed by West and Kumar (1989) on endothelial cells, where 3-10 disaccharide fragments stimulated cell growth, while native HA inhibited cell proliferation (West and Kumar, 1989). HA oligosaccharides (4-25 saccharide range) have been suggested to be implicated in cell proliferation and promotion of angiogenesis (West *et al.*, 1985). In addition to angiogenesis, there is also some evidence that small HA fragments stimulate endothelial cell proliferation, adhesion and migration (Rossler and Hingghofer-Szalkay, 2002; Murai *et al.*, 2004). Conversely, it has been suggested that large HA molecules inhibit endothelial cell growth, exhibiting anti-angiogenic properties (Chen and Abatangelo, 1999; Stern *et al.*, 2006), and being

involved in the promotion of cell quiescence and protection of cells against apoptosis (Morrison *et al.*, 2001; Jiang *et al.*, 2005). There is some evidence suggesting that high levels of HA are present in most cancer malignancies, as well as in the serum of some cancer patients (Dahl and Laurent, 1988; Knudson *et al.*, 1989; Knudson, 1996; Auvinen *et al.*, 1997; Lokeshwar *et al.*, 1997; Ropponen, 1998). Additionally, some studies have evidenced that large HA chain length is found in most normal biological processes, while much smaller fragments are detected in malignant tumours (Kumar *et al.*, 1989; Lokeshwar *et al.*, 1997). Production of HA fragments in the 30-50 saccharide range is seen in highly invasive bladder cancers (Lokeshwar *et al.*, 1997). It has also been reported that HA has the capacity to increase the bioavailability of many drug molecules. The bioavailability promoted by HA is the result of bioadhesion and/or penetration enhancement, which were found to be dependent on the polysaccharide molecular weight (MW). While high MW HA fragments (more than 300 kDa) promote an increase in the bioavailability, low MW fragments (55 kDa) have no effect (Liao *et al.*, 2005).

Since cell proliferation occurs in a balance with apoptosis, the next addressed question was whether HA MW induces apoptosis of tumour-derived cell lines. Apoptosis was assessed by Poly-ADP-Ribose-Polymerase (PARP) cleavage, which is an indicator of apoptosis. PARP is a 113 kD enzyme that it is involved in the DNA repair, binding specifically at DNA strand breaks, and it is also a substrate for certain caspases (including caspase 3 and 7) activated during early stages of apoptosis. These proteases cleave PARP to two fragments of approximately 89 kD and 24 kD. This cleavage neutralises the ability of PARP to participate in DNA repair, and contributes to a cell commitment to undergo apoptosis. Detection of PARP cleavage therefore allows

distinguishing different types of cell death and quantifying apoptotic cells in a population. Detection of the 89 kD PARP fragment with anti-PARP serves as an early marker of apoptosis (Soldani and Scovassi, 2002). To investigate whether HA polymer MW induce apoptosis, cells growing on HA-coated surfaces were immunoblotted for the 89kDa, carboxy-terminal catalytic domain fragment of cleaved PARP, with the amount of cleaved PARP produced following treatment indicating the extent to which the cells have undergone apoptosis. In the present work, a significant apoptosis induction promoted by HA was not shown. Apoptotic marker was only detected in PNT1A cells. Apoptosis study was performed after eight days of cell growth. In order to perform this investigation cells could not be fed over this period of time, since all cells needed to be collected for protein extraction. Therefore, this might be related with the fact that PNT1A cells undergone apoptosis, including control cells. These results may suggest that HA was not involved in the apoptosis, but only on cell proliferation. Hence, the decreased proliferation seen for cells growing on medium and large HA fragments maybe due a decrease of growth kinetics, and not apoptosis mechanism. The role of HA on apoptosis is still controversial. It is reported that tetrasaccharides are anti-apoptotic (Xu *et al.*, 2002). However, a study performed by Pauloin and co-workers (2009) evidenced that high MW hyaluronic acid decreases UVB-induced apoptosis in human epithelial corneal cells (Pauloin *et al.*, 2009). Bourguignon and co-workers (2009) have also proposed a model for HA-CD44-mediated PKC (Protein Kinase C) activation in the regulation of chemoresistance in breast tumour cells. In this model, HA binds to CD44, promoting PKC activity and activating a protein cascade, leading to anti-apoptosis and survival of breast tumour cells (Bourguignon *et al.*, 2009). However, in this study, the molecular size of the HA polymer is not mentioned.

It would be useful to perform more apoptosis studies in order to confirm these results, and using more apoptotic markers, such as Bid and Bax. These markers are pro-apoptotic proteins and their respective levels can also be indicative of apoptosis. Bid is truncated and relocates to the mitochondria at the start of apoptosis (Luo *et al.*, 1998; Kim and Chung, 2007), while Bax is recruited to the mitochondrial membrane to repress the anti-apoptotic protein Bcl-2 and to permeabilise the membrane so cytochrome c can be released to initiate the caspase cascade (Lalier *et al.*, 2007). Cells that are undergoing programmed cell death acquire characteristic nuclear morphology, such as nuclear condensation and fragmentation (Kerr et al., 1972). Another way to visualise the induction of programmed cell death is to assess apoptotic markers using fluorescence microscopy. Although this is a non-quantitative method, through the analysis of the nuclear staining it is possible to observe the different stages of nuclear disruption that occur throughout programmed cell death.

The investigation performed in this chapter indicates that HA affects the proliferation of the cells to varying degrees, but not apoptosis. Proliferation is a tightly controlled process, regulated by the checkpoints of the cell cycle. The cell cycle consists of different stages of DNA replication and division, and progression of a cell through each one is tightly regulated to prevent aberrant cells from proliferating. To determine whether the effects of HA on cell proliferation and viability are related to changes in cell cycle progression, it would be useful to examine the distribution of the cells throughout the cell cycle. This could be performed using propidium iodide (PI) and analysed by flow cytometry. PI is a fluorochrome that intercalates double-stranded nucleic acids and its signal can therefore be used to quantify cellular DNA content. The distinct phases of the cell cycle can be identified, based on relative fluorescence

intensity and hence relative DNA content, and then subsequent quantification of the number of cells within each phase can be performed.

Targeted therapieshat are designed to induce apoptosis selectively in cancer cells are currently the most promising anti-cancer strategies. These strategies aim to target and kill malignant cells with minimal or no collateral damage. Therefore, the toxicity of anti-cancer agents has to be kept to a minimum level. When this cannot be achieved, dosage is reduced. Another important factor is how the immune system deals with the targeted delivery of its potentially highly dangerous effector mechanisms (Bremer, 2006). Although HA was not shown to induce apoptosis, this compound is a biocompatible and biodegradable molecule, reported to increase the bioavailability of many drug molecules. Since proliferation of malignant cells was markedly reduced by the presence of exogenous HA_{234} and HA_{2590}, findings from this work also suggest that these polymers may be potential candidates to be used in cancer therapeutics.

3.5. CONCLUSIONS

To the present knowledge, this represents the first study were HA polymer MW has been suggested to modulate cell adhesion and differentiation of tumour-derived cell lines, with medium and large HA fragments preventing tumour cells from attaching to the surface, and consequently cells do not differentiate and acquire their normal morphology. Therefore, being suggested that the regulation of differentiation of tumour cells is dependent on HA MW. In this chapter of work it was demonstrated that the proliferation of tumour-derived cell lines is specifically HA-molecular size and phenotype dependent; with low MW stimulating increased proliferation in less invasive

cell lines, whereas a sharp decrease was observed in the most malignant cell lines growing in the presence of medium and high molecular weight fragments. Here it was also reported that piecewise nonlinear regression with three linear fragments is a good approach for the calculation of growth kinetic parameters of mammalian cell lines. Despite not being shown that HA promotes apoptosis, findings from this investigation can suggest that medium and large MW polysaccharides may be potential biopolymer candidates to be used in cancer therapeutics.

CHAPTER 4

"Science is a way of thinking much more than it is a body of knowledge" – Carl Sagan

CHAPTER 4

4. INVESTIGATION OF THE EFFECT THAT HA HAS ON THE EXPRESSION OF CD44 AND RHAMM

4.1. INTRODUCTION

As previously discussed in **Chapter 1**, the biological functions presented by hyaluronic acid are mediated through interactions with its cellular receptors: CD44 and RHAMM being the principal HA receptors. CD44 is a cell surface receptor, playing an important role in cell-cell and cell-ECM interactions (Martin *et al*., 2003). It is also involved in cell motility, migration and differentiation, functions intimately associated with the capacity of CD44 to promote cell attachment to HA (Naor *et al.*, 1997). The gene coding for human CD44 is located on the short arm of chromosome 11 location p13 (Francke *et al.*, 1983; Forsberg *et al.*, 1989a, 1989b). It is composed of at least by 20 exons, spanning approximately 60 kb (Screaton *et al.*, 1992; Borland *et al.*, 1998; Günthert, 2001). There are two groups of 10 exons each: one group comprises exons 1-5 and 16-20, being constitutively expressed and described as the standard form of the gene – CD44s; and the other group described as the variable form – CD44v – which in humans comprises exons 7-15 that can be alternatively spliced, resulting in a large number of functionally distinct isoforms (**Figure 4.1**; Tölg *et al.*, 1993). The first five exons (exon 1-5) and exons 16 and 17 are present in all CD44 isoforms, whereas exons 7-15 are subjected to alternative splicing (designated as variant exons, v2-v10; Tölg *et*

al., 1993; van Weering *et al.*, 1993; Martin *et al.*, 2003; Thorne *et al.*, 2004; see **Figure 4.1**).

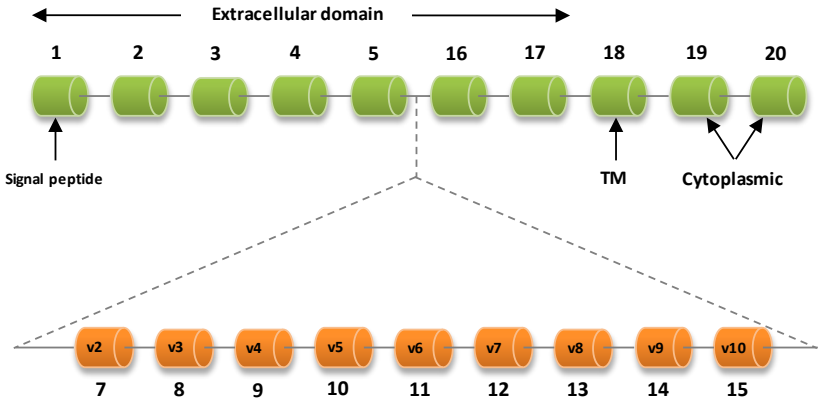

Figure 4.1 – Genomic organisation of human CD44. Orange boxes represent the 9 variant exons v2–v10 which are either all spliced out to produce the standard form of CD44 (CD44s) or combinations to produce alternatively spliced CD44 isoforms (CD44v) [Adapted from Isacke and Yarwood, 2002; Martin *et al.*, 2003].

CD44 is a family of transmembrane glycoproteins (Weber *et al.*, 1996). The standard form of CD44 (CD44s) is a type I transmembrane molecule, composed of 341 amino acids and synthesised as a 37 kDa protein that undergoes extensive post-translational modifications. The protein can be divided into three major domains: a cytoplasmic (70 aa), transmembrane (23 aa) and extracellular (248 aa). The nine exons subjected to alternative splicing (v2-v10) encode up to 381 aa. They are inserted at a single site in the membrane proximal extracellular domain between exons 5 and 16 of the RNA transcript, corresponding to a position between aa 202 and 203 (Martin *et al.*, 2003). The protein modifications following translation result in several isoforms-specific post-translational modifications and therefore to a structural diversity (Bajorath, 2000). Post-translational modifications occurs either due to glycosylation resulting in a protein of 85 kDa, or through the addition of chondroitin sulphate producing a protein

of 180-200 kDa. The cytoplasmic domain of the protein may also undergo to phosphorylation changes. Post-translational modification patterns of CD44 isoforms varies among different cell types and cellular context (Bajorath, 2000; Martin *et al.*, 2003). Consequently, post-translational modifications can modulate the binding characteristics and functional properties of CD44 (Kincade *et al.*, 1997; Lesley *et al.*, 1997; Borland *et al.*, 1998).

In contrast to the other hyaladherins, RHAMM is expressed both intracellularly and at the cell surface. Cell surface RHAMM is involved in promotion of cell motility and invasion, whereas the intracellular form is implicated in the cell cycle control and mitotic spindle formation (Turley *et al.*, 2002; Girish and Kemparaju, 2007). The single gene encoding for human RHAMM is located on chromosome 5 location 5q33.2 (Spicer *et al.*, 1995). The gene is composed of 18 exons, 2 of which can be alternatively spliced (Hardwick *et al.*, 1992; Entwiste *et al.*, 1995; Harrison and Turley, 1999). Similar to CD44, RHAMM can exist in multiple isoforms, with four different transcripts identified in humans (**Figure 4.2**; Harrison and Turley, 1999). These four RHAMM isoforms include full length RHAMM (standard RHAMM), an isoform lacking exon 4 and one lacking exon 13, and a variant lacking both exons 4 and 13 (**Figure 4.2**; Harrison and Turley, 1999; Assmann *et al.*, 1999).

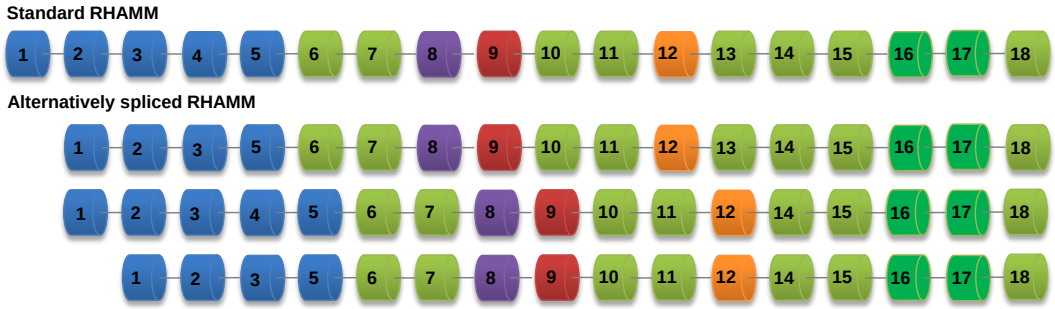

Figure 4.2 – Genomic organisation of standard and alternatively spliced isoforms of human RHAMM [Adapted from Harrison and Turley, 1999].

The constitutively expressed and most common RHAMM mRNA human transcript encodes the largest intracellular RHAMM protein with 85 kDa (**Figure 4.2**). Some isoforms are generated by alternative splicing of the longest RHAMM mRNA transcript (**Figure 4.2**; Harrison and Turley, 1999). The existence of shorter RHAMM proteins ranging 56-80 kDa, have been also reported, the N-terminal truncations of the largest protein (Harrison and Turley, 1999; Lyn *et al.*, 2001).

In a similar fashion to CD44, RHAMM protein also has the potential for post-translational modifications. RHAMM contains many potential sites for post-translational modifications, including N-glycosylation, myristoylation, and multiple serine-threonine phosphorylation sites. The effect that these modifications might have on subcellular localisation and protein interactions remains unclear (Harrison and Turley, 1999; Savani, 2010).

In **Chapter 3** it was shown that surfaces coated with HA polymers of differing molecular weights have the ability to modulate the proliferation of a number of tumour-derived cell lines. Since the biological functions presented by HA are known to be mediated via interactions with its cell receptors, this chapter of work aims to investigate whether HA polymer MW has an effect on the expression of CD44 and RHAMM, in

both standard and variant forms, in the same cell lines previously used in **Chapter 3**. One way of investigating the cellular alterations induced by an artificial or natural agent during a biological process is to look for changes in transcript expression levels; such changes may also produce an effect on expression at the protein level. Therefore, in order to perform the present investigation, both transcriptional and translational studies have been carried out. Transcriptional studies focused upon the presence of mature RNA - mRNA. Thus, RNA was extracted from the cell lines and then reverse transcribed into complementary DNA (cDNA). This cDNA was then used as the template in a PCR reaction. Translational studies investigated the expression of CD44 and RHAMM proteins. The work presented in this chapter can be illustrated by **Figure 4.3**, summarising all the steps and techniques involved in this investigation.

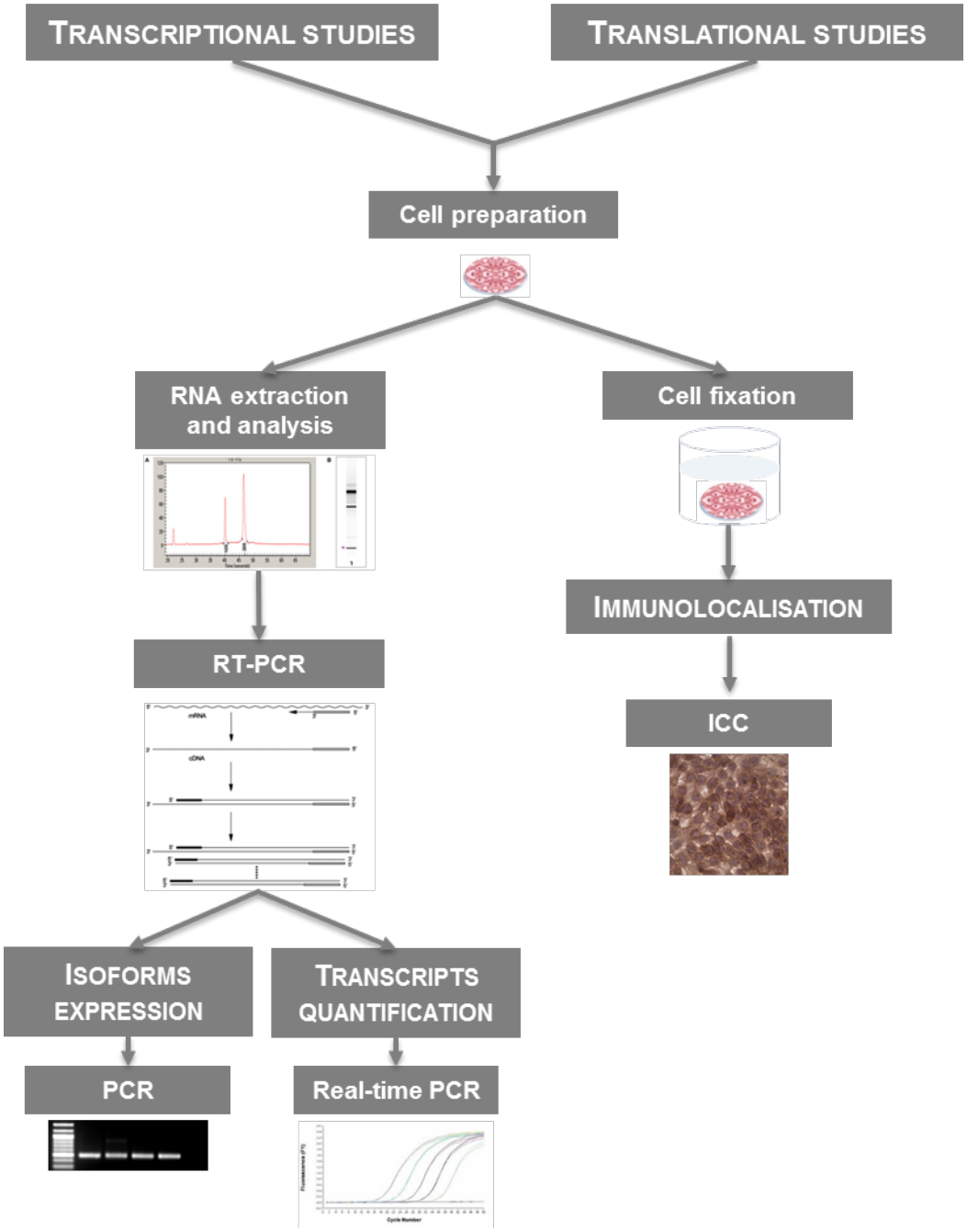

Figure 4.3 – Summary of the steps involved in the investigation carried out in Chapter 4, for both transcriptional and translational studies.

4.2. MATERIAL AND METHODS

4.2.1. CELL CULTURE

Culture and maintenance of RT112, T24, PC3 and PNT1A cell lines was performed as previously described in **Chapter 3** (**section 3.2.1.**).

4.2.2. RNA EXTRACTION

4.2.2.a. Cell preparation

RNA extraction was carried out in T75 flask for control cells and in twelve HA-coated surfaces per film condition previously placed in a 12-well plate. Culture media was removed and cells were washed with sterile PBS. 10 ml of fresh sterile PBS were added to the flask and cells were detached from the surface using a cell scraper (Fisher, UK). The PBS was then removed and placed in a 15 ml centrifuge tube and centrifuged at 307 g at 4ºC for 5 minutes. The supernatant was discarded and the cells resuspended in 1 ml of sterile PBS. This was then transferred to a micro-centrifuge tube and centrifuged again as described previously. The supernatant was discarded and the cell pellet then used for the total RNA extraction.

4.2.2.b. Synopsis of PureLink™ RNA Mini Kit protocol

Total RNA was extracted using PureLink™ RNA Mini Kit (Invitrogen, Paisley, UK) according to the manufacturer's instructions. Briefly, a lysis buffer containing guanidine isothiocyanate and 2-mercaptoethanol was added to the cell pellet and lysate was passed through an 18 gauge needle. Nucleic acids were precipitated in 70% ethanol and then cell homogenate transferred to a spin column, and washed a number of times to remove impurities. This was followed by a centrifugation to remove the ethanol mixture. The RNA allowed to dry and then resuspended in 30 µl of RNase-free water.

4.2.2.c. RNA quantification and integrity analysis

The purified total RNA quantification was performed using Picodrop spectrophotometer (Picodrop Limited, United Kingdom).

RNA integrity was assessed using Experion Automated Electrophoresis System (Bio-Rad, UK) according to the manufacturer's instructions. This method applies combination of microfluidic separation technology and sensitive fluorescent sample detection to perform a rapid and automated analysis of RNA. All gel-based electrophoretic steps, including sample separation, staining, de-staining, imaging, band detection and data analysis, are automatically performed in a RNA chip to generate reproducible separation and quantitative results. In this study, RNA analysis was performed using RNA StdSens analysis kit. The RNA quality indicator (RQI) classification generated by Experion system returns a number between 10 (intact RNA)

and 1 (highly degraded RNA). RQI values ranged 7.4-10, meaning that all RNA samples presented high quality and integrity (see **Appendix XV**).

4.2.3. cDNA PRODUCTION BY REVERSE TRANSCRIPTION (RT)

cDNA production was carried out using a cDNA cycle kit (Invitrogen, Paisley, UK), according to the manufacturer's instructions. RNA from cell extraction was mixed with 1 µl of random-hexamer primers and 2 µl of dNTP mix and RO water for a final volume of 12 µl. This was incubated at 65ºC for 10 minutes before being placed on ice for 2 minutes. Then an RT master mix (**Table 4.1**) was added to the previously described mix. This mix (20 µl in total) was then incubated at 25ºC for 10 min, 50ºC for 50 min, followed by a final step of 85ºC for 5 minutes.

Table 4.1– RT master mix for cDNA production.

	Reaction mix	**Volume (µl)**	**Final concentration**
5x	cDNA synthase buffer	4.0	2.5x
0.1 M	DTT	1.0	12.5 mM
40 U/µl	RNase Out	1.0	5 U
15 U/µl	Cloned AMV RT	1.0	1.88 U
	DEPC H_2O	1.0	
	Total	8.0	

For the construction of Real-Time PCR standard curves, 2 µg of total RNA were used, whereas 1 µg of total RNA was used for Real-Time PCR target gene expression analysis. Between 1-2 µg of total RNA were used for PCR.

4.2.4. PCR

cDNA from the above cycle was used in PCR reactions. For the amplification reaction mixes, Taq PCR Core Kit (Qiagen, UK) was used. The composition of PCR mastermix is shown in **Table 4.2**.

Table 4.2 – Mastermix composition used in PCR reactions.

	Reaction mix	Volume (µl)	Final concentration
10x	PCR buffer	5.0	1x
10 mM	dNTPs	1.0	0.2 mM
25 mM	$MgCl_2$	1.0	0.5 mM
10 mM	F primer	1.0	0.2 mM
10 mM	R primer	1.0	
5 U/µl	Taq DNA polymerase	0.5	2.5 U
	DEPC H_2O	38.5	
	cDNA	2.0	
	Total	50.0	

The primer pair (P1/P4) used in the standard amplification of CD44 (Goodison *et al.*, 1997) amplifies from exon 3 to exon 17, thereby encompassing the whole variant region. A positive result from CD44 standard amplification was indicated by the presence of a number of bands, the smallest of which is 482 bp. Regarding CD44 variants amplification, exon link PCR assay was used. Exon link assay is a PCR-based assay that allows the examination of CD44 exon splicing, focusing upon splicing at the standard/variant exon border (Goodison *et al.*, 1997). This technique uses the standard exon-anchored primer (P1) at exon 3 and a second primer for a particular standard/variant junction between exon 5 and one of the variant exons 7-14 (**Figure**

4.4). Reverse primers used are designated as follows: 5/7, 5/8, 5/9, 5/10, 5/11, 5/12, 5/13 and 5/14. A positive result of variants amplification is a product of 348 bp (Goodison *et al.*, 1997).

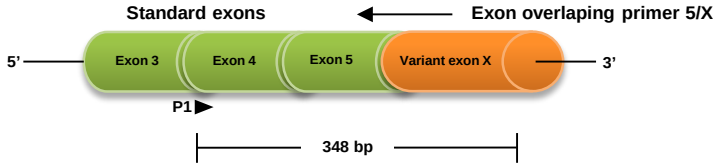

Figure 4.4 – Schematic diagram of the exon link assay design. PCR is performed using the standard exon-anchored primer (P1) at exon 3 and a second primer for a particular standard/variant junction between exon 5 and one of the variant exons 7-14 [Adapted from Goodison *et al.*, 1997].

For the amplification of RHAMM standard form ($RHAMM^{FL}$)**,** a primer pair was designed for exon 7 and exon 11, and therefore encompassing the common region for all the variants. $RHAMM^{-48}$ corresponds to the isoform lacking exon 4, and the primers were designed for amplifying the region encompassing exons 1 to 7. $RHAMM^{-147}$ corresponds to the variant lacking exon 13, and primer pair was designed for the amplification of exons 11 to 16. Positive results correspond to a product amplification of 571 bp for $RHAMM^{FL}$, 646 bp for $RHAMM^{-48}$ and 677 bp for $RHAMM^{-147}$ (Crainie *et al.*, 1999).

Positive and negative controls were included in each reaction. A negative control included everything within the PCR mastermix except the cDNA, to ensure that no contamination was present. β-actin amplification was used as positive control, since it is an abundant protein within eukaryotic cells and therefore is readily detectable by PCR via its mRNA.

CD44 standard and exon link assay, and β-actin PCR amplifications were performed in a DNA Engine (PTC200) Peltier Thermo Cycler (MJ Research, USA) programmed for one initial cycle at 95ºC for 1 minute, followed by 29 cycles at 94ºC for 1 minute, 55ºC for 1 minute and 72ºC for 1 minute. This was followed by 1 cycle at 94ºC for 1 minute, 55ºC for 1 minute and a final extension step at 72ºC for 5 minutes. For $RHAMM^{FL}$ and $RHAMM^{-48}$ amplifications thermocycler was programmed for one initial cycle at 95ºC for 1 minute, followed by 35 cycles at 95ºC for 1 minute, 60ºC for 1 minute and 72ºC for 1 minute, and a final extension step at 72ºC for 5 minutes. For $RHAMM^{-147}$ the same cycling parameters were used, but 58ºC for the annealing temperature.

PCR products were separated by 1.5% agarose gel electrophoresis in 1% TAE buffer, at 80 V for 70 minutes, stained with ethidium bromide and visualised on an UV light transluminator. GeneGenius Bio Imaging System (Syngene, USA). The size of the PCR fragments was estimated comparing to a molecular weight marker (100 bp ladder Promega, UK).

Primer sequences can be found in **Appendix XIII.**

4.2.5. REAL-TIME PCR

For the study of the expression of CD44, a primer pair was designed for standard CD44 form flanking exons 2 and 3. Regarding RHAMM standard form, a primer pair was designed flaking exons 5 to 7. Primers were designed using Primer 3.0 software (Rozen and Skaletsky, 2000), and a BLAST (Altschul *et al.*, 1990) was performed in the

Nacional Center for Biotechnology Information (NCBI), in order to ensure that the proposed primers were only specific to the target sequences. Normaliser genes need to be evaluated and validated regarding the expression stability in each tissue type; hence, ABL1 was selected to be used as housekeeping gene for prostate cell lines (Nna *et al.*, 2010) and HSPCB for bladder cell lines (Anderson *et al.*, 2004). The sequences of the primers used in real-time PCR are shown in **Appendix XIV**.

PCR reactions were performed in a Bio-rad CFX96 thermal cycler (Biorad, UK) programmed for one initial cycle at 95ºC for 15 minutes, followed by 45 cycles at 95ºC for 15 seconds, 60.1ºC for 30 seconds and 72ºC for 30 seconds, and a final melting curve analysis 65ºC-95ºC with an increment of 0.5ºC for 5 seconds. Product formation was detected by incorporation of SYBR green (QuantiTect SYBR Green PCR Kit, Qiagen, UK). The composition of the real-time PCR mastermix is shown in **Table 4.3**.

Table 4.3 – Reaction mixture used in real-time PCR.

	Reaction mix	Volume (µl)	Final concentration
10x	PCR buffer	5.0	5x
10 mM	F primer	0.5	0.5 mM
10 mM	R primer	0.5	0.5 mM
	DEPC H_2O	3.0	
	cDNA	1.0	
	Total	10.0	

4.2.5.a. Data analysis

In the present study relative quantification of gene expression was performed in order to evaluate expression of CD44 and RHAMM using Pfaffl method (Pfaffl, 2001).

In this method, the relative expression ratio (*R*) of a target gene is calculated based on *E* and the C_t deviation of an unknown sample versus a control, and expressed in comparison to a reference gene (**Equation 4.1**). The preparation of standard curves is only required to determine the amplification efficiencies of the target and housekeeping genes in an initial experiment (Pfaffl, 2001).

$$R = \frac{(E_{target})^{\Delta Ct_{target}(control-sample)}}{(E_{reference})^{\Delta Ct_{reference}(control-sample)}} \quad (\textbf{Equation 4.1})$$

Where E_{target} is the real-time PCR efficiency of target gene transcript; $E_{reference}$ is the real-time PCR efficiency of a reference gene transcript. Efficiencies can be calculated according to **Equation 4.2**:

$$E = 10^{[-1/slope]} \quad (\textbf{Equation 4.2})$$

C_t deviations are calculated using **Equations 4.3** and **4.4**:

$$\Delta C_{t_{target}} = C_t \text{ control target gene} - C_t \text{ sample target gene} \quad (\textbf{Equation 4.3})$$

$$\Delta C_{t_{reference}} = C_t \text{ control reference gene} - C_t \text{ sample reference gene} \quad (\textbf{Equation 4.4})$$

The fold change in expression ratios and statistical analysis for quantitative PCR were performed by group-wise comparison based on PCR efficiencies and the mean crossing point of the amplification curve with the threshold deviation between sample and control group using Relative Expression Software Tool - REST© (MCS version)

using randomisation tests with pair-wise reallocation (Pfaffl *et al.*, 2002). This type of test makes no assumptions about distribution of the data, thus allowing for more flexibility than non-parametric ranked tests. Significance was set at $p \leq 0.05$. Graphical representations are presented in logarithmic scale (power of 2).

For the calculation of the RHAMM/CD44 expression ratio, Pfaffl equation was simplified as **Equation 4.5**:

$$R = \frac{(E_{RHAMM})^{\Delta Ct_{RHAMM}(sample)}}{(E_{CD44})^{\Delta Ct_{CD44}(sample)}} \qquad (\textbf{Equation 4.5})$$

Statistical analysis was performed using GraphPad Prism 5.0 software. Analysis of variance (ANOVA) was performed using Kruskal-Wallis test (for nonparametric, and not assuming Gaussian distribution) and Dunns' multiple comparison test. A probability value of < 0.05 was considered statistically significant. Graphical representations are presented in logarithmic scale (power of 2).

4.2.6. IMMUNOCYTOCHEMISTRY

Cells required for immunocytochemistry (ICC) were treated as if for passage and resuspended in fresh media. Control cells were grown in slide flasks with a detachable polystyrene slide as their base (Nunc, Denmark). Cells were seeded in these flasks and were grown until the base of flask was covered by a monolayer of cells. The media was removed and cells were washed in cold sterile PBS, before detaching the flasks from the slides. These slides were then immersed in cold methanol for 10 minutes to fix the cells

and left to dry overnight at 4ºC. Slides were wrapped in foil and stored at -20ºC until required. The same protocol was followed for cells growing on the coverslips coated with hyaluronic acid.

Slides and coverslips were removed from storage at -20ºC and allowed to stand at room temperature for 10 minutes, before being divided into sections using an ImmEdge pen (Vector Laboratories, Peterborough, UK). To block non-specific antibody reactions, 50µl/grid of a 1:5 dilution of goat serum (Biosera Limited, UK) in PBS was applied to the slides, which were then incubated for 1 hour at room temperature in a humid atmosphere. Blocking solution was removed and slides were incubated with 50µl of primary antibody (**Table 4.4**) overnight at 4ºC in a humid atmosphere.

Slides were then incubated 30 minutes at room temperature followed by three washes in PBS of 5 minutes each. This was followed by incubation with secondary antibody (**Table 4.4**) for 1 hour at room temperature in humid atmosphere followed by three 15 minutes washes in PBS. Slides were incubated at room temperature for 30 minutes in ABC (avidin-biotin conjugate), which represents the first stage of the detection system. The ABC (Dako) was made up 30 minutes in advance, consisting in equal amounts of solution A (5 µl) and solution B (5 µl) with 1000 µl of PBS. Slides were then washed three 5 minutes in PBS, and incubated in DAB (diaminobenzidine) solution for 30 minutes. Slides were then washed in water and conterstained in haematoxylin for 30 seconds, followed by washing in running water to produce the true colour of the counterstaining. Slides were then mounted using a glycerol based mountant (Vector, UK) and analysed using a Zeiss microscope with a Zeiss axiocam

camera, and using a Zeiss axiansian software. Staining was evaluated using x800 magnification.

Table 4.4 – Primary and secondary antibodies used in immunocytochemistry.

Primary Antibody	Dilution	Secondary antibody (biotinylated)	Dilution
CD44 mAb (AbD Serotec, UK)	1:100	Rabbit anti-mouse (Dako-Cytomation, UK)	1:200
CD168 mAb (Abcam, UK)	1:25		

Antibodies were diluted in PBS containing 1% of goat serum.

4.3. RESULTS

4.3.1. CD44 AND RHAMM STANDARD FORMS EXPRESSION

4.3.1.a. CD44 expression

In order to confirm the expression of CD44, a screening of CD44 was first carried out among the controls of all four cell lines (**Figure 4.5**). The four cell lines generated an amplification pattern, albeit showing different patterns. All cell lines express a common band of approximately 470 bp. In RT112 cells it can be seen the presence of a number of bands, the lowest of which is approximately 470 bp and the highest approximately 1500 bp. For T24 only a band can be seen (470 bp), whereas for PNT1A the presence of two bands (700 bp and 470 bp) can be observed. In PC3 cells three bands of approximately 850 bp, 650 bp and 470 bp were amplified. The band of approximately 470 bp corresponds to the standard form of CD44, and the other bands

representing CD44 variant forms. For RT112 cells the CD44 standard form band appears to be less expressed comparatively to the other cell lines.

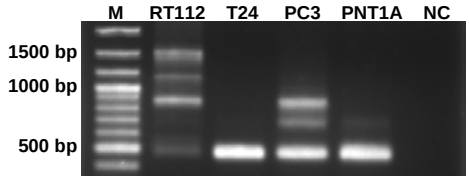

Figure 4.5 – Amplification pattern generated by CD44 standard form using P1-P4 primers for RT112, T24, PC3 and PNT1A cell lines. Pattern marker of 100 bp (M); negative control (NC).

After confirmation of the expression of CD44 in the control cells, the analysis of the expression of this transcript was also performed in those cells growing on HA structured surfaces (**Figures 4.6** to **4.9**).

RT112 cell line

Figure 4.6 presents the amplification pattern generated by CD44 standard form for RT112 cell line. It can be seen that CD44 is expressed in RT112 cells growing in all four HA structured surfaces, with the same pattern generated by control cells amplified.

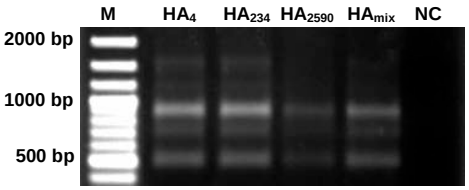

Figure 4.6 – Amplification pattern generated by CD44 standard form using P1-P4 primers for RT112 cells growing on HA-coated surfaces. Pattern marker of 100 bp (M); negative control (NC).

T24 cell line

Figure 4.7 shows the amplification pattern generated by P1-P4 primers for T24 cell line. It can be seen that T24 cells growing on HA-coated surfaces express CD44 standard transcript, and having the same amplification pattern from the control (a band of approximately 470 bp). Cells growing on structured surfaces appear to have similar CD44 expression.

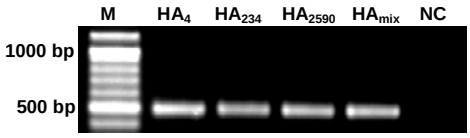

Figure 4.7 – Amplification pattern generated by CD44 P1-P4 primers for T24 cells growing on HA-coated surfaces. Pattern marker of 100 bp (M); negative control (NC).

PC3 cell line

Figure 4.8 shows the amplification pattern generated by CD44 P1-P4 primers for PC3 cell line. As it can be seen CD44 is expressed in cells growing on all four different structured surfaces and showing the same amplification pattern from the control. Stronger bands appear to be amplified in PC3 cells growing on HA_{2590} and HA_{mix} surfaces. In addition, in all four treatments the bands corresponding to CD44 isoforms appear to be less expressed when comparing to the control (see **Figure 4.5**).

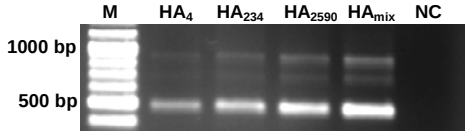

Figure 4.8 – Amplification pattern generated by CD44 P1-P4 primers for PC3 cells growing on HA-coated surfaces. Pattern marker of 100 bp (M); negative control (NC).

PNT1A cell line

In **Figure 4.9** is shown the amplification pattern generated by CD44 P1-P4 primers for PNT1A cell line growing on the HA-coated surfaces. As it can be observed CD44 shows the same amplification pattern from the control. However, interestingly, the band corresponding to the CD44 standard form (470 bp) appears to be less expressed and the band of approximately 700 pb corresponding to variant form being more expressed comparatively to control cells (see **Figure 4.5**). The 700 bp band also appears to be more expressed on PNT1A cells growing on HA_{2590} and HA_{mix}.

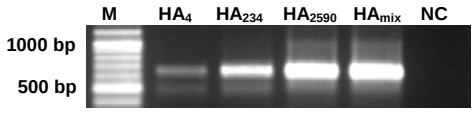

Figure 4.9 –Amplification pattern generated by CD44 P1-P4 primers for PNT1A cells growing on HA-coated surfaces. Pattern marker of 100 bp (M); negative control (NC).

4.3.1.b. RHAMM expression

A RHAMM standard form ($RHAMM^{FL}$) screening was carried among all cell lines in order to verify the presence or absence of this gene (**Figure 4.10**). As it can be observed from **Figure 4.10**, $RHAMM^{FL}$ is highly expressed in all four cell lines, showing a band of approximately 520 bp.

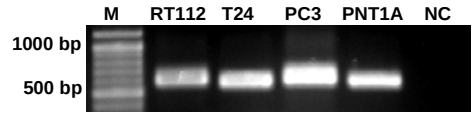

Figure 4.10 – Amplification pattern generated by $RHAMM^{FL}$ primers for RT112, T24, PC3 and PNT1A control cells. Pattern marker of 100 bp (M); negative control (NC).

After confirmation of the presence of RHAMM in control cells, the same investigation was performed in those cells growing on HA structured surfaces (**Figures 4.11** to **4.14**).

RT112 cell line

From **Figure 4.11** it can be seen that $RHAMM^{FL}$ was expressed in RT112 cells growing in all four HA-coated surfaces, presenting similar amplification to the control (see **Figure 4.11**).

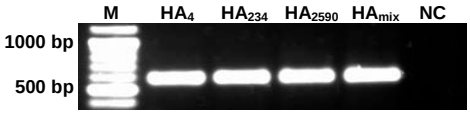

Figure 4.11 – Amplification pattern generated by $RHAMM^{FL}$ primers for RT112 cells growing on HA-coated surfaces. Pattern marker of 100 bp (M); negative control (NC).

T24 cell line

In **Figure 4.12** is presented the amplification pattern generated by $RHAMM^{FL}$ primers, being observed that RHAMM standard form is expressed in T24 growing in the presence of HA.

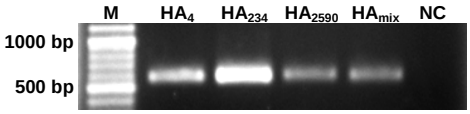

Figure 4.12 – Amplification pattern generated by $RHAMM^{FL}$ primers for T24 cells growing on HA-coated surfaces. Pattern marker of 100 bp (M); negative control (NC).

PC3 cell line

In **Figure 4.13** it can be seen that RHAMM standard form was amplified in PC3 cells growing in the presence of HA, appearing to have similar expression levels to the control (see **Figure 4.13**).

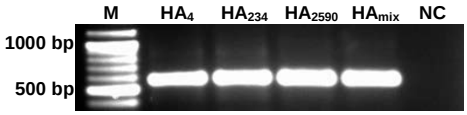

Figure 4.13 – Amplification pattern generated by RHAMM^{FL} primers for PC3 cells growing on HA-coated surfaces. Pattern marker of 100 bp (M); negative control (NC).

PNT1A cell line

In **Figure 4.14** it can be observed that RHAMM^{FL} is amplified in PNT1A cells growing on all four HA structured surfaces

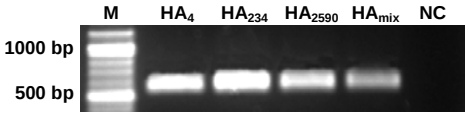

Figure 4.14 – Amplification pattern generated by RHAMM^{FL} primers for PNT1A cells growing on HA-coated surfaces. Pattern marker of 100 bp (M); negative control (NC).

4.3.1.c. Quantitative CD44 and RHAMM expression

Real-time PCR (qPCR) is considered the gold-standard technique for measuring gene expression. It is a quantitative technique that monitors the accumulation kinetics of a specific PCR product, recognised by a specific fluorescent dye. Quantification of

cDNA can be achieved by determining, for each sample, the specific cycle number at which the detection of PCR product reaches an arbitrary threshold value; this value must represent the PCR's exponential phase across all relevant samples in the reaction. In the present study relative quantification of gene expression was performed in order to evaluate expression of CD44 and RHAMM. In **Figures 4.15 - 4.18** is shown the CD44 and RHAMM transcript expression levels in all four cell lines.

RT112 cell line

Results from qPCR assays normalised to HSPCB, showed that both CD44 and RHAMM transcripts are down-regulated in RT112 cells growing on HA-coated surfaces. CD44 appears to be down-regulated to a greater level in cells growing on HA_4 surfaces, with a greater RHAMM decrease in those cells growing in the presence of HA_{mix} (**Figure 4.15**). However, the expression of CD44 and RHAMM in cells growing on HA_{234} are not significantly down-regulated when compared to controls.

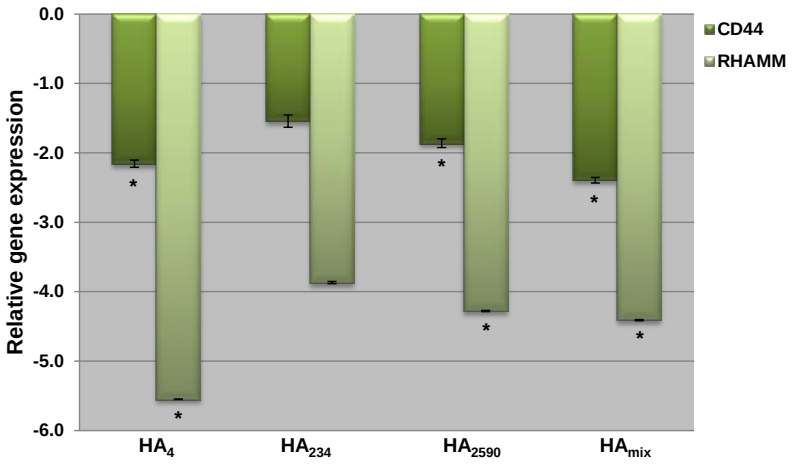

Figure 4.15 – Change in expression of CD44 and RHAMM transcript (expressed as relative gene expression) normalised to HSPCB in RT112 cell line. Data represent the mean ± S.D. of triplicate PCR observations. Cells growing on HA-coated surfaces were compared to control cells using *Pair-Wise Fixed Reallocation Randomization Test*© with significance set at $p \leq 0.05$. The conditions linked by (*) are statistically different to the control, the other one being similar.

T24 cell line

From the CD44 and RHAMM expression normalised to HSPCB in T24 cell line it can be seen that both transcripts are up-regulated for cells growing on HA-coated surfaces. The expression of both transcripts appears to be up-regulated to a greater degree in those cells growing on HA_{mix}, with a lower increased level in cells growing in the presence of HA_{234}. Nevertheless, the cell receptors expression is not significantly up-regulated when compared to the control (**Figure 4.15**).

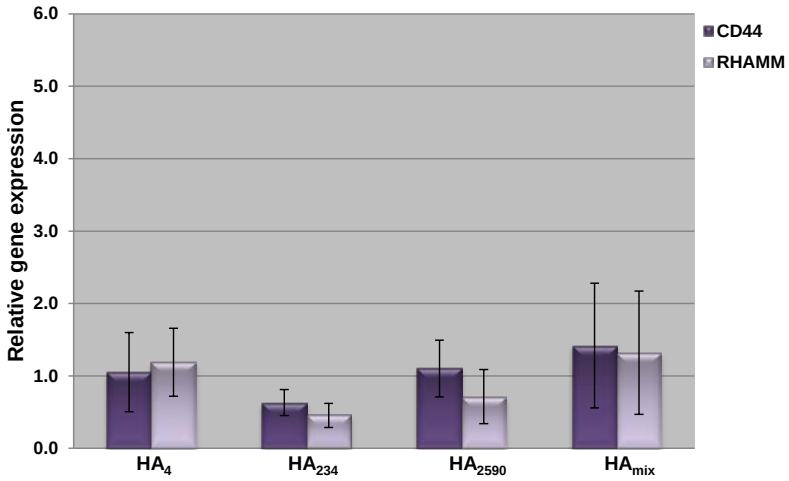

Figure 4.16 – Change in expression of CD44 and RHAMM transcript (expressed as relative gene expression) normalised to HSPCB in T24 cell line. Data represent the mean ± S.D. of triplicate PCR observations. Cells growing on HA-coated surfaces were compared to control cells using *Pair-Wise Fixed Reallocation Randomization Test*© with significance set at $p \leq 0.05$. The conditions linked by (*) are statistically different to the control, the other one being similar.

PC3 cell line

In **Figure 4.17** is shown the CD44 and RHAMM expression normalised to ABL1 in PC3 cell line. It can be observed that CD44 and RHAMM transcript levels are significantly down-regulated for PC3 cells growing on HA structured surfaces. CD44 transcript levels have a greater decrease in cells growing on HA_{2590} surfaces, and lower decrease in those cells growing in the presence of HA_{234}. Regarding RHAMM, this transcript is down-regulated to a greater level in PC3 cells growing on HA_{234} surfaces, and having lower down-regulation level in cells growing on HA_4 surfaces (**Figure 4.17**).

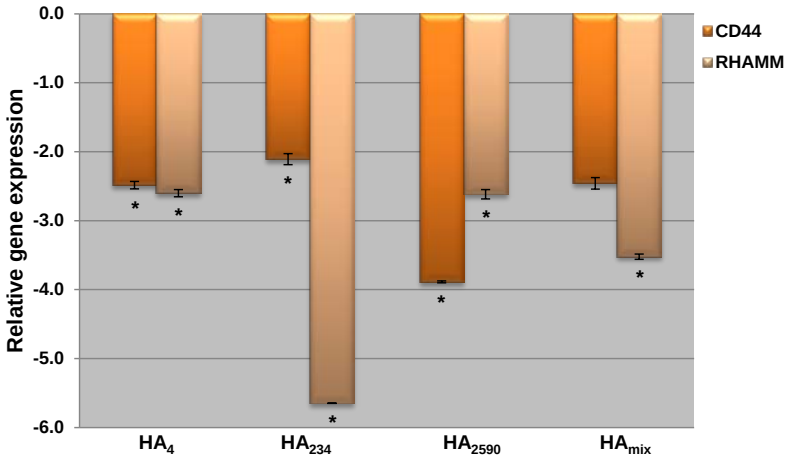

Figure 4.17 – Change in expression of CD44 and RHAMM transcript (expressed as relative gene expression) normalised to ABL1 in PC3 cell line. Data represent the mean ± S.D. of triplicate PCR observations. Cells growing on HA-coated surfaces were compared to control using *Pair-Wise Fixed Reallocation Randomization Test*© with significance set at $p \leq 0.05$. The conditions linked by (*) are statistically different to the control, the other one being similar.

PNT1A cell line

In **Figure 4.18** is presented the CD44 and RHAMM expression normalised to ABL1 in PNT1A cell line. As it can be observed, CD44 transcript is up-regulated in PNT1A cells growing on HA structured surfaces. CD44 is up-regulated to a greater level in PNT1A cells growing on HA_{mix} surfaces, with a lower up-regulation seen in those cells growing in the presence of HA_{234}. However, significant up-regulation is only seen on PNT1A cells growing on HA_{mix}-coated surfaces. Regarding RHAMM, this transcript is up-regulated in cells growing on HA_4 and HA_{234}-coated surfaces, and down-regulated in those cells growing on HA_{2590} and HA_{mix} surfaces. This transcript is up-regulated to a greater degree in cells growing on HA234, with a greater down-regulation seen for cells growing on HA_{mix}. Nevertheless, no significant expression is seen in RHAMM regulation when compared to the control.

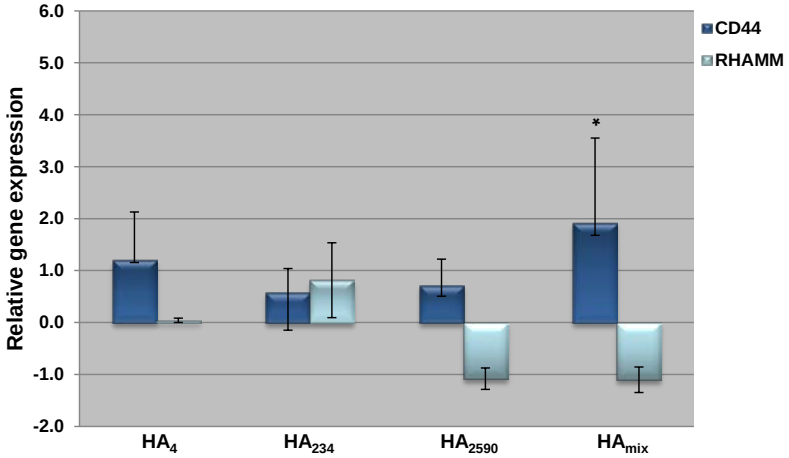

Figure 4.18 – Change in expression of CD44 and RHAMM transcript (expressed as relative gene expression) normalised to ABL1 in PNT1A cell line. Data represent the mean ± S.D. of triplicate PCR observations. Cells growing on HA-coated surfaces were compared to control cells *Pair-Wise Fixed Reallocation Randomization Test*© with significance set at $p \leq 0.05$. The conditions linked by (*) are statistically different to the control, the other one being similar.

Figures 4.19 and **4.20** present graphs summarising the expression of CD44 and RHAMM transcripts in all four cell lines. In **Figure 4.19** is shown the expression of CD44, being observed that CD44 transcript is up-regulated in the less invasive cell lines (T24 and PNT1A), while a down-regulation is seen in the most malignant cells (RT112 and PC3). From **Figure 4.20** it can be observed that RHAMM transcript is also down-regulated in RT112 and PC3 cells, and up-regulated in T24 and PNT1A cell lines; with the exception of PNT1A cells growing on HA_{2590} and HA_{mix} structured surfaces.

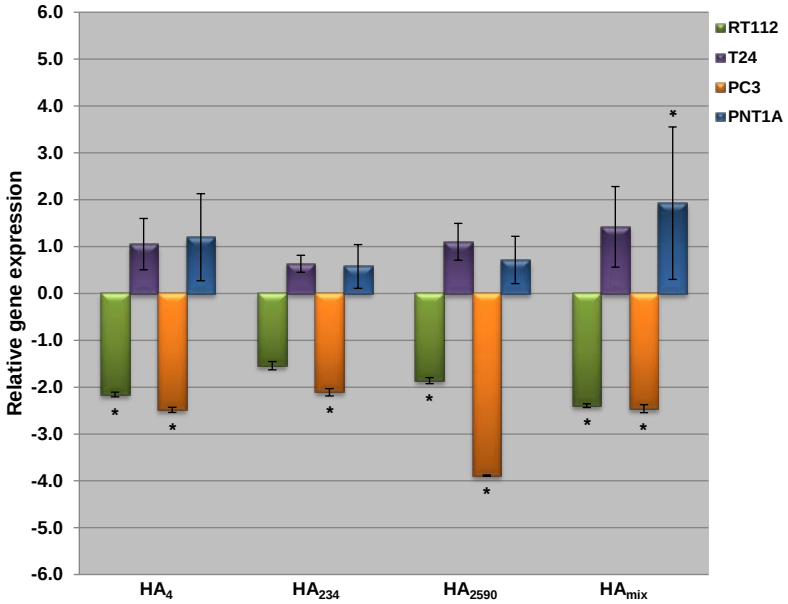

Figure 4.19 – Change in expression of CD44 transcript (expressed as relative gene expression) normalised to the correspondent housekeeping gene in all four cell lines. Data represent the mean ± S.D. of triplicate PCR observations. Cells growing on HA-coated surfaces were compared to control cells using *Pair-Wise Fixed Reallocation Randomization Test*© with significance set at $p \leq 0.05$. The conditions linked by (*) are statistically different to the control, the other one being similar.

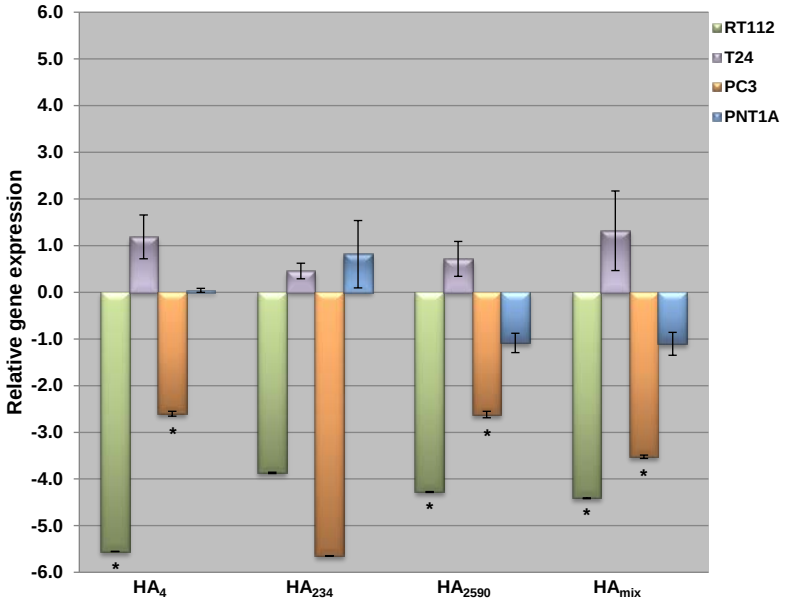

Figure 4.20 – Change in expression of RHAMM transcript (expressed as relative gene expression) normalised to the correspondent housekeeping gene in all four cell lines. Data represent the mean ± S.D. of triplicate PCR observations. Cells growing on HA-coated surfaces were compared to control cells using *Pair-Wise Fixed Reallocation Randomization Test*© with significance set at $p \leq 0.05$. The conditions linked by (*) are statistically different to the control, the other one being similar.

In **Figure 4.21** is presented the RHAMM/CD44 transcript expression ratio.

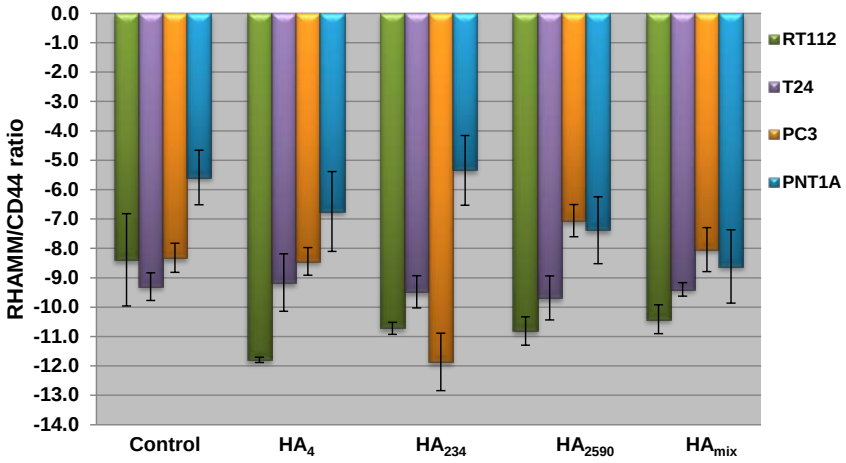

Figure 4.21 – RHAMM/CD44 transcripts ratio in all four cell lines. Data represent the mean ± S.D. of triplicate PCR observations.

From figure above it can be seen that CD44 is more expressed than RHAMM in all four cell lines and all treatments. The RHAMM/CD44 ratio was significantly decreased to a greater degree in RT112 cells growing in the presence of HA_4 comparatively to control and those cells growing in the presence of HA_{mix}. No significant difference between treatments was found in T24 cell lines. PC3 cells growing on HA_{234} surfaces showed a decreased ratio comparatively to control cells and those growing on HA_4 and HA_{2590} surfaces. The RHAMM/CD44 ratio was also significantly decreased to a greater level in PNT1A cells growing in the presence of HA_{mix} when compared to the control and cells growing in the presence of HA_{234} (**Figure 4.21**).

Regarding RHAMM/CD44 ratio no pattern was observed. RHAMM/CD44 transcript ratio in PNT1A control cells showed a significantly lower decrease than the rest of cell lines. For cells growing on HA_4-coated surfaces, the transcript ratio was seen to be decreased to a greater level in RT112 comparatively to the other cell lines; with a

lower ratio decrease seen for PNT1A cells. Again, RHAMM/CD44 ratio was found to be decreased to a lower level in PNT1A cells growing in the presence of HA_{234}; with a greater decreased seen for PC3 cell line growing on HA_{234}-coated surfaces. RT112 cells growing in the presence of HA_{2590} were found to have the transcript ratio decreased to a greater level comparatively to the other cell lines. No significant difference was found for cell lines growing on HA_{mix}-coated surfaces (**Figure 4.21**).

4.3.2. CD44 AND RHAMM ISOFORMS EXPRESSION

4.3.2.a. CD44 expression

After confirmation of the expression of CD44 standard form in the control cells, exon link PCR assay was subsequently performed to study the presence of CD44 variant exons on all four cell lines and cells growing on HA-coated surfaces (**Figures 4.22** to **4.25**).

RT112 cell line

Figure 4.22 presents the amplification pattern generated by the exon link assay for RT112 cell line. Lane 2 shows a standard CD44 amplification pattern, using primers P1 and P4, used here as a positive control. Lanes 3-10 indicate the presence or absence of exon junctions between 5/7, 5/8, 5/9, 5/10, 5/11, 5/12, 5/13 and 5/14. Lane 11 corresponds to β-actin amplification used as positive control to ensure integrity of

cDNA, and lane 12 the negative control. Thus it can be seen that RT112 cell line expresses exon junctions between standard exon 5 and variant exons 7, 8, 9, 11, 12, 13 and 14. This is demonstrated by the presence of a band of approximately 348 bp in each relevant lane. Lane 6 corresponds to exon junction 5/10, being observed an amplification of approximately 680 bp. However, this is an unspecific and unexpected amplification, and the reason for its present remains unclear. The band amplified on lane 9, corresponding to CD44v8 (exon junction 5/13), presented the strongest amplification expression. Conversely, the amplification of CD44v7 and v9 (lanes 8 and 10) presented feint bands (**Figure 4.22**).

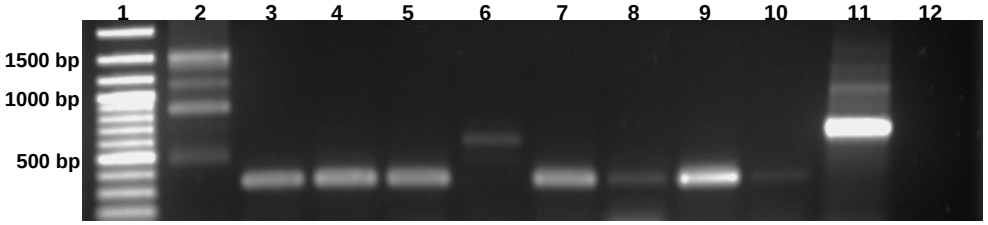

Figure 4.22 – Amplification pattern of RT112 exon link assay. Lanes numbered 1-12 from left to right. Pattern marker of 100 bp (1), P1/P4 primers (2), P1/ 5/7 primers (3), P1/ 5/8 primers (4), P1/ 5/9 primers (5), P1/ 5/10 primers (6), P1/ 5/11 primers (7), P1/ 5/12 primers (8), P1/ 5/13 primers (9), P1/ 5/14 primers (10), β-actin primers (11), negative control (12).

T24 cell line

In **Figure 4.23** is presented the amplification result for exon link assay from T24 cell lines. It can be seen the presence of variant forms, although lesser in number than in RT112 cell line. T24 cell line showed the amplification of 5/8, 5/9, 5/11, 5/12 and 5/13 variant junctions. The band in lane 9 corresponding to exon junction 5/13 (CD44 variant 8) does not appear to be very distinct.

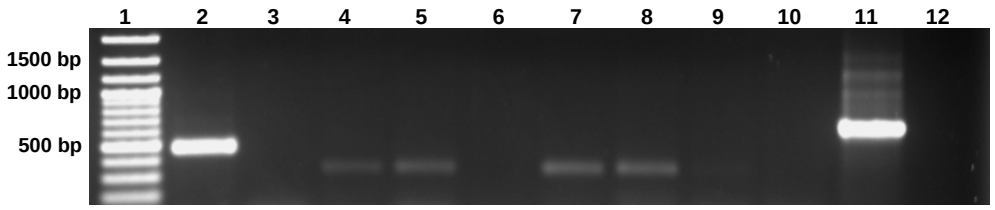

Figure 4.23 – Amplification pattern of T24 exon link assay. Lanes numbered 1-12 from left to right. Pattern marker of 100 bp (1), P1/P4 primers (2), P1/ 5/7 primers (3), P1/ 5/8 primers (4), P1/ 5/9 primers (5), P1/ 5/10 primers (6), P1/ 5/11 primers (7), P1/ 5/12 primers (8), P1/ 5/13 primers (9), P1/ 5/14 primers (10), β-actin primers (11) and negative control (12).

PC3 cell line

Figure 4.24 shows the amplification pattern generated by the exon link assay for PC3 cell line. For this cell line 5/7, 5/8, 5/9, 5/11, 5/13 and 5/14 variant exons are expressed. Two very distinct bands can be seen in lanes 7 and 9, corresponding to CD44v8 and v8 forms (exon junctions 5/11 and 5/13). Conversely, CD44v2 and v4 shown in lanes 3 and 5 appear to be feint.

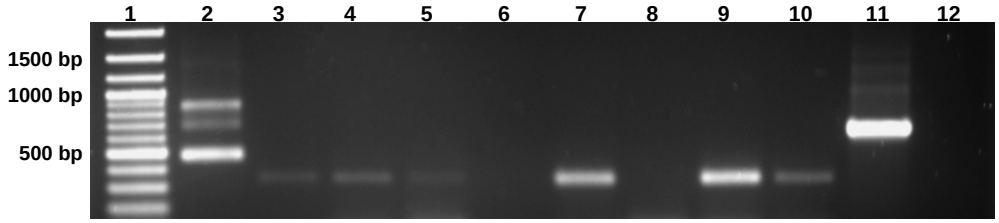

Figure 4.24 – Amplification pattern of PC3 exon link assay. Lanes numbered 1-12 from left to right. Pattern marker of 100 bp (1), P1/P4 primers (2), P1/ 5/7 primers (3), P1/ 5/8 primers (4), P1/ 5/9 primers (5), P1/ 5/10 primers (6), P1/ 5/11 primers (7), P1/ 5/12 primers (8), P1/ 5/13 primers (9), P1/ 5/14 primers (10), β-actin primers (11) and negative control (12).

PNT1A cell line

Figure 4.25 shows the amplification pattern generated by the exon link assay for PNT1A cell line. Of all four cell lines used in this investigation, PNT1A was the cell

line expressing the lowest number of variant exons. Only three out of eight variant exons were expressed: 5/8, 5/11 and 5/13. The bands amplified in lanes 4 and 9 corresponding to CD44v3 and CD44v8 are not very distinct, appearing to be very feint.

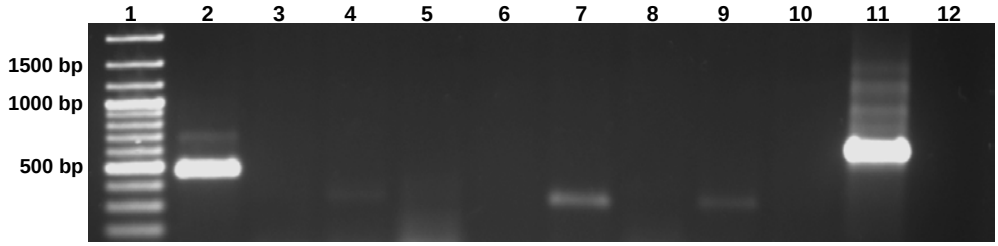

Figure 4.25 – Amplification pattern of PNT1A exon link assay. Lanes numbered 1-12 from left to right. Pattern marker of 100 bp (1), P1/P4 primers (2), P1/ 5/7 primers (3), P1/ 5/8 primers (4), P1/ 5/9 primers (5), P1/ 5/10 primers (6), P1/ 5/11 primers (7), P1/ 5/12 primers (8), P1/ 5/13 primers (9), P1/ 5/14 primers (10), β-actin primers (11) and negative control (12).

In **Table 4.5** is summarised the CD44 variants expression on the controls of all four cell lines.

Table 4.5 – Summary of the CD44s and CD44v forms expression on RT112, T24, PC3 and PNT1A cell lines. + presence of the form, - absence of the form.

	CD44s	CD44v2 (5/7)	CD44v3 (5/8)	CD44v4 (5/9)	CD44v5 (5/10)	CD44v6 (5/11)	CD44v7 (5/12)	CD44v8 (5/13)	CD44v9 (5/14)
RT112 control	+	+	+	+	-	+	+	+	+
T24 control	+	-	+	+	-	+	+	+	-
PC3 control	+	+	+	+	-	+	-	+	+
PNT1A control	+	-	+	-	-	+	-	+	-

The semi-quantitative CD44 expression results within cell lines investigated in this study revealed the expression of a number of variant exon junctions. For bladder models, seven out of eight variants were found to be present in RT112 cell line (v2, v3,

v4, v6, v7, v8 and v9); with the presence of five variants in T24 cell line (v3, v4, v6, v7 and v8). Regarding prostate models, in PC3 cell line six out of eight possible variants of are expressed: v2, v3, v4, v6, v8 and v9; whereas only there variants (v3, v6 and v8) were found to be expressed in PNT1A cell line. It was also noticed the presence of v7 (junction 5/12) only be present in RT112 and T24 cells, being absent in prostate cell lines. It was also observed that v2 and v9 isoforms are only present in RT112 and PC3 cell lines. In addition, CD44v4 appears to be expressed in all cell lines, except in PNT1A cells; with the absence of CD44v5 in all four cell lines (**Table 4.5**).

4.3.2.b. CD44 isoforms expression on cells growing on HA-coated surfaces

After confirmation of the presence of CD44 standard form on HA-coated surfaces and the investigation of variant forms on control cells, CD44 exon link PCR was also carried out on cell lines growing on the HA structured surfaces. Results from the exon link PCR are summarised in **Tables 4.6** to **4.9**.

RT112 cell line

In **Table 4.6** is presented a summary of CD44 variants expressed in RT112 cells growing on HA-coated surfaces. As it can be seen, RT112 cells growing on HA surfaces appear to have similar CD44 variants pattern expression. Although, conversely to control cells CD44 v7 and v9 were not found to be present in those cells growing in the presence of HA (**Table 4.6**).

Table 4.6 – Summary of the CD44s and CD44v forms in RT112cell line. + presence of the form, - absence of the form.

	CD44s	CD44v2 (5/7)	CD44v3 (5/8)	CD44v4 (5/9)	CD44v5 (5/10)	CD44v6 (5/11)	CD44v7 (5/12)	CD44v8 (5/13)	CD44v9 (5/14)
RT112 control	+	+	+	+	-	+	+	+	+
RT112 HA_4	+	+	+	+	-	+	-	+	-
RT112 HA_{234}	+	+	+	+	-	+	-	+	-
RT112 HA_{2590}	+	+	+	+	-	+	-	+	-
RT112 HA_{mix}	+	+	+	+	-	+	-	+	-

T24 cell line

In **Table 4.7** is summarised the amplification pattern generated by CD44 variants on T24 cells. It can be observed that three variants (v3, v6 and v8) expressed in control cells do not appear to be amplified in cells growing on HA structured surfaces (**Table 4.7**).

Table 4.7 – Summary of the CD44s and CD44v forms in T24cell line. + presence of the form, - absence of the form.

	CD44s	CD44v2 (5/7)	CD44v3 (5/8)	CD44v4 (5/9)	CD44v5 (5/10)	CD44v6 (5/11)	CD44v7 (5/12)	CD44v8 (5/13)	CD44v9 (5/14)
T24 control	+	-	+	+	-	+	+	+	-
T24 HA_4	+	-	-	+	-	-	+	-	-
T24 HA_{234}	+	-	-	+	-	-	+	-	-
T24 HA_{2590}	+	-	-	+	-	-	+	-	-
T24 HA_{mix}	+	-	-	+	-	-	+	-	-

PC3 cell line

From the analysis of the results presented in **Table 4.8**, it can be seen that conversely to control cells CD44v2 and v7 are not found to be amplified in PC3 cells growing on HA-coated surfaces. In addition, v3 and v6 do not also appear to be amplified in those cells growing on HA_{234} surfaces.

Table 4.8 – Summary of the CD44s and CD44v forms in PC3 cell line. + presence of the form, - absence of the form.

	CD44s	CD44v2 (5/7)	CD44v3 (5/8)	CD44v4 (5/9)	CD44v5 (5/10)	CD44v6 (5/11)	CD44v7 (5/12)	CD44v8 (5/13)	CD44v9 (5/14)
PC3 control	+	+	+	+	-	+	-	+	+
PC3 HA_4	+	-	+	-	-	+	-	+	+
PC3 HA_{234}	+	-	-	-	-	-	-	+	-
PC3 HA_{2590}	+	-	+	-	-	+	-	+	+
PC3 HA_{mix}	+	-	+	-	-	+	-	+	+

PNT1A cell line

Table 4.9 presents the summary of the amplification of CD44 variants from PNT1A cells. As it can be observed, CD44v3 and v8 appear do not be expressed in PNT1A cells growing on HA_{234} and HA_{2590} surfaces. In addition, CD44v8 appears do not be found in those cells growing on HA_4 surfaces (**Table 4.9**).

Table 4.9 – Summary of the CD44s and CD44v forms in PNT1A cell line. + presence of the form, - absence of the form.

	CD44s	CD44v2 (5/7)	CD44v3 (5/8)	CD44v4 (5/9)	CD44v5 (5/10)	CD44v6 (5/11)	CD44v7 (5/12)	CD44v8 (5/13)	CD44v9 (5/14)
PNT1A control	+	-	+	-	-	+	-	+	-
PNT1A HA_4	+	-	+	-	-	+	-	-	-
PNT1A HA_{234}	+	-	-	-	-	+	-	-	-
PNT1A HA_{2590}	+	-	-	-	-	+	-	-	-
PNT1A HA_{mix}	+	-	+	-	-	+	-	+	-

4.3.2.c. RHAMM expression

After confirmation of the expression of RHAMM standard form in the cell lines, a subsequent study was performed in order to investigate the presence of RHAMM variant forms in both control and cells growing in the presence of HA (**Figures 4.26** to **4.29**).

RT112 cell line

Figure 4.26 presents the amplification generated by RHAMM isoforms for RT112 cell line. Lane 2 shows a standard RHAMM ($RHAMM^{FL}$) amplification pattern used here as positive control. Lane 3 indicates the presence of $RHAMM^{-48}$ and lane 4 the presence of $RHAMM^{-147}$. Lane 5 corresponds to β-actin also used as positive control, and lane 6 the negative control. Thus, it can be seen that both $RHAMM^{-48}$ and $RHAMM^{-147}$ variant forms appear to be expressed in RT112 cells. This is demonstrated by the presence of a band of approximately 646 bp and of 677 bp, for each

correspondent isoform. It can be also observed that both isoforms appear to have very distinct amplification (**Figure 4.26**).

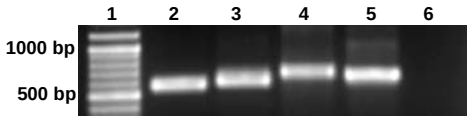

Figure 4.26 – Amplification pattern generated for RT112 cell line. Lanes numbered 1-6 from left to right. Pattern marker of 100 bp (1), $RHAMM^{FL}$ (2), $RHAMM^{-48}$ (3), $RHAMM^{-147}$ (4), β-actin (5) and negative control (6).

T24 cell line

Figure 4.27 shows the result of the RHAMM isoforms amplification pattern generated for T24 cell line. For this cell line very distinct bands were amplified for both $RHAMM^{-48}$ and $RHAMM^{-147}$ isoforms.

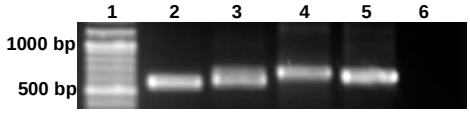

Figure 4.27 – Amplification pattern generated for T24 cell line. Lanes numbered 1-6 from left to right. Pattern marker of 100 bp (1), $RHAMM^{FL}$ (2), $RHAMM^{-48}$ (3), $RHAMM^{-147}$ (4), β-actin (5) and negative control (6).

PC3 cell line

In **Figure 4.28** is presented the RHAMM isoforms amplification pattern generated by PC3 cell line. It can be observed that very distinct bands were amplified for both $RHAMM^{-48}$ and $RHAMM^{-147}$ isoforms in PC3 cells.

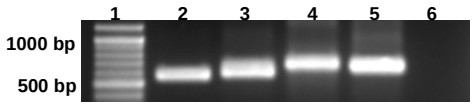

Figure 4.28 – Amplification pattern generated for PC3 cell line. Lanes numbered 1-6 from left to right. Pattern marker of 100 bp (1), $RHAMM^{FL}$ (2), $RHAMM^{-48}$ (3), $RHAMM^{-147}$ (4), β-actin (5) and negative control (6).

PNT1A cell line

From **Figure 4.29** it can be seen that both $RHAMM^{-48}$ and $RHAMM^{-147}$ isoforms were expressed in PNT1A cell line, with very distinct bands being amplified.

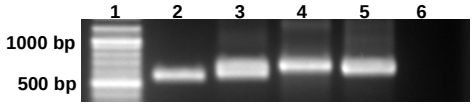

Figure 4.29 – Amplification pattern generated for PNT1A cell line. Lanes numbered 1-6 from left to right. Pattern marker of 100 bp (1), $RHAMM^{FL}$ (2), $RHAMM^{-48}$ (3), $RHAMM^{-147}$ (4), β-actin (5) and negative control (6).

In **Table 4.10** is summarised the RHAMM isoforms expression on the controls of both bladder and prostate cell lines. The semi-quantitative RHAMM expression results within cell lines investigated in this study revealed that both $RHAMM^{-48}$ and $RHAMM^{-147}$ isoforms were present in all four cell lines.

Table 4.10 – Summary of the RHAMM forms expression on RT112, T24, PC3 and PNT1A cell lines. + presence of the form, - absence of the form.

	$RHAMM^{FL}$	**$RHAMM^{-48}$**	**$RHAMM^{-147}$**
RT112	+	+	+
T24	+	+	+
PC3	+	+	+
PNT1A	+	+	+

4.3.2.b. RHAMM isoforms expression on cells growing on HA-coated surfaces

After confirmation of the presence of RHAMM isoforms in control cells, the same investigation was performed in those cells growing on HA structured surfaces. Both $RHAMM^{-48}$ and $RHAMM^{-147}$ variant forms were found to be present in all four cell lines growing on HA-coated surfaces (**Table 4.11**).

Table 4.11 – Summary of the RHAMM forms in RT112, T24, PC3 and PNT1A cell lines growing on HA-coated surfaces. + presence of the form, - absence of the form.

	$RHAMM^{FL}$	**$RHAMM^{-48}$**	**$RHAMM^{-147}$**
RT112 control	+	+	+
RT112 HA_4	+	+	+
RT112 HA_{234}	+	+	+
RT112 HA_{2590}	+	+	+
RT112 HA_{mix}	+	+	+
T24 control	+	+	+
T24 HA_4	+	+	+
T24 HA_{234}	+	+	+
T24 HA_{2590}	+	+	+
T24 HA_{mix}	+	+	+
PC3 control	+	+	+
PC3 HA_4	+	+	+
PC3 HA_{234}	+	+	+
PC3 HA_{2590}	+	+	+
PC3 HA_{mix}	+	+	+
PNT1A control	+	+	+
PNT1A HA_4	+	+	+
PNT1A HA_{234}	+	+	+
PNT1A HA_{2590}	+	+	+
PNT1A HA_{mix}	+	+	+

4.3.3. CD44 AND RHAMM IMMUNOLOCALISATION

Immunocytochemistry (ICC) was performed in order to detect the presence and localisation of CD44 and RHAMM in both cell lines and to compare the expression profile of cells grown under varying conditions. **Figures 4.30 – 4.33** show the immunocytochemical results for each cell line with CD44 and RHAMM antibodies. No staining was seen on any of the negative controls confirming the absence of non-specific binding. All cell lines express CD44 and RHAMM proteins, although as for the mRNA expression, patterns differed between each. As CD44 is a cell adhesion molecule, it would be expected that staining would be concentrated within the cell membrane. However, cytoplasmic and nuclear staining was also noticed in some cells. Regarding RHAMM, membrane, cytoplasmic and nuclear expression was found to be present.

As previously discussed in **Chapter 3**, it is observed the formation of aggregates on cells growing on HA_{234}, HA_{2590} and HA_{mix} structured surfaces. Due all steps involved in immunocytochemistry, including the fixation and staining of cells, most of cellular aggregates have been lost. Therefore, it is not possible to present immunostaining results for all treatments.

4.3.3.a. RT112 cell line

Figure 4.30 shows the result of ICC with CD44 and RHAMM antibodies for RT112 cell line. It can be observed cells growing on HA_4-coated surfaces appear to

have similar morphology to control cells. Conversely, cells growing on HA_{234}, HA_{2590} and HA_{mix} surfaces do not have similar morphology to the controls, forming cell aggregates and displaying spherical somal shape. CD44 was found to be stained in membrane, cytoplasm and nucleus of RT112 control and cells growing in the presence of HA. In addition, a decreased CD44 expression appears to be found in those cells growing on HA-coated surfaces, in comparison to controls. RHAMM appears to be stained in the cytoplasm of control and cells growing in the presence of HA_4 and HA_{2590}; being observed a higher expression in cells undergoing cellular division. Cells growing on HA_{234} and HA_{mix}-coated surfaces appeared to be stained for RHAMM antibody in membrane, cytoplasm and nucleus.

4.3.3.b. T24 cell line

In **Figure 4.31** is shown the result of ICC with CD44 and RHAMM antibodies for T24 cell line. It can be observed that control cells appear to be larger than those cells growing in the presence of HA. Again, cells growing on HA_{234}, HA_{2590} and HA_{mix} surfaces do not have similar morphology to the controls, forming cell aggregates and displaying spherical somal shape. CD44 was found to be stained in membrane, cytoplasm and nucleus of T24 control and cells growing in the presence of HA. Similar findings to those observed for CD44 protein can be also seen for the RHAMM staining in T24 cell line.

4.3.3.c. PC3 cell line

Staining patterns of CD44 and RHAMM in PC3 cell line are shown in **Figure 4.32**. Again, it can be observed that cells growing in the presence of HA are smaller than control cells, with the formation of aggregates in those cells growing on HA_{234}, HA_{2590} and HA_{mix}. PC3 cells positively stained for both CD44 and RHAMM antibodies. CD44 staining pattern of the PC3 on controls and cells growing on HA-coated surfaces appears to be localised in the membrane, cytoplasm and nucleus. However, the CD44 membrane protein appears to be down-regulated in cells growing in the presence of HA_4 comparatively to control. RHAMM also appears to be expressed in cytoplasm and nucleus in both control and cells growing in the presence of HA. An increased cytoplasmic and nuclear expression can be seen in those cells undergoing to cell division. Membrane RHAMM expression also appears to be found in those cells growing on HA_{2590} and HA_{mix}-coated surfaces.

4.3.3.d. PNT1A cell line

Figure 4.33 illustrates the ICC results for PNT1A cell line with CD44 and RHAMM antibodies. Again, PNT1A control cells appear to be slightly larger than those cells growing on HA_4-coated surfaces; with cells growing on HA_{234}, HA_{2590} and HA_{mix} surfaces displaying spherical somal shape and forming cellular clumps. PNT1A cells positively stained for both CD44 and RHAMM antibodies. Both control and cells growing in the presence of HA were found to be stained for CD44 in membrane,

cytoplasm and nucleus. In addition, CD44 expression appears to be up-regulated in cells growing on HA_4, comparatively to control. RHAMM also showed membrane, cytoplasmic and nuclear staining in both control and cells growing in the presence of HA. RHAMM protein expression appears to be up-regulated in those cells growing on HA-coated surfaces. Interestingly, conversely for cells growing in the presence of HA_{2590} surfaces, not all cells growing on HA_{mix} structured surfaces were found to be stained for RHAMM. Indeed, cells growing in the presence of HA_{mix} appear to have a decreased RHAMM expression comparatively to control and the rest of treatments.

CD44 appears to be highly expressed in the controls of all four cell lines. The expression of CD44 protein appears to be decreased in RT112 and PC3 cell lines growing on HA-coated surfaces. A slightly increased CD44 expression can be seen in T24 cells. Regarding PNT1A cell line, CD44 also appears to be slightly increased in those cells growing on HA-coated surfaces. RHAMM protein is also expressed in all four cell lines, with cells appearing to be stained in membrane, cytoplasm and nucleus. RHAMM appears to be more expressed in T24 cell lines, and being less expressed in PNT1A cells. Conversely, RHAMM appears to be down-regulated in RT112 and PC3 cells growing on HA structured surfaces comparatively to controls. In addition, as also found from the qPCR results, RHAMM appears to be less expressed than CD44 in all cell lines.

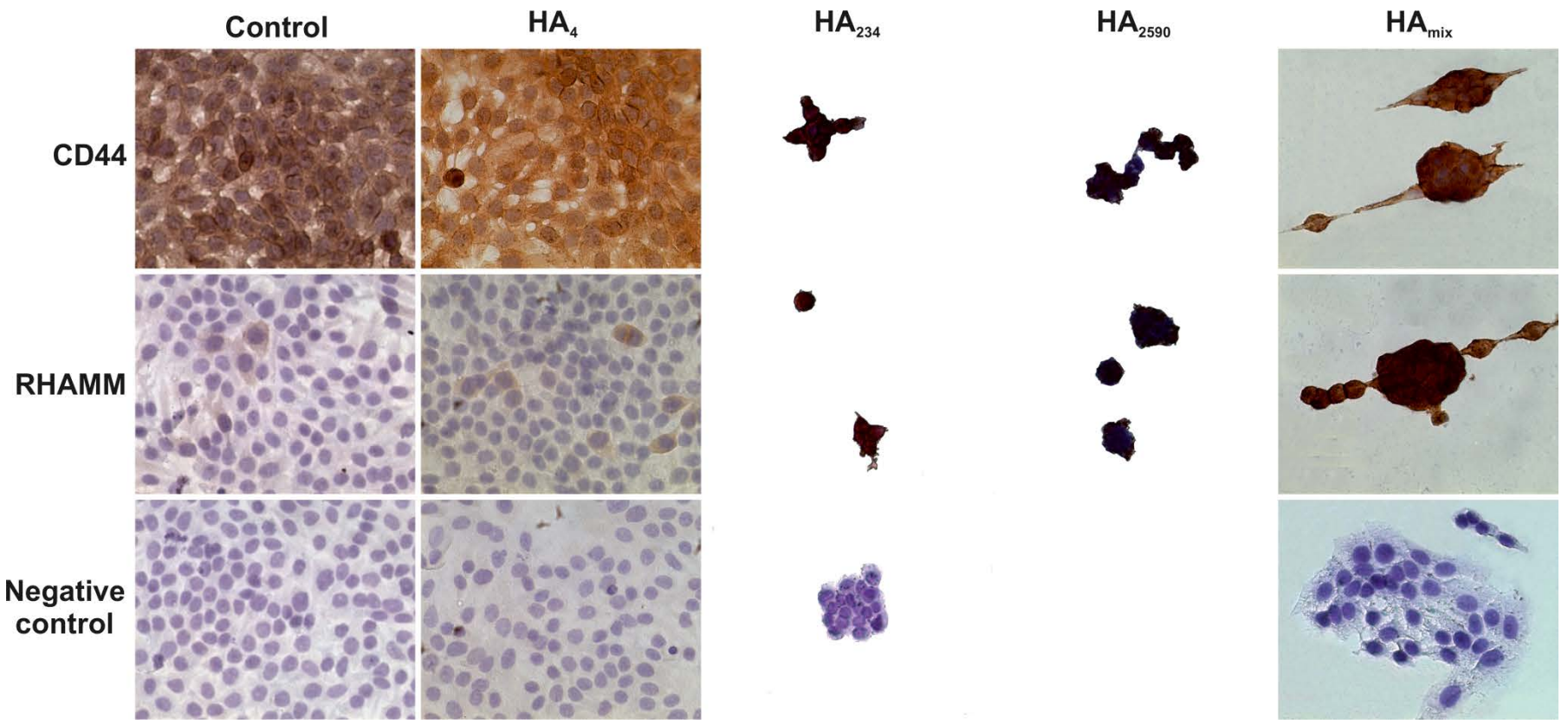

Figure 4.30 – Immunocytochemical staining in RT112 cell line using anti-CD44 and anti-RHAMM antibodies, with nuclei counterstained in haematoxylin.

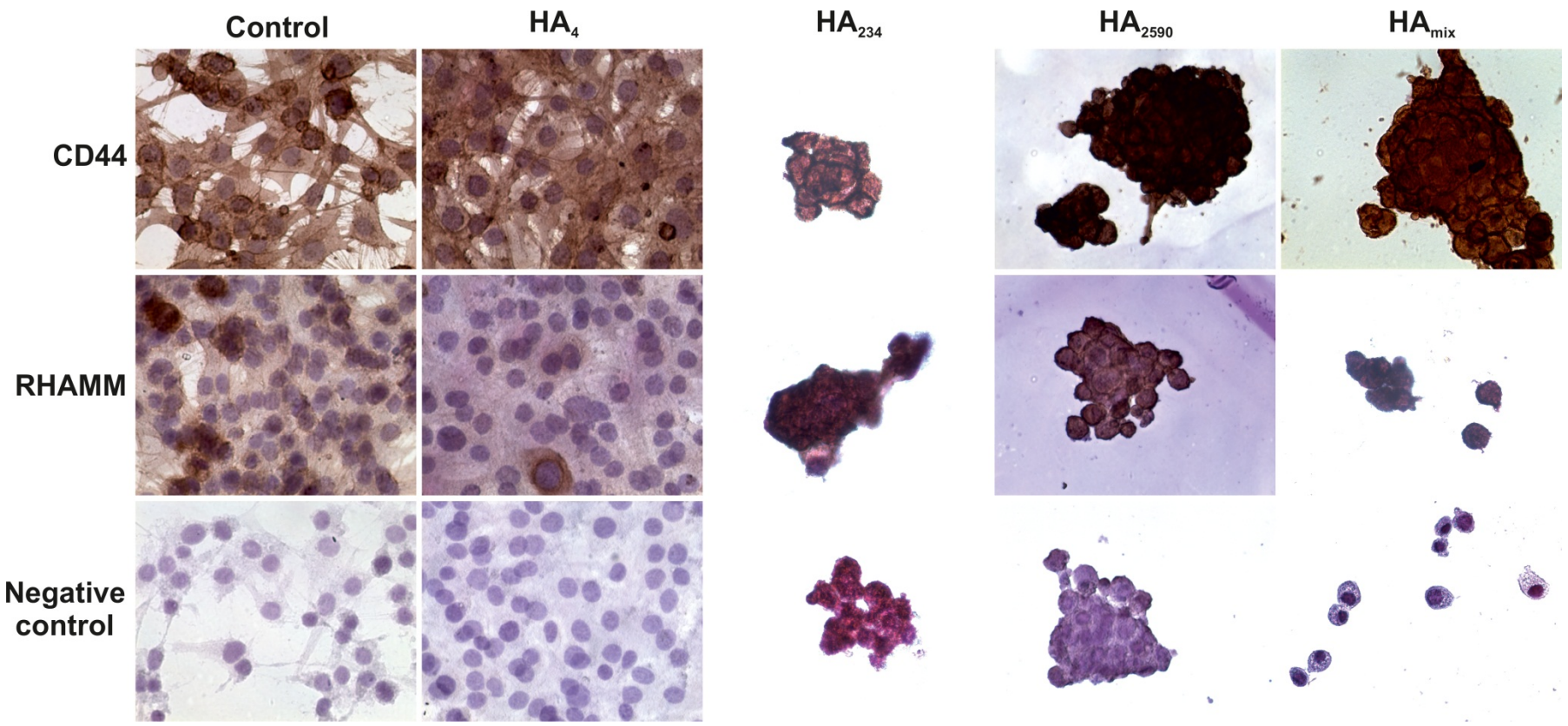

Figure 4.31 – Immunocytochemical staining in T24 cell line using anti-CD44 and anti-RHAMM antibodies, with nuclei counterstained in haematoxylin.

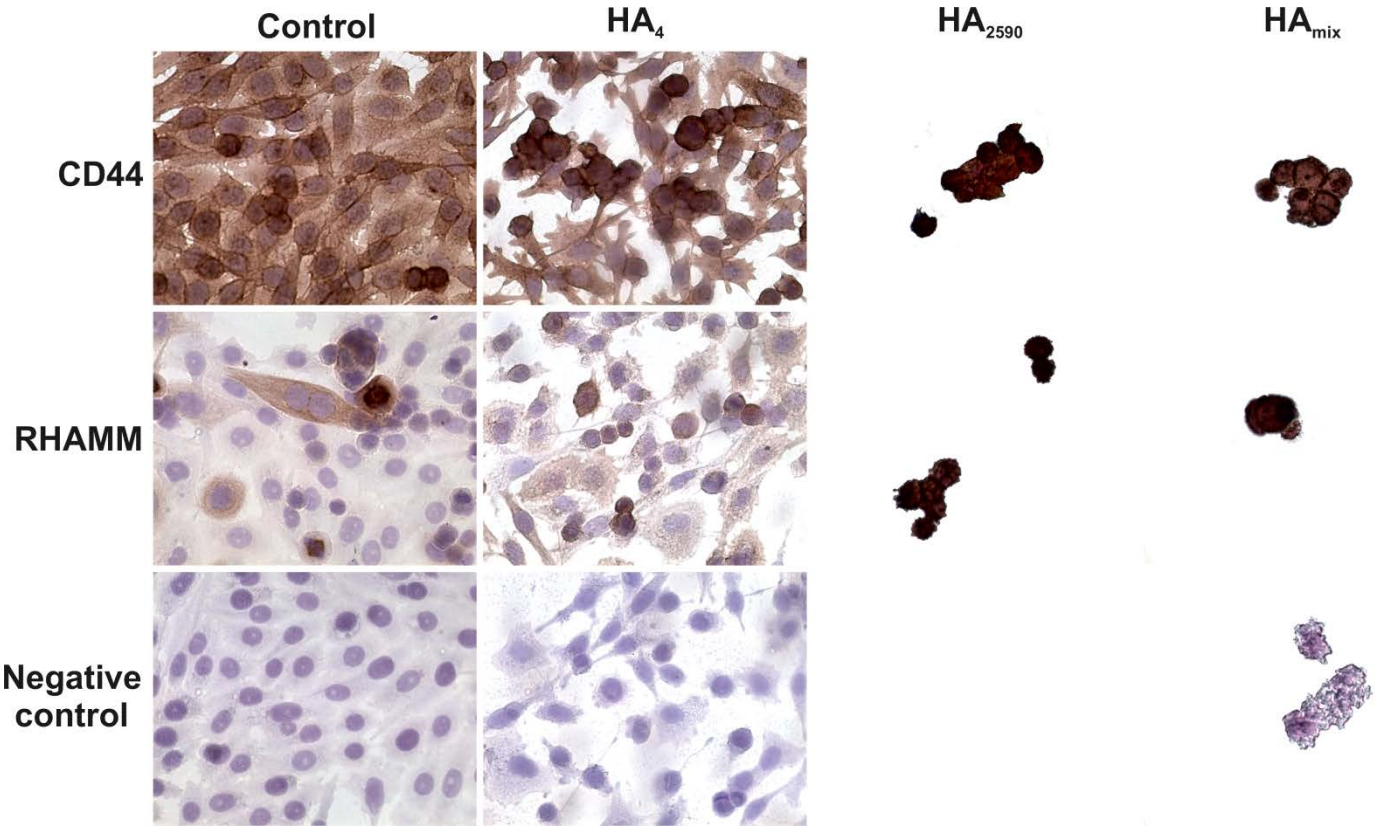

Figure 4.32 – Immunocytochemical staining in PC3 cell line using anti-CD44 and anti-RHAMM antibodies, with nuclei counterstained in haematoxylin

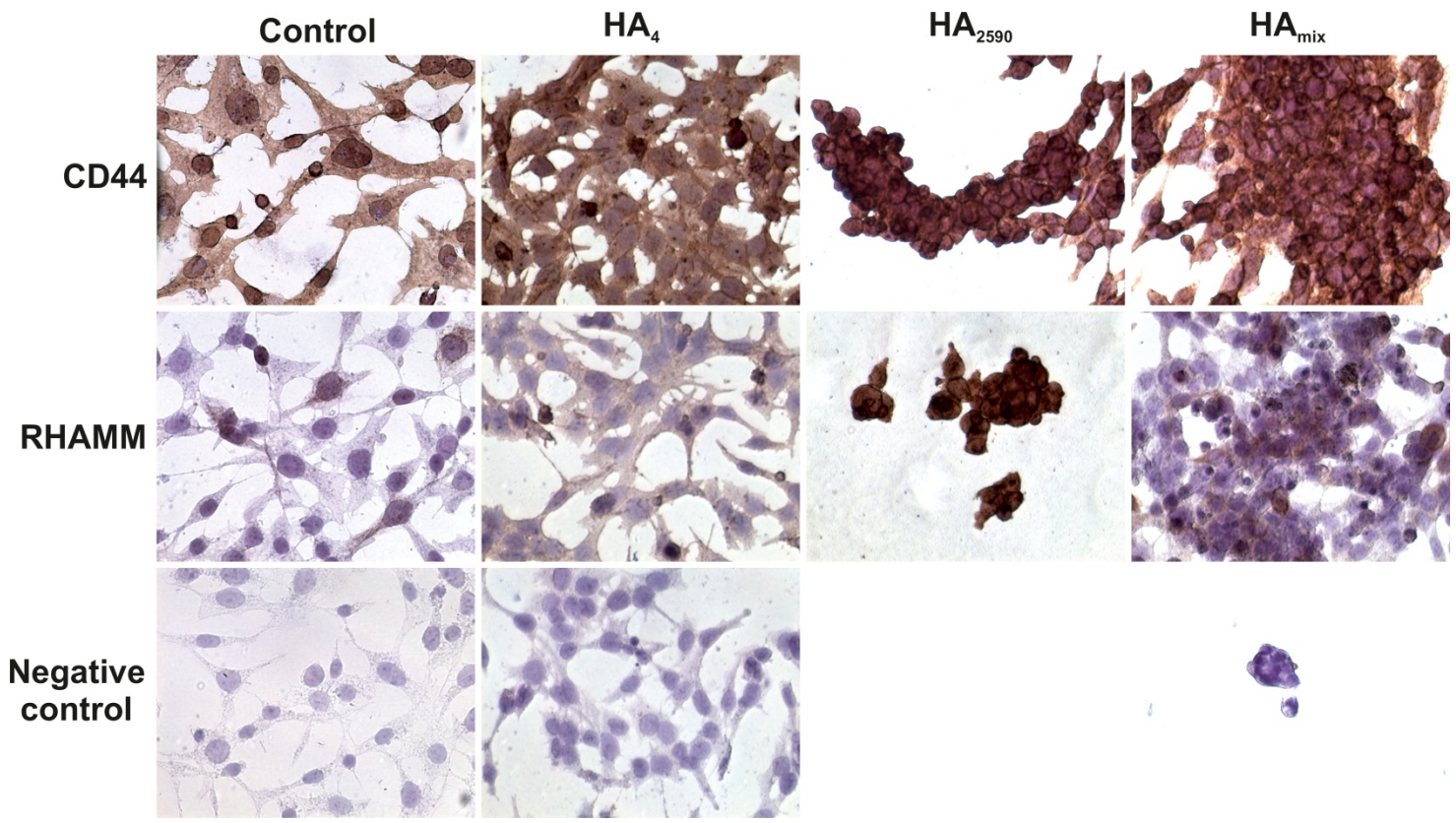

Figure 4.33 – Immunocytochemical staining in PNT1A cell line using anti-CD44 and anti-RHAMM antibodies, with nuclei counterstained in haematoxylin.

4.4. DISCUSSION

This chapter of work aimed to investigate whether HA polymer molecular weight modulates the expression of CD44 and RHAMM within tumour-derived cell lines. In order to perform this investigation transcriptional and translational studies have been carried out.

4.4.1. HA MODULATES TRANSCRIPTION OF CD44 AND RHAMM GENES IN A CELL PHENOTYPE MANNER

From the results presented, it can be seen that all four cell lines used as *in vitro* models express both CD44 and RHAMM at the mRNA level. However, this expression varies between both tissue and cell lines of each tissue type. Interestingly, CD44 and RHAMM expression appear to be phenotype dependent, but not HA molecular weight dependent. CD44 and RHAMM were found to be down-regulated in the most malignant cell lines (RT112 and PC3) and up-regulated in the less invasive cells (T24 and PNT1A). These data suggest that CD44 and RHAMM interrelated, as the expression levels can be correlated: CD44 and RHAMM are either up-regulated or down-regulated. From the RHAMM/CD44 ratio obtained from qPCR, it was also found that CD44 is more expressed than RHAMM transcript in all four cell lines and all different treatments. Previous reports had established that some of the oncogenic effects of RHAMM results from its extracellular HA-binding properties (Yang *et al.*, 1994; Hall *et al.*, 1995). It has also been shown an involvement of the extracellular RHAMM protein in signalling via an association with HA-CD44 complexes, promoting cell motility and invasion (Turley *et al.*, 2002; Toole, 2004). In breast cancer there is some

evidence that in the presence of HA, RHAMM partners with CD44, activating erk1/2, which in turn results in the expression of genes required for cell motility and invasion, and consequently conferring malignant potential (Turley *et al.*, 2002; Toole *et al.*, 2004; Tolg *et al.*, 2006; Hamilton *et al.*, 2007; Maxwell *et al.*, 2008). Evidence presented in this study further suggests that CD44 and RHAMM act in an interrelated fashion in bladder and prostate cancer. However, one cannot conclude that the mechanism active in bladder and prostate carcinomas is the same as that seen in breast cancer. More studies would be required in order to confirm such an assertion.

4.4.2. HA MODULATES EXPRESSION OF CELL RECEPTORS VARIANTS

The semi-quantitative CD44 expression results within the prostate (PC3 and PNT1A cell lines) and bladder (RT112 and T24 cell lines) *in vitro* models revealed the expression of a number of variant exon junctions. This suggests that a characteristic splice pattern can be demonstrated within prostate and bladder cancer. For prostate models, regarding PC3 cell line six out of eight possible variants of are expressed: v2, v3, v4, v6, v8 and v9; whereas only there variants (v3, v6 and v8) were found to be expressed in PNT1A cell line. PC3 cell line shows multiple banding with varied size product; while PNT1A shows two bands. Yang and co-workers (2010) have shown that CD44v7-v10 isoforms constitute a unique prostate cancer signature, consistently expressed in primary and metastatic prostate cancer (Yang *et al.*, 2010). In addition, several studies have shown that cells lose the ability to produce the standard isoform and certain variants, other than CD44 v7-v10, in benign prostate tumour (Iczkowski *et al.*, 1997; Omara-Opyene *et al.*, 2004; Vis *et al.*, 2000, 2002; Harrison *et al.*, 2006;

Yang *et al.*, 2010). Since PNT1A is a cell line derived from normal prostatic epithelial cells, absence of variants would be expected; however, the presence of variant exons might be attributed to the immortalisation of the cells with a plasmid containing SV40 viral gene with a defective replication origin.

For bladder models, in RT112 cell line seven variants were found to be present, namely v2, v3, v4, v6, v7, v8 and v9. For T24 cell line v3, v4, v6, v7 and v8 variants were found to be present. The number of variant exons present within each cell line can be compared to the characteristic banding noted when carrying out a standard P1-P4 amplification across the whole gene. RT112 cell line shows multiple banding with varied size product; therefore the presence of a number of variant could be expected. Conversely, T24 cell line shows only a major band in the agarose gel. However, Morgan (2002) reported that when southern blotting is undertaken, a further band slightly greater in size than the standard band can be seen (Morgan, 2002). Therefore, the presence of lower number in variant exons could be expected in T24 cells. CD44 exon link assay also showed that v7 (junction 5/12) only appears in RT112 and T24 cells, being absent in prostate cell lines. Interestingly, junction 5/12 had previously been demonstrated to be a potentially useful marker for bladder cancer (Morgan, 2002). It was also observed that v2 and v9 isoforms are only present in RT112 and PC3 cell lines, and therefore might be suggestive of a correlation between these variants and the more invasive and malignant phenotype of these cells. Expectedly, CD44v6 isoform was shown to be expressed in all four cells lines, as this isoform is reported to be implicated in cancer progression and metastasis formation in a number of tumours (Günthert, 1991; Ponta *et al.*, 2003; Bendall *et al.*, 2004; Yaqin *et al.*, 2007).

From the analysis of the results of the cell lines growing on the structured surfaces, the absence of v7 and v9 in RT112 cells growing in the presence of HA can be

also observed. Absence of v3, v6 and v8 is also observed for T24 cells growing on HA-coated surfaces. The absence of v2 is seen in PC3 cells growing on HA structured surfaces. Interestingly, the absence of v3, v6 and v9 is seen in PC3 cells growing on HA_{234}-coated surfaces. The presence of v8 in PNT1A cell line is only observed in control cells and cells growing on HA_{mix}-coated surfaces. Additionally, for this prostate cell line, an absence of v3 in cells growing on HA_{234} and HA_{2590} structured surfaces is also observed. As previously described by Morgan (2002), as sometimes no result with agarose gel analysis is obtained due to a very low expression of CD44 variant forms, there is a need for a southern blotting analysis in order to confirm the presence of different CD44 isoforms obtained by exon-link PCR (Morgan, 2002).

It has been reported that certain variant exons are spliced in blocks, and exons rarely appear to be spliced alone in the transcript (Bell *et al.*, 1998). Despite the simply analysis of exon presence may not give rise to any form of distinguishable pattern, it may be demonstrated the level of expression for each exon. Analysis of exon junctions allows for detection of a predominant pattern that may be tissue and/or tumour specific. Normal tissues have preferential splicing patterns, and in tumour cells a desorganised regulation of the transcript assembly is seen; this resulting in the generation of a wide variety of unusual and alternatively spliced transcripts (Goodison *et al.*, 1997). The expression of certain CD44 variant isoforms has been reported to being implicated in tumour metastasis (Henke *et al.*, 1996). However, the regulation of the expression of CD44 variants in tumours is still controversial. For instance, whereas most of studies have shown an increase in CD44v6 expression in colorectal cancer, others have demonstrated a significant decrease in advanced colorectal carcinoma (Ni *et al.*, 2002).

From the semi-quantitative RHAMM expression results it can be seen that $RHAMM^{-48}$ and $RHAMM^{-147}$ variant transcripts were amplified in all four cell lines,

and also in the presence of hyaluronic acid of different molecular weights. It is described that in most of normal tissues RHAMM mRNA expression is low or undetectable. Conversely, high levels of RHAMM are seen in tumour cells, and are also correlated with the neoplastic progression of a variety of tumours, including aggressive human fibromatoses tumours, terminally differentiated multiple myelomas, breast carcinoma cells, blood tumours, adenocarcinomas, small lung carcinoma cells, squamous cell carcinomas, and late stage astrocytoma (Turley *et al.*, 1993; Teder *et al.*, 1995; Mohapara *et al.*, 1996; Assman *et al.*, 1998; Greiner *et al.*, 2002; Tolg *et al.*, 2003; Maxwell *et al.*, 2008). RHAMM splice variants of exon 4 ($RHAMM^{-48}$) and exon 13 ($RHAMM^{-147}$) have also been detected in blood of patients with multiple myeloma (Crainie *et al.*, 1999). $RHAMM^{-48}$ was also described in several tumours and cancer cell lines (Maxwell *et al.*, 2004).

The data presented in this study have demonstrated that CD44 and RHAMM expression do both appear to change in the presence of different weights of HA, but no evidence to conclude its regulatory role. Nevertheless, the significance of these findings in tumourigenesis remains unclear. It would therefore be useful to develop a real-time PCR assay for the quantitative analysis of the isoform expression presented by these genes, as performed for CD44 and RHAMM standard isoforms. This would provide a more accurate analysis of the gene splicing observed.

4.4.3. HA MODULATES EXPRESSION OF CD44 AND RHAMM PROTEINS

After being seen that HA regulates the expression of CD44 and RHAMM at mRNA level, the next addressed question was whether HA also modulates the

expression of these cell receptors at protein level. Immunocytochemistry (ICC) was performed in order to detect and localise CD44 and RHAMM proteins. It was not possible to present immunocytochemical results for all treatments, due to the loss of cell clumps during the steps involved in the cellular fixation and staining. The antibodies used were specific to detect both standard and protein isoforms. From the results obtained it can be seen both CD44 and RHAMM proteins are expressed in all four cell lines, with the protein expression appearing to be somehow correlated with the obtained transcripts expression. In concordance with the results seen during mRNA quantification, CD44 and RHAMM proteins appear to be down-regulated in RT112 and PC3 cells growing on HA-coated surfaces, when compared to control cells. Conversely, cell receptors appear to be slightly up-regulated in T24 and PNT1A cells growing in the presence of exogenous HA. In addition, is it also observed that lower levels of RHAMM are present in PNT1A control cells comparing to the other cell lines. This finding might be correlated with the phenotype nature of this cell line, as it is reported that in most of normal tissues RHAMM mRNA and protein expression is low or undectable (Savani *et al.*, 1995; Mohapara *et al.*, 1996; Tolg *et al.*, 2003; Maxwell *et al.*, 2008). For all cell lines it can be observed a lower expression of RHAMM comparatively to CD44; finding that was also observed for the transcripts expression. From the immunolocalisation results it can be observed that RHAMM protein is expressed at the membrane, cytoplasmic and nuclear level. This is not wholly unexpected, since it has been described that RHAMM is a protein localised at both cell surface and intracellularly, including cytoplasm, mitochondria, and nucleus, being associated with the cytoskeleton, microtubules, centrosomes and mitotic spindle. However, it still remains unclear whether the cell localisation of RHAMM is due to the different isoforms of the transcript or due to post-translational modifications. Sohr and

co-workers (2008) have also reported that RHAMM expression is regulated during the various phases of the cell cycle, with resting cells containing very low levels of RHAMM, with the increase of mRNA and protein levels rising during S phase (DNA synthesis) and peaking during G2/M phase (mitotic phase) (Sohr and Engeland, 2008). Indeed, from immunocytochemical results it can be observed that RHAMM is normally more expressed in cells undergoing division.

From the CD44 immunolocalisation results it can be observed that this protein is expressed at both membrane, cytoplasmic and nuclear level. As CD44 is a transmembrane protein, it would be expected that the majority of CD44 would be present on the membrane alone. However, all four cell lines showed expression in membrane, cytoplasm and nucleus. The regulation of CD44 occurs at multiple levels in addition to splicing, including promoter methylation, transcription, post-translational modifications, ligand binding, and proteolytic processing of the extracellular domain. A possible explanation for the cytoplasmic presence of CD44 may be correlated with post-translational modifications, leading to defective proteins production. Alternatively, it could be associated with the build-up of functional protein that is unable to integrate into the membrane due to saturation. In some cells the cytoplasmic staining appears to be grainy in nature, suggesting aggregation of protein; this may be caused by the removal mechanisms within the cells where proteins are encapsulated in order to facilitate their degradation. Recently, Lee and co-workers (2009) have shown that CD44 is internalised and translocated to the nucleus, forming complexes with STAT3 and p300, binding to cyclin D1 promoter and enhancing cell proliferation. A bipartite nuclear localisation signal was mapped to the cytoplasmic tail of CD44, which is involved in the mediation of its nuclear translocation (Lee *et al.*, 2009). However, the mechanism of the nuclear localisation and the function of nuclear CD44 remains to be

elucidated. Similarly to RHAMM, CD44 protein expression is less expressed in RT112 and PC3 cells growing on HA-coated surfaces, when compared to control cells. In addition, for T24 cells there appears to be an increased expression of membrane protein for cells growing on HA structured surfaces.

CD44 is a cell surface glycoprotein, playing an important role in cell-cell and cell-ECM interactions and mediating tumour-cell adhesion through binding to several ECM components, including hyaluronic acid (Martin et *al.*, 2003). CD44 can be correlated with the oncobiological behaviour, including tumourigenesis, growth, metastasis and prognosis (Liu and Jiang, 2006). The CD44s protein is detected in several types of normal tissues, but an increased expression is seen in neoplastic pathologies (Yoshida *et al.*, 1996). The abnormal expression of CD44v proteins is detected in a variety of human tumours, including gastrointestinal, mammary, urothelial, pulmonary, uterine, bladder, colorectal, thymic and prostate (Yoshida *et al.*, 1996; Lee *et al.*, 2003; Kobel *et al.*, 2004; Kuncová *et al.*, 2007; Afify *et al.*, 2009). Hence, it would be useful to perform detection of CD44 protein variants. In spite of the biological significance of CD44 in tumourigenesis is starting to be elucidated, there are some aspects that need to be clarified. There are cases showing that standard CD44, rather than its variants, enhances tumour progression (Sy *et al.*, 1991; Bartolazzi *et al.*, 1994). Conversely, in prostate cancer and cervical neuroendocrine carcinoma, CD44 suppresses metastasis (Gao *et al.*, 1997; Kuo *et al.*, 2007). Furthermore, there are studies showing that it inhibits prostate cancer progression (Desai *et al.*, 2007; Patrawala *et al.*, 2007). Therefore, the internal and external environment of the tumour appears to have an influence in the relationship of standard CD44 *vs.* CD44 variants. Consequently, this relationship must be analysed for each case and each type of tumour;

heterogeneity in CD44-dependency can be detected in tumours derived from the same histological origin (Naor *et al.*, 2008).

4.5. CONCLUSIONS

In this chapter of work it was demonstrated that the regulation of CD44 and RHAMM expression in tumour-derived cell lines appears to be phenotype dependent but not HA-MW dependent. HA down-regulates CD44 and RHAMM in the most malignant cell lines; and in general, up-regulation of the expression of the cell receptors in the less invasive cell lines is seen.

Findings from this work suggest that CD44 and RHAMM functioning is interrelated as their expression levels can be correlated: both CD44 and RHAMM are either up-regulated or down-regulated. In addition, the presence of exogenous HA appears to be involved in the regulation of CD44 isoform expression. However, the significance of these findings in tumourigenesis remains unclear. As performed for CD44 and RHAMM standard isoforms, it would be useful to develop a real-time PCR assay for the quantitative analysis of the isoform expression pattern presented by these genes. This would facilitate a more accurate analysis of the gene splicing observed in this study.

Findings from this study also suggest that the results obtained for the CD44 and RHAMM gene expression are consistent at both the mRNA and protein level. HA appears to up-regulate CD44 and RHAMM in the less invasive cell lines, and down-regulate the cell receptors in the most malignant cells. In the future, it would be also interesting to perform double immunolocalisation of CD44 and RHAMM, to directly compare the localisation and expression of both proteins. In addition, it would be also

useful to perform a more accurate analysis of CD44 and RHAMM protein expression levels, both standard and variant forms, using techniques such as western blotting and flow cytometry.

CHAPTER 5

“ 1. When a distinguished but elderly scientist states that something is possible, he is almost certainly right; when he states that something is impossible, he is probably wrong.
2. The only way of discovering the limits of the possible is to venture a little way past them into the impossible.
3. Any sufficiently advanced technology is indistinguishable from magic.”

Clarke's three laws

CHAPTER 5

5. FINAL DISCUSSION

Tumour progression is accompanied by various cellular, biochemical and genetic alterations, including the interaction of tumour cells with extracellular matrix (ECM) molecules. Increased synthesis of certain ECM components and/or increased breakdown with generation of ECM cleavage products are known to contribute to tumour progression. Hyaluronic acid (HA) is a major constituent of ECM, and several studies have shown that there is a positive correlation between tumour aggressiveness and stromal HA expression on human cancers from different origins and various malignancy degrees (Hautman *et al.,* 2001; Auvinen *et al.,* 1997; Li *et al.,* 2007; Ropponen *et al.,* 1998; Anttila *et al.,* 2000; Delpech *et al.,* 1993; Horai *et al.,* 1981; Lokeshwar *et al.,* 2001; Lipponen *et al.,* 2001; Aaltomaa *et al.,* 2002; Köbel *et al.,* 2004; Pirinen *et al.,* 2001; Böhm *et al.,* 2002). The high concentrations of HA present in tumours are consistent with the high levels present in the serum of some cancer patients, when compared with the levels found in those normal individuals (Ropponen *et al.,* 1998; Dahland Laurent 1988; Knudson *et al.,* 1989; Knudson 1996). The aberrant amounts of HA seen in cancers can be produced by the tumour cells themselves or by the stromal cells commandeered by the tumour cells (Asplund *et al.,* 1993; Toole 2004). High levels of HA are not only a characteristic seen in tumours; transformed cells, including those infected with oncogenic viruses, exhibit higher levels of HA production as well as abnormal acceleration of cellular growth (Hamerman *et al.,* 1965; Ishimoto *et al.,* 1966; Hopwood and Dorfman, 1978; Leonard *et al.,* 1978). In spite of high levels of HA being also associated with an unfavourable outcome of the disease, some studies

have shown that the accumulation of HA in tumour could serve as a favourable prognostic (Pirinen *et al.,* 2001). Therefore, the role of hyaluronic acid and its association with progression and metastasis remains unclear and cannot be generalised; therefore there is a need to be studied in different cancer entities.

HA has been implicated in migration, differentiation, progression and invasion of cancer cells leading to metastasis. Several studies have shown that HA mediates these cellular functions through interactions with specific binding proteins, including CD44 and RHAMM, which are known to be the principal receptors for HA. Although the major biological function of HA are still unsure, it is well reported that the functions exhibited by HA depend on the chain length, molecular mass and on the conditions under which the polysaccharide is synthesized (Toole, 2004; Noble, 2002; Girish and Kemparaju, 2007). Polymers coming from the HA fragmentation in the course of the catabolic pathway occur in a variety of sizes that have a vast range of properties. High and low molecular weight HA polymers play opposite roles on cell behaviour (Girish and Kemparaju, 2007). It has also been reported that the expression of CD44 and RHAMM are linked with pathologic activities of cancer cells (Bourguignon *et al.*, 1993; Crainie *et al.,* 1999; Martin *et al.,* 2003; Maxwell *et al.*, 2008).

All the previous stated findings were the basis of the present project. Hence, the aim of this work was to investigate whether hyaluronan polymer molecular weight has an effect on the proliferation of tumour-derived cell lines, and to investigate whether different HA molecular weight polymers have an effect on the expression of CD44 and RHAMM.

It is reported that immobilised components on a substrate may more closely stimulate cell responses due to intimate cell contact with the substrate-bound HA, rather than periodic contact with exogenous hyaluronan of media supplementation (Ibrahim *et*

al., 2007). Therefore, in order to perform this investigation, biocompatible surfaces for the immobilisation of cells have been produced and characterised as part of the work, to allow for the study of cell proliferation and subsequent receptor expression. A number of surfaces, coated with polymers of different molecular weights, were constructed. The present strategy relied on the crosslinking of HA, in order to improve the rapid degradation of this polymer in an aqueous environment, while maintaining its biocompatibility and biological activity (Leach and Schimidt, 2004; Segura *et al.*, 2005; Collins and Birkinshaw, 2007). Many strategies exist for crosslinking HA, of which carbodiimide-mediated crosslinking was selected, for its simplicity and in contrast with other crosslinking agents it does not chemically bind to HA polymer molecules (Tomihata and Ikada, 1997; Wrobel *et al.*, 2002). Different approaches using lipid bilayers have also been employed on the construction of HA surfaces. However, these systems require the anchoring of HA films to solid supported membranes through the use of HA binding ligands, including p53 and CD44 (Sengupta *et al.*, 2003; Richter *et al.*, 2007). This in turn could lead to a competition of HA performed by these ligands and the molecular receptors on the cell membrane.

The studies performed in this investigation relied on 2D *in vitro* culture, since the construction of 3D surfaces would require the use of another component (e.g. poly(L-lysine), chitosan, collagen, fibronectin) (Prestwich, 2010), which could stimulate a different response, rather than only HA. It is also reported that matrix stiffness has an effect on cell morphology, adhesion, proliferation, and migration; with cells showing different morphologies and motility rates when cultured on substrates of identical chemical properties but different rigidities (Pelham and Wang, 1997; Ren *et al.*, 2008). For this reason, the structured surfaces were constructed over a range of different crosslinker concentrations (C1, C2 and C3). Using a toolbox of *in situ* characterisation

techniques, including wettability measurements, QCM, AFM and confocal microscopy, the highly HA crosslinked films (C3) were selected to be used in *in vitro* studies.

The definition of low, medium and high molecular weight lacks consistency in studies using HA. In the present work small polymer (H_4), which consists of 4.3 kDa and approximately 22 saccharides was chosen based on the minimum of oligosaccharides that can bind to CD44. It is reported that 6 saccharides is the minimum size binding to CD44 (Kohda *et al.*, 1996). Regarding RHAMM, it is not reported the minimum size of polysaccharide that can bind to this receptor. In some studies, high molecular mass polymers are reported to be larger than 500 kDa, whereas in other studies are considered larger than 400 kDa or 262 kDa; with very-high-molecular size HA polymers reaching 20,000 kDa (Stern, 2006; Kothapalli *et al.*, 2008; Wolny *et al.*, 2010). HA with 2,590 kDa (HA_{2590}) was the chosen high molecular mass polymer, and HA_{234} consisting of 234 kDa the medium MW polymer. It would be also interesting to test different sizes of the polymer; for instance testing HA consisting of 6 saccharides and see whether it also binds to RHAMM. Regarding medium HA size, would be interesting to evaluate a polymer smaller than 234 kDa. In addition, it would be also interesting to investigate the effect of very-high-molecular size HA polymers.

Before investigating whether HA has as effect on proliferation of tumour-derived cell lines, cells were required to adhere and grow on the films. Cells were thus seeded and cultured on HA structured surfaces, coated with polymers of different molecular weights. To the present knowledge, this represents the first study were HA polymer MW has been suggested to modulate cell adhesion and differentiation of tumour-derived cell lines, with medium and large polymers preventing the attachment of tumour cells to the matrix. As a consequence, cells do not differentiate and acquire their normal morphology. Preliminary experiments have also shown that when placing

the cellular clumps on normal plastic tissue culture flask, cells spread and acquire again similar morphology to the control (data not shown). These findings might be correlated with the anti-adhesive properties of HA, also reported by other studies, where it was shown that HA promotes cell detachment (Barnhart *et al.,* 1979; Abatangelo *et al.*, 1982; Koochekpour *et al.*, 1995). Therefore, HA shows to have both adhesive and anti-adhesive properties, being correlated with the size of the polymer. The effects of HA on tumour cells attachment, proliferation and migration have not yet been completely studied and remain to be elucidated. However, findings from this work may suggest that the regulation of the differentiation of tumour cells is dependent on HA MW.

Using the constructed structured surfaces was demonstrated that HA-polymer MW modulates cell proliferation of human bladder (RT112 and T24) and prostate (PC3 and PNT1A) tumour-derived cell lines. Low HA MW (HA_4) increases proliferation, whereas a decrease is seen in the presence of medium (HA_{234}) and high MW fragments (HA_{2590}). Interestingly, the proliferation stimulus performed by HA appears to be phenotype dependent, with HA_4 surfaces stimulating an increased proliferation in those less invasive cell lines (T24 and PNT1A), while HA_{234} and HA_{2590} inducing a sharper decrease in the more malignant tumour cell lines (RT112 and PC3).

Cell proliferation occurs in a balance with apoptosis. In addition, targeted therapies that are designed to induce apoptosis in cancer cells are currently the most promising anti-cancer strategies, aiming to target and kill malignant cells with minimal or no collateral damage (Bremer, 2006). Therefore, after being shown that HA modulates cell proliferation, the next addressed question was whether HA also has an effect on apoptosis of tumour-derived cell lines. However, no production of significant amount of cleaved PARP protein, which serves as an early marker of apoptosis, was detected. These results may suggest that HA is not involved in the apoptosis pathway,

but only on proliferation of tumour-derived cell lines. In addition, the decreased proliferation seen for cells growing on medium and large HA fragments might be only correlated with a decrease of growth kinetics, and not apoptosis mechanism.

The reasons for the unique interactions of different molecular sizes of HA with tumour cells are not fully understood. However, it is believed that the biological functions presented by HA are mediated through interactions with its cellular receptors. CD44 and RHAMM are known to be the principal HA receptors, with CD44 being the most studied among the cell receptors identified. After being shown that HA is involved in the promotion of cell proliferation, the next question was whether the expression of CD44 and RHAMM was also modulated by the different molecular weights of HA. CD44 and RHAMM are hyaluronic acid receptors known to be involved in cell proliferation and development of tumourigenesis. It has been reported that HA fragments ranging 20-500 kDa promote cell cycle progression via CD44/Rac/ERK pathway in smooth muscle cells, whereas fragments with >500 kDa were shown to be inhibitory (Kothapalli *et al.,* 2008). Wolny and co-workers (2010) have shown that small fragments of HA (≤10 kDa) reversible bind to CD44, whereas an irreversible interaction with larger polymers is seen (Wolny *et al.,* 2010). It has also been reported that HA oligomers can induce very different cell responses when bound to CD44, comparatively to high MW fragments, because oligomers can cause clustering of multiple CD44 receptors and thus altering the intracellular responses (Liu *et al.,* 1998). It has been suggested that the interaction of HA oligomers with CD44 promote cell proliferation, due the enhancement of vascular endothelial growth factor (VEGF; Murphy *et al.,* 2005). Therefore, in the present investigation one could speculate that the expression of these receptors could be correlated with the cell proliferation findings obtained, with CD44 and RHAMM transcripts being up-regulated in cells growing in

the presence of HA_4, and down-regulated in the presence of HA_{234} and HA_{2590}. Unexpectedly, CD44 and RHAMM expression were found to be phenotype dependent, but not HA polymer size dependent; with CD44 and RHAMM being down-regulated in the most malignant cell lines (RT112 and PC3) and up-regulated in the less invasive cells (T24 and PNT1A). It can also be suggested that CD44 and RHAMM interplay, as the expression levels can be correlated: CD44 and RHAMM are either significantly up-regulated or down-regulated. Although cellular assays have provided insights into overall molecular pathways, the regulation of the interaction of the different molecular sizes of HA with its cell receptors, and its role in cancer progression, remains unclear. In addition, as previously discussed the definition of low, medium and high molecular weight lacks consistency in these studies, and there is not a consensus of the size of the polymer. For instance, in some studies either oligomers that correspond to a single binding site for CD44, or polymers with more than 100 binding sites are denoted as low MW (Wolny *et al.*, 2010).

It has been reported that the expression of certain CD44 variant isoforms is implicated in tumour metastasis (Henke *et al.*, 1996). In addition, RHAMM splice exon variants have been also detected in several tumours and cancer cell lines (Maxwell *et al.*, 2004). Hence, the next question was whether HA has also a role in the expression of CD44 and RHAMM splice variants transcription. The use of exon link assay revealed the expression of a number of CD44 variant exon junctions within the prostate and bladder *in vitro* models. It was demonstrated that RT112 and PC3 cells present a higher number of variants, which can be correlated with the more invasive and malignant phenotype of these cell lines. The non-appearance of some variants in cells growing in the presence of exogenous HA was also observed. Regarding RHAMM, it was observed that all four cell lines growing on HA structured surfaces express all variant isoforms.

The significance of these findings in tumourigenesis remains unclear. Similarly as performed for standard forms, the development of a real-time PCR assay for cell receptors isoforms would allow a more accurate transcription quantification.

The results from protein expression were found to be somehow correlated with the obtained transcripts expression. It can be seen that both CD44 and RHAMM proteins are detected in all four cell lines, appearing to be less expressed in RT112 and PC3 cells growing on HA-coated surfaces, when compared to control cells. Conversely, cell receptors appear to be more expressed on T24 and PNT1A cells growing in the presence of exogenous HA. In addition, it can be observed that lower levels of RHAMM are present in PNT1A cells, comparing to the other cell lines; being correlated with the phenotype nature of this cell line, as it is reported that in most of the normal tissues RHAMM mRNA and protein expression is low or undectable (Savani *et al.*, 1995; Mohapara *et al.*, 1996; Tolg *et al.*, 2003; Maxwell *et al.*, 2008). For all cell lines it can be observed a lower expression of RHAMM comparatively to CD44, what was previously observed for the transcripts expression. Both proteins appear to be expressed at both membrane, cytoplasmic and nuclei level. Western blotting and flow cytometry techniques, in addition the use of antibodies against CD44 and RHAMM isoforms, could be employed to clearly see whether alterations in mRNA expression were translated down to protein level in the cells.

It has been reported that the ability of cells to bind HA is due to CD44/HA interactions. Some studies have evidenced that melanoma cells in the absence of CD44 were not able to bind to HA, with higher levels of CD44 promoting binding of cancer cell lines to HA (Guo *et al.*, 1994; Herrera-Gayol and Jothy, 2001). Therefore, up-regulation of CD44 expression in the membrane could be expected, leading to increased cell adhesion and proliferation in those cells growing in the presence of HA_4.

Conversely, drop in CD44 expression at the membrane, leading to poorer adhesion and decreased proliferation in cells growing in HA_{234} and HA_{2590}-coated surfaces would also be expected. However, these findings were not observed for all cell lines. The unexpected CD44 and RHAMM expression findings obtained may be correlated with epithelial-mesenchymal transition (EMT) phenomena. EMT and the reverse process, denominated as mesenchymal-epithelial transition (MET), are processes involved in embryonic development. During embryogenesis, epithelial cells are required to change gene expression patterns, lose their adhesion molecules and become motile: mesenchymal-like cells that invade the ECM and differentiate into multiple tissues via EMTs; and later mesodermal cells generate epithelial organs by METs (Mani *et al.,* 2008). A similar process is also a prerequisite in tumour progression, particularly in the metastatic process; which includes the loss of adhesion molecules and the activation of common genes. The relevance of EMT to tumourigenesis has been explored *in vitro* using epithelial cell models. A number of embryonic transcription factors that play crucial roles in early embryogenesis, tissue morphogenesis and wound healing, have also been found to confer malignant characteristics to neoplastic cells (Greenburgand Hay 1986, Klymkowskyand Savagner 2009). Therefore, since active and activated genes during the carcinoma progression and metastasis are also active in other processes, these findings have led to the idea that EMT, as it occurs during developmental events, is also reactivated in the course of tumour development. The term EMT in tumourigenesis only refers to epithelial-derived cancers (carcinomas). However, the loss of cell-cell adhesion in epithelial cells, does not make an EMT phenotype (Klymkowskyand Savagner 2009).

Recent studies have suggested that HA is involved in EMT (Chow *et al.,* 2010). A study performed by Zoltan-Jones and co-workers (2003) have shown that increased

endogenous expression of high molecular weight HA is sufficient to induce EMT and acquisition of transformed properties in phenotypically normal epithelial cells (Zoltan-Jones *et al.,* 2003). These authors infected canine kidney and mammary human cells with a HAS2 adenovirus, leading to an increase in the endogenous levels of HA; they showed that high levels of high MW HA promoted cellular anchorage-independent growth and increased cell invasiveness. They also showed that the addition of HA oligomers and antibody against CD44 could reverse this anchorage independent growth (Zoltan-Jones *et al.,* 2003). Conversely, Chow and co-workers (2010) when transfecting non-small cell lung cancer with HAS3, which is involved in the synthesis of small HA chains, showed that small endogenous HA fragments promotes EMT phenotype and increased cell invasion (Chow *et al.,* 2010). A possible explanation for these differences seen can be correlated with the different types of tissues and tumours. In addition, both authors did not investigate the expression of HYALs that could also have increased expression and have been also reported to be involved in cancer progression; and therefore these results could be also related with the expression of HYALS. A question that arises from these studies is whether cells exhibit the same behaviour and are stimulated in the same way in the presence of exogenous or endogenous HA.

Two possible hypotheses arise from the findings obtained from the present investigation: cells growing in the presence of medium and high MW exogenous HA polymers may either lose their adhesion ability, due the anti-adhesion properties presented by HA; or on the other hand, may gain anchorage-independent growth properties related with the induction of mesenchymal transformed phenotype properties by HA in epithelial cells. In order to test both hypotheses, more studies would need to be performed, namely the investigation of the expression of other transient factors involved in EMT, including β-catenin, vimentin, E-cadherin, N-cadherin, Snail, Slug.

There is some evidence that malignant tumours may contain their own stem cells, denominated as cancer stem cells (CSCs). CSCs represent a small subpopulation of cells within the tumour, possessing a self-renewing ability and can differentiate into multiple lineages (Yu *et al.,* 2008, Fabrizi *et al.,* 2010, Fan *et al.,* 2010). Recently, CSCs have been isolated from leukaemia and several solid tumours, including colorectal, breast, prostate and bladder (Fan *et al.,* 2010, Bonnetand Dick 1997, Singh *et al.,* 2004, O'Brien *et al.,* 2007, Bentivegna *et al.,* 2010). Most of the CSCs have been isolated from clinical tumours specimens and only a few from established cell lines; being described that CSCs can form spheres *in vitro* (Yu *et al.,* 2008, Fan *et al.,* 2010). Another question that arose from this investigation was the nature of the cellular clumps observed, whether or not these clumps are tumourspheres formed by CSCs. It has been reported the prostate sphere formation of PC3 cells, being shown that PC3 cells can either grow in an adherent culture or form spheres in suspension culture system when growing in serum free media (Fan *et al.,* 2010). It is described that cancer stem cells are enriched in $CD44^+$; but since in general tumour prostate cells express CD44, it is difficult to use $CD44^+$ to sort prostate cancer stem cells (PrCSC). It has been described that cells with $CD44^+/CD133^+$ phenotype possess a marked capacity of self-renewal and differentiation into cells expressing androgen receptor and prostatic acid phosphates. Therefore, cell surface markers $CD44^+/CD133^+$ have been used to localise and isolate PrCSC. Fan and co-workers (2010) have shown that there was a markedly increased proportion of $CD44^+/CD133^+$ cells in sphere-forming population, but not in adherent cells (Fan *et al.,* 2010). However, in the present work a decreased expression of CD44 in PC3 cells, and an increased expression of this molecular receptor in PNT1A cells growing in the presence of exogenous HA, comparatively to control cells was observed. Therefore, it would be interesting to investigate the proportion of $CD44^+/CD133^+$ in

prostate cells. $CD133^+$ has been also described as a marker of tumour-initiating cells in other types of human cancer, including bladder carcinomas (Bentivegna *et al.*, 2010, Mizrak *et al.*, 2008). Other stem cell markers have been assessed for bladder cancer disorders, including Oct-3/4, nestin and cytokeratins (Bentivegna *et al.*, 2010). Hence, it would be interesting to investigate the presence of these cancer stem cell molecular markers in RT112 and T24 cell lines.

The work performed in this thesis provides a basis for future research. In this study was shown that HA polymer of medium and high MW decrease proliferation of tumour-derived cell lines. Hence, if it is highlighted that the formation of cellular clumps in the presence of medium and high MW polymers is associated with the anti-adhesion properties of HA, these molecules might be potentially used in cancer therapeutics. On the other hand, if there is some evidence that different molecular weights of HA are involved in EMT and formation of tumourspheres, the understanding of these spheres could lead to ideas for drugs and methods to be used in cancer therapeutic approaches.

CHAPTER 6

“Science... never solves a problem without creating ten more.” - George Bernard Shaw

CHAPTER 6

6. CONCLUSIONS AND FUTURE PERSPECTIVES

The aim of this work was to investigate whether HA polymer molecular weight (MW) alters the proliferation of tumour-derived cell lines, and to investigate the effect that HA has on the expression of CD44 and RHAMM, using HA-tethered culture surfaces. This aim was achieved, through meeting all of the objectives established within **Chapter 1**. Therefore, a variety of novel 2D HA structured surfaces to support cell adhesion have been constructed. These surfaces were coated with HA polymers of different MWs. Surfaces approached was used, since immobilised components on a 2D substract may more closely stimulate cell responses within 3D scaffolds due to intimate cell contact with the substract-bound HA, rather than periodic contact with exogenous HA of media supplementation. To the present knowledge, this represents the first study where surfaces coated with HA polymers of varying MWs have been constructed over a range of film stiffness. It was shown that the stiffness of films and the polymer MW modulate the surface characteristics (**Chapter 2**). Using these structured surfaces, human *in vitro* models have been established, allowing the assessment that HA has on cell proliferation and apoptosis of tumour-derived cell lines. This study demonstrates that HA-polymer molecular weight modulates adhesion, differentiation and proliferation of human bladder (RT112 and T24) and prostate (PC3 and PNT1A) tumour-derived cell lines. It was observed that all four cell lines adhered and grew on the structured surfaces, although different cellular growth patterns were observed depending on the MW of HA chain. It was also observed that HA MW does not appear to be involved in

the promotion of apoptosis (**Chapter 3**). In **Chapter 4** was demonstrated that HA regulates transcription and translation of CD44 and RHAMM cell receptors in a phenotype dependent manner. Findings from this work may also suggest that CD44 and RHAMM functioning is interrelated.

The findings from this investigation can help, not only in highlighting the biological significance that hyaluronic acid has on tumourigenesis, but also in the design and development of biocompatible implants with controlled surface properties to be used in cancer therapeutics. Implications from this work may allow better understanding of the biomaterial/cell interface, which is particularly important in many therapeutics applications, including tissue engineering and implant surgery. In addition, medium and large HA polysaccharides have shown to be potential biopolymer candidates, useful for the development of novel therapies for highly invasive cancer. Therefore, this study can serve as a base for future research, leading to ideas for drugs and methods to be used in cancer therapeutic approaches.

In conclusion, the work presented here has met the aims and objectives addressed to this project. However, a large body of further work arises from this project:

- From a surface side, would be interesting to characterise the amount of HA immobilised on each surface; this could be assessed, with ellipsometry. Some degradation studies would be also interesting to perform, to quantify if there is any loss of polymer and degradation of larger polymers into smaller along the time.

- Studies in 2D cell culture have produced results to help in the interpretation of complex biological phenomena and hypothesis. However, cells cultured in 3D cultures are characterised by several factors differentiating them from 2D dimensions and

providing findings more closely to those produced *in vivo*. Therefore, from an anatomical and physiological point of view, it would be useful to growth the tumour-derived cell lines in 3D constructed surfaces coated with HA polymers of different MWs.

- Confirmation of the absence of bands seen in CD44 exon link PCR by Southern Blotting, and analysis of CD44 and RHAMM isoforms transcript expression by real-time PCR.

- CD44 and RHAMM protein expression analysis by Western blotting and flow cytometry. The use of antibodies against CD44 and RHAMM isoforms would show more clearly whether alterations in mRNA expression were translated down to protein level in the cells.

- Knock-down and transfection of cell lines with CD44 and RHAMM isoforms, in order to disclose the role of each isoform in tumourigenesis.

- Analysis of HA synthases (HAS) expression, since has been demonstrated that the overexpression of HAS genes induces HA production and matrix formation. Additionally, there is some evidence that is due the HA overproduction that cancer cells form a HA-rich matrix, providing a suitable environment for tumour growth, invasion and metastasis. Furthermore, there is also some evidence that HAS isoforms are involved in different stages of malignant tumourigenesis.

- Analysis of hyaluronidases (HYALs) expression, since degradation of HA may be involved in the control of HA accumulation, with HYAL isoforms appearing to play roles in tumourigenesis. It would also be interesting to study the exogenous HYAL expression, to see whether the addition of HA to exogenous cellular environment led to endogenous HYALs production, ultimately leading to a disrupted HA and lower endogenous production.

- The relation of HA production/degradation and its function in cancer progression remains unclear. Therefore, would be interesting to carry out an analysis of the presence of HA in both culture media and cells, in order to detect the size/concentration of polymers present, and localisation of the polymer in the cells, correlating it with the production/degradation ratio.

- It is known that different CD44 and RHAMM isoforms are expressed depending on the cell type and disease pathology, and post-translational modifications modulate binding characteristics and functional properties of these proteins. In addition, for CD44 there is some evidence that post-translational modification patterns lead to differences in the HA binding. Therefore it would be interesting to clarify whether different HA-polymer MW alters expression of CD44 and RHAMM protein isoforms, and how it affects the binding affinity of the protein isoforms to HA.

- Since it was demonstrated in this work that HA modulates proliferation of tumour-derived cell lines, it would be useful to see whether HA polymer MW has an effect on cell adhesion, migration and invasion. In addition, further apoptotic studies by flow

cytometry would be useful to confirm whether HA molecular size is involved in promotion of apoptosis.

- It has been reported that in the presence of HA, RHAMM partners with CD44, activating erk1/2 and resulting in the expression of genes required for cell motility and invasion, and conferring malignant potential. In addition, it has been also evidenced that p53 down-regulates CD44 and RHAMM. Therefore, it would be interesting to investigate the effect that HA polymer MW has on the expression of erk1/2 and p53, correlating it with the expression of CD44 and RHAMM.

- There is some evidence that RHAMM is involved in the activation of the CD44-HA pathway, and in the absence of CD44, RHAMM seems to compensate the loss of CD44. However, it is still unclear how the absence of RHAMM affects CD44 expression. Therefore, through blocking studies, would be interesting to investigate the interplay between RHAMM and CD44, looking at transcripts and protein expression levels of these cell receptors and relating it with cell proliferation.

- One of the challenges of the present investigation was the study of the formed cell aggregates. Therefore, it would be useful to improve the immobilisation/analysis of the cell aggregates. This could be achieved by removing the clumps from the HA-coated slides and then cytospinning the cells in a new slide. It would be also interesting to embed these cellular clumps into paraffin, and then cut them into sections, and analyse these sections.

- Two possible hypotheses may arise from the findings obtained from the present investigation: cells growing in the presence of exogenous medium and high MW HA polymers may either lose their adhesion ability, due the anti-adhesion properties presented by HA; or on the other hand may gain anchorage-independent growth properties related with the induction of mesenchymal transformed phenotype properties by HA in epithelial cells. Therefore, in order to test these hypotheses, would be necessary to investigate the expression of other transient factors involved in EMT, including β-catenin, vimentin, E-cadherin, N-cadherin, Snail, Slug. In addition, it would be also interesting to investigate the expression of prostate and bladder cancer stem cell (CSC) markers, in order to confirm the presence/absence of CSCs.

- *In vivo* studies would be useful to see whether HA polymer MW also modulates proliferation of tumours in animal models. In addition, since HA has been reported to have immunostimulatory properties and a role in inflammation, would be interesting to relate the findings from tumour proliferation with inflammation.

REFERENCES

REFERENCES

Aaltomaa, S., Lipponen, P., Tammi, R., Tammi, M., Viitanen, J., Kankkunen, J. P., Kosma, V. M. (2002) *Strong stromal hyaluronan expression is associated with PSA recurrence in local prostate cancer*, Urologia Internationalis, 69(4): 266-272

Abatangelo, G., Cortivo, R., Martelli, M., Vecchia, P. (1982) *Cell detachment mediated by hyaluronic acid*, Experimental Cell Research 137: 73-78

Abatangelo, G., Cortivo, R., Martelli, M., Vecchia, P. (1982) *Cell detachment mediated by hyaluronic acid*, Experimental Cell Research, 137: 73-78

Adamia, S., Maxwell, C. A., Pilarski, L. M. (2005a) *Hyaluronan and hyaluronan synthases: potential therapeutic target in cancer*, Current Drug Targets, Cardiovascular & Haematological Disorders, 5: 3–14

Adamia, S., Reiman, T., Crainie, M., Mant, M. J., Belch, A. R., Pilarski, L. M. (2005b) *Intronic splicing of hyaluronan synthase 1 (HAS1): a biologically relevant indicator of poor outcome in multiple myeloma*, Blood, 105: 4836-4844

Afify, A., Purnell, P., Nguyen, L. (2009) *Role of CD44s and CD44v6 on human breast cancer cell adhesion, migration and invasion*, Experimental and Molecular Pathology, 86: 95-100

Aguiar, D. J., Knudson, W., Knudson, C. B. (1999) I*nternalization of the hyaluronan receptor CD44 by chondrocytes*, Experimental Cell Research, 252:292-302

Akiyama Y, Jung S, Salhia B, Lee S, Hubbard S, Taylor M, Mainprize T, Akaishi K, Van Furth W, Rutka J. (2001) *Hyaluronate receptors mediating glioma cell migration and proliferation*, Journal of Neuro-Oncology, 53: 2115-2127

Alberts, B., Johnson, A., Lewis, J., Raff, M., Roberts, K., Walter, P. (2002) *Molecular Biology of the Cell*, Fourth edition, Garland Science, London

Altschul, S. F., Gish, W., Miller, W., Myers, E. W., Lipman, D. J. (1990) *Basic local alignment search tool*, Journal of Molecular Biology, 215(3):403-10

Andersen, C. L., Jensen, J. L., Ørntoft , T. F. (2004) *Normalization of Real-Time Quantitative Reverse Transcription-PCR Data: A Model-Based Variance Estimation Approach to Identify Genes Suited for Normalization, Applied to Bladder and Colon Cancer Data Sets*, Cancer Research, 64: 5245-5250

Anttila, M. A., Tammi, R. H., Tammi, M. I., Syrjanen, K.. J., Saarikoski, S. V., Kosma, V. M. (2000) *High levels of stromal hyaluronan predict poor disease outcome in epithelial ovarian cancer,* Cancer Research, 60:150-5

Aruffo, A.; Stamenkovic, I.; Melnick, M.; Underhill, C. B.; Seed, B (1990) *CD44 is the principal cell surface receptor for hyaluronate*, Cell, 61: 1303-1313

Asplund, T., Versnel, M. A., Laurent, T. C., Heldin, P. (1993) *Human mesothelioma cells produce factors that stimulate the production of hyaluronan by mesothelial cells and fibroblasts,* Cancer research, 53: (2) 388-392

Assays for Cell Proliferation Studies: Determining Cell Count, Detecting DNA Synthesis, and Measuring Metabolic Activity (2006) Genetic Engineering & Biotechnology News, Vol. 26, Nº 6 (Accessed on 20 February 2009) http://www.genengnews.com/articles/chitem.aspx?aid=1442

Assman, V., Gillet, C. E., Poulsom, R., Ryder, K., Hart, I. R., Hanby, A. M. (2001) *The pattern of expression of the microtubule-binding protein RHAMM/IHAPB in mammary carcinoma suggests a role in the invasive behaviour of tumour cells*, Journal of Pathology, 195: 191-196

Assman, V., Jenkinson, D., Marshall, J. F., Hart, I. R. (1999) The intracellular hyaluronan receptor RHAMM/IHABP interacts with microtubules and actin filaments, *Journal of Cell Science, 112: 3943-3954*

Assmann, V., Marshall, J. F., Fieber, C., Hofmann, M., Hart, I. R. (1998) *The human hyaluronan receptor RHAMM is expressed as an intracellular protein in breast cancer cells*, Journal of Cell Science, 111: 1685-1694

Auvinen, P. K., Parkkinen, J. J., Johansson, R. T., Agren, U. M., Tammi, R. H., Eskelinen, M. J., Kosma, V. M. (1997) *Expression of hyaluronan in benign and malignant breast lesions*, International Journal of Cancer, 74:477-481

Auvinen, P. K., Tammi, R. Parkkinen, J. J., Tammi, M., Ågren, U. M., Johansson, R. T., Hirvikoski, P., , Eskelinen, M. J., Kosma, V. M. (2000) *Hyaluronan in peritumoral stroma and malignant cells associates with breast cancer spreading and predicts survival*, International, American Journal of Pathology, 156(2): 529-536

Bacáková, L., Filová, E., Rypácek, F., Svorcík, V., Starý, V. (2004) *Cell adhesion on artificial materials for tissue engineering*, Physiological Research, S35-S45

Baier, J. M. (2003) *Hyaluronic acid hydrogel biomaterials for soft tissue engineering applications*, PhD dissertation, University of Texas at Austin, USA

Baker, S. J., Markowitz, S., Fearon, E. R., Willson, J. K., Vogelstein, B. (1990) *Suppression of human colorectal carcinoma cell growth by wild-type p53,* Science ,249 (4971): 912–5

Balazs, E. A., Laurent, T. C., Jeanloz, R. W. (1986) *Nomenclature of hyaluronic acid*, Biochemical Journal, 286: 903

Banerji, S., Ni, J., Wang, S. X., Clasper, S., Su, J., Tammi, R., Jones, M., Jackson, D. G. (1999) *LYVE-1, a new homologue of the CD44 glycoprotein, is a lymph-specific receptor for hyaluronan*, Journal Cell Biology, 144: 789–801

Banhegyi, G., Mandl, J. (2001) *The hepatic glycogenoreticular system*, Pathology and Oncology Research, 7: 107-110

Barnhart, B., J., Cox, S. H., Kraemer, P. M. (1979) *Detachment Variants of chinese hamster cells. Hyaluronic acid as a modulator of cell detachment*, Experimental Cell Research, 119: 327–332

Bartolazzi A, Peach R, Aruffo A, Stamenkovic I. (1994) *Interaction between CD44 and hyaluronate is directly implicated in the regulation of tumor development*, Journal of Experimental Medicine, 180: 53-66

Bartolazzi, A., Nocks, A., Aruffo, A., Spring, F., Stamenkovic, I. (1996) *Glycosylation of CD44 is implicated in CD44-mediated cell adhesion to hyaluronan*, Journal of Cell Biology, 132: 1199-1208

Bast, R. C., Jr, Freeney, M., Lazarus, H., Nadler, L. M., Colvin, R. B., Knapp, R. C. (1981) *Reactivity of a monoclonal antibody with human ovarian carcinoma*, Journal Clinical Investigation, 68: 1331-1337

Bast, R. C., Klug, T. L., St John, E., Jenison, E., Niloff, J. M., Lazarus, H., Berkowitz, R. S., Leavitt, T., Griffiths, C. T., Parker, L., Zurawski, V. R., Jr, Knapp, R. C. (1983) *A radioimmunoassay using a monoclonal antibody to monitor the course of epithelial ovarian cancer*, New England Journal of Medicine, 309: 883-887

Bayliss, M. T., Howat, S. L., Dudhia, J., Murphy, J. M., Barry, F. P., Edwards, J. C., Day, A. J. (2001) *Up-regulating and differential expression of the hyaluronan-binding protein TSG-6 in cartilage and synovium in rheumatoid arthritis and osteoarthritis*, Osteoarthritis and Cartilage, 9: 42-48

Bell, M. V., Cowper, A. E., Lefranc, M-P., Bell, J. I., Screaton, G. R. (1998) *Influence of intron length on alternative splicing of CD44*, Molecular and Cellular Biology, 18(10): 5930-5941

Bendall, L. J., Nilsson, S. K., Khan, N. I., James, A., Bonnet, C., Lock, R. B., Papa, R., K Bradstock, K., F., Gottlieb, D. J. (2004) *Role of CD44 variant exon 6 in acute lymphoblastic leukaemia: association with altered bone marrow localisation and increased tumour burden*, Leukemia, 18: 1308-1311

Bennett, K. L., Modrell, B., Greenfield, B., Bartolazzi, A., Stamenkovic, I., Peach, R., Jackson, D. G., Spring, F., Aruffo, A. (1995) *Regulation of CD44 binding to hyaluronan by glycosylation of variably spliced exons*, Journal of Cell Biology, 131: 1623-1633

Bentivegna, A., Conconi, D., Panzeri, E., Sala, E., Bovo, G., Viganò, P., Brunelli, S., Bossi, M., Tredici, G., Strada, G., Dalprà, L. (2010) *Biological heterogeneity of putative bladder cancer stem-like cell populations from human bladder transitional cell carcinoma samples*, Cancer Science, 101: (2) 416-424

Bishop, J. M., Weinberg, R. A., (1996) *Molecular Oncology*, Scientific American Inc., New York.

Böhm, J., Niskanen, L., Tammi, R., Tammi, M., Eskelinen, M., Pirinen, R., Hollmen, S., Alhava, E., Kosma, V-M. (2002) *Hyaluronan expression in differentiated thyroid carcinoma,* American Journal of Pathology, 196: 180-185

Bonnet, D.Dick, J. E. (1997) *Human acute myeloid leukemia is organized as a hierarchy that originates from a primitive hematopoietic cell,* Nature medicine, 3: (7) 730-737

Bono, P., Cordero, E., Johnson, K., Borowsky, M., Ramesh, V., Jacks, T., Hynes, R. O. (2005) *Layilin, a cell surface hyaluronan receptor, interacts with merlin and radixin*, Experimental Cell Research, 308: 177–187

Borland, G., Ross, J. A., Guy, K. (1998) *Forms and functions of CD44,* Immunology, 93: 139-148

Borrowman, N. J., Myers, R. A. (2000) *Still more spawner-recruitment curves: the hockey stick and its generalizations,* Canadian Journal of Fisheries and Aquatic Sciences, 57: 665-676

Boudreau, N., Turley, E. A., Rabinovitch, M. (1991) *Fibronectin, hyaluronan, and a hyaluronan binding protein contribute to increased ductus arteriosus smooth muscle cell migration*, Dev Biol, 143: 235-247

Bourguignon, L. Y. M., Lokeshwar, V. B., Chen, X, Kerrick, W. G. L. (1993) *Hyaluronic acid-induced lymphocyte signal transduction and HA receptor (GP85/CD44)-cytoskeleton interaction*, Journal of Immunology, 151: 6634-6644

Bourguignon, L. Y. M., Lokeshwar, V. B., Chen, X., Kerrick, W. G. L. (1993) *Hyaluronic acid-induced lymphocyte signal transduction and HA receptor (GP85/CD44)-cytoskeleton interaction*, Journal of Immunology, 151: 6634-6644

Bourguignon, L. Y., Walker, G., Suchard, S. J., Balazovich, K. (1986) *A lymphoma plasma membrane-associated protein with ankyrin-like properties*, Journal of Cell Biology, 102: 2115-2124

Bremer, E. (2006) *Targeted induction of apoptosis for cancer therapy*, PhD dissertation, University of Gronigen, Netherlands

Brown, T. A., Bouchard, T., John, T St., Wayne, E., Carter, W. G. (1991) *Human keratinocytes express a new CD44 core protein (CD44E) as a heparan-snifate intrinsic membrane proteoglycan with additional exons,* The Journal of Cell Biology, 113: 207-221

Brugarolas, J., Chandrasekaran, C., Gordon, J., Beach, D., Jacks, T., Hannon, G. J. (1995) Radiation induced cell cycle arrested compromised by p21 deficiency, Nature, 377: 552-557

Carmichael, J., DeGraff, W. G., Gazdar, A. F., Minna, J. D., Mitchell, J. B. (1987) *Evaluation of a tetrazolium-based semiautomated colorimetric assay: assessment of radiosensitivity,* Cancer Research, 47: 943-946

Carter, W. G., Wayner, E. A. (1988) *Characterization of the class III collagen receptor, a phosphorylated, transmembrane glycoprotein expressed in nucleated human cells,* Journal of Biological Chemistry, 263(9): 4193-4201

Castner, D. G., Ratner, B. D. (2002) *Biomedical surface science: Foundations to frontiers,* Surface Science, 500: 28-60

Chandrasekaran, V., Gopal, G., Thomas, A. (2005) *Piece wise linear growth curve modeling in repeated measures analysis,* Statistics in Medicine, 24(8): 1139-1151

Chang, C. Y. M., Harrison, R., Li, A., Yang, X., Turley, E. A. (1997) Fibronectin-RHAMM interaction regulate cell motility, FASEB Journal, A1095-1397

Chen, W. J. Y.Abatangelo, G. (1999) *Functions of hyaluronan in wound repair,* Wound Repair and Regeneration, 8: 79-89

Cheung, W. F., Cruz, T. F., Turley, E. A. (1999) *Receptor for hyaluronan-mediated motility (RHAMM), a hyaladherins that regulates cell responses to growth factors,* Biochemical Society Transactions, 27: 135-142

Chianella, I. (2010) Personal communication

Chow, G., Tauler, J., Mulshine, J. L. (2010) *Cytokines and growth factors stimulate hyaluronan production: Role of hyaluronan in epithelial to mesenchymal-like transition in non-small cell lung cancer*, Journal of Biomedicine and Biotechnology, 2010:

Cobbold, S. H. (1987) *Human leukocyte differentiation antigens: monoclonal antibody computer databases as a tool for the future*, Molecular and Cellular Probes, 1: 61-72

Coleman, W. B., Tsongalis, G. T. (2002) *Molecular basis of human cancer*, Humana Press, Totowa, New Jersey

Collins, M. N., Birkinshaw, C. (2007) *Comparison of the effectiveness of four different crosslinking agents with hyaluronic acid hydrogel films for tissue-culture applications*, Journal of Applied Polymer Science, 104: 3183–3191

Collins, M. N., Birkinshaw, C. (2008) *Physical properties of crosslinked hyaluronic acid hydrogels*, Journal of Materials Science: Materials in Medicine, 19: 3335–3343

Con, L. M. G. (2009) Personal communication

Cooper, G. M., Hausman, R. E. (2007) *The cell: A molecular approach*, Fourth edition, ASM Press and Sinauer Associates, Inc., USA

Cowman, M. K., Spagnoli, C., Kudasheva, D., Li, M., Dyal, A., Kanai, S., Balazs, E. A. (2005) *Extended, relaxed and condensed conformations of hyaluronan observed by atomic force microscopy*, Biophysical Journal, 88: 590-602

Crainie, M., Belch, A. R., Mant, M. J., Pilarski, L. M. (1999) *Overexpression of the receptor for hyaluronan-mediated motility (RHAMM) characterizes the malignant clone in multiple myeloma: Identification of three distinct RHAMM variants*, Blood, 93:1684-1696

Crainie, M., Belch, A. R., Mant, M. J., Pilarski, L. M. (1999) *Overexpression of the receptor for hyaluronan-mediated motility (RHAMM) characterizes the malignant clone in multiple myeloma: Identification of three distinct RHAMM variants*, Blood, 93: 1684-1696

Csoka, T. B., Frost, G. I., Stern, R. (1997) *Hyaluronidases in tissue invasion*, Invasion Metastasis, 17: 297-311

Culty, M., Nguyen, H. A., Underhill, C. B. (1992) *The hyaluronan receptor (CD44) participates in the uptake and degradation of hyaluronan*, Journal Cell Biology, 116: 1055-1062

Cussenot, O., Berthon, P., Berger, R., Mowszowicz, I., Faille, A., Hojman, F., Teillac, P., Le Duc, A., Calvo, F. (1991) *Immortalization of human adult normal prostatic epithelial cells by liposomes containing large T-SV40 gene*, Journal of Urology, 146(3): 881-886

Dahl, I. M. S., Laurent, T. C. (1988) *Concentration of hyaluronan in serum of untreated cancer patients with special reference to patients with mesothelioma*, Cancer, 62: 326-330

Dahl, L., Hopwood, J. J., Laurent, U. B., Lilja, K., Tengblad, A. (1983) *The concentration of hyaluronate in amniotic fluid*, Biochemical Medicine, 30: 280-283

Dalchau, R., Kirley, J., Fabre, J. W. (1980) *Monoclonal antibody to a human brain-granulocyte-T lymphocyte antigen probably homologous to the W 3/13 antigen of the rat*, European Journal of Immunology, 10: 745-749

Damos, F. S., Mendes, R. K., Kubota, L. K. (2004) *Applications of QCM, EIS and SPR in the investigation of surfaces and interfaces for the development of (bio)sensors*, Química Nova, 27(6): 970-979

David-Raoudi, M., Tranchepain, F., Deschrevel, B., Vincent, J., Bogdanowicz, P., Boumediene, K., Pujol, J. (2008) *Differential effects of hyaluronan and its fragments on fibroblasts: Relation to wound healing*, Wound Repair and Regeneration, 16: 274-287

David-Raoudi, M., Tranchepain, F., Deschrevel, B., Vincent, J-C., Bogdanowicz, P., Boumediene, K., Pujol, J-P. (2008) *Differential effects of hyaluronan and its fragments on fibroblasts: Relation to wound healing*, Wound Repair and Regeneration, 16: 274-287

Day, A. J., de la Motte, C. A. (2005) *Hyaluronan cross-linking: a protective mechanism in inflammation*, Trends in Immunology, 26: 637-643

Day, A. J., Prestwich, G. (2002) *Hyaluronan-binding proteins: tying up the giant*, The Journal of Biological Chemistry, 277(7): 4585-4588

DeAngelis, P. L. (1999) *Hyaluronan synthases: fascinating glycosyltransferases from vertebrates, bacterial pathogens, and algal viruses*, Cellular and Molecular Life Sciences, 56: 670-682

Decker, M., Chiu, E. S., Dollbaum, C., Moiin, A., Hall, J., Spendlove, R., Longaker, M. T., Stern, R. (1989) *Hyaluronic acid-stimulating activity in sera from the bovine fetus and from breast cancer patients*, Cancer Research, 49: 3499-3505

Deed, R., Rooney, P., Kumar, P., Norton, J. D., Smith, J., Freemont, A. J., Kumar, S. (1997) *Early response gene signaling is induced by angiogenic oligosaccharides of hyaluronan in endothelial cells*, Inhibition by non-angiogenic, high-molecular-weight hyaluronan., International Journal of Cancer, 71: 251-256

Deguine, V., Menasche, M., Ferrari, P., Fraisse, L., Pouliquen, Y., Robert, L. (1998) *Free radical depolymerization of hyaluronan by Maillard reaction products: role in liquefaction of aging vitreous*, Int. J. Biol. Macromol, 22: 17-22

Delmage, J. M., Powars, D. R., Jaynes, P. K., Allerton, S. E. (1986) *The selective suppression of immunogenicity by hyaluronic acid*, Annals of Clinical and Laboratory Science, 16: 303-310

Delpech, B., Maingonnat, C., Girard, N., Chauzy, C., Maunoury, R., Olivier, A., Tayot, J, Creissard. P. (1993) *Hyaluronan and hyaluronectin in the extracellular matrix of human brain tumour stroma*, European Journal of Cancer, 29A:1012-1017

Desai, B., Rogers, M. J., Chellaiah, M. A. (2007) *Mechanisms of osteopontin and CD44 as metastatic principles in prostate cancer cells*, Molecular Cancer, 7: 6-18

Dick, S. J., Macchi, B., Papazoglou, S., Oldfield, E. H., Kornblith, P. L., Smith, B. H., and Gately, M. K. (1983) *Lymphoid cell-glioma cell interaction enhances cell coat production by human gliomas: novel suppressor mechanism*, Science, 220: 739-742

Duranti, F., Salti, G., Bovani, B., Calandra, M., Rosati, M. L. (1998) *Injectable hyaluronic acid gel for soft tissue augmentation. A clinical and histological study*, Dermatologic Surgery, 24: 1317-1325

Enegd, B., King, J. A., Stylli, S., Paradiso, L., Kaye, A. H., Novak, U. (2002) *Overexpression of hyaluronan synthase-2 reduces the tumorigenic potential of glioma cells lacking hyaluronidase activity*, Neurosurgery, 50: 1311-1318

Engel, A., Gaub, H. E., Müller, D. J. (1999) *Atomic force microscopy: A forceful way with single molecules*, Current Biology, 9(4): 133-136

Entwistle., J., Hall., C. L., Turley, E. A. (1996) *HA receptors: Regulators of signaling to the cytoskeleton*, Journal of Cell Biochemistry, 61:569-577

Etienne, O., Gasnier, C., Taddei, C., Voegel, J-C., Aunis, D., Schaaf, P., Metz-Boutigue, M. H., Bolcato-Bellemin, A-L., Egles, C. (2005) *Antifungal coating by biofunctionalized polyelectrolyte multilayered films*, Biomaterials, 26: 6704-6712

Evanko, S. P., Tammi, M. I., Tammi, R. H., Wight, T. N. (2007) *Hyaluronan-dependent pericellular matrix*, Advanced Drug Delivery Reviews, 59: 1352-1365

Faassen, A. E., Schrager, J. A., Klein, D. J., Oegema, T. R., Couchman, J. R., McCarthy, J. B. (1992) *A cell surface chondroitin sulfate proteoglycan, immunologically related to CD44, is involved in type I collagen-mediated melanoma cell motility and invasion*, Journal of Cell Biology, 116(2): 521-531

Fabrizi, E., di Martino, S., Pelacchi, F., Ricci-Vitiani, L. (2010) *Therapeutic implications of colon cancer stem cells*, World Journal of Gastroenterology, 16: (31) 3871-3877

Fan, X., Liu, S., Su, F., Pan, Q., Lin, T. (2010) *Effective enrichment of prostate cancer stem cells from spheres in a suspension culture system*, Urologic Oncology: Seminars and Original Investigations,

Feinberg, R. N., Beebe, D. C. (1983) *Hyaluronate in vasculogenesis*, Science, 220: 1177-1179

Fero, M. L., Randel ,E., Gurley, K. E., Roberts, J. M., Kemp, C. J. (1998) T*he murine gene p27Kip1 is haplo-insufficient for tumour suppression*, Nature, 396 (6707): 177-180

Fieber, C., Plug, R., Sleeman, J., Dall, P., Ponta, H., Hofmann, M. (1999) *Characterisation of the murine gene enconding the intracellular hyaluronan receptor IHABP (RHAMM)*, Gene, 226: 41-50

Figueiredo, A., Ferreira, L., Figueiredo, P. (2001) *Impacto psico-social do cancro da mama na mulher*, Enfermagem Oncológica, Porto, 17: 22-27

Forrester, J. V., Balazs, E. A. (1980) *Inhibition of phagocytosis by high molecular weight hyaluronate*, Immunology, 40: 435-446

Forsberg, U. H., Ala-Kapee, M. M., Jalkanen, S., Andersson, L. C., Schroder, J. (1989b) *The gene for human lymphocyte homing receptor is located on chromosome 11*, European Journal of Immunology, 19: 409-412

Forsberg, U. H., Jalkanen, S., Schroder, J. (1989a) *Assignment of the human lymphocyte homing receptor gene to the short arm of chromosome 11*, Immunogenetics 29: 405-407

Foschi, D., Castoldi, L., Radaelli, E., Abelli, P., Calderini, G., Rastrelli, A., Mariscotti, C., Marazzi, M., Trabucchi, E. (1990) *Hyaluronic acid prevents oxygen free-radical damage to granulation tissue: a study in rats*, International Journal Tissue Reactions, 12: 333-339

Francke, U.; Foellmer, B. E.; Haynes, B. F. (1983) *Chromosome mapping of human cell surface molecules: monoclonal anti-human lymphocyte antibodies 4F2, A3D8, and A1G3 define antigens controlled by different regions of chromosome 11*, Somatic Cell and Molecular Genetics, 9: 333-344

Frank, S. A. (2007) *Dynamics of Cancer: Incidence, Inheritance, and Evolution*, Princeton University Press, UK

Fraser, J. R. E., Laurent, T. C., Laurent, U. B. G. (1981) *Hyaluronan: its nature, distribution and turnover*, Journal of Internal Medicine, 242: 27-33

Fraser, J. R., Laurent, T. C., Pertoft, H., Baxter, E. (1981) *Plasma clearance, tissue distribution and metabolism of hyaluronic acid injected intravenously in the rabbit*, Biochemical Journal, 200: 415-424

Freshney, R. I. (2005) *Culture of animal cells: A manual of basic techniques*, Fifth edition, John Wiley & Sons, Inc., New Jersey, USA

Fulop, C., Salustri, A., Hascall, V. C. (1997) *Coding sequence of a hyaluronan synthase homologue expressed during expansion of the mouse cumulus-oocyte complex*, Archives of Biochemistry and Biophysics, 337:261-266

Gabriel, J. A. (2007) *The biology of cancer*, Second edition, John Wiley & Sons Ltd, England

Gadducci, A., Ferdeghini, M., Fanucchi, A., Annicchiarico, C., Cosio, S., Prontera, C., Bianchi, R., Genazzani, A. R. (1997) *Serum assay of soluble CD44 standard (sCD44-st), CD44 splice variant v5 (sCD44-v5), and CD44 splice variant v6 (sCD44-v6) in patients with epithelial ovarian cancer*, Anticancer Research, 17: 4463-4466

Gao, A. C., Lou, W., Dong, J. T., Isaacs, J. T. (1997) *CD44 is a metastasis suppressor gene for prostatic cancer located on human chromosome 11p13*, Cancer Research, 57: 846-9

Gardner, D. K., Rodriegez-Martinez, H., Lane, M. (1999) *Fetal development after transfer is increased by replacing protein with the glycosaminoglycan hyaluronan for mouse embryo culture and transfer*, Human Reproduction, 14: 2575-2580

Gardner, D. K., Rodriegez-Martinez, H., Lane, M. (1999) *Fetal development after transfer is increased by replacing protein with the glycosaminoglycan hyaluronan for mouse embryo culture and transfer*, Human Reproduction, 14: 2575-2580

George, J., Stern, R. (2004) *Serum hyaluronan and hyaluronidase: very early markers of toxic liver injury*, Clinica Chimica Acta, 348: 189-197

Gewies, A. (2003) *Introduction to apoptosis*. *In:* ApoReview (online encyclopedia)

Ghatak, S., Misra, S., Toole, B. P. (2002) *Hyaluronan oligosaccharides inhibit anchorage-independent growth of tumor cells by suppressing the phosphoinositide 3-kinase/Akt cell survival pathway*, Journal of Biological Chemistry, 277: 38013-38020

Girish, K. S., Kemparaju, K. (2007) *The magic glue and its eraser hyaluronidase: A biological overview*, Life Sciences, 80: 1921-1943

Girish, K. S.Kemparaju, K. (2007) *The magic glue and its eraser hyaluronidase: A biological overview*, Life Sciences, 80: (1921) 1943

Goi, T., Yamaguchi, A., Seki, K., Nakagawara, G., Urano, T., Shiku, H., Furukawa, K. (1997) *Soluble protein encoded by CD44 variant exons 8-10 in the serum of patients with colorectal cancer*, British Journal of Surgery, 84: 1452-1453

Gold, P., Freedman, S. O. (1965) *Demonstration of tumor-specific antigens in human colonic carcinomata by immunological tolerance and absortion techniques*, Journal Experimental Medicine, 121(3): 439–462

Goldstein L. A., Zhou D. F., Picker L. J., Minty C. N., Bargatze R. F., Ding J. F., Butcher E. C. (1990) *A human lymphocyte homing receptor, the hermes antigen, is related to cartilage proteoglycan core and link proteins*, Cell, 56*:* 1063-1072

Goodhew, P., Humpreys, J. Beanland, R. (2001) Electron Microscopy and Analysis. Third Edition, Taylor & Francis, London, UK

Goodison, S., Yoshida, K., Sugino, T., Woodman, A., Gorham, H., Bolodeoku, J., Kaufman, M., Tarin, D. (1997) *Rapid analysis of distinctive CD44 RNA splicing preferences that characterize colonic tumors*, Cancer Research, 57: 3140-3144

Gosh, I., Chowdhury, A. R., Rajeswari, M. R., Datta, K. (2004) *Differential expression of hyaluronic acid binding protein 1 (HAPB1)/P32/C1QBP during progression of epidermal carcinoma*, Molecular and Cellular Biochemistry, 267: 133-139

Granger, H. J., Laine, G. A., Barnes, G. E., Lewis, R. E. (1984) *Dynamics and control of transmicrovascular fluid exchange*. In: Staub, N. C., Taylor, A. E., Edema, Raven Press, New York, pp. 189-228

Greenburg, G.Hay, E. D. (1986) *Cytodifferentiation and tissue phenotype change during transformation of embryonic lens epithelium to mesenchyme-like cells in vitro,* Developmental biology, 115: (2) 363-379

Greiner, J., Ringhoffer, M., Taniguchi, M., Schmitt, A., Kirchner, D., Krahn, G., Heilman, V., Gschwend, J., Bergmann, L., Dohner, H., Schmitt, M. (2002) *Receptor for hyaluronan acid-mediated motility (RHAMM) is a immunogenic leukemia-associated antigen in acute and chronic myeloid leukemia*, Experimental Hematology, 30: 1029-1035

Günthert, U. (2001) *CD44: A multitude of isoforms with diverse functions*, Current Topics in Microbiology and Immunology, 184: 45-62

Günthert, U., Hoffman, M., Wolfgang, R., Reber, S., Zoller, M., Hausmann, I., Matzku, S., Wenzel, A., Ponta, H., Herrilich, P. (1991) *A new variant of glycoprotein CD44 confers metastic potential to rat carcinoma cells*, Cell, 65: 13-24

Guo, Y., Ma, J., Wang, J., Che, X., Narula, J., Bigby, M., Wu, M., Sy, M-S. (1994) *Inhibition of human melanoma growth and metastasis in vivo by anti CD44 monoclonal antibody*, Cancer Research, 54: 1561-1565

Güthert, U., Hofmann, M., Rudy, W., Reber, S., Zoller, M., Haussman, I., Matzku, S., Wenzel, A., Ponta, H., Herrich, P. (1991) *A new variant of glycoprotein CD44 confers metastatic potential in rat carcinoma cells*, Cell, 65: 13-24

Hall, C. L., Lange, L. A., Prober, D. A., Zhang, S., Turley, E. A. (1996) *Pp60 (c-scr) is required for cell locomotion regulated by the hyaluronan receptor RHAMM*, Oncogene, 13: 2213-2224

Hall, C. L., Turley, E. A. (1995) *Hyaluronan: RHAMM mediated cell locomotion and signaling in tumorigenesis*, Journal of Neuro-Oncol, 26: 221-229

Hall, C. L., Yang, B., Yang, X., Zhang, S., Turley, M., Samuel, S., Lange, L. A., Wang, C., Curpen, G. D., Savani, R. C., Turley, E. A. (1995) *Overexpression of the hyaluronan receptor RHAMM is transforming and is also required for H-ras transformation*, Cell, 82:19-26

Hamdan, M. H. (2007) *Cancer biomarkers – Analytical techniques for discovery*, John Wiley & Sons, New Jersey

Hamerman, D., Sandson, J. (1963) *Unusual properties of hyaluronateprotein isolated from pathological synovial fluids*, The Journal of Clinical Investigation, 42: 1882-1889

Hamerman, D., Todaro, G. J., Green, H. (1965) *The production of hyaluronate by spontaneously established cell lines and viral transformed lines of fibroblastic origin*, Biochimica et Biophysica Acta, 101:343-351

Hamilton, S. R., Fard, S. F., Paiwand, F. F., Tolg, C., Veiseh, M., Wang, C., McCarthy, J. B., Bissell, M. J., Koropatnick, J., Turley, E. A. (2007) *The hyaluronan receptors CD44 and Rhamm (CD168) form complexes with ERK1,2 that sustain high basal motility in breast cancer cells*, The Journal of Biological Chemistry, 282(22): 16667-16680

Hanahan, D., Weinberg, R. A. (2000) *The hallmarks of cancer*, Cell, 100: 57-70

Hardingham, T. E., Fosang, A. M. (1992) Proteoglycans: many forms and many functions, The FASEB Journal, 6: 861-870

Hardingham, T. E., Muir, H. (1972) *The specific interaction of hyaluronan acid with cartilage proteoglycans*, Biochimica et Biophysicsa Acta, 279: 401-405

Hardwick, C., Hoare, K., Owens, R., Hohn, H. P., Hook, M., Moore, D., Cripps, V., Austen, L. (1992) *Molecular cloning of a novel hyaluronan receptor that mediates tumor cell motility*, The Journal of Cell Biology, 117: 1343-1350

Harrison, G. M., Davies, G., Martin, T. A., Mason, M. D., Jiang, W. G. (2006) *The influence of CD44v3-v10 on adhesion, invasion and MMP-14 expression in prostate cancer cells*, Oncology Reports, 15: 199-206

Hartmann, U., Maurer, P. (2000) *Proteoglycans in the nervous system – the quest for functional roles in vivo*, Matrix Biology, 20: 23-35

Hautman, S. H., Lokeshwar, V. B., Schroeder, G. L., Civantos, F., Duncan, R. C., Gnann, R. Friedrich, M. G., Soloway, M. S. (2001) *Elevated tissue expression of*

hyaluronic acid and hyaluronidase validates the HA-HAase urine test for bladder cancer, Journal of Urology, 165:2068-2075

Heldin, P. (2003) *Importance of hyaluronan biosynthesis and degradation in cell differentiation and tumor formation*, Brazilian Journal of Medical and Biological Research, 36: 967–973

Henke, C., Bitterman, P., Roongta, U., Ingbar, D., Polunovsky, V. (1996) *Induction of fibroblast apoptosis by anti-CD44 antibody: implications for the treatment of fibroproliferative lung disease*, American Journal of Pathology, 149(5): 1639-1650

Herrera-Gayol, A., Jothy, S. (2001) *Effects of hyaluronan on the invasive properties of human breast cancer cells in vitro*, International Journal of Experimental Pathology, 82(3): 193-200

Hiltunen EL, Anttila M, Kultti A, Ropponen K, Penttinen J, Yliskoski M, Kuronen, A. T., Juhola, M., Tammi, R., Tammi, M., Kosma, V-M. (2002) *Elevated hyaluronan concentration without hyaluronidase activation in malignant epithelial ovarian tumors*, Cancer Research, 62: 6410-6413

Hoekstra, D. (1999) *Hyaluronan-Modified Surfaces for Medical Devices*, Medical Device & Diagnostic Industry Magazine

Hofinger, E.S. A., Hoechstetter, J., Oettl M., Bernhardt G., Buschauer A. (2008) Isoenzyme-specific differences in the degradation of hyaluronic acid by mammalian-type hyaluronidases, Glycoconj Journal, 25:101–109

Hollenberg, M. J., Erickson, A. M. (1973) *The scanning electron microscope: potential usefulness for biologists*, Journal of Hystochemistry and Cytochemistry, 21: 109-130

Hopwood, J. J., Dorfman, A. (1977) *Glycosaminoglycan synthesis by cultured human skin fibroblasts after transformation with simian virus 40*, Journal of Biological Chemistry, 252: 4777-4785

Hopwood, J. J., Dorfman, A. (1978) *Glycosaminoglycan synthesis by Wilms' tumor*, Pediatric Research, 12:52-6

Horai, T., Nakamura, N., Tateishi, R., Hattori, S. (1981) *Glycosaminoglycans in human lung cancer*, Cancer. 48:2016-2021

Horst, E., Meijer, C. J. L. M., Radaszkiewicz, T., Ossekopele, G. J., Van Krieken, J. H. J. M., Pals, S. (1990) *Adhesion molecules in the prognosis of diffuse large cell lymphoma: expression of a lymphocyte homing receptor (CD44), LFA-1 (CD11a/18), and ICAM-1 (CD54),* Leukemia, 4(8):595-599

Horton, M. R., McKee, C. M., Bao, C., Liao, F., Farber, J. M., Hodge-DuFour, J., Pure, E., Oliver, B. L., Wright, T. M., Noble, P. W. (1998) *Hyaluronan fragments synergize with interferon-g to induce the C-X-C chemokines Mig and interferon-inducible protein-10 in mouse macrophages,* Journal of Biological Chemistry, 273: 35088-35094

Horton, M. R., Olman, M. A., Bao, C., White, K. E., Choi, A. M., Chin, B. Y., Noble, P. W., Lowenstein, C. J. (2000) *Regulation of plasminogen activator inhibitor-1 and urokinase by hyaluronan fragments in mouse macrophages*, American Journal of Physiology – Lung Cellular and Molecular Physiology, 279: L707–L715

Hua, Q., Knudson, C. B., Knudson, W. (1993) *Internalization of hyaluronan by chondrocytes occurs via receptor-mediated endocytosis*, Journal Cell Science, 106: 365-375

Huet S, Groux H, Caillou B, Valentin, H., Prieur, A. M., Bernard, A. (1989) *CD44 contributes to T-cell activation*, The Journal of Immunology, 143: 798-801

Humphris, A. D. L., Miles, M. J., Hobbs, J. K. (2005) *A mechanical microscope: High-speed atomic force microscopy*, Applied Physics Letters, 86: 034106

Hutmacher, D. W., Loessner, D., Rizzi, S., Kaplan, D. L., Mooney, D. J., Clements, J. A. (2010) *Can tissue engineering concepts advance tumor biology research?* Trends in Biotechnology, 28: (3) 125-133

Ibrahim, S., Joddar, B., Craps, M., Ramamurthia, A. (2007) *A surface-tethered model to assess size-specific effects of hyaluronan (HA) on endothelial cells*, Biomaterials 28: 825-835

Ibrahim, S., Joddar, B., Craps, M., Ramamurthia, A. (2007) *A surface-tethered model to assess size-specific effects of hyaluronan (HA) on endothelial cells,* Biomaterials, 28: 825-835

Iczkowski, K. A., Pantazis, C. G., Collins, J. (1997) *The loss of expression of CD44 standard and variant isoforms is related to prostatic carcinoma development and tumor progression,* Journal of Urologic Pathology, 6:119-129

Isacke, C. M., Yarwood, H. (2002) *The hyaluronan receptor, CD44,* The International Journal of Biochemistry and Cell Biology, 34(7): 718-721

Ishii, S., Ford, R., Thomas, P., Nachman, A., Steele, G. Jr., Jessup, J. M. (1993) *CD44 participates in the adhesion of human colorectal carcinoma cells to laminin and type IV collagen,* Surgical Oncology, 2(4): 255-264

Ishimoto, N., Temin, H. M., Strominger, J. L. (1966) *Studies of Carcinogenesis by Avian Sarcoma Viruses – II Virus-induced in hyaluronic acid synthetase in chicken fibroblasts,* The Journal of Biological Chemistry, 241: 2052-2057

Itano, N., Kimata, K. (1996a) *Expression cloning and molecular characterization of HAS protein, a eukaryotic hyaluronan synthase,* Journal Biological Chemistry, 271(17):9875–9878

Itano, N., Kimata, K. (1996b) *Molecular cloning of human hyaluronan synthase,* Biochemical and Biophysical Research communications, 222: 816-820

Itano, N., Sawai, T., Atsumi, F., Miyaishi, O., Taniguchi, S., Kannagi, R., Hamaguchi, M., Kimata, K. (2004) *Selective expression and functional characteristics of three mammalian hyaluronan synthases in oncogenic malignant transformation, Journal of Biological Chemistry,* **279**: 18679-18687

Itano, N., Sawai, T., Yoshida, M., Lenas, P., Yamada, Y., Imagawa, M., Shinomurai, T., Hamaguchi, M., Yoshida, Y., Ohnuki, Y., Miyauchi, S., Spicer, A., McDonald, J. A., Kimata, K. (1999) *Three isoforms of mammalian hyaluronan synthases have distinct enzymatic properties,* The Journal of Biological Chemistry, (274) 34: 25085-25092

Ito, T., Williams, J. D., Al-Assaf, S., Phillips, G. O., Phillips, A. O. (2004) *Hyaluronan and proximal tubular cell migration*, Kidney International, 65: 823-833

Jackson, D. G. (2003) *The lymphatics revisited: new perspectives from the hyaluronan receptor LYVE-1*, Trends in Cardiovascular Medicine, 13: 1-7

Jackson, D. G. (2004) *Biology of the lymphatic marker LYVE-1 and applications in research into lymphatic trafficking and lymphogiogenesis,* Acta Pathologica, Microbiologica et Immunologica Scadinavica, 112: 526-538

Jackson, D. G., Prevo, R., Clasper, S., Banerji, S. (2001) *LYVE-1, the lymphatic system and tumor lymphagiogenesis,* Trends in Immunogy, 22: 317-321

Jalkanen, S., Bargatze, R., De los Toyos, J., Butcher, E. C (1987) *Lymphocyte recognition of high endothelium: antibodies to distinct epitopes of an 85–95 kD glycoprotein antigen differentially inhibit lymphocyte binding to lymph node, mucosal, or synovial endothelial cells,* Journal of Cell Biology, 105: 983–90

Jalkanen, S., Bargatze, R., Herron, L., Butcher, E. C (1986) *A lymphoid cell surface glycoprotein involved in endothelial cell recognition and lymphocyte homing in man,* European Journal of Immunology, 16: 1195-202

Jalkanen, S., Jalkanen, M. (1992) *Lymphocyte CD44 binds the COOH terminal heparin-binding domain of fibronectin*, Journal of Cell Biology, 116(3): 817-825

Jemal, A., Siegal, R., Ward, E., Murray, T., Xu, J., Thun, M. J. (2007) *Cancer statistics, 2007*, CA – A Cancer Journal for Clinicians, 57: 43-66

Jiang, D., Liang, J., Fan, J., Yu, S., Chen, S., Luo, Y., Prestwich, G. D., Mascarenhas, M. M., Garg, H. G., Quinn, D. A., Homer, R. J., Goldstein, D. R., Bucala, R., Lee, P. J., Medzhitov, R., Noble, P. W. (2005) *Regulation of lung injury and repair by Toll-like receptors and hyaluronan,* Nature Medicine, 11: 1173-1179

Joyce Y. Wong , Jennie B. Leach, Xin Q. Brown (2004) *Balance of chemistry, topography, and mechanics at the cell–biomaterial interface: Issues and challenges for assessing the role of substrate mechanics on cell response,* Surface Science, 570 : 119–133

Kalomiris, E. L., Bourguignon, L. Y. (1988) *Mouse T lymphoma cells contain a transmembrane glycoprotein (GP85) that binds ankyrin*, Journal of Cell Biology, 106(2): 319-327

Katoh, S., Zheng, Z., Ortani, K., Shimozato, T., Kincade, P.W. (1995) *Glycosylation of CD44 negatively regulates its recognition of hyaluronan*, The Journal of Experimental Medicine, 182:419-429

Kefeng Ren, Thomas Crouzier, Christian Roy, and Catherine Picart (2008) *Polyelectrolyte Multilayer Films of Controlled Stiffness Modulate Myoblast Cell Differentiation*, Adv. Funct. Mater, 18: 1378–1389

Kennedy, C. I., Diegelmann, R. F., Haynes, J. H., Yager, D. R. (2000) *Proinflammatory cytokines differencially regulate hyaluronan synthase isoforms in fetal and adult fibrobalsts*, Journal of Pediatric Surgery, 35: 874-879

Kerr, J. F., Wyllie, A. H., Currie, A. R. (1972) *Apoptosis: a basic biological phenomenon with wide-ranging implications in tissue kinetics*, Br J Cancer, 26: 239-57

Kim, B. M., Chung, H. W. (2007) *Hypoxia/reoxygenation induces apoptosis through a ROS-mediated caspase-8/Bid/Bax pathway in human lymphocytes*, Biochem Biophys Res Commun, 363**:** 745-50

Kim, H-Y., Fay, M. P., Feuer, E. J., Midthune, D. N (2000) *Permutation methods for joinpoint regression with applications to cancer rates*, Statistics in Medicine, 19: 335-351

Kimata, K., Honma, Y., Okayama, M., Oguri, K., Hozumi, M., Suzuki, S. (1983) *Increased synthesis of hyaluronic acid by mouse mammary carcinoma cell variants with high metastatic potential*, Cancer Research, 43: 1347-1354

Kincade, P. W., Zheng, Z., Katoh, S., Hanson, L. (1997) *The importance of cellular environment to function of the CD44 matrix receptor*, Current Opinion in Cell Biology, 9: 635-642

King, R. J. B. (2000) *Cancer biology*, Second edition, Prentice Hall, Harlow

King, S. R., Hickerson, W. L., Proctor, K. G. (1991) *Beneficial actions of exogenous hyaluronic acid on wound healing,* Surgery, 109: 76-84

Kittl, E. M., Haberhauer, G., Ruckser, R., Selleny, S., Rech-Weichselbraun, I., W. Hinterberger, W., Bauer, K. (1997) *Serum levels of soluble CD44 variant isoforms are elevated in rheumatoid arthritis*, Rheumatology International, 16: 181–186

Kittl, E. M., Ruckser, R., Selleny, S., Samek, V., Hofmann, J., Huber, K., Reiner, A., Ogris, E., Hinterberger, W., Bauer, K. (1997) *Evaluation of soluble CD44 splice variant v5 in the diagnosis and follow-up in breast cancer patients*, Experimental and Clinical Immunogenetics, 14(4): 264-272

Klymkowsky, M. W.Savagner, P. (2009) *Epithelial-mesenchymal transition: A cancer researcher's conceptual friend and foe,* American Journal of Pathology, 174: (5) 1588-1593

Knudson, C. B. (2003) *Hyaluronan and CD44: strategic players for cell-matrix interactions during chondrogenesis and matrix assembly*, Birth Defects Research (Part C) Embryo Today, 69: 174-196

Knudson, C. B., Knudson, W. (1990) *Similar epithelial interactions in the regulation of hyaluronate production during limb morphogenesis and tumor invasion*, Cancer Letters, 52(2):113-22

Knudson, C. B., Knudson, W. (1993) *Hyaluronan-binding proteins in development, tissue homeostasis, and disease*, The FASEB Journal, 7: 1233-1241

Knudson, W. (1996) *Tumor-associated hyaluronan – Providing an extracellular matrix that facilitates invasion,* American Journal of Pathology, 6: 1721-1726

Knudson, W., Biswas, C., Li, X-Q., Nemec, R. E., Toole, B. P. (1989) The role and regulation of tumor-associated hyaluronan. In: Whelan, J., *The Biology of Hyaluronan*, Ciba Foundation Symposium 143, Wiley Chichester, New York

Knudson, W., Chow, G., Knudson, C. B. (2002) *CD44-mediated uptake and degradation of hyaluronan*, Matrix Biology, 21: 15-23

Ko, L. J., Prives, C. (1996) *p53: Puzzle and paradigm*, Genes and Development, 10-1054-1072

Köbel, M., Weicherd, W., Crüwell, K., Schmitt, W. D., Lautenschlager, C., Hauptmann, S. (2004) *Epithelial hyaluronic acid and CD44v6 are mutually involved in invasion of colorectal adenocarcinomas and linked to patient prognosis*, Virchows Archives, 445: 456-464

Kogan, G., Šoltés, L., Stern, R., Gemeiner, P. (2007) *Hyaluronic acid: a natural biopolymer with a broad range of biomedical and industrial applications*, Biotechnology Letters, 29: 17-25

Koochekpour, S., Pilkington, G. J. Merzak, A. (1995) *Hyaluronic acid/CD44H interaction induces cell detachment and stimulates migration and invasion of human glioma cells in vitro*, International Journal of Cancer, 63: 450-454

Kopp, R., Classen, S., Wolf, H., Gholam, P., Possinger, K., Eiermann, W., Wilmanns, W. (2001) *Predictive relevance of soluble CD44v6 serum levels for the responsiveness to second line hormone- or chemotherapy in patients with metastatic breast cancer*, Anticancer Research, 21: 2995-3000

Kosaki, R., Watanabe, K., Yamaguchi, Y. (1999) *Overproduction of hyaluronan by expression of the hyaluronan synthase Has2 enhances anchorage-independent growth and tumorigenicity*, Cancer Research, 59: 1141-1145

Kothapalli, D., Flowers, J., Xu, T., Puré, E., Assoian, R. K. (2008) *Differential activation of Erk and Rac mediates the proliferative and anti-proliferative effects of hyaluronan and CD44*, Journal of Biological Chemistry, 283: 31823-34393

Kufe, D., Bast, R., Hait, W., Hong, W., Pollack, R., Weichselbaum, R., Holland, J., Frei, E. (2003) *Cancer Medicine 6*, BC Decker Inc, London

Kumar, S., West, D. C., Ponting, J. M., Gattamaneni, H. R. (1989) *Sera of children with renal tumours contain low-molecular-mass hyaluronic acid*, International Journal of Cancer, 44: 445-448

Kuncová, J., Urban, M., Mandys, V. (2007) *Expression of CD44s and CD44v6 in translational cell carcinomas of the urinary bladder: comparison with tumor grade, proliferative activity and p53 immunoreactivity of tumor cells*, Acta Pathologica, Microbiologica et Immunologica Scandinavica, 115: 1194-1205

Kuo, K. T., Liang, C. W., Hsiao, C. H., Lin, C. H., Chen, C. A., Sheu, B. C., Lin, M. C. (2006) *Downregulation of BRG-1 repressed expression of CD44s in cervical neuroendocrine carcinoma and adenocarcinoma*, Modern Pathology, 19: 1570-7

Kurzrock, R., Talpaz, M. (1996) *Molecular biology in cancer medicine*, Martin Dunitz Ltd., UK

Ladam, G., Vonna, L., Sackmann, E. (2003) *Micromechanics of surface-grafted hyaluronic acid gels*, The Journal of Physical Chemistry B, 107: 8965-8971

Lalier, L., Cartron, P. F., Juin, P., Nedelkina, S., Manon, S., Bechinger, B., Vallette, F. M. (2007) *Bax activation and mitochondrial insertion during apoptosis*, Apoptosis, 12: 887-96

Lapčík Jr., L., Lapčík, L., De Smedt, S., Demeester, J., Chabreček, P. (1998) *Hyaluronan: Preparation, structure, properties, and applications*, Chemical reviews, 98: (8) X1-X2

Lapick, L. J., Lapick, L., Demeester, J., Chabrecek, P. (1998) *Hyaluronan: Preparation, Structure, Properties, and Applications*, Chemical Reviews, 98 (8): 2663-2684

Larsson, A., Ocklind, A. (2000) *In:* K. L. Mittal, Editor, Polymer Surface Modification: Relevance to Adhesion, vol 2, VSP, Utrecht (2000), p. 121.

Laurent, T. C. (1970) The structure of hyaluronic acid. In: Balazs, E. A. (Ed.), *Chemistry and Molecular Biology of the Intercellular Matrix*, Academic Press, New York, pp. 703-732

Laurent, T. C., Fraser, J. R. (1992) *Hyaluronan*, FASEB Journal, 6: 2397-2404

Laurent, T. C., Laurent, U. B. G., Fraser, J. R. E. (1995) *Functions of hyaluronan,* Annals of Rheumatoid Diseases, 54: 429-432

Laurent, T. C., Laurent, U. B., Fraser, J. R. (1996) *Serum hyaluronan as a disease marker*, Annals of Medicine, 28: 241–253

Laurent, T. C.Fraser, J. R. (1992) *Hyaluronan,* The FASEB Journal, 6: 2397-2404

Leach, J. B., Schimidt, C. E. (2004) *Hyaluronan*. In: Bowlin, G. L.; Wnek, G., Encyclopedia of Biomaterials and Biomedical Engineering, Informa Healthcare

Lee, J. Y., Spicer, A. P. (2000) *Hyaluronan: a multifunctional, megadalton, stealth molecule,* Current Opinion in Cell Biology, 12: 581-586

Lee, S-C., Harn, H-J., Lin, T-S., Yeh, K-T., Liu, Y-C., Tsai, C-S., Cheng, Y-L. (2003) *Prognostic significance of CD44v5 expression in human thymic epithelial neoplasms*, General Thoracic, 76: 213-218

Legg, J. W., Lewis, C. A., Parsons, M., Ng, T., Isacke, C. M. (2002) *A novel PKC-regulated mechanism controls CD44 ezrin association and directional cell motility,* Nature Cell Biology, 4(6): 399-407

Legras, S., Günthert, U., Stauder, R., Curt, F., Oliferenko, S., Kluin-Nelemans, H. (1998) *A strong expression of CD44-6v correlates with shorter survival of patients with acute myeloid leukemia*, Blood, 91: 3401-3413

Leonard, J. G., Hale, A. H., Roll, D. E., Conrad, H. E., Weber, M. J. (1978) *Turnover of cellular carbohydrates in normal and rous sarcoma virus-transformed cells*, Cancer Research, 38: 185-188

Lepperdinger, G., Fehrer, C., Reitlinger, S. (2004) *Biodegradation of hyaluronan*. In: Garg, H.G., Hales, C.A., Chemistry and Biology of Hyaluronan, Elsevier Press, Amsterdam, pp. 71–82

Lesley, J., English, N., Perschl, A., Gregoroff, J,, Hyman, R. (1995) *Variant cell lines selected for alterations in the function of the hyaluronan receptor CD44 show differences in glycosylation*, The Journal of Experimental Medicine, 182: 431-437

Lesley, J., Hascall, V.C., Tammi, M., Hyman, R. (2000) *Hyaluronan binding by cell surface CD44*, Journal Biological Chemistry, 275: 26967–26975

Lesley, J., Hyman, R., English, N., Catterall, J. B., Turner, G. A. (1997) *CD44 in inflammation and metastasis*, Glycoconjugate Journal, 14: 611-622

Li, Y., Heldin, P. (2001) *Hyaluronan production increases the malignant properties of mesothelioma cells*, British Journal of Cancer, 85: 600-607

Li, Y., Li, L., Brown, T. J., Heldin, P. (2007) *Silencing of hyaluronan synthase 2 supresses the malignant phenotype of invasive breast cancer cells*, International Journal of Cancer, 120(12): 2557-2567

Liao, Y-H., Jones, S. A., Forbes, B., Martin, G. P., Brown, M. B. (2005) *Hyaluronan: pharmaceutical characterization and drug delivery*, Drug Delivery, 12: 327-342

Liotta, L. A., Kohn, E. C. (2001) *The microenvironment of the tumour-host interface*, Nature, 411: 375-379

Lipponen, P., Aaltomaa, S., Tammi, R., Tammi, M., Ågren, U., Kosma, V-M. (2001) *High stromal hyaluronan leve lis associated with poor differentiation metastasis in proatate cancer*, European Journal of Cancer, 37(7): 849-856

Liu, D., Liu, T., Li, R., Sy, M. S. (1998) *Mechanisms regulating the binding activity of CD44 to hyaluronic acid*, Frontiers in Bioscience, 3: d631-d636

Liu, H., Yin, Y., Yao, K., Ma, D., Cui, L., Cao, Y. (2004) *Influence of the concentrations of hyaluronic acid on the properties and biocompatibility of Cs-Gel-HA membranes*, Biomaterials, 25: 3523-3530

Liu, J., Jiang, G. (2006) *CD44 and hematologic malignancies*, Cellular and Molecular Immnunology, 3(5): 359-365

Liu, N., Gao, F., Han, Z., Xu, X., Underhill, C. B., Zhang, L. (2001) *Hyaluronan synthase 3 overexpression promotes the growth of TSU prostate cancer cells*, Cancer Research, 61: 5207-14

Liua, H., Yina, Y., Yaoa, K., Mab, D., Cuib, L., Caob, Y., *Influence of the concentrations of hyaluronic acid on the properties and biocompatibility of Cs–Gel–HA membranes*, Biomaterials, 25: 3523-3530

Lodish, H., Berk, A., Matsudaira, P., Kaiser, C. A., Krieger, M., Scott, M. P., Zipursky, L., Darnell, J. (2004) *Molecular Cell Biology*, Fifth edition, W. H. Freeman & Co., New York

Lokeshwar V. B., Schroeder GL, Selzer MG, Hautmann SH, Posey JT, Duncan RC, Watson, R., Rose, L. Markowitz, S., Soloway, M. S. (2002) *Bladder tumor markers for monitoring recurrence and screening comparison of hyaluronic acid-hyaluronidase and BTA-Stat tests*, Cancer, 95: 61-72

Lokeshwar, V. B., Rubinowicz, D., Schroeder, G. L., Forgacs, E., Minna, J. D., Block, N. L., Nadji, M., Lokeshwar, B. L. (2001) *Stromal and epithelial expression of tumor markers hyaluronic acid and HYAL1 hyaluronidase in prostate cancer*, Journal of Biological Chemistry, 276:11922-11932

Lokeshwar, V. B., Selzer, M. G. (2000) *Differences in hyaluronic acid-mediated functions and signaling in arterial, microvessel, and vein-derived human endothelial cells*, Journal of Biological Chemistry, 275: 27641-27649

Luo, X., Budihardjo, I., Zou, H., Slaughter, C., Wang, X. (1998) *Bid, a Bcl2 interacting protein, mediates cytochrome c release from mitochondria in response to activation of cell surface death receptors*, Cell, 94**:** 481-490

Lutolf, M. P., Lauer-Fields, J. L., Schmoekel, H. G., Metters, A. T., Weber, F. E., Fields, G. B., Hubbell, J. A. (2003) *Synthetic matrix metalloproteinase-sensitive hydrogels for the conduction of tissue regeneration: Engineering cell-invasion characteristics*, Proc. Nutl. Acad. Sci. USA, 100: (9) 5413-5418

Lynn, B. D., Li, X., Cattini, P. A., Turley, E. A., Nagy, J. I. (2001) *Identification of sequence, protein isoforms, and distribution of the hyaluronan-binding protein RHAMM in adult and developing rat brain*, J. Comp. Neurol, 439: 315-330

Lynn, B. D., Turley, E. A., Nagy, J. I. (2001) *Subcellular distribution, calmodulin interaction, and mitochondrial association of the hyaluronan-binding protein RHAMM in rat brain*, Journal of Neurosciences Research, 65: 6-16

Maceina, M. J. (2007) *Use of piecewise nonlinear models to estimate variable size-related mortality rates*, North American Journal of Fisheries Management, 27: 77-84

Mahoney, D. J., Blundell, C. D., Day, A., J. (2001) *Mapping the Hyaluronan Binding Site on the Link Module from Human TSG6 by Site Directed Mutagenesis*, Journal of Biological Chemistry, 276 (25): 22764-22771

Mani, S. A., Guo, W., Liao, M. -., Eaton, E. N., Ayyanan, A., Zhou, A. Y., Brooks, M., Reinhard, F., Zhang, C. C., Shipitsin, M., Campbell, L. L., Polyak, K., Brisken, C., Yang, J., Weinberg, R. A. (2008) *The Epithelial-Mesenchymal Transition Generates Cells with Properties of Stem Cells*, Cell, 133: (4) 704-715

Manzel, E. J., Farr, C. (1988) *Hyaluronidases and its substrate: biochemistry, biological activities and therapeutic use*, Cancer Letters, 131: 3–11

Martin, T. A., Harrison, G., Mansel, R. E., Jiang, W. G. (2003) *The role of the CD44/ezrin complex in cancer metastasis*, Critical Reviews in Oncology/Hematology, 46: 165-186

Masellis-Smith, A., Belch, A. R., Mant, M. J., Turley, E. A., Pilarski, L. M. (1996) *Hyaluronan-dependent motility of B cells and leukemic plasma cells in blood, but not of bone marrow plasma cells, in multiple myeloma: alternate use of receptor for hyaluronan mediated motility (RHAMM) and CD44*, Blood, 87: 1891-1899

Matinlinna, J. P., Lassila, L. V. J., Özcan, M., Yli-Urpo, A., Vallittu, P. K. (2004) *An introduction to silanes and their clinical applications in dentistry*, The International Journal of Prosthontics, 17(2): 155-164

Matsui, Y., Inomata, M., Izumi, K., Sonoda, K., Shiraishi, N., Kitano, S. (2004) *Hyaluronic acid stimulates tumor-cell proliferation at wound sites*, Gastrointestinal Endoscopy, 60: (4) 539-543

Maxwell, C. A., McCarthy, J., Turley, E. (2008) *Cell-surface and mitotic-spindle RHAMM moonlighting or dual oncogenic functions?* Journal of Cell Science, 121: 925-932

McBride, W. H., Bard, J. B. (1979) *Hyaluronidase-sensitive halos around adherent cells. Their role in blocking lymphocyte-mediated cytolysis*, The Journal Experimental Medicine, 149: 507-515

McKee, C. M., Penno, M. B., Cowman, M., Burdick, M. D., Strieter, R. M., Bao, C., Noble, P. W. (1996) *Hyaluronan fragments induce chemokine gene expression in alveolar macrophages. The role of HA size and CD44*, Journal of Clinical Investigation 15: 2403-2413

McKee, T., McKee, J. R. (2008) Biochemistry in perspective: carcinogenesis. *In: Biochemistry: The molecular basis of life*, Fourth edition, Oxford University Press, USA

Menzel, E. J.Farr, C. (1998) *Hyaluronidase and its substrate hyaluronan: biochemistry, biological activities and therapeutic uses*, Cancer Letters, 131: 3-11

Meyer, K. (1971) *Hyaluronidases*. In: Boyer, P. D., The enzymes, Academic Press, New York, pp. 307-320

Meyer, K., Palmer, J. W. (1934) *The polysaccharide of the vitreous humor*, Journal of Biological Chemistry, 107: 629-634

Meyer, K., Palmer, J. W. (1936) *On glycoproteins. The polysaccharides of vitreous humor and of umbilical cord*, J. Biol. Chem., 114: 689-703

Mian, N. (1986) *Characterization of a high-Mr plasma-membrane-bound protein assessment of its role as a constituent of hyaluronate synthase complex*, Biochemistry Journal, 237: 343-357

Miller, D.Stengmann, R. (1983) *Healon (Sodium Hyaluronate). A guide to its use in ophthalmic surgery*,

Miller, K. A., Shao, M., Martin-Deleon, P. A. (2007) *Hyalp in murine sperm function: evidence for unique and overlapping functions with other reproductive hyaluronidases*, Journal of Andrology, 28: 67-76

Milner, C. M., Higman, V. A., Day, A. J. (2006) *TSG-6: a pluripotent inflammatory mediator*?, Biochemical Society Transactions, 34: 446–450

Mizejewski, G. J. (1999) *Role of integrins in cancer: survey of expression patterns*, Proceedings of the Society for Experimental Biology and Medicine, 222: 124-138

Mizrak, D., Brittan, M., Alison, M. R. (2008) *CD 133: Molecule of the moment*, Journal of Pathology, 214: (1) 3-9

Mohapatra, S., Yang, X., Wright, J. A., Turley, E. A., Greenberg, A. H. (1996) *Soluble hyaluronan receptor RHAMM induces mitotic arrest by suppressing Cdc2 and cyclin B1 expression*, Journal of Experimental Medicine, 183: 1663-1668

Morgan, S. (2002) *Towards the molecular diagnosis of bladder and colorectal cancer: analysis of CD44 exon splicing*, PhD dissertation, Cranfield University, Cranfield, UK

Mori, H., Tomari, T., Koshikawa, N., Kajita, M., Itoh, Y., Sato, H., Tojo, H., Yana, I., Seiki, M. (2002) *CD44 directs membrane-type 1 matrix metalloproteinase to lamellipodia by associating with its hemopexin-like domain*, European Molecular Biology Organization Journal, 21: 3949-3959

Morraa, M., Cassinellia, C., Carpib, A., Giardinoc, R., Finic, M. (2006) *Effects of molecular weight and surface functionalization on surface composition and cell adhesion to Hyaluronan coated titanium*, Biomedicine & Pharmacotherapy, 60: 365-369

Morrison, H., Sherman, L. S., Legg, J., Banine, F., Isacke, C., Haipek, C. A., Gutmann, D. H., Ponta, H., and Herrlich, P. (2001) *The NF2 tumor suppressor gene product, merlin, mediates contact inhibition of growth through interactions with CD44*, Genes and Development, 15(8): 968-980

Mosmann, **T.** (1983) *Rapid colorimetric assay for cellular growth and survival: Application to proliferation and cytotoxicity assays*, Journal of immunological Methods, 65 (1-2): 55–63

Murai, T., Miyazaki, Y., Nishinakamura, H., Sugahara, K. N., Miyauchi, T., Sako, Y., Yanagida, T., Miyasaka, M. (2004) *Engagement of CD44 promotes Rac activation and CD44 cleavage during tumor cell migration*, Journal of Biological Chemistry, 279: 4541-4550

Murard, A. (1996) *Principios de farmacología e do uso clínico dos agentes antineopásicos*. In: Murard., A., Katz, A., Oncologia – Bases clínicas do tratamento, Guanabara koogan, Rio de Janeiro, Brazil

Murphy, J. F., Lennon, F., Steele, C., Kelleher, D., Fitzgerald, D., Long, A. C. (2005) *Engagement of CD44 modulates cyclooxygenase induction, VEGF generation, and proliferation in human vascular endothelial cells,* FASEB Journal, 19: (3) 446-448

Myint, P., Deeble, D. J., Beaumont, P. C., Blake, S. M., Phillips, G. O. (1987) *The reactivity of various free radicals with hyaluronic acid: steady-state and pulse radiolysis studies*, Biochimica and Biophysica Acta, 925: 194-202

Nagano, O., Murakami, D., Hartmann, D., De Strooper, B., Saftig, P., Iwatsubo, T., Nakajima, M., Shinohara, M., Saya, H. (2004) *Cell-matrix interaction via CD44 is independently regulated by different metalloproteinases activated in response to extracellular Ca21 influx and PKC activation*, Journal of Cell Biology, 165 (6): 893-902

Nagy, J. I., Hacking, J., Frankenstein, U. N., Turley, E. A. (1995) *Requirement of the hyaluronan receptor RHAMM in neurite extension and motility as demonstrated in primary neurons and neuronal cell lines*, The Journal of Neuroscience, 15(1): 241-252

Naor, D., Nedvetzki, S, Golan, I., Melnik, L., Faitelson, Y. (2002) *CD44 in cancer*, Critical Reviews in Clinical Laboratory Sciences, 39: 527-79

Naor, D., Sionov, R. V., Ish-Shalom, D. (1997) *CD44: structure, function, and association with the malignant process*, Advances in Cancer Research, 71: 241-319

Naor, D., Wallach-Dayan, S. B., Muayad A. Zahalka, M. A., Ronit Vogt Sionov, R. V. (2008) *Involvement of CD44, a molecule with a thousand faces, in cancer dissemination*, Seminars in Cancer Biology, 18: 260-267

Naujokas, M. F., Morin, M, Anderson, M. S., Peterson, M., Miller, J. (1993) *The chondroitin sulfate form of invariant chain can enhance stimulation of T cell responses through interaction with CD44*, Cell, 74(2):257-268

Nedvetzki, S., Golan, I., Assayag, N., Gonen, E., Caspi, D., Gladnikoff, M., Yayon, A., Naor, D. (2003) *A mutation in a CD44 variant of inflammatory cells enhances the mitogenic interaction of FGF with its receptor*, Journal of Clinical Investigation, 111: 1211-1220

Nedvetzki, S., Gonen, E., Assayag, N., Reich, R., Williams, R. O., Thurmond, R. L., Huang, J-F., Neudecker, B. A., Wang, F-S., Turley, E. A., Naor, D. (2004) *RHAMM, a receptor for hyaluronan-mediated motility, compensates for CD44 in inflamed CD44-knockout mice: A different interpretation of redundancy*, Proceedings of the National Academy of Sciences, 101(52): 18081-18086

Ni, H-M., Leong, A. F. P., Cheong, D., Hooi, S. C. (2002) *Expression of CD44 variants in colorectal carcinoma quantified by real-time reverse transcriptasepolymerase chain reaction*, Journal of Laboratory and Clinical Medicine, 139(1): 59-65

Nishida, Y., Knudson, W., Knudson, C. B., Ishiguro, N. (2005) *Antisense inhibition of hyaluronan synthase-2 in human osteosarcoma cells inhibits hyaluronan retention and tumorigenicity*, Experimental Cell Research, 307: 194–203

Nixdorf, S., Grimm, M-O., Lorberg, R., Marreiros, A., Russel, P. J., Pienta, K. J., Jackson, P. (2004) *Expression and regulation of MIM (Missing in Metastasis), a novel putative metastasis supressor gene, and MIM-B, in bladder cancer cell lines*, Cancer Letters, 215(2): 209-220

Nna, E., Tothill, I. E., Ludeman, L., Bailey, T. (2010) *Endogenous Control Genes in Prostate Cells: Evaluation of Gene Expression Using 'Real-Time' Quantitative Polymerase Chain Reaction*, Medical Principles and Practice,19:433–439

Noble, P. W. (2002) *Hyaluronan and its catabolic products in tissue injury and repair,* Matrix Biology, 21: (1) 25-29

Noble, P. W., Lake, F. R., Henson, P. M., Riches, D. W. H. (1993) *Hyaluronate activation of CD44 induces insulin-like growth factor-2 expression by a tumor necrosis factor-α dependent mechanism in murine macrophages*, Journal of Clinical Investigation, 91: 2368-2377

O'Brien, C. A., Pollett, A., Gallinger, S., Dick, J. E. (2007) *A human colon cancer cell capable of initiating tumour growth in immunodeficient mice,* Nature, 445: (7123) 106-110

Ohno, S., Im, H. J., Knudson, C. B., Knudson, W. (2005) *Hyaluronan oligosaccharide-induced activation of transcription factors in bovine articular chondrocytes,* Arthritis and Rheumatism, 52: 800-809

Okamoto, I., Kawano, Y., Murakami, D., Sasayama, T., Araki, N., Miki, T., Albert J. Wong, A. J., Saya, H. (2001) *Proteolytic release of CD44 intracellular domain and its role in the CD44 signaling pathway*, Journal of Cell Biology, 155: 755-762

Omara-Opyene, A. L., Qiu, J., Shah, G. V., Iczkowski, K. A. (2004) *Prostate cancer invasion is influenced more by expression of a CD44 isoform including variant 9 than by Muc18*, Laboratory Investigation, 84: 894–907

Oswald, S., Reiche, R. (2001) *Binding state information from XPS-depth profiles - capabilities and limits,* Applied Surface Science, 179: 307-315

Pasqui, D., Atrei, A, Barbucci, R. (2007) *A novel strategy to obtain hyaluronan monolayer on solid substrates*, Biomacromolecules, 8: 3531-3539

Patrawala, L., Calhoun-Davis, T., Schneider-Broussard, R., Tang, D. G. (2007) *Hierarchical organization of prostate cancer cells in xenograft tumors: the CD44+alpha2beta1+cell population is enriched in tumor-initiating cells,* Cancer Research, 67: 6796-805

Pauloin, T., Dutot, M., Joly, F. Warnet, J-M., Rat, P. (2009) *High molecular weight hyaluronan decreases UVB-induced apoptosis and inflammation in human epithelial corneal cells*, Molecular Vision, 15:577-583

Pavia, P., Van Damme, M-P., Tellbach, M., Jones, R. L., Jobling, T., Salamonsen, L. A. (2005) *Expression patterns of hyaluronan, hyaluronan synthases and hyaluronidases indicate a role in the progression of endometrial cancer*, Ginecologic Oncology, 98: 193-202

Pecorino, L. (2005) *Molecular biology of cancer – mechanisms, targets, and therapeutics*, Oxford University Press, UK

Peifer, K. (2000) Cirúrgia. In: Otto, S., *Enfermagem em Oncologia*, Lusociência, Loures, Portugal

Pelham, R. J. Jr., and Y-I. Wang (1997) *Cell locomotion and focal adhesions are regulated by substrate flexibility*, Proc. Nutl. Acad. Sci. USA, 94:13661-13665

Pelletier, L., Guillaumot, P., Freche, B., Luquain, C., Christiansen, D., Brugière, S., Garin, J., Manié, S. N. (2006) *Gamma-secretase-dependent proteolysis of CD44 promotes neoplastic transformation of rat fibroblastic cells*, Cancer Research, 66: 3681-3687

Peramo, A., Meads, M. B., Dalton, W. S., Matthews, W. G. (2008) *Static adhesion of cancer cells to glass surfaces coated with glycosaminoglycans*, Colloids and Surfaces B: Biointerfaces, 67: 140-144

Peyron, J. G. (1993) *A new approach to the treatment of osteoarthritis: viscosupplementation*, Osteoarthritis Cartilage, 1: 85-87

Pfaffl, M. W. (2001) *A new mathematical model for relative quantification in real-time RT–PCR*, Nucleic Acids Research, 29(9): 2002-2007

Picart, C., Lavalle, Ph., Hubert, P., Cuisinier, F. J. G., Decher, G., Schaaf, P., Voegel, J.-C. (2001) *Buildup mechanism for poly(L-lysine)/hyaluronic acid films onto a solid surface*, Langmuir, 17: 7414-7424

Picker, L. J., Nakache, M., Butcher, E. C. (1989) *Monoclonal antibodies to human lymphocyte homing receptors define a novel class of adhesion molecules on diverse cell types*, Journal of Cell Biology, 109(2):927-937

Pilarski, L., Maxwell, C. A., Gares, S. L. (2001) *RHAMM (CD168, IHAPB)*, Protein reviews on the web, 2:76-84

Pirinen, R., Tammi, R., Tammi, M., Hirvikoski, P., Parkkinen, J. J., Johansson, R., Böhm, J., Hollmén, S., Kosma, V-M. (2001) *Prognostic value of hyaluronan expression in non-small-cell lung cancer: increased stromal expression indicates unfavourable outcome in patients with adenocarcinoma*, International Journal of Cancer, 95: 12-17

Ponta, H., Sherman, L., Herrlich, P. A. (2003) *CD44: From adhesion molecules to signalling regulators*, Nature Reviews Molecular Cell Biology, 4: 33-45

Ponta, H., Wainwright, D., Herrlich, P. A. (1998) *Molecules in focus The CD44 protein family*, The International Journal of Biochemistry & Cell Biology, 30(3): 299-305

Pozo, M. A., Balazs, E. A., Belmonte, C. (1997) *Reduction of sensory responses to passive movements of inflamed knee joints by hylan, a hyaluronan derivative*, Experimental Brain Research, 116: 3-9

Prem, P. (1984) *Hyaluronate is synthesized at plasma membranes*, Biochemical Journal, 220(2):597-600

Prestwich, G. (2010) Personal communication

Quackenbush, E. J., Vera, S., Greaves, A., Letarte. M. (1990) *Confirmation by peptide sequence and co-expression on various cell types of the identity of CD44 and P85 glycoprotein*, Molecular Immunology, 27: 947-955

Rauch, U., Karthikeyan, L., Maurel, P., Margolis, R. U., and Margolis, R. K. (1992) *Cloning and primary sequence of neurocan, a developmentally regulated, aggregating chondroitin sulfate proteoglycan of brain*, Journal of Biological Chemistry, 267: 19536-19547

Reitinger, S., Laschober, G. T., Feher, C., Greiderer, B., Lepperdinger, G. (2007) *Mouse testicular hyaluronidase-like proteins, SPAM 1 and Hyall5 but not Hyalp 1 degrade hyaluronan*, Biochemical Journal, 401: 79-85

Ren, K., Crouzier, T., Roy, C., Picart, C. (2008) *Polyelectrolyte multilayer films of controlled stiffness modulate myoblast cell differentiation*, Advanced Functional Materials, 18: 1378-1389

Richert, L., Boulmedais, F., Lavalle, P., Mutterer, J., Ferreux, E., Decher, G., Schaaf, P., Voegel, J-C., Picart, C. (2004) *Improvement of the stability and cell adhesion properties of polyectrolyte multilayer films by chemical cross-linking*, Biomacromolecules, 5: 284-294

Richert, L., Lavalle, P., Payan, E., Xiao Zheng Shu, X. Z., Prestwich, G. D., Stoltz, J-F., Schaaf, P., Voegel, J-C, Picart, C. (2004) *Layer by layer buildup of polysaccharide films: physical chemistry and cellular adhesion aspects*, Langmuir, 20: 448-458

Richter, R. P., Hock, K. K. Burkhartsmeyer, J., Boehm, H., Bingen, P., Wang, G., Steinmetz, N. F., Evans, D. J., Spatz, J. P. (2007) *Membrane-grafted hyaluronan films: A well-defined model system of glycoconjugate cell coats*, *Journal* of the American Chemical Society, 129: 5306 – 5307

Rilla, K., Siiskonen, H., Spicer, A. P., Hyttinen, J. M. T., Tammi, M. I., Tammi, R. H. (2005) *Plasma Membrane Residence of Hyaluronan Synthase Is Coupled to Its Enzymatic Activity*, The Journal of Biological Chemistry, 280 (36): 31890–31897

Rodahl, M., Kasemo, B. (2004) *Frequency and dissipation-factor responses to localized liquid deposits on a QCM electrode*, Sensors and Actuators, B37: 111-116

Roden, L., Campbell, P., Fraser, J. R., Laurent, T. C., Pertoft, H., Thompson, J. N. (1989), *Enzymic pathways of hyaluronan catabolism*, Ciba Foundation Symposium, 143: 60-76

Romaris, M., Bassols, A., David, G. (1995) *Effect of transforming growth factor-beta 1 and basic fibroblast growth factor on the expression of cell surface proteoglycans in*

human lung fibroblasts. Enhanced glycanation and fibronectin-binding of CD44 proteoglycan, and down-regulation of glypican, Biochemical Journal, 310(1): 73-81

Rooney, P., Kumar, S., Ponting, J., Wang, M. (1995) *The role of hyaluronan in tumour neovascularisation*, International Journal of Cancer, 60: 632-636

Ropponen, K., Tammi, M., Parkkinen, J., Eskelinen, M., Tammi, R., Lipponen, P., Agren, U., Alhava, E., Kosma, V. M. (1998) *Tumor cell-associated hyaluronan as an unfavorable prognostic factor in colorectal cancer*, Cancer Research, 58:342-347

Rossler, A., Hinghofer-Szalkay, H. (2002) *Hyaluronan fragments: an information-carrying system?*, Hormone and Metabolic Research, 35: 67-68

Rozen, S., Skaletsky, H. J. (2000) *Primer3 on the WWW for general users and for biologist programmers.* In: Krawetz S, Misener S (eds) *Bioinformatics Methods and Protocols: Methods in Molecular Biology.* Humana Press, Totowa, NJ, 365-386

Rudon, R. W. (2007) *Cancer biology*, Fouth edition, Oxford University Press, USA

Saari, H., Konttinen, Y. T., Friman, C., Sorsa, T., (1993) *Differential effects of reactive oxygen species on native synovial fluid and purified human umbilical cord hyaluronate*, Inflammation, 17: 403–415

Saiki, I. (1997) *Cell adhesion molecules and cancer metastasis*, Japanese Journal of Pharmacology, 75: 215-242

Saito, H., Tsujitani, S., Katano, K., Ikeguchi, M., Maeta, M, Kaibara, N. (1998) *Serum concentration of CD44 variant 6 and its relation to prognosis in patients with gastric carcinoma*, Cancer, 83: 1094-1101

Sandson, J., Hamerman, D., and Schwick, G. (1965) *Altered properties of pathological hyaluronate due to a bound inter-alpha trypsin inhibitor,* Trans Assoc. Am. Physicians, 78: 304-313

Sato, N., Funayama, N., Nagafuchi, A., Yonemura, S., Tsukita, S., Tsukita, S. (1992) *A gene family consisting of ezrin, radixin and moesin. Its specific localization at*

actin filament/plasma membrane association sites, Journal of Cell Science, 103: 131-143

Savani, R. C. (2010) Personal communication

Savani, R. C., Khalil, N., Turley, E. A. (1995) *Hyaluronan receptor antagonists alter skin inflammation and fibrosis following injury*, Proceedings of the Western Pharmacology Society, 38: 131-136

Savani, R. C., Wang, C., Yang, B., Zhang, S., Kinsella, M. G., Wight, T. N., Stern, R., Nanee, D. M, Turley. E. A. (1995) *Migration of bovine aortic smooth muscle cells after wounding injury*, The Journal Clinical Investigation, 95:1158-1168

Savani,, R. C., Turley, E. A. (1995) *The role of hyaluronan and its receptors in restenosis after balloon angioplasty: development of a potential therapy*, International Journal of Tissue Reactions, 17: 141-151

Savitski, K., Bar-Shira, A., Gilad, S., **Rotman, G., Ziv, Y., Vanagaite, L., Tagle, D. A., Smith, S., Uziel, T., Sfez, S., Ashkenazi, M., Pecker, I., Frydman, M., Harnik, R., Patanjali, S. R., Simmons, A., Clines, G. A., Sartiel, A., Gatti, R. A., Luciana Chessa, L., Ozden Sanal, O., Martin F. Lavin, M. F., Jaspers, N. G. J., Taylor, A. M. R., Arlett, C. F., Miki, T., Weissman, S. M., Lovett, M., Collins, F. S., Shiloht, Y.** (1995) *A single ataxia-teleangiectasia gene with a product similar to PI-3 kinase*, Science, 268: 1749-1753

Scaltriti1, M., Bettuzzi, S., Sharrard, R. M., Caporali, A. Caccamo, A. E., Maitland, N. J. (2004) *Clusterin overexpression in both malignant and nonmalignant prostate epithelial cells induces cell cycle arrest and apoptosis*, British Journal of Cancer, 9: 1842-1850

Schneider, A. Picart, C., Senger, B., Schaaf, P., Voegel, J-P., Frisch, B. (2007) *Layer-by-Layer Films from Hyaluronan and Amine-Modified Hyaluronan*, Langmuir, 23, 2655-2662

Schneider, A., Francius, G., Obeid, R., Schwinte´, P Hemmerle´, J., Frisch, B., Schaaf, P., Voegel, J-C., Senger, B., Picart, C. (2006) *Polyelectrolyte multilayers with*

a tunable young's modulus: influence of film stiffness on cell adhesion, Langmuir, 22, 1193-1200

Schultz, G. S., Ladwig, G., Wysocki, A. (2005) *Extracellular matrix: Review of its roles in acute and chronic wounds*. In: World Wide Wounds (accessed on 27 May 2008). http://www.worldwidewounds.com/2005/august/Schultz/Extrace-Matric-Acute-Chronic-Wounds.html

Schumacher, P. P. (2004) *Innhibition of hyaluronan export from human fibroblasts by inhibitors of multidrug resistance transporters*, Biochem Pharmacol, 68: 1401-1410

Scott, D. A., Stapleton, J. A., Palmer, R. M., Wilson, R. F., Sutherland, G., Coward, P. Y., Gustavsson, G., Odell, E. W., Poston, R. N. (2000) *Plasma concentrations of reputed tumor-associated soluble CD44 isoforms (v5 and v6) in smokers are dose related and decline on smoking cessation*, Cancer Epidemiology Biomarkers and Prevention, 9: 1211-1214

Scott, J. E., Heatley, F. (2002) *Biological properties of hyaluronan in aqueous solution are controlled and sequestered by reversible tertiary structures, defined by NMR spectroscopy, Biomacromolecules*, 3:547-553

Screaton, G. R., Bell, M. V., Jackson, D. G., Cornelis, F. B., Gerth, U., Bell, J. I. (1992) *The identification of a new alternative exon with highly restricted tissue expression in transcripts encoding the mouse Pgp-1 (CD44) homing receptor: comparison of all 10 variable exons between mouse, human, and rat*, Journal of Biological Chemistry, 268(17): 12235-12238

Segura, T., Anderson, B. C., Chung, P. H., Webber, R. E., Shull, K. R., She, L. D. (2005) *Crosslinked hyaluronic acid hydrogels: a strategy to functionalize and pattern*, Biomaterials, 26 :359–371

Sengupta, K., Schilling, J., Marx, S., Fischer, M., Bacher, A., Erich Sackmann, E. (2003) *Mimicking tissue surfaces by supported membrane coupled ultra-thin layer of hyaluronic acid*, Langmuir 19(5): 1775-1781

Sheen-Chen, S. M., Chen,W. J., Eng, H. L., Sheen, C. C., Chou, F. F., Cheng, Y. F. (1999) *Evaluation of the prognostic value of serum soluble CD 44 in patients with breast cancer*, Cancer Investigation, 17: 581-585

Shimizu, Y., Van Seventer, G. A., Siraganian, R, Wahl, L., Shaw, S. (1989) *Dual role of the CD44 molecule in T-cell adhesion and activation*, The Journal of Immunology, 143: 2457-63

Shin, H., Jo, S., Mikos, A. G. (2003) *Biomimetic materials for tissue engineering*, Biomaterials, 24: 4353-4364

Shyjan, A. M., Heldin, P., Butcher, E. C., Yoshino, T., Briskin, M. J. (1996) *Functional cloning of the cDNA for a human hyaluronan synthase*, The Journal of Biological Chemistry, 271(38): 23395-23399

Sillanpää, S., Anttila, M. A., Voutilainen, K., Tammi, R. H., Tammi, M. I., Saarikoski, S. V., Kosma, V-M. (2003) *CD44 expression indicates favorable prognosis in epithelial ovarian cancer*, Clinical Cancer Research, 9: 5318-5324

Simmons, K. (2007) The plant cell wall. *In: Cells and cellular processes* (assessed on 12 December 2010)
http://kentsimmons.uwinnipeg.ca/cm1504/cellwall.htm

Simon, A., Safran, A., Revel, A., Aizenman, E., Reubinoff, B., Porat-Katz, A., Lewin, A., Laufer, N. (2003) *Hyaluronic acid can successfully replace albumin as the sole macromolecule in a human embryo transfer medium*, Fertility and Sterility, 79: 1434-1438

Simpson, M. A., Wilson, C. M., Furcht, L. T., Spicer, A. P., Oegema Jr, T. R,, McCarthy, J. B. (2002a) *Manipulation of hyaluronan synthase expression in prostate adenocarcinoma cells alters pericellular matrix retention and adhesion to bone marrow endothelial cells*, Journal of Biological Chemistry, 277: 10050-10057

Simpson, M. A., Wilson, C. M., McCarthy, J. B. (2002b) *Inhibition of prostate tumor cell hyaluronan synthesis impairs subcutaneous growth and vascularization in immunocompromised mice*, American Journal of Pathology, 161: 849-57

Singh, S. K., Hawkins, C., Clarke, I. D., Squire, J. A., Bayani, J., Hide, T., Henkelman, R. M., Cusimano, M. D., Dirks, P. B. (2004) *Identification of human brain tumour initiating cells,* Nature, 432: (7015) 396-401

Sliutz, G., Tempfer, C., Winkler, S., Kohlberger, P., Reinthaller, A., Kainz, C. (1995) *Immunohistochemical and serological evaluation of CD44 splice variants in human ovarian cancer*, British Journal of Cancer, 72: 1494-1497

Smedsrod, B., Pertoft, H. (1985) *Preparation of pure hepatocytes and reticuloendothelial cells in high yield from a single rat liver by means of Percoll centrifugation and selective adherence,* Journal Leukocyte Biology, 38: 213-230

Sobin, L. H., Wittekind *C.* (2002) *TNM Classification of Malignant Tumors,* Sixth edition, John Wiley & Sons, Inc., USA

Sohn, D. K., Chang, H. J., Choi, H. S., Jeong S-Y., Kook, M-C., Kim, C. G., Choi, J. (2008) *Does hyaluronic acid stimulate tumor growth after endoscopic mucosal resection?,* Gastroenterology, 23: 1204-1207

Sohr, S., Engeland, K. (2008) *RHAMM is differentially expressed in the cell cycle and downregulated by the tumor suppressor p53,* Cell Cycle, **7**: 3448-3460

Soldani, C., Scovassi, A. I. (2002) *Poly(ADP-ribose) polymerase-1 cleavage during apoptosis: an update,* Apoptosis, 7: 321-328

Soltes, L., Stankovska, M., Kogan, G., Gemeiner, P., Stern, R., (2005) Contribution of oxidative–reductive reactions to high molecular weight hyaluronan catabolism, Chemistry and Biodiversity, 2: 1242-1245

Spagnoli, C., Korniakov, A., Ulman, A., Balazs, E. A., Lyubchenko, Y. L., Cowman, M. K. (2005) *Hyaluronan conformations on surfaces: effect of surface charge and hydrophobicity,* Carbohydrate Research, 340: 929-941

Spevak, L. Y. W., Wong, C. C., Xia, G., W., Gilad, E. (2009) *Hyaluronan-CD44 interaction with protein kinase C_{ϵ} promotes oncogenic signaling by the stem cell marker nanog and the production of microRNA-21, leading to down-regulation of the*

tumor suppressor protein PDCD4, anti-apoptosis, and chemotherapy resistance in breast tumor cells, The Journal of Biological Chemistry, 284(39): 26533–26546

Spicer, A. P., Augustine, M. L., McDonald, J. A. (1997a) *Characterization and molecular evolution of a vertebrate hyaluronan synthase gene family*, The Journal of Biological Chemistry, 273: 1923-1932

Spicer, A. P., Joo, A., Bowling, R. A. (2003) *A hyaluronan binding link protein gene family whose members are physically linked adjacent to chondroitin sulfate proteoglycan core protein genes: the missing links*, The Journal of Biological Chemistry, 278(23): 21083-21091

Spicer, A. P., McDonald, J. A. (1998) *Characterization and molecular evolution of a vertebrate hyaluronan synthase gene family*, The Journal of Biological Chemistry, 273: 1923-1932

Spicer, A. P., Olson, J. S., McDonald, J. A. (1997b) *Molecular cloning and characterization of cDNA enconding the third putative mammalian hyaluronase synthase*, The Journal of Biological Chemistry, 272(14): 8957-8961

Spicer, A. P., Seldin, M. F., Olsen, A. S., Brown, N., Wells, D. E., Doggett, N. A., Itano, N., Kimata, K., Inazawa, J., McDonald, J. A. (1997c) *Chromosomal Localization of the Human and Mouse Hyaluronan Synthase Genes*, Genomics, 41: 493-497

Spicer, A. P., Tien, J. Y .L. (2004) *Hyaluronan and morphogenesis*, Birth defects research. Part C, Embryo today : reviews, 72: 89–108

Stamenkovic, I., Amiot, M., Pesando, J. M.., Seed, B. (1989) *A lymphocyte molecule implicated in lymph node homing is a member of the cartilage link protein family*, Cell, 56: 1057-1062

Stamenkovic, I., Aruffo, A., Amiot, M., Seed, B. (1991) *The hematopoietic and epithelial forms of CD44 are distinct polypeptides with different adhesion potentials for hyaluronate bearing cells*, Eur. Mol. Biol. Organ Journal, 10: 343-348

Staros, J. V., Wright, R. W., Swingle, D. M. (1986) *Enhancement by N-hydroxysulfosuccinimide of water-soluble carbodiimide-mediated coupling reactions*, Analytical Biochemistry, 156: 220-222

Stein G. S., Pardee A. B. (2004) *Cell cycle and growth control: Biomolecular regulation and cancer*, Second edition, John Wiley & Sons, Hoboken, New Jersey

Stern, R. (2003) *Devising a pathway for hyaluronan catabolism. Are we there yet?* In: Glycobiology Advance Access, Oxford University Press

Stern, R. (2004) *Hyaluronan catabolism: a new metabolic pathway*, European Journal of Cell Biology , 83: 317-325

Stern, R. (2005) *Hyaluronan metabolism: a major paradox in cancer biology*, Pathologie Biologie, 53: 371-382

Stern, R. (2008) *Hyaluronidases in cancer biology*, Seminars in Cancer Biology, Seminars in Cancer Biology, 18485730 article in press

Stern, R., Asari, A. A., Sugahara, K. N. (2006) *Hyaluronan fragments: An information-rich system*, European Journal of Cell Biology, 85: 699-715

Stern, R., Maibach, H. I. (2008) *Hyaluronan in skin: aspects of aging and its pharmacologic modulation*, Clinics in Dermathology, 26: 106-122

Studznski, G. P. (1999) *Overview of apoptosis*. *In:* Apoptosis – a pratical approach, Oxford University Press Inc., New York

Sugiyama, Y., Shimada, A., Sayo, T., Sakai, S., Inoue, S. (1998) *Putative hyaluronan synthase mRNA are expressed in mouse skin and TGF-beta upregulates their expression in cultured human skin cells*, Journal Investigative Dermatology, 110: 116-121

Sundstrom, G. (2006) *Hyaluronan in normal and malignant bone marrow – A clinical and morphological study with emphasis on myelofibrosis*, Umeå University, Umeå, Sweden

Sy, M. S., Guo, Y. J., Stamenkovic, I. (1991) *Distinct effects of two CD44 isoforms on tumor growth in vivo*, Journal of Experimental Medicine, 174: 859-66

Takahashi, Y., Li, L., Kamiryo, M., Asteriou, T., Moustakas, A., Yamashita, H., Heldin, P. (2005) *Hyaluronan fragments induce endothelial cell differentiation in a CD44 and CXCL1/GRO1-dependent manner*, Journal of Biological Chemistry, 280: 24195-24204

Tamayo, R. P. (1987) *Introducción a la patologia: Mecanismos de enfermedad*, Third edition, Editorial Médica Panamericana, Buenos Aires

Tammi, M. I., Day, A. J., Turley, E. A., (2002) *Hyaluronan and homeostasis: a balancing act*, Journal of Biological Chemistry, 277: 4581–4584

Tavernor, A. S., Deverson, E. V., W. Coadwell, W. J., Lunn, D. P., Zhang, C., Davis, W., Butcher, G. W. (1993) *Molecular cloning of equine CD44 eDNA by a COS cell expression system*, Immunogenetics, 3: 474-477

Taylor, K. R., Gallo, R. L. (2006) *Glycosaminoglycans and their proteoglycans: host-associated molecular patterns for initiation and modulation of inflammation*, FASEB Journal, 20: 9–22

Teder. P.. Bergh, J., Heldin., P. (1995) *Functional hyaluronan receptors are expressed on squamous cell lung carcinoma cell line but not on other lung carcinoma cell lines*, Cancer Research, 55: 3908-3914

Termeer, C. C., Hennies, J., Voith, U., Ahrens, T., Weiss, J. M., Prehm, P., Simon, J. C. (2000) *Oligosaccharides of hyaluronan are potent activators of dendritic cells*, Journal of Immunology, 165: 1863-1870

Termeer, C., Benedix, F., Sleeman, J., Fieber, C., Voith, U., Ahrens, T., Miyake, K., Freudenberg, M., Galanos, C., Simon, J. C. (2002) *Oligosaccharides of hyaluronan activate dendritic cells via toll-like receptor 4*, Journal of Experimental Medicine, 195: 99-111

Termeer, C., Sleeman, J. P., Simon, J. C. (2003) *Hyaluronan – magic glue for the regulation of the immune response?*, Trends in Immunology, 24: 112-114

Tilkorn, D. J., Lokmic, Z., Chaffer, C. L., Mitchell, G. M., Morrison, W. A., Thompson, E. W. (2010) *Disparate companions: tissue engineering meets cancer research,* Cells Tissues Organs, 192: 141-157

Tirone, E., D'Alessandris, C., Hascall, V. C., Siracusa G., Salustri, A. (1997) *Hyaluronan synthesis by mouse cumulus cells is regulated by interactions between follicle-stimulating hormone (or epidermal growth factor) and a soluble oocyte factor (or transforming growth factor beta1),* Journal of Biological Chemistry, 279 (8): 4787–4794

Tiwari, R. C., Cronin, K. A., Davis, W., Feuer, E. J., Yu, B., Chib, S. (2005) *Bayesian model selection for jointpoint regression with application to age-adjusted cancer rates,* Applied Statistcs, 54: 919-939

Tölg, C., Hofmann, M., Herrlich, P., Ponta, H. (1993) *Splicing choice from ten variant exons establishes CD44 variability*, Nucleic Acids Research, 21: 1225-1229

Tölg, C., Poon, R., Fodde, R., Turley, E. A., Alman, B. A. (2003) *Genetic delection of receptor for hyaluronan-mediated motility (Rhamm) attenuates the formation of aggressive fibromatosis (desmoids tumor),* Oncogene, 22: 6873-6882

Tomihata, K. and Ikada, Y. (1997) *Crosslinking of hyaluronic acid with water-soluble carbodiimide*, Journal of Biomedical Materials Research, 37: 243-251

Toole, B. P. (1990) *Hyaluronan and its binding proteins, the hyaladherins,* Current Opinion in Cell Biology, 2: 839-844

Toole, B. P. (2001) *Hyaluronan in morphogenesis,* Cell and Developmental Biology, 12: 79-87

Toole, B. P. (2004) *Hyaluronan: from extracellular glue to pericellular cue,* Nature Reviews Cancer, 4: 528-539

Toole, B. P., Biswas, C., Gross, J. (1979) *Hyaluronate and invasiveness of the rabbit V2 carcinoma,* The Proceedings of National Academy of Sciences U. S. A., 76: 6299-6303

Toole, B. P., Goldberg, R. L., Chi-Rosso, G., Underhill, C. B., and Orkin, R. W. (1984) In: Trelstad, R. C., *The Role of Extracellular Matrix in Development,* New York, Alan R. Liss Inc.

Toole, B. P., Hascall, V. C. (2002) *Hyaluronan and tumor growth,* The American Journal of Pathology, 161:745-747

Toole, B. P., Wight, T. N., Tammi, M. I. (2002) *Hyaluronan-cell interactions in cancer and vascular disease,* The Journal of Biological Chemistry, 277(7): 4593–4596

Toyama-Sorimachi, N., Miyasaka, M. (1994) *A sulfated proteoglycan as a novel ligand for CD44,* The Journal of Dermatology, 21(11): 795-801

Toyama-Sorimachi, N., Sorimachi, H., Tobita, Y., Kitamura, F., Yagita, H., Suzuki, K., Miyasaka, M. (1995) *A novel ligand for CD44 is serglycin, a hematopoietic cell lineage-specific proteoglycan. Possible involvement in lymphoid cell adherence and activation,* Journal of Biological Chemistry, 270(13): 7437-7444

Trommer, H., Wartewig, S., Böttcher, R., Pöppl, A. Hoentsch, J., Ozegowski, J. H., Neubert, R. H. H. (2003) *The effects of hyaluronan and its fragments on lipid models exposed to UV irradiation,* International Journal of Pharmaceutics, 254: 223-234

Tsukita, S., Oishi, K., Sato, N., Sagara, J., Kawai, A., Tsukita, S. (1994) *ERM family members as molecular linkers between the cell surface glycoprotein CD44 and actin-based cytoskeletons,* Journal of Cell Biology, 126: 391-401

Turley, E. A. (1982) *Purification of a hyaluronate binding protein fraction that modifies cell social behaviour,* Biochemical and Biophysical Research Communications, 108: 1016-1024

Turley, E. A. (1992) *Hyaluronan and cell locomotion,* Cancer Metastasis Reviews, 11: 21-30

Turley, E. A., Blech , A. R., Poppema, S., Pilarsky, L. M. (1993) *Expression and function of a receptor for hyaluronan mediated motility (RHAMM) on normal and malignant B lymphocytes*, Blood, 81:446-453

Turley, E. A., Noble, P. W., Bourguignon, L. Y. W. (2002) *Signaling properties of hyaluronan receptors*, Journal of Biological Chemistry, 277: 4589–4592

Turley, E. A., Tretiak, M. (1985) *Glycosaminoglycan Production by Murine Melanoma Variants in Vivo and in Vitro*, Cancer Research, 45: 5098-5105

Turley, E., Harrison, R. (1999) RHAMM, a member of the hyaladherins. In: Glycoforum (accessed on 28 May 2008).
http://www.glycoforum.gr.jp/science/hyaluronan/HA11/HA11E.html

Turley, E.A. (1982) *Purification of a hyaluronate-binding protein fraction that modifies cell social behavior*, Biochemical and Biophysical Research Communications, 108:1016-1024

Tzanakakis, G. N., Karamanos, N. K., Hjerpe, A. (1995) *Effects on glycosaminoglycan synthesis in cultured human mesothelioma cells of transforming, epidermal, and fibroblast growth factors and their combinations with platelet-derived growth factor*, Experimental Cell Research, 220 (1): 130-137

Uchiyama, H., Dobashi, Y., Ohkouchi, K., Nagasawa, K. (1990) *Chemical change involved in the oxidative reductive depolymerization of hyaluronic acid*, Journal Biological Chemistry, 265: 7753-7759

Udabage L., Brownlee, G. R., Waltham, M., Blick, T., Walker, E. C., Heldin, P., Nilsson, S. K., Thompson, E. W., Brown, T. J. (2005) *Antisense-mediated suppression of hyaluronan synthase 2 inhibits the tumourigenesis and progression of breast cancer*, Cancer Research, 65: 6139-50

Underhill, C. (1992) *CD44: The hyaluronan receptor*, Journal of Cell Science, 103: 293-298

Van den Heuvel, S. (2005) Cell cycle regulation. In: Eisenmann, D. M., *WormBook*, ed. The *C. elegans* Research Community, WormBook, doi/10.1895/wormbook.1.7.1

Van der Schueren, E., Kesteloot, K., Cleemput, I. (2000) *Federation of European Cancer Societies. Full Report. Economic evaluation in cancer care questions and answers on how to alleviate conflicts between rising needs and expectations and tightening budgets*, European Journal of Cancer, 36: 13-36

Vaux, D.L., S.J. Korsmeyer (1999) *Cell death in development*, Cell, 96: 245-254

Vercruysse, K. P., Prestwich, G. D. (1998) *Hyaluronate derivatives in drug delivery*, Critical Reviews in Therapeutic Drug Carrier Systems, 15: 513-555

Vercruysse, K. P., Ziebell, M. R., Prestwich, G. D. (1999) *Control of enzymatic degradation of hyaluronan by divalent cations*, Carbohydrate Research 318: 26–37

Verma, H. R. (2007) Atomic and nuclear analytical methods : XRF, Mössbauer, XPS, NAA and ion-beam spectroscopic techniques, Springer, Berlin

Vis, A. N., Noordzij, M. A., Fitoz, K., Wildhagen, M. F., Schroder, F. H., Kwast, T. H. van der (2000) *Prognostic value of cell cycle proteins p27(kip1) and MIB-1, and the cell adhesion protein CD44s in surgically treated patients with prostate cancer*, The Journal of Urology, 164: 2156-2161

Vis, A. N., van Rhijn, B. W., Noordzij, M. A., Schroder, F. H., Kwast, T. H. van der (2002) *Value of tissue markers p27(kip1), MIB-1, and CD44s for the pre-operative prediction of tumour features in screen-detected prostate cancer*, The Journal of Pathology, 197: 148-154

Vogelstein, B., Kinzler, K. W. (1992) p53 function and dysfunction, Cell, 70: 523–526

Wang, M. C., Valenzuela, L. A., Murphy, G. P., Chu, T. M. (1979) *Purification of a human prostate specific antigen*, Invest Urology, 17(2):159–163

Watanabe, H. Cheung, S. C., Itano, N., Kimata, K., Yamada, Y. (1997) *Identification of hyaluronan-binding domains of aggrecan*, Journal of Biological Chemistry, 272: 28057-28065

Watanabe, K., Yamaguchi, Y. (1996) *Molecular identification of a putative human hyaluronan synthase*, Journal of Biological Chemistry, 271(38): 22945-22948

Weber, G. F., Ashkar, S., Glimcher, M. J., Cantor, H. (1996) *Receptor-ligand interaction between CD44 and osteopontin (Eta-1),* Science, 271: 509-512

Weigel, P. H., DeAngelis, P. L. (2007) *Hyaluronan synthases: a decade-plus novel glycosyltransferases*, The Journal of Biological Chemistry, 282(51): 36777-36781

Weigel, P. H., Hascall, V. C., Tammi, M. (1997) *Hyaluronan synthases*, The Journal of Biological Chemistry, 272(22): 13997-14000

Weinberg, R. A. (1995) *The retinoblastoma protein and cell cycle control*, Cell, 81: 323-330

Weinberg, R. A. (1996) *How cancer arises*, Scientific American, 275: 32-40

Weissman, B., Meyer, K. J. (1954), *The structure of hyalobiuronic acid and of hyaluronic acid from umbilical cord,* American Chemical Society, 76: 1753-1757

West, D. C., Hampson, I. N., Arnold, F., Kumar, S. (1985) *Angiogenesis induced by degradation products of hyaluronic acid,* Science, 228: 1324-1326

West, D. C., Kumar, S. (1989) *The effect of hyaluronate and its oligosaccharides on endothelial cell proliferation and monolayer integrity,* Experimental Cell Research, 183: 179-196

Whitcombe, M. J. (2010) Personal communication

Willoughby, D. A. (1994) *First International Workshop on Hyaluronan in Drug Delivery*, Royal Society of Medicine Press, Windsor, UK

Wolny, P. M., Banerji, S., Gounou, C., Brisson, A. R., Day, A. J., Jackson, D. G., Richter, R. P. (2010) Analysis of CD44-Hyaluronan interactions in artificial membrane system: insights into the distinct binding properties of high and low molecular weight hyaluronan, The Journal of Biological Chemistry, 285: 30170-30180

Wong, J. Y., Leach, J. B., Brown, X. Q. (2004) *Balance of chemistry, topography, and mechanics at the cell-biomaterial interface: issues and challenges for assessing the role of substrate mechanics on cell response,* Surface Science, 570: 119-133

Wrobel, N., Schinkinger, M., Mirsky, V. M. (2002) *A Novel Ultraviolet Assay for Testing Side Reactions of Carbodiimides,* Analytical Biochemistry, 305(2): 135-8

Xu, X., Ito, T., Tawada, A., Maeda, H., Yamanokuchi, H., Isahara, K., Yoshida, K., Uchiyama, Y., Asari, A. (2002) *Effect of hyaluronan oligosaccharides on the expression of heat shock protein 72*, Journal of Biological Chemistry, 277: 17308-17314

Yabushita, H., Noguchi, M., Kishida, T., Fusano, K., Noguchi, Y., Itano, N., Kimata, K., Noguchi, M. (2004) *Hyaluronan synthase expression in ovarian cancer*, Oncology Reports, 12: 739-743

Yadav, A. K., Mishra, P., Agrawal, G. P. (2008) *An insight on hyaluronic acid in drug targeting and drug delivery*, Journal of Drug Targeting, 16(2): 91-107

Yamada, Y., Itano, N., Narimatsu, H., Kudo, T., Morozumi, K., Hirohashi, S., Ochiai, A., Ueda, M., Kimata, K. (2004) *Elevated transcript level of hyaluronan synthase1 gene correlates with poor prognosis of human colon cancer*, Clinical and Experimental Metastasis, 21: 57–63

Yamaguchi, A., Goi, T., Taguchi, S., Ohtaki, N., Seki, K., Hirose, K., Nakagawara, G., Urano, T., Furukawa, K. (1998) *Clinical significance of serum levels of CD44 variant exons 8-10 protein in colorectal cancer*, Journal of Gastroenterologia, 33: 349-353

Yamaguchi, Y. (2000) *Lecticans: organizers of the brain extracellular matrix*, Cell Molecular Life Sciences, 57:276–289

Yamane, N., Tsujitani, S., Makino, M., Maeta, M., Kaibara, N. (1999) *Soluble CD44 variant 6 as a prognostic indicator in patients with colorectal cancer*, Oncology, 56: 232–238

Yang, B., Hall, C. L., Yang, B. L., Savani, R. C., Turley, E. A. (1994) *Identification of a novel heparin binding domain in RHAMM and evidence that it modifies HA mediated locomotion of ras-transformed cells*, Journal of Cell Biochemistry, 56: 455-468

Yang, B., Yang, B. L., Savani, R. C.,Turley, E. A. (1994) *Identification of a common hyaluronan binding motif in the hyaluronan binding proteins RHAMM, CD44 and link Protein*, The EMBO Journal, 13(2): 286-296

Yang, B., Zhang, L., Turley, E. A. (1993) *Identification of two hyaluronan-binding domains in the hyduronan receptor RHAMM*, Journal of Biological Chemistry, 268: 8617-8623

Yang, K., Tang, Y., Habermehl, G. K., Iczkowski, K. A. (2010) *Stable alterations of CD44 isoform expression in prostate cancer cells decrease invasion and growth and alter ligand binding and chemosensitivity*, BMC Cancer 2010, 10:1

Yaqin, M., Runhua, L., Fuxi, Z. (2007) *Analyses of Bcl-2, Survivin, and CD44v6 expressions and human papillomavirus infection in cervical carcinomas*, Scandinavian Journal of Infectious Diseases, 39(5): 441-8

Yonemura, S., Hirao, M., Doi, Y., Takahashi, N., Kondo, T., Tsukita, S., Tsukita, S. (1998) *Ezrin/radixin/moesin (ERM) proteins bind to a positively charged amino acid cluster in the juxta-membrane cytoplasmic domain of CD44, CD43 and ICAM-2*, Journal of Cell Biology, 140(4): 885-895

Yoshida, K., Goodison, S., Sugino, T., Bolodeoku, J., Churchman, M., Warren, B. F., Tarin, D. (1996) *Semiquantitative detection of abnormal CD44 transcripts in colon carcinomas by reverse transcription-polymerase chain reaction enzyme-linked immunosorbant assay (RT-PCR ELISA)*, Molecular Diagnosis, 1(3): 167-173

Yu, Q., Stamenkovic, I. (1999) *Localization of matrix metalloproteinase 9 to the cell surface provides a mechanism for CD44-mediated tumor invasion*, Genes and Development, 13: 35-48

Yu, Q., Stamenkovic, I. (2000) *Cell surface-localized matrix metalloproteinase-9 proteolytically activates TGF-beta and promotes tumor invasion and angiogenesis*, Genes and Development, 14: 163-176

Yu, S., Ping, Y., Yi, L., Zhou, Z., Chen, J., Yao, X., Gao, L., Wang, J. M., Bian, X. (2008) *Isolation and characterization of cancer stem cells from a human glioblastoma cell line U87,* Cancer letters, 265(1): 124-134

Yu, W. H., Woessner, J. F. Jr., McNeish, J. D., Stamenkovic, I. (2002) *CD44 anchors the assembly of matrilysin/MMP-7 with heparin-binding epidermal growth factor precursor and ErbB4 and regulates female reproductive organ remodelling,* Genes and Development, 16: 307-323

Zhang, L., Underhill, C. B., Chen, L. (1995) *Hyaluronan on the Surface of Tumor Cells Is Correlated with Metastatic Behavior,* Cancer Research, 55: 428-433

Zhang, S., Chang, M. C., Zylka, D., Turley, S., Harrison, R., Turley, E.A. (1998) *The hyaluronan receptor RHAMM regulates extracellular-regulated kinase,* Journal Biological Chemistry, 273: 11342–11348

Zhou, B., Weigel, J.A., Fauss, L., Weigel, P.H. (2000) *Identification of the hyaluronan receptor for endocytosis (HARE),* Journal of Biological Chemistry, 275: 37733-37741

Zhuo, L., Hascall, V. C., Kimata, K. (2004) *Inter-α-trypsin inhibitor, a covalent protein-glycosaminoglycan-protein complex,* Journal of Biological Chemistry, 279: 38079–38082

Zoltan-Jones, A., Huang, L., Ghatak, S., Toole, B. P. (2003) *Elevated Hyaluronan Production Induces Mesenchymal and Transformed Properties in Epithelial Cells,* Journal of Biological Chemistry, 278: (46) 45801-45810

APPENDICES

Appendix I

Solution formulations

General solutions

PBS PBS is made using tablets (Sigma, UK) dissolved in 500 ml of RO H_2O. PBS for sell culture was sterilised by autoclaving.

Protein extraction

Protease inhibitor Protease inhibitor cocktail arrives in kit form with four separate constituents (EDTA disodium dihydrate, pepstatin A, leupeptin hemisulfate and AEBSF hydrochloride). Each bottle is resuspended in RO H_2O, and the four bottles mixed. The volume is then made up to 100 ml with RO H_2O.

CHAPS lysis buffer
20 mM Tris pH 8.0
0.15 M NaCl
5 mM EDTA
310 mg of CHAPS
1 ml of protease inhibitor cocktail
Made to a final volume of 50 ml with RO H_2O

ICC

DAB solution
30 mg of DAB
50 ml PBS
100 µl of hydrogen peroxide

Appendix I

Western Blot

5x Sample buffer

10 ml 0.5M Tris (pH 6.8) – final concentration 250mM
8 ml Glycerol - final concentration 40% (v/v)
2 g SDS – final concentration 10% (w/v)
0.1 mg Bromophenol blue – final concentration 0.5% (w/v)
Made up to 20ml with distilled water, and pH set to 6.8
The solution was aliquoted and stored at -20°C for future use. Directly before use 125µl β-mercaptoethanol was added to 875µl of 5x sample buffer. A working solution of either 1x or 2x sample buffer was used. These were prepared by diluting the 5x buffer in RO H_2O as appropriate.

10x Running buffer

30.2g Tris - final concentration 0.025M
144g Glycine - final concentration 0.192M
10g SDS - final concentration 0.1% (w/v)
Made up to 1 L with RO H_2O.
The 10x running buffer solution was stored at room temperature for future use. A 1x working solution was made fresh on the day of use by diluting 100 ml 10x running buffer with 900ml RO H_2O.

10x Transfer/Blotting buffer

30.2g Tris - final concentration 0.025M
144g Glycine - final concentration 0.192M
Made up to 1 L in RO H_2O.
The 10x transfer buffer solution was stored at room temperature for future use. A 1x working solution was made fresh on the day of use by diluting 100ml 10x transfer buffer with 200ml methanol and 700ml distilled water. The 1x working solution of transfer buffer was cooled to 4°C prior to use.

Appendix II

Surface wettability measurements assessed by contact angle

	θ (angle formed)
Glass	64.78 ± 1.65
Activated glass	22.16 ± 1.58
Aminosilane	34.26 ± 2.81
HA_4 C1	42.17 ± 5.39
HA_4 C2	41.76 ± 3.75
HA_4 C3	43.62 ± 2.69
HA_{234} C1	27.98 ± 3.06
HA_{234} C2	29.17 ± 2.74
HA_{234} C3	35.30 ± 2.04
HA_{2590} C1	17.05 ± 4.48
HA_{2590} C2	19.89 ± 3.26
HA_{2590} C3	18.74 ± 2.03
HA_{mix} C1	28.60 ± 3.065
HA_{mix} C2	34.44 ± 2.09
HA_{mix} C3	33.82 ± 2.17

Appendix III

Surface wettability statistics

	Glass	Activated glass	Aminosilane	HA_4 C1	HA_4 C2	HA_4 C3	HA_{234} C1	HA_{234} C2	HA_{234} C3	HA_{2590} C1	HA_{2590} C2	HA_{2590} C3	HA_{mix} C1	HA_{mix} C2	HA_{mix} C3
Number of values	12	12	25	99	85	72	113	64	55	60	78	91	117	56	50
Minimum	60.99	19.19	31.28	28.90	35.10	26.56	23.63	24.09	31.16	10.03	15.02	15.34	23.56	31.04	31.18
25% Percentile	63.52	20.57	33.27	38.94	39.34	42.35	25.57	26.79	33.92	12.66	16.92	17.15	26.55	32.61	31.92
Median	64.78	22.16	34.26	43.07	41.13	43.95	27.09	29.17	35.45	17.43	19.17	18.53	28.15	34.27	33.06
75% Percentile	65.34	22.66	37.38	46.56	44.80	45.32	30.68	31.92	36.73	21.00	22.49	19.97	29.84	36.46	36.15
Maximum	67.06	24.93	41.37	53.00	48.97	46.63	33.91	33.38	38.94	23.69	25.97	23.66	37.95	37.97	37.64
Mean	64.55	21.86	35.41	42.17	41.76	43.62	27.98	29.17	35.30	17.05	19.89	18.74	28.60	34.44	33.82
Std. Deviation	1.653	1.578	2.809	5.389	3.750	2.686	3.061	2.741	2.039	4.475	3.263	2.029	3.065	2.094	2.172
Std. Error	0.4772	0.4556	0.5619	0.5416	0.4068	0.3165	0.2880	0.3427	0.2750	0.5778	0.3695	0.2127	0.2834	0.2798	0.3072
Lower 95% CI of mean	63.50	20.86	34.25	41.10	40.95	42.99	27.41	28.48	34.75	15.89	19.16	18.32	28.03	33.88	33.20
Upper 95% CI of mean	65.60	22.86	36.57	43.25	42.57	44.25	28.55	29.85	35.85	18.20	20.63	19.17	29.16	35.00	34.44
Sum	774.6	262.3	885.2	4175	3550	3140	3162	1867	1942	1023	1552	1706	3346	1929	1691

Appendix III

One-way analysis of variance			
P value	< 0.0001		
P value summary	***		
Are means signif. different? (P < 0.05)	Yes		
Number of groups	15		
F	581.6		
R square	0.8932		
Bartlett's test for equal variances			
Bartlett's statistic (corrected)	189.9		
P value	< 0.0001		
P value summary	***		
Do the variances differ signif. (P < 0.05)	Yes		
ANOVA Table	SS	df	MS
Treatment (between columns)	87512	14	6251
Residual (within columns)	10468	974	10.75
Total	97980	988	

Appendix III

Tukey's Multiple Comparison Test	Mean Diff.	q	Significant? P < 0.05?	Summary	95% CI of diff
Glass vs Activated glass	42.69	45.11	Yes	***	38.08 to 47.30
Glass vs Aminosilane	29.14	35.80	Yes	***	25.18 to 33.11
Glass vs HA_4 C1	22.38	31.58	Yes	***	18.93 to 25.83
Glass vs HA_4 C2	22.79	31.88	Yes	***	19.31 to 26.27
Glass vs HA_4 C3	20.93	28.96	Yes	***	17.41 to 24.45
Glass vs HA_{234} C1	36.57	51.96	Yes	***	33.14 to 39.99
Glass vs HA_{234} C2	35.38	48.52	Yes	***	31.83 to 38.93
Glass vs HA_{234} C3	29.25	39.60	Yes	***	25.65 to 32.84
Glass vs HA_{2590} C1	47.50	64.80	Yes	***	43.94 to 51.07
Glass vs HA_{2590} C2	44.66	62.12	Yes	***	41.16 to 48.16
Glass vs HA_{2590} C3	45.81	64.34	Yes	***	42.34 to 49.27
Glass vs HA_{mix} C1	35.95	51.17	Yes	***	32.53 to 39.37
Glass vs HA_{mix} C2	30.11	40.83	Yes	***	26.52 to 33.70
Glass vs HA_{mix} C3	30.73	41.24	Yes	***	27.10 to 34.36
Activated glass vs Aminosilane	-13.55	16.64	Yes	***	-17.51 to -9.584
Activated glass vs HA_4 C1	-20.31	28.66	Yes	***	-23.76 to -16.86
Activated glass vs HA_4 C2	-19.90	27.84	Yes	***	-23.38 to -16.42
Activated glass vs HA_4 C3	-21.76	30.10	Yes	***	-25.27 to -18.24
Activated glass vs HA_{234} C1	-6.122	8.698	Yes	***	-9.548 to -2.696
Activated glass vs HA_{234} C2	-7.308	10.02	Yes	***	-10.86 to -3.758
Activated glass vs HA_{234} C3	-13.44	18.20	Yes	***	-17.04 to -9.846
Activated glass vs HA_{2590} C1	4.815	6.568	Yes	***	1.247 to 8.383
Activated glass vs HA_{2590} C2	1.967	2.737	No	ns	-1.532 to 5.466
Activated glass vs HA_{2590} C3	3.118	4.380	No	ns	-0.3476 to 6.584
Activated glass vs HA_{mix} C1	-6.735	9.584	Yes	***	-10.16 to -3.314
Activated glass vs HA_{mix} C2	-12.58	17.06	Yes	***	-16.17 to -8.988
Activated glass vs HA_{mix} C3	-11.96	16.05	Yes	***	-15.59 to -8.331
Aminosilane vs HA_4 C1	-6.763	13.03	Yes	***	-9.289 to -4.237
Aminosilane vs HA_4 C2	-6.356	12.05	Yes	***	-8.923 to -3.788
Aminosilane vs HA_4 C3	-8.210	15.26	Yes	***	-10.83 to -5.590
Aminosilane vs HA_{234} C1	7.425	14.49	Yes	***	4.931 to 9.919
Aminosilane vs HA_{234} C2	6.239	11.41	Yes	***	3.577 to 8.900
Aminosilane vs HA_{234} C3	0.1054	0.1885	No	ns	-2.616 to 2.827
Aminosilane vs HA_{2590} C1	18.36	33.27	Yes	***	15.68 to 21.05
Aminosilane vs HA_{2590} C2	15.51	29.12	Yes	***	12.92 to 18.11
Aminosilane vs HA_{2590} C3	16.66	31.84	Yes	***	14.12 to 19.21
Aminosilane vs HA_{mix} C1	6.812	13.34	Yes	***	4.326 to 9.298
Aminosilane vs HA_{mix} C2	0.9694	1.739	No	ns	-1.745 to 3.684
Aminosilane vs HA_{mix} C3	1.588	2.797	No	ns	-1.176 to 4.352
HA_4 C1 vs HA_4 C2	0.4074	1.189	No	ns	-1.261 to 2.076
HA_4 C1 vs HA_4 C3	-1.447	4.029	No	ns	-3.194 to 0.3012
HA_4 C1 vs HA_{234} C1	14.19	44.46	Yes	***	12.63 to 15.74
HA_4 C1 vs HA_{234} C2	13.00	34.97	Yes	***	11.19 to 14.81
HA_4 C1 vs HA_{234} C3	6.869	17.62	Yes	***	4.971 to 8.766
HA_4 C1 vs HA_{2590} C1	25.12	66.25	Yes	***	23.28 to 26.97
HA_4 C1 vs HA_{2590} C2	22.28	63.47	Yes	***	20.57 to 23.99
HA_4 C1 vs HA_{2590} C3	23.43	69.59	Yes	***	21.79 to 25.07
HA_4 C1 vs HA_{mix} C1	13.58	42.88	Yes	***	12.03 to 15.12
HA_4 C1 vs HA_{mix} C2	7.732	19.95	Yes	***	5.846 to 9.619
HA_4 C1 vs HA_{mix} C3	8.351	20.76	Yes	***	6.394 to 10.31
HA_4 C2 vs HA_4 C3	-1.854	4.993	Yes	*	-3.661 to -0.04658
HA_4 C2 vs HA_{234} C1	13.78	41.40	Yes	***	12.16 to 15.40
HA_4 C2 vs HA_{234} C2	12.59	32.83	Yes	***	10.73 to 14.46
HA_4 C2 vs HA_{234} C3	6.461	16.11	Yes	***	4.508 to 8.414
HA_4 C2 vs HA_{2590} C1	24.72	63.24	Yes	***	22.81 to 26.62
HA_4 C2 vs HA_{2590} C2	21.87	60.17	Yes	***	20.10 to 23.64
HA_4 C2 vs HA_{2590} C3	23.02	65.83	Yes	***	21.32 to 24.72

Appendix III

Tukey's Multiple Comparison Test	Mean Diff.	q	Significant? P < 0.05?	Summary	95% CI of diff
HA_4 C2 vs HA_{mix} C1	13.17	39.86	Yes	***	11.56 to 14.78
HA_4 C2 vs HA_{mix} C2	7.325	18.36	Yes	***	5.383 to 9.267
HA_4 C2 vs HA_{mix} C3	7.944	19.23	Yes	***	5.933 to 9.955
HA_4 C3 vs HA_{234} C1	15.63	44.73	Yes	***	13.93 to 17.34
HA_4 C3 vs HA_{234} C2	14.45	36.28	Yes	***	12.51 to 16.39
HA_4 C3 vs HA_{234} C3	8.315	20.03	Yes	***	6.294 to 10.34
HA_4 C3 vs HA_{2590} C1	26.57	65.57	Yes	***	24.60 to 28.54
HA_4 C3 vs HA_{2590} C2	23.72	62.62	Yes	***	21.88 to 25.57
HA_4 C3 vs HA_{2590} C3	24.87	68.03	Yes	***	23.09 to 26.65
HA_4 C3 vs HA_{mix} C1	15.02	43.26	Yes	***	13.33 to 16.71
HA_4 C3 vs HA_{mix} C2	9.179	22.22	Yes	***	7.168 to 11.19
HA_4 C3 vs HA_{mix} C3	9.798	22.96	Yes	***	7.721 to 11.88
HA_{234} C1 vs HA_{234} C2	-1.186	3.271	No	ns	-2.952 to 0.5790
HA_{234} C1 vs HA_{234} C3	-7.320	19.21	Yes	***	-9.175 to -5.464
HA_{234} C1 vs HA_{2590} C1	10.94	29.54	Yes	***	9.134 to 12.74
HA_{234} C1 vs HA_{2590} C2	8.089	23.70	Yes	***	6.428 to 9.750
HA_{234} C1 vs HA_{2590} C3	9.240	28.30	Yes	***	7.650 to 10.83
HA_{234} C1 vs HA_{mix} C1	-0.6129	2.005	No	ns	-2.101 to 0.8754
HA_{234} C1 vs HA_{mix} C2	-6.456	17.04	Yes	***	-8.300 to -4.612
HA_{234} C1 vs HA_{mix} C3	-5.837	14.82	Yes	***	-7.753 to -3.920
HA_{234} C2 vs HA_{234} C3	-6.133	14.39	Yes	***	-8.208 to -4.059
HA_{234} C2 vs HA_{2590} C1	12.12	29.10	Yes	***	10.10 to 14.15
HA_{234} C2 vs HA_{2590} C2	9.275	23.72	Yes	***	7.372 to 11.18
HA_{234} C2 vs HA_{2590} C3	10.43	27.57	Yes	***	8.585 to 12.27
HA_{234} C2 vs HA_{mix} C1	0.5734	1.591	No	ns	-1.181 to 2.328
HA_{234} C2 vs HA_{mix} C2	-5.269	12.42	Yes	***	-7.334 to -3.205
HA_{234} C2 vs HA_{mix} C3	-4.650	10.63	Yes	***	-6.780 to -2.521
HA_{234} C3 vs HA_{2590} C1	18.26	42.19	Yes	***	16.15 to 20.36
HA_{234} C3 vs HA_{2590} C2	15.41	37.75	Yes	***	13.42 to 17.40
HA_{234} C3 vs HA_{2590} C3	16.56	41.82	Yes	***	14.63 to 18.49
HA_{234} C3 vs HA_{mix} C1	6.707	17.70	Yes	***	4.862 to 8.552
HA_{234} C3 vs HA_{mix} C2	0.8640	1.963	No	ns	-1.278 to 3.006
HA_{234} C3 vs HA_{mix} C3	1.483	3.273	No	ns	-0.7222 to 3.688
HA_{2590} C1 vs HA_{2590} C2	-2.848	7.154	Yes	***	-4.785 to -0.9099
HA_{2590} C1 vs HA_{2590} C3	-1.697	4.402	No	ns	-3.574 to 0.1795
HA_{2590} C1 vs HA_{mix} C1	-11.55	31.38	Yes	***	-13.34 to -9.758
HA_{2590} C1 vs HA_{mix} C2	-17.39	40.38	Yes	***	-19.49 to -15.30
HA_{2590} C1 vs HA_{mix} C3	-16.77	37.79	Yes	***	-18.93 to -14.61
HA_{2590} C2 vs HA_{2590} C3	1.151	3.217	No	ns	-0.5906 to 2.892
HA_{2590} C2 vs HA_{mix} C1	-8.702	25.68	Yes	***	-10.35 to -7.053
HA_{2590} C2 vs HA_{mix} C2	-14.54	35.82	Yes	***	-16.52 to -12.57
HA_{2590} C2 vs HA_{mix} C3	-13.93	33.16	Yes	***	-15.97 to -11.88
HA_{2590} C3 vs HA_{mix} C1	-9.853	30.41	Yes	***	-11.43 to -8.275
HA_{2590} C3 vs HA_{mix} C2	-15.70	39.86	Yes	***	-17.61 to -13.78
HA_{2590} C3 vs HA_{mix} C3	-15.08	36.95	Yes	***	-17.06 to -13.09
HA_{mix} C1 vs HA_{mix} C2	-5.843	15.51	Yes	***	-7.676 to -4.009
HA_{mix} C1 vs HA_{mix} C3	-5.224	13.34	Yes	***	-7.130 to -3.317
HA_{mix} C2 vs HA_{mix} C3	0.6188	1.372	No	ns	-1.577 to 2.814

Appendix IV

Cell counting raw data

	RT112				T24			
Day	**Cell density ($x10^4$)**	**Cell density ($x10^4$)**	**Cell density ($x10^4$)**	**Cell density Average ($x10^4$)**	**Cell density ($x10^4$)**	**Cell density ($x10^4$)**	**Cell density ($x10^4$)**	**Cell density Average ($x10^4$)**
0	10	10	10	10	10	10	10	10
1	8	11	10	10	11	17	15	14
2	8	19	19	15	31	20	24	25
3	29	37	35	34	32	17	14	21
4	69	93	71	78	29	31	18	26
5	125	152	130	136	52	47	46	48
6	103	127	122	117	79	65	67	70
7	168	179	125	157	69	73	70	71
8	175	148	127	150	74	-	74	74

	PC3				PNT1A			
Day	**Cell density ($x10^4$)**	**Cell density ($x10^4$)**	**Cell density ($x10^4$)**	**Cell density Average ($x10^4$)**	**Cell density ($x10^4$)**	**Cell density ($x10^4$)**	**Cell density ($x10^4$)**	**Cell density Average ($x10^4$)**
0	10	10	10	10	10	10	10	10
1	10	11	8	10	14	11	10	12
2	11	13	11	12	16	14	13	14
3	38	20	30	29	12	11	12	12
4	56	62	58	59	26	31	17	25
5	81	58	58	66	30	-	28	29
6	72	100	63	78	-	47	31	39
7	117	73	68	86	57	52	66	58
8	105	108	113	109	-	72	72	72

Appendix V

Cell counting statistics

	RT112	T24	PC3	PNT1A
Number of values	9	9	9	9
Minimum	9.667	10.00	9.667	10.00
25% Percentile	12.67	17.67	10.83	11.67
Median	77.67	26.00	58.67	24.67
75% Percentile	142.8	70.50	82.17	48.67
Maximum	157.3	74.00	108.7	72.00
Mean	78.52	39.96	50.89	30.07
Std. Deviation	62.78	26.05	37.04	22.35
Std. Error	20.93	8.682	12.35	7.449
Lower 95% CI of mean	30.26	19.94	22.42	12.90
Upper 95% CI of mean	126.8	59.98	79.36	47.25
Sum	706.7	359.7	458.0	270.7

Appendix VI

Cell counting – curve fitting using SigmaPlot 10.0

a) RT112 cell line

Nonlinear Regression - Dynamic Fitting

Data Source: RT112 in Notebook2
Equation: Piecewise; 3 segment linear
t1 = min(t)
t3 = max(t)
region1(t) = (y1*(T1-t) + y2*(t-t1))/(T1-t1)
region2(t) = (y2*(T2-t) + y3*(t-T1))/(T2-T1)
region3(t) = (y3*(t3-t) + y4*(t-T2))/(t3-T2)
f = if(t <= T1; region1(t); if(t <= T2; region2(t); region3(t)))

Dynamic Fit Options:

Total Number of Fits	200
Maximum Number of Iterations	200

Parameter Ranges for Initial Estimates:

	Minimum	Maximum
y1	-12.9378	38.8135
y2	-34.2869	102.8607
y3	-121.9138	365.7414
y4	-150.0692	450.2075
T1	-2.6667	8.0000
T2	-5.3333	16.0000

Summary of Fit Results:

Converged	97.0%
Singular Solutions	68.0%
Ill-Conditioned Solutions	20.0%
Iterations Exceeding 200	3.0%

Results for the Overall Best-Fit Solution:

R	Rsqr	Adj Rsqr	Standard Error of Estimate
0.9903	0.9807	0.9485	14.2342

	Coefficient	Std. Error	t	P	VIF
y1	9.1573	12.9940	0.7047	0.5318	1.1997
y2	15.7376	19.3622	0.8128	0.4758	2.9825
y3	126.8762	25.9483	4.8896	0.0164	6.3669<
y4	152.6963	12.5937	12.1248	0.0012	1.2177
T1	2.6242	0.5890	4.4556	0.0210	3.3266
T2	5.0000	0.9876	5.0629	0.0149	7.1465<

Appendix VI

Analysis of Variance:

Uncorrected for the mean of the observations:

	DF	SS	MS
Regression	6	86391.1614	14398.5269
Residual	3	607.8386	202.6129
Total	9	86999.0000	9666.5556

Corrected for the mean of the observations:

	DF	SS	MS	F	P
Regression	5	30852.3836	6170.4767	30.4545	0.0090
Residual	3	607.8386	202.6129		
Total	8	31460.2222	3932.5278		

Statistical Tests:

PRESS 3831.7618

Durbin-Watson Statistic 3.5164 Failed

Normality Test Passed (P = 0.4742)

K-S Statistic = 0.2674 Significance Level = 0.4742

Constant Variance Test Passed (P = 0,0200)

Power of performed test with alpha = <0.0001: 0.0000

The power of the performed test (0.0000) is below the desired power of 0,8000.
You should interpret the negative findings cautiously.

Appendix VI

b) T24 cell line

Nonlinear Regression - Dynamic Fitting

Data Source: T24 in Notebook2
Equation: Piecewise; 3 segment linear
t1 = min(t)
t3 = max(t)
region1(t) = (y1*(T1-t) + y2*(t-t1))/(T1-t1)
region2(t) = (y2*(T2-t) + y3*(t-T1))/(T2-T1)
region3(t) = (y3*(t3-t) + y4*(t-T2))/(t3-T2)
f = if(t <= T1; region1(t); if(t <= T2; region2(t); region3(t)))

Dynamic Fit Options:

Total Number of Fits	200
Maximum Number of Iterations	200

Parameter Ranges for Initial Estimates:

	Minimum	Maximum
y1	-9.3419	28.0256
y2	-20.6710	62.0130
y3	-52.2951	156.8854
y4	-72.5136	217.5408
T1	-2.6667	8.0000
T2	-5.3333	16.0000

Summary of Fit Results:

Converged	96.5%
Singular Solutions	77.5%
Ill-Conditioned Solutions	19.0%
Iterations Exceeding 200	3.5%

Results for the Overall Best-Fit Solution:

R	Rsqr	Adj Rsqr	Standard Error of Estimate
0.9960	0.9920	0.9787	3.8020

	Coefficient	Std. Error	t	P	VIF
y1	11.4000	2.9451	3.8709	0.0305	0.0000
y2	28.5187	3.9760	7.1727	0.0056	0.0000
y3	68.9819	4.2242	16.3302	0.0005	0.0000
y4	73.6667	3.4708	21.2248	0.0002	0.0000
T1	4.3894	0.3203	13.7028	0.0008	0.0000
T2	5.6576	0.0159	356.5576	<0.0001	0.0000

Analysis of Variance:

Uncorrected for the mean of the observations:

	DF	SS	MS
Regression	6	19715.6333	3285.9389
Residual	3	43.3667	14.4556
Total	9	19759.0000	2195.4444

Appendix VI

Corrected for the mean of the observations:

	DF	SS	MS	F	P
Regression	5	5395.5222	1079.1044	74.6498	0.0024
Residual	3	43.3667	14.4556		
Total	8	5438.8889	679.8611		

Statistical Tests:

PRESS 1.0727E+014

Durbin-Watson Statistic 2.7014 Failed

Normality Test Passed (P = 0.2221)

K-S Statistic = 0.3320 Significance Level = 0.2221

Constant Variance Test Passed (P = 0.0158)

Power of performed test with alpha = <0.0001: 0.0000

The power of the performed test (0.0000) is below the desired power of 0,8000.
You should interpret the negative findings cautiously.

Appendix VI

c) PC3 cell line

Nonlinear Regression - Dynamic Fitting

Data Source: PC3 in Notebook2
Equation: Piecewise; 3 segment linear
t1 = min(t)
t3 = max(t)
region1(t) = (y1*(T1-t) + y2*(t-t1))/(T1-t1)
region2(t) = (y2*(T2-t) + y3*(t-T1))/(T2-T1)
region3(t) = (y3*(t3-t) + y4*(t-T2))/(t3-T2)
f = if(t <= T1; region1(t); if(t <= T2; region2(t); region3(t)))

Dynamic Fit Options:

Total Number of Fits	200
Maximum Number of Iterations	200

Parameter Ranges for Initial Estimates:

	Minimum	**Maximum**
y1	-11.8733	35.6200
y2	-27.8087	83.4261
y3	-70.6345	211.9035
y4	-108.0754	324.2261
T1	-2.6667	8.0000
T2	-5.3333	16.0000

Summary of Fit Results:

Converged	96.0%
Singular Solutions	69.0%
Ill-Conditioned Solutions	19.5%
Iterations Exceeding 200	4.0%

Results for the Overall Best-Fit Solution:

R	**Rsqr**	**Adj Rsqr**	**Standard Error of Estimate**
0.9964	0.9929	0.9811	5.0947

	Coefficient	**Std. Error**	**t**	**P**	**VIF**
y1	9.6667	4.6508	2.0785	0.1292	1.1885
y2	12.2487	5519374.9572	2.2192E-006	1.0000	1.2409E+012<
y3	49.8395	114675676.7255	4.3461E-007	1.0000	8.5791E+014<
y4	103.6000	4.1067	25.2269	0.0001	1.3193
T1	2.5820	5519374.9845	4.6781E-007	1.0000	5.8031E+014<
T2	3.5200	9556306.4227	3.6834E-007	1.0000	1.8796E+015<

Appendix VI

Analysis of Variance:

Uncorrected for the mean of the observations:

	DF	SS	MS
Regression	6	34305.1333	5717.5222
Residual	3	77.8667	25.9556
Total	9	34383.0000	3820.3333

Corrected for the mean of the observations:

	DF	SS	MS	F	P
Regression	5	10896.1333	2179.2267	83.9599	0.0020
Residual	3	77.8667	25.9556		
Total	8	10974.0000	1371.7500		

Statistical Tests:

PRESS 2968.3867

Durbin-Watson Statistic 2.2561 Failed

Normality Test Passed (P = 0.6397)

K-S Statistic = 0.2352 Significance Level = 0.6397

Constant Variance Test Passed (P = 0.0039)

Power of performed test with alpha = <0.0001: 0.0000

The power of the performed test (0.0000) is below the desired power of 0,8000.
You should interpret the negative findings cautiously.

Appendix VI

d) PNT1A cell line

Nonlinear Regression - Dynamic Fitting

Data Source: PNT1A in Notebook2
Equation: Piecewise; 3 segment linear
t1 = min(t)
t3 = max(t)
region1(t) = (y1*(T1-t) + y2*(t-t1))/(T1-t1)
region2(t) = (y2*(T2-t) + y3*(t-T1))/(T2-T1)
region3(t) = (y3*(t3-t) + y4*(t-T2))/(t3-T2)
f = if(t <= T1; region1(t); if(t <= T2; region2(t); region3(t)))

Dynamic Fit Options:

Total Number of Fits	200
Maximum Number of Iterations	200

Parameter Ranges for Initial Estimates:

	Minimum	**Maximum**
y1	-10.1158	30.3473
y2	-14.5247	43.5742
y3	-33.1283	99.3849
y4	-72.4390	217.3170
T1	-2.6667	8.0000
T2	-5.3333	16.0000

Summary of Fit Results:

Converged	96.0%
Singular Solutions	67.5%
Ill-Conditioned Solutions	18.5%
Iterations Exceeding 200	4.0%

Results for the Overall Best-Fit Solution:

R	**Rsqr**	**Adj Rsqr**	**Standard Error of Estimate**
0.9975	0.9950	0.9867	2.5695

	Coefficient	**Std. Error**	**t**	**P**	**VIF**
y1	10.5363	2.2703	4.6409	0.0189	1.2144
y2	14.1077	4.3057	3.2765	0.0465	5.8577<
y3	38.3246	9.9875	3.8372	0.0312	26.2816<
y4	72.8226	2.3456	31.0467	<0.0001	1.0601
T1	3.0000	0.9596	3.1261	0.0522	7.7772<
T2	5.9163	0.6563	9.0146	0.0029	23.,2375<

Appendix VI

Analysis of Variance:

Uncorrected for the mean of the observations:

	DF	SS	MS
Regression	6	12099.1937	2016.5323
Residual	3	19.8063	6.6021
Total	9	12119.0000	1346.5556

Corrected for the mean of the observations:

	DF	SS	MS	F	P
Regression	5	3939.0826	787.8165	119.3280	0.0012
Residual	3	19.8063	6.6021		
Total	8	3958.8889	494.8611		

Statistical Tests:

PRESS 773.7495

Durbin-Watson Statistic 3.3112 Failed

Normality Test Passed (P = 0.8689)

K-S Statistic = 0.1890 Significance Level = 0.8689

Constant Variance Test Passed (P = 0.3558)

Power of performed test with alpha = <0.0001: 0.0000

The power of the performed test (0.0000) is below the desired power of 0.8000.
You should interpret the negative findings cautiously.

Appendix VII

MTT assay raw data

	RT112															
	5 x 10^4 cells/well				2.5 x 10^4 cells/well				1.25 x 10^4 cells/well				6.25 x 10^3 cells/well			
Day	**OD**	**OD**	**OD**	**OD Average**	**OD**	**OD**	**OD**	**OD Average**	**OD**	**OD**	**OD**	**OD Average**	**OD**	**OD**	**OD**	**OD Average**
1	0,121098	0,132753	0,123470	0,125774	0,095271	0,102409	0,090952	0,096211	0,075069	0,068748	0,066768	0,070195	0,096373	0,067866	0,074302	0,079514
2	0,233944	0,236996	0,191767	0,220902	0,187385	0,218359	0,180280	0,195341	0,154890	0,140851	0,086731	0,127491	0,102085	0,135241	0,160578	0,132635
3	0,462192	0,499506	0,706911	0,556203	0,361141	0,318832	0,396644	0,358872	0,227792	0,188246	0,173079	0,196372	0,108411	0,143664	0,114478	0,122184
4	0,490042	0,783793	0,679699	0,651178	0,453061	0,458324	0,440470	0,450618	0,348387	0,319244	0,229465	0,299032	0,237593	0,164646	0,162242	0,188160
5	-	-	-	-	-	-	-	-	-	-	-	-	-	-	-	-
6	0,931375	0,956415	0,878249	0,922013	0,764141	0,697791	0,817968	0,759967	0,479049	0,591917	0,693637	0,588201	0,360303	0,379873	0,453982	0,398053
7	0,978242	0,747502	0,792431	0,839392	0,719865	0,761657	0,712742	0,731421	0,671882	0,593287	0,801570	0,688913	0,717500	0,513409	0,575102	0,602004
8	0,770693	0,835520	0,978109	0,861441	0,702665	0,620979	0,981363	0,768336	0,675917	0,847879	0,933055	0,818950	0,877655	0,798094	0,731169	0,802306

	T24															
	5 x 10^4 cells/well				2.5 x 10^4 cells/well				1.25 x 10^4 cells/well				6.25 x 10^3 cells/well			
Day	**OD**	**OD**	**OD**	**OD Average**	**OD**	**OD**	**OD**	**OD Average**	**OD**	**OD**	**OD**	**OD Average**	**OD**	**OD**	**OD**	**OD Average**
1	0.1878	0.1677	0.1725	0.1760	0.1173	0.0935	0.1194	0.1101	0.1247	0.1298	0.0793	0.1113	0.0975	0.0782	0.1240	0.0999
2	0.1889	0.2011	0.1837	0.1912	0.1598	0.1632	0.1542	0.1591	0.1441	0.1334	0.1292	0.1356	0.1151	0.1112	0.1476	0.1246
3	0.4058	0.4319	0.3400	0.3926	0.3403	0.2719	0.1902	0.2675	0.1760	0.2223	0.1835	0.1940	0.1424	0.1387	0.1264	0.1358
4	0.5787	0.6248	0.6214	0.6083	0.4114	0.4457	0.4351	0.4307	0.2857	0.2724	0.3009	0.2863	0.2018	0.1742	0.2535	0.2098
5	0.5494	0.5843	0.6173	0.5837	0.5166	0.4979	0.5102	0.5083	0.3783	0.4281	0.3736	0.3933	0.2649	0.3215	0.2990	0.2951
6	0.8259	0.8854	0.8417	0.8510	0.7048	0.7530	0.8121	0.7566	0.5887	0.6528	0.6882	0.6432	0.5089	0.5369	0.5376	0.5278
7	0.8981	0.8941	0.9327	0.9083	0.7783	0.9231	0.9841	0.8952	0.6674	0.8562	0.9210	0.8148	0.7291	0.6541	0.7323	0.7052
8	0.8585	0.7607	0.7918	0.8037	0.8481	0.8480	0.7714	0.8225	0.8298	0.8299	0.7366	0.7987	0.6968	0.6326	0.6248	0.6514

Appendix VII

	PC3															
	5×10^4 cells/well				2.5×10^4 cells/well				1.25×10^4 cells/well				6.25×10^3 cells/well			
Day	**OD**	**OD**	**OD**	**OD Average**	**OD**	**OD**	**OD**	**OD Average**	**OD**	**OD**	**OD**	**OD Average**	**OD**	**OD**	**OD**	**OD Average**
1	0.1523	0.1275	0.1637	0.1478	0.0861	0.1241	0.0993	0.1032	0.0865	0.0940	0.0971	0.0925	0.0786	0.0949	0.0958	0.0897
2	0.2042	0.1669	0.1882	0.1864	0.1467	0.1774	0.1630	0.1624	0.1480	0.1418	0.1788	0.1562	0.1052	0.1169	0.1257	0.1159
3	0.2252	0.2386	0.2359	0.2332	0.1664	0.1626	0.1364	0.1551	0.1279	0.1429	0.1631	0.1447	0.1124	0.1157	0.1372	0.1218
4	0.2695	0.2742	0.3148	0.2861	0.1923	0.1855	0.1900	0.1893	0.1410	0.1572	0.1950	0.1644	0.1252	0.1272	0.0951	0.1158
5	0.5017	0.5100	0.5856	0.5324	0.2855	0.3174	0.3417	0.3149	0.2444	0.2193	0.2173	0.2270	0.1834	0.1527	0.1668	0.1676
6	0.6338	0.5767	0.5349	0.5818	0.4062	0.4110	0.4003	0.4059	0.2144	0.2176	0.2276	0.2199	0.1479	0.1498	0.1541	0.1506
7	0.6382	0.6016	0.6300	0.6233	0.5147	0.4688	0.4929	0.4921	0.3425	0.3487	0.3072	0.3328	0.2021	0.2165	0.2483	0.2223
8	0.6520	0.6779	0.6933	0.6744	0.6146	0.6204	0.5484	0.5944	0.5740	0.5401	0.5284	0.5475	0.3652	0.4328	0.4113	0.4031

	PNT1A															
	5×10^4 cells/well				2.5×10^4 cells/well				1.25×10^4 cells/well				6.25×10^3 cells/well			
Day	**OD**	**OD**	**OD**	**OD Average**	**OD**	**OD**	**OD**	**OD Average**	**OD**	**OD**	**OD**	**OD Average**	**OD**	**OD**	**OD**	**OD Average**
1	0.1718	0.0963	0.1255	0.1312	0.1042	0.0568	0.0802	0.0804	0.0834	0.0816	0.0819	0.0823	0.0713	0.0729	0.0705	0.0716
2	0.1370	0.1398	0.1197	0.1322	0.1064	0.0806	0.0974	0.0948	0.1146	0.0888	0.1009	0.1014	0.0778	0.0815	0.0684	0.0759
3	0.1634	0.1625	0.1660	0.1639	0.1101	0.1079	0.1114	0.1098	0.0833	0.0823	0.0810	0.0822	0.0742	0.0729	0.0783	0.0751
4	0.2058	0.2404	0.2301	0.2254	0.1533	0.1754	0.1736	0.1675	0.1037	0.1147	0.1092	0.1092	0.0882	0.0857	0.0864	0.0868
5	0.1900	0.2279	0.2505	0.2228	0.1808	0.1688	0.1435	0.1644	0.0966	0.1198	0.1228	0.1131	0.1161	0.1233	0.1124	0.1173
6	0.2643	0.3122	0.3131	0.2965	0.2032	0.2132	0.2008	0.2057	0.1326	0.1408	0.1518	0.1417	0.1305	0.1000	0.1085	0.1130
7	0.3335	0.3689	0.3382	0.3469	0.2409	-	0.2521	0.2465	0.1567	0.1536	0.1687	0.1597	0.1316	0.0945	0.1010	0.1090
8	0.3235	0.3458	0.3182	0.3291	-	0.2816	0.3524	0.3170	0.3413	0.2237	0.2539	0.2730	0.2012	0.1250	0.1373	0.1545

Appendix VIII

MTT assay statistics

RT112				
	5 x 10^4 cells/well	**2.5 x 10^4 cells/well**	**1.25 x 10^4 cells/well**	**6.25 x 10^3 cells/well**
Number of values	7	7	7	7
Minimum	0.1258	0.09621	0.07020	0.07951
25% Percentile	0.2209	0.1953	0.1275	0.1222
Median	0.6512	0.4506	0.2990	0.1882
75% Percentile	0.8614	0.7600	0.6889	0.6020
Maximum	0.9220	0.7683	0.8190	0.8023
Mean	0.5967	0.4801	0.3985	0.3321
Std. Deviation	0.3169	0.2795	0.2970	0.2789
Std. Error	0.1198	0.1056	0.1122	0.1054
Lower 95% CI of mean	0.3036	0.2216	0.1238	0.07419
Upper 95% CI of mean	0.8898	0.7386	0.6731	0.5900
Sum	4.177	3.361	2.789	2.325

T24				
	5 x 10^4 cells/well	**2.5 x 10^4 cells/well**	**1.25 x 10^4 cells/well**	**6.25 x 10^3 cells/well**
Number of values	8	8	8	8
Minimum	0.1760	0.1101	0.1113	0.09990
25% Percentile	0.2415	0.1862	0.1502	0.1274
Median	0.5960	0.4695	0.3398	0.2525
75% Percentile	0.8391	0.8060	0.7599	0.6205
Maximum	0.9083	0.8952	0.8148	0.7052
Mean	0.5643	0.4937	0.4222	0.3437
Std. Deviation	0.2877	0.3054	0.2916	0.2479
Std. Error	0.1017	0.1080	0.1031	0.08764
Lower 95% CI of mean	0.3238	0.2384	0.1784	0.1365
Upper 95% CI of mean	0.8049	0.7491	0.6659	0.5510
Sum	4.515	3.950	3.377	2.750

Appendix VIII

PC3				
	5 x 10^4 cells/well	**2.5 x 10^4 cells/well**	**1.25 x 10^4 cells/well**	**6.25 x 10^3 cells/well**
Number of values	8	8	8	8
Minimum	0.1478	0.1032	0.09251	0.08974
25% Percentile	0.1981	0.1569	0.1475	0.1159
Median	0.4093	0.2521	0.1921	0.1362
75% Percentile	0.6129	0.4705	0.3064	0.2086
Maximum	0.6744	0.5944	0.5475	0.4031
Mean	0.4082	0.3022	0.2356	0.1734
Std. Deviation	0.2155	0.1797	0.1450	0.1014
Std. Error	0.07620	0.06352	0.05127	0.03586
Lower 95% CI of mean	0.2280	0.1520	0.1144	0.08858
Upper 95% CI of mean	0.5884	0.4524	0.3569	0.2582
Sum	3.265	2.417	1.885	1.387

PNT1A				
	5 x 10^4 cells/well	**2.5 x 10^4 cells/well**	**1.25 x 10^4 cells/well**	**6.25 x 10^3 cells/well**
Number of values	8	8	8	8
Minimum	0.1312	0.08038	0.08218	0.07156
25% Percentile	0.1401	0.09853	0.08708	0.07531
Median	0.2241	0.1659	0.1111	0.09791
75% Percentile	0.3210	0.2363	0.1552	0.1162
Maximum	0.3469	0.3170	0.2730	0.1545
Mean	0.2310	0.1733	0.1328	0.1004
Std. Deviation	0.08592	0.08107	0.06268	0.02855
Std. Error	0.03038	0.02866	0.02216	0.01009
Lower 95% CI of mean	0.1592	0.1055	0.08042	0.07653
Upper 95% CI of mean	0.3028	0.2410	0.1852	0.1243
Sum	1.848	1.386	1.063	0.8032

Appendix IX

MTT assay – curve fitting

a) RT112 cell line

i) 5 x 10^4 cells/well

Nonlinear Regression - Dynamic Fitting

Dynamic Fit Options:

Total Number of Fits	200
Maximum Number of Iterations	200

Parameter Ranges for Initial Estimates:

	Minimum	Maximum
y1	-0.1195	0.3585
y2	-0.5678	1.7035
y3	-0.,8833	2.6499
y4	-0.8563	2.5690
T1	-3.,3333	10.,0000
T2	-5.6667	17.0000

Summary of Fit Results:

Converged	100.0%
Singular Solutions	84.5%
Ill-Conditioned Solutions	13.0%

Results for the Overall Best-Fit Solution:

R	Rsqr	Adj Rsqr	Standard Error of Estimate
0.9905	0.9810	0.8861	0.1070

	Coefficient	Std. Error	t	P	VIF
y1	0.0857	0.0976	0.8782	0.5412	0.0000
y2	0.5292	7.2156	0.0733	0.9534	0.0000
y3	0.9058	1.1326	0.7997	0.5706	0.0000
y4	0.8440	0.0976	8.6442	0.0733	0.0000
T1	3.0606	33.5406	0.0913	0.9421	0.0000
T2	5.9609	37.2503	0.1600	0.8990	0.0000

Analysis of Variance:

Uncorrected for the mean of the observations:

	DF	SS	MS
Regression	6	3.0833	0.5139
Residual	1	0.0114	0.0114
Total	7	3.0948	0.4421

Corrected for the mean of the observations:

	DF	SS	MS	F	P
Regression	5	0.5910	0.1182	10.3320	0.2317
Residual	1	0.0114	0.0114		
Total	6	0.6024	0.1004		

Appendix IX

Statistical Tests:

PRESS 197324537.6713

Durbin-Watson Statistic 3.1667 Failed

Normality Test Passed (P = 0.8128)

K-S Statistic = 0.2267 Significance Level = 0.8128

Constant Variance Test Passed (P = 0.0545)

Power of performed test with alpha = <0.0001: 0.0000

The power of the performed test (0.0000) is below the desired power of 0.8000.
You should interpret the negative findings cautiously.

ii) 2.5 x 10^4 cells/well

Nonlinear Regression - Dynamic Fitting

Dynamic Fit Options:

Total Number of Fits	200
Maximum Number of Iterations	200

Parameter Ranges for Initial Estimates:

	Minimum	Maximum
y1	-0.0980	0.2940
y2	-0.3868	1.1605
y3	-0.6902	2.0705
y4	-0.7594	2.2781
T1	-3.3333	10.0000
T2	-5.6667	17.0000

Summary of Fit Results:

Converged	98.0%
Singular Solutions	86.0%
Ill-Conditioned Solutions	10.5%
Iterations Exceeding 200	2.0%

Results for the Overall Best-Fit Solution:

R	Rsqr	Adj Rsqr	Standard Error of Estimate
0.9982	0.9965	0.9788	0.0407

	Coefficient	Std. Error	t	P	VIF
y1	0.0912	0.0352	2.5932	0.2343	1.6015
y2	0.6955338923	5.0839	2.0521E-007	1.0000	4.0046E+015<
y3	0.74378711	9.5516	8.5361E-006	1.0000	2.1187E+012<
y4	0.7574	0.0617	12.2790	0.0517	3.7660
T1	5.92582762766	9.1123	2.1449E-007	1.0000	4.0046E+015<
T2	4.71032081959	4.9007	2.2624E-007	1.0000	2.1187E+012<

Appendix IX

Analysis of Variance:

Uncorrected for the mean of the observations:

	DF	SS	MS
Regression	6	2.0805	0.3467
Residual	1	0.0017	0.0017
Total	7	2.0821	0.2974

Corrected for the mean of the observations:

	DF	SS	MS	F	P
Regression	5	0.4669	0.0934	56.4233	0.1007
Residual	1	0.0017	0.0017		
Total	6	0.4686	0.0781		

Statistical Tests:

PRESS 56548.6550

Durbin-Watson Statistic 3.4472 Failed

Normality Test Passed (P = 0.9412)

K-S Statistic = 0.1889 Significance Level = 0.9412

Constant Variance Test Passed (P = 0.6602)

Power of performed test with alpha = <0.0001: 0.0000

The power of the performed test (0.0000) is below the desired power of 0.8000.
You should interpret the negative findings cautiously.

iii) 1.25×10^4 cells/well

Nonlinear Regression - Dynamic Fitting

Dynamic Fit Options:

Total Number of Fits	200
Maximum Number of Iterations	200

Parameter Ranges for Initial Estimates:

	Minimum	Maximum
y1	-0.0728	0.2184
y2	-0.2323	0.6970
y3	-0.5255	1.5765
y4	-0.8148	2.4445
T1	-3.3333	10.0000
T2	-5.6667	17.0000

Summary of Fit Results:

Converged	97.0%
Singular Solutions	83.0%
Ill-Conditioned Solutions	13.0%
Iterations Exceeding 200	3.0%

Appendix IX

Results for the Overall Best-Fit Solution:

R	Rsqr	Adj Rsqr	Standard Error of Estimate
0.9998	0.9997	0.9981	0.0129

	Coefficient	Std. Error	t	P	VIF
y1	0.0683	0.0118	5.8092	0.1085	1.2519
y2	0.246428946	7.2124	8.5129E-007	1.0000	5.1377E+014<
y3	0.3862112761	2.5216	3.4253E-007	1.0000	3.8768E+015<
y4	0.8141	0.0178	45.7892	0.0139	3.3296
T1	3.8239458826	5.0730	8.3341E-007	1.0000	4.7294E+015<
T2	4.2919977348	4.9239	4.3913E-007	1.0000	1.0077E+016<

Analysis of Variance:

Uncorrected for the mean of the observations:

	DF	SS	MS
Regression	6	1.6403	0.2734
Residual	1	0.0002	0.0002
Total	7	1.6404	0.2343

Corrected for the mean of the observations:

	DF	SS	MS	F	P
Regression	5	0,5289	0,1058	638,3953	0,0300
Residual	1	0,0002	0,0002		
Total	6	0,5291	0,0882		

Statistical Tests:

PRESS 0.0003

Durbin-Watson Statistic 3.1667 Failed

Normality Test Passed (P = 0.8603)

K-S Statistic = 0.2148 Significance Level = 0.8603

Constant Variance Test Passed (P = 0.0956)

Power of performed test with alpha = <0,0001: 0,0000

The power of the performed test (0.0000) is below the desired power of 0.8000.
You should interpret the negative findings cautiously.

iv) 6.25×10^3 cells/well

Nonlinear Regression - Dynamic Fitting

Dynamic Fit Options:

Total Number of Fits	200
Maximum Number of Iterations	200

Appendix IX

Parameter Ranges for Initial Estimates:

	Minimum	Maximum
y1	-0.0812	0.2436
y2	-0.1466	0.4397
y3	-0.3511	1.0534
y4	-0.8033	2.4099
T1	-3.3333	10.0000
T2	-5.6667	17.0000

Summary of Fit Results:

Converged	94.0%
Singular Solutions	79.5%
Ill-Conditioned Solutions	14.5%
Iterations Exceeding 200	6.0%

Results for the Overall Best-Fit Solution:

R	Rsqr	Adj Rsqr	Standard Error of Estimate
0.9993	0.9986	0.9913	0.0260

	Coefficient	Std. Error	t	P	VIF
y1	0.0901	0.0237	3.7971	0.1639	1.1659
y2	0.14346601	1.4901	2.1721E-006	1.0000	9.0240E+012<
y3	0.3406127355	4.7036	2.6744E-007	1.0000	2.4177E+015<
y4	0.8029	0.0238	33.7262	0.0189	1.1176
T1	3.4969309400	8.2702	1.1302E-006	1.0000	7.2217E+013<
T2	5.7128 630077	4.9573	9.0668E-007	1.0000	2.3180E+015<

Analysis of Variance:

Uncorrected for the mean of the observations:

	DF	SS	MS
Regression	6	1.2381	0.2064
Residual	1	0.0007	0.0007
Total	7	1.2388	0.1770

Corrected for the mean of the observations:

	DF	SS	MS	F	P
Regression	5	0.4660	0.0932	137.9127	0.0646
Residual	1	0.0007	0.0007		
Total	6	0.4667	0.0778		

Statistical Tests:

PRESS 0.0092

Durbin-Watson Statistic 3.1667 Failed

Normality Test Passed (P = 0.4288)

K-S Statistic = 0.3115 Significance Level = 0,4288

Constant Variance Test Passed (P = 0.0956)

Power of performed test with alpha = <0.0001: 0.0000

Appendix IX

a) T24 cell line

i) 5 x 10^4 cells/well

Nonlinear Regression - Dynamic Fitting

Dynamic Fit Options:

Total Number of Fits	200
Maximum Number of Iterations	200

Parameter Ranges for Initial Estimates:

	Minimum	Maximum
y1	-0.1601	0.4802
y2	-0.4196	1.2587
y3	-0.7869	2.3606
y4	-0.8142	2.4426
T1	-3.3333	10.0000
T2	-5.6667	17.0000

Summary of Fit Results:

Converged	100.0%
Singular Solutions	87.0%
Ill-Conditioned Solutions	13.0%

Results for the Overall Best-Fit Solution:

R	Rsqr	Adj Rsqr	Standard Error of Estimate
0.9849	0.9700	0.8950	0.0932

	Coefficient	Std. Error	t	P	VIF
y1	0.1760	0.0932	1.8874	0.1997	1.0000
y2	0.1872144981	8.9801	1.2914E-007	1.0000	4.6256E+014<
y3	0.9370	0.0815	11.4933	0.0075	1.5581
y4	0.8037	0.0932	8.6193	0.0132	1.0465
T1	1.7618959718	3.2488	1.8357E-007	1.0000	4.6256E+014<
T2	6.7251	0.6016	11.1796	0.0079	1.6315

Analysis of Variance:

Uncorrected for the mean of the observations:

	DF	SS	MS
Regression	6	3.1100	0.5183
Residual	2	0.0174	0.0087
Total	8	3.1274	0.3909

Corrected for the mean of the observations:

	DF	SS	MS	F	P
Regression	5	0.5622	0.1124	12.9331	0.0733
Residual	2	0.0174	0.0087		
Total	7	0.5796	0.0828		

Appendix IX

Statistical Tests:

PRESS 2.6206E+014

Durbin-Watson Statistic 3.0280 Failed

Normality Test Passed (P = 0.6325)

K-S Statistic = 0.2500 Significance Level = 0.6325

Constant Variance Test Passed (P = 0.8393)

Power of performed test with alpha = <0.0001: 0.0000

The power of the performed test (0.0000) is below the desired power of 0.8000.
You should interpret the negative findings cautiously.

ii) 2.5 x 10^4 cells/well

Nonlinear Regression - Dynamic Fitting

Dynamic Fit Options:

Total Number of Fits	200
Maximum Number of Iterations	200

Parameter Ranges for Initial Estimates:

	Minimum	Maximum
y1	-0.1024	0.3072
y2	-0.2964	0.8893
y3	-0.6893	2.0680
y4	-0.8288	2.4864
T1	-3.3333	10.0000
T2	-5.6667	17.0000

Summary of Fit Results:

Converged	99.0%
Singular Solutions	84.0%
Ill-Conditioned Solutions	14.0%
Iterations Exceeding 200	1.0%

Results for the Overall Best-Fit Solution:

R	Rsqr	Adj Rsqr	Standard Error of Estimate
0.9975	0.9950	0.9825	0.0404

	Coefficient	Std. Error	t	P	VIF
y1	0.0815	0.0324	2.5162	0.1283	1.2055
y2	0.5092	2914937.6284	1.7469E-007	1.0000	1.0551E+016<
y3	0.9200	578102.4842	1.5915E-006	1.0000	1.8768E+014<
y4	0.8225	0.0404	20.3490	0.0024	1.0651
T1	5.0047	27293299.3931	1.8337E-007	1.0000	1.4186E+016<
T2	6.6575	7957180.7253	8.3667E-007	1.0000	9.8169E+014<

Appendix IX

Analysis of Variance:

Uncorrected for the mean of the observations:

	DF	SS	MS
Regression	6	2.5999	0.4333
Residual	2	0.0033	0.0016
Total	8	2.6031	0.3254

Corrected for the mean of the observations:

	DF	SS	MS	F	P
Regression	5	0.6496	0.1299	79.5250	0.0125
Residual	2	0.0033	0.0016		
Total	7	0.6529	0.0933		

Statistical Tests:

PRESS 0.0162

Durbin-Watson Statistic 2.2626 Failed

Normality Test Passed (P = 0.6325)

K-S Statistic = 0.2500 Significance Level = 0.6325

Constant Variance Test Passed (P = 0.0018)

Power of performed test with alpha = <0.0001: 0.0000

The power of the performed test (0.0000) is below the desired power of 0.8000.
You should interpret the negative findings cautiously.

iii) 1.25×10^4 cells/well

Nonlinear Regression - Dynamic Fitting

Dynamic Fit Options:

Total Number of Fits	200
Maximum Number of Iterations	200

Parameter Ranges for Initial Estimates:

	Minimum	Maximum
y1	-0.1056	0.3168
y2	-0.2008	0.6025
y3	-0.5646	1.6937
y4	-0.8022	2.4066
T1	-3.3333	10.0000
T2	-5.6667	17.0000

Summary of Fit Results:

Converged	99.0%
Singular Solutions	85.5%
Ill-Conditioned Solutions	12.5%
Iterations Exceeding 200	1.0%

Appendix IX

Results for the Overall Best-Fit Solution:

R	Rsqr	Adj Rsqr	Standard Error of Estimate
0.9990	0.9981	0.9932	0.0241

	Coefficient	Std. Error	t	P	VIF
y1	0.0943	0.0201	4.6829	0.0427	1.2359
y2	0.3077	0.0356	8.6462	0.0131	4.0666<
y3	0.8196	0.0301	27.2126	0.0013	1.6531
y4	0.7987	0.0241	33.2033	0.0009	1.0517
T1	4.6572	0.2212	21.0585	0.0022	4.5874<
T2	6.7057	0.2056	32.6129	0.0009	2.0994

Analysis of Variance:

Uncorrected for the mean of the observations:

	DF	SS	MS
Regression	6	2.0196	0.3366
Residual	2	0.0012	0.0006
Total	8	2.0207	0.2526

Corrected for the mean of the observations:

	DF	SS	MS	F	P
Regression	5	0.5939	0.1188	205.2436	0.0049
Residual	2	0.0012	0.0006		
Total	7	0.5950	0.0850		

Statistical Tests:

PRESS 501338760288.7576

Durbin-Watson Statistic 2.2499 Failed

Normality Test Passed (P = 0.6325)

K-S Statistic = 0.2500 Significance Level = 0.6325

Constant Variance Test Passed (P = <0.0001)

Power of performed test with alpha = <0.0001: 0.0000
The power of the performed test (0.0000) is below the desired power of 0.8000.
You should interpret the negative findings cautiously.

iv) 6.25×10^3 cells/well

Nonlinear Regression - Dynamic Fitting

Dynamic Fit Options:

Total Number of Fits	200
Maximum Number of Iterations	200

Appendix IX

Parameter Ranges for Initial Estimates:

	Minimum	Maximum
y1	-0.0953	0.2858
y2	-0.1399	0.4197
y3	-0.4577	1.3732
y4	-0.6557	1.9670
T1	-3.3333	10.0000
T2	-5.6667	17.0000

Summary of Fit Results:

Converged	97.0%
Singular Solutions	82.5%
Ill-Conditioned Solutions	13.5%
Iterations Exceeding 200	3.0%

Results for the Overall Best-Fit Solution:

R	Rsqr	Adj Rsqr	Standard Error of Estimate
0.9990	0.9979	0.9927	0.0212

	Coefficient	Std. Error	t	P	VIF
y1	0.0914	0.0177	5.1573	0.0356	1.2367
y2	0.2162	0.0275	7.8711	0.0158	3.1866
y3	0.7155	0.0222	32.1801	0.0010	1.2305
y4	0.6514	0.0212	30.7479	0.0011	1.0262
T1	4.6608	0.1876	24.8426	0.0016	3.7051
T2	6.8070	0.1715	39.6906	0.0006	1.6030

Analysis of Variance:

Uncorrected for the mean of the observations:

	DF	SS	MS
Regression	6	1.3743	0.2291
Residual	2	0.0009	0.0004
Total	8	1.3752	0.1719

Corrected for the mean of the observations:

	DF	SS	MS	F	P
Regression	5	0.4292	0.0858	191.2805	0.0052
Residual	2	0.0009	0.0004		
Total	7	0.4301	0.0614		

Statistical Tests:

PRESS 6.1959E+013

Durbin-Watson Statistic 2.7441 Failed

Normality Test Passed (P = 0.2396)

K-S Statistic = 0.3447 Significance Level = 0.2396

Constant Variance Test Passed (P = 0.0149)

Power of performed test with alpha = <0.0001: 0.0000
The power of the performed test (0.0000) is below the desired power of 0.8000.
You should interpret the negative findings cautiously.

Appendix IX

a) PC3 cell line

i) 5 x 10^4 cells/well

Nonlinear Regression - Dynamic Fitting

Dynamic Fit Options:

Total Number of Fits	200
Maximum Number of Iterations	200

Parameter Ranges for Initial Estimates:

	Minimum	Maximum
y1	-0.1571	0.4713
y2	-0.2695	0.8086
y3	-0.5464	1.6393
y4	-0.6650	1.9950
T1	-3.3333	10.0000
T2	-5.6667	17.0000

Summary of Fit Results:

Converged	97.5%
Singular Solutions	81.0%
Ill-Conditioned Solutions	15.0%
Iterations Exceeding 200	2.5%

Results for the Overall Best-Fit Solution:

R	Rsqr	Adj Rsqr	Standard Error of Estimate
1.0000	0.9999	0.9997	0.0037

	Coefficient	Std. Error	t	P	VIF
y1	0.1465	0.0033	43.7279	0.0005	1.2821
y2	0.2721	0.0067	40.8303	0.0006	4.8607<
y3	0.5342	0.0069	77.0355	0.0002	5.5286<
y4	0.6728	0.0033	200.8733	<0.0001	1.2945
T1	3.9430	0.0329	119.6935	<0.0001	4.4655<
T2	5.0071	0.0335	149.4766	<0.0001	5.1031<

Analysis of Variance:

Uncorrected for the mean of the observations:

	DF	SS	MS
Regression	6	1.6581	0.2763
Residual	2	2.6923E-005	1.3461E-005
Total	8	1.6581	0.2073

Corrected for the mean of the observations:

	DF	SS	MS	F	P
Regression	5	0.3251	0.0650	4830.7099	0.0002
Residual	2	2.6923E-005	1.3461E-005		
Total	7	0.3252	0.0465		

Statistical Tests:

Appendix IX

PRESS 0.0002

Durbin-Watson Statistic 3.1667 Failed

Normality Test Passed (P = 0.5886)

K-S Statistic = 0.2588 Significance Level = 0.5886

Constant Variance Test Passed (P = 0.4228)

Power of performed test with alpha = 0.0500: 1.0000

ii) 2.5×10^4 cells/well

Nonlinear Regression - Dynamic Fitting

Dynamic Fit Options:

Total Number of Fits	200
Maximum Number of Iterations	200

Parameter Ranges for Initial Estimates:

	Minimum	Maximum
y1	-0.0951	0.2852
y2	-0.4506	1.3518
y3	-0.3936	1.1807
y4	-0.5945	1.7835
T1	-0.1942	0.5826
T2	-0.2987	0.8960

Summary of Fit Results:

Converged	100.0%
Singular Solutions	92.5%
Ill-Conditioned Solutions	7.5%

Results for the Overall Best-Fit Solution:

R	Rsqr	Adj Rsqr	Standard Error of Estimate
0.9768	0.9541	0.8392	0.0716

	Coefficient	Std. Error	t	P	VIF
y1	0.1067	0.0725	1.4721	0.2789	1.3782
y2	0.2029	7760751.8463	2.6149E-008	1.0000	1.5818E+016<
y3	0.3089	859976.9417	3.5918E-007	1.0000	2.0881E+014<
y4	0.6044	0.0716	8.4447	0.0137	1.3163
T1	0.1319	3398540.7405	3.8806E-008	1.0000	1.5818E+016<
T2	0.0792	942585.6078	8.4073E-008	1.0000	2.0881E+014<

Appendix IX

Analysis of Variance:

Uncorrected for the mean of the observations:

	DF	SS	MS
Regression	6	0.9490	0.1582
Residual	2	0.0103	0.0051
Total	8	0.9593	0.1199

Corrected for the mean of the observations:

	DF	SS	MS	F	P
Regression	5	0.2130	0.0426	8.3051	0.1109
Residual	2	0.0103	0.0051		
Total	7	0.2233	0.0319		

Statistical Tests:

PRESS 0.0212

Durbin-Watson Statistic 2.6154 Failed

Normality Test Passed (P = 0.7841)

K-S Statistic = 0.2193 Significance Level = 0.7841

Constant Variance Test Passed (P = 0.1597)

Power of performed test with alpha = 0.0500: 0.9987

iii) 1.25×10^4 cells/well

Nonlinear Regression - Dynamic Fitting

Dynamic Fit Options:

Total Number of Fits	200
Maximum Number of Iterations	200

Parameter Ranges for Initial Estimates:

	Minimum	Maximum
y1	-0.0982	0.2947
y2	-0.1692	0.5075
y3	-0.2164	0.6492
y4	-0.5454	1.6363
T1	-3.3333	10.0000
T2	-5.6667	17.0000

Summary of Fit Results:

Converged	98.5%
Singular Solutions	86.5%
Ill-Conditioned Solutions	10.0%
Iterations Exceeding 200	1.5%

Appendix IX

Results for the Overall Best-Fit Solution:

R	Rsqr	Adj Rsqr	Standard Error of Estimate
0.9951	0.9903	0.9659	0.0268

	Coefficient	Std. Error	t	P	VIF
y1	0.0925	0.0268	3.4553	0.0745	1.0000
y2	0.1323	1303742.5010	1.0146E-007	1.0000	4.1287E+015<
y3	0.2359	0.0535	4.4083	0.0478	8.2121<
y4	0.5475	0.0268	20.4500	0.0024	1.0968
T1	1.6094	62155100.0116	2.5894E-008	1.0000	4.1287E+015<
T2	6.5483	0.3254	20.1239	0.0025	3.3325

Analysis of Variance:

Uncorrected for the mean of the observations:

	DF	SS	MS
Regression	6	0.5899	0.0983
Residual	2	0.0014	0.0007
Total	8	0.5913	0.0739

Corrected for the mean of the observations:

	DF	SS	MS	F	P
Regression	5	0.1458	0.0292	40.6686	0.0242
Residual	2	0.0014	0.0007		
Total	7	0.1472	0.0210		

Statistical Tests:

PRESS 0.0000

Durbin-Watson Statistic 2.6890 Failed

Normality Test Passed (P = 0.6325)

K-S Statistic = 0.2500 Significance Level = 0.6325

Constant Variance Test Passed (P = 0.7941)

Power of performed test with alpha = 0.0500: 1.0000

iv) 6.25×10^3 cells/well

Nonlinear Regression - Dynamic Fitting

Dynamic Fit Options:

Total Number of Fits	200
Maximum Number of Iterations	200

Parameter Ranges for Initial Estimates:

	Minimum	Maximum
y1	-0.0897	0.2692
y2	-0.1942	0.5826
y3	-0.2987	0.8960
y4	-0.4031	1.2094

Appendix IX

T1	-0.1942	0.5826
T2	-0.2987	0.8960

Summary of Fit Results:

Converged	99.5%
Singular Solutions	94.0%
Ill-Conditioned Solutions	5.5%
Iterations Exceeding 200	0.5%

Results for the Overall Best-Fit Solution:

R	**Rsqr**	**Adj Rsqr**	**Standard Error of Estimate**
1.0000	1.0000	1.0000	0.0000

	Coefficient
y1	0.0897
y2	0.2094
y3	1.8482
y4	1.1160
T1	0.2094
T2	1.8482

Analysis of Variance:

Uncorrected for the mean of the observations:

	DF	**SS**	**MS**
Regression	6	0.3125	0.0521
Residual	2	0.0000	0.0000
Total	8	0.3125	0.0391

Corrected for the mean of the observations:

	DF	**SS**	**MS**	**F**	**P**
Regression	5	0.0720	0.0144	(+inf)	(NAN)
Residual	2	0.0000	0.0000		
Total	7	0.0720	0.0103		

Statistical Tests:

PRESS 0.0000

Durbin-Watson Statistic (+inf) Failed

Normality Test Failed (P = <0.0001)

K-S Statistic = <0.0001 Significance Level = <0.0001

Constant Variance Test Passed (P = 0.1823)

Power of performed test with alpha = 0.0500: 1.0000

Appendix IX

a) PNT1A cell line

i) 5 x 10^4 cells/well

Nonlinear Regression - Dynamic Fitting

Dynamic Fit Options:

Total Number of Fits	200
Maximum Number of Iterations	200

Parameter Ranges for Initial Estimates:

	Minimum	**Maximum**
y1	-0.1275	0.3825
y2	-0.1744	0.5232
y3	-0.2820	0.8459
y4	-0.3331	0.9993
T1	-3.3333	10.0000
T2	-5.6667	17.0000

Summary of Fit Results:

Converged	98.5%
Singular Solutions	87.5%
Ill-Conditioned Solutions	10.5%
Iterations Exceeding 200	1.5%

Results for the Overall Best-Fit Solution:

R	**Rsqr**	**Adj Rsqr**	**Standard Error of Estimate**
0.9897	0.9795	0.9282	0.0230

	Coefficient	**Std. Error**	**t**	**P**	**VIF**
y1	0.1198	0.0178	6.7195	0.0214	0.0000
y2	0.2408	0.5121	0.4702	0.6845	0.0000
y3	0.3533	0.1949	1.8129	0.2115	0.0000
y4	0.3291	0.0230	14.2974	0.0049	0.0000
T1	5.3756	18.4984	0.2906	0.7987	0.0000
T2	6.6363	10.8430	0.6120	0.6028	0.0000

Analysis of Variance:

Uncorrected for the mean of the observations:

	DF	**SS**	**MS**
Regression	6	0.4775	0.0796
Residual	2	0.0011	0.0005
Total	8	0.4786	0.0598

Corrected for the mean of the observations:

	DF	**SS**	**MS**	**F**	**P**
Regression	5	0.0506	0.0101	19.0983	0.0505
Residual	2	0.0011	0.0005		
Total	7	0.0517	0.0074		

Appendix IX

Statistical Tests:

PRESS 47335729508.8559

Durbin-Watson Statistic 2.6863 Failed

Normality Test Passed (P = 0.6325)

K-S Statistic = 0.2500 Significance Level = 0.6325

Constant Variance Test Failed (P = 0.0212)

Power of performed test with alpha = 0.0500: 1.0000

ii) 2.5×10^4 cells/well

Nonlinear Regression - Dynamic Fitting

Dynamic Fit Options:

Total Number of Fits	200
Maximum Number of Iterations	200

Parameter Ranges for Initial Estimates:

	Minimum	Maximum
y1	-0.0804	0.2413
y2	-0.1304	0.3911
y3	-0.1944	0.5832
y4	-0.3179	0.9537
T1	-3.3333	10.0000
T2	-5.6667	17.0000

Summary of Fit Results:

Converged	97.0%
Singular Solutions	83.5%
Ill-Conditioned Solutions	9.0%
Iterations Exceeding 200	3.0%

Results for the Overall Best-Fit Solution:

R	Rsqr	Adj Rsqr	Standard Error of Estimate
0.9932	0.9865	0.9529	0.0176

	Coefficient	Std. Error	t	P	VIF
y1	0.0804	0.0176	4.5689	0.0447	1.0503
y2	0.0989	0.0510	1.9380	0.1922	15.5463<
y3	0.2239	0.0361	6.1941	0.0251	7.7946<
y4	0.3170	0.0176	18.0192	0.0031	1.0591
T1	2.2890	2.1552	1.0621	0.3995	17.0014<
T2	6.6788	0.7306	9.1419	0.0118	6.6902<

Appendix IX

Analysis of Variance:

Uncorrected for the mean of the observations:

	DF	SS	MS
Regression	6	0.2855	0.0476
Residual	2	0.0006	0.0003
Total	8	0.2861	0.0358

Corrected for the mean of the observations:

	DF	SS	MS	F	P
Regression	5	0.0454	0.0091	29.3287	0.0333
Residual	2	0.0006	0.0003		
Total	7	0.0460	0.0066		

Statistical Tests:

PRESS 48616480789.2878

Durbin-Watson Statistic 3.3934 Failed

Normality Test Passed (P = 0.3047)

K-S Statistic = 0.3244 Significance Level = 0.3047

Constant Variance Test Passed (P = 0.3873)

Power of performed test with alpha = 0.0500: 1.0000

iii) 1.25×10^4 cells/well

Nonlinear Regression - Dynamic Fitting

Dynamic Fit Options:

Total Number of Fits	200
Maximum Number of Iterations	200

Parameter Ranges for Initial Estimates:

	Minimum	Maximum
y1	-0.0862	0.2585
y2	-0.1009	0.3026
y3	-0.1225	0.3675
y4	-0.2695	0.8085
T1	-3.3333	10.0000
T2	-5.6667	17.0000

Summary of Fit Results:

Converged	97.5%
Singular Solutions	87.5%
Ill-Conditioned Solutions	7.5%
Iterations Exceeding 200	2.5%

Appendix IX

Results for the Overall Best-Fit Solution:

R	Rsqr	Adj Rsqr	Standard Error of Estimate
0.9936	0.9873	0.9556	0.0132

	Coefficient	Std. Error	t	P	VIF
y1	0.0885	0.0121	7.3343	0.0181	1.0417
y2	0.0893	0.0124	7.2041	0.0187	1.8486
y3	0.1515	0.0228	6.6334	0.0220	5.2978<
y4	0.2730	0.0132	20.6572	0.0023	1.0050
T1	3.0000	1.5223	1.9706	0.1876	2.8431
T2	6.9241	0.2492	27.7892	0.0013	3.9961

Analysis of Variance:

Uncorrected for the mean of the observations:

	DF	SS	MS
Regression	6	0.1683	0.0280
Residual	2	0.0003	0.0002
Total	8	0.1686	0.0211

Corrected for the mean of the observations:

	DF	SS	MS	F	P
Regression	5	0.0272	0.0054	31.1019	0.0314
Residual	2	0.0003	0.0002		
Total	7	0.0275	0.0039		

Statistical Tests:

PRESS >1e20

Durbin-Watson Statistic 3.4265 Failed

Normality Test Passed (P = 0.9238)

K-S Statistic = 0.1838 Significance Level = 0.9238

Constant Variance Test Failed (P = 0.0374)

Power of performed test with alpha = 0.0500: 1.0000

iv) 6.25×10^3 cells/well

Nonlinear Regression - Dynamic Fitting

Dynamic Fit Options:

Total Number of Fits	200
Maximum Number of Iterations	200

Appendix IX

Parameter Ranges for Initial Estimates:

	Minimum	Maximum
y1	-0.0741	0.2222
y2	-0.0855	0.2566
y3	-0.1103	0.3308
y4	-0.1525	0.4574
T1	-3.3333	10.0000
T2	-5.6667	17.0000

Summary of Fit Results:

Converged	99.5%
Singular Solutions	88.5%
Ill-Conditioned Solutions	11.0%
Iterations Exceeding 200	0.5%

Results for the Overall Best-Fit Solution:

R	Rsqr	Adj Rsqr	Standard Error of Estimate
0.9712	0.9433	0.8015	0.0129

	Coefficient	Std. Error	t	P	VIF
y1	0.0716	0.0129	5.5470	0.0310	1.2500
y2	0.0800	0.0477	1.6762	0.2357	31.9373<
y3	0.1305	481447.9227	2.7103E-007	1.0000	1.9277E+015<
y4	0.1545	0.0129	11.9703	0.0069	1.0000
T1	3.0000	4.7513	0.6314	0.5923	33.9078<
T2	7.6527	44355169.9462	1.7253E-007	1.0000	1.9277E+015<

Analysis of Variance:

Uncorrected for the mean of the observations:

	DF	SS	MS
Regression	6	0.0876	0.0146
Residual	2	0.0003	0.0002
Total	8	0.0880	0.0110

Corrected for the mean of the observations:

	DF	SS	MS	F	P
Regression	5	0.0055	0.0011	6.6530	0.1358
Residual	2	0.0003	0.0002		
Total	7	0.0059	0.0008		

Statistical Tests:

PRESS >1e20

Durbin-Watson Statistic 2.2405 Passed

Normality Test Passed (P = 0.2296)

K-S Statistic = 0.3481 Significance Level = 0.2296

Constant Variance Test Passed (P = 0.7494)

Power of performed test with alpha = 0.0500: 0.9972

Appendix X

MTT assay raw data

RT112 cell line

	Control							Aminosilane						
Day	**OD**	**OD**	**OD**	**OD**	**OD**	**OD**	**OD Average**	**OD**	**OD**	**OD**	**OD**	**OD**	**OD**	**OD Average**
1	0.1493	0.1557	0.1526	0.1448	0.1523	0.1519	0.1511	0.1864	0.1758	0.1642	0.1816	0.1733	0.1624	0.1739
2	0.2230	0.2801	0.1884	0.2260	0.2918	0.1939	0.2339	0.2729	0.2783	0.2971	0.2699	0.2852	0.3031	0.2844
3	0.4489	0.4760	0.5104	0.4379	0.4488	0.4813	0.4672	0.6567	0.4975	0.4320	0.6362	0.4988	0.4096	0.5218
4	0.3764	0.8924	0.6519	0.3529	0.8282	0.6271	0.6215	0.4956	0.4015	0.8344	0.4781	0.4029	0.7901	0.5671
5	0.7215	0.8058	0.9166	0.7005	0.7720	0.8968	0.8022	1.0707	1.0135	0.9613	0.7166	0.7209	0.6913	0.8624
6	0.8857	1.0613	0.7061	0.8855	1.0605	0.6948	0.8823	1.1405	1.1853	1.0043	1.1518	1.1736	0.9770	1.1054
7	0.7828	0.8463	0.8896	0.9905	1.0961	1.0556	0.9435	0.9374	0.9875	0.9636	1.1381	1.1631	1.1288	1.0531
8	0.9704	1.0905	1.0274	0.9857	1.0801	1.0141	1.0280	0.9586	1.0124	1.0655	0.9389	1.0515	1.0936	1.0201

	HA_4							HA_{234}						
Day	**OD**	**OD**	**OD**	**OD**	**OD**	**OD**	**OD Average**	**OD**	**OD**	**OD**	**OD**	**OD**	**OD**	**OD Average**
1	0.2085	0.2678	0.2007	0.2041	0.2616	0.2000	0.2238	0.1861	0.2115	0.2005	0.1861	0.2124	0.1974	0.1990
2	0.2958	0.4537	0.2605	0.3036	0.4410	0.2579	0.3354	0.2790	0.2569	0.2600	0.2846	0.2867	0.2704	0.2729
3	0.3548	0.3497	0.3471	0.3383	0.3649	0.3749	0.3549	0.3963	0.3936	0.3839	0.3662	0.3865	0.3672	0.3823
4	0.3727	0.3636	0.3620	0.3576	0.3443	0.3416	0.3570	0.4452	0.4329	0.4339	0.3782	0.3742	0.3704	0.4058
5	0.5424	0.7220	0.6648	0.5492	0.7101	0.6672	0.6426	0.5450	0.5359	0.5325	0.5960	0.5980	0.6011	0.5681
6	1.0442	0.9999	0.9902	0.9164	0.8806	0.8703	0.9503	0.7784	0.7110	0.5752	0.6698	0.7362	0.6103	0.6802
7	0.9443	0.8679	0.8416	0.9265	0.8679	0.8653	0.8856	0.6609	0.6652	0.6222	0.7258	0.7633	0.7858	0.7039
8	1.0115	1.0762	1.0804	0.9929	1.0709	1.1411	1.0621	0.8202	0.7927	0.7024	0.7816	0.6782	0.6399	0.7358

Appendix X

	HA_{2590}							HA_{mix}						
Day	**OD**	**OD**	**OD**	**OD**	**OD**	**OD**	**OD Average**	**OD**	**OD**	**OD**	**OD**	**OD**	**OD**	**OD Average**
1	0.1441	0.1800	0.2008	0.1488	0.1804	0.1925	0.1744	0.1883	0.1393	0.2193	0.1886	0.1393	0.2142	0.1815
2	0.3116	0.2762	0.3082	0.3277	0.2972	0.3091	0.3050	0.2616	0.2655	0.3028	0.2653	0.2668	0.2949	0.2762
3	0.3971	0.3836	0.3782	0.4004	0.4097	0.3766	0.3909	0.3971	0.3836	0.3782	0.4004	0.4097	0.3766	0.3909
4	0.5330	0.5309	0.2726	0.6056	0.2751	0.6286	0.4743	0.5728	0.4930	0.6219	0.5635	0.4721	0.6121	0.5559
5	0.5167	0.5323	0.5456	0.5105	0.5316	0.5631	0.5333	0.5976	0.5889	0.5827	0.7631	0.7682	0.8008	0.6836
6	0.8823	0.7992	0.7919	0.5403	0.5281	0.5187	0.6768	0.9941	0.8540	0.5642	0.9390	0.8157	0.5393	0.7844
7	0.6302	0.6160	0.5794	0.5915	0.6847	0.6364	0.6230	0.9579	0.9492	0.9173	0.9198	0.8923	0.8602	0.9161
8	0.5600	0.5777	0.5729	0.6919	0.7054	0.6356	0.6239	1.0002	1.0023	0.9767	0.9642	0.9809	0.9193	0.9739

T24 cell line

	Control							**Aminosilane**						
Day	**OD**	**OD**	**OD**	**OD**	**OD**	**OD**	**OD Average**	**OD**	**OD**	**OD**	**OD**	**OD**	**OD**	**OD Average**
1	-	-	-	0.3043	0.2549	0.2174	0.2589	-	-	-	0.2207	0.2178	0.1749	0.2044
2	0.2238	0.2655	0.2934	0.2137	0.2683	0.2993	0.2607	0.2057	0.2505	0.2661	0.2051	0.2522	0.2744	0.2423
3	0.2965	0.3149	0.2705	0.2816	0.3123	0.2716	0.2912	0.2546	0.2654	0.3104	0.2424	0.2633	0.3138	0.2750
4	0.5783	0.3531	0.3630	0.5828	0.3670	0.3598	0.4340	0.4225	0.2361	0.2792	0.4221	0.2524	0.2869	0.3165
5	0.4396	0.4288	0.4692	0.4293	0.4357	0.4623	0.4442	0.4329	0.3897	0.4342	0.4302	0.4046	0.4289	0.4201
6	0.6656	0.5620	0.7431	0.6608	0.5859	0.7562	0.6623	0.6455	0.6110	0.7047	0.6447	0.6250	0.7006	0.6553
7	0.9510	0.9124	0.9142	0.9148	0.8737	0.8512	0.9029	0.8558	0.8527	1.0782	0.8423	0.8621	1.0878	0.9298
8	0.7312	0.8403	0.9145	0.7162	0.8395	0.8593	0.8168	0.8184	0.8468	0.9907	0.7700	0.8195	1.0170	0.8771

Appendix X

	HA_4							HA_{234}						
Day	**OD**	**OD**	**OD**	**OD**	**OD**	**OD**	**OD Average**	**OD**	**OD**	**OD**	**OD**	**OD**	**OD**	**OD Average**
1	-	-	-	0.1864	0.2116	0.2131	0.2037	-	-	-	0.2048	0.2530	0.2057	0.2212
2	0.2427	0.2464	0.2437	0.2405	0.2443	0.2434	0.2435	0.2478	0.2478	0.2359	0.2452	0.2496	0.2365	0.2438
3	0.1853	0.2275	0.2245	0.1774	0.2227	0.2262	0.2106	0.2054	0.2549	0.2365	0.1955	0.2569	0.2330	0.2304
4	0.2963	0.4041	0.3141	0.2971	0.4105	0.3307	0.3421	0.4310	0.3958	0.2995	0.4316	0.4240	0.3078	0.3816
5	0.3512	0.4033	0.4367	0.3416	0.4055	0.4627	0.4002	0.3023	0.4235	0.3128	0.3213	0.4495	0.3334	0.3571
6	0.7489	0.6672	0.6906	0.7617	0.6735	0.6735	0.7026	0.5198	0.4349	0.5583	0.5296	0.4370	0.5559	0.5059
7	0.9443	0.8679	0.8416	0.9265	0.8679	0.8318	0.8800	0.6609	0.5071	0.7258	0.6222	0.5396	0.7858	0.6402
8	0.9610	1.0390	0.9518	0.9128	1.0154	1.0251	0.9842	0.9464	0.5596	0.8582	0.8850	0.5247	0.8866	0.7767

	HA_{2590}							HA_{mix}						
Day	**OD**	**OD**	**OD**	**OD**	**OD**	**OD**	**OD Average**	**OD**	**OD**	**OD**	**OD**	**OD**	**OD**	**OD Average**
1	-	-	-	0.2164	0.2605	0.2179	0.2316	-	-	-	0.2420	0.2679	0.3456	0.2801
2	0.1853	0.3069	0.2283	0.1838	0.3323	0.2253	0.2436	0.3197	0.2461	0.2622	0.3209	0.2541	0.2624	0.2776
3	0.2852	0.2374	0.2333	0.2731	0.2357	0.2289	0.2489	0.2116	0.2508	0.2601	0.1996	0.2419	0.2500	0.2357
4	0.4321	0.2572	0.3994	0.4171	0.2683	0.4048	0.3632	0.3235	0.3081	0.3296	0.3263	0.3149	0.3265	0.3215
5	0.3230	0.3969	0.3357	0.3292	0.4022	0.3420	0.3548	0.3721	0.3792	0.4456	0.3652	0.3723	0.4488	0.3972
6	0.4208	0.4090	0.4212	0.4283	0.3719	0.3742	0.4042	0.5535	0.5834	0.6545	0.5419	0.5966	0.6470	0.5961
7	0.6160	0.5471	0.5915	0.5674	0.5415	0.6364	0.5833	1.0275	0.9198	1.0102	0.9492	0.8923	0.9706	0.9616
8	0.6090	0.6264	0.8324	0.5683	0.6059	0.7143	0.6594	0.8430	0.8886	1.0585	0.8541	0.9531	1.0734	0.9451

Appendix X

PC3 cell line

	Control							Aminosilane						
Day	**OD**	**OD**	**OD**	**OD**	**OD**	**OD**	**OD Average**	**OD**	**OD**	**OD**	**OD**	**OD**	**OD**	**OD Average**
1	0.2393	0.2240	0.2133	0.2395	0.2262	0.2119	0.2257	0.2200	0.2834	0.1872	0.2217	0.2819	0.1753	0.2282
2	0.4794	0.2458	0.4703	0.4794	0.2458	0.4703	0.3985	0.4441	0.4302	0.3996	0.4422	0.4172	0.4030	0.4227
3	0.6520	0.6500	0.6374	0.5330	0.5529	0.5469	0.5953	0.6604	0.3910	0.5198	0.6418	0.3866	0.5268	0.5211
4	0.5137	0.5402	0.5925	0.5302	0.6340	0.6080	0.5698	0.6636	0.6147	0.6193	0.6710	0.6463	0.6863	0.6502
5	0.6643	0.6608	0.6543	0.6718	0.6828	0.6942	0.6714	0.7950	0.7997	0.6939	0.6636	0.6147	0.6193	0.6977
6	1.1821	1.1222	1.1052	1.1343	1.1094	1.1176	1.1285	-	-	1.0554	1.0367	1.0402	1.0270	1.0398
7	1.2685	1.1351	1.1302	1.2035	1.1234	1.1672	1.1713	1.1062	1.0568	1.0639	1.0884	-	1.0510	1.0732
8	1.3761	1.2711	1.2302	1.3343	1.3397	1.3396	1.3151	1.2978	1.3184	1.2770	1.2819	1.3470	1.2765	1.2998

	HA_4							HA_{234}						
Day	**OD**	**OD**	**OD**	**OD**	**OD**	**OD**	**OD Average**	**OD**	**OD**	**OD**	**OD**	**OD**	**OD**	**OD Average**
1	0.2576	0.2611	0.2598	0.2062	0.2090	0.2048	0.2331	0.2799	0.1751	0.2715	0.2738	0.1891	0.2875	0.2461
2	0.4905	0.4154	0.4497	0.5146	0.4334	0.4687	0.4620	0.1845	0.3538	0.2956	0.1877	0.3903	0.3138	0.2876
3	0.4449	0.4484	0.4461	0.5406	0.5552	0.5506	0.4976	0.2575	0.2616	0.2664	0.3419	0.3575	0.3552	0.3067
4	0.5637	0.5715	0.5753	0.5454	0.5609	0.5735	0.5651	0.4140	0.4282	0.4255	0.3290	0.3386	0.3507	0.3810
5	0.5394	0.5670	0.5681	0.5519	0.5734	0.5814	0.5635	0.4692	0.5731	0.4388	0.4671	0.5778	0.4660	0.4987
6	1.0608	1.0984	1.0271	1.0483	1.1014	1.0071	1.0572	0.7215	0.7287	0.6774	0.7032	0.7213	0.6830	0.7058
7	0.9451	1.0888	1.1306	0.9580	1.1324	1.1223	1.0629	0.7206	0.7466	0.7746	0.7404	0.7047	0.7715	0.7431
8	1.2009	1.4051	1.3643	1.2001	1.3781	1.3605	1.3182	0.5988	0.6974	0.7466	0.6133	0.7289	0.8233	0.7014

Appendix X

	HA_{2590}							HA_{mix}						
Day	**OD**	**OD**	**OD**	**OD**	**OD**	**OD**	**OD Average**	**OD**	**OD**	**OD**	**OD**	**OD**	**OD**	**OD Average**
1	0.2486	0.2490	0.2441	0.3139	0.3132	0.3174	0.2810	0.2980	0.3067	0.3052	0.1386	0.1456	0.1544	0.2248
2	0.4171	0.1974	0.3386	0.4262	0.2031	0.3586	0.3235	0.2793	0.2837	0.2869	0.3935	0.4081	0.4050	0.3428
3	0.3545	0.3617	0.3589	0.3250	0.3450	0.3379	0.3472	0.4128	0.4221	0.4196	0.3559	0.3721	0.3708	0.3922
4	0.4394	0.4526	0.4500	0.5625	0.5723	0.5752	0.5087	0.5567	0.5688	0.5743	0.4468	0.4537	0.4494	0.5083
5	0.5602	0.6212	0.5806	-	-	-	0.5873	0.5453	0.5722	0.5644	0.4607	0.4782	0.4613	0.5137
6	0.8178	0.8477	0.8237	0.8474	0.8528	0.8523	0.8403	0.7650	0.7764	0.7525	-	-	-	0.7646
7	0.7427	0.7531	0.6935	0.8029	0.8435	0.8053	0.7735	1.0475	1.0828	1.0391	1.1430	1.0851	1.0387	1.0727
8	0.7271	0.7754	0.8008	0.6614	0.7532	0.7867	0.7508	1.1759	1.2041	1.2053	1.2079	1.2408	1.2181	1.2087

PNT1A cell line

	Control							**Aminosilane**						
Day	**OD**	**OD**	**OD**	**OD**	**OD**	**OD**	**OD Average**	**OD**	**OD**	**OD**	**OD**	**OD**	**OD**	**OD Average**
1	0.2419	0.2561	0.1789	0.2420	0.2558	0.1801	0.2258	0.2622	0.2208	0.2116	0.2612	0.2213	0.2132	0.2317
2	0.4311	0.2524	0.4283	0.2567	0.4275	0.2513	0.3412	0.3765	0.4186	0.4818	0.3776	0.4187	0.4900	0.4272
3	0.3616	0.3357	0.3572	0.3414	0.3550	0.3379	0.3481	0.3776	0.3865	0.3784	0.3762	0.3954	0.3856	0.3833
4	0.3874	0.5209	0.3874	0.3937	0.5233	0.5174	0.4550	0.4741	0.4701	0.4137	0.4716	0.4804	0.4282	0.4563
5	0.4990	0.5011	0.5543	0.4874	0.5458	0.5497	0.5229	0.4851	0.4843	0.4546	0.4792	0.4500	0.4446	0.4663
6	0.7773	0.8817	0.7512	0.8042	0.7503	0.7931	0.7930	0.7561	0.8204	0.8003	0.7497	0.8173	0.8130	0.7928
7	0.6993	0.7046	0.7065	0.6874	0.6760	0.6863	0.6933	0.7032	0.7539	0.7488	0.6915	0.7378	0.7365	0.7286
8	0.6473	0.6446	0.6652	0.6687	0.6918	0.6632	0.6635	0.5582	0.6449	0.6525	0.5539	0.6515	0.6408	0.6170

Appendix X

	HA_4							HA_{234}						
Day	**OD**	**OD**	**OD**	**OD**	**OD**	**OD**	**OD Average**	**OD**	**OD**	**OD**	**OD**	**OD**	**OD**	**OD Average**
1	0.1865	0.1803	0.1652	0.1875	0.1793	0.1664	0.1776	0.1782	0.1785	0.1820	0.1788	0.1792	0.1855	0.1804
2	0.2373	0.2582	0.2442	0.2654	0.2440	0.2709	0.2534	0.3204	0.3462	0.3306	0.3564	-	-	0.3384
3	0.2510	0.2621	0.2628	0.2574	0.2650	0.2692	0.2613	0.2518	0.2477	0.2489	0.2397	0.2598	0.2554	0.2506
4	0.3522	0.3014	0.3464	0.3544	0.3084	0.3500	0.3355	0.3055	0.2778	0.3141	0.2823	0.3110	0.2815	0.2954
5	0.4019	0.4570	0.4246	0.3902	0.4499	0.4273	0.4251	0.3132	0.3001	0.3850	0.3055	0.3728	0.3562	0.3388
6	0.5406	0.5125	0.5371	0.5054	0.5294	0.4947	0.5199	0.5537	0.5366	0.5262	0.5419	0.5407	0.5258	0.5375
7	0.7791	0.7337	0.7656	0.7418	0.7513	0.7201	0.7486	0.6670	0.6484	0.6656	0.6547	0.6658	0.6495	0.6585
8	0.7901	0.9472	0.7708	0.9169	0.7643	0.9156	0.8508	0.7173	0.6244	0.6957	0.6517	0.6848	0.6256	0.6666

	HA_{2590}							HA_{mix}						
Day	**OD**	**OD**	**OD**	**OD**	**OD**	**OD**	**OD Average**	**OD**	**OD**	**OD**	**OD**	**OD**	**OD**	**OD Average**
1	0.1760	0.2134	0.1930	0.1828	0.2131	0.1965	0.1958	0.2491	0.2437	0.2466	0.2383	0.2388	0.2411	0.2429
2	0.3301	0.2973	0.3496	0.3413	0.3143	0.3648	0.3329	0.3725	0.3774	0.3748	0.4278	0.4291	0.4227	0.4007
3	0.2525	0.2764	0.2638	0.2472	0.2693	0.2738	0.2638	0.2686	0.2626	0.2916	0.2654	0.2676	0.2868	0.2738
4	0.2698	0.3127	0.3033	0.2636	0.3003	0.3079	0.2929	0.3213	0.3003	0.3478	0.3269	0.3053	0.3466	0.3247
5	0.3419	0.3280	0.3452	0.3139	0.3188	0.3407	0.3314	0.4038	0.3996	0.3926	0.3956	0.3947	0.3769	0.3939
6	0.5686	0.5974	0.5669	0.5768	0.5462	0.5750	0.5718	0.3649	0.3660	0.3577	0.4797	0.5050	0.4940	0.4279
7	0.4832	0.4728	0.4728	0.4919	0.4562	0.4719	0.4748	0.4797	0.5050	0.4940	0.6172	0.6200	0.6260	0.5570
8	0.5620	0.6441	0.6632	0.6229	0.5860	0.6237	0.6170	0.8890	0.8788	0.8494	0.8916	0.9046	0.8939	0.8845

Appendix XI

MTT assay statistics

RT112 cell line

Column A vs Column B	Control vs Aminosilane	Control vs HA4	Control vs HA234	Control vs HA2590	Control vs HAmix
Unpaired t test					
P value	0.8087	0.2748	P<0.0001	P<0.0001	0.0440
P value summary	ns	ns	***	***	*
Are means signif. different? (P <	No	No	Yes	Yes	Yes
One- or two-tailed P value?	Two-tailed	Two-tailed	Two-tailed	Two-tailed	Two-tailed
t, df	t=0.2486 df=10	t=1.155 df=10	t=8.210 df=10	t=12.34 df=10	t=2.304 df=10
How big is the difference?					
Mean ± SEM of column A	1.028 ± 0.01994 N=6	1.028 ± 0.01994 N=6	1.028 ± 0.01994 N=6	1.028 ± 0.01994 N=6	1.028 ± 0.01994 N=6
Mean ± SEM of column B	1.020 ± 0.02509 N=6	1.062 ± 0.02175 N=6	0.7358 ± 0.02948 N=6	0.6239 ± 0.02597 N=6	0.9739 ± 0.01242 N=6
Difference between means	0.007968 ± 0.03205	-0.03410 ± 0.02951	0.2922 ± 0.03559	0.4041 ± 0.03274	0.05413 ± 0.02350
95% confidence interval	-0.06343 to 0.07937	-0.09985 to 0.03166	0.2129 to 0.3715	0.3312 to 0.4771	0.001778 to 0.1065
R squared	0.006144	0.1178	0.8708	0.9384	0.3467
F test to compare variances					
F,DFn, Dfd	1.583, 5, 5	1.190, 5, 5	2.186, 5, 5	1.696, 5, 5	2.576, 5, 5
P value	0.6267	0.8532	0.4110	0.5761	0.3223
P value summary	ns	ns	ns	ns	ns
Are variances significantly different?	No	No	No	No	No

Appendix XI

T24 cell line

Column A vs Column B	Control vs Aminosilane	Control vs HA4	Control vs HA234	Control vs HA2590	Control vs HAmix
Unpaired t test					
P value	0.2747	0.0012	0.6339	0.0113	0.0333
P value summary	ns	**	ns	*	*
Are means signif. different? (P <	No	Yes	No	Yes	Yes
One- or two-tailed P value?	Two-tailed	Two-tailed	Two-tailed	Two-tailed	Two-tailed
t, df	t=1.156 df=10	t=4.461 df=10	t=0.4912 df=10	t=3.095 df=10	t=2.466 df=10
How big is the difference?					
Mean ± SEM of column A	0.8168 ± 0.03156 N=6	0.8168 ± 0.03156 N=6	0.8168 ± 0.03156 N=6	0.8168 ± 0.03156 N=6	0.8168 ± 0.03156 N=6
Mean ± SEM of column B	0.8771 ± 0.04148 N=6	0.9842 ± 0.02027 N=6	0.7767 ± 0.07526 N=6	0.6594 ± 0.03990 N=6	0.9451 ± 0.04134 N=6
Difference between means	-0.06024 ± 0.05212	-0.1673 ± 0.03751	0.04009 ± 0.08161	0.1575 ± 0.05087	-0.1283 ± 0.05201
95% confidence interval	-0.1764 to 0.05589	-0.2509 to -0.08376	-0.1417 to 0.2219	0.04411 to 0.2708	-0.2442 to -0.01240
R squared	0.1178	0.6656	0.02356	0.4893	0.3782
F test to compare variances					
F,DFn, Dfd	1.727, 5, 5	2.424, 5, 5	5.687, 5, 5	1.598, 5, 5	1.716, 5, 5
P value	0.5632	0.3534	0.0794	0.6195	0.5678
P value summary	ns	ns	ns	ns	ns
Are variances significantly different?	No	No	No	No	No

Appendix XI

PC3 cell line

Column A vs Column B	Control vs Aminosilane	Control vs HA4	Control vs HA234	Control vs HA2590	Control vs HAmix
Unpaired t test					
P value	0.5490	0.9463	P<0.0001	P<0.0001	0.0011
P value summary	ns	ns	***	***	**
Are means signif. different? (P <	No	No	Yes	Yes	Yes
One- or two-tailed P value?	Two-tailed	Two-tailed	Two-tailed	Two-tailed	Two-tailed
t, df	t=0.6202 df=10	t=0.06905 df=10	t=14.98 df=10	t=18.68 df=10	t=4.518 df=10
How big is the difference?					
Mean ± SEM of column A	1.315 ± 0.02193 N=6	1.315 ± 0.02193 N=6	1.315 ± 0.02193 N=6	1.315 ± 0.02193 N=6	1.315 ± 0.02193 N=6
Mean ± SEM of column B	1.300 ± 0.01150 N=6	1.318 ± 0.03776 N=6	0.7014 ± 0.03462 N=6	0.7508 ± 0.02078 N=6	1.209 ± 0.008625 N=6
Difference between means	0.01536 ± 0.02476	-0.003015 ± 0.04366	0.6138 ± 0.04098	0.5644 ± 0.03021	0.1065 ± 0.02356
95% confidence interval	-0.03981 to 0.07052	-0.1003 to 0.09426	0.5225 to 0.7051	0.4971 to 0.6317	0.05397 to 0.1590
R squared	0.03704	0.0004766	0.9573	0.9721	0.6712
F test to compare variances					
F,DFn, Dfd	3.639, 5, 5	2.964, 5, 5	2.492, 5, 5	1.114, 5, 5	6.465, 5, 5
P value	0.1826	0.2582	0.3389	0.9088	0.0614
P value summary	ns	ns	ns	ns	ns
Are variances significantly different?	No	No	No	No	No

Appendix XI

PNT1A cell line

Column A vs Column B	Control vs Aminosilane	Control vs HA4	Control vs HA234	Control vs HA2590	Control vs HAmix
Unpaired t test					
P value	0.0210	0.0003	0.3231	0.1041	0.0002
P value summary	*	***	ns	ns	***
Are means signif. different? (P <	Yes	Yes	No	No	Yes
One- or two-tailed P value?	Two-tailed	Two-tailed	Two-tailed	Two-tailed	Two-tailed
t, df	t=2.736 df=10	t=5.343 df=10	t=1.039 df=10	t=1.788 df=10	t=5.664 df=10
How big is the difference?					
Mean ± SEM of column A	0.6635 ± 0.006954	0.6635 ± 0.006954 N=6	0.6635 ± 0.006954 N=6	0.6635 ± 0.006954 N=6	0.6635 ± 0.006954
Mean ± SEM of column B	0.6387 ± 0.005775	0.8508 ± 0.03436 N=6	0.6801 ± 0.01438 N=6	0.6370 ± 0.01306 N=6	0.8156 ± 0.02595 N=6
Difference between means	0.02473 ± 0.009040	-0.1873 ± 0.03506	-0.01660 ± 0.01597	0.02646 ± 0.01480	-0.1521 ± 0.02686
95% confidence interval	0.004590 to 0.04487	-0.2655 to -0.1092	-0.05218 to 0.01898	-0.006518 to 0.05943	-0.2120 to -0.09229
R squared	0.4281	0.7406	0.09750	0.2422	0.7623
F test to compare variances					
F,DFn, Dfd	1.450, 5, 5	24.42, 5, 5	4.274, 5, 5	3.529, 5, 5	13.92, 5, 5
P value	0.6934	0.0032	0.1368	0.1926	0.0117
P value summary	ns	**	ns	ns	*
Are variances significantly different?	No	Yes	No	No	Yes

Appendix XII

MTT assay – curve fitting

RT112 cell line

a) Control

Equation: Piecewise, 3 segment linear
t1 = min(t)
t3 = max(t)
region1(t) = (y1*(T1-t) + y2*(t-t1))/(T1-t1)
region2(t) = (y2*(T2-t) + y3*(t-T1))/(T2-T1)
region3(t) = (y3*(t3-t) + y4*(t-T2))/(t3-T2)
f = if(t <= T1, region1(t), if(t <= T2, region2(t), region3(t)))

Dynamic Fit Options:

Total Number of Fits	200
Maximum Number of Iterations	200

Parameter Ranges for Initial Estimates:

	Minimum	Maximum
y1	-0.1480	0.4441
y2	-0.5120	1.5360
y3	-0.8605	2.5816
y4	-1.0287	3.0860
T1	-3.3333	10.0000
T2	-5.6667	17.0000

Summary of Fit Results:

Converged	99.5%
Singular Solutions	84.0%
Ill-Conditioned Solutions	14.0%
Iterations Exceeding 200	0.5%

Results for the Overall Best-Fit Solution:

R	Rsqr	Adj Rsqr	Standard Error of Estimate
0.9993	0.9985	0.9948	0.0238

	Coefficient	Std. Error	t	P
y1	0.1511	0.0238	6.3387	0.0240
y2	0.2303	1122127.9199	2.0527E-007	1.0000
y3	0.7876	0.0526	14.9641	0.0044
y4	1.0248	0.0199	51.3911	0.0004
T1	1.9138	5789797.4524	3.3055E-007	1.0000
T2	4.7891	0.5599	8.5538	0.0134

Analysis of Variance:

Analysis of Variance:

	DF	SS	MS
Regression	6	4.0499	0.6750
Residual	2	0.0011	0.0006
Total	8	4.0510	0.5064

Appendix XII

Corrected for the mean of the observations:

	DF	SS	MS	F	P
Regression	5	0.7607	0.1521	267.8172	0.0037
Residual	2	0.0011	0.0006		
Total	7	0.7619	0.1088		

Statistical Tests:

Normality Test (Shapiro-Wilk) Passed (P = 0.2004)

W Statistic= 0.8828 Significance Level = 0.0500

Constant Variance Test Passed (P = 0.7941)

iterations=200
stepsize=1
tolerance=1e-10

Number of Iterations Performed = 14

a) Aminosilane

Equation: Piecewise, 3 segment linear
t1 = min(t)
t3 = max(t)
region1(t) = (y1*(T1-t) + y2*(t-t1))/(T1-t1)
region2(t) = (y2*(T2-t) + y3*(t-T1))/(T2-T1)
region3(t) = (y3*(t3-t) + y4*(t-T2))/(t3-T2)
f = if(t <= T1, region1(t), if(t <= T2, region2(t), region3(t)))

Dynamic Fit Options:

Total Number of Fits	200
Maximum Number of Iterations	200

Parameter Ranges for Initial Estimates:

	Minimum	Maximum
y1	-0.1739	0.5217
y2	-0.5183	1.5549
y3	-0.9808	2.9425
y4	-1.0049	3.0148
T1	-3.3333	10.0000
T2	-5.6667	17.0000

Summary of Fit Results:

Converged	99.0%
Singular Solutions	87.0%
Ill-Conditioned Solutions	11.0%
Iterations Exceeding 200	1.0%

Appendix XII

Results for the Overall Best-Fit Solution:

R	Rsqr	Adj Rsqr	Standard Error of Estimate
0.9966	0.9932	0.9763	0.0557

	Coefficient	Std. Error	t	P
y1	0.1743	0.0479	3.6363	0.0680
y2	0.6310	2366771.1322	2.6660E-007	1.0000
y3	1.1095	349170.1357	3.1775E-006	1.0000
y4	1.0169	0.0511	19.9019	0.0025
T1	4.2233	16704407.3780	2.5283E-007	1.0000
T2	5.8293	8182604.2214	7.1240E-007	1.0000

Analysis of Variance:

Analysis of Variance:

	DF	SS	MS
Regression	6	4.8140	0.8023
Residual	2	0.0062	0.0031
Total	8	4.8202	0.6025

Corrected for the mean of the observations:

	DF	SS	MS	F	P
Regression	5	0.9105	0.1821	58.6115	0.0169
Residual	2	0.0062	0.0031		
Total	7	0.9167	0.1310		

Statistical Tests:

Normality Test (Shapiro-Wilk) Failed (P = 0.0386)

W Statistic= 0.8122 Significance Level = 0.0500

Constant Variance Test Passed (P = 0.6194)

iterations=200
stepsize=1
tolerance=1e-10

Number of Iterations Performed = 7

c) HA_4

Equation: Piecewise, 3 segment linear
t1 = min(t)
t3 = max(t)
region1(t) = (y1*(T1-t) + y2*(t-t1))/(T1-t1)
region2(t) = (y2*(T2-t) + y3*(t-T1))/(T2-T1)
region3(t) = (y3*(t3-t) + y4*(t-T2))/(t3-T2)
f = if(t <= T1, region1(t), if(t <= T2, region2(t), region3(t)))

Dynamic Fit Options:

Total Number of Fits	200
Maximum Number of Iterations	200

Appendix XII

Parameter Ranges for Initial Estimates:

	Minimum	Maximum
y1	-0.2154	0.6461
y2	-0.3616	1.0847
y3	-0.7646	2.2938
y4	-1.0334	3.1002
T1	-3.3333	10.0000
T2	-5.6667	17.0000

Summary of Fit Results:

Converged	96.5%
Singular Solutions	84.5%
Ill-Conditioned Solutions	12.0%
Iterations Exceeding 200	3.5%

Results for the Overall Best-Fit Solution:

R	Rsqr	Adj Rsqr	Standard Error of Estimate
0.9928	0.9857	0.9498	0.0756

	Coefficient	Std. Error	t	P
y1	0.2184	0.0633	3.4511	0.0747
y2	0.4012	0.1303	3.0798	0.0912
y3	0.8884	0.1321	6.7248	0.0214
y4	1.0219	0.0690	14.8019	0.0045
T1	4.3980	1.8303	2.4029	0.1382
T2	5.6131	1.7918	3.1326	0.0886

Analysis of Variance:

Analysis of Variance:

	DF	SS	MS
Regression	6	3.5909	0.5985
Residual	2	0.0114	0.0057
Total	8	3.6024	0.4503

Corrected for the mean of the observations:

	DF	SS	MS	F	P
Regression	5	0.7861	0.1572	27.4868	0.0355
Residual	2	0.0114	0.0057		
Total	7	0.7976	0.1139		

Statistical Tests:

Normality Test (Shapiro-Wilk) Passed (P = 0.2755)

W Statistic= 0.8977 Significance Level = 0.0500

Constant Variance Test Passed (P = 0.0716)

iterations=200
stepsize=1
tolerance=1e-10

Number of Iterations Performed = 10

Appendix XII

d) HA_{234}

Equation: Piecewise, 3 segment linear

t1 = min(t)
t3 = max(t)
region1(t) = (y1*(T1-t) + y2*(t-t1))/(T1-t1)
region2(t) = (y2*(T2-t) + y3*(t-T1))/(T2-T1)
region3(t) = (y3*(t3-t) + y4*(t-T2))/(t3-T2)
f = if(t <= T1, region1(t), if(t <= T2, region2(t), region3(t)))

Dynamic Fit Options:

Total Number of Fits	200
Maximum Number of Iterations	200

Parameter Ranges for Initial Estimates:

	Minimum	Maximum
y1	-0.1999	0.5998
y2	-0.3850	1.1549
y3	-0.6236	1.8708
y4	-0.7292	2.1877
T1	-3.3333	10.0000
T2	-5.6667	17.0000

Summary of Fit Results:

Converged	97.5%
Singular Solutions	85.5%
Ill-Conditioned Solutions	11.0%
Iterations Exceeding 200	2.5%

Results for the Overall Best-Fit Solution:

R	Rsqr	Adj Rsqr	Standard Error of Estimate
0.9977	0.9954	0.9838	0.0263

	Coefficient	Std. Error	t	P
y1	0.2055	0.0267	7.6902	0.0165
y2	0.4382	2444164.8645	1.7927E-007	1.0000
y3	0.6685	473366.0928	1.4122E-006	1.0000
y4	0.7344	0.0257	28.5381	0.0012
T1	4.1877	33490886.8464	1.2504E-007	1.0000
T2	5.6276	17027556.4370	3.3050E-007	1.0000

Analysis of Variance:

Analysis of Variance:

	DF	SS	MS
Regression	6	2.2458	0.3743
Residual	2	0.0014	0.0007
Total	8	2.2472	0.2809

Appendix XII

Corrected for the mean of the observations:

	DF	SS	MS	F	P
Regression	5	0.2975	0.0595	86.0265	0.0115
Residual	2	0.0014	0.0007		
Total	7	0.2989	0.0427		

Statistical Tests:

Normality Test (Shapiro-Wilk) Passed (P = 0.0547)

W Statistic= 0.8266 Significance Level = 0.0500

Constant Variance Test Passed (P = 0.1020)

iterations=200
stepsize=1
tolerance=1e-10

Number of Iterations Performed = 7

e) HA_{2590}

Equation: Piecewise, 3 segment linear
t1 = min(t)
t3 = max(t)
region1(t) = (y1*(T1-t) + y2*(t-t1))/(T1-t1)
region2(t) = (y2*(T2-t) + y3*(t-T1))/(T2-T1)
region3(t) = (y3*(t3-t) + y4*(t-T2))/(t3-T2)
f = if(t <= T1, region1(t), if(t <= T2, region2(t), region3(t)))

Dynamic Fit Options:

Total Number of Fits	200
Maximum Number of Iterations	200

Parameter Ranges for Initial Estimates:

	Minimum	Maximum
y1	-0.1773	0.5320
y2	-0.4204	1.2613
y3	-0.6064	1.8191
y4	-0.6155	1.8464
T1	-3.3333	10.0000
T2	-5.6667	17.0000

Summary of Fit Results:

Converged	99.0%
Singular Solutions	86.0%
Ill-Conditioned Solutions	10.0%
Iterations Exceeding 200	1.0%

Results for the Overall Best-Fit Solution:

R	Rsqr	Adj Rsqr	Standard Error of Estimate
0.9959	0.9918	0.9713	0.0297

Appendix XII

	Coefficient	Std. Error	t	P
y1	0.1744	0.0318	5.4814	0.0317
y2	0.2970	1057265.3717	2.8089E-007	1.0000
y3	0.6496	0.0566	11.4844	0.0075
y4	0.6190	0.0297	20.8617	0.0023
T1	1.9614	12109909.9548	1.6197E-007	1.0000
T2	6.0000	0.6862	8.7433	0.0128

Analysis of Variance:

Analysis of Variance:

	DF	SS	MS
Regression	6	2.0193	0.3366
Residual	2	0.0018	0.0009
Total	8	2.0211	0.2526

Corrected for the mean of the observations:

	DF	SS	MS	F	P
Regression	5	0.2128	0.0426	48.3365	0.0204
Residual	2	0.0018	0.0009		
Total	7	0.2145	0.0306		

Statistical Tests:

Normality Test (Shapiro-Wilk) Passed (P = 0.4130)

W Statistic= 0.9179 Significance Level = 0.0500

Constant Variance Test Failed (P = 0.0212)

iterations=200
stepsize=1
tolerance=1e-10

Number of Iterations Performed = 26

f) HA_{mix}

Equation: Piecewise, 3 segment linear
t1 = min(t)
t3 = max(t)
region1(t) = (y1*(T1-t) + y2*(t-t1))/(T1-t1)
region2(t) = (y2*(T2-t) + y3*(t-T1))/(T2-T1)
region3(t) = (y3*(t3-t) + y4*(t-T2))/(t3-T2)
f = if(t <= T1, region1(t), if(t <= T2, region2(t), region3(t)))

Dynamic Fit Options:

Total Number of Fits	200
Maximum Number of Iterations	200

Appendix XII

Parameter Ranges for Initial Estimates:

	Minimum	Maximum
y1	-0.1813	0.5440
y2	-0.4482	1.3445
y3	-0.7642	2.2926
y4	-0.9773	2.9320
T1	-3.3333	10.0000
T2	-5.6667	17.0000

Summary of Fit Results:

Converged	99.0%
Singular Solutions	85.0%
Ill-Conditioned Solutions	10.5%
Iterations Exceeding 200	1.0%

Results for the Overall Best-Fit Solution:

R	Rsqr	Adj Rsqr	Standard Error of Estimate
0.9992	0.9983	0.9942	0.0225

	Coefficient	Std. Error	t	P
y1	0.1815	0.0225	8.0686	0.0150
y2	0.3437	0.1058	3.2492	0.0831
y3	0.6398	0.0807	7.9254	0.0156
y4	0.9899	0.0188	52.5960	0.0004
T1	2.7138	0.7283	3.7264	0.0651
T2	4.5086	0.6578	6.8537	0.0206

Analysis of Variance:

Analysis of Variance:

	DF	SS	MS
Regression	6	3.4403	0.5734
Residual	2	0.0010	0.0005
Total	8	3.4413	0.4302

Corrected for the mean of the observations:

	DF	SS	MS	F	P
Regression	5	0.6052	0.1210	239.1890	0.0042
Residual	2	0.0010	0.0005		
Total	7	0.6062	0.0866		

Statistical Tests:

Normality Test (Shapiro-Wilk) Failed (P = 0.0236)

W Statistic= 0.7922 Significance Level = 0.0500

Constant Variance Test Failed (P = 0.0149)

iterations=200
stepsize=1
tolerance=1e-10

Number of Iterations Performed = 17

Appendix XII

T24 cell line

a) Control

Equation: Piecewise, 3 segment linear
t1 = min(t)
t3 = max(t)
region1(t) = (y1*(T1-t) + y2*(t-t1))/(T1-t1)
region2(t) = (y2*(T2-t) + y3*(t-T1))/(T2-T1)
region3(t) = (y3*(t3-t) + y4*(t-T2))/(t3-T2)
f = if(t <= T1, region1(t), if(t <= T2, region2(t), region3(t)))

Dynamic Fit Options:

Total Number of Fits	200
Maximum Number of Iterations	200

Parameter Ranges for Initial Estimates:

	Minimum	Maximum
y1	-0.2512	0.7537
y2	-0.2884	0.8653
y3	-0.6116	1.8349
y4	-0.8267	2.4800
T1	-3.3333	10.0000
T2	-5.6667	17.0000

Summary of Fit Results:

Converged	97.5%
Singular Solutions	85.0%
Ill-Conditioned Solutions	12.5%
Iterations Exceeding 200	2.5%

Results for the Overall Best-Fit Solution:

R	Rsqr	Adj Rsqr	Standard Error of Estimate
0.9990	0.9981	0.9932	0.0212

	Coefficient	Std. Error	t	P
y1	0.2508	0.0177	14.1584	0.0050
y2	0.3668	0.0271	13.5129	0.0054
y3	0.9076	835110.5664	1.0868E-006	1.0000
y4	0.8168	0.0212	38.5730	0.0007
T1	4.6790	0.1662	28.1499	0.0013
T2	7.0370	3640944.1371	1.9327E-006	1.0000

Analysis of Variance:

Analysis of Variance:

	DF	SS	MS
Regression	6	2.4786	0.4131
Residual	2	0.0009	0.0004
Total	8	2.4795	0.3099

Appendix XII

Corrected for the mean of the observations:

	DF	SS	MS	F	P
Regression	5	0.4600	0.0920	205.1691	0.0049
Residual	2	0.0009	0.0004		
Total	7	0.4609	0.0658		

Statistical Tests:

Normality Test (Shapiro-Wilk) Passed (P = 0.5163)

W Statistic= 0.9300 Significance Level = 0.0500

Constant Variance Test Passed (P = 0.2327)

iterations=200
stepsize=1
tolerance=1e-10

Number of Iterations Performed = 8

b) Aminosilane

Equation: Piecewise, 3 segment linear
t1 = min(t)
t3 = max(t)
region1(t) = (y1*(T1-t) + y2*(t-t1))/(T1-t1)
region2(t) = (y2*(T2-t) + y3*(t-T1))/(T2-T1)
region3(t) = (y3*(t3-t) + y4*(t-T2))/(t3-T2)
f = if(t <= T1, region1(t), if(t <= T2, region2(t), region3(t)))

Dynamic Fit Options:

Total Number of Fits	200
Maximum Number of Iterations	200

Parameter Ranges for Initial Estimates:

	Minimum	Maximum
y1	-0.1977	0.5932
y2	-0.2309	0.6927
y3	-0.5873	1.7618
y4	-0.8837	2.6512
T1	-3.3333	10.0000
T2	-5.6667	17.0000

Summary of Fit Results:

Converged	98.0%
Singular Solutions	84.5%
Ill-Conditioned Solutions	13.5%
Iterations Exceeding 200	2.0%

Appendix XII

Results for the Overall Best-Fit Solution:

R	Rsqr	Adj Rsqr	Standard Error of Estimate
0.9996	0.9992	0.9972	0.0159

	Coefficient	Std. Error	t	P
y1	0.2130	0.0133	15.9829	0.0039
y2	0.2795	0.0175	15.9328	0.0039
y3	0.9315	1027237.4394	9.0681E-007	1.0000
y4	0.8771	0.0159	55.0726	0.0003
T1	4.4743	0.1075	41.6339	0.0006
T2	7.0324	4030500.2338	1.7448E-006	1.0000

Analysis of Variance:

Analysis of Variance:

	DF	SS	MS
Regression	6	2.4749	0.4125
Residual	2	0.0005	0.0003
Total	8	2.4754	0.3094

Corrected for the mean of the observations:

	DF	SS	MS	F	P
Regression	5	0.6230	0.1246	491.2757	0.0020
Residual	2	0.0005	0.0003		
Total	7	0.6235	0.0891		

Statistical Tests:

Normality Test (Shapiro-Wilk) Passed (P = 0.3717)

W Statistic= 0.9125 Significance Level = 0.0500

Constant Variance Test Passed (P = 0.2897)

iterations=200
stepsize=1
tolerance=1e-10

Number of Iterations Performed = 8

c) HA_4

Equation: Piecewise, 3 segment linear
t1 = min(t)
t3 = max(t)
region1(t) = (y1*(T1-t) + y2*(t-t1))/(T1-t1)
region2(t) = (y2*(T2-t) + y3*(t-T1))/(T2-T1)
region3(t) = (y3*(t3-t) + y4*(t-T2))/(t3-T2)
f = if(t <= T1, region1(t), if(t <= T2, region2(t), region3(t)))

Dynamic Fit Options:

Total Number of Fits	200
Maximum Number of Iterations	200

Appendix XII

Parameter Ranges for Initial Estimates:

	Minimum	Maximum
y1	-0.2049	0.6148
y2	-0.2475	0.7426
y3	-0.5925	1.7774
y4	-0.9823	2.9470
T1	-3.3333	10.0000
T2	-5.6667	17.0000

Summary of Fit Results:

Converged	95.5%
Singular Solutions	75.0%
Ill-Conditioned Solutions	18.0%
Iterations Exceeding 200	4.5%

Results for the Overall Best-Fit Solution:

R	Rsqr	Adj Rsqr	Standard Error of Estimate
0.9964	0.9929	0.9751	0.0496

	Coefficient	Std. Error	t	P
y1	0.1926	0.0415	4.6428	0.0434
y2	0.3377	0.0654	5.1664	0.0355
y3	0.8143	0.1373	5.9304	0.0273
y4	0.9842	0.0496	19.8474	0.0025
T1	4.7934	0.3141	15.2589	0.0043
T2	6.3694	0.5631	11.3107	0.0077

Analysis of Variance:

Analysis of Variance:

	DF	SS	MS
Regression	6	2.6540	0.4423
Residual	2	0.0049	0.0025
Total	8	2.6589	0.3324

Corrected for the mean of the observations:

	DF	SS	MS	F	P
Regression	5	0.6870	0.1374	55.8826	0.0177
Residual	2	0.0049	0.0025		
Total	7	0.6919	0.0988		

Statistical Tests:

Normality Test (Shapiro-Wilk) Failed (P = 0.0234)

W Statistic= 0.7918 Significance Level = 0.0500

Constant Variance Test Passed (P = 0.0860)

iterations=200
stepsize=1
tolerance=1e-10

Number of Iterations Performed = 8

Appendix XII

d) HA_{234}

Equation: Piecewise, 3 segment linear
t1 = min(t)
t3 = max(t)
region1(t) = (y1*(T1-t) + y2*(t-t1))/(T1-t1)
region2(t) = (y2*(T2-t) + y3*(t-T1))/(T2-T1)
region3(t) = (y3*(t3-t) + y4*(t-T2))/(t3-T2)
f = if(t <= T1, region1(t), if(t <= T2, region2(t), region3(t)))
Dynamic Fit Options:

Total Number of Fits	200
Maximum Number of Iterations	200

Parameter Ranges for Initial Estimates:

	Minimum	Maximum
y1	-0.2208	0.6623
y2	-0.2710	0.8130
y3	-0.4547	1.3642
y4	-0.7793	2.3378
T1	-3.3333	10.0000
T2	-5.6667	17.0000

Summary of Fit Results:

Converged	98.0%
Singular Solutions	84.0%
Ill-Conditioned Solutions	10.5%
Iterations Exceeding 200	2.0%

Results for the Overall Best-Fit Solution:

R	Rsqr	Adj Rsqr	Standard Error of Estimate
0.9938	0.9875	0.9564	0.0432

	Coefficient	Std. Error	t	P
y1	0.2234	0.0422	5.2960	0.0339
y2	0.2555	0.1356	1.8845	0.2002
y3	0.3701	0.0839	4.4102	0.0478
y4	0.7785	0.0394	19.7346	0.0026
T1	3.0000	3.3914	0.8846	0.4697
T2	5.0517	0.9369	5.3917	0.0327

Analysis of Variance:

Analysis of Variance:

	DF	SS	MS
Regression	6	1.6702	0.2784
Residual	2	0.0037	0.0019
Total	8	1.6739	0.2092

Corrected for the mean of the observations:

	DF	SS	MS	F	P
Regression	5	0.2961	0.0592	31.7120	0.0309
Residual	2	0.0037	0.0019		
Total	7	0.2998	0.0428		

Statistical Tests:

Normality Test (Shapiro-Wilk) Passed (P = 0.1102)

Appendix XII

W Statistic= 0.8563 Significance Level = 0.0500

Constant Variance Test Passed (P = 0.4228)

iterations=200
stepsize=1
tolerance=1e-10
Number of Iterations Performed = 88

e) HA_{2590}

Equation: Piecewise, 3 segment linear
t1 = min(t)
t3 = max(t)
region1(t) = (y1*(T1-t) + y2*(t-t1))/(T1-t1)
region2(t) = (y2*(T2-t) + y3*(t-T1))/(T2-T1)
region3(t) = (y3*(t3-t) + y4*(t-T2))/(t3-T2)
f = if(t <= T1, region1(t), if(t <= T2, region2(t), region3(t)))

Dynamic Fit Options:
Total Number of Fits 200
Maximum Number of Iterations

Parameter Ranges for Initial Estimates:

	Minimum	Maximum
y1	-0.2300	0.6901
y2	-0.2652	0.7956
y3	-0.4074	1.2222
y4	-0.6657	1.9971
T1	-3.3333	10.0000
T2	-5.6667	17.0000

Summary of Fit Results:

Converged	97.5%
Singular Solutions	83.0%
Ill-Conditioned Solutions	10.5%
Iterations Exceeding 200	2.5%

Results for the Overall Best-Fit Solution:

R	Rsqr	Adj Rsqr	Standard Error of Estimate
0.9936	0.9872	0.9550	0.0343

	Coefficient	Std. Error	t	P
y1	0.2326	0.0318	7.3083	0.0182
y2	0.2507	0.0604	4.1536	0.0534
y3	0.3754	0.0973	3.8568	0.0611
y4	0.6704	0.0313	21.4053	0.0022
T1	3.0000	2.4673	1.2159	0.3481
T2	5.5378	0.9665	5.7296	0.0291

Appendix XII

Analysis of Variance:

Analysis of Variance:

	DF	SS	MS
Regression	6	1.3253	0.2209
Residual	2	0.0024	0.0012
Total	8	1.3277	0.1660

Corrected for the mean of the observations:

	DF	SS	MS	F	P
Regression	5	0.1809	0.0362	30.7336	0.0318
Residual	2	0.0024	0.0012		
Total	7	0.1833	0.0262		

Statistical Tests:

Normality Test (Shapiro-Wilk) Passed (P = 0.1176)

W Statistic= 0.8591 Significance Level = 0.0500

Constant Variance Test Passed (P = 0.2897)

iterations=200
stepsize=1
tolerance=1e-10
Number of Iterations Performed = 22

e) HA_{mix}

Equation: Piecewise, 3 segment linear

t1 = min(t)
t3 = max(t)
region1(t) = (y1*(T1-t) + y2*(t-t1))/(T1-t1)
region2(t) = (y2*(T2-t) + y3*(t-T1))/(T2-T1)
region3(t) = (y3*(t3-t) + y4*(t-T2))/(t3-T2)
f = if(t <= T1, region1(t), if(t <= T2, region2(t), region3(t)))

Dynamic Fit Options:

Total Number of Fits	200
Maximum Number of Iterations	200

Parameter Ranges for Initial Estimates:

	Minimum	Maximum
y1	-0.2690	0.8071
y2	-0.2425	0.7274
y3	-0.5712	1.7136
y4	-0.9628	2.8884
T1	-3.3333	10.0000
T2	-5.6667	17.0000

Appendix XII

Summary of Fit Results:

Converged	98.5%
Singular Solutions	83.0%
Ill-Conditioned Solutions	14.0%
Iterations Exceeding 200	1.5%

Results for the Overall Best-Fit Solution:

R	**Rsqr**	**Adj Rsqr**	**Standard Error of Estimate**
0.9955	0.9910	0.9685	0.0534

	Coefficient	**Std. Error**	**t**	**P**
y1	0.2414	0.0414	5.8368	0.0281
y2	0.3747	321682.6360	1.1647E-006	1.0000
y3	0.9633	262022.6307	3.6763E-006	1.0000
y4	0.9451	0.0561	16.8505	0.0035
T1	5.4587	10764125.5337	5.0712E-007	1.0000
T2	6.8974	15900716.8503	4.3378E-007	1.0000

Analysis of Variance:

Analysis of Variance:

	DF	**SS**	**MS**
Regression	6	2.6358	0.4393
Residual	2	0.0057	0.0029
Total	8	2.6415	0.3302

Corrected for the mean of the observations:

	DF	**SS**	**MS**	**F**	**P**
Regression	5	0.6270	0.1254	43.9847	0.0224
Residual	2	0.0057	0.0029		
Total	7	0.6327	0.0904		

Statistical Tests:

Normality Test (Shapiro-Wilk) Passed (P = 0.3582)

W Statistic= 0.9106 Significance Level = 0.0500

Constant Variance Test Failed (P = 0.0053)

iterations=200
stepsize=1
tolerance=1e-10

Number of Iterations Performed = 7

Appendix XII

PC3 cell line

a) Control

Equation: Piecewise, 3 segment linear
t1 = min(t)
t3 = max(t)
region1(t) = (y1*(T1-t) + y2*(t-t1))/(T1-t1)
region2(t) = (y2*(T2-t) + y3*(t-T1))/(T2-T1)
region3(t) = (y3*(t3-t) + y4*(t-T2))/(t3-T2)
f = if(t <= T1, region1(t), if(t <= T2, region2(t), region3(t)))

Dynamic Fit Options:

Total Number of Fits	200
Maximum Number of Iterations	200

Parameter Ranges for Initial Estimates:

	Minimum	Maximum
y1	-0.2167	0.6501
y2	-0.5369	1.6106
y3	-0.9161	2.7482
y4	-1.3014	3.9042
T1	-3.3333	10.0000
T2	-5.6667	17.0000

Summary of Fit Results:

Converged	96.0%
Singular Solutions	85.0%
Ill-Conditioned Solutions	11.0%
Iterations Exceeding 200	4.0%

Results for the Overall Best-Fit Solution:

R	Rsqr	Adj Rsqr	Standard Error of Estimate
0.9921	0.9842	0.9448	0.0931

	Coefficient	Std. Error	t	P
y1	0.2796	0.0735	3.8032	0.0627
y2	0.7262	4168008.6997	1.7423E-007	1.0000
y3	1.0963	4666853.6247	2.3492E-007	1.0000
y4	1.2983	0.0950	13.6646	0.0053
T1	5.2025	39223045.9324	1.3264E-007	1.0000
T2	5.8361	49999769.1479	1.1672E-007	1.0000

Analysis of Variance:

Analysis of Variance:

	DF	SS	MS
Regression	6	5.6973	0.9495
Residual	2	0.0173	0.0087
Total	8	5.7146	0.7143

Corrected for the mean of the observations:

	DF	SS	MS	F	P
Regression	5	1.0831	0.2166	24.9755	0.0389
Residual	2	0.0173	0.0087		
Total	7	1.1005	0.1572		

Appendix XII

Statistical Tests:

Normality Test (Shapiro-Wilk) Passed (P = 0.1205)

W Statistic= 0.8602 Significance Level = 0.0500

Constant Variance Test Passed (P = 0.4597)

iterations=200
stepsize=1
tolerance=1e-10

Number of Iterations Performed = 7

b) Aminosilane

Equation: Piecewise, 3 segment linear
t1 = min(t)
t3 = max(t)
region1(t) = (y1*(T1-t) + y2*(t-t1))/(T1-t1)
region2(t) = (y2*(T2-t) + y3*(t-T1))/(T2-T1)
region3(t) = (y3*(t3-t) + y4*(t-T2))/(t3-T2)
f = if(t <= T1, region1(t), if(t <= T2, region2(t), region3(t)))

Dynamic Fit Options:

Total Number of Fits	200
Maximum Number of Iterations	200

Parameter Ranges for Initial Estimates:

	Minimum	Maximum
y1	-0.2314	0.6942
y2	-0.5595	1.6784
y3	-0.8806	2.6419
y4	-1.2863	3.8590
T1	-3.3333	10.0000
T2	-5.6667	17.0000

Summary of Fit Results:

Converged	98.0%
Singular Solutions	84.5%
Ill-Conditioned Solutions	13.5%
Iterations Exceeding 200	2.0%

Results for the Overall Best-Fit Solution:

R	Rsqr	Adj Rsqr	Standard Error of Estimate
0.9936	0.9872	0.9551	0.0775

	Coefficient	Std. Error	t	P
y1	0.2707	0.0852	3.1762	0.0865
y2	0.7612	13720119.3452	5.5483E-008	1.0000
y3	0.9756	0.6069	1.6076	0.2492
y4	1.2676	0.0707	17.9256	0.0031
T1	5.2056	117629492.3518	4.4254E-008	1.0000
T2	5.7537	4.6259	1.2438	0.3396

Appendix XII

Analysis of Variance:

Analysis of Variance:

	DF	SS	MS
Regression	6	5.3223	0.8871
Residual	2	0.0120	0.0060
Total	8	5.3343	0.6668

Corrected for the mean of the observations:

	DF	SS	MS	F	P
Regression	5	0.9226	0.1845	30.7507	0.0318
Residual	2	0.0120	0.0060		
Total	7	0.9346	0.1335		

Statistical Tests:

Normality Test (Shapiro-Wilk) Failed (P = 0.0211)

W Statistic= 0.7877 Significance Level = 0.0500

Constant Variance Test Passed (P = 0.8849)

iterations=200
stepsize=1
tolerance=1e-10

Number of Iterations Performed = 7

c) HA_4

Equation: Piecewise, 3 segment linear
t1 = min(t)
t3 = max(t)
region1(t) = (y1*(T1-t) + y2*(t-t1))/(T1-t1)
region2(t) = (y2*(T2-t) + y3*(t-T1))/(T2-T1)
region3(t) = (y3*(t3-t) + y4*(t-T2))/(t3-T2)
f = if(t <= T1, region1(t), if(t <= T2, region2(t), region3(t)))

Dynamic Fit Options:

Total Number of Fits	200
Maximum Number of Iterations	200

Parameter Ranges for Initial Estimates:

	Minimum	Maximum
y1	-0.2375	0.7124
y2	-0.5073	1.5218
y3	-0.8167	2.4501
y4	-1.2965	3.8896
T1	-3.3333	10.0000
T2	-5.6667	17.0000

Summary of Fit Results:

Converged	99.5%
Singular Solutions	86.5%
Ill-Conditioned Solutions	13.0%
Iterations Exceeding 200	0.5%

Appendix XII

Results for the Overall Best-Fit Solution:

R	Rsqr	Adj Rsqr	Standard Error of Estimate
0.9865	0.9731	0.9060	0.1153

	Coefficient	Std. Error	t	P
y1	0.3115	0.0981	3.1763	0.0865
y2	0.6214	3575551.6669	1.7378E-007	1.0000
y3	1.0081	8079635.6953	1.2477E-007	1.0000
y4	1.2766	0.1053	12.1250	0.0067
T1	5.0563	46806246.9374	1.0803E-007	1.0000
T2	5.9425	61918844.6003	9.5972E-008	1.0000

Analysis of Variance:

Analysis of Variance:

	DF	SS	MS
Regression	6	5.1106	0.8518
Residual	2	0.0266	0.0133
Total	8	5.1372	0.6422

Corrected for the mean of the observations:

	DF	SS	MS	F	P
Regression	5	0.9640	0.1928	14.4947	0.0658
Residual	2	0.0266	0.0133		
Total	7	0.9906	0.1415		

Statistical Tests:

Normality Test (Shapiro-Wilk) Passed (P = 0.0942)

W Statistic= 0.8495 Significance Level = 0.0500

Constant Variance Test Passed (P = 0.8849)

iterations=200
stepsize=1
tolerance=1e-10

Number of Iterations Performed = 13

d) HA_{234}

Equation: Piecewise, 3 segment linear
t1 = min(t)
t3 = max(t)
region1(t) = (y1*(T1-t) + y2*(t-t1))/(T1-t1)
region2(t) = (y2*(T2-t) + y3*(t-T1))/(T2-T1)
region3(t) = (y3*(t3-t) + y4*(t-T2))/(t3-T2)
f = if(t <= T1, region1(t), if(t <= T2, region2(t), region3(t)))

Dynamic Fit Options:

Total Number of Fits	200
Maximum Number of Iterations	200

Appendix XII

Parameter Ranges for Initial Estimates:

	Minimum	Maximum
y1	-0.2487	0.7461
y2	-0.3270	0.9810
y3	-0.6193	1.8579
y4	-0.6950	2.0849
T1	-3.3333	10.0000
T2	-5.6667	17.0000

Summary of Fit Results:

Converged	98.0%
Singular Solutions	86.5%
Ill-Conditioned Solutions	9.0%
Iterations Exceeding 200	2.0%

Results for the Overall Best-Fit Solution:

R	Rsqr	Adj Rsqr	Standard Error of Estimate
0.9991	0.9981	0.9934	0.0169

	Coefficient	Std. Error	t	P
y1	0.2418	0.0141	17.1059	0.0034
y2	0.3888	0.0226	17.1776	0.0034
y3	0.7715	0.0258	29.8688	0.0011
y4	0.7014	0.0169	41.5106	0.0006
T1	4.4698	0.1958	22.8231	0.0019
T2	6.3172	0.1538	41.0641	0.0006

Analysis of Variance:

Analysis of Variance:

	DF	SS	MS
Regression	6	2.1729	0.3622
Residual	2	0.0006	0.0003
Total	8	2.1735	0.2717

Corrected for the mean of the observations:

	DF	SS	MS	F	P
Regression	5	0.3004	0.0601	210.4517	0.0047
Residual	2	0.0006	0.0003		
Total	7	0.3010	0.0430		

Statistical Tests:

Normality Test (Shapiro-Wilk) Failed (P = 0.0251)

W Statistic= 0.7946 Significance Level = 0.0500

Constant Variance Test Failed (P = 0.0287)
iterations=200
stepsize=1
tolerance=1e-10

Number of Iterations Performed = 8

Appendix XII

e) HA_{2590}

Equation: Piecewise, 3 segment linear
t1 = min(t)
t3 = max(t)
region1(t) = (y1*(T1-t) + y2*(t-t1))/(T1-t1)
region2(t) = (y2*(T2-t) + y3*(t-T1))/(T2-T1)
region3(t) = (y3*(t3-t) + y4*(t-T2))/(t3-T2)
f = if(t <= T1, region1(t), if(t <= T2, region2(t), region3(t)))

Dynamic Fit Options:

Total Number of Fits	200
Maximum Number of Iterations	200

Parameter Ranges for Initial Estimates:

	Minimum	Maximum
y1	-0.2876	0.8629
y2	-0.4060	1.2181
y3	-0.7263	2.1790
y4	-0.7385	2.2154
T1	-3.3333	10.0000
T2	-5.6667	17.0000

Summary of Fit Results:

Converged	96.5%
Singular Solutions	87.5%
Ill-Conditioned Solutions	7.0%
Iterations Exceeding 200	3.5%

Results for the Overall Best-Fit Solution:

R	Rsqr	Adj Rsqr	Standard Error of Estimate
0.9925	0.9851	0.9479	0.0505

	Coefficient	Std. Error	t	P
y1	0.2597	0.0423	6.1451	0.0255
y2	0.5199	0.0900	5.7760	0.0287
y3	0.8340	0.0602	13.8470	0.0052
y4	0.7435	0.0505	14.7206	0.0046
T1	4.7169	0.7051	6.6899	0.0216
T2	6.0000	1.4217	4.2202	0.0518

Analysis of Variance:

Analysis of Variance:

	DF	SS	MS
Regression	6	2.7709	0.4618
Residual	2	0.0051	0.0026
Total	8	2.7760	0.3470

Corrected for the mean of the observations:

	DF	SS	MS	F	P
Regression	5	0.3373	0.0675	26.4483	0.0368
Residual	2	0.0051	0.0026		
Total	7	0.3424	0.0489		

Statistical Tests:

Appendix XII

Normality Test (Shapiro-Wilk) Passed (P = 0.7522)
W Statistic= 0.9541 Significance Level = 0.0500

Constant Variance Test Passed (P = 0.4597)

iterations=200
stepsize=1
tolerance=1e-10

Number of Iterations Performed = 34

e) HA_{mix}

Equation: Piecewise, 3 segment linear
t1 = min(t)
t3 = max(t)
region1(t) = (y1*(T1-t) + y2*(t-t1))/(T1-t1)
region2(t) = (y2*(T2-t) + y3*(t-T1))/(T2-T1)
region3(t) = (y3*(t3-t) + y4*(t-T2))/(t3-T2)
f = if(t <= T1, region1(t), if(t <= T2, region2(t), region3(t)))

Dynamic Fit Options:

Total Number of Fits	200
Maximum Number of Iterations	200

Parameter Ranges for Initial Estimates:

	Minimum	Maximum
y1	-0.2159	0.6477
y2	-0.4069	1.2206
y3	-0.7022	2.1065
y4	-1.2201	3.6604
T1	-3.3333	10.0000
T2	-5.6667	17.0000

Summary of Fit Results:

Converged	98.5%
Singular Solutions	84.0%
Ill-Conditioned Solutions	11.5%
Iterations Exceeding 200	1.5%

Results for the Overall Best-Fit Solution:

R	Rsqr	Adj Rsqr	Standard Error of Estimate
0.9981	0.9962	0.9866	0.0410

	Coefficient	Std. Error	t	P
y1	0.2477	0.0318	7.7924	0.0161
y2	0.5797	0.0704	8.2404	0.0144
y3	1.0477	0.1813	5.7794	0.0287
y4	1.2087	0.0410	29.4567	0.0012
T1	5.4672	0.7176	7.6187	0.0168
T2	6.8159	1.2834	5.3109	0.0337

Analysis of Variance:

Analysis of Variance:

	DF	SS	MS
Regression	6	4.0370	0.6728

Appendix XII

Residual	2	0.0034	0.0017		
Total	8	4.0403	0.5050		

Corrected for the mean of the observations:

	DF	**SS**	**MS**	**F**	**P**
Regression	5	0.8772	0.1754	104.2030	0.0095
Residual	2	0.0034	0.0017		
Total	7	0.8806	0.1258		

Statistical Tests:

Normality Test (Shapiro-Wilk) Passed (P = 0.6022)

W Statistic= 0.9391 Significance Level = 0.0500

Constant Variance Test Passed (P = 0.0716)

iterations=200
stepsize=1
tolerance=1e-10

Number of Iterations Performed = 8

Appendix XII

PNT1A cell line

a) Control

Equation: Piecewise, 3 segment linear
t1 = min(t)
t3 = max(t)
region1(t) = (y1*(T1-t) + y2*(t-t1))/(T1-t1)
region2(t) = (y2*(T2-t) + y3*(t-T1))/(T2-T1)
region3(t) = (y3*(t3-t) + y4*(t-T2))/(t3-T2)
f = if(t <= T1, region1(t), if(t <= T2, region2(t), region3(t)))

Dynamic Fit Options:

Total Number of Fits	200
Maximum Number of Iterations	200

Parameter Ranges for Initial Estimates:

	Minimum	Maximum
y1	-0.2344	0.7033
y2	-0.3912	1.1735
y3	-0.6578	1.9733
y4	-0.6465	1.9395
T1	-3.3333	10.0000
T2	-5.6667	17.0000

Summary of Fit Results:

Converged	95.5%
Singular Solutions	84.5%
Ill-Conditioned Solutions	9.0%
Iterations Exceeding 200	4.5%

Results for the Overall Best-Fit Solution:

R	Rsqr	Adj Rsqr	Standard Error of Estimate
0.9945	0.9891	0.9619	0.0387

	Coefficient	Std. Error	t	P
y1	0.2383	0.0324	7.3521	0.0180
y2	0.5146	316727.6410	1.6249E-006	1.0000
y3	0.7980	6814941.4132	1.1709E-007	1.0000
y4	0.6518	0.0497	13.1172	0.0058
T1	4.9777	4559674.1669	1.0917E-006	1.0000
T2	5.7432	105246534.0202	5.4569E-008	1.0000

Analysis of Variance:

Analysis of Variance:

	DF	SS	MS
Regression	6	2.3158	0.3860
Residual	2	0.0030	0.0015
Total	8	2.3188	0.2898

Corrected for the mean of the observations:

	DF	SS	MS	F	P
Regression	5	0.2727	0.0545	36.3343	0.0270
Residual	2	0.0030	0.0015		
Total	7	0.2757	0.0394		

Appendix XII

Statistical Tests:

Normality Test (Shapiro-Wilk) Passed (P = 0.7722)

W Statistic= 0.9561 Significance Level = 0.0500

Constant Variance Test Passed (P = 0.3533)

iterations=200
stepsize=1
tolerance=1e-10

Number of Iterations Performed = 12

b) Aminosilane

Equation: Piecewise, 3 segment linear
t1 = min(t)
t3 = max(t)
region1(t) = (y1*(T1-t) + y2*(t-t1))/(T1-t1)
region2(t) = (y2*(T2-t) + y3*(t-T1))/(T2-T1)
region3(t) = (y3*(t3-t) + y4*(t-T2))/(t3-T2)
f = if(t <= T1, region1(t), if(t <= T2, region2(t), region3(t)))

Dynamic Fit Options:

Total Number of Fits	200
Maximum Number of Iterations	200

Parameter Ranges for Initial Estimates:

	Minimum	Maximum
y1	-0.2389	0.7167
y2	-0.4095	1.2286
y3	-0.6401	1.9202
y4	-0.6019	1.8057
T1	-3.3333	10.0000
T2	-5.6667	17.0000

Summary of Fit Results:

Converged	96.0%
Singular Solutions	85.5%
Ill-Conditioned Solutions	10.5%
Iterations Exceeding 200	4.0%

Results for the Overall Best-Fit Solution:

R	Rsqr	Adj Rsqr	Standard Error of Estimate
0.9755	0.9516	0.8305	0.0769

	Coefficient	Std. Error	t	P
y1	0.2933	0.0853	3.4369	0.0752
y2	0.5013	4655067.8338	1.0769E-007	1.0000
y3	0.8289	842205.0005	9.8418E-007	1.0000
y4	0.6170	0.0769	8.0221	0.0152
T1	5.1743	93419732.7629	5.5388E-008	1.0000
T2	6.1022	7542336.6478	8.0905E-007	1.0000

Appendix XII

Analysis of Variance:

Analysis of Variance:

	DF	SS	MS
Regression	6	2.3370	0.3895
Residual	2	0.0118	0.0059
Total	8	2.3489	0.2936

Corrected for the mean of the observations:

	DF	SS	MS	F	P
Regression	5	0.2325	0.0465	7.8602	0.1167
Residual	2	0.0118	0.0059		
Total	7	0.2443	0.0349		

Statistical Tests:

Normality Test (Shapiro-Wilk) Passed (P = 0.2191)

W Statistic= 0.8869 Significance Level = 0.0500

Constant Variance Test Failed (P = 0.0018)

iterations=200
stepsize=1
tolerance=1e-10

Number of Iterations Performed = 8

c) HA_4

Equation: Piecewise, 3 segment linear
t1 = min(t)
t3 = max(t)
region1(t) = (y1*(T1-t) + y2*(t-t1))/(T1-t1)
region2(t) = (y2*(T2-t) + y3*(t-T1))/(T2-T1)
region3(t) = (y3*(t3-t) + y4*(t-T2))/(t3-T2)
f = if(t <= T1, region1(t), if(t <= T2, region2(t), region3(t)))

Dynamic Fit Options:

Total Number of Fits	200
Maximum Number of Iterations	200

Parameter Ranges for Initial Estimates:

	Minimum	Maximum
y1	-0.1773	0.5318
y2	-0.2870	0.8609
y3	-0.5034	1.5103
y4	-0.8568	2.5704
T1	-3.3333	10.0000
T2	-5.6667	17.0000

Summary of Fit Results:

Converged	99.5%
Singular Solutions	83.0%
Ill-Conditioned Solutions	14.0%
Iterations Exceeding 200	0.5%

Appendix XII

Results for the Overall Best-Fit Solution:

R	Rsqr	Adj Rsqr	Standard Error of Estimate
0.9978	0.9956	0.9848	0.0301

	Coefficient	Std. Error	t	P
y1	0.1751	0.0233	7.5037	0.0173
y2	0.4582	0.0382	11.9834	0.0069
y3	0.6703	0.0990	6.7693	0.0211
y4	0.8508	0.0301	28.2421	0.0013
T1	5.9039	0.3138	18.8114	0.0028
T2	6.2339	0.7853	7.9386	0.0155

Analysis of Variance:

Analysis of Variance:

	DF	SS	MS
Regression	6	2.0101	0.3350
Residual	2	0.0018	0.0009
Total	8	2.0119	0.2515

Corrected for the mean of the observations:

	DF	SS	MS	F	P
Regression	5	0.4150	0.0830	91.4646	0.0109
Residual	2	0.0018	0.0009		
Total	7	0.4169	0.0596		

Statistical Tests:

Normality Test (Shapiro-Wilk) Passed (P = 0.3639)

W Statistic= 0.9114 Significance Level = 0.0500

Constant Variance Test Failed (P = 0.0474)

iterations=200
stepsize=1
tolerance=1e-10

Number of Iterations Performed = 7

d) HA_{234}

Equation: Piecewise, 3 segment linear
t1 = min(t)
t3 = max(t)
region1(t) = (y1*(T1-t) + y2*(t-t1))/(T1-t1)
region2(t) = (y2*(T2-t) + y3*(t-T1))/(T2-T1)
region3(t) = (y3*(t3-t) + y4*(t-T2))/(t3-T2)
f = if(t <= T1, region1(t), if(t <= T2, region2(t), region3(t)))

Dynamic Fit Options:

Total Number of Fits	200
Maximum Number of Iterations	200

Appendix XII

Parameter Ranges for Initial Estimates:

	Minimum	Maximum
y1	-0.1858	0.5574
y2	-0.2725	0.8174
y3	-0.4570	1.3709
y4	-0.6623	1.9870
T1	-3.3333	10.0000
T2	-5.6667	17.0000

Summary of Fit Results:

Converged	98.5%
Singular Solutions	86.5%
Ill-Conditioned Solutions	10.0%
Iterations Exceeding 200	1.5%

Results for the Overall Best-Fit Solution:

R	Rsqr	Adj Rsqr	Standard Error of Estimate
0.9831	0.9665	0.8826	0.0644

	Coefficient	Std. Error	t	P
y1	0.2224	0.0539	4.1287	0.0540
y2	0.3292	0.0904	3.6399	0.0679
y3	0.6552	0.0985	6.6527	0.0219
y4	0.6666	0.0644	10.3515	0.0092
T1	4.9515	0.5994	8.2614	0.0143
T2	6.5924	0.7581	8.6964	0.0130

Analysis of Variance:

Analysis of Variance:

	DF	SS	MS
Regression	6	1.5619	0.2603
Residual	2	0.0083	0.0041
Total	8	1.5702	0.1963

Corrected for the mean of the observations:

	DF	SS	MS	F	P
Regression	5	0.2390	0.0478	11.5250	0.0818
Residual	2	0.0083	0.0041		
Total	7	0.2473	0.0353		

Statistical Tests:

Normality Test (Shapiro-Wilk) Failed (P = 0.0241)

W Statistic= 0.7930 Significance Level = 0.0500

Constant Variance Test Failed (P = <0.0001)

iterations=200
stepsize=1
tolerance=1e-10

Number of Iterations Performed = 8

Appendix XII

f) HA_{2590}

Equation: Piecewise, 3 segment linear
t1 = min(t)
t3 = max(t)
region1(t) = (y1*(T1-t) + y2*(t-t1))/(T1-t1)
region2(t) = (y2*(T2-t) + y3*(t-T1))/(T2-T1)
region3(t) = (y3*(t3-t) + y4*(t-T2))/(t3-T2)
f = if(t <= T1, region1(t), if(t <= T2, region2(t), region3(t)))

Dynamic Fit Options:

Total Number of Fits	200
Maximum Number of Iterations	200

Parameter Ranges for Initial Estimates:

	Minimum	Maximum
y1	-0.2100	0.6299
y2	-0.2943	0.8829
y3	-0.4265	1.2796
y4	-0.5758	1.7273
T1	-3.3333	10.0000
T2	-5.6667	17.0000

Summary of Fit Results:

Converged	94.0%
Singular Solutions	85.5%
Ill-Conditioned Solutions	8.5%
Iterations Exceeding 200	6.0%

Results for the Overall Best-Fit Solution:

R	Rsqr	Adj Rsqr	Standard Error of Estimate
0.9474	0.8976	0.6416	0.0885

	Coefficient	Std. Error	t	P
y1	0.2380	0.0741	3.2130	0.0847
y2	0.3266	30025.9941	1.0879E-005	1.0000
y3	0.5293	729392.8187	7.2574E-007	1.0000
y4	0.5618	0.0886	6.3419	0.0240
T1	4.9860	1350463.3135	3.6920E-006	1.0000
T2	5.5797	54326371.3029	1.0271E-007	1.0000

Analysis of Variance:

Analysis of Variance:

	DF	SS	MS
Regression	6	1.3095	0.2183
Residual	2	0.0157	0.0078
Total	8	1.3252	0.1656

Corrected for the mean of the observations:

	DF	SS	MS	F	P
Regression	5	0.1374	0.0275	3.5059	0.2367
Residual	2	0.0157	0.0078		
Total	7	0.1531	0.0219		

Appendix XII

Statistical Tests:

Normality Test (Shapiro-Wilk) Passed (P = 0.9570)
W Statistic= 0.9788 Significance Level = 0.0500

Constant Variance Test Passed (P = 0.8849)

iterations=200
stepsize=1
tolerance=1e-10

Number of Iterations Performed = 7

f) HA_{mix}

Equation: Piecewise, 3 segment linear
t1 = min(t)
t3 = max(t)
region1(t) = (y1*(T1-t) + y2*(t-t1))/(T1-t1)
region2(t) = (y2*(T2-t) + y3*(t-T1))/(T2-T1)
region3(t) = (y3*(t3-t) + y4*(t-T2))/(t3-T2)
f = if(t <= T1, region1(t), if(t <= T2, region2(t), region3(t)))

Dynamic Fit Options:

Total Number of Fits	200
Maximum Number of Iterations	200

Parameter Ranges for Initial Estimates:

	Minimum	Maximum
y1	-0.2641	0.7923
y2	-0.3383	1.0150
y3	-0.4316	1.2947
y4	-0.8630	2.5891
T1	-3.3333	10.0000
T2	-5.6667	17.0000

Summary of Fit Results:

Converged	98.5%
Singular Solutions	85.5%
Ill-Conditioned Solutions	11.5%
Iterations Exceeding 200	1.5%

Results for the Overall Best-Fit Solution:

R	Rsqr	Adj Rsqr	Standard Error of Estimate
0.9731	0.9469	0.8140	0.0897

	Coefficient	Std. Error	t	P
y1	0.2925	0.0751	3.8968	0.0600
y2	0.3292	0.0911	3.6133	0.0688
y3	0.5874	0.7487	0.7846	0.5149
y4	0.8845	0.0897	9.8579	0.0101
T1	4.0000	2.2029	1.8158	0.2111
T2	7.1060	8.9429	0.7946	0.5102

Appendix XII

Analysis of Variance:

Analysis of Variance:

	DF	SS	MS
Regression	6	1.9202	0.3200
Residual	2	0.0161	0.0081
Total	8	1.9363	0.2420

Corrected for the mean of the observations:

	DF	SS	MS	F	P
Regression	5	0.2869	0.0574	7.1282	0.1276
Residual	2	0.0161	0.0081		
Total	7	0.3030	0.0433		

Statistical Tests:

Normality Test (Shapiro-Wilk) Passed (P = 0.2192)

W Statistic= 0.8870 Significance Level = 0.0500

Constant Variance Test Failed (P = 0.0212)

iterations=200
stepsize=1
tolerance=1e-10

Number of Iterations Performed = 24

Appendix XII

MTT assay – curve fitting

RT112 cell line

a) Control

Equation: Piecewise, 3 segment linear
t1 = min(t)
t3 = max(t)
region1(t) = (y1*(T1-t) + y2*(t-t1))/(T1-t1)
region2(t) = (y2*(T2-t) + y3*(t-T1))/(T2-T1)
region3(t) = (y3*(t3-t) + y4*(t-T2))/(t3-T2)
f = if(t <= T1, region1(t), if(t <= T2, region2(t), region3(t)))

Dynamic Fit Options:

Total Number of Fits	200
Maximum Number of Iterations	200

Parameter Ranges for Initial Estimates:

	Minimum	Maximum
y1	-0.1480	0.4441
y2	-0.5120	1.5360
y3	-0.8605	2.5816
y4	-1.0287	3.0860
T1	-3.3333	10.0000
T2	-5.6667	17.0000

Summary of Fit Results:

Converged	99.5%
Singular Solutions	84.0%
Ill-Conditioned Solutions	14.0%
Iterations Exceeding 200	0.5%

Results for the Overall Best-Fit Solution:

R	Rsqr	Adj Rsqr	Standard Error of Estimate
0.9993	0.9985	0.9948	0.0238

	Coefficient	Std. Error	t	P
y1	0.1511	0.0238	6.3387	0.0240
y2	0.2303	1122127.9199	2.0527E-007	1.0000
y3	0.7876	0.0526	14.9641	0.0044
y4	1.0248	0.0199	51.3911	0.0004
T1	1.9138	5789797.4524	3.3055E-007	1.0000
T2	4.7891	0.5599	8.5538	0.0134

Analysis of Variance:

Analysis of Variance:

	DF	SS	MS
Regression	6	4.0499	0.6750
Residual	2	0.0011	0.0006
Total	8	4.0510	0.5064

Appendix XII

Corrected for the mean of the observations:

	DF	SS	MS	F	P
Regression	5	0.7607	0.1521	267.8172	0.0037
Residual	2	0.0011	0.0006		
Total	7	0.7619	0.1088		

Statistical Tests:

Normality Test (Shapiro-Wilk) Passed (P = 0.2004)

W Statistic= 0.8828 Significance Level = 0.0500

Constant Variance Test Passed (P = 0.7941)

iterations=200
stepsize=1
tolerance=1e-10

Number of Iterations Performed = 14

a) Aminosilane

Equation: Piecewise, 3 segment linear
t1 = min(t)
t3 = max(t)
region1(t) = (y1*(T1-t) + y2*(t-t1))/(T1-t1)
region2(t) = (y2*(T2-t) + y3*(t-T1))/(T2-T1)
region3(t) = (y3*(t3-t) + y4*(t-T2))/(t3-T2)
f = if(t <= T1, region1(t), if(t <= T2, region2(t), region3(t)))

Dynamic Fit Options:

Total Number of Fits	200
Maximum Number of Iterations	200

Parameter Ranges for Initial Estimates:

	Minimum	Maximum
y1	-0.1739	0.5217
y2	-0.5183	1.5549
y3	-0.9808	2.9425
y4	-1.0049	3.0148
T1	-3.3333	10.0000
T2	-5.6667	17.0000

Summary of Fit Results:

Converged	99.0%
Singular Solutions	87.0%
Ill-Conditioned Solutions	11.0%
Iterations Exceeding 200	1.0%

Results for the Overall Best-Fit Solution:

R	Rsqr	Adj Rsqr	Standard Error of Estimate
0.9966	0.9932	0.9763	0.0557

Appendix XII

	Coefficient	Std. Error	t	P
y1	0.1743	0.0479	3.6363	0.0680
y2	0.6310	2366771.1322	2.6660E-007	1.0000
y3	1.1095	349170.1357	3.1775E-006	1.0000
y4	1.0169	0.0511	19.9019	0.0025
T1	4.2233	16704407.3780	2.5283E-007	1.0000
T2	5.8293	8182604.2214	7.1240E-007	1.0000

Analysis of Variance:

Analysis of Variance:

	DF	SS	MS
Regression	6	4.8140	0.8023
Residual	2	0.0062	0.0031
Total	8	4.8202	0.6025

Corrected for the mean of the observations:

	DF	SS	MS	F	P
Regression	5	0.9105	0.1821	58.6115	0.0169
Residual	2	0.0062	0.0031		
Total	7	0.9167	0.1310		

Statistical Tests:

Normality Test (Shapiro-Wilk) Failed (P = 0.0386)

W Statistic= 0.8122 Significance Level = 0.0500

Constant Variance Test Passed (P = 0.6194)

iterations=200
stepsize=1
tolerance=1e-10

Number of Iterations Performed = 7

c) HA_4

Equation: Piecewise, 3 segment linear
t1 = min(t)
t3 = max(t)
region1(t) = (y1*(T1-t) + y2*(t-t1))/(T1-t1)
region2(t) = (y2*(T2-t) + y3*(t-T1))/(T2-T1)
region3(t) = (y3*(t3-t) + y4*(t-T2))/(t3-T2)
f = if(t <= T1, region1(t), if(t <= T2, region2(t), region3(t)))

Dynamic Fit Options:

Total Number of Fits	200
Maximum Number of Iterations	200

Appendix XII

Parameter Ranges for Initial Estimates:

	Minimum	Maximum
y1	-0.2154	0.6461
y2	-0.3616	1.0847
y3	-0.7646	2.2938
y4	-1.0334	3.1002
T1	-3.3333	10.0000
T2	-5.6667	17.0000

Summary of Fit Results:

Converged	96.5%
Singular Solutions	84.5%
Ill-Conditioned Solutions	12.0%
Iterations Exceeding 200	3.5%

Results for the Overall Best-Fit Solution:

R	Rsqr	Adj Rsqr	Standard Error of Estimate
0.9928	0.9857	0.9498	0.0756

	Coefficient	Std. Error	t	P
y1	0.2184	0.0633	3.4511	0.0747
y2	0.4012	0.1303	3.0798	0.0912
y3	0.8884	0.1321	6.7248	0.0214
y4	1.0219	0.0690	14.8019	0.0045
T1	4.3980	1.8303	2.4029	0.1382
T2	5.6131	1.7918	3.1326	0.0886

Analysis of Variance:

Analysis of Variance:

	DF	SS	MS
Regression	6	3.5909	0.5985
Residual	2	0.0114	0.0057
Total	8	3.6024	0.4503

Corrected for the mean of the observations:

	DF	SS	MS	F	P
Regression	5	0.7861	0.1572	27.4868	0.0355
Residual	2	0.0114	0.0057		
Total	7	0.7976	0.1139		

Statistical Tests:

Normality Test (Shapiro-Wilk) Passed (P = 0.2755)

W Statistic= 0.8977 Significance Level = 0.0500

Constant Variance Test Passed (P = 0.0716)

iterations=200
stepsize=1
tolerance=1e-10

Number of Iterations Performed = 10

Appendix XII

d) HA_{234}

Equation: Piecewise, 3 segment linear
t1 = min(t)
t3 = max(t)
region1(t) = (y1*(T1-t) + y2*(t-t1))/(T1-t1)
region2(t) = (y2*(T2-t) + y3*(t-T1))/(T2-T1)
region3(t) = (y3*(t3-t) + y4*(t-T2))/(t3-T2)
f = if(t <= T1, region1(t), if(t <= T2, region2(t), region3(t)))

Dynamic Fit Options:

Total Number of Fits	200
Maximum Number of Iterations	200

Parameter Ranges for Initial Estimates:

	Minimum	Maximum
y1	-0.1999	0.5998
y2	-0.3850	1.1549
y3	-0.6236	1.8708
y4	-0.7292	2.1877
T1	-3.3333	10.0000
T2	-5.6667	17.0000

Summary of Fit Results:

Converged	97.5%
Singular Solutions	85.5%
Ill-Conditioned Solutions	11.0%
Iterations Exceeding 200	2.5%

Results for the Overall Best-Fit Solution:

R	Rsqr	Adj Rsqr	Standard Error of Estimate
0.9977	0.9954	0.9838	0.0263

	Coefficient	Std. Error	t	P
y1	0.2055	0.0267	7.6902	0.0165
y2	0.4382	2444164.8645	1.7927E-007	1.0000
y3	0.6685	473366.0928	1.4122E-006	1.0000
y4	0.7344	0.0257	28.5381	0.0012
T1	4.1877	33490886.8464	1.2504E-007	1.0000
T2	5.6276	17027556.4370	3.3050E-007	1.0000

Analysis of Variance:

Analysis of Variance:

	DF	SS	MS
Regression	6	2.2458	0.3743
Residual	2	0.0014	0.0007
Total	8	2.2472	0.2809

Appendix XII

Corrected for the mean of the observations:

	DF	SS	MS	F	P
Regression	5	0.2975	0.0595	86.0265	0.0115
Residual	2	0.0014	0.0007		
Total	7	0.2989	0.0427		

Statistical Tests:

Normality Test (Shapiro-Wilk) Passed (P = 0.0547)

W Statistic= 0.8266 Significance Level = 0.0500

Constant Variance Test Passed (P = 0.1020)

iterations=200
stepsize=1
tolerance=1e-10

Number of Iterations Performed = 7

e) HA_{2590}

Equation: Piecewise, 3 segment linear
t1 = min(t)
t3 = max(t)
region1(t) = (y1*(T1-t) + y2*(t-t1))/(T1-t1)
region2(t) = (y2*(T2-t) + y3*(t-T1))/(T2-T1)
region3(t) = (y3*(t3-t) + y4*(t-T2))/(t3-T2)
f = if(t <= T1, region1(t), if(t <= T2, region2(t), region3(t)))

Dynamic Fit Options:

Total Number of Fits	200
Maximum Number of Iterations	200

Parameter Ranges for Initial Estimates:

	Minimum	Maximum
y1	-0.1773	0.5320
y2	-0.4204	1.2613
y3	-0.6064	1.8191
y4	-0.6155	1.8464
T1	-3.3333	10.0000
T2	-5.6667	17.0000

Summary of Fit Results:

Converged	99.0%
Singular Solutions	86.0%
Ill-Conditioned Solutions	10.0%
Iterations Exceeding 200	1.0%

Results for the Overall Best-Fit Solution:

R	Rsqr	Adj Rsqr	Standard Error of Estimate
0.9959	0.9918	0.9713	0.0297

Appendix XII

	Coefficient	Std. Error	t	P
y1	0.1744	0.0318	5.4814	0.0317
y2	0.2970	1057265.3717	2.8089E-007	1.0000
y3	0.6496	0.0566	11.4844	0.0075
y4	0.6190	0.0297	20.8617	0.0023
T1	1.9614	12109909.9548	1.6197E-007	1.0000
T2	6.0000	0.6862	8.7433	0.0128

Analysis of Variance:

Analysis of Variance:

	DF	SS	MS
Regression	6	2.0193	0.3366
Residual	2	0.0018	0.0009
Total	8	2.0211	0.2526

Corrected for the mean of the observations:

	DF	SS	MS	F	P
Regression	5	0.2128	0.0426	48.3365	0.0204
Residual	2	0.0018	0.0009		
Total	7	0.2145	0.0306		

Statistical Tests:

Normality Test (Shapiro-Wilk) Passed (P = 0.4130)

W Statistic= 0.9179 Significance Level = 0.0500

Constant Variance Test Failed (P = 0.0212)

iterations=200
stepsize=1
tolerance=1e-10

Number of Iterations Performed = 26

f) HA_{mix}

Equation: Piecewise, 3 segment linear
t1 = min(t)
t3 = max(t)
region1(t) = (y1*(T1-t) + y2*(t-t1))/(T1-t1)
region2(t) = (y2*(T2-t) + y3*(t-T1))/(T2-T1)
region3(t) = (y3*(t3-t) + y4*(t-T2))/(t3-T2)
f = if(t <= T1, region1(t), if(t <= T2, region2(t), region3(t)))

Dynamic Fit Options:

Total Number of Fits	200
Maximum Number of Iterations	200

Appendix XII

Parameter Ranges for Initial Estimates:

	Minimum	Maximum
y1	-0.1813	0.5440
y2	-0.4482	1.3445
y3	-0.7642	2.2926
y4	-0.9773	2.9320
T1	-3.3333	10.0000
T2	-5.6667	17.0000

Summary of Fit Results:

Converged	99.0%
Singular Solutions	85.0%
Ill-Conditioned Solutions	10.5%
Iterations Exceeding 200	1.0%

Results for the Overall Best-Fit Solution:

R	Rsqr	Adj Rsqr	Standard Error of Estimate
0.9992	0.9983	0.9942	0.0225

	Coefficient	Std. Error	t	P
y1	0.1815	0.0225	8.0686	0.0150
y2	0.3437	0.1058	3.2492	0.0831
y3	0.6398	0.0807	7.9254	0.0156
y4	0.9899	0.0188	52.5960	0.0004
T1	2.7138	0.7283	3.7264	0.0651
T2	4.5086	0.6578	6.8537	0.0206

Analysis of Variance:

Analysis of Variance:

	DF	SS	MS
Regression	6	3.4403	0.5734
Residual	2	0.0010	0.0005
Total	8	3.4413	0.4302

Corrected for the mean of the observations:

	DF	SS	MS	F	P
Regression	5	0.6052	0.1210	239.1890	0.0042
Residual	2	0.0010	0.0005		
Total	7	0.6062	0.0866		

Statistical Tests:

Normality Test (Shapiro-Wilk) Failed (P = 0.0236)

W Statistic= 0.7922 Significance Level = 0.0500

Constant Variance Test Failed (P = 0.0149)

iterations=200
stepsize=1
tolerance=1e-10

Number of Iterations Performed = 17

Appendix XII

T24 cell line

a) Control

Equation: Piecewise, 3 segment linear
t1 = min(t)
t3 = max(t)
region1(t) = (y1*(T1-t) + y2*(t-t1))/(T1-t1)
region2(t) = (y2*(T2-t) + y3*(t-T1))/(T2-T1)
region3(t) = (y3*(t3-t) + y4*(t-T2))/(t3-T2)
f = if(t <= T1, region1(t), if(t <= T2, region2(t), region3(t)))

Dynamic Fit Options:

Total Number of Fits	200
Maximum Number of Iterations	200

Parameter Ranges for Initial Estimates:

	Minimum	Maximum
y1	-0.2512	0.7537
y2	-0.2884	0.8653
y3	-0.6116	1.8349
y4	-0.8267	2.4800
T1	-3.3333	10.0000
T2	-5.6667	17.0000

Summary of Fit Results:

Converged	97.5%
Singular Solutions	85.0%
Ill-Conditioned Solutions	12.5%
Iterations Exceeding 200	2.5%

Results for the Overall Best-Fit Solution:

R	Rsqr	Adj Rsqr	Standard Error of Estimate
0.9990	0.9981	0.9932	0.0212

	Coefficient	Std. Error	t	P
y1	0.2508	0.0177	14.1584	0.0050
y2	0.3668	0.0271	13.5129	0.0054
y3	0.9076	835110.5664	1.0868E-006	1.0000
y4	0.8168	0.0212	38.5730	0.0007
T1	4.6790	0.1662	28.1499	0.0013
T2	7.0370	3640944.1371	1.9327E-006	1.0000

Analysis of Variance:

Analysis of Variance:

	DF	SS	MS
Regression	6	2.4786	0.4131
Residual	2	0.0009	0.0004
Total	8	2.4795	0.3099

Appendix XII

Corrected for the mean of the observations:

	DF	SS	MS	F	P
Regression	5	0.4600	0.0920	205.1691	0.0049
Residual	2	0.0009	0.0004		
Total	7	0.4609	0.0658		

Statistical Tests:

Normality Test (Shapiro-Wilk) Passed (P = 0.5163)

W Statistic= 0.9300 Significance Level = 0.0500

Constant Variance Test Passed (P = 0.2327)

iterations=200
stepsize=1
tolerance=1e-10

Number of Iterations Performed = 8

b) Aminosilane

Equation: Piecewise, 3 segment linear
t1 = min(t)
t3 = max(t)
region1(t) = (y1*(T1-t) + y2*(t-t1))/(T1-t1)
region2(t) = (y2*(T2-t) + y3*(t-T1))/(T2-T1)
region3(t) = (y3*(t3-t) + y4*(t-T2))/(t3-T2)
f = if(t <= T1, region1(t), if(t <= T2, region2(t), region3(t)))

Dynamic Fit Options:

Total Number of Fits	200
Maximum Number of Iterations	200

Parameter Ranges for Initial Estimates:

	Minimum	Maximum
y1	-0.1977	0.5932
y2	-0.2309	0.6927
y3	-0.5873	1.7618
y4	-0.8837	2.6512
T1	-3.3333	10.0000
T2	-5.6667	17.0000

Summary of Fit Results:

Converged	98.0%
Singular Solutions	84.5%
Ill-Conditioned Solutions	13.5%
Iterations Exceeding 200	2.0%

Results for the Overall Best-Fit Solution:

R	Rsqr	Adj Rsqr	Standard Error of Estimate
0.9996	0.9992	0.9972	0.0159

Appendix XII

	Coefficient	Std. Error	t	P
y1	0.2130	0.0133	15.9829	0.0039
y2	0.2795	0.0175	15.9328	0.0039
y3	0.9315	1027237.4394	9.0681E-007	1.0000
y4	0.8771	0.0159	55.0726	0.0003
T1	4.4743	0.1075	41.6339	0.0006
T2	7.0324	4030500.2338	1.7448E-006	1.0000

Analysis of Variance:

Analysis of Variance:

	DF	SS	MS
Regression	6	2.4749	0.4125
Residual	2	0.0005	0.0003
Total	8	2.4754	0.3094

Corrected for the mean of the observations:

	DF	SS	MS	F	P
Regression	5	0.6230	0.1246	491.2757	0.0020
Residual	2	0.0005	0.0003		
Total	7	0.6235	0.0891		

Statistical Tests:

Normality Test (Shapiro-Wilk) Passed (P = 0.3717)

W Statistic= 0.9125 Significance Level = 0.0500

Constant Variance Test Passed (P = 0.2897)

iterations=200
stepsize=1
tolerance=1e-10

Number of Iterations Performed = 8

c) HA_4

Equation: Piecewise, 3 segment linear
t1 = min(t)
t3 = max(t)
region1(t) = (y1*(T1-t) + y2*(t-t1))/(T1-t1)
region2(t) = (y2*(T2-t) + y3*(t-T1))/(T2-T1)
region3(t) = (y3*(t3-t) + y4*(t-T2))/(t3-T2)
f = if(t <= T1, region1(t), if(t <= T2, region2(t), region3(t)))

Dynamic Fit Options:

Total Number of Fits	200
Maximum Number of Iterations	200

Appendix XII

Parameter Ranges for Initial Estimates:

	Minimum	Maximum
y1	-0.2049	0.6148
y2	-0.2475	0.7426
y3	-0.5925	1.7774
y4	-0.9823	2.9470
T1	-3.3333	10.0000
T2	-5.6667	17.0000

Summary of Fit Results:

Converged	95.5%
Singular Solutions	75.0%
Ill-Conditioned Solutions	18.0%
Iterations Exceeding 200	4.5%

Results for the Overall Best-Fit Solution:

R	Rsqr	Adj Rsqr	Standard Error of Estimate
0.9964	0.9929	0.9751	0.0496

	Coefficient	Std. Error	t	P
y1	0.1926	0.0415	4.6428	0.0434
y2	0.3377	0.0654	5.1664	0.0355
y3	0.8143	0.1373	5.9304	0.0273
y4	0.9842	0.0496	19.8474	0.0025
T1	4.7934	0.3141	15.2589	0.0043
T2	6.3694	0.5631	11.3107	0.0077

Analysis of Variance:

Analysis of Variance:

	DF	SS	MS
Regression	6	2.6540	0.4423
Residual	2	0.0049	0.0025
Total	8	2.6589	0.3324

Corrected for the mean of the observations:

	DF	SS	MS	F	P
Regression	5	0.6870	0.1374	55.8826	0.0177
Residual	2	0.0049	0.0025		
Total	7	0.6919	0.0988		

Statistical Tests:

Normality Test (Shapiro-Wilk) Failed (P = 0.0234)

W Statistic= 0.7918 Significance Level = 0.0500

Constant Variance Test Passed (P = 0.0860)

iterations=200
stepsize=1
tolerance=1e-10

Number of Iterations Performed = 8

Appendix XII

d) HA_{234}

Equation: Piecewise, 3 segment linear

t1 = min(t)
t3 = max(t)
region1(t) = (y1*(T1-t) + y2*(t-t1))/(T1-t1)
region2(t) = (y2*(T2-t) + y3*(t-T1))/(T2-T1)
region3(t) = (y3*(t3-t) + y4*(t-T2))/(t3-T2)
f = if(t <= T1, region1(t), if(t <= T2, region2(t), region3(t)))

Dynamic Fit Options:

Total Number of Fits	200
Maximum Number of Iterations	200

Parameter Ranges for Initial Estimates:

	Minimum	Maximum
y1	-0.2208	0.6623
y2	-0.2710	0.8130
y3	-0.4547	1.3642
y4	-0.7793	2.3378
T1	-3.3333	10.0000
T2	-5.6667	17.0000

Summary of Fit Results:

Converged	98.0%
Singular Solutions	84.0%
Ill-Conditioned Solutions	10.5%
Iterations Exceeding 200	2.0%

Results for the Overall Best-Fit Solution:

R	Rsqr	Adj Rsqr	Standard Error of Estimate
0.9938	0.9875	0.9564	0.0432

	Coefficient	Std. Error	t	P
y1	0.2234	0.0422	5.2960	0.0339
y2	0.2555	0.1356	1.8845	0.2002
y3	0.3701	0.0839	4.4102	0.0478
y4	0.7785	0.0394	19.7346	0.0026
T1	3.0000	3.3914	0.8846	0.4697
T2	5.0517	0.9369	5.3917	0.0327

Analysis of Variance:

Analysis of Variance:

	DF	SS	MS
Regression	6	1.6702	0.2784
Residual	2	0.0037	0.0019
Total	8	1.6739	0.2092

Corrected for the mean of the observations:

	DF	SS	MS	F	P
Regression	5	0.2961	0.0592	31.7120	0.0309
Residual	2	0.0037	0.0019		
Total	7	0.2998	0.0428		

Appendix XII

Statistical Tests:

Normality Test (Shapiro-Wilk) Passed (P = 0.1102)

W Statistic= 0.8563 Significance Level = 0.0500

Constant Variance Test Passed (P = 0.4228)

iterations=200
stepsize=1
tolerance=1e-10
Number of Iterations Performed = 88

e) HA_{2590}

Equation: Piecewise, 3 segment linear
t1 = min(t)
t3 = max(t)
region1(t) = (y1*(T1-t) + y2*(t-t1))/(T1-t1)
region2(t) = (y2*(T2-t) + y3*(t-T1))/(T2-T1)
region3(t) = (y3*(t3-t) + y4*(t-T2))/(t3-T2)
f = if(t <= T1, region1(t), if(t <= T2, region2(t), region3(t)))

Dynamic Fit Options:
Total Number of Fits 200
Maximum Number of Iterations

Parameter Ranges for Initial Estimates:

	Minimum	Maximum
y1	-0.2300	0.6901
y2	-0.2652	0.7956
y3	-0.4074	1.2222
y4	-0.6657	1.9971
T1	-3.3333	10.0000
T2	-5.6667	17.0000

Summary of Fit Results:

Converged	97.5%
Singular Solutions	83.0%
Ill-Conditioned Solutions	10.5%
Iterations Exceeding 200	2.5%

Results for the Overall Best-Fit Solution:

R	Rsqr	Adj Rsqr	Standard Error of Estimate
0.9936	0.9872	0.9550	0.0343

	Coefficient	Std. Error	t	P
y1	0.2326	0.0318	7.3083	0.0182
y2	0.2507	0.0604	4.1536	0.0534
y3	0.3754	0.0973	3.8568	0.0611
y4	0.6704	0.0313	21.4053	0.0022
T1	3.0000	2.4673	1.2159	0.3481
T2	5.5378	0.9665	5.7296	0.0291

Analysis of Variance:

Analysis of Variance:

Appendix XII

	DF	SS	MS
Regression	6	1.3253	0.2209
Residual	2	0.0024	0.0012
Total	8	1.3277	0.1660

Corrected for the mean of the observations:

	DF	SS	MS	F	P
Regression	5	0.1809	0.0362	30.7336	0.0318
Residual	2	0.0024	0.0012		
Total	7	0.1833	0.0262		

Statistical Tests:

Normality Test (Shapiro-Wilk) Passed (P = 0.1176)

W Statistic= 0.8591 Significance Level = 0.0500

Constant Variance Test Passed (P = 0.2897)

iterations=200
stepsize=1
tolerance=1e-10
Number of Iterations Performed = 22

e) HA_{mix}

Equation: Piecewise, 3 segment linear

t1 = min(t)
t3 = max(t)
region1(t) = (y1*(T1-t) + y2*(t-t1))/(T1-t1)
region2(t) = (y2*(T2-t) + y3*(t-T1))/(T2-T1)
region3(t) = (y3*(t3-t) + y4*(t-T2))/(t3-T2)
f = if(t <= T1, region1(t), if(t <= T2, region2(t), region3(t)))

Dynamic Fit Options:

Total Number of Fits	200
Maximum Number of Iterations	200

Parameter Ranges for Initial Estimates:

	Minimum	Maximum
y1	-0.2690	0.8071
y2	-0.2425	0.7274
y3	-0.5712	1.7136
y4	-0.9628	2.8884
T1	-3.3333	10.0000
T2	-5.6667	17.0000

Summary of Fit Results:

Converged	98.5%
Singular Solutions	83.0%
Ill-Conditioned Solutions	14.0%
Iterations Exceeding 200	1.5%

Results for the Overall Best-Fit Solution:

Appendix XII

R	Rsqr	Adj Rsqr	Standard Error of Estimate
0.9955	0.9910	0.9685	0.0534

	Coefficient	Std. Error	t	P
y1	0.2414	0.0414	5.8368	0.0281
y2	0.3747	321682.6360	1.1647E-006	1.0000
y3	0.9633	262022.6307	3.6763E-006	1.0000
y4	0.9451	0.0561	16.8505	0.0035
T1	5.4587	10764125.5337	5.0712E-007	1.0000
T2	6.8974	15900716.8503	4.3378E-007	1.0000

Analysis of Variance:

Analysis of Variance:

	DF	SS	MS
Regression	6	2.6358	0.4393
Residual	2	0.0057	0.0029
Total	8	2.6415	0.3302

Corrected for the mean of the observations:

	DF	SS	MS	F	P
Regression	5	0.6270	0.1254	43.9847	0.0224
Residual	2	0.0057	0.0029		
Total	7	0.6327	0.0904		

Statistical Tests:

Normality Test (Shapiro-Wilk) Passed (P = 0.3582)

W Statistic= 0.9106 Significance Level = 0.0500

Constant Variance Test Failed (P = 0.0053)

iterations=200
stepsize=1
tolerance=1e-10

Number of Iterations Performed = 7

Appendix XII

PC3 cell line

a) Control

Equation: Piecewise, 3 segment linear
t1 = min(t)
t3 = max(t)
region1(t) = (y1*(T1-t) + y2*(t-t1))/(T1-t1)
region2(t) = (y2*(T2-t) + y3*(t-T1))/(T2-T1)
region3(t) = (y3*(t3-t) + y4*(t-T2))/(t3-T2)
f = if(t <= T1, region1(t), if(t <= T2, region2(t), region3(t)))

Dynamic Fit Options:

Total Number of Fits	200
Maximum Number of Iterations	200

Parameter Ranges for Initial Estimates:

	Minimum	Maximum
y1	-0.2167	0.6501
y2	-0.5369	1.6106
y3	-0.9161	2.7482
y4	-1.3014	3.9042
T1	-3.3333	10.0000
T2	-5.6667	17.0000

Summary of Fit Results:

Converged	96.0%
Singular Solutions	85.0%
Ill-Conditioned Solutions	11.0%
Iterations Exceeding 200	4.0%

Results for the Overall Best-Fit Solution:

R	Rsqr	Adj Rsqr	Standard Error of Estimate
0.9921	0.9842	0.9448	0.0931

	Coefficient	Std. Error	t	P
y1	0.2796	0.0735	3.8032	0.0627
y2	0.7262	4168008.6997	1.7423E-007	1.0000
y3	1.0963	4666853.6247	2.3492E-007	1.0000
y4	1.2983	0.0950	13.6646	0.0053
T1	5.2025	39223045.9324	1.3264E-007	1.0000
T2	5.8361	49999769.1479	1.1672E-007	1.0000

Analysis of Variance:

Analysis of Variance:

	DF	SS	MS
Regression	6	5.6973	0.9495
Residual	2	0.0173	0.0087
Total	8	5.7146	0.7143

Corrected for the mean of the observations:

	DF	SS	MS	F	P
Regression	5	1.0831	0.2166	24.9755	0.0389
Residual	2	0.0173	0.0087		
Total	7	1.1005	0.1572		

Appendix XII

Statistical Tests:

Normality Test (Shapiro-Wilk) Passed (P = 0.1205)

W Statistic= 0.8602 Significance Level = 0.0500

Constant Variance Test Passed (P = 0.4597)

iterations=200
stepsize=1
tolerance=1e-10

Number of Iterations Performed = 7

b) Aminosilane

Equation: Piecewise, 3 segment linear
t1 = min(t)
t3 = max(t)
region1(t) = (y1*(T1-t) + y2*(t-t1))/(T1-t1)
region2(t) = (y2*(T2-t) + y3*(t-T1))/(T2-T1)
region3(t) = (y3*(t3-t) + y4*(t-T2))/(t3-T2)
f = if(t <= T1, region1(t), if(t <= T2, region2(t), region3(t)))

Dynamic Fit Options:

Total Number of Fits	200
Maximum Number of Iterations	200

Parameter Ranges for Initial Estimates:

	Minimum	Maximum
y1	-0.2314	0.6942
y2	-0.5595	1.6784
y3	-0.8806	2.6419
y4	-1.2863	3.8590
T1	-3.3333	10.0000
T2	-5.6667	17.0000

Summary of Fit Results:

Converged	98.0%
Singular Solutions	84.5%
Ill-Conditioned Solutions	13.5%
Iterations Exceeding 200	2.0%

Results for the Overall Best-Fit Solution:

R	Rsqr	Adj Rsqr	Standard Error of Estimate
0.9936	0.9872	0.9551	0.0775

	Coefficient	Std. Error	t	P
y1	0.2707	0.0852	3.1762	0.0865
y2	0.7612	13720119.3452	5.5483E-008	1.0000
y3	0.9756	0.6069	1.6076	0.2492
y4	1.2676	0.0707	17.9256	0.0031
T1	5.2056	117629492.3518	4.4254E-008	1.0000
T2	5.7537	4.6259	1.2438	0.3396

Appendix XII

Analysis of Variance:

Analysis of Variance:

	DF	SS	MS
Regression	6	5.3223	0.8871
Residual	2	0.0120	0.0060
Total	8	5.3343	0.6668

Corrected for the mean of the observations:

	DF	SS	MS	F	P
Regression	5	0.9226	0.1845	30.7507	0.0318
Residual	2	0.0120	0.0060		
Total	7	0.9346	0.1335		

Statistical Tests:

Normality Test (Shapiro-Wilk) Failed (P = 0.0211)

W Statistic= 0.7877 Significance Level = 0.0500

Constant Variance Test Passed (P = 0.8849)

iterations=200
stepsize=1
tolerance=1e-10

Number of Iterations Performed = 7

c) HA_4

Equation: Piecewise, 3 segment linear
t1 = min(t)
t3 = max(t)
region1(t) = (y1*(T1-t) + y2*(t-t1))/(T1-t1)
region2(t) = (y2*(T2-t) + y3*(t-T1))/(T2-T1)
region3(t) = (y3*(t3-t) + y4*(t-T2))/(t3-T2)
f = if(t <= T1, region1(t), if(t <= T2, region2(t), region3(t)))

Dynamic Fit Options:

Total Number of Fits	200
Maximum Number of Iterations	200

Parameter Ranges for Initial Estimates:

	Minimum	Maximum
y1	-0.2375	0.7124
y2	-0.5073	1.5218
y3	-0.8167	2.4501
y4	-1.2965	3.8896
T1	-3.3333	10.0000
T2	-5.6667	17.0000

Summary of Fit Results:

Converged	99.5%
Singular Solutions	86.5%
Ill-Conditioned Solutions	13.0%
Iterations Exceeding 200	0.5%

Appendix XII

Results for the Overall Best-Fit Solution:

R	Rsqr	Adj Rsqr	Standard Error of Estimate
0.9865	0.9731	0.9060	0.1153

	Coefficient	Std. Error	t	P
y1	0.3115	0.0981	3.1763	0.0865
y2	0.6214	3575551.6669	1.7378E-007	1.0000
y3	1.0081	8079635.6953	1.2477E-007	1.0000
y4	1.2766	0.1053	12.1250	0.0067
T1	5.0563	46806246.9374	1.0803E-007	1.0000
T2	5.9425	61918844.6003	9.5972E-008	1.0000

Analysis of Variance:

Analysis of Variance:

	DF	SS	MS
Regression	6	5.1106	0.8518
Residual	2	0.0266	0.0133
Total	8	5.1372	0.6422

Corrected for the mean of the observations:

	DF	SS	MS	F	P
Regression	5	0.9640	0.1928	14.4947	0.0658
Residual	2	0.0266	0.0133		
Total	7	0.9906	0.1415		

Statistical Tests:

Normality Test (Shapiro-Wilk) Passed (P = 0.0942)

W Statistic= 0.8495 Significance Level = 0.0500

Constant Variance Test Passed (P = 0.8849)

iterations=200
stepsize=1
tolerance=1e-10

Number of Iterations Performed = 13

d) HA_{234}

Equation: Piecewise, 3 segment linear
t1 = min(t)
t3 = max(t)
region1(t) = (y1*(T1-t) + y2*(t-t1))/(T1-t1)
region2(t) = (y2*(T2-t) + y3*(t-T1))/(T2-T1)
region3(t) = (y3*(t3-t) + y4*(t-T2))/(t3-T2)
f = if(t <= T1, region1(t), if(t <= T2, region2(t), region3(t)))

Dynamic Fit Options:

Total Number of Fits	200
Maximum Number of Iterations	200

Appendix XII

Parameter Ranges for Initial Estimates:

	Minimum	Maximum
y1	-0.2487	0.7461
y2	-0.3270	0.9810
y3	-0.6193	1.8579
y4	-0.6950	2.0849
T1	-3.3333	10.0000
T2	-5.6667	17.0000

Summary of Fit Results:

Converged	98.0%
Singular Solutions	86.5%
Ill-Conditioned Solutions	9.0%
Iterations Exceeding 200	2.0%

Results for the Overall Best-Fit Solution:

R	Rsqr	Adj Rsqr	Standard Error of Estimate
0.9991	0.9981	0.9934	0.0169

	Coefficient	Std. Error	t	P
y1	0.2418	0.0141	17.1059	0.0034
y2	0.3888	0.0226	17.1776	0.0034
y3	0.7715	0.0258	29.8688	0.0011
y4	0.7014	0.0169	41.5106	0.0006
T1	4.4698	0.1958	22.8231	0.0019
T2	6.3172	0.1538	41.0641	0.0006

Analysis of Variance:

Analysis of Variance:

	DF	SS	MS
Regression	6	2.1729	0.3622
Residual	2	0.0006	0.0003
Total	8	2.1735	0.2717

Corrected for the mean of the observations:

	DF	SS	MS	F	P
Regression	5	0.3004	0.0601	210.4517	0.0047
Residual	2	0.0006	0.0003		
Total	7	0.3010	0.0430		

Statistical Tests:

Normality Test (Shapiro-Wilk) Failed (P = 0.0251)

W Statistic= 0.7946 Significance Level = 0.0500

Constant Variance Test Failed (P = 0.0287)
iterations=200
stepsize=1
tolerance=1e-10

Number of Iterations Performed = 8

Appendix XII

e) HA_{2590}

Equation: Piecewise, 3 segment linear
t1 = min(t)
t3 = max(t)
region1(t) = (y1*(T1-t) + y2*(t-t1))/(T1-t1)
region2(t) = (y2*(T2-t) + y3*(t-T1))/(T2-T1)
region3(t) = (y3*(t3-t) + y4*(t-T2))/(t3-T2)
f = if(t <= T1, region1(t), if(t <= T2, region2(t), region3(t)))

Dynamic Fit Options:

Total Number of Fits	200
Maximum Number of Iterations	200

Parameter Ranges for Initial Estimates:

	Minimum	Maximum
y1	-0.2876	0.8629
y2	-0.4060	1.2181
y3	-0.7263	2.1790
y4	-0.7385	2.2154
T1	-3.3333	10.0000
T2	-5.6667	17.0000

Summary of Fit Results:

Converged	96.5%
Singular Solutions	87.5%
Ill-Conditioned Solutions	7.0%
Iterations Exceeding 200	3.5%

Results for the Overall Best-Fit Solution:

R	Rsqr	Adj Rsqr	Standard Error of Estimate
0.9925	0.9851	0.9479	0.0505

	Coefficient	Std. Error	t	P
y1	0.2597	0.0423	6.1451	0.0255
y2	0.5199	0.0900	5.7760	0.0287
y3	0.8340	0.0602	13.8470	0.0052
y4	0.7435	0.0505	14.7206	0.0046
T1	4.7169	0.7051	6.6899	0.0216
T2	6.0000	1.4217	4.2202	0.0518

Analysis of Variance:

Analysis of Variance:

	DF	SS	MS
Regression	6	2.7709	0.4618
Residual	2	0.0051	0.0026
Total	8	2.7760	0.3470

Corrected for the mean of the observations:

	DF	SS	MS	F	P
Regression	5	0.3373	0.0675	26.4483	0.0368
Residual	2	0.0051	0.0026		
Total	7	0.3424	0.0489		

Appendix XII

Statistical Tests:

Normality Test (Shapiro-Wilk) Passed (P = 0.7522)
W Statistic= 0.9541 Significance Level = 0.0500

Constant Variance Test Passed (P = 0.4597)

iterations=200
stepsize=1
tolerance=1e-10

Number of Iterations Performed = 34

e) HA_{mix}

Equation: Piecewise, 3 segment linear
t1 = min(t)
t3 = max(t)
region1(t) = (y1*(T1-t) + y2*(t-t1))/(T1-t1)
region2(t) = (y2*(T2-t) + y3*(t-T1))/(T2-T1)
region3(t) = (y3*(t3-t) + y4*(t-T2))/(t3-T2)
f = if(t <= T1, region1(t), if(t <= T2, region2(t), region3(t)))

Dynamic Fit Options:

Total Number of Fits	200
Maximum Number of Iterations	200

Parameter Ranges for Initial Estimates:

	Minimum	Maximum
y1	-0.2159	0.6477
y2	-0.4069	1.2206
y3	-0.7022	2.1065
y4	-1.2201	3.6604
T1	-3.3333	10.0000
T2	-5.6667	17.0000

Summary of Fit Results:

Converged	98.5%
Singular Solutions	84.0%
Ill-Conditioned Solutions	11.5%
Iterations Exceeding 200	1.5%

Results for the Overall Best-Fit Solution:

R	Rsqr	Adj Rsqr	Standard Error of Estimate
0.9981	0.9962	0.9866	0.0410

	Coefficient	Std. Error	t	P
y1	0.2477	0.0318	7.7924	0.0161
y2	0.5797	0.0704	8.2404	0.0144
y3	1.0477	0.1813	5.7794	0.0287
y4	1.2087	0.0410	29.4567	0.0012
T1	5.4672	0.7176	7.6187	0.0168
T2	6.8159	1.2834	5.3109	0.0337

Appendix XII

Analysis of Variance:

Analysis of Variance:

	DF	SS	MS
Regression	6	4.0370	0.6728
Residual	2	0.0034	0.0017
Total	8	4.0403	0.5050

Corrected for the mean of the observations:

	DF	SS	MS	F	P
Regression	5	0.8772	0.1754	104.2030	0.0095
Residual	2	0.0034	0.0017		
Total	7	0.8806	0.1258		

Statistical Tests:

Normality Test (Shapiro-Wilk) Passed (P = 0.6022)

W Statistic= 0.9391 Significance Level = 0.0500

Constant Variance Test Passed (P = 0.0716)

iterations=200
stepsize=1
tolerance=1e-10

Number of Iterations Performed = 8

Appendix XII

PNT1A cell line

a) Control

Equation: Piecewise, 3 segment linear
t1 = min(t)
t3 = max(t)
region1(t) = (y1*(T1-t) + y2*(t-t1))/(T1-t1)
region2(t) = (y2*(T2-t) + y3*(t-T1))/(T2-T1)
region3(t) = (y3*(t3-t) + y4*(t-T2))/(t3-T2)
f = if(t <= T1, region1(t), if(t <= T2, region2(t), region3(t)))

Dynamic Fit Options:

Total Number of Fits	200
Maximum Number of Iterations	200

Parameter Ranges for Initial Estimates:

	Minimum	Maximum
y1	-0.2344	0.7033
y2	-0.3912	1.1735
y3	-0.6578	1.9733
y4	-0.6465	1.9395
T1	-3.3333	10.0000
T2	-5.6667	17.0000

Summary of Fit Results:

Converged	95.5%
Singular Solutions	84.5%
Ill-Conditioned Solutions	9.0%
Iterations Exceeding 200	4.5%

Results for the Overall Best-Fit Solution:

R	Rsqr	Adj Rsqr	Standard Error of Estimate
0.9945	0.9891	0.9619	0.0387

	Coefficient	Std. Error	t	P
y1	0.2383	0.0324	7.3521	0.0180
y2	0.5146	316727.6410	1.6249E-006	1.0000
y3	0.7980	6814941.4132	1.1709E-007	1.0000
y4	0.6518	0.0497	13.1172	0.0058
T1	4.9777	4559674.1669	1.0917E-006	1.0000
T2	5.7432	105246534.0202	5.4569E-008	1.0000

Analysis of Variance:

Analysis of Variance:

	DF	SS	MS
Regression	6	2.3158	0.3860
Residual	2	0.0030	0.0015
Total	8	2.3188	0.2898

Corrected for the mean of the observations:

	DF	SS	MS	F	P
Regression	5	0.2727	0.0545	36.3343	0.0270
Residual	2	0.0030	0.0015		
Total	7	0.2757	0.0394		

Appendix XII

Statistical Tests:

Normality Test (Shapiro-Wilk) Passed (P = 0.7722)

W Statistic= 0.9561 Significance Level = 0.0500

Constant Variance Test Passed (P = 0.3533)

iterations=200
stepsize=1
tolerance=1e-10

Number of Iterations Performed = 12

b) Aminosilane

Equation: Piecewise, 3 segment linear
t1 = min(t)
t3 = max(t)
region1(t) = (y1*(T1-t) + y2*(t-t1))/(T1-t1)
region2(t) = (y2*(T2-t) + y3*(t-T1))/(T2-T1)
region3(t) = (y3*(t3-t) + y4*(t-T2))/(t3-T2)
f = if(t <= T1, region1(t), if(t <= T2, region2(t), region3(t)))

Dynamic Fit Options:

Total Number of Fits	200
Maximum Number of Iterations	200

Parameter Ranges for Initial Estimates:

	Minimum	Maximum
y1	-0.2389	0.7167
y2	-0.4095	1.2286
y3	-0.6401	1.9202
y4	-0.6019	1.8057
T1	-3.3333	10.0000
T2	-5.6667	17.0000

Summary of Fit Results:

Converged	96.0%
Singular Solutions	85.5%
Ill-Conditioned Solutions	10.5%
Iterations Exceeding 200	4.0%

Results for the Overall Best-Fit Solution:

R	Rsqr	Adj Rsqr	Standard Error of Estimate
0.9755	0.9516	0.8305	0.0769

	Coefficient	Std. Error	t	P
y1	0.2933	0.0853	3.4369	0.0752
y2	0.5013	4655067.8338	1.0769E-007	1.0000
y3	0.8289	842205.0005	9.8418E-007	1.0000
y4	0.6170	0.0769	8.0221	0.0152
T1	5.1743	93419732.7629	5.5388E-008	1.0000
T2	6.1022	7542336.6478	8.0905E-007	1.0000

Appendix XII

Analysis of Variance:

Analysis of Variance:

	DF	SS	MS
Regression	6	2.3370	0.3895
Residual	2	0.0118	0.0059
Total	8	2.3489	0.2936

Corrected for the mean of the observations:

	DF	SS	MS	F	P
Regression	5	0.2325	0.0465	7.8602	0.1167
Residual	2	0.0118	0.0059		
Total	7	0.2443	0.0349		

Statistical Tests:

Normality Test (Shapiro-Wilk) Passed (P = 0.2191)

W Statistic= 0.8869 Significance Level = 0.0500

Constant Variance Test Failed (P = 0.0018)

iterations=200
stepsize=1
tolerance=1e-10

Number of Iterations Performed = 8

c) HA_4

Equation: Piecewise, 3 segment linear
t1 = min(t)
t3 = max(t)
region1(t) = (y1*(T1-t) + y2*(t-t1))/(T1-t1)
region2(t) = (y2*(T2-t) + y3*(t-T1))/(T2-T1)
region3(t) = (y3*(t3-t) + y4*(t-T2))/(t3-T2)
f = if(t <= T1, region1(t), if(t <= T2, region2(t), region3(t)))

Dynamic Fit Options:

Total Number of Fits	200
Maximum Number of Iterations	200

Parameter Ranges for Initial Estimates:

	Minimum	Maximum
y1	-0.1773	0.5318
y2	-0.2870	0.8609
y3	-0.5034	1.5103
y4	-0.8568	2.5704
T1	-3.3333	10.0000
T2	-5.6667	17.0000

Summary of Fit Results:

Converged	99.5%
Singular Solutions	83.0%
Ill-Conditioned Solutions	14.0%
Iterations Exceeding 200	0.5%

Appendix XII

Results for the Overall Best-Fit Solution:

R	Rsqr	Adj Rsqr	Standard Error of Estimate
0.9978	0.9956	0.9848	0.0301

	Coefficient	Std. Error	t	P
y1	0.1751	0.0233	7.5037	0.0173
y2	0.4582	0.0382	11.9834	0.0069
y3	0.6703	0.0990	6.7693	0.0211
y4	0.8508	0.0301	28.2421	0.0013
T1	5.9039	0.3138	18.8114	0.0028
T2	6.2339	0.7853	7.9386	0.0155

Analysis of Variance:

Analysis of Variance:

	DF	SS	MS
Regression	6	2.0101	0.3350
Residual	2	0.0018	0.0009
Total	8	2.0119	0.2515

Corrected for the mean of the observations:

	DF	SS	MS	F	P
Regression	5	0.4150	0.0830	91.4646	0.0109
Residual	2	0.0018	0.0009		
Total	7	0.4169	0.0596		

Statistical Tests:

Normality Test (Shapiro-Wilk) Passed (P = 0.3639)

W Statistic= 0.9114 Significance Level = 0.0500

Constant Variance Test Failed (P = 0.0474)

iterations=200
stepsize=1
tolerance=1e-10

Number of Iterations Performed = 7

d) HA_{234}

Equation: Piecewise, 3 segment linear
t1 = min(t)
t3 = max(t)
region1(t) = (y1*(T1-t) + y2*(t-t1))/(T1-t1)
region2(t) = (y2*(T2-t) + y3*(t-T1))/(T2-T1)
region3(t) = (y3*(t3-t) + y4*(t-T2))/(t3-T2)
f = if(t <= T1, region1(t), if(t <= T2, region2(t), region3(t)))

Dynamic Fit Options:

Total Number of Fits	200
Maximum Number of Iterations	200

Appendix XII

Parameter Ranges for Initial Estimates:

	Minimum	Maximum
y1	-0.1858	0.5574
y2	-0.2725	0.8174
y3	-0.4570	1.3709
y4	-0.6623	1.9870
T1	-3.3333	10.0000
T2	-5.6667	17.0000

Summary of Fit Results:

Converged	98.5%
Singular Solutions	86.5%
Ill-Conditioned Solutions	10.0%
Iterations Exceeding 200	1.5%

Results for the Overall Best-Fit Solution:

R	Rsqr	Adj Rsqr	Standard Error of Estimate
0.9831	0.9665	0.8826	0.0644

	Coefficient	Std. Error	t	P
y1	0.2224	0.0539	4.1287	0.0540
y2	0.3292	0.0904	3.6399	0.0679
y3	0.6552	0.0985	6.6527	0.0219
y4	0.6666	0.0644	10.3515	0.0092
T1	4.9515	0.5994	8.2614	0.0143
T2	6.5924	0.7581	8.6964	0.0130

Analysis of Variance:

Analysis of Variance:

	DF	SS	MS
Regression	6	1.5619	0.2603
Residual	2	0.0083	0.0041
Total	8	1.5702	0.1963

Corrected for the mean of the observations:

	DF	SS	MS	F	P
Regression	5	0.2390	0.0478	11.5250	0.0818
Residual	2	0.0083	0.0041		
Total	7	0.2473	0.0353		

Statistical Tests:

Normality Test (Shapiro-Wilk) Failed (P = 0.0241)

W Statistic= 0.7930 Significance Level = 0.0500

Constant Variance Test Failed (P = <0.0001)

iterations=200
stepsize=1
tolerance=1e-10

Number of Iterations Performed = 8

Appendix XII

f) HA_{2590}

Equation: Piecewise, 3 segment linear
t1 = min(t)
t3 = max(t)
region1(t) = (y1*(T1-t) + y2*(t-t1))/(T1-t1)
region2(t) = (y2*(T2-t) + y3*(t-T1))/(T2-T1)
region3(t) = (y3*(t3-t) + y4*(t-T2))/(t3-T2)
f = if(t <= T1, region1(t), if(t <= T2, region2(t), region3(t)))

Dynamic Fit Options:

Total Number of Fits	200
Maximum Number of Iterations	200

Parameter Ranges for Initial Estimates:

	Minimum	Maximum
y1	-0.2100	0.6299
y2	-0.2943	0.8829
y3	-0.4265	1.2796
y4	-0.5758	1.7273
T1	-3.3333	10.0000
T2	-5.6667	17.0000

Summary of Fit Results:

Converged	94.0%
Singular Solutions	85.5%
Ill-Conditioned Solutions	8.5%
Iterations Exceeding 200	6.0%

Results for the Overall Best-Fit Solution:

R	Rsqr	Adj Rsqr	Standard Error of Estimate
0.9474	0.8976	0.6416	0.0885

	Coefficient	Std. Error	t	P
y1	0.2380	0.0741	3.2130	0.0847
y2	0.3266	30025.9941	1.0879E-005	1.0000
y3	0.5293	729392.8187	7.2574E-007	1.0000
y4	0.5618	0.0886	6.3419	0.0240
T1	4.9860	1350463.3135	3.6920E-006	1.0000
T2	5.5797	54326371.3029	1.0271E-007	1.0000

Analysis of Variance:

Analysis of Variance:

	DF	SS	MS
Regression	6	1.3095	0.2183
Residual	2	0.0157	0.0078
Total	8	1.3252	0.1656

Corrected for the mean of the observations:

	DF	SS	MS	F	P
Regression	5	0.1374	0.0275	3.5059	0.2367
Residual	2	0.0157	0.0078		
Total	7	0.1531	0.0219		

Appendix XII

Statistical Tests:

Normality Test (Shapiro-Wilk) Passed (P = 0.9570)
W Statistic= 0.9788 Significance Level = 0.0500

Constant Variance Test Passed (P = 0.8849)

iterations=200
stepsize=1
tolerance=1e-10

Number of Iterations Performed = 7

f) HA_{mix}

Equation: Piecewise, 3 segment linear
t1 = min(t)
t3 = max(t)
region1(t) = (y1*(T1-t) + y2*(t-t1))/(T1-t1)
region2(t) = (y2*(T2-t) + y3*(t-T1))/(T2-T1)
region3(t) = (y3*(t3-t) + y4*(t-T2))/(t3-T2)
f = if(t <= T1, region1(t), if(t <= T2, region2(t), region3(t)))

Dynamic Fit Options:

Total Number of Fits	200
Maximum Number of Iterations	200

Parameter Ranges for Initial Estimates:

	Minimum	Maximum
y1	-0.2641	0.7923
y2	-0.3383	1.0150
y3	-0.4316	1.2947
y4	-0.8630	2.5891
T1	-3.3333	10.0000
T2	-5.6667	17.0000

Summary of Fit Results:

Converged	98.5%
Singular Solutions	85.5%
Ill-Conditioned Solutions	11.5%
Iterations Exceeding 200	1.5%

Results for the Overall Best-Fit Solution:

R	Rsqr	Adj Rsqr	Standard Error of Estimate
0.9731	0.9469	0.8140	0.0897

	Coefficient	Std. Error	t	P
y1	0.2925	0.0751	3.8968	0.0600
y2	0.3292	0.0911	3.6133	0.0688
y3	0.5874	0.7487	0.7846	0.5149
y4	0.8845	0.0897	9.8579	0.0101
T1	4.0000	2.2029	1.8158	0.2111
T2	7.1060	8.9429	0.7946	0.5102

Appendix XII

Analysis of Variance:

Analysis of Variance:

	DF	SS	MS
Regression	6	1.9202	0.3200
Residual	2	0.0161	0.0081
Total	8	1.9363	0.2420

Corrected for the mean of the observations:

	DF	SS	MS	F	P
Regression	5	0.2869	0.0574	7.1282	0.1276
Residual	2	0.0161	0.0081		
Total	7	0.3030	0.0433		

Statistical Tests:

Normality Test (Shapiro-Wilk) Passed (P = 0.2192)

W Statistic= 0.8870 Significance Level = 0.0500

Constant Variance Test Failed (P = 0.0212)

iterations=200
stepsize=1
tolerance=1e-10

Number of Iterations Performed = 24

Appendix XIII

PCR primers

Primer		Sequence (5' – 3')
P1		GACACATATTGCTTCAATGCTTCAGC
P4		GATGCCAAGATGATCAGCCATTCTGGAA
5/7		CACTAGTGCTCATCAAAGTGGTAG
5/8		TGGTATTTGAAGACGTACTGGTAG
5/9		CCCGTG GTGTGGTTGAAATGGTAG
5/10		TGCCATTTCTGTCTACATTGGTAG
5/11		TACTAGGAGTTGCCTGGATGGTAG
5/12		TGGTATGAGCTGAGGCTGTGGTAG
5/13		TATGACTGGAGTCCATATTGGTAG
5/14		TCTGAGAATTACTCTGCTTGGTAG
$RHAMM^{FL}$	F	CAGGTCACCCAAAGGAGTCTCG
	R	CAAGCTCATCCAGTGTTTGC
$RHAMM^{-48}$	F	GGCCGTCAACATGTCCTTTCCTA
	R	TTGGGCTATTTTCCCTTGAGACTC
$RHAMM^{-147}$	F	AGGAGGAACAAGCTGAAAGG
	R	TTCCTGAGCTGCACCATGTT
β-actin	F	CTAGAAGCATTTGCGGTGGAC
	R	TGACGGGGTCACCCATGT

Appendix XIV

Real-time PCR

Primer		Sequence (5' – 3')	Amplicon Size (bp)
HSPCB	F	AAGAGAGCAAGGCAAAGTTTGAG	120
	R	TGGTCACAATGCAGCAAGGT	
ABL1	F	GATACGAAGGGAGGGTGTACCA	94
	R	CTCGGCCAGGGTGTTGAA	
CD44	F	GGCTTTCAATAGCACCTTGC	152
	R	ACACCCCTGTGTTGTTTGCT	
RHAMM	F	GTTGTGCACCATCTCCAGGT	152
	R	AGCTGAAGCAGGCAAGGTAG	

Calculation of the real-time PCR efficiency

For the relative gene quantification using *Plaff* method, the preparation of standard curves is only required to determine the amplification efficiencies of the target and housekeeping genes in an initial experiment. The calculation of the real-time PCR efficiencies of the housekeeping and target genes constituted the first step for quantification of gene expression. The accuracy of qPCR is dependent on the linearity and efficiency of PCR amplification. Both of these were determined using a standard curve generated by dilution series using a pool of cDNA from both cell lines, in order to have high representativity of gene expression. For the establishment of a standard curve for each gene, five concentrations of cDNA of the targets and the normalisers: 1:1 (neat), 1:10, 1:100, 1:1,000 and 1:10,000 were prepared, and using three replicates of each template (**Figures I – IV**).

Appendix XIV

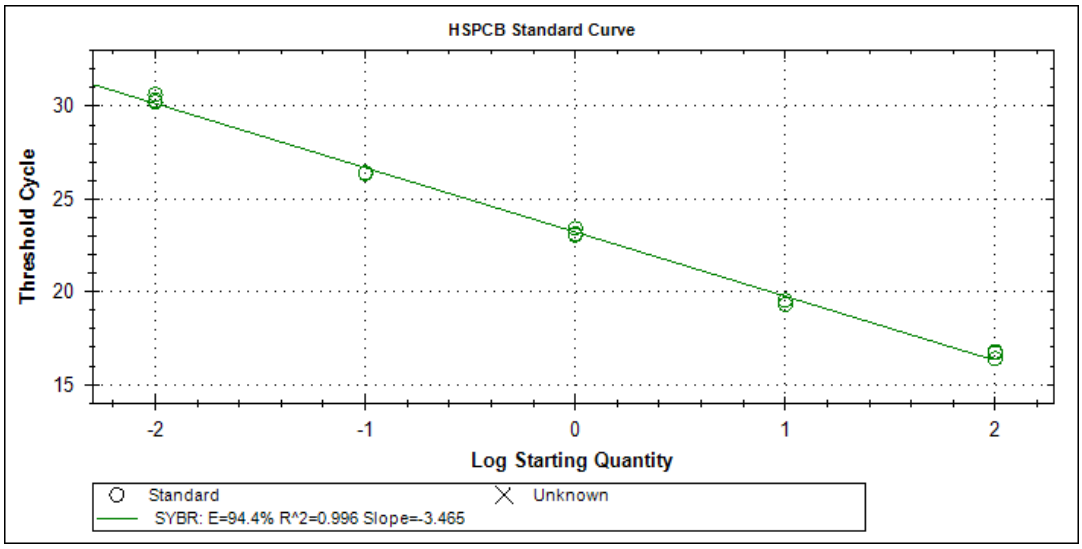

Figure I – HSPCB standard curve. Five dilutions were used: 1:1 (neat), 1:10, 1:100, 1:1,000 and 1:10,000, with three replicates per dilution, using a pool of RT112 and T24 cells cDNA. In the x-axis is represented the logarithm of cDNA concentration value and in the y-axis is represented the amplification cycle.

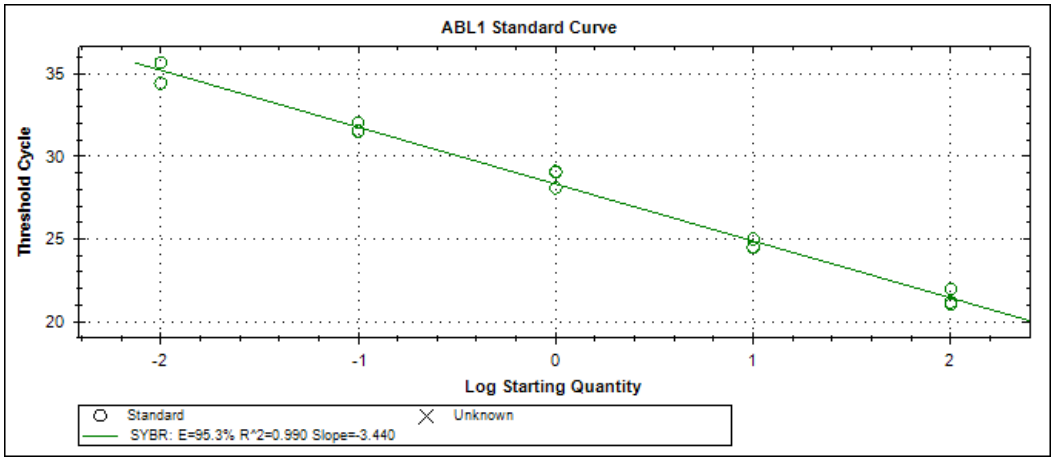

Figure II – ABL1 standard curve. Five dilutions were used: 1:1 (neat), 1:10, 1:100, 1:1,000 and 1:10,000, with three replicates per dilution, using a pool of PC3 and PNT1A cells cDNA. In the x-axis is represented the logarithm of cDNA concentration value and in the y-axis is represented the amplification cycle.

Appendix XIV

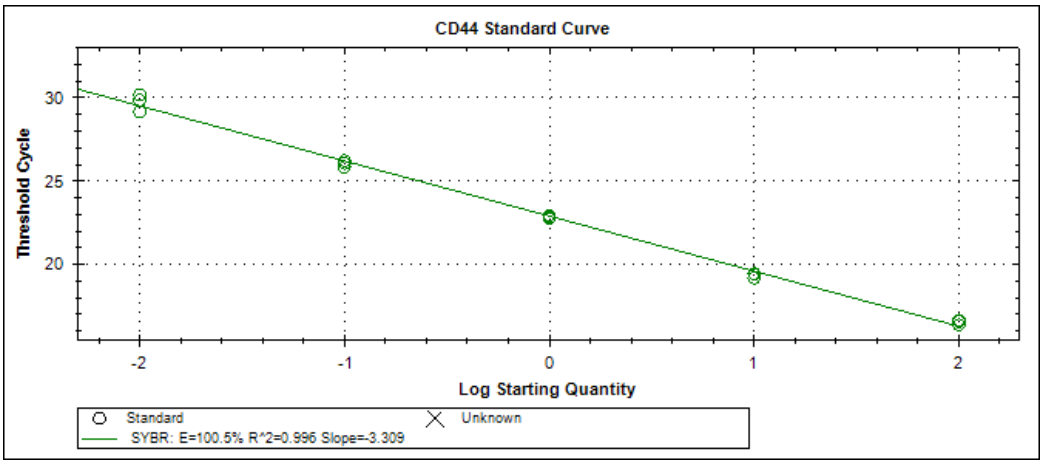

Figure III – CD44 standard curve. Five dilutions were used: 1:1 (neat), 1:10, 1:100, 1:1,000 and 1:10,000, with three replicates per dilution, using a pool of RT112, T24, PC3 and PNT1A cells cDNA. In the x-axis is represented the logarithm of cDNA concentration value and in the y-axis is represented the amplification cycle.

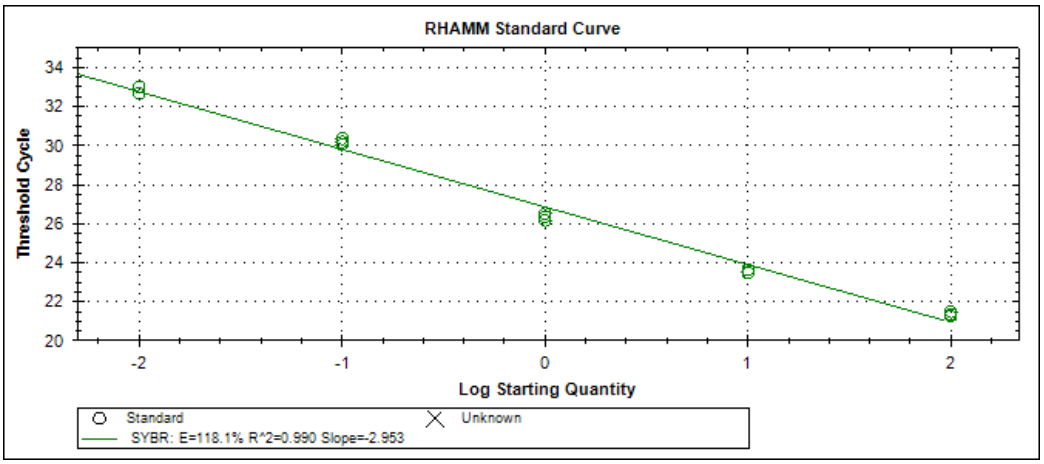

Figure IV – RHAMM standard curve. Five dilutions were used: 1:1 (neat), 1:10, 1:100, 1:1,000 and 1:10,000, with three replicates per dilution, using a pool of RT112, T24, PC3 and PNT1A cells cDNA. In the x-axis is represented the logarithm of cDNA concentration value and in the y-axis is represented the amplification cycle.

Negative control

For all experiments a negative control was used in order to assure the efficiency of the method and absence of contaminations. The negative control consists on a normal qPCR amplification procedure in a sample where water was added instead of cDNA template. The figures below describe the results of the negative controls amplification for each primer pair.

These are indicated by an arrow, whereas the other peaks correspond to the various cDNA templates (**Figures V** to **VIII**).

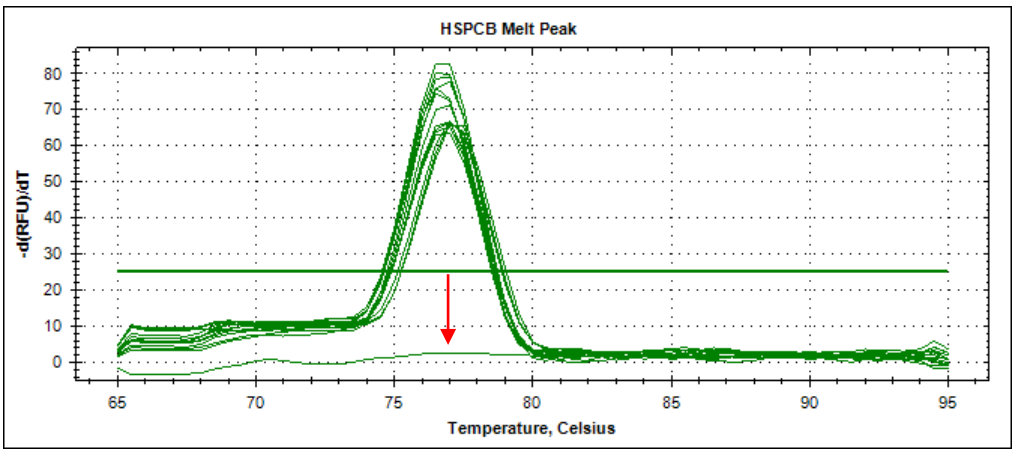

Figure V – HSPCB melt curves characteristic for a specific amplification, illustrating the negative control importance. The arrow points to the negative control.

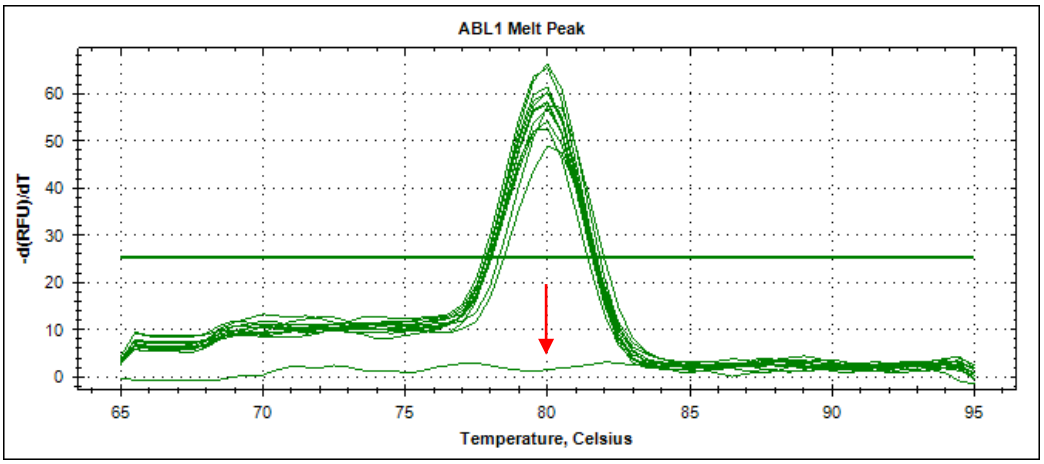

Figure VI – ABL1 melt curves characteristic for a specific amplification, illustrating the negative control importance. The arrow points to the negative control.

Appendix XIV

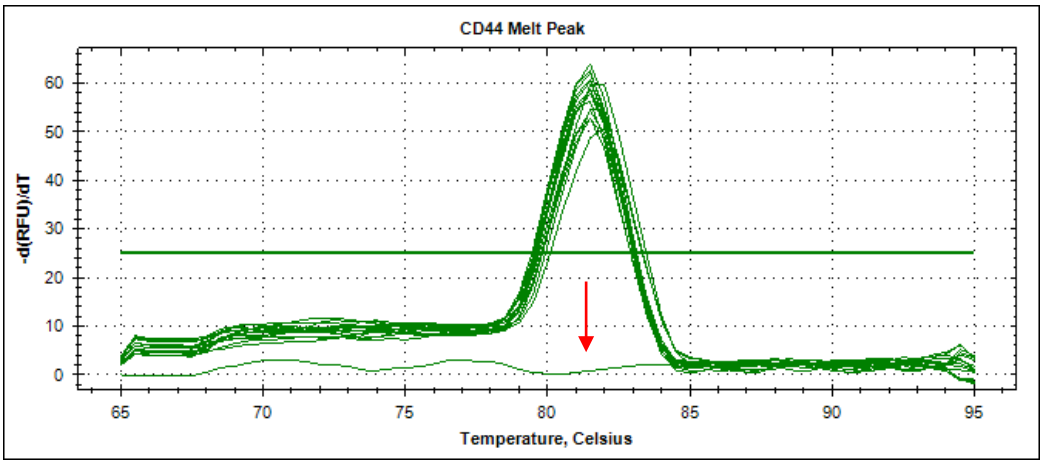

Figure VII – CD44 melt curves characteristic for a specific amplification, illustrating the negative control importance. The arrow points to the negative control.

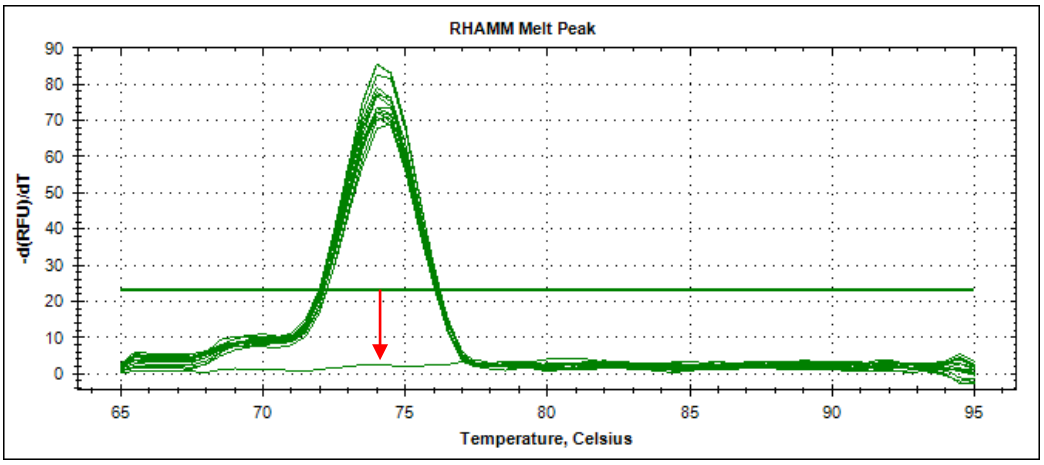

Figure VIII – RHAMM melt curves characteristic for a specific amplification, illustrating the negative control importance. The arrow points to the negative control.

Analysis of the qPCR products

An analysis of the obtained products from standard curves amplification was carried out in order to confirm the fragments size resulting from the qPCR amplification for each primer pair. This analysis was performed by electrophoresis using 1.5% agarose gel (**Figures IX** to **XII**).

Appendix XIV

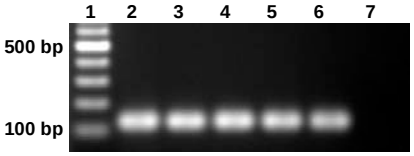

Figure IX – Amplification pattern generated by HSPCB primer pair at 60.1ºC annealing temperature, in a pool of RT112 and T24 cells cDNA. Lanes numbered 1-7 from left to right. Pattern marker of 100 bp (1), negative control (7).

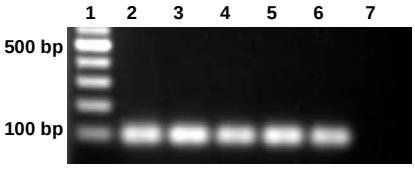

Figure X – Amplification pattern generated by ABL1 primer pair at 60.1ºC annealing temperature, in a pool of PC3 and PNT1A cells cDNA. Lanes numbered 1-7 from left to right. Pattern marker of 100 bp (1), negative control (7).

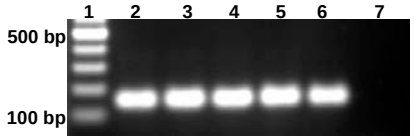

Figure XI – Amplification pattern generated by CD44 primer pair at 60.1ºC annealing temperature, in a pool of RT112, T24, PC3 and PNT1A cells cDNA. Lanes numbered 1-7 from left to right. Pattern marker of 100 bp (1), negative control (7).

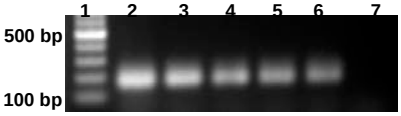

Figure XII – Amplification pattern generated by RHAMM primer pair at 60.1ºC annealing temperature, in a pool of RT112, T24, PC3 and PNT1A cells cDNA. Lanes numbered 1-7 from left to right. Pattern marker of 100 bp (1), negative control (7).

Appendix XV

RNA integrity analysis generated by Experion Automated Electrophoresis System (Bio-Rad)

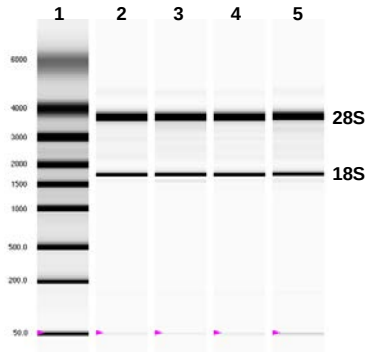

Figure I – Virtual gel generated by Experion Automated Electrophoresis System. Lanes numbered 1-5 from left to right. RNA ladder (1), RT112 cells (2), T24 cells (3), PC3 cells (4) and PNT1A cells (5).

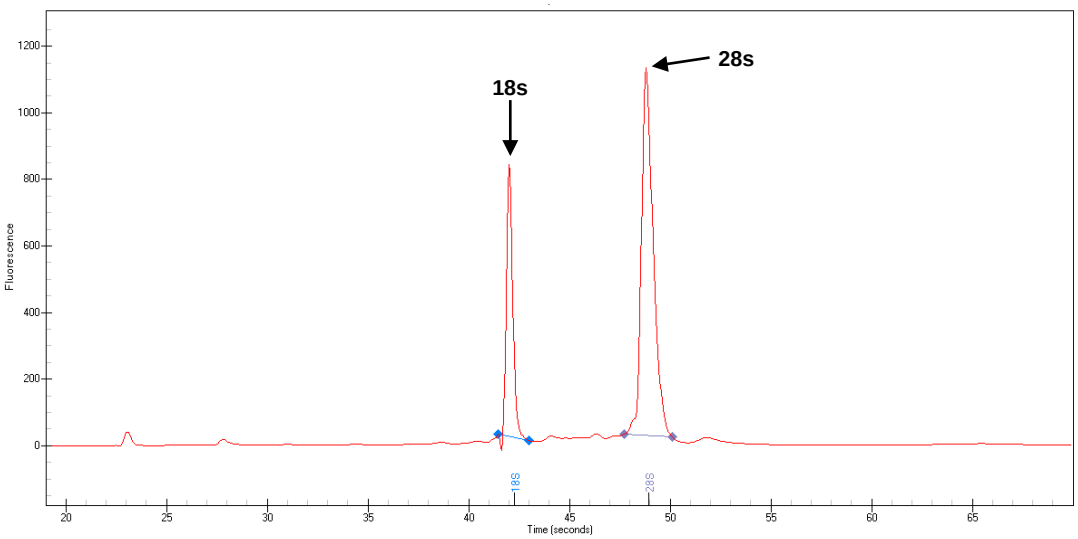

Figure II – Electropherogram of a total RNA sample from RT112 cell line, showing the 18s/28s RNA peaks.

Appendix XV

Run summary generated by Experion Automated Electrophoresis System. RQI refers to RNA quality indicator.

Sample Name	RNA Area	RNA Concentration (ng/µl)	Ratio [28S:18S]	RQI	RQI Classification
Ladder	817.11	160.00			
RT112 control	3,024.07	592.15	2.15	10.0	
RT112 HA_4	548.09	153.60	1.22	7.4	
RT112 HA_{234}	927.02	259.80	1.31	8.1	
RT112 HA_{2590}	1,161.79	325.59	1.08	7.8	
RT112 HA_{mix}	965.64	270.62	1.53	8.2	
T24 control	3,621.88	709.20	2.11	10.0	
T24 HA_4	609.89	170.92	2.26	10.0	
T24 HA_{234}	884.36	247.84	2.02	9.9	
T24 HA_{2590}	1,178.12	330.17	1.84	9.9	
T24 HA_{mix}	1,184.09	331.84	1.96	10.0	
PC3 control	2,728.31	534.23	2.00	10.0	
PC3 HA_4	518.59	405.94	1.73	7.8	
PC3 HA_{234}	666.73	521.90	1.57	7.9	
PC3 HA_{2590}	316.36	247.63	1.47	9.3	
PC3 HA_{mix}	324.11	253.70	1.49	7.6	
PNT1A control	1,441.07	282.18	2.04	10.0	
PNT1A HA_4	1,940.00	543.72	2.04	10.0	
PNT1A HA_{234}	2,301.55	645.01	1.84	10.0	
PNT1A HA_{2590}	1,824.69	511.37	1.88	10.0	
PNT1A HA_{mix}	3,691.44	1034.52	1.84	10.0	

Appendix XVI

Real-time PCR – RHAMM/CD44 ratio statistics

One-way analysis of variance	
P value	< 0.0001
P value summary	***
Are means signif. different? (P < 0.05)	Yes
Number of groups	20
F	20.15
R square	0.7336

Bartlett's test for equal variances	
Bartlett's statistic (corrected)	95.71
P value	< 0.0001
P value summary	***
Do the variances differ signif. (P < 0.05)	Yes

ANOVA Table	SS	df	MS
Treatment (between columns)	457.5	19	24.08
Residual (within columns)	166.1	139	1.195
Total	623.6	158	

Tukey's Multiple Comparison Test	Mean Diff.	q	Significant? P < 0.05?	Summary	95% CI of diff
RT112 control vs RT112 HA4	3.403	7.625	Yes	***	1.116 to 5.690
RT112 control vs RT112 HA234	2.331	5.721	Yes	*	0.2429 to 4.419
RT112 control vs RT112 HA2590	2.422	5.428	Yes	*	0.1351 to 4.710
RT112 control vs RT112 HAmix	2.022	4.964	No	ns	-0.06571 to 4.110
RT112 control vs T24 control	0.9092	2.232	No	ns	-1.179 to 2.997
RT112 control vs T24 HA4	0.7741	1.900	No	ns	-1.314 to 2.862
RT112 control vs T24 HA234	1.088	2.439	No	ns	-1.199 to 3.376
RT112 control vs T24 HA2590	1.296	3.182	No	ns	-0.7918 to 3.384
RT112 control vs T24 HAmix	1.009	2.476	No	ns	-1.079 to 3.097
RT112 control vs PC3 control	-0.06734	0.1653	No	ns	-2.155 to 2.021
RT112 control vs PC3 HA4	0.05173	0.1270	No	ns	-2.036 to 2.140
RT112 control vs PC3 HA234	3.477	8.535	Yes	***	1.389 to 5.565
RT112 control vs PC3 HA2590	-1.336	3.278	No	ns	-3.424 to 0.7524
RT112 control vs PC3 HAmix	0.9991	2.452	No	ns	-1.089 to 3.087
RT112 control vs PNT1A control	-2.803	6.282	Yes	**	-5.091 to -0.5161
RT112 control vs PNT1A HA4	-1.647	4.043	No	ns	-3.735 to 0.4409
RT112 control vs PNT1A HA234	-3.045	6.823	Yes	***	-5.332 to -0.7579
RT112 control vs PNT1A HA2590	-1.007	2.471	No	ns	-3.095 to 1.081
RT112 control vs PNT1A HAmix	0.2256	0.5056	No	ns	-2.062 to 2.513
RT112 HA4 vs RT112 HA234	-1.072	2.632	No	ns	-3.160 to 1.016
RT112 HA4 vs RT112 HA2590	-0.9806	2.197	No	ns	-3.268 to 1.307
RT112 HA4 vs RT112 HAmix	-1.381	3.389	No	ns	-3.469 to 0.7073
RT112 HA4 vs T24 control	-2.494	6.121	Yes	**	-4.582 to -0.4058
RT112 HA4 vs T24 HA4	-2.629	6.453	Yes	**	-4.717 to -0.5409
RT112 HA4 vs T24 HA234	-2.315	5.187	Yes	*	-4.602 to -0.02746
RT112 HA4 vs T24 HA2590	-2.107	5.171	Yes	*	-4.195 to -0.01883
RT112 HA4 vs T24 HAmix	-2.394	5.877	Yes	**	-4.482 to -0.3063
RT112 HA4 vs PC3 control	-3.470	8.518	Yes	***	-5.558 to -1.382
RT112 HA4 vs PC3 HA4	-3.351	8.226	Yes	***	-5.439 to -1.263
RT112 HA4 vs PC3 HA234	0.07402	0.1817	No	ns	-2.014 to 2.162
RT112 HA4 vs PC3 HA2590	-4.739	11.63	Yes	***	-6.827 to -2.651

Appendix XVI

Tukey's Multiple Comparison Test	Mean Diff.	q	Significant? P < 0.05?	Summary		95% CI of diff
T24 control vs PC3 HA4	-0.8575	2.353	No	ns	-2.725 to 1.010
T24 control vs PC3 HA234	2.568	7.047	Yes	***	0.7003 to 4.435
T24 control vs PC3 HA2590	-2.245	6.161	Yes	**	-4.112 to -0.3772
T24 control vs PC3 HAmix	0.08986	0.2466	No	ns	-1.778 to 1.957
T24 control vs PNT1A control	-3.713	9.113	Yes	***	-5.801 to -1.625
T24 control vs PNT1A HA4	-2.556	7.015	Yes	***	-4.424 to -0.6888
T24 control vs PNT1A HA234	-3.954	9.706	Yes	***	-6.042 to -1.866
T24 control vs PNT1A HA2590	-1.916	5.258	Yes	*	-3.784 to -0.04839
T24 control vs PNT1A HAmix	-0.6836	1.678	No	ns	-2.772 to 1.404
T24 HA4 vs T24 HA234	0.3141	0.7711	No	ns	-1.774 to 2.402
T24 HA4 vs T24 HA2590	0.5221	1.433	No	ns	-1.346 to 2.390
T24 HA4 vs T24 HAmix	0.2346	0.6439	No	ns	-1.633 to 2.102
T24 HA4 vs PC3 control	-0.8415	2.309	No	ns	-2.709 to 1.026
T24 HA4 vs PC3 HA4	-0.7224	1.983	No	ns	-2.590 to 1.145
T24 HA4 vs PC3 HA234	2.703	7.418	Yes	***	0.8353 to 4.570
T24 HA4 vs PC3 HA2590	-2.110	5.790	Yes	*	-3.977 to -0.2422
T24 HA4 vs PC3 HAmix	0.2249	0.6173	No	ns	-1.643 to 2.092
T24 HA4 vs PNT1A control	-3.578	8.781	Yes	***	-5.666 to -1.490
T24 HA4 vs PNT1A HA4	-2.421	6.645	Yes	**	-4.289 to -0.5537
T24 HA4 vs PNT1A HA234	-3.819	9.375	Yes	***	-5.907 to -1.731
T24 HA4 vs PNT1A HA2590	-1.781	4.887	No	ns	-3.648 to 0.08668
T24 HA4 vs PNT1A HAmix	-0.5485	1.346	No	ns	-2.637 to 1.539
T24 HA234 vs T24 HA2590	0.2079	0.5104	No	ns	-1.880 to 2.296
T24 HA234 vs T24 HAmix	-0.07950	0.1952	No	ns	-2.168 to 2.008
T24 HA234 vs PC3 control	-1.156	2.837	No	ns	-3.244 to 0.9324
T24 HA234 vs PC3 HA4	-1.037	2.544	No	ns	-3.125 to 1.051
T24 HA234 vs PC3 HA234	2.389	5.864	Yes	**	0.3008 to 4.477
T24 HA234 vs PC3 HA2590	-2.424	5.950	Yes	**	-4.512 to -0.3359
T24 HA234 vs PC3 HAmix	-0.08922	0.2190	No	ns	-2.177 to 1.999
T24 HA234 vs PNT1A control	-3.892	8.720	Yes	***	-6.179 to -1.604
T24 HA234 vs PNT1A HA4	-2.735	6.714	Yes	***	-4.823 to -0.6474
T24 HA234 vs PNT1A HA234	-4.133	9.262	Yes	***	-6.421 to -1.846
T24 HA234 vs PNT1A HA2590	-2.095	5.142	Yes	*	-4.183 to -0.007025
T24 HA234 vs PNT1A HAmix	-0.8626	1.933	No	ns	-3.150 to 1.425
T24 HA2590 vs T24 HAmix	-0.2874	0.7888	No	ns	-2.155 to 1.580
T24 HA2590 vs PC3 control	-1.364	3.742	No	ns	-3.231 to 0.5040
T24 HA2590 vs PC3 HA4	-1.244	3.415	No	ns	-3.112 to 0.6231
T24 HA2590 vs PC3 HA234	2.181	5.985	Yes	**	0.3133 to 4.048
T24 HA2590 vs PC3 HA2590	-2.632	7.223	Yes	***	-4.499 to -0.7642
T24 HA2590 vs PC3 HAmix	-0.2971	0.8154	No	ns	-2.165 to 1.570
T24 HA2590 vs PNT1A control	-4.100	10.06	Yes	***	-6.188 to -2.012
T24 HA2590 vs PNT1A HA4	-2.943	8.077	Yes	***	-4.811 to -1.076
T24 HA2590 vs PNT1A HA234	-4.341	10.66	Yes	***	-6.429 to -2.253
T24 HA2590 vs PNT1A HA2590	-2.303	6.320	Yes	**	-4.171 to -0.4354
T24 HA2590 vs PNT1A HAmix	-1.071	2.628	No	ns	-3.159 to 1.017
T24 HAmix vs PC3 control	-1.076	2.953	No	ns	-2.944 to 0.7914
T24 HAmix vs PC3 HA4	-0.9570	2.626	No	ns	-2.825 to 0.9105
T24 HAmix vs PC3 HA234	2.468	6.774	Yes	***	0.6007 to 4.336
T24 HAmix vs PC3 HA2590	-2.344	6.434	Yes	**	-4.212 to -0.4768
T24 HAmix vs PC3 HAmix	-0.009711	0.02665	No	ns	-1.877 to 1.858
T24 HAmix vs PNT1A control	-3.812	9.357	Yes	***	-5.900 to -1.724
T24 HAmix vs PNT1A HA4	-2.656	7.289	Yes	***	-4.523 to -0.7883
T24 HAmix vs PNT1A HA234	-4.054	9.951	Yes	***	-6.142 to -1.966
T24 HAmix vs PNT1A HA2590	-2.016	5.531	Yes	*	-3.883 to -0.1480
T24 HAmix vs PNT1A HAmix	-0.7831	1.922	No	ns	-2.871 to 1.305
PC3 control vs PC3 HA4	0.1191	0.3268	No	ns	-1.748 to 1.987
PC3 control vs PC3 HA234	3.544	9.727	Yes	***	1.677 to 5.412

Appendix XVI

Tukey's Multiple Comparison Test	Mean Diff.	q	Significant? P < 0.05?	Summary	95% CI of diff
PC3 control vs PC3 HA2590	-1.268	3.481	No	ns	-3.136 to 0.5993
PC3 control vs PC3 HAmix	1.066	2.927	No	ns	-0.8012 to 2.934
PC3 control vs PNT1A control	-2.736	6.716	Yes	***	-4.824 to -0.6480
PC3 control vs PNT1A HA4	-1.580	4.335	No	ns	-3.447 to 0.2878
PC3 control vs PNT1A HA234	-2.978	7.309	Yes	***	-5.066 to -0.8898
PC3 control vs PNT1A HA2590	-0.9394	2.578	No	ns	-2.807 to 0.9282
PC3 control vs PNT1A HAmix	0.2930	0.7191	No	ns	-1.795 to 2.381
PC3 HA4 vs PC3 HA234	3.425	9.400	Yes	***	1.558 to 5.293
PC3 HA4 vs PC3 HA2590	-1.387	3.807	No	ns	-3.255 to 0.4802
PC3 HA4 vs PC3 HAmix	0.9473	2.600	No	ns	-0.9202 to 2.815
PC3 HA4 vs PNT1A control	-2.855	7.008	Yes	***	-4.943 to -0.7671
PC3 HA4 vs PNT1A HA4	-1.699	4.662	No	ns	-3.566 to 0.1687
PC3 HA4 vs PNT1A HA234	-3.097	7.602	Yes	***	-5.185 to -1.009
PC3 HA4 vs PNT1A HA2590	-1.058	2.905	No	ns	-2.926 to 0.8091
PC3 HA4 vs PNT1A HAmix	0.1739	0.4269	No	ns	-1.914 to 2.262
PC3 HA234 vs PC3 HA2590	-4.813	13.21	Yes	***	-6.680 to -2.945
PC3 HA234 vs PC3 HAmix	-2.478	6.800	Yes	***	-4.346 to -0.6104
PC3 HA234 vs PNT1A control	-6.280	15.42	Yes	***	-8.368 to -4.192
PC3 HA234 vs PNT1A HA4	-5.124	14.06	Yes	***	-6.992 to -3.257
PC3 HA234 vs PNT1A HA234	-6.522	16.01	Yes	***	-8.610 to -4.434
PC3 HA234 vs PNT1A HA2590	-4.484	12.31	Yes	***	-6.351 to -2.616
PC3 HA234 vs PNT1A HAmix	-3.251	7.981	Yes	***	-5.339 to -1.163
PC3 HA2590 vs PC3 HAmix	2.335	6.407	Yes	**	0.4671 to 4.202
PC3 HA2590 vs PNT1A control	-1.468	3.603	No	ns	-3.556 to 0.6202
PC3 HA2590 vs PNT1A HA4	-0.3115	0.8549	No	ns	-2.179 to 1.556
PC3 HA2590 vs PNT1A HA234	-1.710	4.196	No	ns	-3.798 to 0.3784
PC3 HA2590 vs PNT1A HA2590	0.3289	0.9025	No	ns	-1.539 to 2.196
PC3 HA2590 vs PNT1A HAmix	1.561	3.832	No	ns	-0.5268 to 3.649
PC3 HAmix vs PNT1A control	-3.802	9.334	Yes	***	-5.890 to -1.714
PC3 HAmix vs PNT1A HA4	-2.646	7.262	Yes	***	-4.514 to -0.7786
PC3 HAmix vs PNT1A HA234	-4.044	9.927	Yes	***	-6.132 to -1.956
PC3 HAmix vs PNT1A HA2590	-2.006	5.505	Yes	*	-3.873 to -0.1382
PC3 HAmix vs PNT1A HAmix	-0.7734	1.898	No	ns	-2.861 to 1.315
PNT1A control vs PNT1A HA4	1.156	2.838	No	ns	-0.9318 to 3.244
PNT1A control vs PNT1A HA234	-0.2418	0.5418	No	ns	-2.529 to 2.045
PNT1A control vs PNT1A HA2590	1.797	4.410	No	ns	-0.2914 to 3.885
PNT1A control vs PNT1A HAmix	3.029	6.787	Yes	***	0.7417 to 5.316
PNT1A HA4 vs PNT1A HA234	-1.398	3.432	No	ns	-3.486 to 0.6900
PNT1A HA4 vs PNT1A HA2590	0.6404	1.757	No	ns	-1.227 to 2.508
PNT1A HA4 vs PNT1A HAmix	1.873	4.597	No	ns	-0.2152 to 3.961
PNT1A HA234 vs PNT1A HA2590	2.038	5.004	No	ns	-0.04958 to 4.126
PNT1A HA234 vs PNT1A HAmix	3.271	7.329	Yes	***	0.9835 to 5.558
PNT1A HA2590 vs PNT1A HAmix	1.232	3.025	No	ns	-0.8556 to 3.320

Appendix XVII

Protein quantification

$y = 13.693\ x - 0.0467$

$R^2 = 0.997$

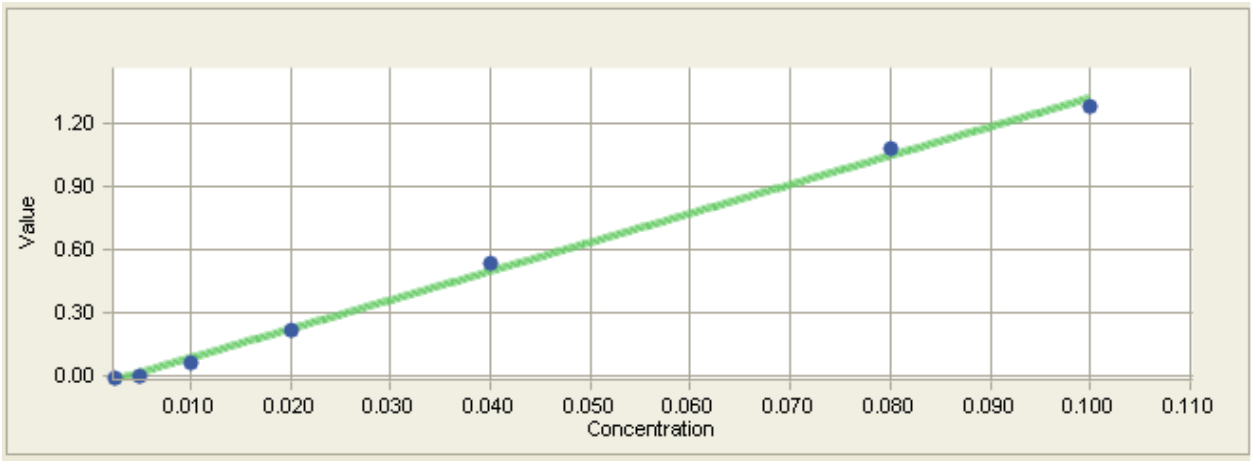

Appendix XVIII

AFM statistics

	Glass	Aminosilane	HA_4 C1	HA_4 C2	HA_4 C3	HA_{234} C1	HA_{234} C2	HA_{234} C3	HA_{2590} C1	HA_{2590} C2	HA_{2590} C3	HA_{mix} C1	HA_{mix} C2	HA_{mix} C3
Minimum	0.0500	0.2100	0.1000	0.0800	0.0700	0.0700	0.0800	0.0800	0.0600	0.0650	0.0740	0.0400	0.0600	0.1100
25% Percentile	0.0500	0.2100	0.1100	0.1100	0.1400	0.0800	0.1000	0.1100	0.0700	0.0730	0.0800	0.0470	0.0740	0.1300
Median	0.0600	0.2300	0.1300	0.1600	0.1800	0.1000	0.1200	0.1700	0.0800	0.0800	0.1200	0.0500	0.0870	0.1500
75% Percentile	0.0600	0.2650	0.1500	0.1800	0.2000	0.1200	0.1400	0.1900	0.0800	0.0990	0.1300	0.0600	0.0930	0.1800
Maximum	0.0600	0.2900	0.1800	0.2000	0.2200	0.1600	0.1600	0.2100	0.0900	0.1400	0.1600	0.0660	0.1180	0.2100
Mean	0.0560	0.2360	0.1307	0.1500	0.1688	0.1021	0.1200	0.1533	0.07533	0.08687	0.1143	0.05287	0.08507	0.1533
Std. Deviation	0.005477	0.03286	0.02520	0.03817	0.04241	0.02438	0.02563	0.04117	0.009155	0.01927	0.02715	0.008417	0.01468	0.03155
Std. Error	0.002449	0.01470	0.006508	0.009856	0.01029	0.006296	0.006619	0.01063	0.002364	0.004975	0.007011	0.002173	0.003792	0.008146
Lower 95% CI of mean	0.04920	0.1952	0.1167	0.1289	0.1470	0.08863	0.1058	0.1305	0.07026	0.07620	0.09930	0.04821	0.07693	0.1359
Upper 95% CI of mean	0.06280	0.2768	0.1446	0.1711	0.1906	0.1156	0.1342	0.1761	0.08040	0.09754	0.1294	0.05753	0.09320	0.1708
Sum	0.2800	1.180	1.960	2.250	2.870	1.532	1.800	2.300	1.130	1.303	1.715	0.7930	1.276	2.300

Appendix XVIII

One-way analysis of variance	
P value	< 0.0001
P value summary	***
Are means signif. different? (P < 0.05)	Yes
Number of groups	14
F	31.04
R square	0.6939

Bartlett's test for equal variances	
Bartlett's statistic (corrected)	75.26
P value	< 0.0001
P value summary	***
Do the variances differ signif. (P < 0.05)	Yes

ANOVA Table	SS	df	MS
Treatment (between columns)	0.3138	13	0.02413
Residual (within columns)	0.1384	178	0.0007776
Total	0.4522	191	

Tukey's Multiple Comparison Test	Mean Diff.	q	Significant? P < 0.05?	Summary	95% CI of diff
Glass vs Aminosilane	-0.1800	14.43	Yes	***	-0.2404 to -0.1196
Glass vs HA4 C1	-0.07467	7.333	Yes	***	-0.1239 to -0.02539
Glass vs HA4 C2	-0.09400	9.232	Yes	***	-0.1433 to -0.04472
Glass vs HA4 C3	-0.1128	11.25	Yes	***	-0.1614 to -0.06427
Glass vs HA234 C1	-0.04613	4.531	No	ns	-0.09541 to 0.003148
Glass vs HA234 C2	-0.0640	6.286	Yes	**	-0.1133 to -0.01472
Glass vs HA234 C3	-0.09733	9.559	Yes	***	-0.1466 to -0.04805
Glass vs HA2590 C1	-0.01933	1.899	No	ns	-0.06861 to 0.02995
Glass vs HA2590 C2	-0.03087	3.031	No	ns	-0.08015 to 0.01841
Glass vs HA2590 C3	-0.05833	5.729	Yes	**	-0.1076 to -0.009052
Glass vs HAmix C1	0.003133	0.3077	No	ns	-0.04615 to 0.05241
Glass vs HAmix C2	-0.02907	2.855	No	ns	-0.07835 to 0.02021
Glass vs HAmix C3	-0.09733	9.559	Yes	***	-0.1466 to -0.04805
Aminosilane vs HA4 C1	0.1053	10.34	Yes	***	0.05605 to 0.1546
Aminosilane vs HA4 C2	0.0860	8.446	Yes	***	0.03672 to 0.1353
Aminosilane vs HA4 C3	0.06718	6.697	Yes	***	0.01863 to 0.1157
Aminosilane vs HA234 C1	0.1339	13.15	Yes	***	0.08459 to 0.1831
Aminosilane vs HA234 C2	0.1160	11.39	Yes	***	0.06672 to 0.1653
Aminosilane vs HA234 C3	0.08267	8.119	Yes	***	0.03339 to 0.1319
Aminosilane vs HA2590 C1	0.1607	15.78	Yes	***	0.1114 to 0.2099
Aminosilane vs HA2590 C2	0.1491	14.65	Yes	***	0.09985 to 0.1984
Aminosilane vs HA2590 C3	0.1217	11.95	Yes	***	0.07239 to 0.1709
Aminosilane vs HAmix C1	0.1831	17.99	Yes	***	0.1339 to 0.2324
Aminosilane vs HAmix C2	0.1509	14.82	Yes	***	0.1017 to 0.2002
Aminosilane vs HAmix C3	0.08267	8.119	Yes	***	0.03339 to 0.1319

Appendix XVIII

Tukey's Multiple Comparison Test	Mean Diff.	q	Significant? P < 0.05?	Summary	95% CI of diff
HA4 C1 vs HA4 C2	-0.01933	2.685	No	ns	-0.05418 to 0.01551
HA4 C1 vs HA4 C3	-0.03816	5.463	Yes	*	-0.07196 to -0.004350
HA4 C1 vs HA234 C1	0.02853	3.963	No	ns	-0.006314 to 0.06338
HA4 C1 vs HA234 C2	0.01067	1.482	No	ns	-0.02418 to 0.04551
HA4 C1 vs HA234 C3	-0.02267	3.148	No	ns	-0.05751 to 0.01218
HA4 C1 vs HA2590 C1	0.05533	7.685	Yes	***	0.02049 to 0.09018
HA4 C1 vs HA2590 C2	0.0438	6.083	Yes	**	0.008953 to 0.07865
HA4 C1 vs HA2590 C3	0.01633	2.269	No	ns	-0.01851 to 0.05118
HA4 C1 vs HAmix C1	0.07780	10.81	Yes	***	0.04295 to 0.1126
HA4 C1 vs HAmix C2	0.0456	6.334	Yes	**	0.01075 to 0.08045
HA4 C1 vs HAmix C3	-0.02267	3.148	No	ns	-0.05751 to 0.01218
HA4 C2 vs HA4 C3	-0.01882	2.695	No	ns	-0.05263 to 0.01498
HA4 C2 vs HA234 C1	0.04787	6.648	Yes	***	0.01302 to 0.08271
HA4 C2 vs HA234 C2	0.03000	4.167	No	ns	-0.004847 to 0.06485
HA4 C2 vs HA234 C3	-0.003333	0.4630	No	ns	-0.03818 to 0.03151
HA4 C2 vs HA2590 C1	0.07467	10.37	Yes	***	0.03982 to 0.1095
HA4 C2 vs HA2590 C2	0.06313	8.769	Yes	***	0.02829 to 0.09798
HA4 C2 vs HA2590 C3	0.03567	4.954	Yes	*	0.0008196 to 0.07051
HA4 C2 vs HAmix C1	0.09713	13.49	Yes	***	0.06229 to 0.1320
HA4 C2 vs HAmix C2	0.06493	9.019	Yes	***	0.03009 to 0.09978
HA4 C2 vs HAmix C3	-0.003333	0.4630	No	ns	-0.03818 to 0.03151
HA4 C3 vs HA234 C1	0.06669	9.548	Yes	***	0.03288 to 0.1005
HA4 C3 vs HA234 C2	0.04882	6.990	Yes	***	0.01502 to 0.08263
HA4 C3 vs HA234 C3	0.01549	2.218	No	ns	-0.01832 to 0.04930
HA4 C3 vs HA2590 C1	0.09349	13.38	Yes	***	0.05968 to 0.1273
HA4 C3 vs HA2590 C2	0.08196	11.73	Yes	***	0.04815 to 0.1158
HA4 C3 vs HA2590 C3	0.05449	7.801	Yes	***	0.02068 to 0.08830
HA4 C3 vs HAmix C1	0.1160	16.60	Yes	***	0.08215 to 0.1498
HA4 C3 vs HAmix C2	0.08376	11.99	Yes	***	0.04995 to 0.1176
HA4 C3 vs HAmix C3	0.01549	2.218	No	ns	-0.01832 to 0.04930
HA234 C1 vs HA234 C2	-0.01787	2.482	No	ns	-0.05271 to 0.01698
HA234 C1 vs HA234 C3	-0.0512	7.111	Yes	***	-0.08605 to -0.01635
HA234 C1 vs HA2590 C1	0.0268	3.722	No	ns	-0.008047 to 0.06165
HA234 C1 vs HA2590 C2	0.01527	2.120	No	ns	-0.01958 to 0.05011
HA234 C1 vs HA2590 C3	-0.0122	1.694	No	ns	-0.04705 to 0.02265
HA234 C1 vs HAmix C1	0.04927	6.843	Yes	***	0.01442 to 0.08411
HA234 C1 vs HAmix C2	0.01707	2.370	No	ns	-0.01778 to 0.05191
HA234 C1 vs HAmix C3	-0.0512	7.111	Yes	***	-0.08605 to -0.01635
HA234 C2 vs HA234 C3	-0.03333	4.630	No	ns	-0.06818 to 0.001514
HA234 C2 vs HA2590 C1	0.04467	6.204	Yes	**	0.009820 to 0.07951
HA234 C2 vs HA2590 C2	0.03313	4.602	No	ns	-0.001714 to 0.06798
HA234 C2 vs HA2590 C3	0.005667	0.7871	No	ns	-0.02918 to 0.04051
HA234 C2 vs HAmix C1	0.06713	9.324	Yes	***	0.03229 to 0.1020
HA234 C2 vs HAmix C2	0.03493	4.852	Yes	*	8.623e-005 to 0.06978
HA234 C2 vs HAmix C3	-0.03333	4.630	No	ns	-0.06818 to 0.001514
HA234 C3 vs HA2590 C1	0.0780	10.83	Yes	***	0.04315 to 0.1128
HA234 C3 vs HA2590 C2	0.06647	9.232	Yes	***	0.03162 to 0.1013
HA234 C3 vs HA2590 C3	0.0390	5.417	Yes	*	0.004153 to 0.07385
HA234 C3 vs HAmix C1	0.1005	13.95	Yes	***	0.06562 to 0.1353
HA234 C3 vs HAmix C2	0.06827	9.482	Yes	***	0.03342 to 0.1031
HA234 C3 vs HAmix C3	0.0	0.0	No	ns	-0.03485 to 0.03485

Appendix XVIII

Tukey's Multiple Comparison Test	Mean Diff.	q	Significant? P < 0.05?	Summary		95% CI of diff
HA2590 C1 vs HA2590 C2	-0.01153	1.602	No	ns		-0.04638 to 0.02331
HA2590 C1 vs HA2590 C3	-0.0390	5.417	Yes	*		-0.07385 to -0.004153
HA2590 C1 vs HAmix C1	0.02247	3.120	No	ns		-0.01238 to 0.05731
HA2590 C1 vs HAmix C2	-0.009733	1.352	No	ns		-0.04458 to 0.02511
HA2590 C1 vs HAmix C3	-0.0780	10.83	Yes	***		-0.1128 to -0.04315
HA2590 C2 vs HA2590 C3	-0.02747	3.815	No	ns		-0.06231 to 0.007380
HA2590 C2 vs HAmix C1	0.0340	4.722	No	ns		-0.0008471 to 0.06885
HA2590 C2 vs HAmix C2	0.001800	0.2500	No	ns		-0.03305 to 0.03665
HA2590 C2 vs HAmix C3	-0.06647	9.232	Yes	***		-0.1013 to -0.03162
HA2590 C3 vs HAmix C1	0.06147	8.537	Yes	***		0.02662 to 0.09631
HA2590 C3 vs HAmix C2	0.02927	4.065	No	ns		-0.005580 to 0.06411
HA2590 C3 vs HAmix C3	-0.0390	5.417	Yes	*		-0.07385 to -0.004153
HAmix C1 vs HAmix C2	-0.0322	4.472	No	ns		-0.06705 to 0.002647
HAmix C1 vs HAmix C3	-0.1005	13.95	Yes	***		-0.1353 to -0.06562
HAmix C2 vs HAmix C3	-0.06827	9.482	Yes	***		-0.1031 to -0.03342

Appendix XIX

APPROVAL SIGNATURE

Dept/Date:	**Effective Date:** (Document Control Use Only)
QA/Date:	

Purpose and Scope

To define the testing and specifications for Dried Sodium Hyaluronate, pH 4.0 Process, Medical Grade.

Chemical Structure

[-β-Sodium Glucuronic Acid-(1→3)-β-N-Acetyl Glucosamine-(1→4)-]$_n$

Acceptance Criteria

Test	Method	Specification
Intrinsic Viscosity	QATM 136	≥ 3.0 dl/g
Endotoxin	QATM 092	0.07 EU/mg NaHy maximum
Bioburden	QATM 208	≤ 100 cfu/g
Microbial Identification[1]	QATM 075	None of the following observed: *E. coli, Pseudomonas aeruginosa, Staphylococcus aureus, Salmonella sp.* & *Streptococcus pyogenes*
Water Content	QATM 256	≤ 10.0%
pH (1% solution in water)	QATM 021	6.2 -7.8
Osmolality (1% solution in water)	QATM 069	75 mOsm/kg maximum
Visual Appearance	QATM 071	White to off white, fluffy to small grain powder
Odor	QATM 071	None
IR Spectrum (4000-800 cm^{-1}) (1% solution in water)	QATM 081	Matches Standard
UV-VIS Spectrum (820-190nm) (1% solution in water)	QATM 086	Matches Standard
Nucleic Acid (1% solution in water)	QATM 086	A260 ≤ 0.5
Hyaluronidase sensitivity (1% solution in water)	QATM 065	Positive
Acetate Concentration	QATM 030	1.0 % maximum
Protein Concentration	QATM 001	0.1% maximum
Ethanol	QATM 229	0.5% maximum
Isopropanol	QATM 229	0.5% maximum
Methanol	QATM 229	0.25% maximum

Continued on next page

[1] Microbial identification is necessary only if microorganisms were found using QATM 208.

Acceptance Criteria (continued)

Test	Method	Specification
Arsenic	SOP 9011	2 ppm maximum
Cadmium	SOP 9011	5 ppm maximum
Chromium	SOP 9011	5 ppm maximum
Cobalt	SOP 9011	10 ppm maximum
Copper	SOP 9011	10 ppm maximum
Iron	SOP 9011	51 ppm maximum
Lead	SOP 9011	10 ppm maximum
Mercury	SOP 9011	10 ppm maximum
Nickel	SOP 9011	5 ppm maximum
Rabbit Ocular Toxicity Testing (2% solution in ROPBS)	SOP 9011	• Mean vitreal score ≤ 175 cells/mm^3 • No spike > 400 cells/mm^3 • Mean clinical score < 2.0

Labeling

Method	Stage	Characteristic Present and Accounted For on Date of Inspection
Visual	WIP	• Product Name: Dried Sodium Hyaluronate • Lot Number • SPEC Number • Expiration date per SOP 0340 • Product Weight • Bottle Weight • Bottle Number

Additional Information

Sampling Plan	Sample per MPR 0059 for QC Testing and Archiving
Storage Requirements	≤ -15°C
Retest Date	per SOP 0340

References

MPR 0059, Vacuum Drying and Packaging of Sodium Hyaluronate
QATM 001, Protein Assay
QATM 021, Hydrogen Ion Concentration (pH)
QATM 030, Acetic Acid Test
QATM 065, Hyaluronidase Test for Hyaluronan
QATM 069, Solution Osmolality
QATM 071, Sensory Testing for Raw Materials, In-Process, Final Products and NaHy Powder
QATM 075, Microbial Differentiation/Identification
QATM 081, Identification by Infra-red Spectroscopy
QATM 086, UV/VIS Scan and Optical Density
QATM 092, Photometric Endotoxin Assay
QATM 136, Determination of Intrinsic Viscosity and Average Molecular Weight
QATM 208, Aerobic Plate Count, Total Yeasts and Mold Count
QATM 229, Alcohol Quantification of NaHy Powder By Gas Chromatography With Headspace Sampler
QATM 256, Moisture Determination using MM710 Infrared Gauge
SOP 0340, Expiration Dating and Monitoring
SOP 9011, Outside Lab Testing of Materials

SUMMARY OF REVISION CHANGES

Rev.	Change	Change #	Eff. Date
0	Initial release.	13315	11/06/96
1	Add specification for viscosity in 0.9% saline.	14358	02/19/97
2	Add Lifecore part number and remove SPEC 801 requirement. Change bioburden, protein, and ethanol for specifications. Change viscosity on 3% . Add expiration date.	15550	09/23/97
3	Change QATM 130 to 229. Change lower limit of intrinsic viscosity from 14 to 20. Bioburden BAP & SAP $\leq$ 100 CFU/g.	50909	8/5/98
4	Remove reference to QATM 037, add reference to QATM 208.	53673	2/1/99
5	Remove reference to SOP 1341, add MPR 0059.	54153	5/5/99
6	Add Volatile Organic Compounds Testing.	56502	8/21/00
7	Chang QATM's 060, 251, and 033 to Sop 9011. Update references. Change word to read mean not average.	57094	03/19/01
8	Add Methanol SPEC.	57439	04/30/01
9	Add new test method QATM 256. Remove record retention section. Update references. Remove VOC testing.	58773	11/4/02
10	Update format to InfoAccess. Add chemical structure section. Change pH from 5.5-7.8, to 6.2 – 7.8, change protein concentration from 0.3% max to, 0.1% max, change water from 8.0% max to, 10.0%max, change ethanol from 1.5% to, 0.5%, change iron from 25ppm to, 51ppm, change nucleic acid <0.5 absorbance to, 0.5 max.	60083	10/27/2003
11	Add 260nm to Nucleic Acid Test.	60143	12/1/2003
12	Change title of QATM 001 in references section.	60605	6/14/04
13	Add streptococcus pyogenes to microbial identification.	60872	10/14/04
14	Update format. No changes were made to test specifications	61647	11/23/05
15	Removed molecular weight and viscosity. Lowered intrinsic viscosity and ROTT specification.	62312	

Lifecore report for HA_4

ASTRA 4.90.07 summary Report for 101004_01

File	:	H:\...\Astra\QC Astra files\2007\1007\101007 A1\101004_01.ADF $
Sample ID	:	014735 Sample #8 #1
Operator	:	

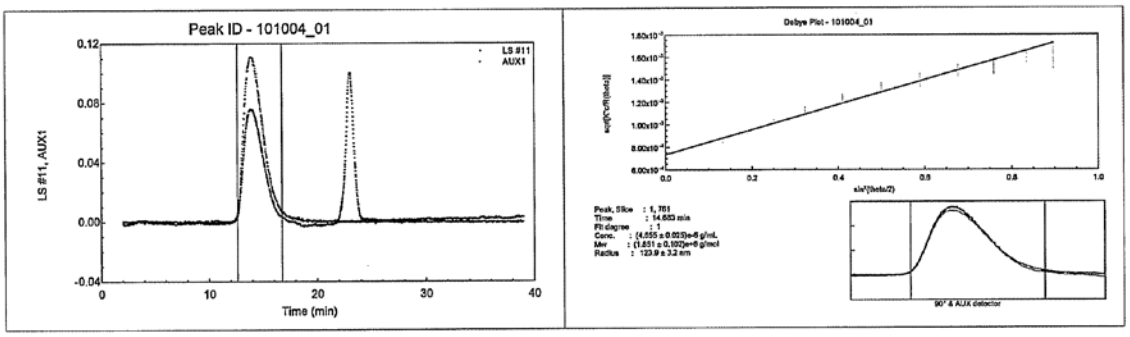

COLLECTION INFORMATION

Collection time	:	Wed Oct 10, 2007 12:31 PM Central Daylight Time
Instrument type	:	DAWN EOS
Cell type	:	K5
Laser wavelength	:	690.0 nm
Solvent name	:	0.15M NaCl/50mM PBS
Solvent RI	:	1.331
Calibration constants		
DAWN	:	8.7560e-06
» AUX1	:	2.2378e-05
Flow rate	:	0.800 mL/min

PROCESSING INFORMATION

Processing time	:	Wed Oct 10, 2007 02:22 PM Central Daylight Time
Smoothing	:	Normal despiking, No smoothing
DAWN/AUX1 delay	:	0.173 mL
Fit method / model	:	Berry
Calculation method	:	dn/dc + AUX Constant
USING FITTED DATA	:	MM fit = 1st order, Polynomial
		Radius fit = 1st order, Polynomial
Detectors used	:	6 7 8 9 10 11 12 13 14 15 16

RESULTS

		PEAK #1
Time (min.)	:	12.617 - 16.750
Slices	:	249
A2 (mol mL/g²)	:	0.000e+00
Fit degree	:	1
Injected Mass (g)	:	0.0000e+00
Calc. Mass (g)	:	1.0430e-05
dn/dc (mL/g)	:	0.150
Polydispersity(Mw/Mn)	:	1.010±0.012 (1.2%)
Polydispersity(Mz/Mn)	:	1.020±0.022 (2.2%)

Molar Mass Moments (g/mol)

Mn	:	1.973e+06 (0.9%)
Mw	:	1.993e+06 (0.9%)
Mz	:	2.013e+06 (2.0%)

Lifecore report for HA_4

R.M.S. Radius Moments (nm)

Rn	:	127.1 (0.24%)
Rw	:	128.2 (0.24%)
Rz	:	129.2 (0.25%)

Peak Areas Module v1.01 Report

Detector #		PEAK #1
3	:	1.20075
4	:	0.99740
5	:	0.75002
6	:	0.58795
7	:	0.47034
8	:	0.38894
9	:	0.31746
10	:	0.27049
11	:	0.22963
12	:	0.20605
13	:	0.18301
14	:	0.17429
15	:	0.15935
16	:	0.16060
17	:	0.10122
18	:	0.14120
A1	:	0.08739
A2	:	-0.00887

Units are (baseline adjusted, normalized volts) * (minutes).

Lifecore report for HA_4

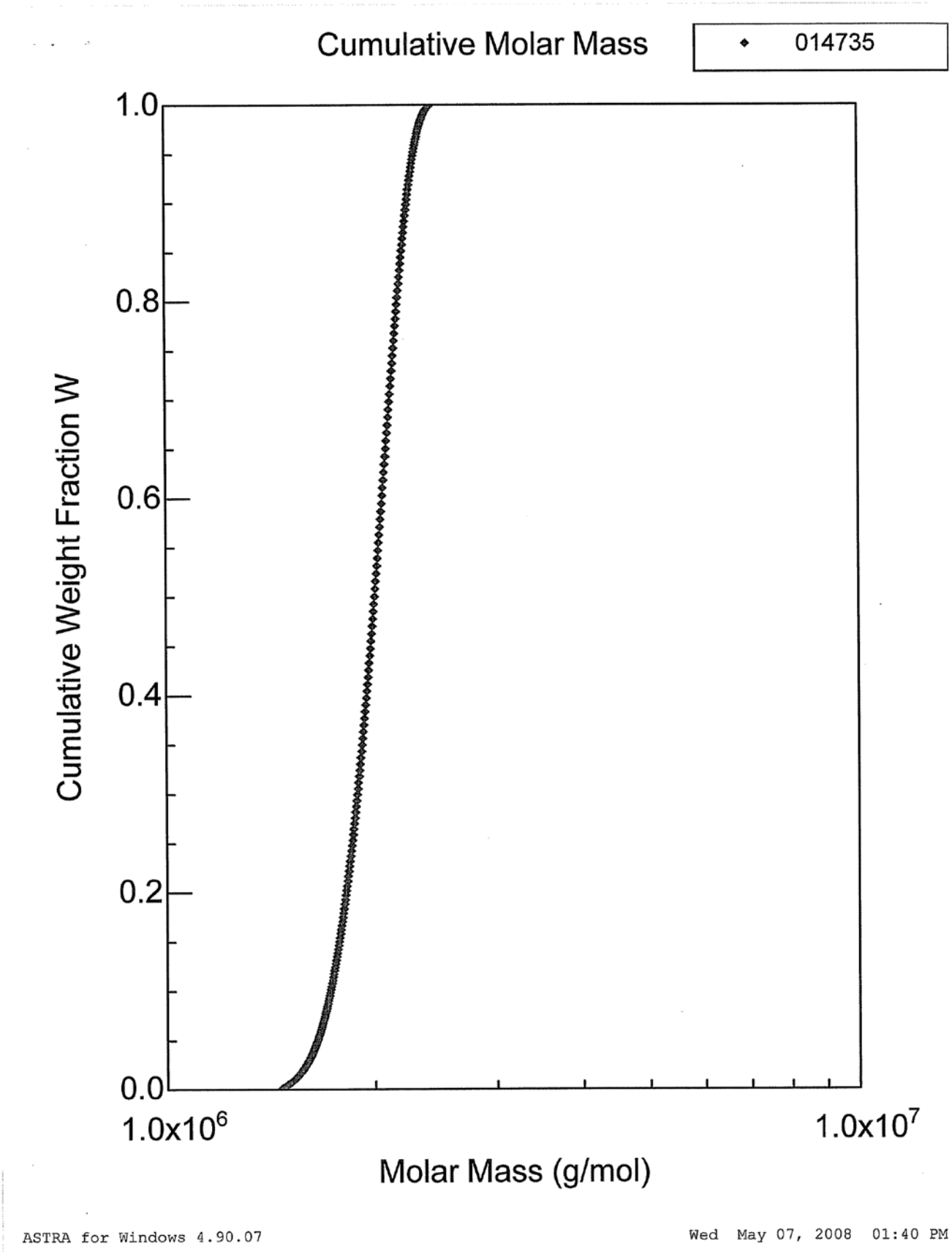

ASTRA for Windows 4.90.07

Wed May 07, 2008 01:40 PM

Lifecore report for HA_{234}

ASTRA 4.90.07 summary Report for 111610_01

File	:	H:\...\Astra\QC Astra files\2006\1106\111606 A1\111610_01.ADF
Sample ID	:	GSP252-5-5 #2
Operator	:	

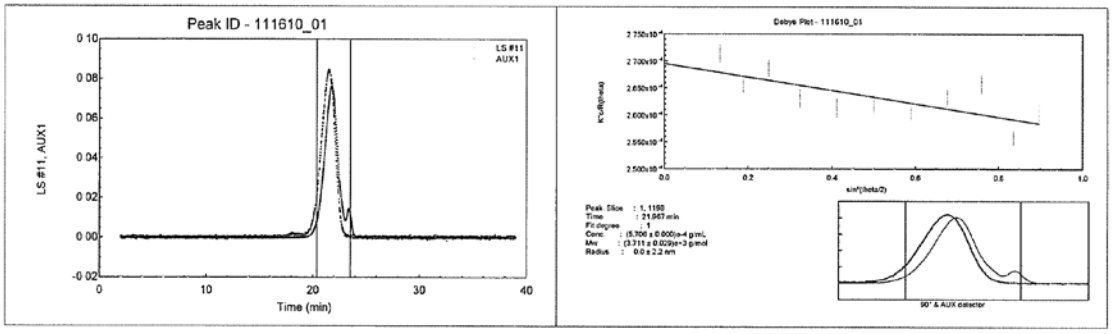

COLLECTION INFORMATION

Collection time	:	Fri Nov 17, 2006 02:04 AM Central Standard Time
Instrument type	:	DAWN EOS
Cell type	:	K5
Laser wavelength	:	690.0 nm
Solvent name	:	0.15M NaCl/50mM PBS
Solvent RI	:	1.331
Calibration constants		
DAWN	:	9.0300e-06
» AUX1	:	2.2439e-05
Flow rate	:	0.800 mL/min

PROCESSING INFORMATION

Processing time	:	Sun Nov 19, 2006 05:20 PM Central Standard Time
DAWN/AUX1 delay	:	0.160 mL
Fit method / model	:	Zimm
Calculation method	:	dn/dc + AUX Constant
USING FITTED DATA	:	MM fit = 1st order, Polynomial Radius fit = 1st order, Polynomial
Detectors used	:	6 7 8 9 10 11 12 13 14 15 16

RESULTS

		PEAK #1
Time (min.)	:	20.383 - 23.567
Slices	:	192
A2 (mol mL/g²)	:	0.000e+00
Fit degree	:	1
Injected Mass (g)	:	0.0000e+00
Calc. Mass (g)	:	7.2562e-04
dn/dc (mL/g)	:	0.150
Polydispersity(Mw/Mn)	:	1.264±0.010 (0.8%)
Polydispersity(Mz/Mn)	:	1.534±0.018 (1.2%)

Molar Mass Moments (g/mol)

Mn	:	3.679e+03 (0.6%)
Mw	:	4.650e+03 (0.5%)
Mz	:	5.644e+03 (1.0%)

R.M.S. Radius Moments (nm)

Lifecore report for HA_{234}

Rn	:	25.1 (28%)
Rw	:	20.3 (24%)
Rz	:	16.8 (20%)

Peak Areas Module v1.01 Report

Detector #		PEAK #1
3	:	0.12035
4	:	0.11205
5	:	0.12779
6	:	0.12033
7	:	0.12156
8	:	0.12312
9	:	0.12361
10	:	0.12366
11	:	0.12386
12	:	0.12386
13	:	0.12358
14	:	0.12309
15	:	0.12393
16	:	0.12368
17	:	0.12189
18	:	0.14797
A1	:	6.06325
A2	:	-0.00586

Units are (baseline adjusted, normalized volts) * (minutes).

Lifecore report for HA_{234}

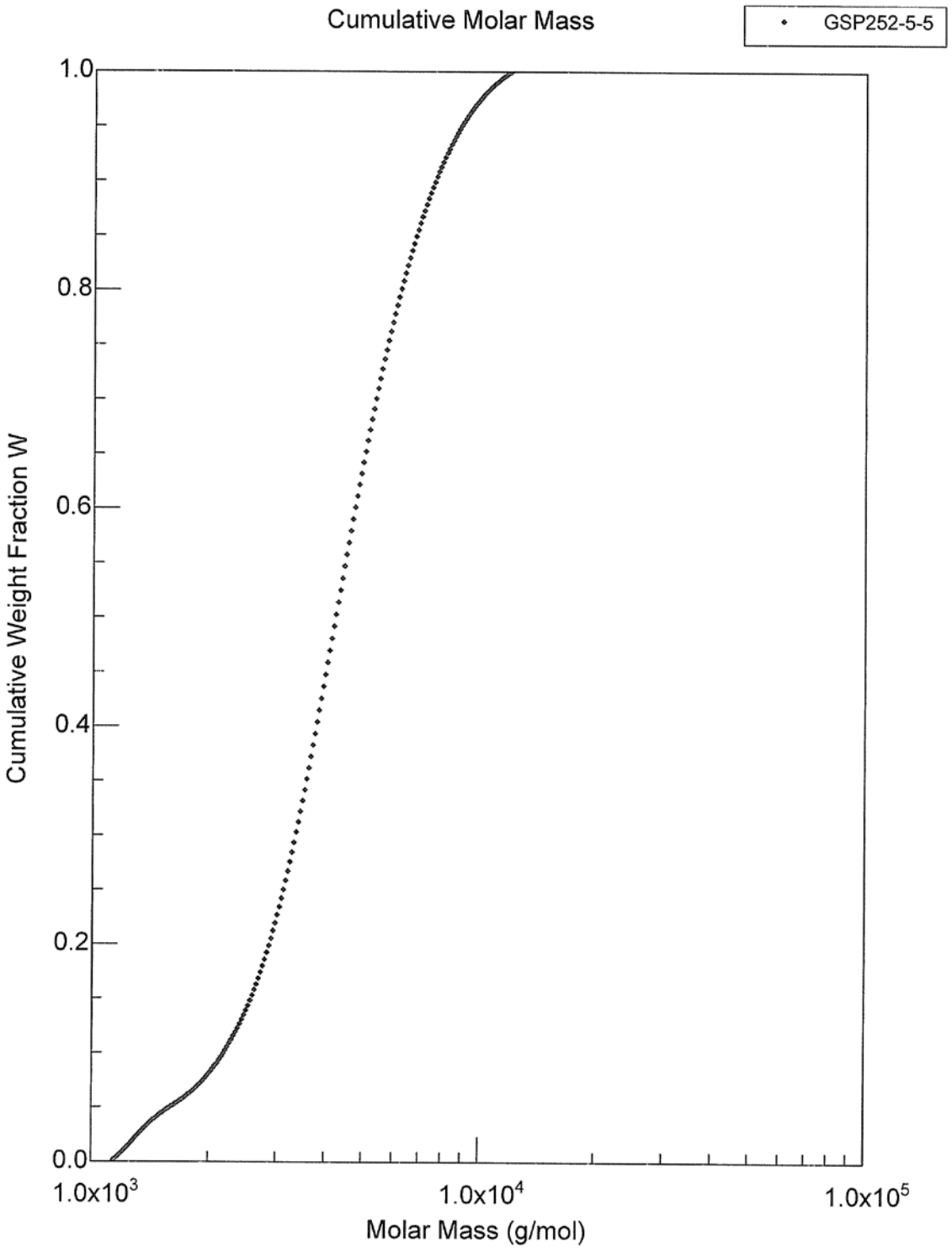

GSP252-5-5
ASTRA for Windows 4.90.07

Wed Dec 19, 2007 03:13 PM

Lifecore report for HA_{2590}

ASTRA 4.90.07 summary Report for 061604_01

File	:	H:\Analytical\Astra\QC Astra files\2004\061604\061604_01.ADF
Sample ID	:	002799 final powder #2
Operator	:	

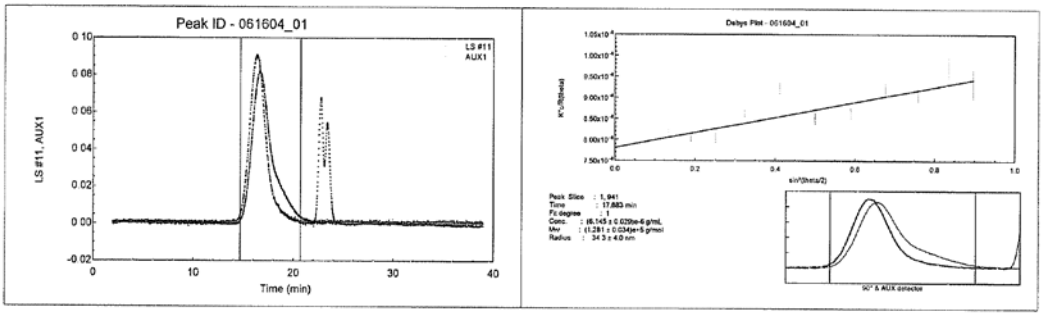

COLLECTION INFORMATION

Collection time	:	Wed Jun 16, 2004 07:50 PM Central Daylight Time
Instrument type	:	DAWN EOS
Cell type	:	K5
Laser wavelength	:	690.0 nm
Solvent name	:	0.15M NaCl/50mM PBS
Solvent RI	:	1.331
Calibration constants		
DAWN	:	8.2530e-06
» AUX1	:	2.2902e-05
Flow rate	:	0.800 mL/min

PROCESSING INFORMATION

Processing time	:	Thu Jun 17, 2004 08:26 AM Central Daylight Time
DAWN/AUX1 delay	:	0.173 mL
Fit method / model	:	Zimm
Calculation method	:	dn/dc + AUX Constant
USING FITTED DATA	:	MM fit = 1st order, Polynomial Radius fit = 1st order, Polynomial
Detectors used	:	6 7 8 9 10 11 12 13 14 15 16

RESULTS

		PEAK #1
Time (min.)	:	14.667 - 20.717
Slices	:	364
A2 (mol mL/g²)	:	0.000e+00
Fit degree	:	1
Injected Mass (g)	:	0.0000e+00
Calc. Mass (g)	:	2.3374e-05
dn/dc (mL/g)	:	0.150
Polydispersity(Mw/Mn)	:	1.746±0.010 (0.6%)
Polydispersity(Mz/Mn)	:	2.424±0.020 (0.8%)

Molar Mass Moments (g/mol)

Mn	:	1.322e+05 (0.5%)
Mw	:	2.307e+05 (0.29%)
Mz	:	3.204e+05 (0.7%)

R.M.S. Radius Moments (nm)

Rn	:	33.5 (0.8%)
Rw	:	45.3 (0.6%)
Rz	:	54.1 (0.5%)

Peak Areas Module v1.01 Report

Detector #		PEAK #1
3	:	0.18427
4	:	0.20936
5	:	0.21696
6	:	0.19931
7	:	0.19965
8	:	0.19294
9	:	0.18771
10	:	0.17760
11	:	0.17921
12	:	0.16787
13	:	0.16043
14	:	0.15375
15	:	0.15007
16	:	0.14844
17	:	0.12280
18	:	0.06936
A1	:	0.19136
A2	:	-0.00555

Units are (baseline adjusted, normalized volts) * (minutes).

Lifecore report for HA_{2590}

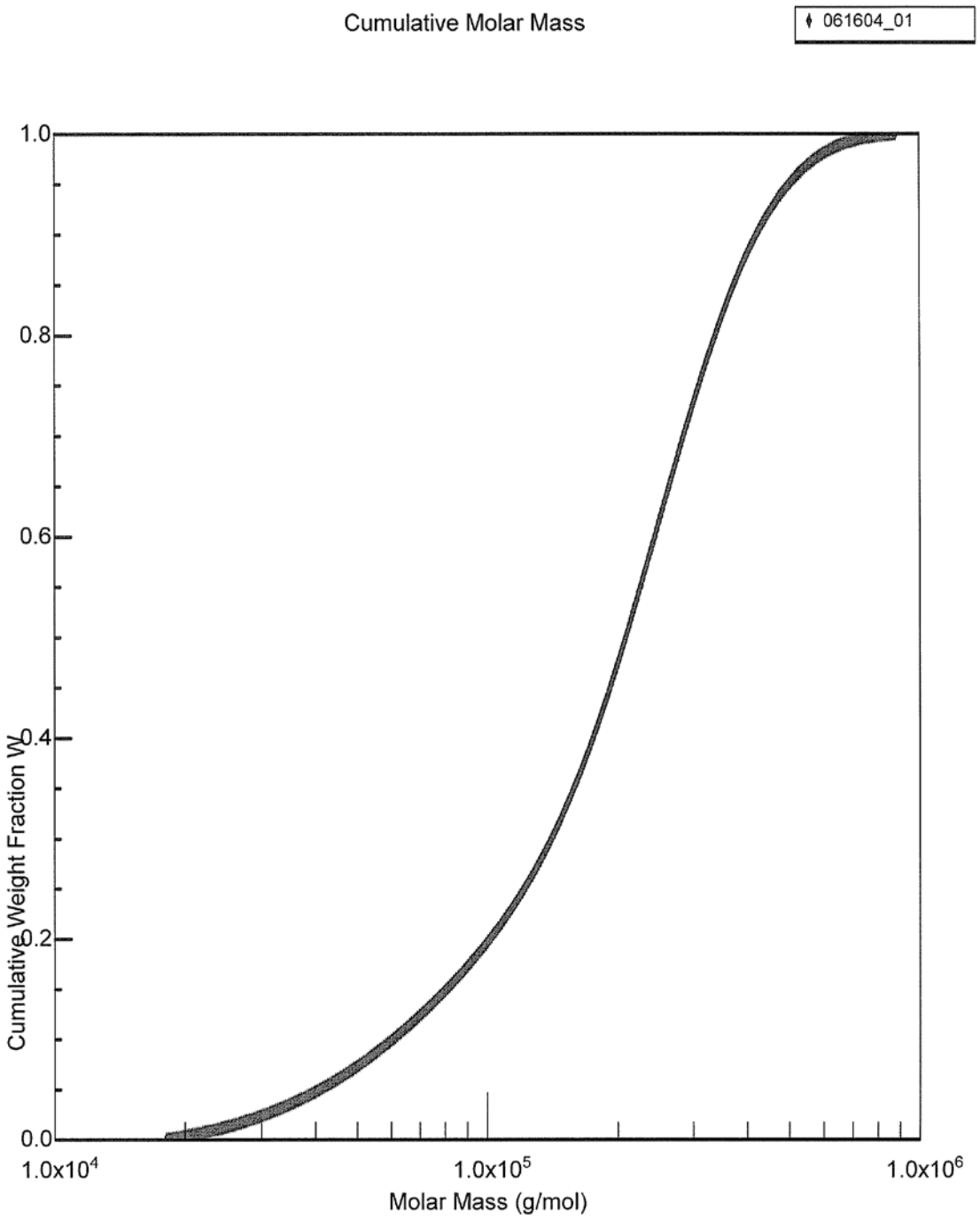

002799
ASTRA for Windows 4.90.07 Tue Apr 01, 2008 10:32 AM

Appendix XX

µLibra Technical Note

µLibra

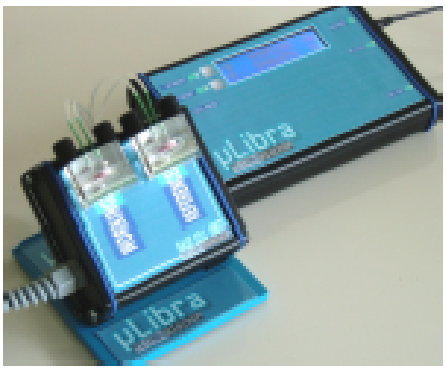

µLibra is a Quartz Crystal Microbalance (QCM) system, composed by a Main Unit and a Cell Base Unit which can support two measuring chambers.

µLibra allows experiments from biology to chemistry, to physics. As biosensor, it can monitor ligand-receptor interactions. The instrument offers a rapid and easy way to detect and measure mass deposition or adsorption as well as film thickness. Alternatively, density and viscosity variation of fluids can be measured, if mass deposition/adsorption is known.

µLibra Introduction

Quartz crystals are widely used to build up resonators. In a QCM instruments the resonator frequency is sampled in order to measure mass deposition/adsorption or viscosity variations. For this applications, AT-cut quartz are suited, because of their great temperature stability, few ppm in a range of 0 C° to 40 C°. For an AT-cut quartz crystal the oscillation frequency f_0 is given by the following equation:

$$f_0 = \frac{n}{2l}\sqrt{\frac{\rho_q}{\mu_q}}$$

where n is the overtone number, l is the thickness of the quartz, ρ_q and μ_q are respectively the density (2.648 g/cm^3) and shear modulus (2.947 10^{11} g/cm s^2) of the quartz.

Theoretical backgrounds for using quartzes as mass sensors take origin in Sauerbrey equation, witch takes into account the frequency shift due to mass deposition on quartz surfaces.

$$\Delta f = -2nf_0^2 \frac{\Delta m}{A\sqrt{\rho_q \mu_q}}$$

Sauerbrey equation

where Δf is the frequency shift, f_0 is the unloaded quartz frequency, A is the piezoelectric active area and Δm is the mass deposited/adsorpted.

For liquid phase working quartzes, Kanazawa equation focuses on frequency shift dependence on liquid's density-viscosity product.

Appendix XX

$$\Delta f = -f_0^{\frac{3}{2}} \sqrt{\frac{\rho_l \eta_l}{\pi \rho_q \mu_q}}$$ **Kanazawa equation**

where ρ_l and η_l are respectively the density and viscosity of the liquid.

For example, according to Sauerbrey equation, for a 10 MHz crystal, a Δf of 1 Hz corresponds to a $\Delta m/A$ of 4.41ng/cm^2. Mass resolution of a QCM instrument can be therefore much greater of a precision balance, making this technique very attractive for a large range of applications.

When a quartz works in liquid phase, several physical phenomena, such as dielectric constant and conductibility variations, can result into frequency variation. Great care has been taken in oscillators design, in order to ensure good sensitivity while maintaining small dependence on environmental factors. **µLibra** oscillators force quartzes at fundamental series frequency (Fs) oscillation, assuring the best reliability and minimizing effects of unwanted parasitic phenomena. The oscillators are well suitable for use in viscous liquids and have been tested for viscosity greater than 20 mPa•s (70% Glycerol in water solution @25°).

µLibra Applications of QCM

A QCM is a mass sensing instrument, which is able to measure in real time very small mass changes. The sensitivity of a QCM can be 100 higher than an electronic balance with a resolution of 0.1ng, allowing extremely small measurements in physical, chemical and biological fields. This technique offers a rapid and easy way to detect and measure mass deposition or adsorption as well as film thickness. The possibility to extend measurements to the liquid phase have increased the interest in this technique during last years. The use of QCM as biosensors allows high sensitivity label-free detection of molecules and take benefits from the small amount of sample needed. **µLibra** cells have a chamber volume as small as only 25 µl.

Below there is a list of possible applications.

- real time monitoring of ligand/receptor interactions
- measure of kinetics and affinity constants
- monoclonal antibody characterization
- kinetic studies in DNA hybridisation
- thin film measurement
- viscosity tracking

Appendix XX

µLibra Working principle of µLibra instrument

The **µLibra** measuring principle is based on quartz fundamental frequency sampling.

µLibra is composed by a Main Unit and a Cell Base Unit which contains oscillators circuitry and can support one or two measuring chambers. The oscillators force quartzes in each measuring chamber at fundamental series frequency oscillation. Frequency is sampled by an high precision and high stability frequency counter, ensuring resolution of 1 Hz and temperature stability of less than 0.1ppm in the range 0° - 60°. Control electronics and frequency counter are housed in the Main Unit.

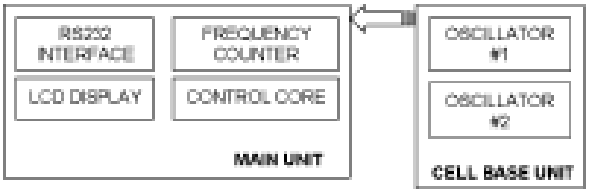

Double channel acquisition system allows single cell operation as well as working/reference measurements. Whatever the experimental set up, **UbraVIEW** software represents a powerful tool to track and record frequency values data.

µLibra Cells

µLibra can be equipped with two low-volume flow-through cells. Housing the transducers inside the cells is rapid and secure. The provided cells have been designed for a wide range of static and flow measurement experiments, however, on requests, custom measuring cells can be made on design.

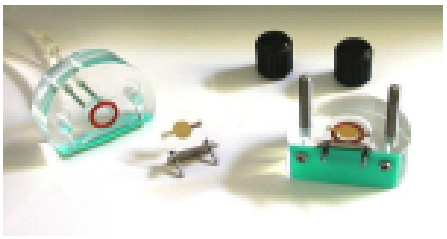

For further information contact:

Technobiochip
Via Provinciale Pianura, 5 (Loc. S. Martino)
80078 Pozzuoli (NA)
Tel. 081 5264315 / 5263169
Fax: 081 5265116
e-mail: lab@technobiochip.com
www.technobiochip.com